Influence du trou d'ozone antarctique et la dynamique atmosphérique sur l'ozone dans le sud du Brésil

Gabriela Dornelles Bittencourt

THÈSE

EN VUE DE L'OBTENTION DU GRADE DE

DOCTEUR ÈS SCIENCES

SPECIALITE: PHYSIQUE DE L'ATMOSPHERE

Présentée et soutenue le vendredi 22 août 2022 par:

Gabriela Dornelles BITTENCOURT

Influence of the Antarctic Ozone Hole and Atmospheric Dynamics on Ozone in Southern Brazil

Jury

Dr. Nelson BÈGUE	LACy, Saint Denis, FR	Examinateur
Dr. Luiz A. STEFFENEL	URCA, Reims, FR	Examinateur
Dr. Vagner ANABOR	UFSM, Santa Maria, BR	Examinateur
Dr. Lucas Vaz PERES	UFOPA, Santarém, BR	Rapporteur
Dra. Nathalie BOIASKI	UFSM, Santa Maria, BR	Rapporteur
Hassan BENCHERIF	LACy, Saint Denis, FR	Directeur de these
Dra. Damaris PINHEIRO	UFSM, Santa Maria, BR	Co-directice de thèse

ÉCOLE DOCTORALE, SPECIALITE:

Sciences Technologies Santé (ED542), Physique de l'Atmosphère

UNITE DE RECHERCHE:

Laboratoire de l'Atmosphère et des Cyclones – LACy UMR 8105

DIRECTEUR ET CO-DIRECTRICE DE THESE:

Hassan BENCHERIF et Damaris PINHEIRO

UNIVERSIDADE FEDERAL DE SANTA MARIA
CENTRO DE CIÊNCIAS NATURAIS E EXATAS
PROGRAMA DE PÓS-GRADUAÇÃO EM METEOROLOGIA

UNIVERSITÉ DE LA RÉUNION
SCIENCES TECHNOLOGIES SANTÉ, PHYSIQUE DE L'ATMOSPHÈRE

Gabriela Dornelles Bittencourt

INFLUENCE OF THE ANTARCTIC OZONE HOLE AND ATMOSPHERIC DYNAMICS ON OZONE IN SOUTHERN BRAZIL

Santa Maria, RS, Brazil

2022

Influence of the Antarctic Ozone Hole and Atmospheric Dynamics on Ozone in Southern Brazil

by

Gabriela Dornelles Bittencourt

Submitted in fulfillment of the requirements for the degree
Doctor in Meteorology in the Graduate Program
in Meteorology, Federal University of Santa Maria

Supervisor: Dra, Damaris Kirsch PINHEIRO

and

Docteur és Sciences (Physique de l'atmosphere)
Sciences Technologies Santé (ED542), Physique de l'Atmosphère,
Laboratoire de l'Atmosphère et des Cyclones – LACy UMR 8105
Université de La Réunion

Supervisor: Hassan BENCHERIF

22 August 2022

INFLUENCE OF THE ANTARCTIC OZONE HOLE AND ATMOSPHERIC DYNAMICS ON OZONE IN SOUTHERN BRAZIL

Thesis presented with Cotutelle to the Graduate Program in Meteorology, Federal University of Santa Maria (UFSM, RS)/ Sciences Technologies Santé, Physique de l'Atmosphère, Université de La Rèunion (UR, FR), as a partial requirement for obtaining the title of **Doctor in Meteorology/ Doctor in Atmosphere Physics.**

Approved in 22 August 2022:

Damaris Kirsch Pinheiro, Dra. (UFSM)
(President/Advisor)

Hassan Bencherif, Dr. (UR)
(Co-Advisor)

Nelson Bègue, Dr. (UR)

Luiz Angelo Steffenel, Dr. (URCA)

Lucas Vaz Peres, Dr. (UFOPA)

Vagner Anabor, Dr. (UFSM)

Nathalie T. Boiaski, Dra. (UFSM)

Santa Maria, RS, Brazil
2022

RESUMO

INFLUÊNCIA DO BURACO DE OZÔNIO ANTÁRTICO E DINÂMICA ATMOSFÉRICA SOBRE O OZÔNIO NO SUL DO BRASIL

AUTORA: Gabriela Dornelles Bittencourt
ORIENTADORA: Damaris Kirsch Pinheiro
CO-ORIENTADOR: Hassan Bencherif

A primavera austral no Hemisfério Sul apresenta reduções temporárias do conteúdo de ozônio principalmente na região Antártica conhecida como Buraco de Ozônio Antártico (BOA). Porém, estudos mostram uma influência sob regiões de médias latitudes, como o Sul do Brasil, onde são identificados dias com diminuições temporárias da coluna total de ozônio (CTO). Com isso, o objetivo principal dessa tese é investigar essa influência do BOA sobre a região sul do Brasil, utilizando dados da coluna total de ozônio e de perfis verticais que vão ajudar a identificar a altura preferencial em que essas diminuições ocorrem no sul do Brasil, além de analisar o comportamento dinâmico atmosférico durante esses eventos no período 42 anos de dados (1979 a 2020). A metodologia utilizada compreende a análise de dados médios diários da coluna total de ozônio através de instrumentos de superfície (Espectrofotômetro Brewer), dados de satélites (TOMS e OMI), e para comparação dados de reanálise do ECMWF-ERA5, para a identificação de eventos de influência do BOA sobre a região Sul do Brasil. A análise do conteúdo vertical de O3 dados do satélite TIMED/SABER disponibiliza dados diários de 15 a 110 km de altura e possuem 17 anos de perfis de O3 disponíveis no período de 2002 a 2018. A validação desses dados se fez necessária, e para isso foi utilizada a rede SHADOZ de medidas de ozonesondes para realizar essa validação através da estação tropical em Natal/RN como referência. Essa validação apresentou uma boa concordância entre os dois instrumentos, viabilizando o uso do SABER para as análises dos eventos de influência do BOA. A partir disso, foram identificados 102 eventos que influenciaram Santa Maria/RS com diminuição temporária no conteúdo de O3 durante o período, e com queda média entre 24 e 28,1 km de altitude. Nas análises dinâmicas os campos estratosféricos mostraram o aumento da vorticidade potencial na média dos eventos, principalmente nos meses de setembro e outubro. Os modelos conceituais no corte horizontal e vertical da atmosfera explicam a atuação do jato estratosférico e troposférico durante a ocorrência de eventos de diminuição do conteúdo de O3 em Santa Maria/RS. Foi possível identificar a forte influência no desenvolvimento desses eventos através da conexão do jato estratosférico (vórtice polar) com os jatos troposféricos (jato polar e subtropical) em níveis médios e altos da atmosfera.

Palavras-chave: Ozônio. Buraco de Ozônio Antártico. Perfil Vertical. Dinâmica Atmosférica.

ABSTRACT

INFLUENCE OF THE ANTARCTIC OZONE HOLE AND ATMOSPHERIC DYNAMICS ON OZONE IN SOUTHERN BRAZIL

AUTHOR: Gabriela Dornelles Bittencourt
ADVISOR: Damaris Kirsch Pinheiro
CO-ADVISOR: Hassan Bencherif

The austral spring in the Southern Hemisphere presents temporary reductions in ozone content mainly in the Antarctic region known as the Antarctic Ozone Hole (AOH). However, studies show an influence in mid-latitude regions, such as southern Brazil, where days with temporary decreases in the total ozone column (TCO) are identified. The main objective of this thesis is to investigate this influence of AOH on the southern region of Brazil, using data from the total ozone column and vertical profiles that will help to identify the preferential height at which these decreases occur in southern Brazil, in addition to analyzing the atmospheric dynamic behavior during these events in the period 42 years of data (1979 to 2020). The methodology used comprises the analysis of average daily data of the total column of ozone through surface instruments (Brewer Spectrophotometer), satellite data (TOMS and OMI), and to compare reanalysis data from the ECMWF-ERA5, for the identification of events of influence of the AOH on the southern region of Brazil. The analysis of the vertical content of O3 data from the TIMED/SABER satellite provides daily data from 15 to 105 km in height and has 17 years of O3 profiles available in the period from 2002 to 2018. The validation of these data was necessary, and for that the SHADOZ network of ozonesondes measurements was used to carry out this validation through the tropical season in Natal/RN as a reference. This validation showed a good agreement between the two instruments, enabling the use of SABER for the analysis of AOH influence events. From this, 102 events were identified that influenced Santa Maria/RS with a temporary decrease in O3 content during the period, and with an average drop between 24 - 28.1 km in altitude. In the dynamic analysis, the stratospheric fields showed an increase in the potential vorticity in the average of the events, mainly in the months of September and October. The conceptual models in the horizontal and vertical section of the atmosphere explain the action of the stratospheric and tropospheric jet during the occurrence of events of decrease in the O3 content in Santa Maria/RS. It was possible to identify the strong influence on the development of these events through the connection of the stratospheric jet (polar vortex) with the tropospheric jets (polar and subtropical jet) at medium and high levels of the atmosphere.

Keywords: Ozone. Antarctic Ozone Hole. Vertical Profile. Atmospheric Dynamics.

RÉSUMÉ

INFLUENCE DU TROU D'OZONE ANTARCTIQUE ET DE LA DYNAMIQUE ATMOSPHÉRIQUE SUR L'OZONE DANS LE SUD DU BRÉSIL

AUTEUR: Gabriela Dornelles Bittencourt
CONSEILLER: Damaris Kirsch Pinheiro
CO-CONSEIL: Hassan Bencherif

Le printemps austral dans l'hémisphère sud présente des réductions temporaires de la teneur en ozone principalement dans la région antarctique connue sous le nom de trou d'ozone antarctique (AOH). Cependant, des études montrent une influence dans les régions de latitude moyenne, comme le sud du Brésil, où des jours avec des diminutions temporaires de la colonne d'ozone totale (COT) sont identifiés. L'objectif principal de cette thèse est d'étudier cette influence de l'AOH sur la région sud du Brésil, en utilisant les données de la colonne d'ozone totale et des profils verticaux qui aideront à identifier la hauteur préférentielle à laquelle ces diminutions se produisent dans le sud du Brésil, en plus à analyser le comportement dynamique de l'atmosphère lors de ces événements dans la période de 42 ans de données (1979-2020). La méthodologie utilisée comprend l'analyse des données quotidiennes moyennes de la colonne totale d'ozone à travers des instruments de surface (spectrophotomètre Brewer), des données satellitaires (TOMS et OMI), et de comparer les données de réanalyse de l'ECMWF-ERA5, pour l'identification des événements d'influence de l'AOH sur la région sud du Brésil. L'analyse du contenu vertical des données O3 du satellite TIMED/SABRE fournit des données quotidiennes de 15 a 105 km d'altitude et dispose de 17 années de profils O3 disponibles sur la période de 2002 à 2018. La validation de ces données était nécessaire, et pour cela le réseau SHADOZ de mesures de sondes d'ozone a été utilisé pour effectuer cette validation à travers la saison tropicale au Natal/RN comme référence. Cette validation a montré un bon accord entre les deux instruments, permettant l'utilisation de SABER pour l'analyse des événements d'influence AOH. A partir de là, 102 événements ont été identifiés qui ont influencé Santa Maria/RS avec une diminution temporaire de la tem eur en O3 au cours de la période, et avec une chute moyenne entre 24 et 28,1 km d'altitude. Dans l'analyse dynamique, les champs stratosphériques ont montré une augmentation du tourbillon potentiel dans la moyenne des événements, principalement dans les mois de septembre et octobre. Les modèles conceptuels dans la coupe horizontale et verticale de l'atmosphère expliquent l'action du jet stratosphérique et troposphérique lors de la survenue d'événements de diminution de la teneur en O3 à Santa Maria/RS. Il a été possible d'identifier la forte influence sur le développement de ces événements à travers la connexion du jet stratosphérique (vortex polaire) avec les jets troposphériques (jet polaire et subtropical) aux niveaux moyens et élevés de l'atmosphère.

Mots-clés: Ozone. Trou d'ozone antarctique. Profil vertical. Dynamique Atmosphérique.

LIST OF FIGURES

CONTENTS

1 INTRODUCTION

The maintenance of life on Earth, maintaining the energy balance of the planet, of all living beings, whether humans, animals, or plants, is due to the existence of ozone gas (SEINFELD; PANDIS, 2016). In 1840, when scientists discovered the existence of ozone gas (O3), studies show that it is the most important trace gas supporting life on Earth, due to its ability to absorb ultraviolet (UV) radiation incident in the atmosphere. Water vapor (H2O), along with carbon dioxide (CO2) and O3, become essential for the planet's energy balance (DOBSON et al., 1968; SALBY et al., 1996). Ozone (O3) is formed by photochemical processes, discovered by Chapman in 1930. Its highest concentration (about 90%) is found in the stratosphere, around 15 to 35 km altitude in a region known as the "Ozone Layer" (LONDON et al., 1985).

The large-scale stratospheric circulation known as the "Brewer Dobson Circulation" (BREWER, 1949; BUCHART et al., 2014; DOBSON, 1930) explains why large amounts of O3 are found in the polar regions, and not in the region where O3 naturally forms. This large-scale meridional circulation transports ozone formed in the tropical region towards the poles and then to the troposphere in regions of mid and high latitudes (BUCHART et al., 2014). Farman et al., (1985) detected a massive reduction in ozone content over the Antarctic region during the austral spring. This significant decrease, indicated as the region with values of the total column of O3 (TCO) lower than 220 Dobson units (DU), was named as the "Antarctic Ozone Hole".

The polar vortex acts as a barrier to the exit of stratospheric air masses from the polar holes during the winter months and vice versa. With the arrival of spring, the polar vortex becomes unstable due to the return of solar radiation and warming due to increased planetary wave activity. The instability of this vortex allows ozone-deficient air masses to be ejected from the polar regions as filaments, reaching mid-latitudes (MANNEY et al., 1994; STHOL et al., 2003; MARCHAND et al., 2005) and affecting southern South America (FARMAN et al., 1985).

The temporary destruction of O3 directly influences the behavior of this gas in and around the polar region, due to the passage of its edge over these areas, resulting

in increased levels of ultraviolet radiation reaching the surface (CASICCIA et al., 2008; MARCHAND et al., 2005). Kirchhoff et al., 1996 presented the first results that identified an “Antarctic Ozone Hole Secondary Effect” event over the mid-latitude region through O3 sounding data, satellites and surface data that documented this O3 decrease. These temporary reductions in O3 content continue to be studied. BITTENCOURT et al., (2018) analyzed an extreme ozone depletion event under mid-latitude regions. On the other hand, there is an increase in solar ultraviolet (UV) radiation that reaches the earth's surface (GUARNIERI et al., 2004; LAAT et al., 2010).

The need to understand the dynamics behind these AOH secondary influence events over mid-latitudes regions is still a point of analysis. The dynamics of the stratospheric vortex together with the jet streams can help in the exchange of air mass between the layers, in the known stratosphere-troposphere exchange (STE) (STHOL, 2003; OHRING, 2010). The behavior of O3 can be influenced by variabilities such as the Quasi-Biennial Oscillation (QBO), modulates the winds in the middle stratosphere and is the main variability that influences O3 in tropical latitudes (PLUMB, 1997; BALDWIN, 2001). This influence in the tropics can interfere with the distribution of O3 to other latitudes, such as mid-latitudes accelerating/decelerating large-scale movement through the Brewer-Dobson Circulation (BDC).

Several instruments have been used over the years to improve the analysis and understanding of this atmospheric gas. Historically, satellite data as well as surface instruments present a large period of data where important discoveries of O3 content have been found. Vertical ozone profile data, through ozonesondes (REMSBERG et al., 2003, THOMPSON et al., 2017), are an important tool in the study of atmospheric variables, such as O3. They provide the main atmospheric variables, helping to understand the behavior of O3 at different atmospheric levels, from the troposphere to the stratosphere.

Recent studies have shown that the greatest decreases in O3 content in southern Brazil occur with the action of jet streams that can help in these transport of air masses between stratosphere-troposphere (BITTENCOURT et al, 2019). Knowing the

importance of monitoring atmospheric O3, this work aims to investigate these temporary decreases in southern Brazil, especially during the period when the Antarctic Ozone Hole is operating during the austral spring. During the 42 years (1979-2020) of data analyzed in the study region, with the use of satellite and ground instruments, it was possible to identify the climatological behavior of the total column of ozone (TCO) in this period, helping to identify 102 events of influence of AOH on mid-latitude regions in Santa Maria/RS, the focus region of this work. These temporary decreases in O3 content, during the austral spring, were analyzed with vertical profiles, where at first data from the TIMED/SABER satellite were used, which provides 17 years of vertical profiles (2002-2018). This study made it possible to identify with greater precision the time at which these O3 decreases predominate during the occurrence of events over the southern region of Brazil.

The performance of atmospheric dynamics during the events identified over Santa Maria/RS requires a more detailed understanding to explain how this transport of air masses between the stratosphere and the troposphere occurs. Data with the new generation of ECMWF ERA5 reanalysis were used in this work, helping to show the stratospheric dynamic behavior using potential vorticity data, in addition to showing the dynamic behavior of the jets (stratospheric and tropospheric) during the occurrence of AOH influence events.

1.1 OBJECTIVES

1.1.1 General objectives

Investigate the influence of the Antarctic Ozone Hole and the action of atmospheric dynamics on the total ozone column and its vertical profile in southern Brazil during the period from 1979 to 2020.

1.1.2 Specific objectives

- Identify the secondary effect events of the Antarctic Ozone Hole that occurred in southern Brazil through the analysis of ozone total column data on surface (Brewer Spectrophotometer), satellite (TOMS, OMI) instruments and from reanalysis data from ECMWF-ERA5 for the period of 42 years of available between 1979 to 2020.
- Analyze data from vertical profiles to verify the behavior of O_3 using the TIMED/SABER satellite from 2002 to 2018.
    - Validate SABER satellite data using in situ O_3 measurements (ozonesondes launch by balloons) from the SHADOZ network available for the tropical region of Brazil in Natal/RN.
    - Analyze the vertical profiles of AOH influence events identified within the SABER data period.
- To characterize the climatological behavior of the TCO and of the vertical profiles during the events of influence of the AOH.
- Identify the main climatic variabilities that modulate the behavior of Ozone.
- Analyze the dynamic stratospheric behavior of secondary effect events through potential vorticity fields.
- Analyze the behavior of tropospheric and stratospheric jets up to 5 hPa during secondary effect events using reanalysis data from ERA5, with the aim of devising a conceptual model of this mechanism.

This Doctoral thesis is divided into three main parts. Chapter 2 presents a theoretical review of the main points relevant to the analysis of this study. Chapter 3 describes the study region, the data that were used and the methodologies used in this study. Chapter 4 presents the results and relevant discussions about them. In Chapter 5, the conclusions of the study and some recommendations for future work are presented. The Appendix section presents all the events of influence of the AOH on the southern region of Brazil that were identified during the 42 years.

2 THEORETICAL REVIEW

2.1 ATMOSPHERIC OZONE

Ozone is a gas that is naturally present throughout the atmosphere where its distribution is in your atmosphere and as specific characteristics it agrees with. The first contact with ozone gas was in 1840 by Christian Frederich Schonbein who discovered ozone while carrying out experiments due to a particular odor that the oxygen molecule released. At the beginning of the 20th century, the French Charles Fabryand and Henri Buisson estimated the first measurements of ozone based on the absorption of ultraviolet (UV) radiation, which if brought to the Earth's surface at normal temperature and pressure (CNTP), the total column ozone would have layers about 3 mm thick (FABRY; BUISSON, 1913). Later, studies showed that ozone is a molecule composed of three oxygen atoms with the ability to absorb ultraviolet radiation, releasing energy in the form of heat. Thus, in the stratosphere, the temperature begins to increase with altitude and its concentration is higher. (SLUSSER, 1999; LIOU, 2002).

In 1930, Sydney Chapman proposed that the continuous production of ozone in the atmosphere was a cycle triggered by the photolysis of O2 in the upper stratosphere. This photochemical mechanism to produce ozone in the stratosphere is called the Chapman Mechanism. Basically, Chapman's mechanism proposes four main reactions for the formation and destruction of ozone. Ozone formation occurs in the stratosphere at an altitude of about 30 km, where solar ultraviolet radiation with wavelengths less than 242 nanometers slowly breaks down oxygen molecules (O2):

$$O_2 + h\nu \rightarrow O + O \qquad (2.1)$$

In the presence of the third body M (N2 or O2), oxygen atoms (O) react rapidly with O2 to form an ozone molecule:

$$O + O_2 + M \rightarrow O_3 + M \qquad (2.2)$$

The formed ozone molecules strongly absorb UV radiation in the wavelength range from 240 to 320 nm, decomposing into O2 and O, or the ozone can react with the oxygen atom, generating two O2 molecules:

$$O_3 + hv \rightarrow O_2 + O \quad (2.3)$$

$$O_3 + O \rightarrow O_2 + O_2 \quad (2.4)$$

However, studies showed that Chapman's theory overestimated the ozone profile that was observed in the stratosphere, inspiring several studies that led to the addition of new chemical reactions to eliminate ozone losses, the so-called "catalytic cycle" (WARNECK, 1988).

$$X + O_3 \rightarrow XO + O_2 \quad (2.5)$$
$$XO + O \rightarrow X + O_2 \quad (2.6)$$

$$O + O_3 \rightarrow 2O_2 \quad (2.7)$$

These new cycles elucidate the roles of hydrogen, nitrogen oxides, chlorine and fluorine, bromine in the effect of stratospheric ozone chemistry, replacing the X in equations 2.5 and 2.6 (BATES; NICOLET, 1950; CRUTZEN, 1970; STOLARSKI; CICERONE et al., 1974; WOFSY; MCELROY; YUNG et al., 1975). Mario Molina and F. Sherwood Roland were awarded the 1974 Nobel Prize in Chemistry for their discovery that the release of man-made chlorofluorocarbons (CFCs) would be the main source of ozone-depleting chlorine in the stratosphere (MOLINA; ROWLAND et al., 1974).

These reactions occur continuously if solar ultraviolet radiation is present in the stratosphere, with the tropical stratosphere being the region where the greatest production of ozone occurs. In the stratosphere, the production of ozone is balanced by its destruction in chemical reactions, thus ozone constantly reacts with sunlight and

various natural and artificial (anthropogenic) chemicals in the stratosphere. In each reaction, a molecule of ozone is lost, and other compounds are produced. The reactive gases that deplete the ozone content are the oxides of hydrogen and nitrogen and those containing chlorine and bromine.

The vertical distribution of O3 content varies according to latitude and season, and the availability of sunlight becomes an important factor in O3 formation. Due to this, the greatest production of O3 occurs in the tropical stratosphere, because in this region the sunlight falls with more intensity, but the largest amounts of O3 occur in medium and high latitudes. This is explained by winds that circulate in the stratosphere, bringing tropical air rich in O3 to the poles in autumn and winter (Brewer-Dobson circulation).

In the tropics, seasonal variations can be ignored as solar radiation is constant throughout the year (WARKAMATZU et al., 1989). O3 production is higher near the equator and increases with increasing altitude, this characterizes a condition for O3 formation to occur:

- latitudinal variation, dependence on the zenith solar angle and intensity of solar radiation (SEINFELD and PANDIS, 1998).

With increasing latitude (Fig. 2.1), the seasonal variation of stratospheric ozone is greater, with a greater concentration during spring. Meanwhile regions near the poles are characterized by strong downdrafts transporting the ozone produced by the layers above at 20 km altitude towards the poles in the upper stratosphere and towards the equator in the lower stratosphere. During autumn, minimum values of O3 are observed, according to figure 2.1, which shows the behavior of TCO as a function of latitude and season (SEINFELD e PANDIS, 2016).

Figure 2.1: Average zonal density of the total ozone column (in Dobson units) as a function of latitude and time of year.

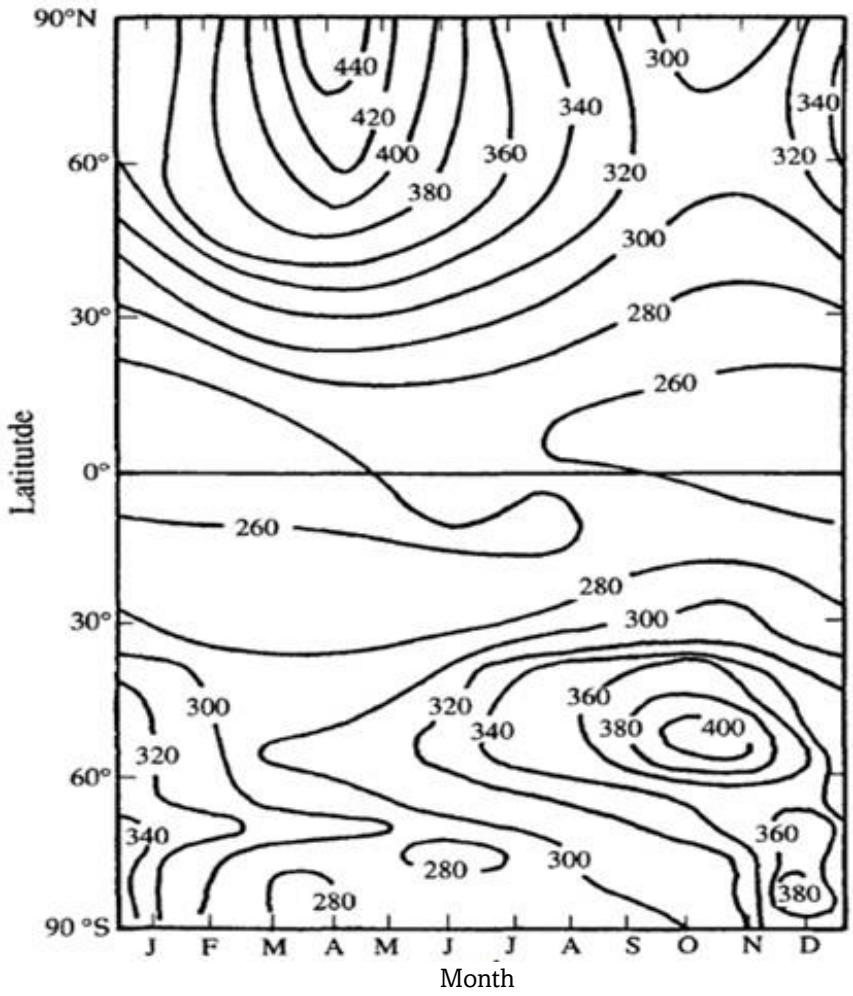

Source: Adapted by Seinfeld and Pandis (2016).

Ozone is found primarily in two important regions of the atmosphere. The two main layers where O3 content is identified are the troposphere and stratosphere. In the troposphere, a layer that goes from the surface to about 10-15 km in altitude depending on the region observed, to the region of the tropopause, O3 is formed by a different set of chemical reactions involving naturally occurring gases, as well as from sources of air pollution. As a result, about 10% of the atmospheric O3 content is found (FISHMAN et al., 1990). In this layer, O3 has negative impacts in several aspects, functioning as a toxic

gas for human health, in addition to causing damage to agriculture and various ecosystems, in addition to being an important greenhouse gas on the planet.

Most of the ozone content is found in the stratospheric layer which is defined between 15 and 50 km altitude. The temperature increases as the latitude increases, this is explained by the absorption of ultraviolet radiation by the O3 molecules available in that region. These molecules release energy in the form of heat, this causes the reduction of at least 1% of the stratospheric ozone content to increase the amount of UVB incidence by up to 2%, further increasing the risks to living beings, including diseases such as cancer of the skin. skin due to overexposure to the sun (SEINFELD; PANDIS, 2016). In Brazil, a 1% reduction in stratospheric O3 content corresponds to an average increase of 1.2% in type B UV radiation. (GUARNIERI et al., 2004). Between 15 and 35 km of altitude, 90% of the total O3 content is identified (LONDON, 1985; WMO, 1996) in the well-known "Ozone Layer". In this layer, O3 works as an absorber of UV radiation, where together with water vapor (H2O) and carbon dioxide (CO2) they become essential for life and the energy balance of the planet, working as a support for the life on the earth's surface due to its ability to absorb ultraviolet (UV) type C (UVC) radiation and part of UVB, the most harmful to living beings. Figure 2.2 shows the vertical behavior of O3 in the atmosphere, where the region of the O3 layer between 15-35 km is clearly observed.

Recent studies have shown that there is an increase in tropospheric O3 concentration. LIU et al. (2022) used numerical models to simulate changes in ozone levels in the upper and lower atmosphere between the years 1955 and 2000, isolating them from other influences and increasing the current understanding of their impact on the heat absorption of the Southern Ocean. The simulations showed that a decrease in ozone in the upper atmosphere and an increase in the lower atmosphere contributed to a warming observed in the upper 2 km of ocean waters at high latitudes by the general increase in greenhouse gases.

Figure 2.2: Vertical profile of O3 in the atmosphere.

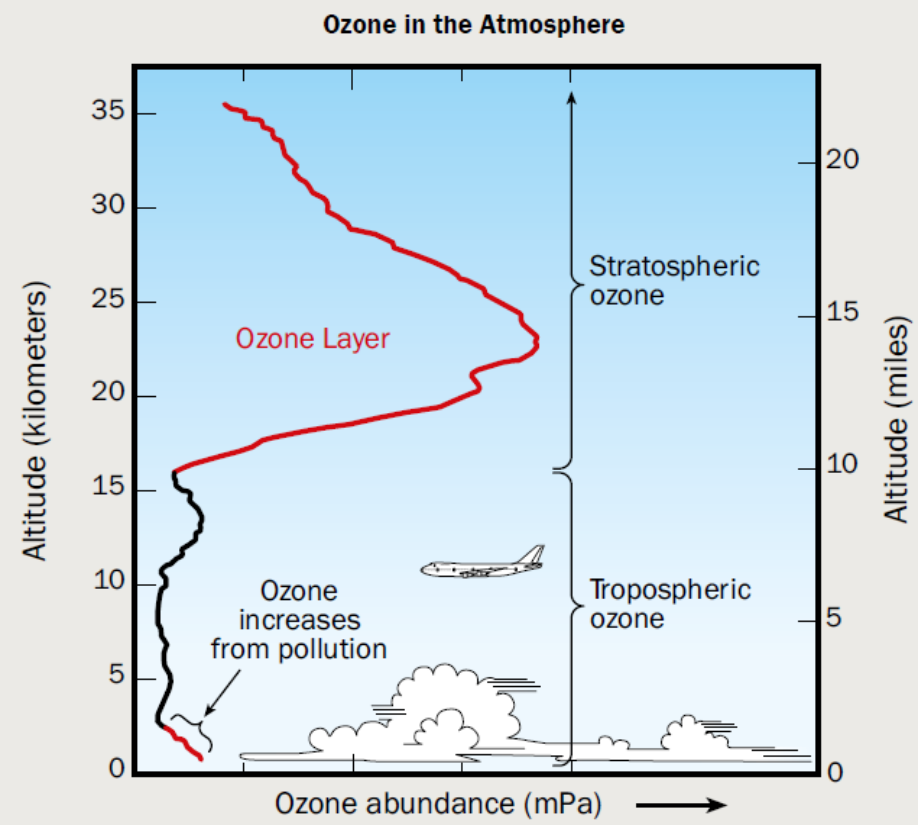

Source: WMO, 2018.

O3 molecules found in the lower stratosphere have a long lifetime and are used as tracers in studies regarding air mass transport, stratosphere-troposphere exchange. (STE). As is known, the O3 content in the upper troposphere and lower stratosphere strongly depends on dynamic factors such as seasonal variation in the atmospheric circulation regime, which is associated with the position, intensity, and interactions of the subtropical and polar jet due to the latitudinal thermal gradient. (BUKIN et al., 2011).

2.2 BREWER DOBSON STRATHOPHERIC CIRCULATION

The Brewer-Dobson circulation (BDC) is a meridional circulation driven primarily by the deposition of planet-scale fluctuating quantities. Changes in BDC lead to changes in ozone through transport and chemical reactions. Brewer (1949) and Dobson (1968) showed that the highest concentration of ozone is found in regions with high latitudes at

the poles, although the highest production of O_3 is in the equatorial region at approximately 40 km of altitude.

This characteristic of O3 presenting higher concentrations in areas distant from its formation made the scientific community suggest that the lifetime of O3 in the stratosphere is longer than the time required for this transport to occur. According to these statements, both the O3 content and its formation rate depend on the latitudinal and altitude variation, the O3 residence time will also vary in the stratosphere. For example, transport from the tropics to the poles takes about 3 to 4 months, at altitudes below 20 km in low latitudes, in the tropics, and above 40 km in high latitudes. Meanwhile, in tropical latitudes where the greatest O3 formation occurs, the residence time is approximately 3 years at altitudes around 15 km and about 1 day at altitudes above 40 km. These new observations cast doubt on the Chapman Mechanism in the O3 destruction process, from which new processes were added to characterize the O3 destruction correctly, according to the equations shown above for the catalytic cycles.

The Brewer-Dobson circulation (BDC) is then a large-scale circulation that is driven by the tropospheric circulation in the tropics up into the stratosphere and then moves towards the poles as it descends. This pattern of atmospheric circulation explains why air in the tropics has less O_3 content than air at the poles, even though the tropical stratosphere is the region where this content is produced (BUTCHART, 2014).

The existence of two distinct branches of the Brewer-Dobson stratospheric circulation characterizes the large-scale distribution of movement with the shallow and deep branches (BIRNER and BÖNISCH, 2011). The shallow branch is found in the lower stratosphere, where there is ancestry in the tropics and subsidence in the subtropics and mid-latitudes. The deep branch of the BDC reaches the upper stratosphere, extending to mid and high latitudes (WMO, 2010). Studies show that climate model simulations predict an acceleration of the Brewer-Dobson circulation in response to increasing concentrations of greenhouse gases with an average increase of about 2%/decade in the 21st century (WMO, 2014).

Figure 2.3: Schematic illustration of the shallow and deep branches of the Brewer-Dobson circulation in the stratosphere at the solstice.

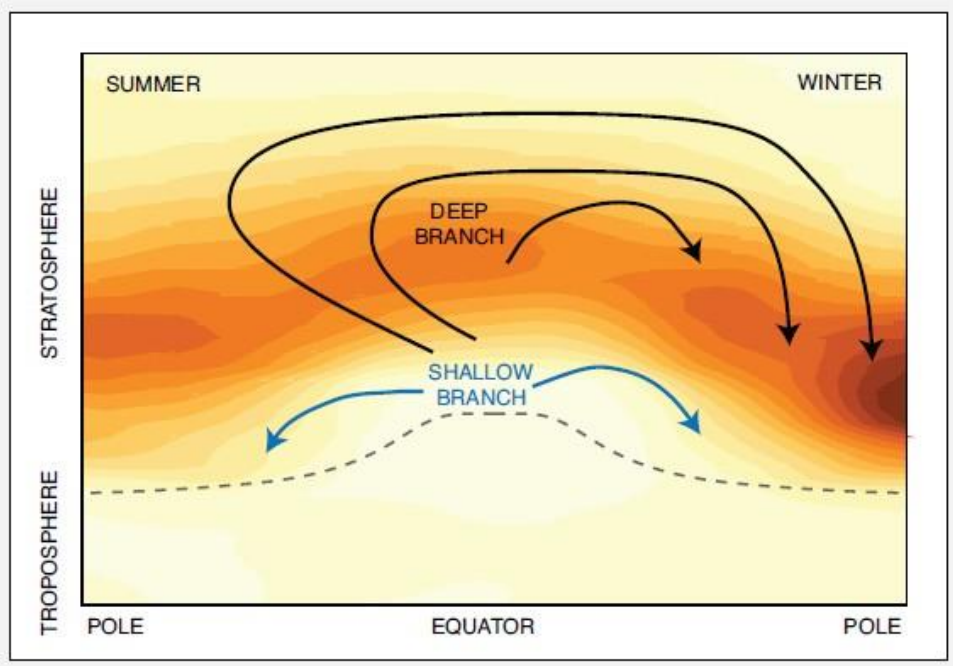

Source: WMO, 2018.

NEU et al. (2014) showed that changes in tropical upwelling have a significant effect on the distribution of stratospheric ozone in mid and low latitudes. In addition to this increase in the concentration of greenhouse gases directly influencing the BDC acceleration, this acceleration can also be estimated through chemical components, for example, ozone and water vapor. FLURY et al. (2013) analyzed the velocities of the deep and shallow branches of the BDC, in both hemispheres, and identified a variability compatible with signals from the Quasi-Biennial Oscillation (QBO). Regarding the average speed of the branches, the NH showed a speed 2 times higher when compared to the SH, this is because the planetary waves there in the NH are more unstable and break more easily than in the SH, where it is more stable mainly during the winter season.

2.3 ANTARCTIC OZONE HOLE

Ozone-depleting substances are found throughout the stratospheric layer because they are transported over long distances by large-scale motion in the atmosphere. The

large depletion of Antarctica's ozone layer, known as the "Antarctic Ozone Hole", is due to the climate and chemical reactions taking place there, which are not identified anywhere else on Earth. In the early 1980s, the first drop in the total ozone column in Antarctica was observed at research stations located on the Antarctic continent, where measurements were made using a surface instrument, the Dobson Spectrophotometer.

Observations indicated that total ozone is exceptionally low during the late winter/early spring months of September, October, and November. The first published reports were from the Japan Meteorological Agency and the British Antarctic Survey. In 1985, three scientists from the British Antarctic Survey published their observations in the prestigious scientific journal Nature that the depletion of stratospheric ozone over Antarctica during the polar spring is known as the "Antarctic Ozone Hole", a result that was widely known worldwide. (FARMAN et al., 1985). Observations showed that the average monthly value of the total column of surface ozone at a British station in Antarctica has been decreasing since 1977, where values above 350 DU (Dobson units) have been observed until then for values close to or below 100 DU. Many theories try to explain the existence of this hole in the ozone layer, but the one that was most accepted by the scientific community is the heterogeneous chemistry of halogens (chlorine and bromine) in a catalytic cycle of O_3 destruction.

Solomon (1999) and Dessler (2000) showed that human activities, in the emission of chemical compounds, chlorofluorocarbons, CFCs, play an important role in this drastic drop in ozone content during the southern spring. The Ozone Hole area is defined where there is a region with values lower than 220 DU (figure 2.4), a value lower than two thirds of the historical level (HOFMANN et al., 1997). Antarctica has the highest concentration of ozone on Earth practically throughout the year. With the deficiency of atomic oxygen in the stratosphere of Antarctica and due to the absence of intense ultraviolet radiation, the photolysis of O2 does not occur, thus causing a low local production of ozone. However, this O3 that accumulates in polar regions such as Antarctica, and the Arctic in NH, is produced in the tropics and transported by the large-scale movements of air in the stratosphere through the BDC.

Figure 2.4: Antarctic Ozone Hone area in 2017. White circle is with values less 220 DU.

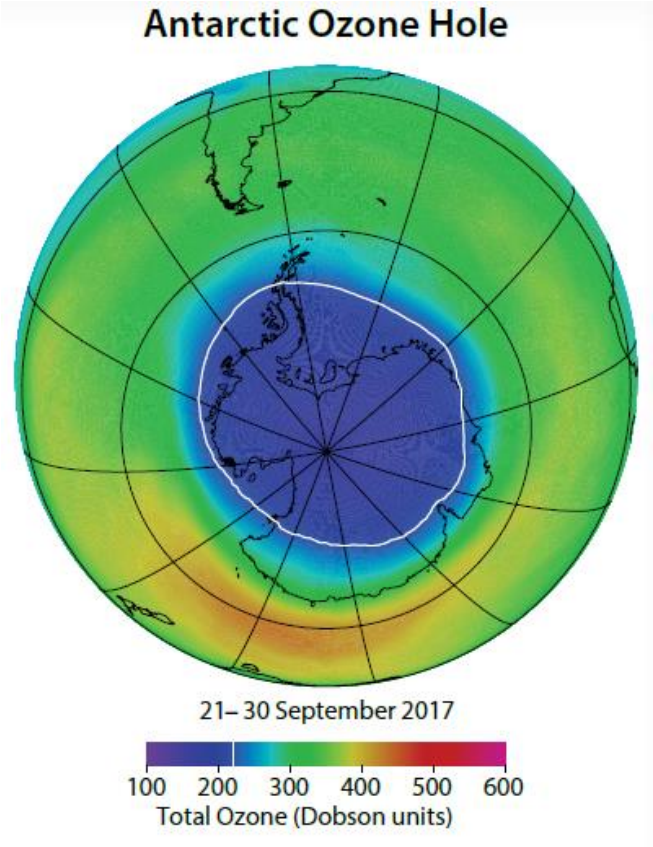

Source: WMO, 2018.

The first step in the formation of the AOH is the formation of the polar vortex (SCHOEBERL; HARTMAN et al., 1991). With the arrival of the polar night in winter, due to the absence of terrestrial radiation during this period, a cooling occurs in the lower stratosphere of Antarctica. Added to this, the relatively warm temperatures in the mid-latitudes result in a strong north-south pressure gradient between these regions, creating a strong zonal wind called the "polar night jet" due to the Coriolis force.

During the polar winter, the formation of a “Polar Vortex” occurs, which has a very cold and extremely stable core of air, mainly in the SH, keeping the cold air inside it throughout the winter. This vortex conserves the ozone that was transported at high levels from the tropics, causing Antarctica to have a higher concentration. With the end of the polar winter and the return of the sun, the vortex tends to weaken, and the amount of ozone begins to decrease during the spring. The destruction of polar ozone depends on

the temperature in the stratospheric, as it is the temperature that “controls” the formation of polar stratospheric clouds (PSC) and therefore the rate of heterogeneous reactions.

The minimum values that are found in the AOH, on average, between late September and mid-October are around 120 DU, equivalent to practically two thirds below the values observed in the early 1970s, according to the figure 2.5 which presents the monthly average for October since the discovery of total O3 destruction in Antarctica. The low O3 content inside the AOH during its active period shows a contrast with the distribution of higher values outside the ozone hole. This feature can be seen in Figure 2.2, where a region with values around 400 DU can be observed that surrounds the AOH area, revealing the edge of the polar vortex that acts as a barrier in the transport of ozone-rich mid-latitudes air to the polar region, due to stratospheric winds at the edge of the vortex.

Figure 2.5: October monthly average of Antarctica total ozone showing the long-term changes in ozone content in Antarctica.

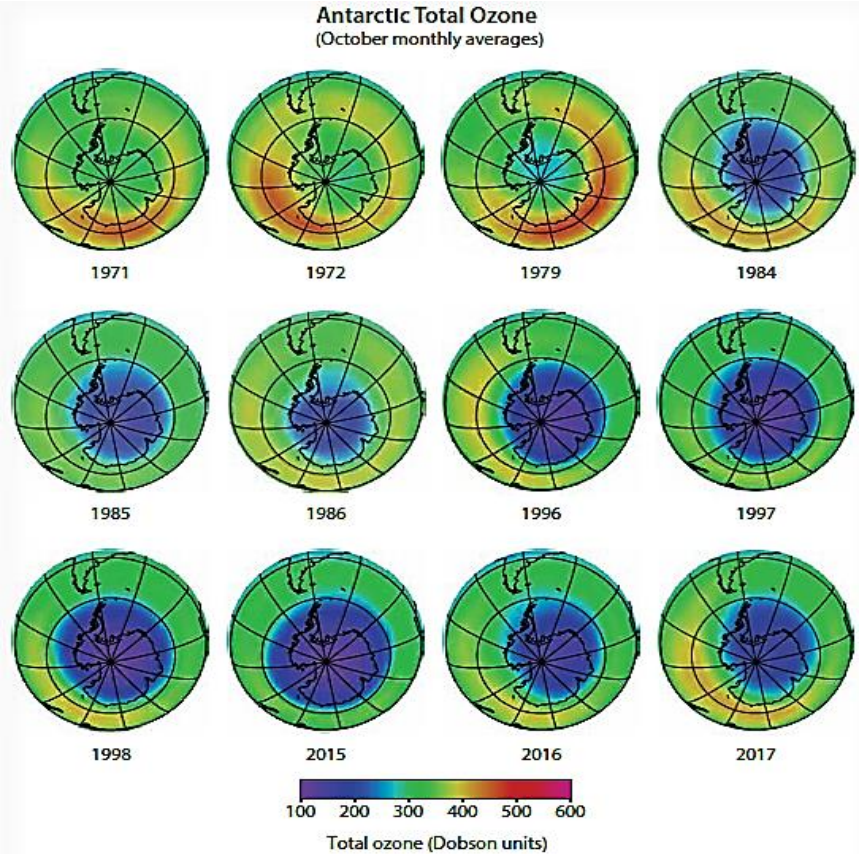

Source: WMO, 2018.

2.3.1 Polar Vortex

Polar vortices are large continuous cyclones located in the upper layers of the atmosphere (stratosphere) at the north and south poles. During the austral winter, the arrival of the polar night stops the heating of the region through the non-incidence of solar radiation in the high polar latitudes (DESSLER, 2000). With this, a strong pressure gradient is observed where the warmer temperatures of the mid-latitudes in contrast with the colder temperatures of the poles creates an intense vortex known as the "Polar Night Jet". This polar vortex forms an air core with very low temperatures and remains stable throughout the winter by trapping all the cold air inside and separating it from the outside air. With the return of solar radiation and the end of the polar night, the temperature starts to increase, and the vortex loses intensity, becoming unstable (MARCHAND et al., 2005).

The polar atmosphere during the austral winter tends to cool intensely, favoring a subsidence movement, which consequently increases the pressure gradient between medium and high latitudes, at the poles, thus forming the Antarctic Polar Vortex (APV) (SOLOMON et al., 1999). This vortex has an intense westward circulation, strengthening then during the coldest period increasing the latitudinal variation of the O3 content in this region, a dynamic barrier is created around 60º S, where the low temperatures and the O3 content that was transported from the tropics (by the Brewer Dobson circulation) are trapped, until this vortex breaks.

Thus, the polar vortex is the first step towards the formation of the Antarctic ozone hole in the southern spring and has two important characteristics that directly affect its formation. The first is due to the low temperature that is trapped inside the vortex, because during the polar night in winter, the absorption of solar radiation ceases, causing the lower part of the Antarctic stratosphere to cool during this period. The low temperature inside the vortex supports the formation of stratospheric polar clouds, which play an important role in the chemical process of the ozone hole. These clouds have a temperature of about 183 K or -90°C in a vortex with a height of about 15 to 20 km. Polar stratospheric clouds are formed in the presence of a small amount of water

vapor and nitric acid condensation, and only appear in polar winters.

The circulation of the polar vortex in the Southern Hemisphere is stronger than the vortex that forms in the Northern Hemisphere, this can be explained by the fact that northern polar latitudes have more topographical surfaces and mountainous regions than southern polar latitudes. As a result, the occurrence of meteorological disturbances in the Northern Hemisphere is greater, increasing the mixing of air from lower latitudes, warming the Arctic stratosphere.

.

2.3.1.1 Polar Stratospheric Clouds

The mechanisms of O3 destruction in the Antarctic region during the austral spring, despite being identified and analyzed by the data available at the time, could not explain how this massive destruction occurred (MOLINA, 1987). It was then that SOLOMON et al., (1986) suggested that chlorine could be activated on the surface of Polar Stratospheric Clouds (PSC), and thus serve as a basis for accelerating the temporary destruction of O3 in the Antarctic region.

PSCs form during the austral winter due to the low temperatures in this period. During the polar night, without the incidence of solar radiation, and because the vortex in Antarctica is more stable compared to the vortex in NH, the temperature inside the PV can reach 183 K, or -93ºC, with that the formation of stratospheric clouds occur. Polar stratospheric clouds (PSCs) form between 15 and 22 km high, where the minimum temperatures for their formation must be at least -78°C. In the Arctic, these low temperatures occur on average for 1 to 2 months, whereas in Antarctica this phenomenon occurs throughout the winter period, for at least 5 months. These meteorological differences between the two poles are due to variations in the distributions of land, ocean, and mountains at mid and high latitudes in both hemispheres. The presence of these clouds in the stratosphere supports chemical reactions and, consequently, the destruction of O3 in the Antarctic region.

On the surface of the PSC, the release of reactive chlorine from the reservoir species ClONO2 and N2O5 occurs, which react with the clouds in which the HCl was

absorbed, producing the gases Cl2, HOCl e Cl_2NO_2. The return of sunlight in the austral spring is then necessary as its photolysis Cl2, HOCl and Cl2NO2 releasing reactive chlorine that generates a new mechanism of destruction of the ozone content in the polar regions.

Figure 2.6: Minimum air temperatures in the polar stratosphere showing the PSC formation in SH and NH.

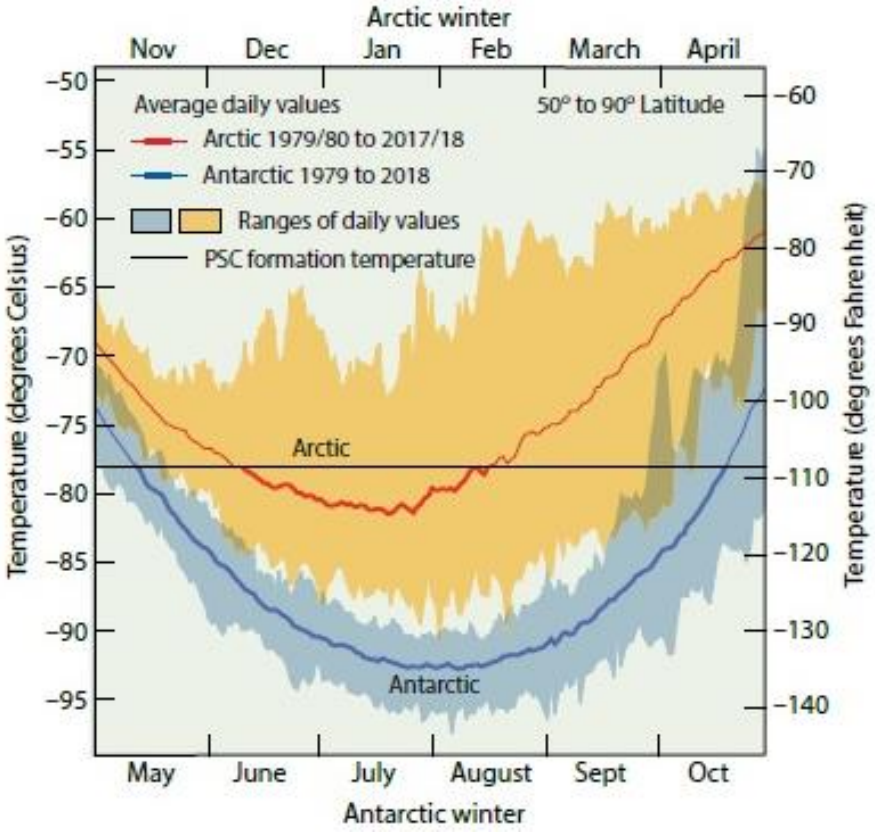

Source: WMO,2018.

In the last two years, the dynamics of O3 destruction in the Antarctic region ensured the occurrence of an AOH different from what normally occurs. This is because the temperature in the polar stratosphere region was much lower than in previous years. This negative temperature ensured the destruction of O3 in the stratospheric region in Antarctica until at least early November, when the temperature in the stratosphere began to increase dissolving the polar stratospheric clouds. This fact made the AOH last for a longer period than usually occurs and it closed only at the end of December 2020/2021. In addition to a longer duration of AOH in 2020/2021, AOH reached a large area in both

seasons recording approximately 25 million km^2, unlike what was observed in 2019, where a sudden stratospheric warming in the stratospheric polar region of Antarctica rapidly dissolved the polar stratospheric clouds, recording an area of 16 million km2, closing in October.

Figure 2.7: a) Relative frequency of appearance of NEPs in SAMII satellite observations, as a function of height and month, over Arctic and Antarctica, and b) photograph of an Arctic polar stratospheric cloud (PSC) was taken in Kiruna, Sweden (67°N) on January 27, 2000.

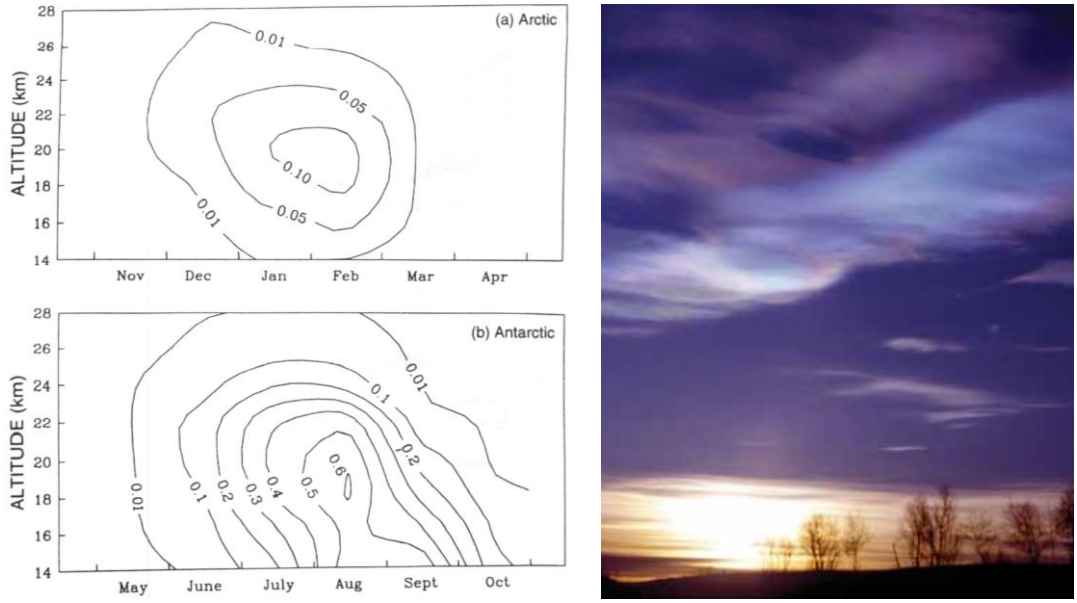

Source: Adapted by Salby, 1996; WMO, 2018.

SALBY et al., (1996) showed that these clouds occur much more frequently in the Antarctic region than in the Arctic region. Thus, for the formation of the AOH, two important points must be analyzed:

1. Low temperatures in the polar region;

As seen, low temperatures are essential for the formation of polar stratospheric clouds during the austral winter in the Antarctic region, with the help of the polar vortex these negative temperatures are isolated creating a barrier that makes it impossible for this cold air to leave the vortex to other regions.

2. Solar radiation;

The end of the polar night, a period in which there is no incidence of solar radiation during the austral winter, causes the vortex to lose its stability and break, in addition, the

stratosphere warms up again, dissolving the stratospheric clouds and ceasing the destruction of O3 in Antarctica.

2.3.2 Secondary Effect of The Antarctic Ozone Hole

As a primary effect, of the Antarctic Ozone Hole, during the austral spring, it directly influences the ozone content of the polar region, where there are drops greater than 25% in relation to the climatological average of the region, which means, values less than 220 DU (HOFMANN et al., 1997). Due to its extreme importance, this phenomenon has been studied and monitored since the 1980s (KIRCHHOFF et al., 1996; SALBY et al., 2012; SOLOMON et al., 1999; PERES et al., 2017; 2019; BITTENCOURT et al., 2019).

The regions of medium and low latitudes can be directly or indirectly influenced by the Ozone Hole. Direct influence occurs when the edge of the polar vortex, together with the Ozone Hole itself, passes directly over mid-latitude regions, such as over southern Chile and Argentina, which are populated regions, causing drastic reductions in the ozone content and respective increase in ultraviolet radiation reaching the surface (LARRY et al., 1995). The indirect influence, on the other hand, occurs when the polar vortex destabilizes, with the arrival of spring, due to increased temperatures and increased planetary wave activity (SEMANE et al., 2006). The satellite image in Figure 2.8 represents this poor O3 air mass filament acting indirectly over mid-latitudes regions in southern Brazil, during the active period of the AOH.

The passage of air masses originating from the Antarctic Ozone Hole over southern Brazil was first observed by Kirchhoff et al., (1996), based on data from two Brewer spectrophotometers installed in Santa Maria and from ozonesondes in October 1993, it was observed that a local reduction of ozone was associated with the entry of a polar air mass. This type of phenomenon was called the “Antarctic Ozone Hole Secondary Effect” event (Figure 2.9).

Figure 2.8: Influence of the Antarctic Ozone Hole on mid-latitudes regions. Blue and purple colors have the lowest O3 values in DU.

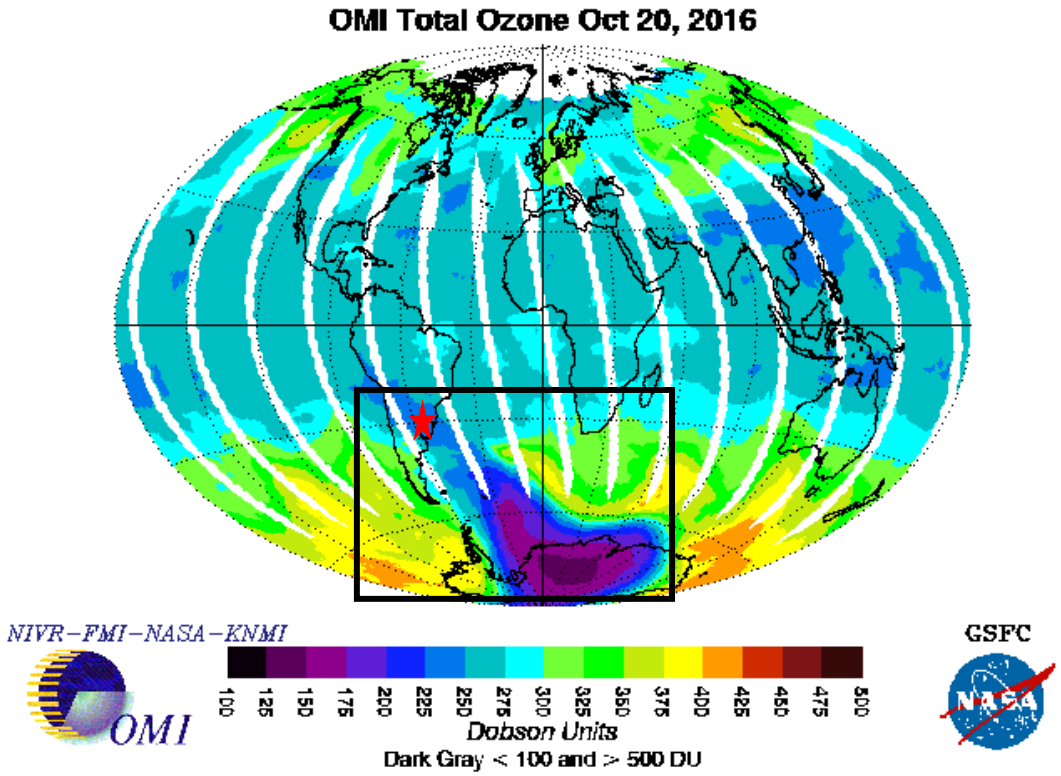

Source: OMI satellite.

Peres et al., (2019) used 35 years of data to analyze the behavior of O_3 in the central region of RS, identifying 62 events through mean fields and potential vorticity anomalies of the events. Bittencourt et al., (2019) presented a 12-year analysis of data from the study region, where 37 secondary effect events that hit, the region were identified, including the event of October 20, 2016, which was the second most intense event ever recorded on the central region of Rio Grande do Sul, where the synoptic condition in the region showed that the event occurred after the passage of a frontal system (BITTENCOURT et al., 2018).

Bresciani et al., (2018) presented the 2016 event through a multi-instrumental study with data from ozonesondes, satellite data, surface instruments that identified at ~24 km of altitude the most significant drop of the event. Steffenel et al., (2021) used "deep learning" to predict changes in ozone content during secondary effect events in southern Brazil. Schuch et al., (2015) showed that amphibian species were in decline

during the months of influence of AOH (August to November) in relation to the increased incidence of UV radiation over the region.

The arrival of austral spring, with the return of sunlight over the Antarctic region and consequently increasing temperatures in the stratosphere, weakens the stability of the Antarctic polar vortex. In this way, poor O3 air masses detach from the AOH area reaching mid-latitudes and causing a temporary decrease in the total ozone column in the region.

Figure 2.9: Vertical ozone profile for October 26 and 28 (a) and total ozone column by Brewer spectrophotometer between September and October 1993 (b) for Santa Maria/RS (c) Backward trajectory of air masses at 25 km height and METEOR 3 TOMS satellite image to October 28, 1993.

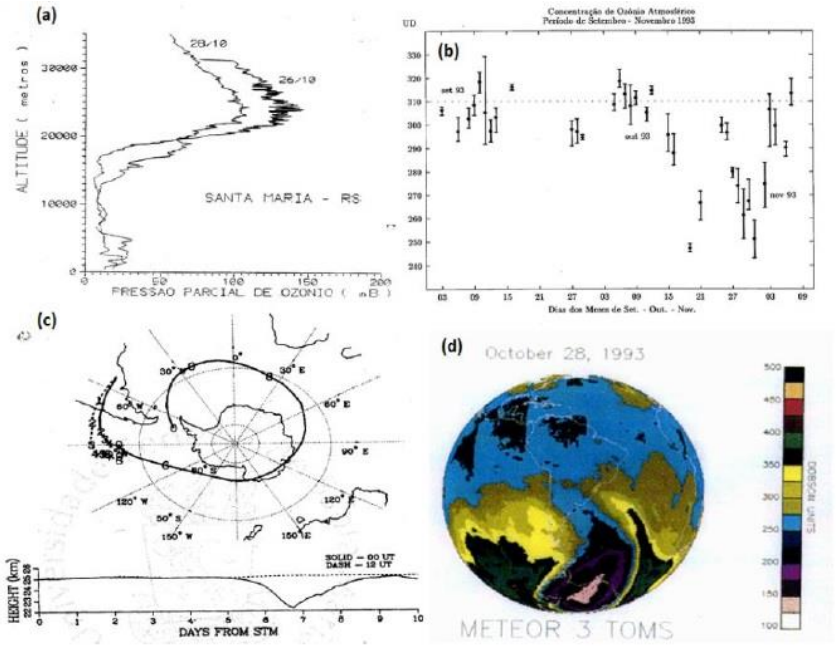

Source: Adapted by Kirchhoff et al., 1996.

2.4 POTENTIAL VORTICITY IN THE DYNAMICS OF STRATHOPHERIC OZONE

The potential vorticity term (PV) works as a dynamic tracer for large-scale air masses, where the potential temperature is conserved and can be used as a horizontal coordinate (HOSKINS et al., 1985). Potential temperature is defined as the temperature that the parcel of air would have if it were expanded or compressed adiabatically from its

pressure and temperature to a standard pressure. It can also be defined as a mark on the vertical position of the air parcel, slowly increasing in tropospheric layers and rapidly increasing in stratospheric levels.

Holton (1995) showed that troposphere-stratosphere exchanges with chemical constituents such as O_3 can be identified through PV on isentropic surfaces relating to events where there is a break in the tropopause and consequent intrusion of air from the stratosphere to the troposphere. On isentropic surfaces, PV can be used as a vertical coordinate for studies with tracer gases such as O_3. Equation 1 shows the PV in the form of Ertel's potential vorticity in isentropic coordinates:

$$PV \equiv (\zeta_\theta + f) - (g \frac{\partial \theta}{\partial p} = cte \qquad (8)$$

Where θ is the potential temperature, p is the pressure, g gravity, $\zeta\theta = \left(\frac{\partial v}{\partial x} - \frac{\partial u}{\partial y}\right)_\theta$ designates the vertical component of the relative vorticity evaluated on an isentropic surface and (ζ_θ+f) is the absolutes vorticity in the isentropic surfaces, $\frac{\partial \theta}{\partial p}$ is the atmospheric stability (HOLTON, 2004). For PV the unit used is $10^{-6}m^2s^{-1}Kkg^{-1}$ called potential vorticity unit (PVU), thus 1 PVU = $10^{-6}m^2s^{-1}Kkg^{-1}$ (HOLTON, 2004). According to equation 8, the potential vorticity is conserved following the motion in an adiabatic and frictionless flow, so it can be said that the PV is a measure of the absolute vorticity ratio in relation to the effective thickness of the vortex.

The PV presents positive values in the HN and negative in the HS, so in the isentropic analyzes we use the absolute potential vorticity (APV), where APV = |PV|. Therefore, when an increase in APV is observed, it is understood that the air mass has a polar origin, whereas when a decrease in the absolute value of PV is observed, it is concluded that the origin of the mass is equatorial (BENCHERIF et al., 2011; PINHEIRO, 2011; SEMANE et al., 2006).

The conservation of potential vorticity in the atmosphere induces changes through the effects of stretching and/or vertical flattening of the air mass between two isentropic surfaces. Potential Vorticity can also be used to identify the dynamic tropopause, on a

surface in the Northern Hemisphere (Sourthern Hemisphere) of 1.5 PVU or 2 PVU (-1.5 PVU or -2 PVU), representing a transition between low values of VP in the troposphere and high values in the stratosphere (HOLTON, 2004).

Danielsen et al., (1985) positively correlated potential vorticity (PV) with the mixing ratio of O3 below its maximum concentration in the stratosphere. The correlations showed that on a global scale, it was possible to differentiate the effects of O3 transport from the effects that are produced by photochemical processes. The region that limits stratospheric air from tropospheric air coincides with the jet axis in the upper troposphere, between 10 and 15 km (HOLTON, 1995).

Many studies have used potential vorticity as a tool to identify and analyze the dynamic evolution of COLs (Cut Off Lows) and Tropopause Folding. Low pressure shear systems (COLs) are defined as low pressure systems with a cold core located in the middle and upper troposphere and that form after their separation from the western mid-latitude winds. COLs develop from pre-existing cold lows in the upper airstream that have moved toward the equatorial side of the jet stream, leaving an isolated cold cyclone vortex. (PALMÉN, NEWTON et al., 1969). Price and Vaughan (1993) studied COLs and identified that they play an important role in stratosphere-troposphere exchanges, resulting in significant changes in O3 concentration at high latitude locations (RONDANELLI et al., 2002).

The region between the upper troposphere and lower stratosphere (UTLS) is a coupling layer in the atmosphere. This area was defined as the region ± 5 km around the tropopause, the region that forms the boundary between the troposphere and the stratosphere. Important dynamic processes occur in this region of the UTLS, because of the transition between the troposphere and the stratosphere altering both the troposphere and the stratosphere. The stratosphere-troposphere exchange (STE) through the tropopause is one of the important processes that influence the chemistry of the upper troposphere and lower stratosphere (HOLTON, 1995; GETTELMAN et al., 2011), figure 2.9, adapted from Gettelman et al., (2011) schematically shows how UTLS behaves.

When a drop (increase) of the dynamic tropopause is observed, there is an intrusion (injection) of stratospheric (tropospheric) air, facilitating the transport of the STE. This

phenomenon became known as tropopause warping where anomalies of this tropopause interact directly with the jet stream, unleashing in the fold (DANIELSEN et al., 1968). STOHL et al., (2003) identified that folds in the tropopause when close to the jet streams, subtropical and polar, are important for the transport of air masses between the stratosphere and troposphere (STE), due to the displacement of the tropopause on isentropic surfaces. This tropopause fold presents high values of the ozone mixing ratio, which consequently increase the temperature of the layer, driven by the downward movement that transports ozone from the middle stratosphere to the UTLS or even lower levels of the troposphere.

2.5 CLIMATE VARIABILITY AND OZONE

Climatic variability can determine the behavior of several meteorological parameters, in addition to dictating how the functioning of the systems should proceed, in relation to small and large-scale events. The variability of stratospheric ozone can be analyzed on daily, seasonal, annual scales and over long periods of time. Some of these variabilities provide important information to explain the behavior of O3 content in certain regions, and the most important ones that will be analyzed in this study are: Almost Biennial Oscillation, ENSO – Southern Oscillation, and the 11-year Solar Cycle.

Domeisen and Butler (2020) identified that climate variability modes, such as El Niño Southern Oscillation (ENSO), Quasi-Biennial Oscillation (OQB) and the Antarctic Oscillation or Southern Annular Mode are important teleconnections in the processes that involve coupling between the stratosphere and troposphere.

2.5.1 Quasi-Biennial Oscillation

The Quasi-Biennial Oscillation is an oscillation that predominates variability in the equatorial stratospheric layer (REED et al., 1961; 1964). This oscillation is characterized by a downward wind shift, in the lower stratosphere, from east to west in an approximate period of 22 to 34 months with an average time of 28 months of duration (LINDZEN; HOLTON, 1968). The QBO is generated by the interaction between the

zonal mean flux and equatorial planetary waves (PLUMB et al., 1997), in addition it is an important interannual variability in the dynamic behavior and in the stratospheric composition both in the tropics and in the polar regions due to changes in the circulation of winds. That end up directly affecting the behavior of different important chemical constituents in the stratosphere, such as O3, H20 and CH4 (BALDWIN, 2001).

Figure 2.10: Monthly zonal mean wind U (m s^{-1}) between 70 and 10 hPa for 1981 to July 2016. Easterly winds are shown in cyan/blue, while westerly winds are shown in green/brown.

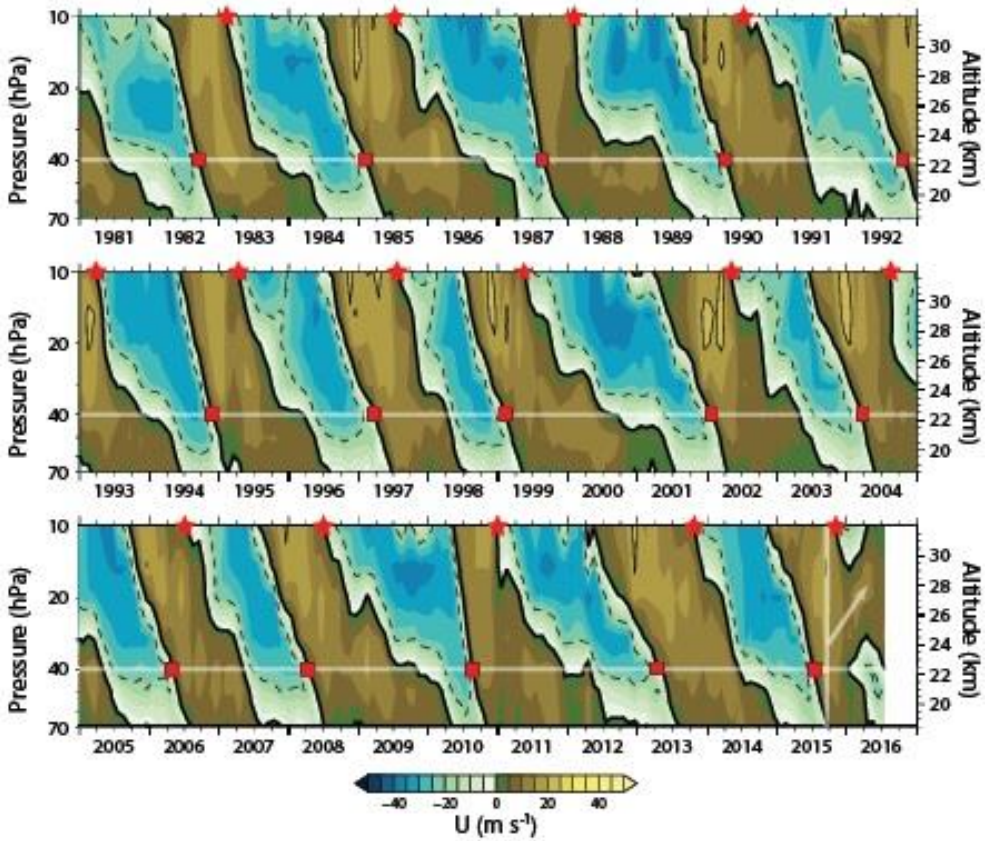

Source: Adapted by Newman, 2016.

Through modulation and propagation of winds, changes in temperature and meridional circulation, QBO directly affects the distribution and transport of trace chemical constituents and can be related to the decrease in stratospheric O3 content. The zonal mean circulation in the extratropical stratospheric layer, compared to the troposphere, presents a much more intense seasonal cycle with the inversion of the winds in the change of seasons. The movement of planetary waves, during the eastern phase of

the QBO, goes towards the winter hemisphere, intensifying the polar vortex and inducing it to strong oscillations. In the western phase of the QBO, a more isolated and radioactively balanced polar vortex is observed (SALBY, 1996).

Fadnavis et al., (2007) analyzed that the equatorial QBO is seasonally asynchronous and presents a slow downward propagation, in addition the results showed that there is a maximum positive equatorial seasonal variation close to 10 hPa during winter in the Northern Hemisphere and autumn in the Southern Hemisphere. Equatorial negative maximum near 22 hPa occurs during January-June in both hemispheres. Peres (2017) identified that QBO is the main mode of interannual variability in the southern region of Brazil through TCO anomalies during 23 years of analysis.

The 2015-2016 NH winter was marked by a strong QBO outage (NEWMAN et al., 2016; DUNKERTON et al., 2016). The alternating regime of zonal winds from west to east propagate downwards over an approximate period of 28 months, but in 2016 an anomalous upward shift in the west phase from ~30 hPa to 15 hPa was recorded, and winds in the east phase were recorded at 40 hPa. This anomalous pattern generated a decrease (increase) in upwelling from 50 to 30 hPa (>50 hPa) which was associated with a positive (negative) O3 anomaly. (WMO, 2018).

Therefore, QBO is defined as the main mode of TCO variability in the equatorial region. The phases of this oscillation (westerly/easterly) in regions with the active winter hemisphere, present equatorial ozone anomalies anti-correlated with the anomalies in the mid/high latitudes (BOWMAN et al., 1989).

2.5.2 El Niño – Sourthern Oscilation (ENSO)

El Niño–Southern Oscillation (ENSO) is an atmospheric-oceanic phenomenon that occurs in the Equatorial Pacific Ocean (and the adjacent atmosphere), called El Niño Southern Oscillation (ENSO). Changes in the temperature of the Equatorial Pacific Ocean are directly reflected in direct effects of temperature and precipitation. It is closely related to the Southern Oscillation (OS), which involves changes in the trade winds and associated tropical circulation. Thus, El Niño is the warm phase of ENSO, and La Niña

(LN) is the cold phase. Historically, EN events have occurred every 3-7 years, alternating with opposite phases of below-average temperatures in the tropical Pacific (LN). ENSO has a global reach, showing greater intensity during winter in both hemispheres. Sea level pressure anomalies (PNM) are much greater in temperate regions, while precipitation variability is greater in tropical regions (BJERKNES, 1969; AMBRIZZI et al., 2006).

Figure 2.11: Coupled ocean-atmosphere system during La Niña and El Niño phenomena.

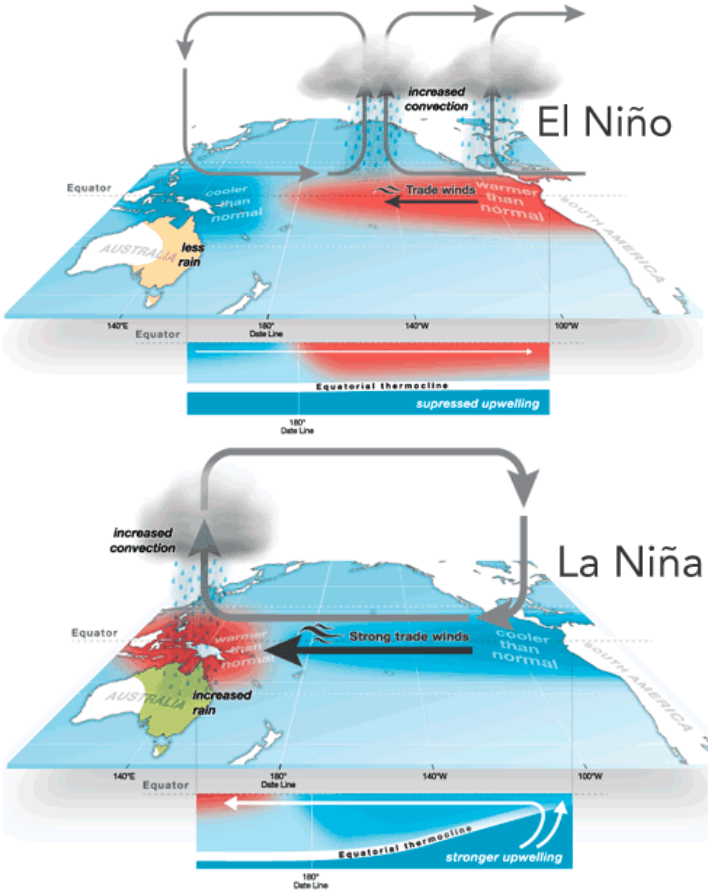

Source: Adapted from Australian Bureau of Meteorology.

ENSO affects tropical upwelling, which in turn leads to fluctuations in temperature and ozone in the tropical lower stratosphere (RANDEL et al., 2009). In the tropical upper troposphere and lower stratosphere (UTLS), the ENSO coefficient is negative, with low ozone during El Niño years and high ozone during La Niña years, the opposite sign is seen at mid-latitudes (OMAN et al., 2013; NEU et al., 2014).

Kawatani et al., (2019) identified that tropical upwelling associated with the BDC is reinforced during active El Niño, consistent with changes in wave propagation due to westerly wind anomalies at mid-latitudes. However, the expected effects of enhanced BDC during El Niño in delaying the progression of the descending QBO phase are outweighed by the improved wave conduction, resulting in a shorter QBO period in El Niño than in La Niña.

Figure 2.12: Schematic illustration of the Walker circulation (thick vector), gravity waves (black vector), QBO zonal wind (blue and pink), and equatorial residual vertical velocity (dashed vector) for (left) El Niño and (right) La Niña.

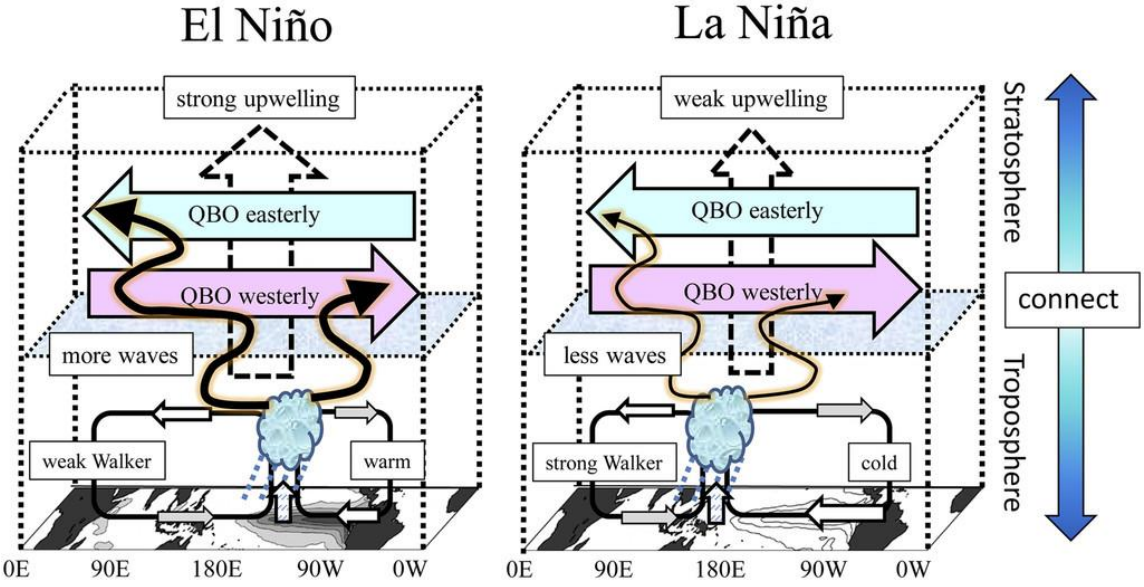

Source: Adapted by Kawatani (2019).

ENSO's effects on tropical convection characterize a good example of the teleconnections that can be represented by ENSO's influence on other modes of variability. It can be said then that ENSO modulates QBO in the tropical region (figure 2.11 by KAWATANI et al., 2019). With an increase in large-scale upwelling in the equatorial stratosphere, the propagation of the QBO phase can be reduced, prolonging its phase.

2.5.3 Solar Cycle – 11 Years

The solar cycle influences ozone through photochemical and dynamic processes in the stratospheric layer. The solar cycle shows the sun's activities at 11-year intervals, and each cycle is determined by the dark spots that appear on the solar surface. During this cycle, the star goes through a period of maximum and minimum of its activity, being able to wreak havoc depending on its location. Ozone concentrations and temperature control in the stratospheric layer are largely due to the variability of solar flux in the ultraviolet spectrum that are associated with the 11-year solar cycle.

Figure 2.13: Progression of the Solar Cycle from 1979 with the prediction of the number of sunspots expected for the solar maximum until 2025.

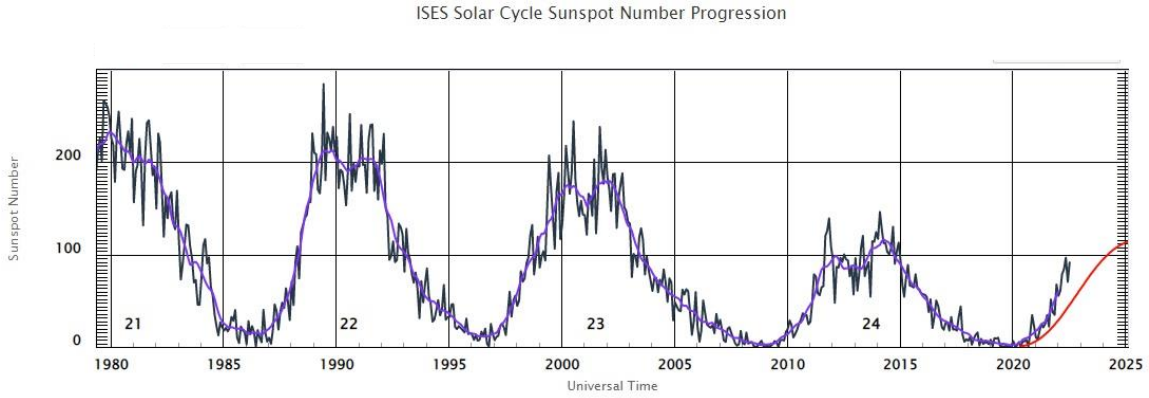

Source: Adapted by Space Weather Prediction Center.

As ozone is produced at wavelengths smaller than 242 nm and mainly destroyed at longer wavelengths through photochemical processes, understanding how these changes in UV irradiance is of paramount importance for the balance of ozone and atmospheric radiation (GRAY, 2010). Due to its radiative properties, the change in ozone content alters the temperature in the stratospheric layer, which in turn alters the upward propagation in the tropics and the consequent breaking of planetary waves that drive large-scale motions such as the Brewer-Dobson circulation.

The variability of ozone content also depends on dynamic forcing and chemical evolution of ozone-depleting substances (ODSs). The global concentration of O3 has

been decreasing since 1980, where anthropogenic emissions of ODS reaching the stratosphere fell after the Montreal Protocol (SINNHUBER et al., 2009). Many studies show that the behavior of the solar cycle does not directly affect the O3 content, but the variations and changes in the solar cycle, with maximums and minimums, end up interfering in the modulation of QBO, which is an important variability in relation to the behavior of stratospheric O3 (WMO, 2006). The dynamics of the Brewer-Dobson circulation can also be modified by solar cycle modulations, for example Kodera and Kuroda (2002) found changes in large-scale circulation through minimum/maximum solar cycle variations resulted in a decrease in O3 content. in the tropical lower stratosphere.

LEE and SMITH (2003) used a two-dimensional chemical-dynamic-radiative model with QBO data to identify the influences that may occur and lead to small or even negative differences in the lower and middle stratosphere equator relating O3 to the solar cycle. The results showed that when one wants to analyze the solar cycle forcing in the O3 data, the models cannot represent this analysis well, and this can be explained, in addition to the influence of the QBO by the large volcanic eruptions that occurred in El Chichón in 1982 and Mount Pinatubo in 1991. Bencherif et al., (2020) investigated the main variability and trends of tropospheric and stratospheric O3 over the station in Irene, South Africa. The results showed that the site located in the subtropical region of the African continent has four dominant modes of variability, where the solar cycle had a great influence on the stratospheric O3 column (SCO).

3 METHODOLOGY

3.1 REGION OF STUDY AND INSTRUMENTS USED TO OBTAIN THE TOTAL OZONE COLUMN

The study area of this work comprises the central region of the state of Rio Grande do Sul in the city of Santa Maria (29.4ºS and 53.7ºW), and the tropical region of Brazil in Natal in Rio Grande do Norte () used in the validation of the vertical profile data. The monitoring of the total column of Ozone has more than 40 years of data available in Santa Maria/RS, which will be used surface instruments (Brewer Spectrophotometer) and satellite data (TOMS, OMI) to analyze the total column of O3, in the identification of AOH side effect events in the region.

Figure 3.1: Study regions used in this work. Santa Maria located in subtropical latitudes and Natal/RN located in tropical latitudes of Brazil.

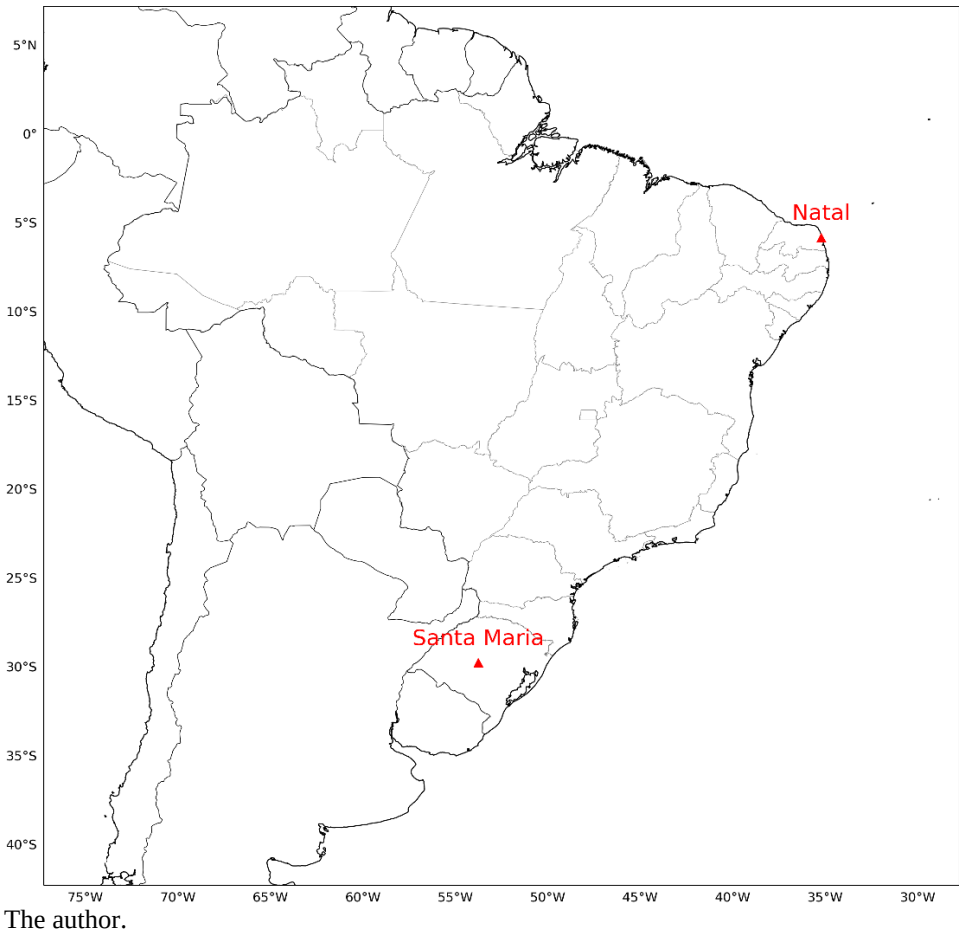

Source: The author.

The database has made measurements available since 1979 with satellites and from 1992 onwards surface measurements began to be carried out in the region. The region will be used as a reference for the analysis and understanding of the AOH influenced events that affect the region during the AOH performance in Antarctica in the southern spring.

3.1.1 Brewer Spectrophotometer

The Brewer spectrophotometer is one of the most important surface instruments that perform daily measurements of ultraviolet radiation, in addition to measurements of the total column of ozone (O_3) and sulfur oxide (SO_2). The beginning of measurements in the central region began with the Brewer Spectrophotometer model MKIV #081 during the period 1992 to 1999, while the model MKII #056 operated from 2000 to 2002 and the model MKIII #167 from 2002 to 2017, initially installed in the Southern Space Observatory – OES/CRS/INPE – MCTI (29.4°S; 53.8°W; 488.7m), in São Martinho da Serra.

The Brewer MKIII #167 Spectrophotometer, Figure 3.1, is a modern and automated surface instrument that measures global solar radiation in the ultraviolet type B (UVB) band of five wavelengths 306.3; 310.1; 313.5; 316.8; 320.1 nm, where each 0.5 nm determines the spectral distribution of incident radiation intensity. The total column allows the deduction of some important atmospheric gases, such as: sulfur dioxide (SO2), nitrogen dioxide (NO2) and ozone (O3). Furthermore, it is possible to obtain the vertical profile of O3, the total column of sulfur dioxide (SO2) and nitrogen dioxide (NO2) in addition to the optical thickness in wavelengths in the UV channel.

Brewer Spectrophotometers are composed of monochromators and detectors to observe and measure the spectrum of solar radiation. The monochromator essentially consists of a dispersion element and devices for controlling the width of the desired wavelength range. The energy source (the Sun) to be analyzed must present a continuous spectrum and is formed by a spectrophotometer and a tracking system of the Sun that are coupled to a microcomputer. From there, the system performs the acquisition and storage

of data and controls the instruments through its own software. The user himself develops a measurement scheme so that the device works individually.

Figure 3.2: Brewer Spectrophotometer #167 installed of the Southern Space Observatory - OES/CRS/INPE - MCTI in São Martinho da Serra (29.42°S, 53.87°W), Rio Grande do Sul, Brazil.

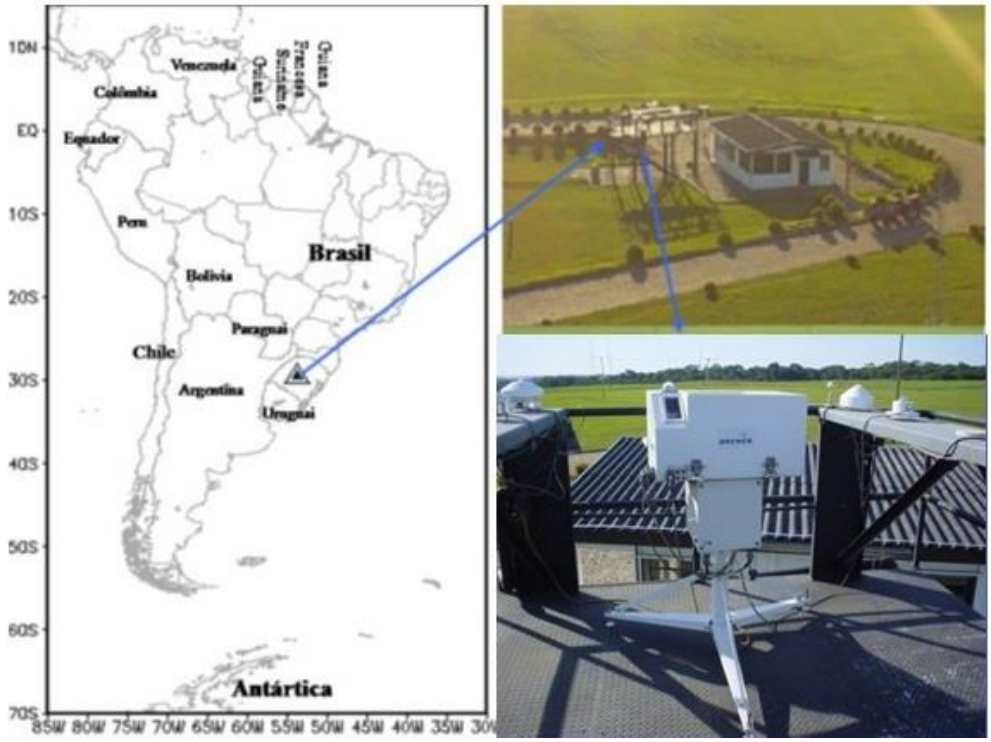

Source: PMOA.

Brewer spectrophotometers have a complete set of programs that control various points in data collection and some analysis. It is programmed to automatically adjust to the settings of the measurement site and will follow a user-defined observation schedule. The individual observations of O3 obtained by the Brewer Spectrophotometer use a method called: Direct to the Sun (DS) measurement. On days without significant cloudiness, the instrument measures individually for half an hour 5 times for 3 minutes, using five wavelengths (306.3; 310.1; 313.5; 316.8; 320.1 nm) to infer the TCO with a resolution of 0.5 nm.

According to this information, to determine the total ozone column, the most appropriate method is by measuring direct solar radiation in the UV range (305 and 340 nm), using the Lambert-Beer law method, which defines the direct spectral irradiance that reaches the Earth's surface and that is attenuated by the amount of certain atmospheric

components. It is necessary to measure the irradiations in more than one wavelength and to determine the total ozone by techniques of differential optical absorption spectroscopy, because the dispersion of particles through aerosols and thin clouds can significantly affect the amount of transmitted irradiance. At the end of each day, daily averages of O3 are calculated at the location where TCO monitoring is performed, and these same averages generated by surface data by Brewer are compared with satellite measurements.

3.1.2 Total Column Ozone Satellites

The Total Ozone Mapping Spectrometer (TOMS) and the Ozone Monitoring Instrument (OMI) are the instruments on board satellites that complement the database for the analysis of the total column of ozone in the study region of this work during the period from 1979 to 2020. The TOMS satellite was one of the first satellite instruments with continuous observations that were available for studies related to monitoring O3 content with global and regional trends. The TOMS (Total Ozone Mapping Spectrometer) satellite was developed by the National Aeronautics and Space Agency (NASA) and began its activities in 1978, with the launch of the Nimbus-7 instrument. Between 1991 and 1994 the satellite was on board the Meteor-3 instrument until 1996, when it was replaced by the Earth Probe, and at the end of 2005 the TOMS satellite ended its activities of measuring the total column of O3.

TOMS provides measurements of tropospheric aerosol content, ultraviolet irradiance, erythematic UV exposure, and effective reflectivity from the Earth's surface and from clouds. In addition to ozone, it also measures sulfur dioxide released in volcanic eruptions. The TOMS instrument is an ozone probe that performs total ozone measurements using incoming solar energy and backscattered ultraviolet (UV) radiation at six wavelengths between 310 and 380 nm (312.5; 317.5; 331.3; 339.8; 360.0 and 380.0 nm). This set of discrete wavelengths 1 nm apart is measured at 35 scanning positions at 3° intervals to cover all regions of the orbital paths that provide spatial coverage at all latitudes from a polar orbit synchronous with the Sun. The spatial resolution will depend on the satellite's orbital altitude, where, for example, the nadir is about 50X50 km and at the extreme points of the satellite scan the resolution is 75x200 km. The TOMS satellite

also has a dataset with individual measurements almost coincident with specific geographic locations, called overpass. This dataset includes measurements of TCO (in DU) at 333 sites during its period of operation.

The OMI derives from NASA's Total Ozone Mapping Spectrometer (TOMS) instrument and the European Space Agency's (ESA) Global Ozone Monitering Experiment (GOME) (aboard the ERS-2 satellite). This new generation of satellite can measure more atmospheric constituents than TOMS and offers much better ground resolution than GOME (13 km x 25 km for OMI vs. 40 km x 320 km for GOME). The OMI instrument was launched in July 2004 aboard the ERS-2 satellite and continued the records of the TOMS satellite, which ended its activities in 2005. The OMI measurements continue to be recorded until today, where measurements of the total column of ozone, as well as some atmospheric data that relate to O3 chemistry such as NO2, SO2, some types of aerosols and cloud cover. Earth is observed in 740 bands along the satellite's path, large enough to provide global coverage in 14 orbits (1 day). It uses Backscatter Ultraviolet (BUV) technology, with two images fed into a spectrometer grid and a spatial resolution of 13 x 25 km, in the two UV bands: UV-1 (270 to 314 nm) and UV-2 (306 to 380 nm) nm) with spectral resolutions of 0.45 and 1 nm, respectively.

The OMI instrument employs hyperspectral imaging in scan mode to observe solar radiation backscattered in the visible and ultraviolet regions of the electromagnetic spectrum. The hyperspectral capability improves the accuracy of the TCO data and allows for accurate long-term self-calibration for wavelengths.

3.2 CRITERIOUS FOR DEFINITION OF INFLUENCED EVENTS OF THE ANTARCTIC OZONE HOLE

The daily average data obtained by satellite and ground instruments provided the analysis of 42 years of TCO data on Santa Maria/RS. This analysis approach has been used to identify days with reduced O3 content over subtropical latitudes (BITTENCOURT et al., 2019). To quantify the temporary reductions in O3 content over the region, tests have shown that the use of -1.5σ is sufficient to quantify these temporary

reductions (WILKS, 2006; PERES, 2016).

The first step is a climatological analysis of the TCO data on MS, during the 42 years of O3 monitoring. Monthly averages during this period were also calculated and with this, during the period in which the AOH is active, it was possible to quantify the possible reductions in O3 content, from August to September. Days in which the TCO_d presented values lower than the monthly mean ($\overline{TCO_m}$) minus 1.5σ the standard deviation of the month are selected for stratospheric analysis.

$$TCO_d < \overline{TCO_m} - 1.5\sigma_m \quad (3.1)$$

The second step after identifying these events is the analysis of potential vorticity fields. Reductions are presented in percent (%) and in absolute values (DU).

3.3 ECMWF REANALYSIS DATA

In the analysis of the TCO database, the days of possible influence events of the Antarctic Ozone Hole in the region of Santa Maria/RS were identified and chosen. With the identification of events, the reanalysis data helped to better understand the behavior of the atmosphere during the occurrence of these events through potential vorticity fields and vertical sections of the atmosphere. The dynamic analysis of the events includes the use of the new generation of meteorological data from the reanalysis of the ECMWF (European Center for Medium-Term Weather Forecasts) with the new ERA-5. The ECMWF ERA-5 reanalysis has a horizontal resolution of 0.25º x 0.25º latitude-longitude and a temporal resolution of 1 hour. Hoffmann et al. (2019) showed significant improvements in potential temperature conservation, especially at stratospheric levels, when comparing data from the new reanalysis database, ERA5, with the ERA-Interim reanalysis.

The data used in this study were:

- total O3 column (*tco3*), for comparisons with TCO surface data over the reference region.

- potential vorticity and O3 mixing ratio, for the analysis the stratospheric dynamics of AOH influence events.
- temperature and u, v, and w components of the wind, for the vertical cuts in the identification of the jets (stratospheric and tropospheric).

The data used in this work are diaries where only the time of 18 UTC was selected, for the 37 isobaric levels (1000 to 1 hPa) during the period 1979 - 2020. The domain region was comprised between 10 ºN to -90 ºS and -100 ºW - 20 ºE. This region covers well the south-central region of South America and part of the South Pole, presenting in detail the behavior of the poor O3 air mass advancing, after the definition of the event.

The potential vorticity fields help to monitor the dynamic behavior of the stratosphere, in addition, it makes it possible to identify the origin of the O3 poor air mass, where the increase in absolute potential vorticity is analyzed, characterizing a polar origin of this air mass, that is, air mass coming directly from the Antarctic region where AOH is active, when there is a decrease in APV) the origin is characterized as equatorial (SEMANE et al., 2006; PERES, 2016; BITTENCOURT et al., 2019). After identifying the events (through TCO data) and determining the height (SABER data) at which temporary decreases in O3 content occurred, PV analysis were performed at pressure levels and at three preferred heights: 30 hPa, 20 hPa and 10 hPa.

To identify the behavior of the jet streams during the active period of the AOH, fields with the vertical cut of the atmosphere help in this matter. In this way, the vertical section of the atmosphere between 1000 and 5 hPa of potential temperature (in Kelvin) and wind (in m/s) for the longitude of 54º west, presents the behavior of the stratospheric jet (polar vortex) and the tropospheric jets (subtropical and polar). Furthermore, one can infer where there was a break in the tropopause and the intrusion of stratospheric air into the troposphere.

3.4 HYSPLIT MODEL AND OZONE SATELLITES

To assist in the identification of AOH influence events on the study region, the HYSPLIT/NOAA model was used. The HYSPLIT model calculates simple trajectories of air parcels, in addition to complex transport, chemical transformation and deposition simulations (ROLPH et al., 2017). HYSPLIT is used in various simulations to describe atmospheric air transport, diffusion and deposition of pollutants and particulate matter. The model calculation method is a mixture of the Lagrangian method (using a reference moving through convection and diffusion calculations) and the Eulerian method (using a fixed 3D grid as a reference to calculate the concentration of pollutants in the air). In this study, the backward trajectory was used, which aims to show the behavior of the air mass for days before, and an isentropic vertical velocity model. With this tool it is possible to confirm the events by making retroactive trajectories showing the path of air masses from the Antarctic region to the region of interest, available at (HYSPLIT, 2017). Satellite images helped to characterize the region of influence of the Ozone Hole in the Antarctic region and possible indirect influences with the regions of medium latitudes. Ozone Watch and TEMIS satellite were used in this work.

3.5 VERTICAL ANALYSIS OF OZONE CONTENT

The analysis of the vertical profile of O3 is extremely important for this work, mainly because it allows investigating the behavior of O3 at different height levels, and at which heights the decrease in O3 content over the study region was greater. The analyzes performed here were carried out through measurements of the SABER instrument (Atmosphere Survey using Broadband Emission Radiometry) on board the TIMED (Thermosphere-Ionosphere-Mesosphere Energetics and Dynamics) satellite, which provides data from 2002 to 2018.

TIMED was a mission developed by NASA that conducted an intensive investigation of the mesospheric region and of the lower thermosphere, which comprises a poorly studied region between 60 and 180 km in altitude. SABER are measured through

soundings of the atmosphere using radiometry with broadband emission. It observes the Earth in narrow spectral ranges, with high accuracy of carbon dioxide (15), ozone (9.6) and nitric oxide (5.3) emissions (MLYNCZAK et al., 1997). The main objective of the SABER experiment is to understand the thermosphere and achieve a major improvement in the understanding of fundamental atmospheric processes (RUSSELL et al., 1999). SABER is one of four experiments on NASA's TIMED mission that was scheduled to be launched in May 2000 by a Delta II rocket into a circular orbit of 74.1º ± 0.1° inclined, 625 ± 25 km.

Many studies present analyzes of the SABER data to identify the main variability through the vertical behavior of temperature and O3 content. For example, REMSBERG (2003) presented the behavior of the temperature profiles for February 2002 between 52 ºS to 83 ºN, the results showed that the dataset is useful for analyzes that relate the dynamics and transport of tracer chemical constituents in the middle atmosphere. Nath et al., (2014) identified the main variability and trends in O3 content and temperature behavior using SABER data between 20 - 100 km altitudes in the 10 - 15 ºN region between 2002 - 2012. The results showed an intense semi-annual oscillation during the months of March-May and August-September (between 25 - 30 km of altitude).

Joshi et al. (2020) analyzed the seasonal and interannual variability of atmospheric O3 from 14 years of SABER data (2002-2015) in mid-latitude regions of both hemispheres. The observed data showed an accumulation of O3 starting in late winter and peaking in early spring in both hemispheres, characterizing the dynamics of the polar vortex, pre-formation of AOH. In addition, the annual oscillation stood out in both hemispheres in the middle atmosphere (between stratosphere and lower mesosphere), the semi-annual oscillation showed peaks between 40-60 km and between 80-100 km of altitude.

For this work, the study region was selected through a box of ±2º of latitude and longitude of the reference point in Santa Maria/RS (29.4ºS and 53.7ºW). During the 17 years of data (2002-2018), approximately 5,982 vertical profiles were identified where the satellite mapped the selected region. The profiles were interpolated with a vertical resolution of 0.1 km providing 954 altitude levels in the range of 15 to 105 km in height.

The SABER satellite provides data on altitude (in km), latitude and longitude, temperature (in Kelvin) and mixture ratio O3 - OMR - (ξO3).

3.5.1 TIMED/SABER satellite data validation

As one of the objectives of this work is to analyze the vertical behavior of O3 content during the AOH influence events over southern Brazil, it was necessary to validate these SABER data to obtain adequate and more accurate results. For this validation, the SHADOZ network (Southern Hemisphere ADditional OZonesondes) was used, which are data from ozonesondes launched by balloons to monitor the vertical behavior of ozone between the surface and the stratosphere. Thus, data from a reference station of the SHADOZ network, the Natal station in Rio Grande do Norte (5.42ºS and 35.40ºW) were used.

The SHADOZ station in Natal/RN has been in operation since 1998, when a campaign was started by NASA providing nine stations, and which today already operates with 14 measurement stations providing data continuously (THOMPSON et al., 2017). The SHADOZ data consists of the new version (V06) available at, and offers some variables such as ozone, temperature, pressure, relative humidity, wind direction and speed. Based on this information, at the station in Natal/RN, about 530 profiles were identified for the period of analysis (2002 - 2018) with 604 vertical levels. Validation was based on SHADOZ data and SABER satellite data for the Natal/RN station. From the SABER data, 3,304 daily profiles were identified for the same period (2002-2018), with 954 vertical levels. The vertical resolution is 0.1 km interpolated also in a ± 2º lat/lon box in the Natal/RN region.

Some studies have already shown the behavior of O3 using SHADOZ and SABER data for different regions of the world. Over the southern region of Brazil, Santa Maria/RS, Bresciani et al., (2018) performed a multi-instrumental analysis to study an intense side effect event that influenced the region in 2016. The study showed comparisons between satellite data, surface instrument, Brewer, and an ozonsondes was launched to monitor the event. Toihir et al., (2018) identified the long-term variability of

O3 at eight points between the tropics and subtropics, from January 1998 to December 2012, using TCO data with surface instruments, satellites, and vertical profiles, by ozone soundings. The results showed that the main variability that dominates the behavior of O3 in the regions of the study is the annual oscillation, with a greater influence in the subtropics than in the tropics. Unlike the QBO which is in phase in tropical regions showing a strong link with the large-scale circulation through the BDC. The solar cycle is in phase with total O3.

3.5.2 Vertical profile analysis of TIMED/SABER O_3 satellite

After identifying the events on 42 years of data, the SABER satellite analysis is used to characterize the vertical behavior of the atmosphere during the events of influence of the AOH on the region. The analyzes were generated from 17 years of data available on the platform, where the daily behavior of the data was observed through vertical profiles, identifying the height where the greatest drops in ozone content happen during the occurrence of an event.

The climatology and monthly averages were generated, so it was possible to make comparisons of the events with the monthly climatology. To quantify the decrease that occurs during the event, the calculation of the relative differences (in percentage) helps to show this temporary decrease in numbers. The calculation of the difference is based on the difference between the profile of the day of the event and the climatology profile for the reference month (August to November - spring months), following equation (3.2):

$$RD\ (\%) = 100 * \frac{(EventDay - Climatologicalmonth)}{(Climatologicalmonth)} \qquad (3.2)$$

3.6 STATISTICS, COMPARISONS AND VARIABILITIES

The monitoring of ozone content over the Santa Maria/RS region during these 42 years of data, composed of instruments on board satellites (TOMS, OMI, SABER) and surface instruments (Brewer Spectrophotometer, ozonesonde) presents particularities and

importance of the ozone content in southern Brazil.

Statistical analyzes were performed with available TCO data to understand O3 behavior. Comparisons were made between the different types of instruments (TOMS/OMI x BREWER x ERA5). In addition to the daily analysis, the climatology and monthly averages were obtained for the 42 years, with the following calculations:

- ✓ Pearson's correlation coefficient (R);

$$R = \frac{\sum_m \sum_n (SATÉLITE - \overline{SATÉLITE})(BREWER - \overline{BREWER})}{\sqrt{\left(\sum_m \sum_n (SATÉLITE - \overline{SATÉLITE})^2 (\sum_m \sum_n (BREWER - \overline{BREWER}^2)\right)}} \quad (3.3)$$

The R^2 that is shown in the results is the value of the squared correlation coefficient. The mean square error (RMSE), often used to estimate the difference between the values predicted by a model (or satellite) and the observed values (Brewer Spectrophotometer), also called residuals, aggregates the predictive strength of the variable in a simple measure:

- ✓ Mean square error (RMSE);

$$RMSE = \sqrt{\sum_{i=1}^{n} \frac{(SATÉLITEi - BREWERi)^2}{n}} \quad (3.4)$$

The mean bias error (MBE) represents a systematic error where positive values of MBE represent an overestimation of the data, and negative values an underestimation of the data observed by the model:

- ✓ Mean bias error (MBE)

$$MBE = \frac{100}{n} \sum_{i=1}^{n} \frac{(SATÉLITEi - BREWERi)}{BREWERi} \quad (3.5)$$

To quantify and visualize the behavior of O3 in the events of influence of the

AOH, in addition to the monthly and climatological averages ($\overline{TCO_m}$), the anomalies in relation to the events ($Events_m$) identified were calculated:

$$\text{Anomaly} = Events_m - \overline{TCO_m} \quad (3.6)$$

3.6.1 Variabilities the Ozone

The identification of the predominant variability of O3 content for the 42 years of available data was studied in this work mainly for the region that is the focus of this study. The wavelet transforms allow identifying the periodicities that stand out the most in time series analyzed along with their evolution (TORRENCE & COMPO, 1998). Monthly TCO anomaly data were used in the wavelet transform method to reveal the main modes of ozone variability (HADJINICOLAOU et al, 2005). In this work, the Morlet transformed wavelet consists of a plane wave modulated by a Gaussian function, represented by:

$$\Psi 0(\eta) = \pi \frac{1}{4} e^{i\omega 0 \eta} e^{\frac{-\eta^2}{2}} \quad (3.7)$$

where ω0 is the non-dimensional frequency; η is the non-dimensional time parameter.

$$W_n(s) = \sum_{n'=0}^{N-1} X_n \Psi * \quad (3.8)$$

Considering the discrete time series (X_n), with a fixed time spacing (Δt) and = 0,..., N-1, the continuous wavelet transform is in Equation (7) where (*) is the complex conjugate es is the period (wavelet scale). The global wavelet spectrum Equation (8) allows to calculate the unbiased estimate of the real power spectrum of the time series, by calculating the average wavelet spectrum over a period.

$$W^2(s) = \frac{1}{N} \sum_{n=0}^{N-1} |W_n(s)| \quad (3.9)$$

The wavelet is composed of the power spectrum, where the edges are closed by a 'U' curve called the influence cone, where there is a 95% confidence level. The global wavelet spectrum contains the most significant values and on the right side of the dotted line indicates a confidence level of 95%, the curve that passes through this line being statistically significant.

4. RESULTS AND DISCUSSION

4.1 TCO VARIABILITY ANALYSIS FOR SANTA MARIA/RS

Daily data of the total column of ozone for the SM region through satellite instruments (TOMS and OMI), the Brewer spectrophotometer, and the reanalysis data from the ECMWF ERA5, from 1979 to 2020. Figure 4.1 presents the TCO time series for each of the instruments used in this work, they are: ground based (a), satellite and reanalysis (b) used in monitoring the TCO over the Santa Maria/RS station between 1979 and 2020. The periods of absence of data in the Brewer Spectrophotometer records between 1999-2000, 2009-2011 and 2017 – current, are due to instrument replacement and/or some technical problem. In the TOMS satellite records, there is a lack of data between 1994 and 1996, which can be explained by the replacement of satellite instruments from Meteor-3 to Earth Probe.

In figures 4.1a) and 4.1b) it is possible to observe the daily series of TCO in Santa Maria/RS, through the different surface, satellite and reanalysis instruments used in the analysis of the behavior of TCO in the subtropical region of Brazil. There is a well-defined annual cycle in all data sets presented, in addition to the comparison between the instruments showing good agreement. Toihir et al., (2018) analyzed satellite data and ground instrument trends and changes in O3 at tropical and subtropical latitudes in the southern hemisphere. One of their results showed good correlation between the instruments and showed that they were used correctly, mainly satellite data for O3 content analysis. Peres (2017), showed a good correlation in the TCO data for a shorter period of data, indicating a good agreement between satellite and surface data in the southern region of Brazil. Figure 4.1c presents the daily series for the region of Santa Maria/RS of the 42 years of data analyzed in this work, from TCO using reanalysis of the ECMWF ERA5.

Figure 4.1: Time series of daily average TCO for each instrument (Brewer, satellite, and reanalysis) in Santa Maria/RS between 1979 and 2020. (a) Brewer spectrophotometer (#081 in red triangle, #056 in gray circle and #167 in black cross), (b) Toms satellite instruments (Nimbus 7 in cyan circle, Meteor-3 in green triangle and Earth Prob in blue circle), OMI satellite in red, c) and ERA5 reanalysis data in gray cross.

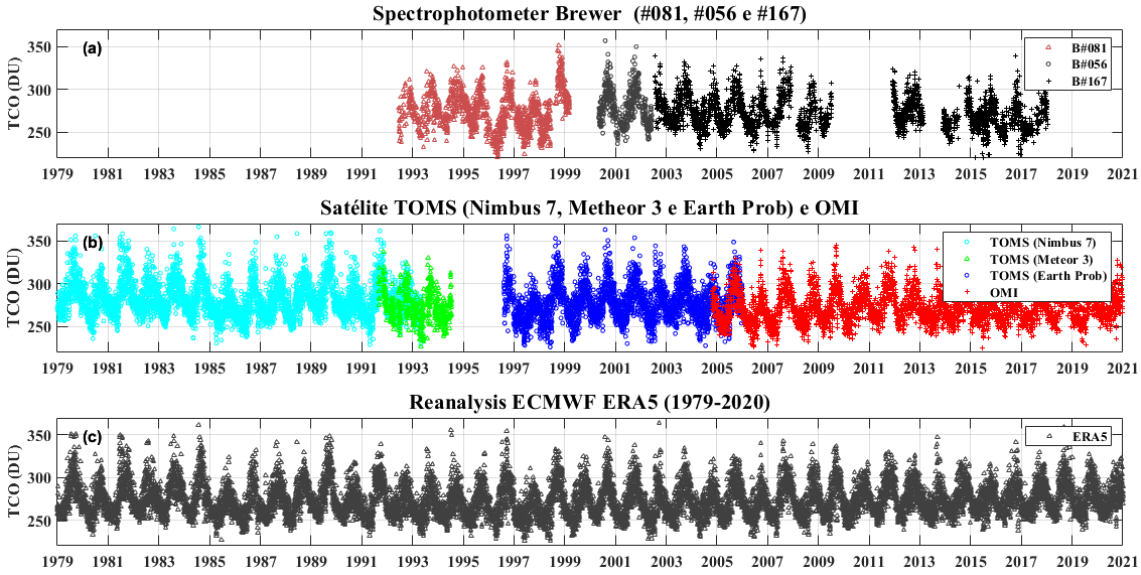

Source: The author.

Thinking about quantifying the differences between the instruments, a linear regression analysis of the TCO data for Santa Maria, in the study period of this work (1979 - 2020). Figure 4.2 presents a schematic diagram among the available instruments, they are:

- Dataset #1 = BREWER x TOMS.
- Dataset #2 = BREWER x OMI.
- Dataset #3 = BREWER x ERA5.

The comparison was performed through the difference between the surface and satellite instruments, in addition to the comparison between surface and reanalysis data. Thus, Dataset #1 presents (Brewer vs. TOMS) for the period from June 1992 to December 2005, containing 2164 pairs of data (Fig. 4.2a), Dataset #2 presents (Brewer vs. OMI) between the period from October 2004 to December 2017, with 4621 pairs of data (Fig. 4.2b), and to finish Dataset #3 presents (Brewer vs. ERA5) for the period from January 1979 to December 2020, with about 5065 data pairs. Each dataset represents the monthly

series of each instrument, it is observed that the correlation coefficient (R^2) with respect to the instruments presented considerably good values, where the values of the correlation coefficient were: 0.88 (BREWERxTOMS) and 0.94 (BREWERxOMI). Improvements in satellite equipment over the years and developers may explain this improvement between TOMS and OMI. The exception was the set between BREWER and ERA5 where R^2 presented a value around 0.83. Despite not being such a low value, the use of TCO reanalysis data cannot represent the behavior of O3 with a good quality. Regarding data from TOMS and OMI satellites, previous studies have shown similar results in relation to comparisons between these TCO measurement instruments over different regions. Anton et al., (2009) compared data from the OMI satellite with different surface instruments in the Iberian Peninsula and identified a good correlation between the instruments in the behavior of the TCO.

Toihir (2015) analyzed the average monthly behavior of TCO at 13 locations in tropical and subtropical latitudes comparing satellite data from the EUMETSAT program, OMI, and surface data SAOZ and DOBSON available at these stations, the results found were good correlations between these instruments with values around 0.87. Peres (2017), showed a good correlation in the TCO data for a shorter period of data, indicating a good agreement between satellite and surface data in the southern region of Brazil.

The root means square error (RMSE) showed differences of less than 3% in almost all data sets, which explains the high correlation values between the instruments, presented above by R^2, except for Dataset#2, which presented an RMSE in around 2.94, corroborating a low R^2. The mean bias error (MBE) in the analysis of daily TCO data showed:

- ✓ overestimation between the following data sets: BREWERxTOMS, BREWERxOMI;
- ✓ underestimation was identified in the dataset between the BREWER instrument with the ERA5 reanalysis.

These results confirm the effectiveness of the TCO measurements on the Santa Maria station, during the 42 years of data analyzed in this work and agree with works already presented that carry out these similar analyses.

Figure 4.2: Scatter diagram of the total column of ozone in SM obtained using the Brewer spectrophotometer and satellites (a) Brewer and TOMS, (b) Brewer and OMI, and (c) Brewer and ERA. The dashed line (blue) represents the slope for which the data would be in complete compliance, and the solid line (red) is the linear regression line.

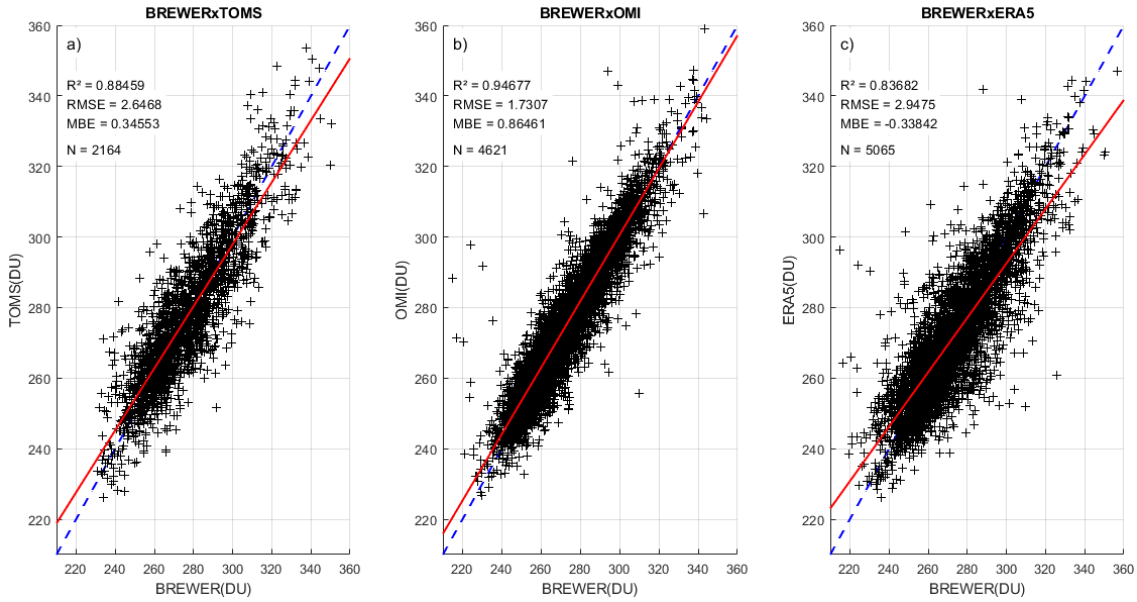

Source: The author.

4.2 OZONE VERTICAL PROFILE DATA VALIDATION

Vertical analysis makes it possible to identify the behavior of the O3 content at different altitudes. Validation of SABER data was performed to understand the behavior of O3 in Natal/RN (5.40ºS, 35.40ºW), using data from balloon soundings through the tropical station SHADOZ, during the 17 years of available data. Figure 4.3 a) shows the seasonal variability in relation to the tropical season in Natal/RN, showing the monthly average of the vertical profiles with SHADOZ data, and 4.3 b) shows the monthly average analyzes for Natal/RN with SABER data during the 17 years of data, also in O3 mixing ratio units (ppmv). The blanks show a failure of drilling measurements in this period, mainly between 2011 and early 2014 due to a malfunction of the instruments (THOMPSON, 2017).

The vertical profiles of O3 SHADOZ presented here are in units of O3 Mixing Ratio (OMR), where it is observed, in Figure 4.3a, a higher content of O3, mainly between 23 and 30 km of height with values that vary from 6 to 10 ppmv, showing a well-established

seasonal behavior during the study period in the tropical stratospheric region. Thompson (2017) presented a study comparing the data available from the SHADOZ station at different latitudes in relation to satellite and surface data at these stations. In Natal, a good correlation was observed between satellite data and surface data with ozonesondes, despite the data gaps presented during the analysis period. In Figure 4.3 b) the highest O3 content is observed in the stratospheric region, between 25-40 km of height with values between 6-10 ppmv, being more intense in early spring, late August to late summer, mid-March to April. Nath et al., 2014 showed that there is a strong biennial trend in relation to SABER analysis between 10 – 15 ºN, mainly in the stratosphere, in addition to the direct relationship of the quasi-biennial oscillation (QBO) with the O3 variability at these latitudes.

Figure 4.3: Monthly average (a) SHADOZ network, between 0 to 30 km in height, and b) SABER satellite, between 15-50 km height of the entire data period (2002 - 2018) in Natal/RN.

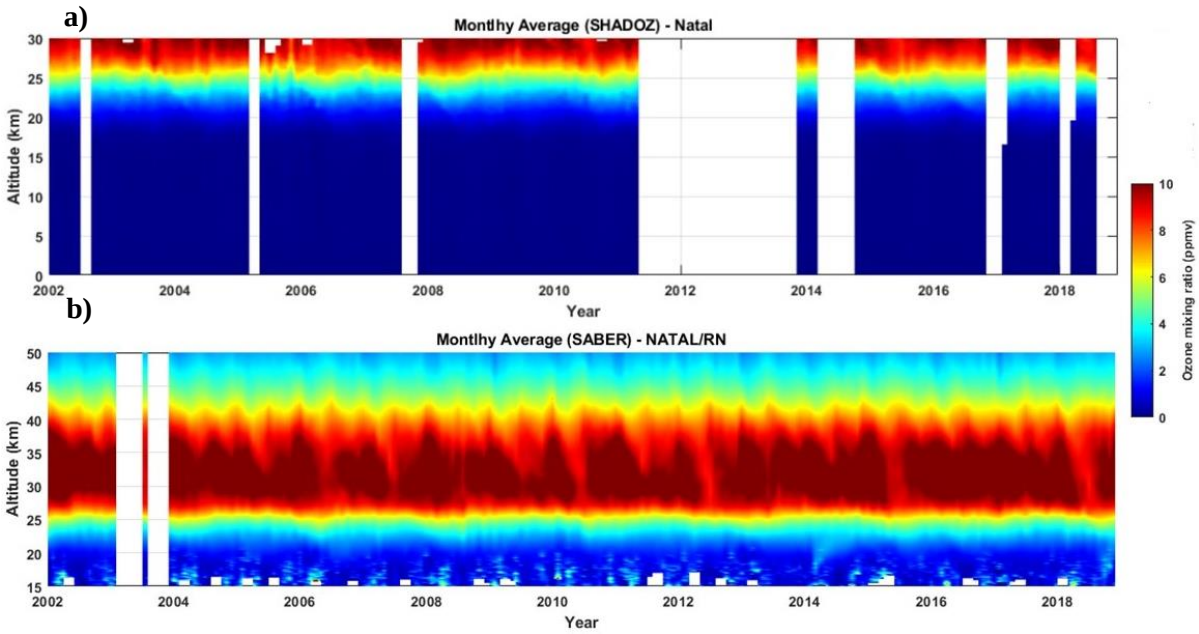

Source: The author.

4.2.1 SABER x SHADOZ comparisons

In the validation of data from the SABER satellite, the relative differences were calculated, allowing to analyze how the two databases (satellite and soundings) behave in the tropical region of Brazil. Thus, the analysis of concomitant profiles was performed, that is, profiles identified for the same days of analysis through the climatology performed for each database. The first difference found is in the heights, while SABER provides data between 15 and 110 km high, the SHADOZ network data provides measurements ranging from the surface to 26-30 km high where the balloon bursts, so comparisons will be made only between heights starting at ~18 km high and going up to 30 km. Figure 4.4 shows this comparison in OMR units (ppmv) of the O3 vertical profile from 2002 to 2018 using the monthly average. It is observed that the two instruments present similar behavior in almost the entire layer and in the entire period. Some points stand out, the first is in relation to the comparisons in the initial heights of the analysis, around 15-20 km of height. There is a more accentuated instability, which can be explained by the divergences and errors, mainly in the SABER satellite measurements.

Estimating these long-term ozone changes below 20 km from satellite data is still a challenge (WMO 2006). There is no significant relative difference above that, proving that the stratosphere can be used through these instruments. In practically every period of analysis, it is observed that the layer does not present significant differences, which could invalidate the use of satellite data in the analysis of the vertical behavior of O3.

Figure 4.4: Vertical profile comparison between SABER and SHADOZ, in O_3 mixing ratio (ppmv), of the monthly average of 2002 – 2018 in Natal/RN, in relation to height.

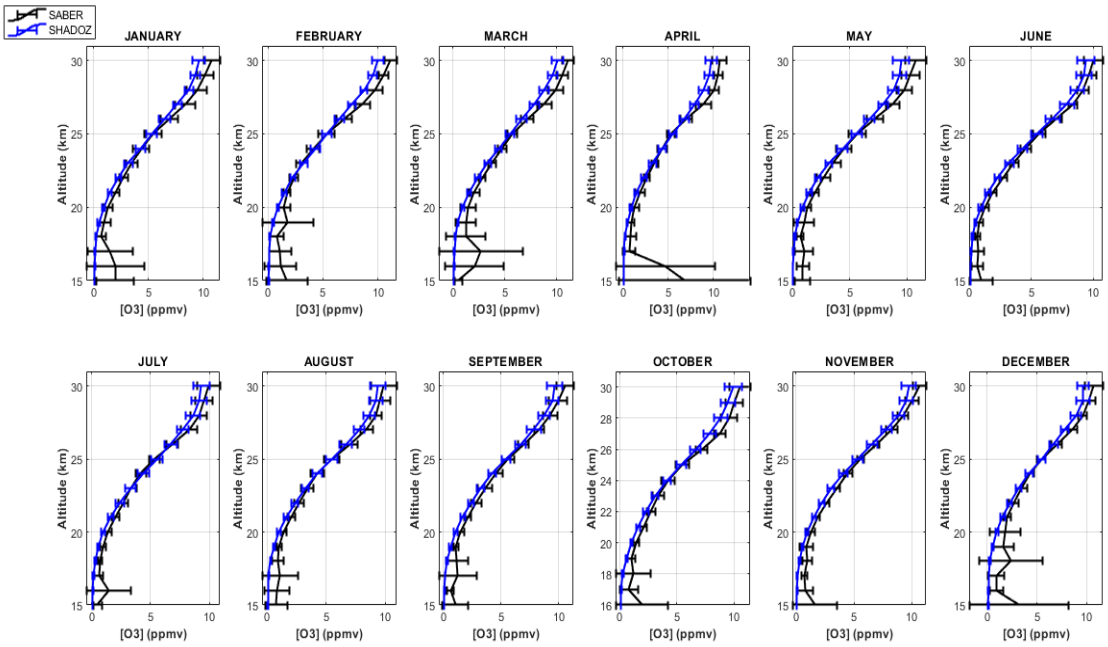

Source: The author.

The most significant differences occur between 15 and 20 km in height, in the summer months (December, January and February), March and April also show the greatest differences. In the middle stratosphere, between 20 – 26 km, the two corresponding profiles of each instrument show similar behavior and begin to diverge in the uppermost layer of the stratosphere. Regarding the analysis of the SABER satellite, it was decided to start the comparisons at 18 km height, and not at 15 km as the satellite provides, because below that, only instabilities are observed in the satellite measurements, according to figure 4.4, that directly interfere in the comparison between the SHADOZ and SABER instruments. These results show that it is reliable to use vertical profile data provided by the TIMED/SABER satellite to analyze the vertical atmospheric behavior of AOH influence events over the southern region of Brazil. Over 17 years of data, it will be possible to visualize the average heights at which the greatest temporary decreases in O3 content over Santa Maria/RS occur.

4.3 CLIMATOLOGY SEASONAL AND VARIABILITIES

4.3.1 TCO Climatology in Santa Maria/RS

The monthly climatology and standard deviation presented in Figure 4.5 for the four main instruments for measuring TCO in the subtropical season in Santa Maria during the period 1979 to 2020, where we have Brewer (black), TOMS (blue), OMI (red) and reanalysis of the new version of ECMWF ERA5 (green). As already seen in previous works, the annual variability stands out in the TCO data in Santa Maria, highlighting minimum values in autumn (April and May) between ~255 and 260 DU, and maximum values during the austral spring (September and October) with values between ~295 and 300 DU. This variability with lows in autumn and highs during spring is mainly explained by the large-scale movement known as Brewer-Dobson circulation (BDC). This transport is the dominant process that determines through its meridional movement that the O3 produced in low latitudes is transported to medium and high latitudes, causing this maximum to occur during late winter/early spring (LONDON et al., 1985).

Sivakumar et al., (2007) carried out a study on the climatology and stratospheric ozone variability over the Ile de La Réunion, France, for 15 years of data available in satellite instruments (HALOE, SAGE-II, TOMS), ozonesondes, where they were also identified maximum O3 values in spring and minimum values in autumn. Peres (2017) identified a similar behavior in the analysis of O3 content on the Southern Space Observatory. The maximums and minimums showing minimums in the austral winter and maximum in the austral spring. Oliveira, 2016 showed the stratosphere-troposphere exchanges (STE) where a greater number of exchanges was identified during the winter and spring months, with a lower frequency during the summer, also explained by the large-scale circulation (BDC).

Figure 4.5: Monthly climatology for SM of TCO in DU between the period 1979 to 2020, TOMS (blue) and OMI (red) satellites, Brewer spectrophotometer (black), and reanalysis ERA5 (green).

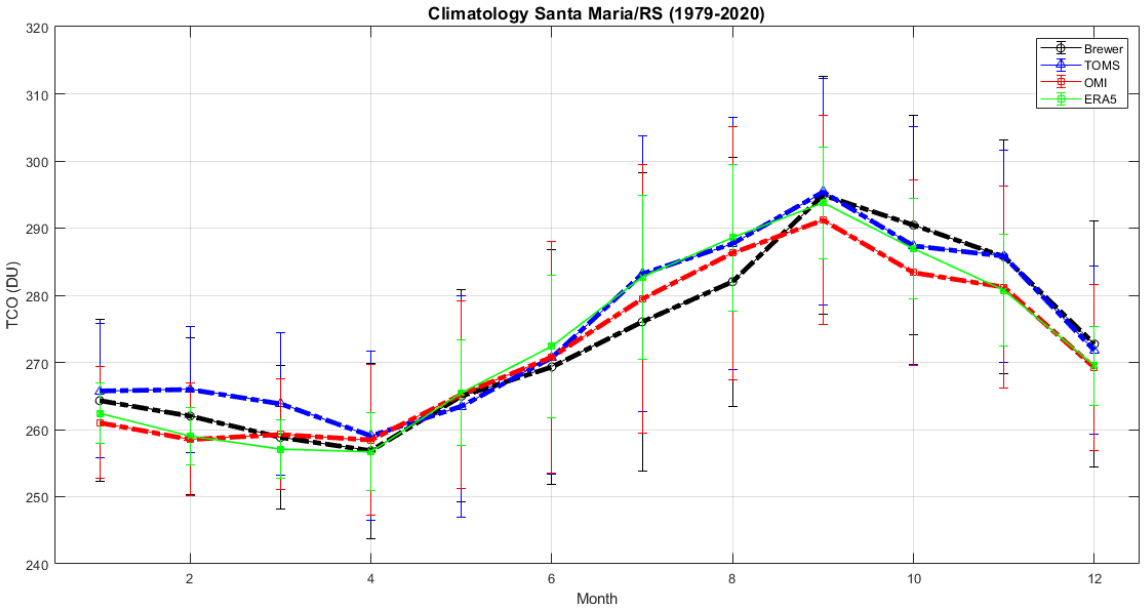

Source: The author.

4.3.2 Climatology O_3 vertical profile

Figure 4.6 shows the distribution of O3 over the period of the data analyzed by the SABER satellite for the subtropical station of Santa Maria/RS. In the monthly average (4.8a) and the climatology (4.8b) for the 17 years of data, it is possible to identify the variability of the ozone content in this period, between 20 to 50 km in height, with values due to the O_3 mixing ratio (ppmv). A high concentration of ozone is observed in the stratospheric layer (~25 - 40 km high) with values between 8 and 12 ppmv, being more intense in early spring, late August to late summer, mid-March to April, corresponding to values already found for mid-latitude regions such as southern Brazil (PERES, 2019; TOIHIR, 2018).

Figure 4.6: Monthly average (a) and climatology (b) for the entire period (2002 - 2018), SABER satellite in Santa Maria/RS, between 18 to 50 km high.

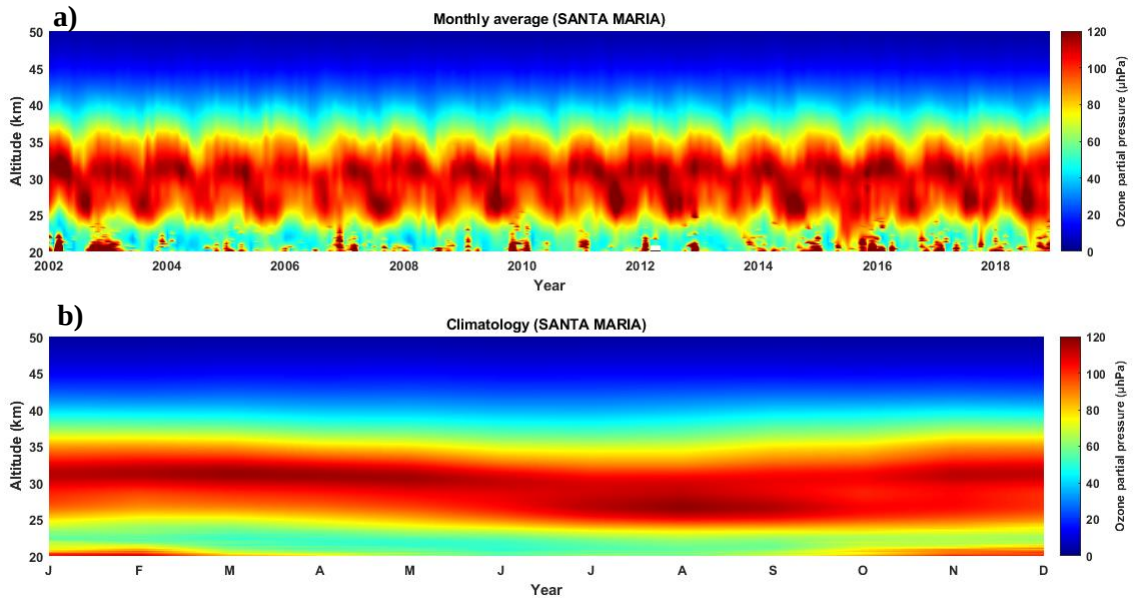

Source: The author.

The monthly climatology for the vertical profile data (SABER) presented in figure 4.7 shows the behavior of O3 at different altitudes, presenting the particularities that this component plays at each specific altitude. The heights chosen for this analysis were: 20 km (blue), 24 km (red), 28 km (green), and 30 km (black). The heights between 20 and 24 km comprise the lower and middle stratosphere, at these altitudes the O3 layer is already established. Ozone at these altitudes undergoes dynamic changes that occur between high troposphere/low stratosphere. It is observed that in 20 km the annual variation is well represented, being like the TCO climatology, with minimums in autumn and maximums in spring, shown in figure 4.9. At 24 km, a behavior without major variations stands out. The O3 variation is between ±20 µhPa in relation to the average, showing a small similarity with the altitude of 20 km. At altitudes of 28 and 30 km, the behavior of O3 is influenced by photochemistry, with higher values during the hottest seasons (spring and summer), and minimum values in the cold season (winter).

Figure 4.7: Monthly climatology for SM using SABER data between the period 2002 to 2018. Differences altitudes, in blue (20 km), red (24 km), green (28 km) and black (30 km), in ozone partial pressure (μhPa).

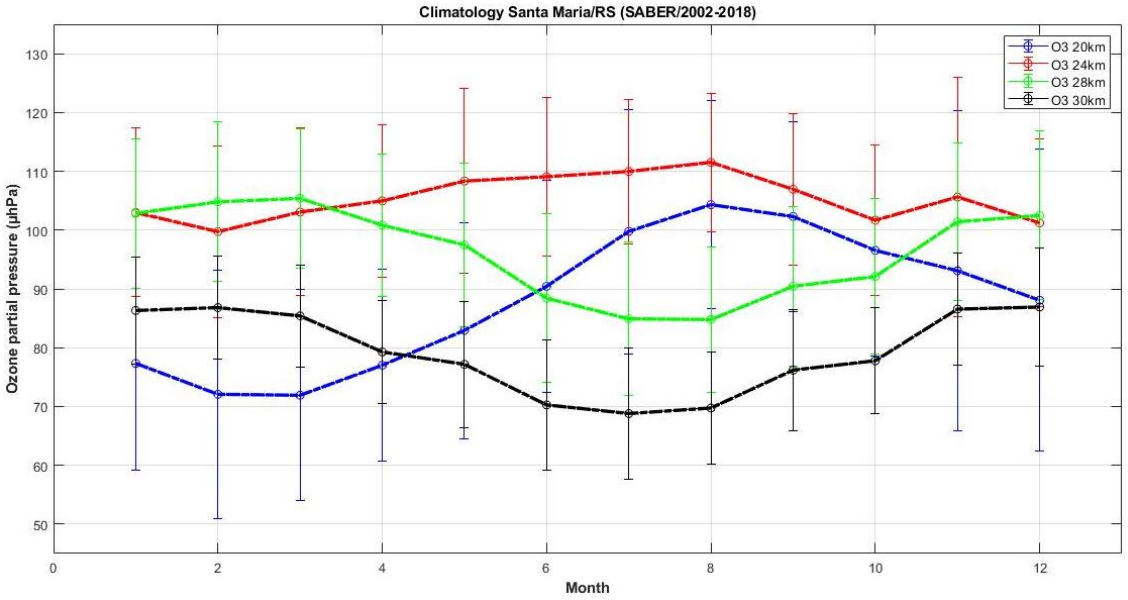

Source: The author.

4.3.3 Variabilities in subtropical latitudes (Santa Maria/RS)

The study of wavelet transforms in a database allows identifying the behavior of the main periodicities that occur in each region. In Santa Maria/RS, this analysis was performed by applying monthly series of TCO anomalies in wavelets for a period of 42 years of data (1979-2020) combining satellite and terrestrial instruments. Figure 4.8 presents this analysis where annual periodicities were removed so as not to mask other important variability in the region. The left axis is the Fourier period (in month), the wavelet power scale on the right axis and the time (years) on the lower axis. The white outline includes regions with a confidence level greater than 95% and the U-shaped curve indicates the cone of influence. However, in the period from 8 to 16 months, a strong influence of annual variability is observed in subtropical latitudes, such as southern Brazil, with a well-marked seasonal cycle at this latitude.

From the power spectrum, the 11-year solar cycle, in the range of 132 months, stands out as an important variability in subtropical latitudes in relation to the O3 content. Bencherif (2020) analyzed the variability and trend of O3 over 20 years of data, in Irene,

South Africa. The variability during this study period showed a strong influence of the annual cycle in the database, being the dominant mode of the TCO over the season.

Other periodicities such as the Quasi-Biennial Oscillation (QBO) between 16 - 32 months also stand out, despite having a low frequency, this signal was observed in other studies in subtropical latitudes (RIGOZO, 2011; TOIHIR, 2018; BENCHERIF, 2020). Peres (2017) presented the TCO monitoring using surface and satellite instruments for Santa Maria/RS from 1992 to 2014, where the main periodicities related to this station were identified.

The solar cycle proved to be an important periodicity, even being outside the cone of influence, the QBO showed an important variability over the region in antiphase with the TCO over the SM region. With a frequency below the 95% reliability axis, signs of ENSO variability between 64 - 128 months showed two prominent periods, one between 1980 to 1990 and another period between 2009 to 2019. Studies show that ENSO variability is the dominant mode in the troposphere, where its impact directly affects tropospheric circulation, in tropical upwelling, causing significant changes in the distribution of O3 content (OMAN et al., 2013).

The variabilities in the O3 content will depend mainly on the time of year and the latitude in which they will be analyzed. The influence of QBO on the behavior of stratospheric ozone is explained by its impact on the chemical and dynamic processes of the gas. The variation of the QBO signal mainly in the tropics, where O3 is formed, consists of maximum primary peaks between 7 -10 hPa in the upper stratosphere and secondary peaks between 20-30 hPa, in addition other periodicities can influence the behavior of ozone, even that in antiphase, such as ENSO and aerosols, in the release of SO2 into the stratosphere through volcanic activities, among other variability (WMO, 2018; NEDOLUHA et al., 2015a).

Figure 4.8: a) Anomaly monthly series of TCO satellite used for wavelet analysis over the Santa Maria/RS between 1979 and 2020. (b) Morlet wavelet power spectrum, normalized by 1 / σ2. (c) The global wavelet spectrum of (a) where the dashed line is the 95% confidence.

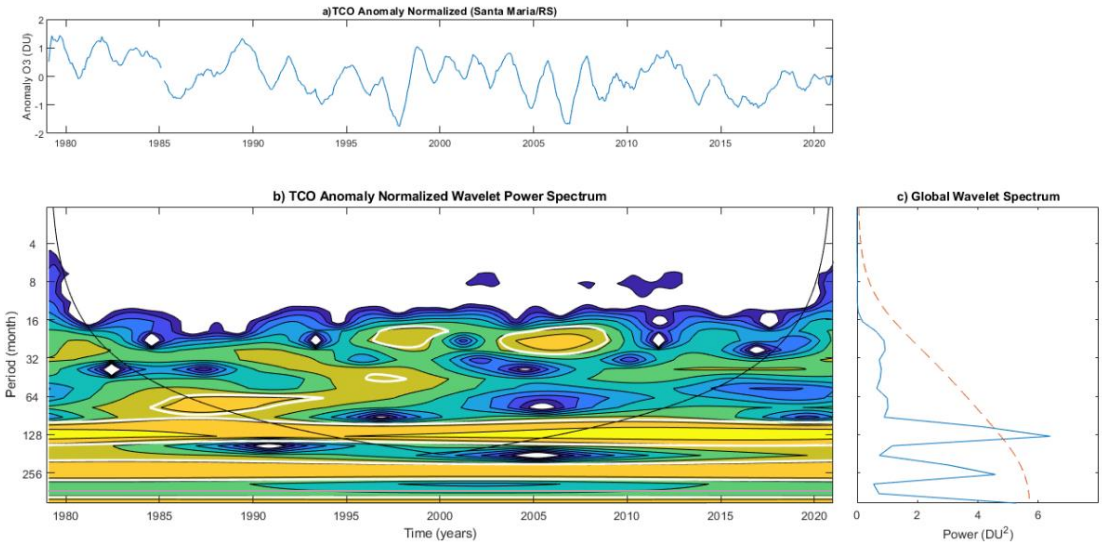

Source: The author.

Changes in the Brewer-Dobson circulation (BDC) also modulate the behavior of ozone in the stratosphere, both by its transport, which is influenced by the strongest and/or weakest impulse in the tropics, and by the chemistry in the formation of O3 in tropical latitudes.

4.3.4 Variabilities in tropical latitudes (Natal/RN)

The Natal/RN tropical station, from TCO satellite data available for latitude, TOMS and OMI, plus ozonesondes data, by the SHADOZ platform, during the study period of this work (1979 to 2020), it was possible to identify the variabilities that dominate this region by the wavelet method. Semi-annual and annual variability were removed from the analysis so that others would not be masked. With the TCO dataset, figure 4.9 presents the average monthly anomaly for these data, in the period 1979-2020, and these results showed a variability between 16 and 32 months predominant in the TCO over Natal/RN, with the QBO being the main one. variability that stands out in this region. Studies show that QBO is the variability that dominates the behavior of O3 in tropical latitudes. In addition to starting its formation in the equatorial stratospheric region, this

oscillation dissipates to other latitudes, alternating the wind direction from east to west, thus influencing the behavior of O3 at these latitudes (BALDWIN, 2001).

The monthly mean anomaly in relation to the stratospheric O3 column showed that the QBO is the predominant variability in the tropical season of Natal/RN. QBO directly affects chemical and dynamic processes in stratospheric ozone and can alter the dynamics of large-scale circulation (BDC). The solar cycle was also influential in the stratospheric layer in the tropical season, mainly from 1993 to mid-2005 with 95% of this variability within the cone of influence.

Naoe et al., (2017) analyzed the future of OBO in ozone in the tropical stratospheric region, where through simulations, related to the increase of study effect gases and the decrease of O3-depleting substances, identified a maximum in the amplitude of OBO between 5-10 hPa suggesting that at that time the photochemistry of the region will depend on temperature to modulate ozone in the tropical stratosphere. Newman (2016) showed an anomalous phase shift of the QBO in the last 60 years of years. The anomaly showed a rapid upward shift from the westerly phase of equatorial winds to an easterly phase between 2015-2016. This sudden QBO phase shift resulted in the shortest eastern phase ever seen in the 1953-2016 records.

As previously described, the 11-year solar cycle also stands out in the periodicities related to TCO in the tropical region, where at least one complete cycle is observed within the cone of influence (between 1993 and 2005). The tropical region presents important characteristics in relation to this periodicity and together with the QBO below 30 hPa they modulate the wind direction (SALBY AND CALLAGHAN, 2000). The variability of O3 in relation to ENSO has little influence on the data analyzed in this work, in relation to subtropical and tropical latitudes. Toihir et al., (2018) analyzed the variability using ozone probe data and identified that the influence of ENSO on the behavior of stratospheric O3 is less than 1%, being more representative in the modulation of tropospheric O3 (RANDEL, THOMPSON, 2011).

Figure 4.9: a) Anomaly monthly series of TCO satellite used for wavelet analysis over the Natal/RN between 1979 and 2020. (b) Morlet wavelet power spectrum, normalized by 1 / σ2. (c) The global wavelet spectrum of (a) where the dashed line is the 95% confidence.

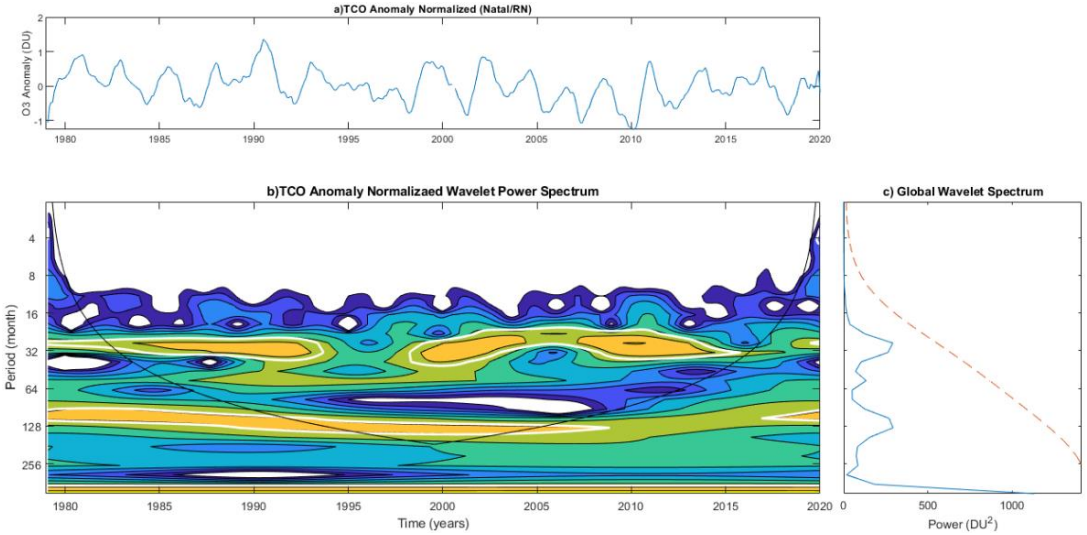

Source: The author.

Ozone's response to changes in solar irradiance also plays a potentially important role in climate change, regulating temperatures and stratospheric winds. These changes in the stratosphere can affect tropospheric climate through direct radiative effects and dynamic coupling, which in turn affects patterns of extratropical variability (WMO,2018).

4.4 INFLUENCE EVENTS OF THE ANTARCTIC OZONE HOLE

The identification of the events of influence of the Antarctic Ozone Hole in the SM region follows the methodology described in item 3.4, where the average daily data for the 42 years available are analyzed. With the climatology established, the first analysis is made for the months of occurrence of the events during the southern spring (August to November), when the AOH is active. Table 4.1 presents the monthly climatology for the daily analyzes of the decrease in O3 content during the occurrence of AOH, in addition to its respective standard deviation and the values of the limits of -1.5 of the standard deviation (μ-1.5σ). The possible events are selected based on the analysis of the average daily value of O3, which must be less than the threshold for the month of the event. Using

this methodology, approximately 102 events were identified that influenced the study region with temporary drops in O3 content during the 42 years of data analyzed to date. At the end of this work, each of these events of decrease in O3 content in the appendix area will be presented, presenting the stratospheric fields of potential vorticity, analysis of the vertical profile (when it exists), and vertical section of the atmosphere showing the dynamic behavior of the atmosphere.

Table 4.1: Monthly climatological values, their standard deviations and -1.5σ limit for August, September, October, and November for the Santa Maria station.

Month	O_3 Climatology in DU (μ)	Standard Deviation in DU (σ)	Limit -1.5σ in DU (μ-1.5σ)
August	290.4	12,1	272.2
September	296.8	9.4	282.7
October	289	11.8	271.3
November	285	8,9	271,6

Source: The author.

4.5 CASE STUDY

4.5.1 Event 20 October 2016

The AOH side effect event that occurred on October 20, 2020, in Southern Brazil was one of the most intense ever recorded in the last 25 years (BITTENCOURT, 2018). Kirchoff and collaborators (1996) identified one of the first extreme events of secondary effect of AOH on the southern region of Brazil that occurred on October 28, 1993. The study analyzed vertical profile data, through the launch of ozonesondes that identified this decrease in TCO in the region, in addition to surface instrument measurements (BREWER) and TOMS satellite data. BRESCIANI (2018) and collaborators performed a multi-instrumental analysis of this event. Vertical profile data with satellite instruments (AURA and SABER), ozonesondes showed how much this event impacted the region with an extreme temporary decrease in O3 content.

In this work, a complete analysis of this extreme event of 2016 will be shown. The first part is the analysis of the TCO data made available by the surface and satellite

instruments. For this event, TCO recorded a minimum amount on October 20th. Brewer Spectrophotometer recorded in the TCO of the day a value of 225.5 DU, representing a reduction of around 23% in the ozone content in relation to the climatological average of October which was 291.4 ± 8.2 DU. On October 21, the secondary event continued to influence the region, where 233 DU was recorded, resulting in a reduction of around 20% in relation to October's climatology.

Figure 4.10 shows the average daily TCO values for October 2020, with the values from the OMI (red) and Brewer (blue) satellites. The black line represents the limit – 1.5σ of the standard deviation for the month, which according to table 4.1 was 271.3 DU. The yellow circle is the day of the event on which the BREWER recorded the lowest O3 content value. Blank spaces represent lack of data from both study instruments.

Figure 4.10: TCO values in October 2016 with satellite (red) and Brewer (blue) data and the -1.5σ limit (black line).

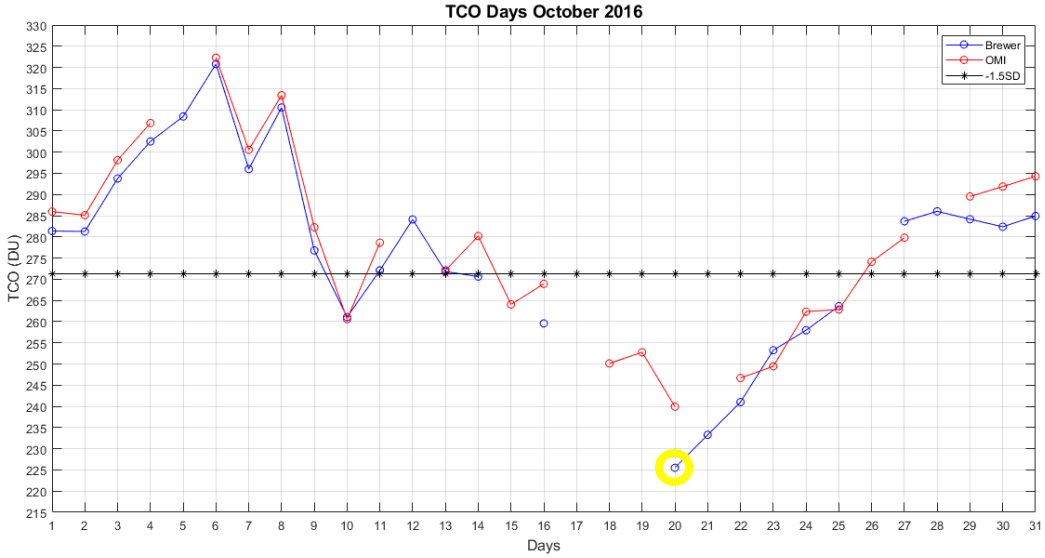

Source: The author.

The beginning of October, according to figure 4.12, presents TCO values ranging from 300 to 320 DU in the first 10 days of the month. Between the 14th and 15th, it is possible to identify that the TCO begins to show a drop in relation to the limit of the climatological average, which despite showing flaws in the data, identifies a recurring decrease in O3, where on October 20 it presents its greatest decrease. of the month of October. Temporary decreases in O3 content were recurrent, and according to the data

they influenced the region until at least 10/23/2016 (BITTENCOURT et al., 2019).

The October 2016 event was also identified with data from the O3 vertical profile by SABER. Figure 4.11 shows the vertical O3 profile of October 20, 2016 (red) compared to the climatology of the event month (black). This climatology was performed for the 17 years of data from the SABER satellite (figure 4.5), allowing a more in-depth analysis of the event in relation to the vertical behavior of the O3 content. Figure 4.11a shows the vertical profile in O3 partial pressure (μhPa) data for the day of the event, October 20, 2016, and the climatology for the SABER data analysis period. The region marked in the figure in yellow, between ~22 to 29 km in height, highlights the significant reduction that occurred during the event in relation to climatology, ranging from 100 to 60 (μhPa) with a peak at ~24 km. Bresciani et al., (2018) presented a multi-instrumental analysis of the event identified in October 2016. The results showed the decrease in O3 content according to data from different vertical profile instruments, during the occurrence of this extreme event.

Figure 4.11: Vertical profile of O_3 by the SABER satellite for the October 20, 2016 (in red) and climatology for the month of October (in black).

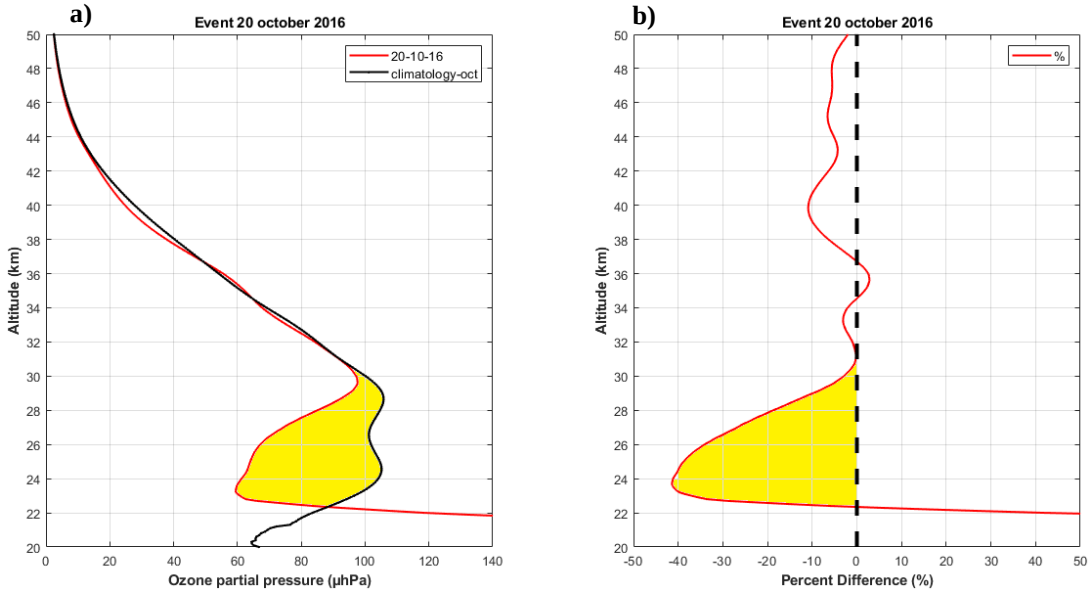

Source: The author.

This reduction is observed when calculating the percentage differences for the day of the event, as shown in Figure 4.11b. Highlighted in yellow, the stratospheric region between 22 - 29 km of altitude, presents high values of reduction of the O3 content in the region during the event which was around -43% in relation to the October climatology by the SABER satellite.

4.5.2 Dynamic Event Analysis

The second part of the confirmation of the secondary effect event is the dynamic analysis of this event, through stratospheric dynamics using potential vorticity on isentropic surfaces. Figure 4.12 shows the daily monitoring of PV at height of 20 hPa, around 25-30 km height, at pressure levels, through ECMWF ERA 5 reanalysis data for two previous days (18 and 19 October 2016), on the day when the lowest O3 content was observed (10/20/2016), and one day after the event (10/21/2016). The increase in vorticity over the region is evident in the sequence of days, where the arrival of a poor O3 air mass from the polar regions to the mid-latitudes regions is observed, identified by the increase in APV. The stratospheric potential vorticity fields mapped the behavior of O3 during the days of the event.

On 10/18/2016 (Fig. 4.12a) high APV values were observed advancing towards southern Brazil, with values ranging from 60 to 140 between the extreme south of Argentina and Uruguay. On October 19, 2016 (Fig. 4.12b) the southern region of Brazil was already showing signs of influence of the poor O3 air mass, with an increase in APV, ranging from 80 to 120 potential vorticity units (PVU). On day 20 (Fig. 4.12c), the poor O3 air mass advanced under the region, with an intensification of UPV values, ranging from 160 to 200 UPV over SM. Also noteworthy is a waveform advancing over the region as the O3-poor air mass moved over Brazil. Bittencourt et al., (2018) showed that the simulations of the MIMOSA model identified the direct influence of the ozone hole in southern Brazil at 550 K potential temperature at 22 km height. On the following day, 10/21/2016 (Fig. 4.12d) there is a stabilization of this mass, but with a decrease in UPV values compared to previous days, around 160 to 180 UPV in the region, in addition to

Bittencourt et al., (2019) presented an analysis of 11 years of TCO data, where AOH influence events on the SM region were investigated using ECMWF ERA-INTERIM data in the dynamic study of events, showing the secondary effect events tend to act in the region up to at least 3 days after the event itself is registered.

Figure 4.12: Potential vorticity fields at 20 hPa of potential temperature for October 18-21, 2016.

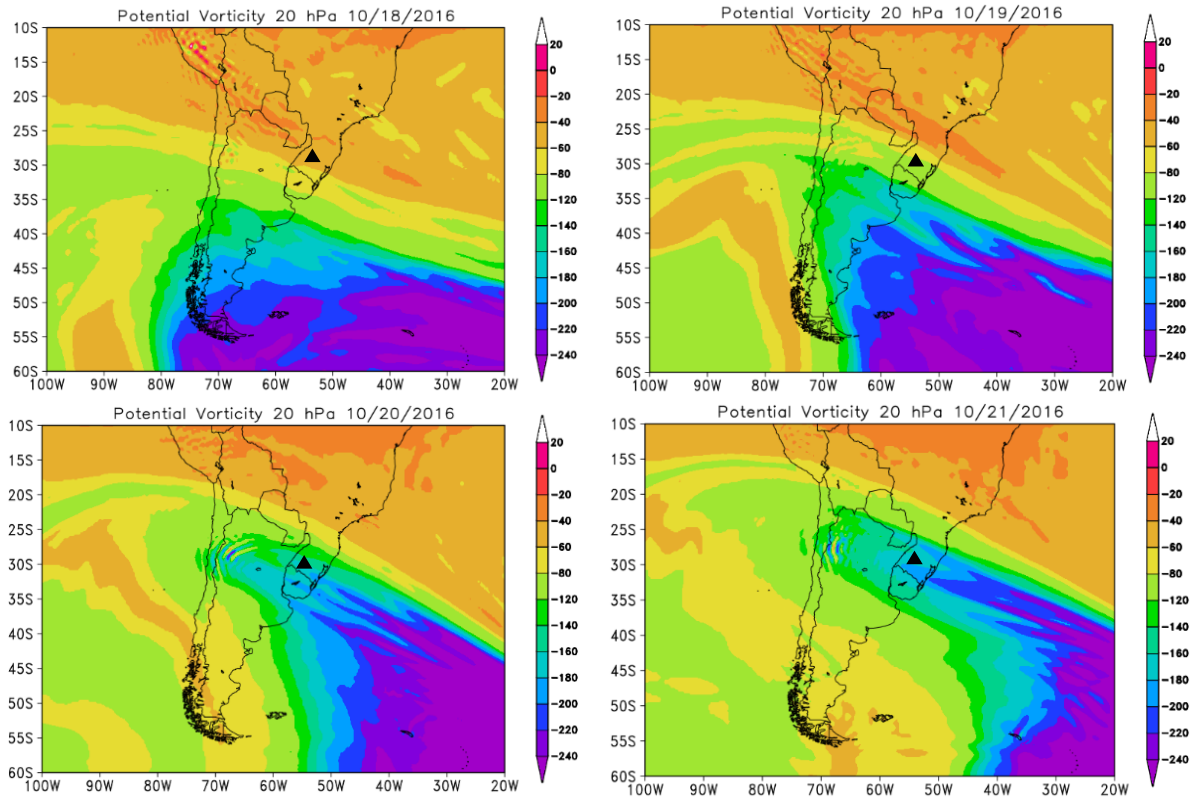

Source: The author.

Peres et al., (2014) presented results that show the identification of events in the region for the year 2012, using surface and satellite data, and reanalysis data from NCEP/NCAR to monitor the dynamics of the stratosphere. Two events were identified influencing the region (PERES et al, 2014a; 2014b).

The decrease in O3 content during the event identified in October 2016 was detailed by Bittencourt et al. (2018) where through the MIMOSA model (Modélisation Isentrope du transport Mésoéchelle de l'Ozone Stratosphérique par Advection) it was possible to identify the advance of a poor O3 polar air mass over mid-latitudes regions. MIMOSA is a high-resolution model developed by the Service d'Aéronomie within the framework of the European METRO project (MERidional TRansport of Ozone in the lower stratosphere) (Hauchecorne et al. 2001).

Figure 4.13: MIMOSA model during the ozone hole influence event under the study region, in October 2016.

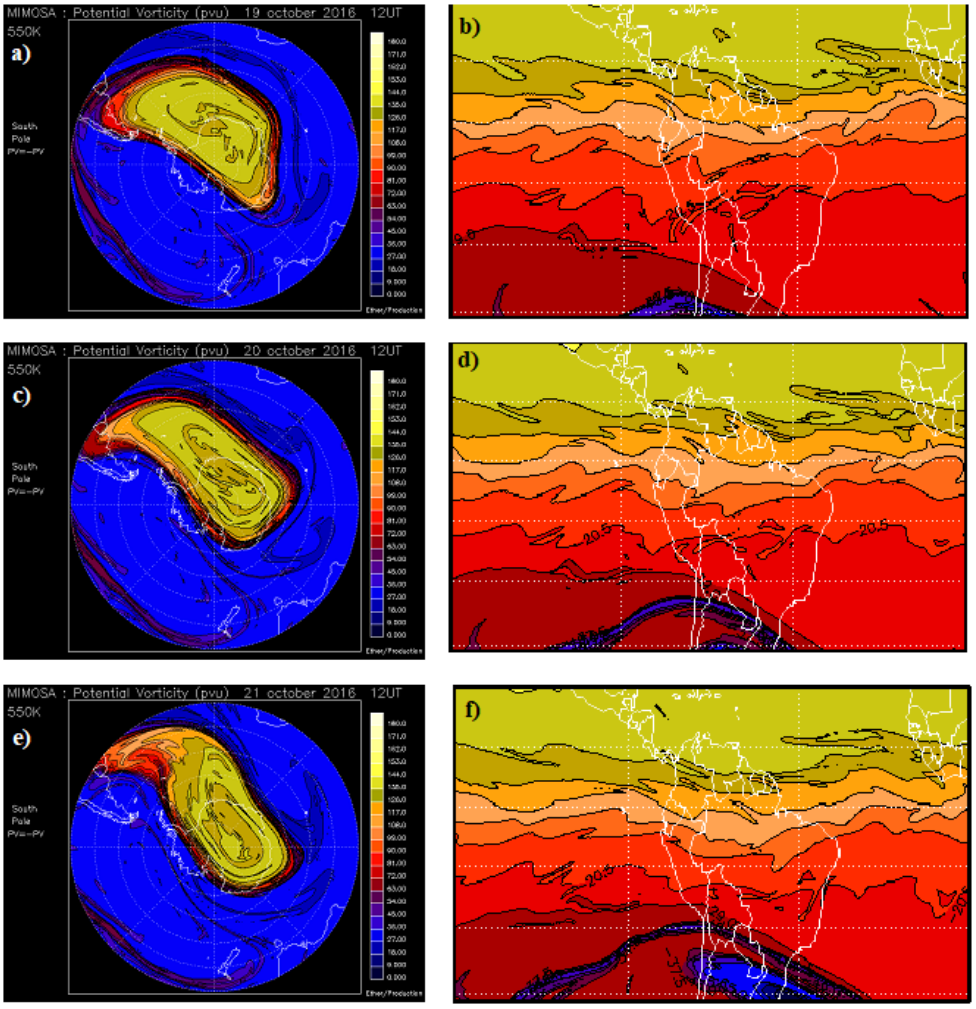

Source: Bittencourt et al., 2018.

The results found by Bittencourt et al. 2018 with the MIMOSA model (Figure 4.13) showed the direct impact of the ozone hole in southern Brazil at a potential

temperature of 550 Kelvin and an altitude of approximately 22 km. The MIMOSA model presents the isentropic level at 550K in the figure for October 2016 (19, 20 and 21), and it is possible to identify the advance of an O3-poor air mass represented by figure 4.13, over regions of medium latitudes, as is the case of the study region of this work in Santa Maria/RS.

The retroactive trajectory of the HYSPLIT/NOAA model presents the trajectory of this poor O3 air parcel. In figure 4.13a, the advance of the parcel from October 16, 2016, can be identified, passing through the Antarctic region where the AOH is acting and taking this air mass to regions of medium latitudes at three different heights, 26 km (red), 24 km (blue) and 22 km altitude (green), at 18 UTC. To complement the confirmation of the secondary effect event over the southern region of Brazil, the TEMIS satellite images (PS and global view, figure 4.14b).

Figure 4.14: a) Retroactive trajectory by the HYSPLIT/NOAA model arriving over the study region, trajectory at 22 km, 24 km, and 26 km of altitude; b) DU satellite image with O3 content by the OMI satellite for the day of the event, showing the AOH influence over southern South America, South Pole, and global view.

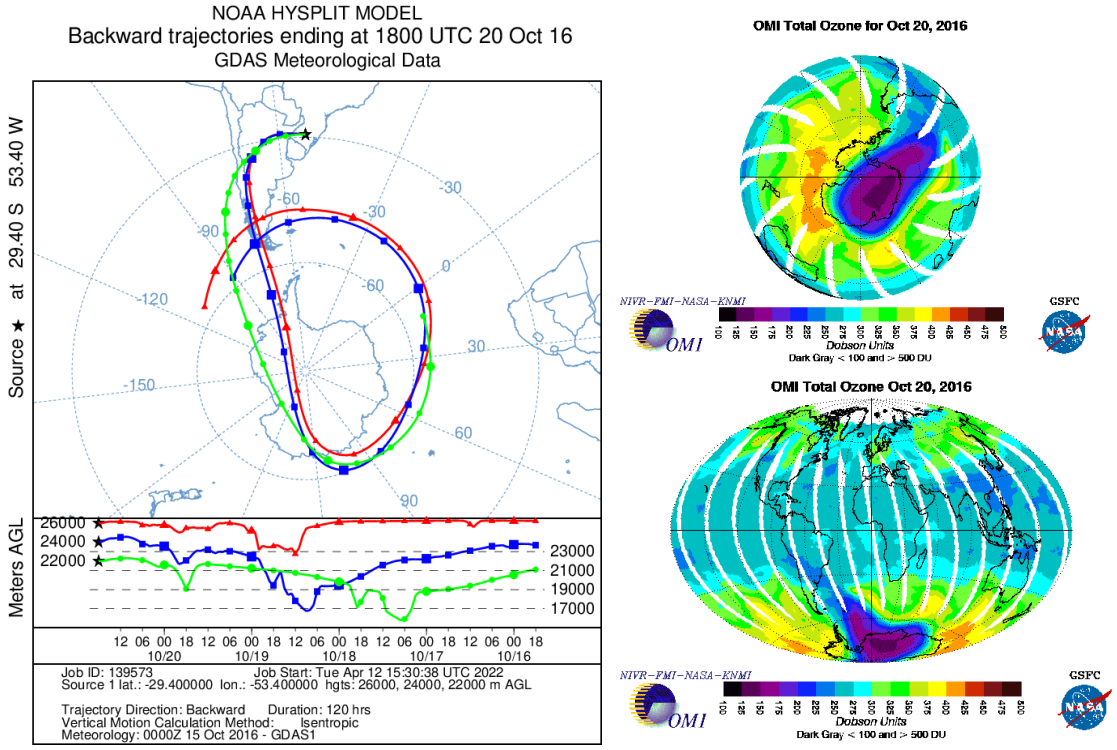

Source: HYSPLIT/NOAA; OMI.

The colors in shades of blue and purple show the lowest TCO values over Antarctica, ranging from 275 to 150 DU in the interior of the continent. For the October 2016 event, a strong influence is observed with low TCO values for the day, where the AOH influence connects directly to the middle latitude's regions. The figure with global vision is more noticeable this influence.

The vertical section of the atmosphere was analyzed after the identification and confirmation of the extreme event of influence of the AOH in the south of Brazil. This field shows the behavior of jet streams with a vertical cut of the atmosphere between 1000 and 10 hPa at pressure levels of potential temperature and wind. The presence of stratospheric (polar vortex) and tropospheric (subtropical and polar) jets can be inferred in figure 4.15 between October 18 - 21, 2016.

The presence of the stratospheric jet, or polar vortex, is identified on 10/18/2016 (Figure 4.15a) between 70 and 80 ºS with a moderate intensity (~50 m/s) above 50 hPa. Below 200 hPa the weak polar jet is observed acting in the more polar regions, while the subtropical jet stands out between latitudes of 30 - 40 ºS coupled with the polar vortex (above 100 hPa). On the 19th of October (figure 4.15b) this stratospheric jet moved eastward, still coupled with the polar jet, but now between 55 - 70 ºS. At high levels of the atmosphere (between 200 hPa) the coupling between the jets is visible, and its influence reaches the mid-latitudes regions analyzed in this work (~30ºS). With a moderate intensity, the polar and subtropical jets extend to the middle troposphere around 500 hPa reaching up to 600 hPa.

On the day of the event, 10/20/2016, (figure 4.15c) and one day after the event (figure 4.14d) the influence of the polar vortex reaches high levels of the atmosphere beyond the coupling between the stratospheric jet and the polar jet that intensifies, between 50 - 60 ºS. On October 21st, the coupling between them reaches 700 hPa, and the subtropical jet also shows an intensification on these two days.

The funneling of the isentropic observed in these days of decreasing O3 content, through the analysis of vertical sections of the atmosphere, helps to explain the stratosphere-troposphere exchanges. These large-scale systems help to understand that they have a direct influence on this movement of air masses between atmospheric layers.

Previous studies show that this exchange between stratosphere and troposphere during the occurrence of AOH influences events on the region of study, it usually occurs after the passage of frontal systems so that the presence of jets helps this exchange of air masses between the layers. (SANTOS, 2016; BITTENCOURT et al., 2019).

Figure 4.15: Vertical section of the atmosphere between 1000 and 5 hPa for the days of the event in October 2016.

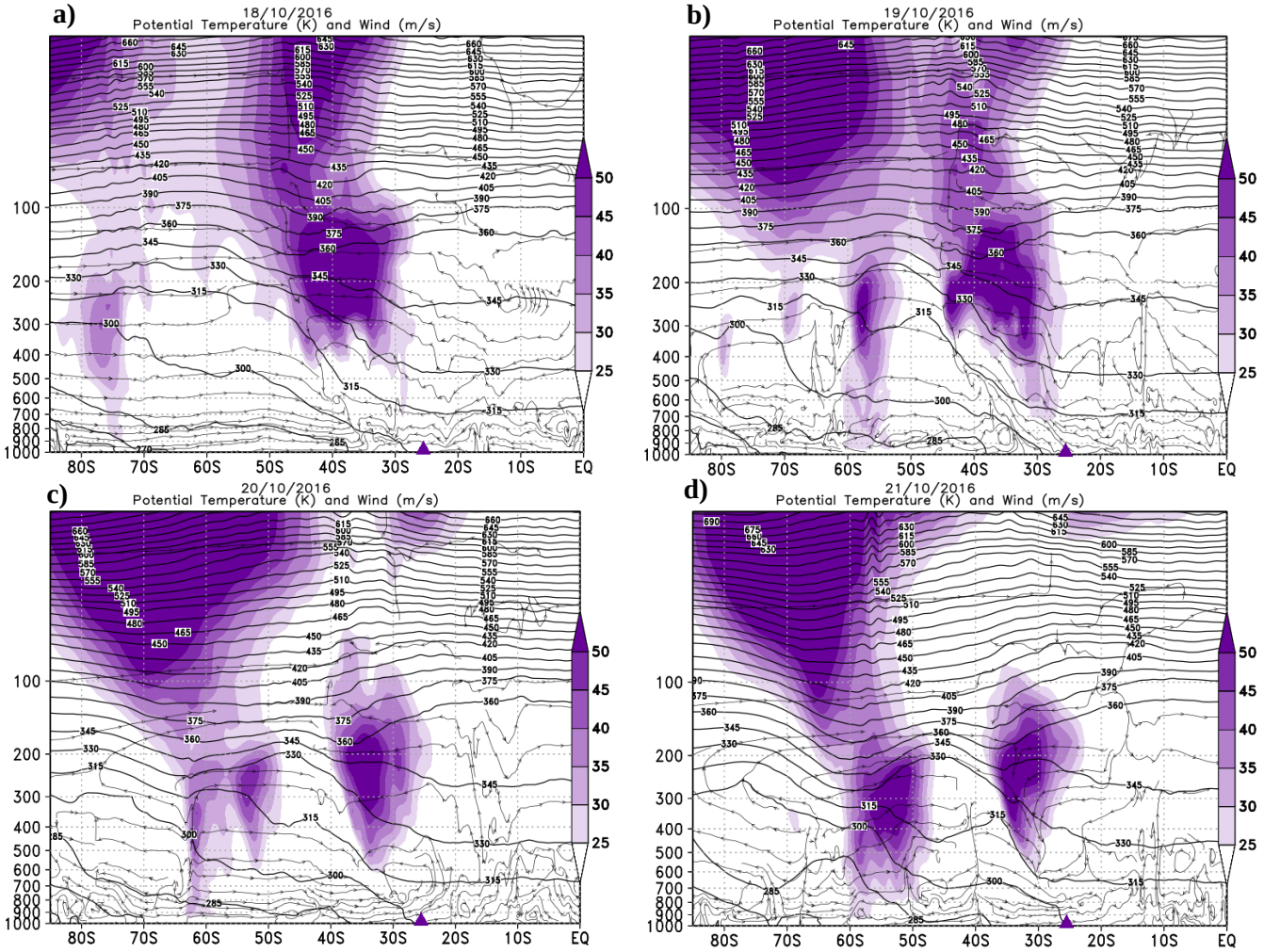

Source: The author.

4.6 EVENTS STATISTICS

In this section, results obtained in relation to the main statistical analysis of the behavior of O3 will be presented, through the potential vorticity fields, analysis of the vertical profiles identified during the events (by the SABER satellite) and the dynamics of the jets.

4.6.1 TCO statistics events

During the 42 years, the identification of AOH side effect events in the SM region occurred through the analysis of average daily data available with different O3 measurement instruments already described here. Table 4.2 presents a summary of all events that were identified in the region through the methodology described above, where the day of the event and the reduction of O3 in percentage (%). During the austral spring (August to November) more than 5124 days were analyzed during the study period (1979-2020). Among this total number of days available in the 4 months, about 735 days were selected because they had a daily TCO value below the limit of -1.5σ. Of this total, 102 AOH influence events were identified influencing the study region, Santa Maria/RS, in the period from 1979 to 2020. Peres et al., (2019) presented the climatological analysis for 35 years of data, 1979 to 2013, on the central region of RS where they identified about 62 events that affected the region. Bittencourt et al., (2019) showed, in 11 years of data, 37 events of influence of AOH over the southern region of Brazil from 2006 to 2017, in addition to presenting the dynamic stratospheric and tropospheric behavior during the occurrence of these events over the region.

Table 4.2 also presents the phase the QBO was in during the event. According to the analysis of the variability of O3 content, it was highlighted that the influence of QBO is more significant in tropical regions, while in regions of subtropical latitudes this variability does not stand out, as is the case of SM. PERES et al., (2017) showed that there is an antiphase between average monthly TCO anomaly data over the SM region compared to QBO modulation. Toihir et al., (2018) also identified that the most important

variabilities in O3 content are, in addition to annual oscillations, the zonal wind modulation at 30 hPa with the QBO. It was possible to observe that this predominant variability is modulated in a cycle of approximately 2 years linked to the QBO, where tropical latitudes are in phase with the QBO, while regions in subtropical latitudes have an anti-phase.

The importance of studying the behavior of the QBO under subtropical and tropical latitudes is due to its influence on the modulation of temperature in the stratosphere, affecting the photochemical dynamics in the lower stratosphere, and consequently influencing the behavior of large-scale circulation (BDC) throughout the atmosphere, which distributes the O3 content from the formation regions (in the tropics) to regions of mid and high latitudes (CORDERO et al., 2012).

The mean reduction, in mean percentage, of TCO in the 102 AOH influence events identified in the study region during the 42 years of analysis was 8.3 ± 3.5%. These events showed that September and October, months in which AOH is at its maximum activity peak, were the months in which the greatest number of temporary decreases in O3 occurred due to these secondary influences. In the period 1979-2020, during the austral spring, about 32.3% and 37.2% of the events identified were in September (33 events) and October (38 events). Meanwhile, in August, when the polar vortex begins to lose its intensity due to the end of winter and the return of radiation, 22 (21.5%) events influenced the study region, while in November only 9 (8.8%) events were registered.

According to table 4.2 of the 102 events of influence of AOH identified over the region of Santa Maria/RS, about 63 events (61.8%) occurred during the QBO in its positive phase, while 39 (38.2%) remainder occurred during the negative phase of the QBO. More studies should be carried out to explain why most events occur during the positive phase of QBO over our study region.

Table 4.2 – AOH influence events from 1979 to 2018, for SM. The table presents the day of the event in MMDDYYYY format, and ozone content reductions relative to climatology in %, and QBO phase.

Event day	O_3 reduction (%)	QBO phase	Event day	O_3 reduction (%)	QBO phase	Event day	O_3 reduction (%)	QBO phase
09/27/1979	4,2	Negative	09/17/1994	6,1	Negative	10/12/2008	8,3	Positive
08/05/1982	11,4	Positive	10/01/1995	7,7	Positive	10/26/2008	7,8	Positive
09/09/1982	13,2	Positive	09/20/1996	17,4	Negative	11/01/2008	10,5	Positive
09/23/1982	6,2	Positive	08/18/1997	16,5	Positive	09/02/2009	16,1	Negative
10/08/1982	5	Positive	09/14/1997	14	Positive	09/29/2009	8,9	Negative
10/08/1982	4,7	Positive	10/16/1997	8,3	Positive	08/08/2010	7,2	Positive
10/15/1982	7,3	Positive	11/02/1997	6	Positive	09/08/2010	5,4	Positive
10/21/1982	9,4	Positive	11/19/1997	6,5	Positive	10/13/2010	5,2	Positive
09/30/1983	7,8	Negative	10/24/1998	10	Negative	10/22/2010	10,1	Positive
10/14/1983	4	Negative	08/21/1999	8,1	Positive	09/05/2011	4,4	Negative
10/16/1984	9,2	Negative	10/07/1999	4,7	Positive	09/14/2012	9,7	Negative
11/05/1984	7,5	Negative	09/23/2000	8,9	Negative	09/22/2012	6,5	Negative
08/09/1985	7,3	Positive	10/12/2000	7,2	Negative	10/14/2012	12,5	Negative
08/23/1985	11	Positive	10/26/2000	6,7	Negative	10/23/2013	13,6	Positive
09/03/1985	16	Positive	08/15/2001	5,8	Negative	08/10/2014	7,5	Negative
10/15/1985	10,6	Positive	09/23/2001	7,7	Negative	08/22/2014	12	Negative
11/07/1985	7,6	Positive	08/18/2002	12,5	Positive	10/13/2014	4,7	Negative
08/09/1987	5	Positive	10/15/2003	10,6	Negative	11/03/2014	5,3	Negative
07/07/1987	7,6	Positive	08/22/2004	9,3	Positive	09/22/2015	7,7	Positive
10/16/1987	6,1	Positive	09/12/2004	6,8	Positive	11/03/2015	8,3	Positive
09/02/1988	5,7	Negative	10/03/2004	4,6	Positive	08/25/2016	12,9	Positive
08/24/1990	8,9	Positive	10/16/2004	12,3	Positive	09//05/2016	10,5	Positive
09/06/1990	16,8	Positive	09/29/2005	5,5	Negative	09/12/2016	9,4	Positive
09/16/1990	9,1	Positive	10/11/2005	5,2	Negative	10/20/2016	22	Positive
10/01/1990	4,2	Positive	11/16/2005	4,6	Negative	08/26/2017	12,6	Negative
10/09/1990	9,7	Positive	08/07/2006	10,9	Positive	09/18/2017	8	Negative
09/03/1992	8,5	Positive	08/23/2006	11,4	Positive	11/11/2018	13,8	Negative
10/10/1992	7,5	Positive	09/19/2006	6,6	Positive	09/16/2019	14,8	Positive
08/15/1993	9	Negative	10/07/2006	9,7	Positive	08/28/2020	15.4	Positive
08/25/1993	8,5	Negative	10/15/2006	9,1	Positive	09/03/2020	17.7	Positive
10/19/1993	13,2	Negative	08/16/2007	6,1	Positive	10/21/2020	11	Positive
10/31/1993	16,8	Negative	09/13/2007	7,4	Negative	11/22/2020	10,7	Positive
08/16/1994	4,2	Negative	10/07/2007	10	Negative			

Source: The author.

4.6.2 Vertical Profile Statistics

In this section, the results related to the vertical profile analysis using data from the SABER satellite will be presented. After identifying the events of influence of the AOH in the period 1979 - 2020 with surface and satellite instruments (table 4.2), it was possible to study the vertical profiles of the SABER satellite for the period of 17 years in which the satellite maintained its activities. During this period (2002-2018) 38 vertical profiles of AOH influence events over the study region were found, according to satellite availability.

Figure 4.16 presents a histogram with the frequency of occurrence of events according to times defined for this analysis. Starting the verification at 20 km altitude, the following altitude groups were separated:

20 – 24 km	Blue
24.1 – 28 km	Red
28.1 – 32 km	Yellow
32.1 – 36 km	Purple
36.1 – 40 km	Green

According to the histogram, the predominance of events is in the months of September (31.6%) and in October (37%), August and November continue to be the months with the lowest occurrence of event identification, 18.4% and 13.2%, corroborating the analyzes made with TCO data. The heights that predominate the temporary decreases in O3 content during the AOH influence events are the height between 24.1 - 28 km, followed by the lowest layer of the stratosphere between 20 - 24 km of altitude, in the months of greater occurrence of the events.

This most intermediate layer of the stratosphere comprises the O3 layer region, thus with active AOH, and influencing the mid-latitudes regions with the advance of poor O3 air masses explains these greater decreases in O3 content at these heights. Dynamic influences that alter the behavior of O3 in the lower stratosphere explain these decreases

at these altitudes. In addition, O3 at altitudes between 32 to 40 km has photochemical changes, according to the climatological analyzes presented in section 4.3.

Figure 4.16: Histogram with the frequency of occurrence of events for each altitude group, using SABER satellite data from 2002-2018.

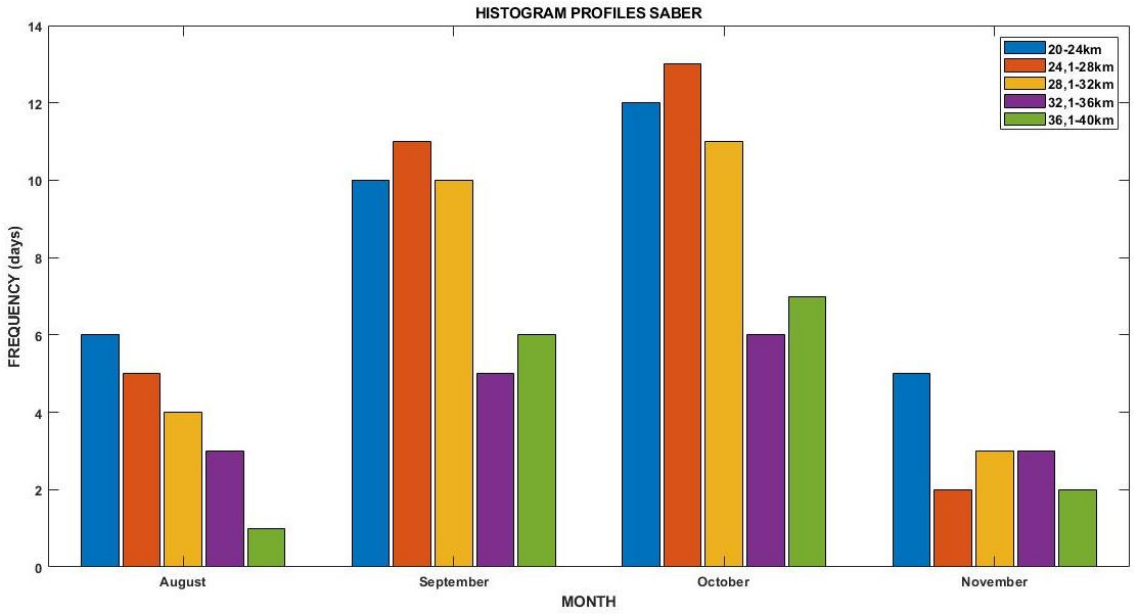

Source: The author.

From these results, it was established to analyze the events at altitudes of 24.1 - 28 km, due to the predominance of these altitudes in the identification of O3 decreases over the region. Figure 4.17 presents vertical profiles relative to the average of events in each month with their respective monthly climatology, in units of partial pressure of O3 at the altitude of 24.1 to 28 km. Regarding climatology, the months of September and October also stand out here, presenting reductions with values significantly lower than their climatology, around ~15-25 μhPa of reduction. The month of November presents a series of factors that must be considered: the AOH begins to close in that month, due to the weakening of the polar vortex and rising temperatures. Thus, as a way of recovering the average profile in relation to the climatology of the period, this average behavior of the profile is observed.

Figure 4.17: Monthly vertical profile in the layer 24.1-28 km altitude, with the average of events per month (a) August, b) September, c) October, d) November) in red and the monthly climatology in black, in partial pressure unit of O3 (μhPa).

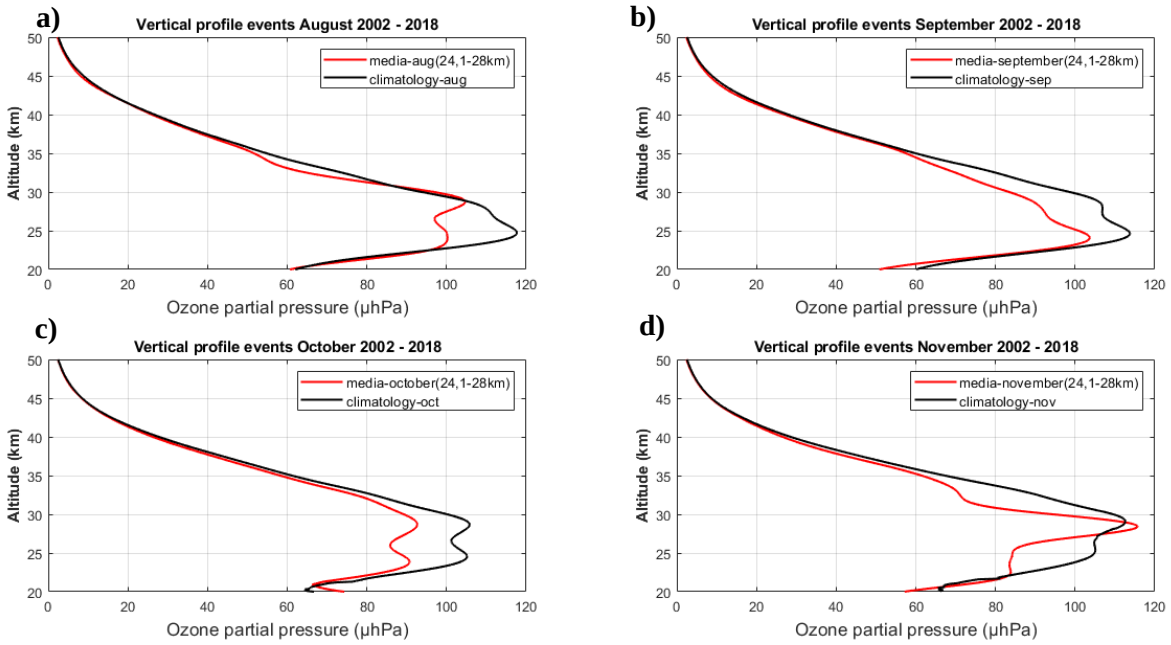

Source: The author.

Figure 4.18 shows the percentage differences for the 38 vertical profiles of events identified in the SABER analysis period (2002 to 2018). The differences are presented for heights between 24.1 and 28 km in height, and there are differences around 20% for the months of August, September and October, the month of November presents, on average, differences around 15%. In agreement with previous studies, these results show that most events occurred in the peak months of AOH (September -12 events and October - 14 events) and a smaller number of events at the beginning (August - 7 events) and at the end (November - 5 events) from AOH (BITTENCOURT et al., 2019).

The 38 events found by the vertical profiles between the period 2002 - 2018 are in the analysis of AOH side effect events in the appendix section.

Figure 4.18: Monthly percentage difference in the 24.1 – 28 km high layer, in relation to the mean of events influence of the AOH on the region in the period 2002 to 2018 of SABER.

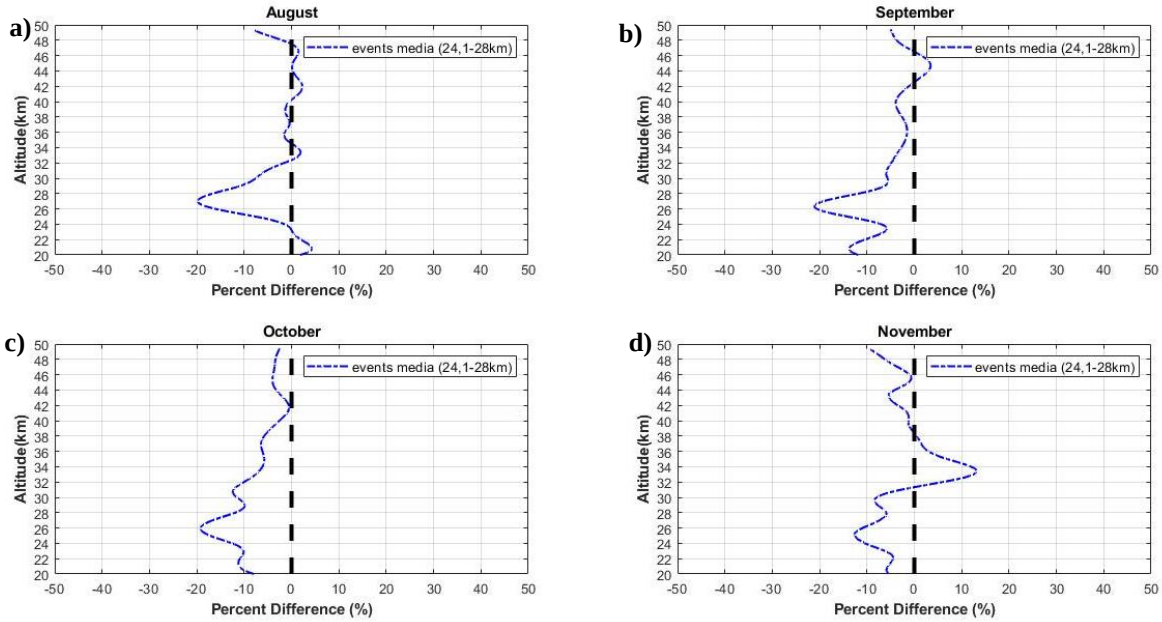

Source: The author.

4.6.3 Dynamic Statistics Events

The climatological analysis, monthly average of events and monthly anomaly of the stratospheric dynamics, during the period of occurrence of the secondary effects of the AOH on the average latitudes, in relation to the climatology of the month are presented in this section. Figure 4.19 shows the monthly climatology of the potential vorticity field at 20 hPa for the entire study period (1979-2020). A gradual increase in APV is observed from August onwards (~55 ºS), the study region presents values around 60 - 80 PVU, and in September these values remain stable between 25 - 40 ºS. This gradual increase in the first months when AOH is active can be explained by the dynamics of the Antarctic polar vortex, which is at its maximum intensity between late winter and early spring, when sunlight returns and destabilizes this vortex.

The return of sunlight, and the consequent destabilization of the polar vortex with increasing temperature, causes the poor O3 air that is trapped within this vortex to move to other regions. The month of October (figure 4.19c) already presents a considerable increase in latitudes below 50 ºS, with values ranging from 80 - 140 PVU. In November,

when the vortex is already weak and starting to break down, there is a greater increase in APV over mid-latitudes (25 - 35 ºS), as is the case with SM, which shows a variation of 60 - 120 PVU.

Figure 4.19: Climatology monthly (a,b,c,d) of potential vorticity at 20 hPa of potential vorticity in the months of occurrence of the AOH influence events on SM from 1979 to 2020.

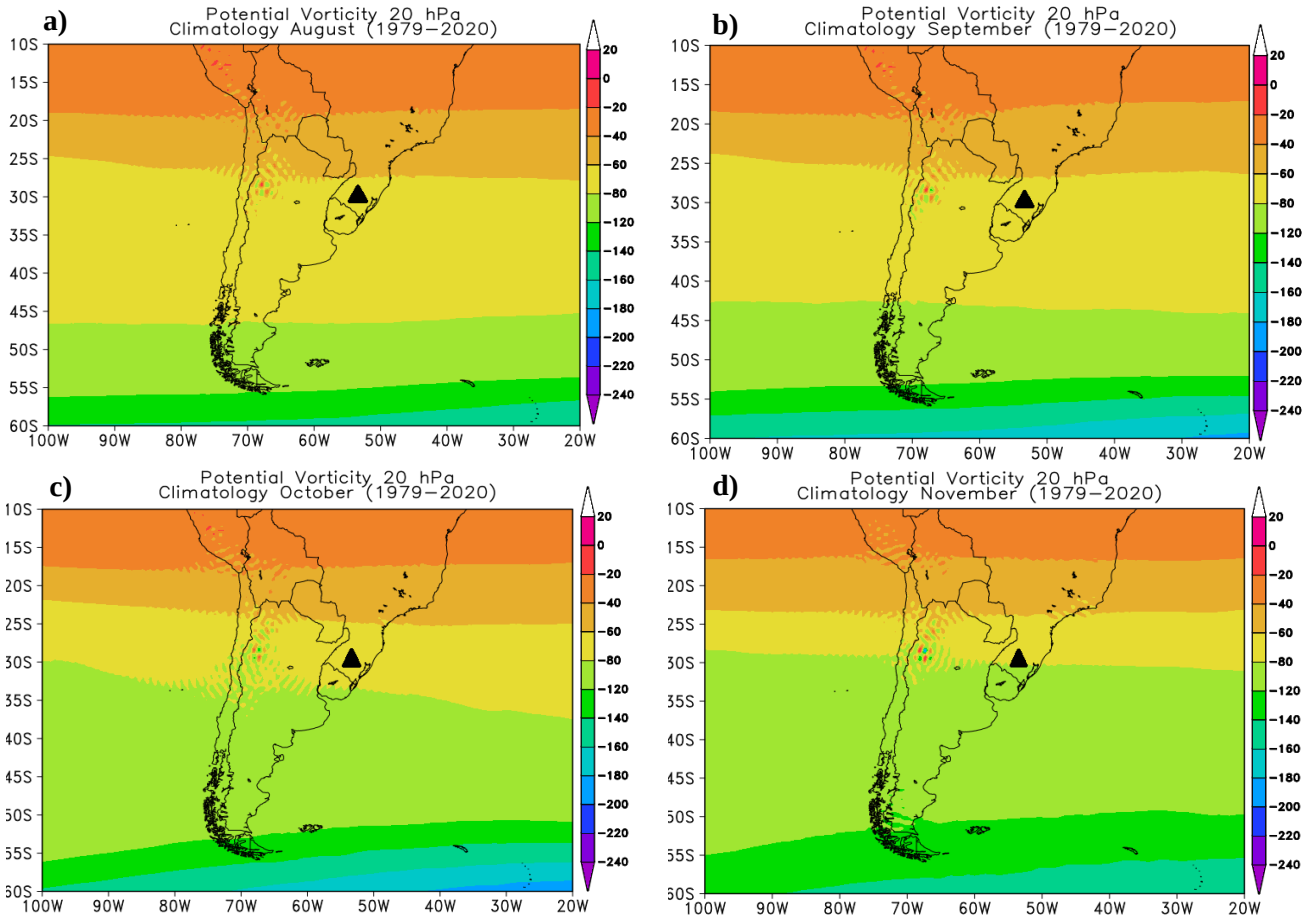

Source: The author.

The monthly average in relation to the number of events in each month is in accordance with the results presented in Table 4.2. The highest number of events between September and October are shown in figure 4.20b and figure 4.20c where an increase in PVU from 60 to 140 APV is observed. These analyses agree with the results obtained in this work, showing the highest occurrence of events in the months of September and October. In addition, the results agree with the work of Bittencourt et al., (2019) where

they identified that the events of influence of the AOH occurred more frequently in the months of September and October. The study also identified that, on average, an event can continue to influence the region with O3-poor air for at least 3 days.

Figure 4.20: Events mean fields (a, b, c, d) of potential vorticity at 20 hPa of potential vorticity in the months of occurrence of the AOH influence events on SM from 1979 to 2020.

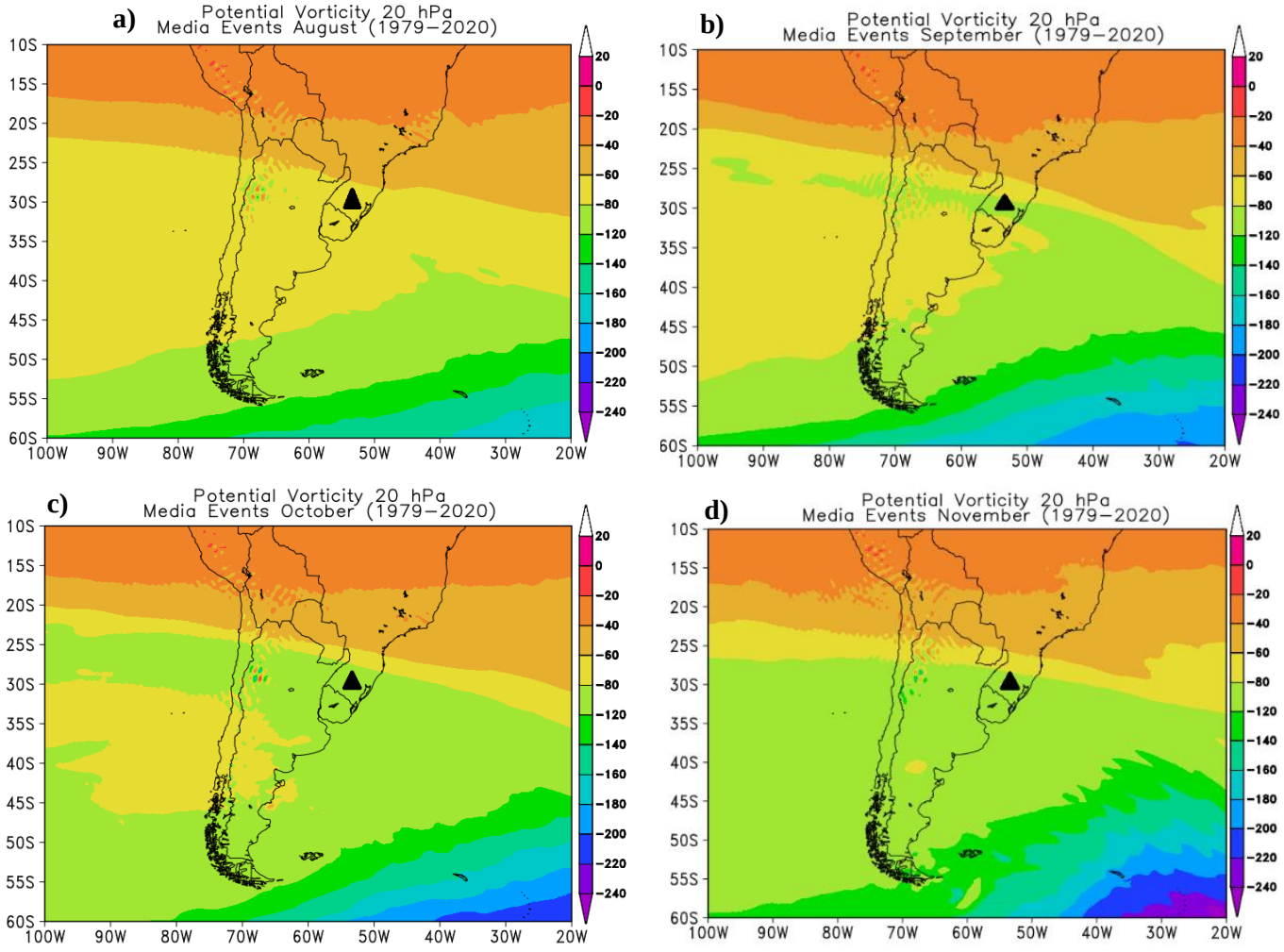

Source: The author.

The stratospheric field anomaly is shown in figure 4.21, where they follow the same configuration as in the figures above, at 20 hPa in the mid-stratosphere region. The calculation considers the monthly events identified in this work (Table 4.2), thus positive PV anomalies act over the entire mid-latitude region in southern Brazil, including SM/RS. As seen above, the months of September and October stand out with the highest number

of AOH influence events, so in Figure 4.21b and 4.21c the values range from -5 to -20 $mKs^{-2}hPa^{-1}$, reaching -40 $mKs^{-2}hPa^{-1}$ in October.

From this analysis, the influence of secondary effect events on mid-latitudes regions during the active period of the AOH in the austral spring is highlighted. The increase and predominance of negative anomalies under the southern region of Brazil stands out from August onwards, with a maximum peak in October and decreasing intensity in November, when the AOH begins to close in Antarctica.

Figure 4.21: Monthly anomaly (a,b,c,d) of potential vorticity at 20 hPa of potential vorticity in the months of occurrence of the AOH influence events on SM from 1979 to 2020.

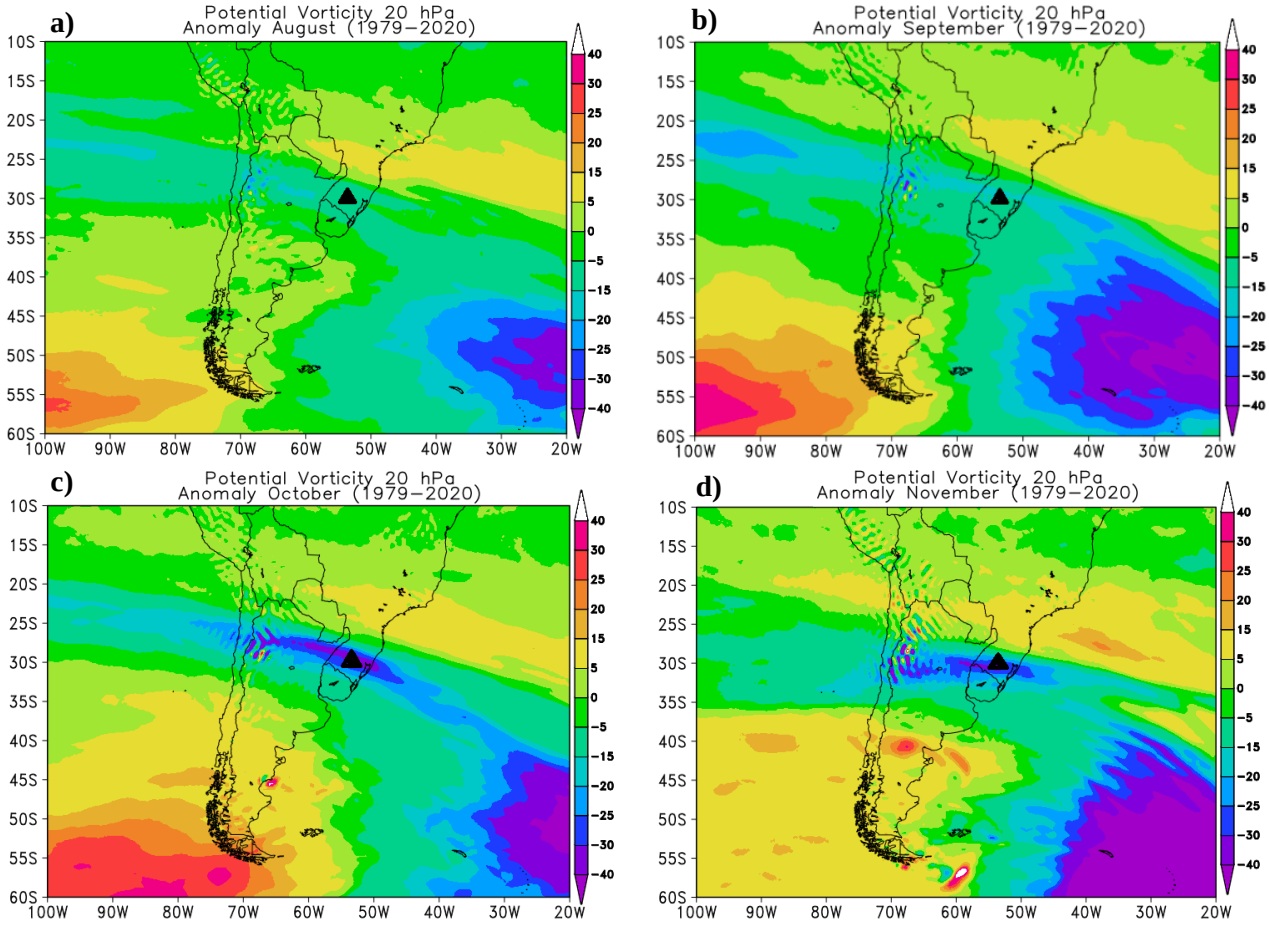

Source: The author.

Regarding the 102 events identified between 1979-2020 and the climatology for the period, it is highlighted in figure 4.22 where a waveform with a predominance of

negative anomalies over the region of study of this work is observed, where negative anomaly values range from -15 to -25 PVU. This analysis agrees with the results presented by Peres et al., (2019) who analyzed the TCO for 35 years using data from the reanalysis II NCEP/DOE in the potential vorticity analyses.

Figure 4.22: Anomaly of the 102 events found. Potential vorticity field at 20 hPa between 1979 to 2020.

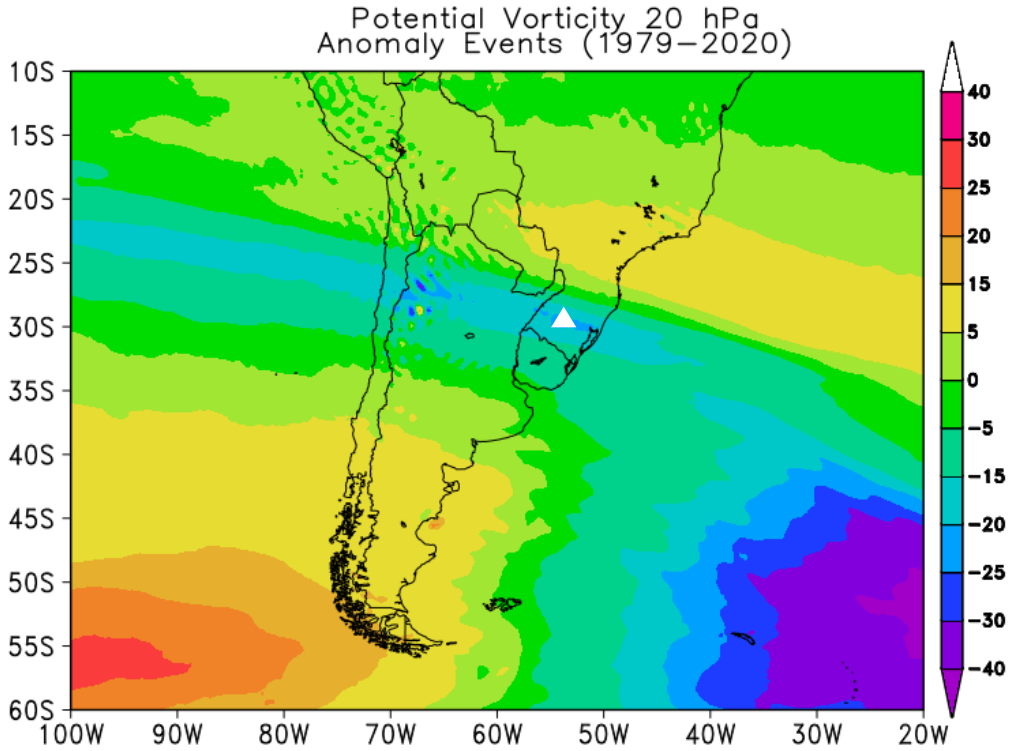

Source: The author.

The dynamic behavior of the atmosphere during the events of AOH influence over the mid-latitudes regions is of paramount importance to understand how these events manage to advance modifying the O3 content. Vertical analysis of the atmosphere shows us how jet streams, important large-scale systems, help transport air masses between the two atmospheric layers (stratosphere-troposphere). According to the events identified in the 42 years of study, figure 4.23 (a, b, c, d) presents the climatological average for each month of active AOH, and the average of events per month (fig. 4.24 a, b, c, d) in the vertical section of the atmosphere between 1000 and 5 hPa.

The influence of the stratospheric jet, or polar vortex, stands out at higher levels

of the atmosphere (100 – 5 hPa) and at high latitudes (45ºS – 70ºS). As previously described, August and September present an extremely strong and very active vortex, which is explained by the low temperatures that are stored inside the vortex during the polar night, making it a stable vortex during this period.

Figure 4.23: Monthly climatology of the vertical section of the atmosphere during the months of identification of the AOH influence events, from 1979 to 2020, between 1000 and 5 hPa showing the presence of the jet (shaded).

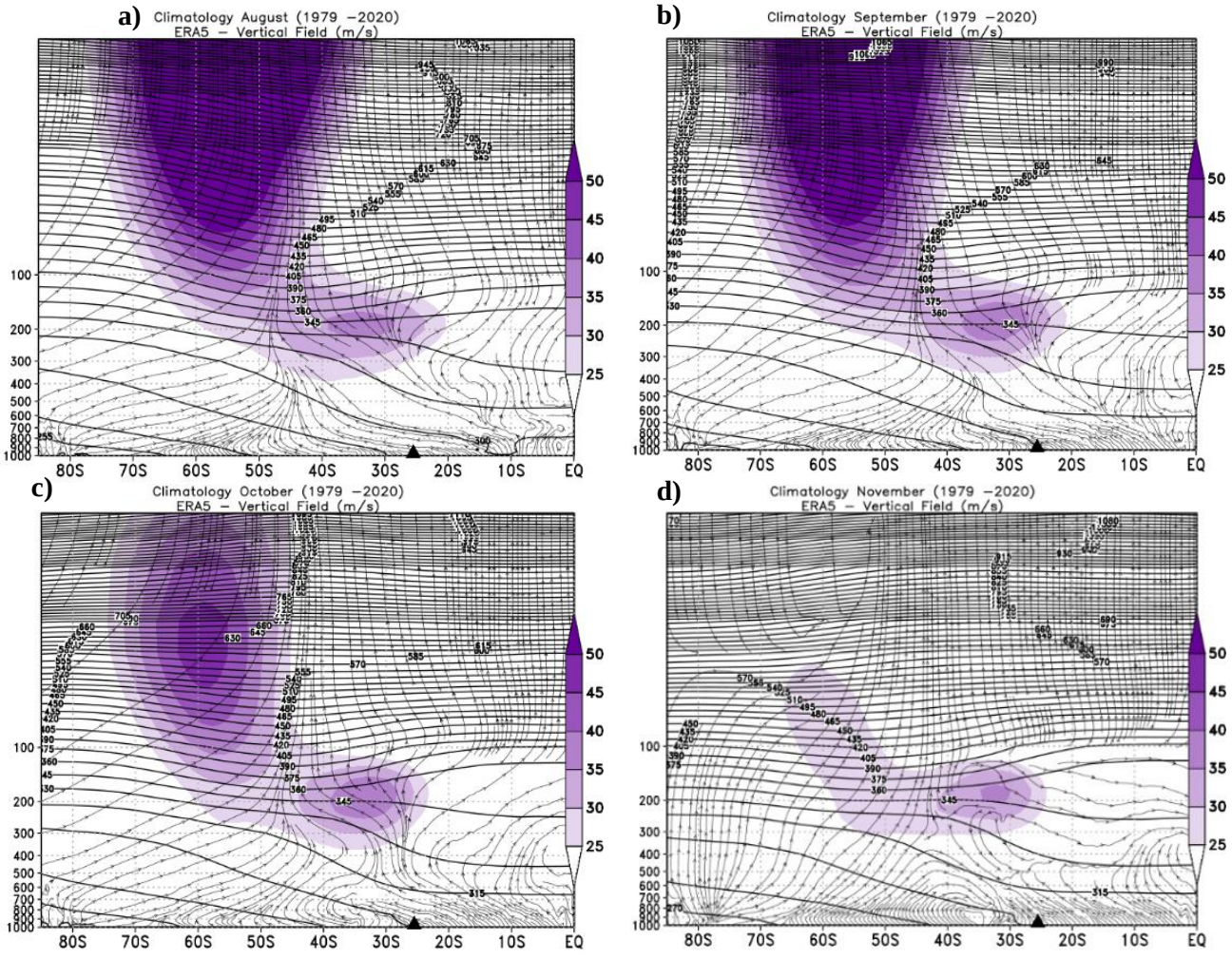

Source: The author.

During the months of October and mainly in November, the climatology shows that the vortex tends to de-intensify, this is because the return of sunlight in the austral spring raises the temperature causing the vortex to destabilize. During the entire period,

the subtropical tropospheric jet remains coupled with the polar vortex (between August-September) and coupled with the polar jet (between 100 - 250 hPa and 50 - 70ºS) in November.

Figure 4.24: Monthly average of the events of AOH influence events of the vertical section of the atmosphere from 1979 to 2020, between 1000 and 5 hPa showing the presence of the jet (shaded).

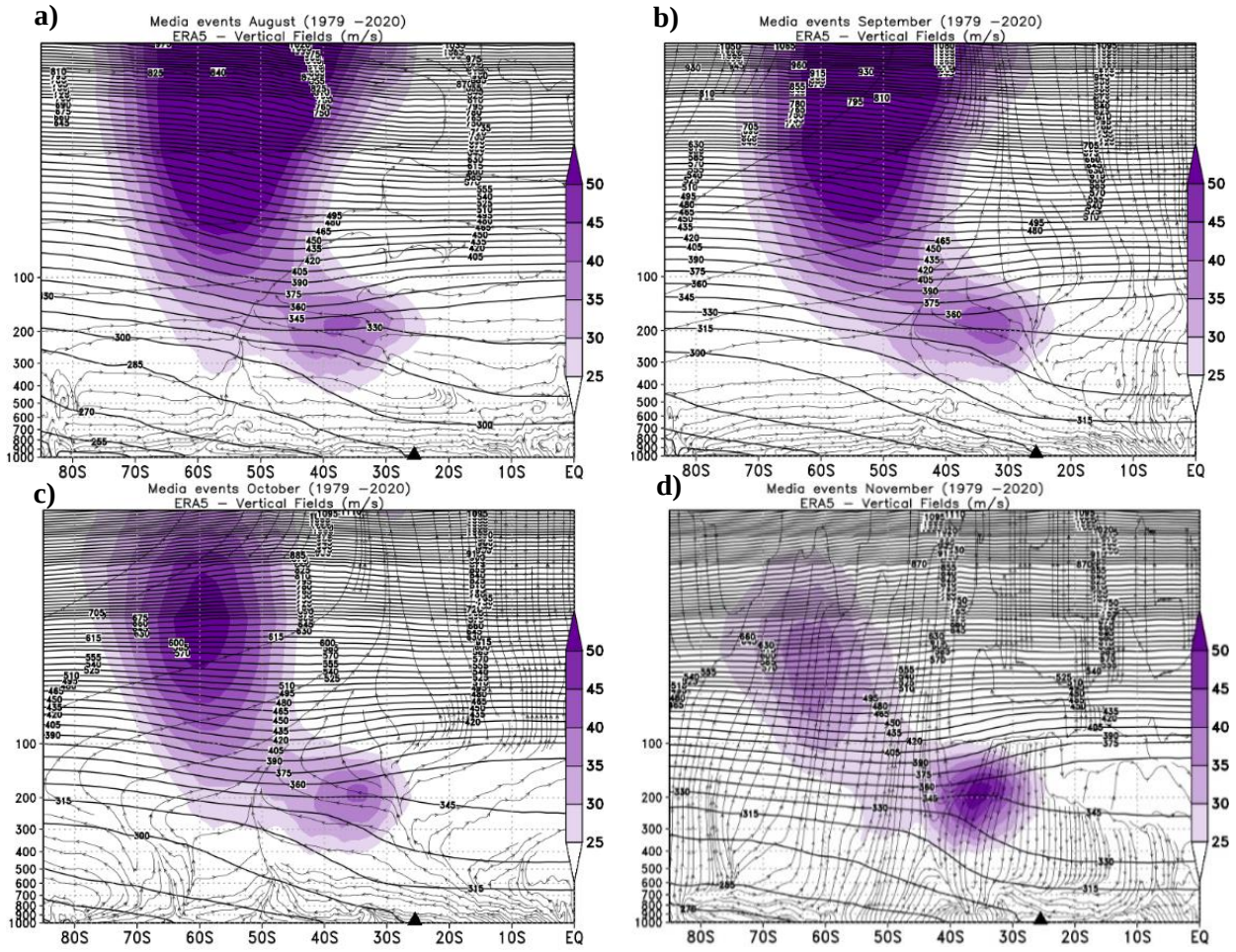

Source: The author

The coupling between the jets together with the funneling of the isentropic ones physically explains how the stratosphere-troposphere exchanges occur. SANTOS (2016) presents important results regarding air exchange between the stratosphere and troposphere, noting the importance of the jet stream helping this exchange mechanism, being more intense in the winter and spring months. GÚZMAN (2021) identified that the

position and intensity of the subtropical jet directly affects the position of the dynamic tropopause, which ends up influencing the mechanism of air mass exchanges by increasing/decreasing the amount of O3 at stratospheric levels.

The monthly mean of the events showed a similar pattern to the climatology for each month. The coupling between the stratospheric and tropospheric jets is visible, highlighting a greater intensity of these jets compared to their climatology. This pattern is confirmed in the average of all events identified in this work (102) in figure 4.25. The coupling between the jets is shown to be an important dynamic pattern during the occurrence of O3 content decrease events over the southern region of Brazil.

Figure 4.25: Monthly average of all 102 AOH events identified during the period 1979 - 2020 of the vertical section of the atmosphere between 1000 and 5 hPa.

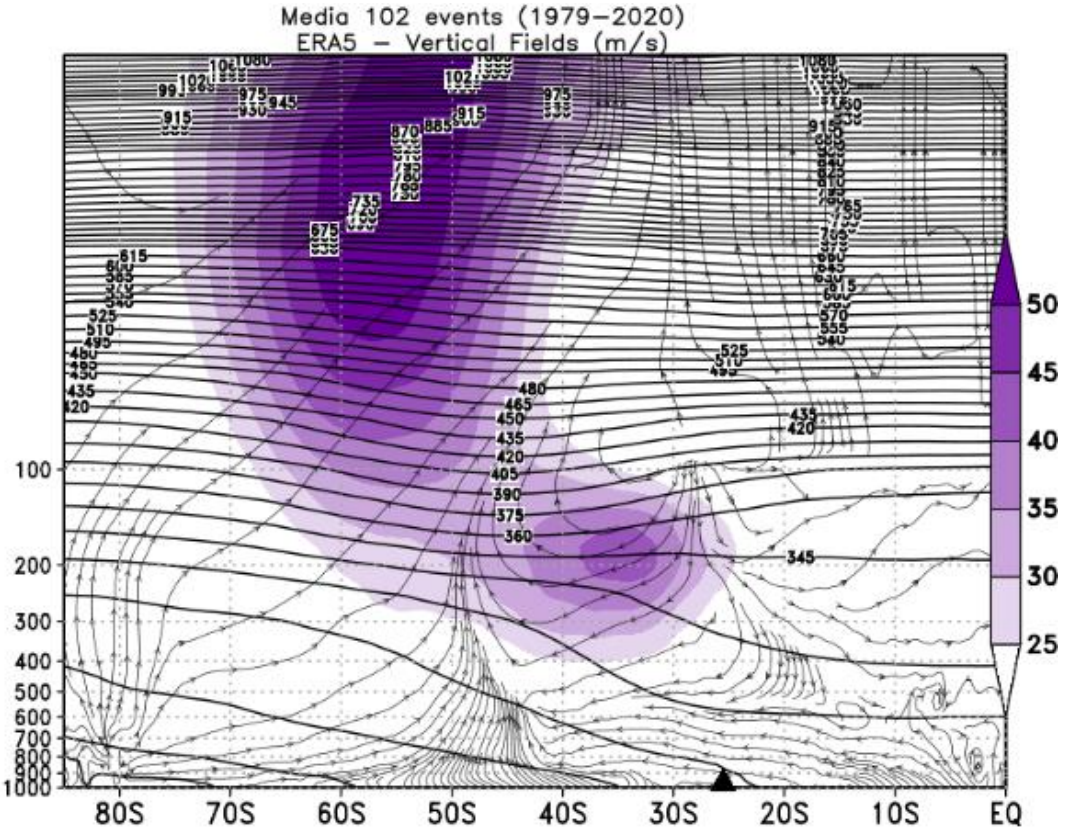

Source: The author.

4.6.4 Conceptual model analysis

The elaboration of the conceptual models allowed a better visualization of how the atmospheric dynamics behaves during the occurrence of events of influence of the Antarctic Ozone Hole on regions of medium latitudes, as the city of Santa Maria/RS focus of this study. Figure 4.26 shows the meridional/horizontal behavior of the stratospheric and tropospheric jets during the analysis period of this study, which is 42 years during the AOH active period.

At 20 hPa is where the stratospheric jet, or polar night jet, is found, intensely present during the winter/early spring period. During winter, the stratospheric polar region has very negative temperatures inside the vortex, mainly due to the absence of solar radiation, making the polar stratospheric clouds that form in this period serve as a basis for the destruction of O3 during this period. As presented in the climatology during the events of decrease in the O3 content, the polar jet is persistent and intense until the beginning of October, being able to influence up to 50 ºS of latitude at high levels.

At the average levels of the atmosphere, around 200 hPa, the position of the tropospheric jets follows the climatological pattern. The subtropical jet influencing mainly mid-latitudes, as is the case of Santa Maria/RS, and the polar jet being more important at high latitudes helping to transport air masses. The isentropic coupling is noticeable in the analyses, dynamically explaining the movement of air masses from the stratosphere to the troposphere. The results also showed that the stratospheric and tropospheric jets couple during the occurrence of the events, showing that these transfers of air masses between the layers occur with the help of these large-scale systems, such as the jets.

According to figure 4.29 the air parcels with a low concentration of O3 are "closed" inside the polar vortex. Despite being stable, the Antarctic Ozone Hole is very dynamic and therefore, air masses can "release" from this vortex reaching regions of medium latitudes. This release occurs, as shown by previous works (Bittencourt et al. 2019) after the passage of frontal systems and according to the analysis presented here, the coupling between the layers occurs through the connection between the subtropical

and polar jets with the stratospheric jet. This coupling between the jets reveals that during events of decrease in O3 content over the Santa Maria/RS region, they occur in practically 90% of all events identified in this study. The connection between the jets dynamically explains how parcels of air with less O3 that are found in the upper levels of the atmosphere, in the region of the stratosphere, and in high latitudes, reach regions of medium latitudes.

Figure 4.26: Conceptual model showing the position of the stratospheric and tropospheric jets at 20 and 200 hPa with the meridional section of the field.

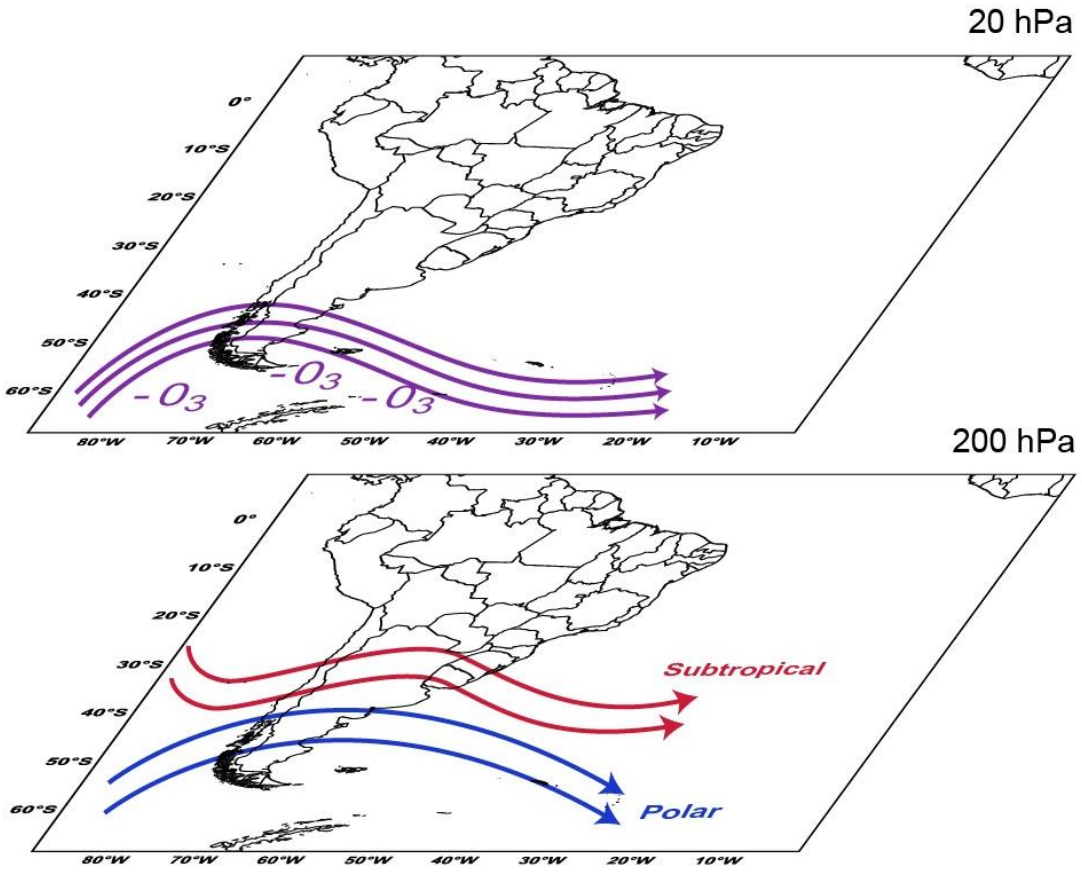

Source: The author.

Conceptually, figure 4.27 symbolizes the dynamic behavior of the atmosphere during the 42 years of data analyzed over Santa Maria/RS in relation to the identification of events of decrease in O3 content, in the active period of the Antarctic Ozone Hole, which occurs from August to November. Shades in purple show the intensity of the jet

both the stratospheric and the two tropospheric jets (left polar between 70ºS - 50ºS, and the subtropical between 40ºS to 20ºS).

The blue line represents the movement of the air mass poor in O3, from the region of the poles where the AOH is active to regions of medium latitudes, such as the city of Santa Maria/RS. The connection of the jets helps in this transport, causing a funneling of the isentropic, also affecting the height of the tropopause, causing this air content with little O3 to reach these regions.

Figure 4.27: Conceptual model showing the dynamic behavior in the vertical section of the atmosphere, during the events of influence of the AOH on regions of medium latitudes in the 42 years of analysis.

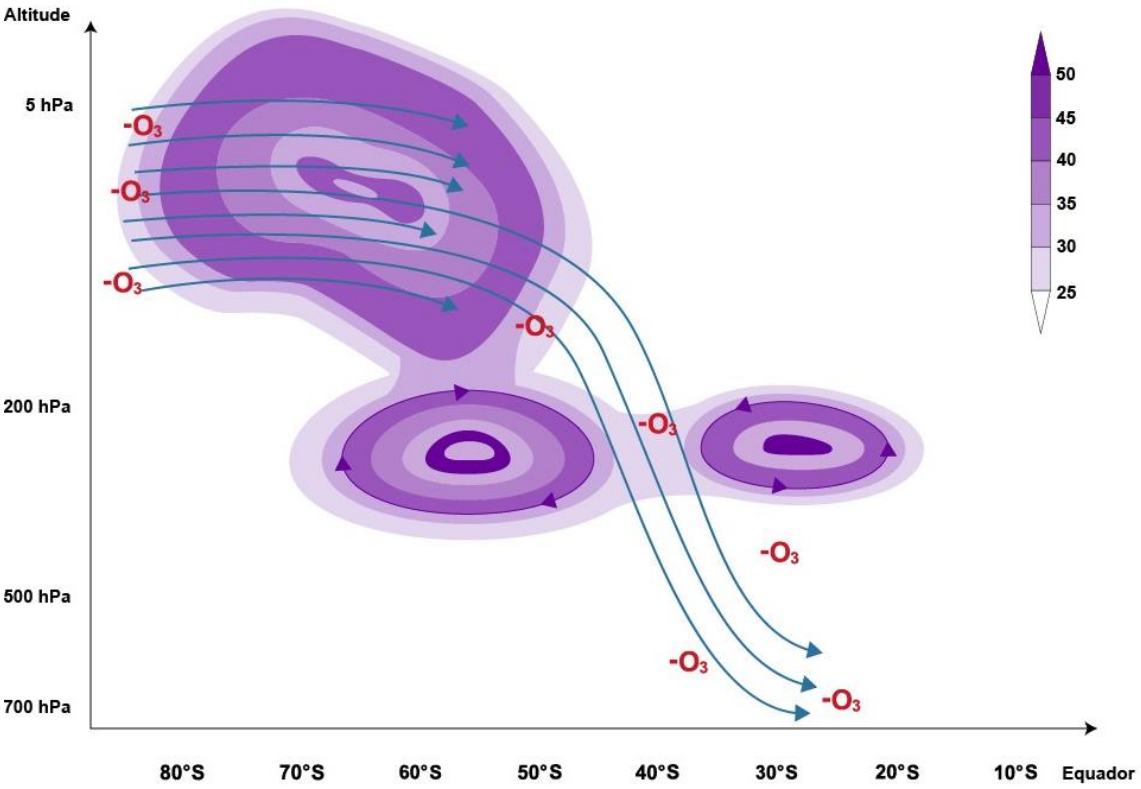

Source: The author.

5 SUMMARY

Dans la présente thèse de doctorat, les données moyennes quotidiennes de la colonne totale d'ozone sur la ville de Santa Maria/RS région des latitudes moyennes ont été analysées. Le comportement de l'O3 sur ces régions reposait sur l'analyse d'instruments de surface, le spectrophotomètre Brewer, des instruments satellites (TOMS et OMI) fournissant des mesures de TCO pour les 42 années de données analysées entre 1979 et 2020.

L'objectif principal de ce travail est d'étudier l'influence du trou d'ozone antarctique ainsi que l'analyse de la dynamique atmosphérique sur la colonne d'ozone totale et son profil vertical dans le sud du Brésil. Les comparaisons des données TCO journalières moyennes ont montré une sous-estimation de la réanalyse ERA5 par rapport aux données BREWER, ce qui explique le R2 de 0,83 constaté. Par conséquent, ERA5 n'est pas une bonne base de données pour représenter ce type de variable. D'autre part, le satellite OMI comparé à BREWER a montré un R2 de 0,94 et des valeurs MBE faibles indiquant une légère surestimation du satellite. Ces résultats concordent avec d'autres études qui présentent une analyse similaire (ÁNTON et al., 2009; PERES et al., 2017).

Les profils verticaux utilisés avec les données TIMED/SABER ont d'abord été validés pour une utilisation plus fiable dans l'analyse des événements. Ainsi, la comparaison entre les données satellitaires (SABRE) et les sondes d'ozone de la station SHADOZ/NASA a été utilisée. A titre de comparaison, la saison tropicale du Natal/RN, qui compte plus de 20 ans de mesures de profils verticaux, a été choisie pour cette validation. Les résultats ont montré que les plus grandes différences relatives entre les satellites et les sondes d'ozone se situent en dessous de 20 km d'altitude. Ces grandes différences, entre 15 et 20 km, peuvent s'expliquer par des incohérences satellitaires, ne représentant pas très bien les mesures initiales. Ainsi, la couche stratosphérique au-dessus de 20 km, dans l'analyse des profils verticaux lors de la survenue d'événements de diminution temporaire de la teneur en O3, est bien représentée par le satellite SABER.

La climatologie TCO montre une variation saisonnière bien définie au cours des 42 années d'analyse sur la région sud du Brésil, avec des valeurs maximales au printemps

et des valeurs minimales en hiver. Cette variation s'explique principalement par la circulation à grande échelle (BDC) qui transporte l'air riche en O3 de sa région de formation dans la stratosphère tropicale vers les régions des moyennes et hautes latitudes, aux pôles. Ce transport dure des mois, provoquant des valeurs élevées au printemps dans la région de Santa Maria/RS. Les profils verticaux présentaient une climatologie différente selon les altitudes choisies. La hauteur de 20 km présentait une climatologie comme l'analyse climatologique du TCO. Influencée par des processus dynamiques, la variation saisonnière se distingue également à cette altitude. Aux altitudes comprises entre 28 et 30 km, région stratosphérique moyenne, le facteur photochimique est ce qui contrôle la teneur en O3. Maximums pendant les saisons chaudes et valeurs minimales en hiver en raison de la faible incidence du rayonnement.

La variabilité climatique montre une forte influence du cycle solaire, suivi du QBO du TCO sur la région subtropicale analysée dans cette étude. Le cycle annuel est également la variabilité dominante du TCO de Santa Maria/RS, même s'il n'est pas retiré des analyses en ondelettes, la climatologie montre ce schéma bien défini (BITTENCOURT, 2019). Aux latitudes tropicales, l'influence qui ressort dans l'analyse du TCO est le QBO, qui module le comportement de l'O3 dans la région tropicale où se produisent les processus photochimiques pour la formation du gaz. Des changements dans l'oscillation quasi-biennale peuvent interférer avec le mouvement à grande échelle de la circulation de Brewer-Dobson, modulant la distribution d'O3 vers les autres régions, où dans la phase occidentale il y a une accumulation d'O3 dans les tropiques en raison d'une décélération du BDC, c'est le contraire qui se produit. dans la phase orientale (phase positive) lorsqu'il y a une accélération du BDC (CORDERO, 2012). Pour les travaux futurs, une analyse plus précise concernant la phase QBO lors des événements de diminution de la teneur en O3 sur le sud du Brésil devrait être analysée plus attentivement.

L'identification des événements d'influence AOH sur la région d'étude, grâce à la méthodologie utilisée dans ce travail entre 1979 et 2020, a permis de trouver 102 événements qui ont diminué la teneur en O3 sur la région. L'étude de cas présentée dans les résultats est un événement extrême de diminution de la teneur en O3 sur le sud du Brésil, qui s'est produit en octobre 2016 (BITTENCOURT, 2018). Selon les données

TCO, la valeur le jour de l'événement était de 225 DU, puisque la région AOH présente des valeurs inférieures à 220 DU (HOFFMAN, 1997), l'événement a réduit d'environ 23% la teneur en O3. Le jour de l'événement, le profil vertical a identifié des réductions d'environ -40% entre 23 et 26 km d'altitude, par rapport à la climatologie pour la période de données. Les réductions observées dans le profil vertical le jour de l'événement ont montré que toute la couche stratosphérique, jusqu'au moins à la stratosphère moyenne, présentait des réductions significatives de la teneur en O3 au-dessus de Santa Maria/RS. Les champs de tourbillon potentiel stratosphérique ont identifié à 20 hPa l'augmentation du tourbillon potentiel absolu sur la région entre le 19 octobre et au moins le 21 octobre.

L'analyse statistique a montré qu'en ce qui concerne le TCO, les réductions moyennes des événements d'influence AOH sont d'environ 8,3 ± 3,5 %. La plupart des événements identifiés sont survenus en septembre avec 33 événements (32,3%) et en octobre avec 38 événements identifiés (37,2%). Ce résultat concorde avec l'analyse des profils verticaux utilisés par le satellite SABRE entre 2002 et 2018, où 38 profils des événements sélectionnés ont été analysés et décrits dans ce travail. Les profils identifiés ont montré la plupart des diminutions de la teneur totale en O3 en septembre et octobre. De plus, la hauteur préférée à laquelle ces diminutions ont été trouvées se situait dans une couche comprise entre 24 et 28,1 km dans la plupart des événements. Certaines épreuves montrent des diminutions dans d'autres attitudes, comme au 20 km et au 30 km. Ces baisses sont constantes et avec une réduction de 20% durant les mois de septembre et octobre, par rapport aux 38 profils verticaux d'événements. Pour les travaux futurs, des périodes d'étude plus longues seront analysées pour caractériser et identifier un plus grand nombre d'événements d'effets secondaires AOH sur les régions de latitude moyenne.

La dynamique des champs stratosphériques à travers le tourbillon potentiel a réussi à montrer certains points plus clairement. En utilisant les données de la nouvelle génération de réanalyse ECMWF avec ERA5, les champs de vorticité potentielle ont été analysés pour caractériser la trajectoire de la masse d'air pauvre en O3 pendant l'événement, où l'augmentation de la vorticité potentielle absolue (APV) entraîne l'origine polaire de l'événement masse d'air. A 20 hPa, où les champs ont été analysés, le comportement dynamique de l'atmosphère moyenne, vers 23 à 26 km d'altitude, a montré

les plus fortes réductions de teneur en O3 lors des événements d'influence AOH identifiés sous les régions de latitude moyenne. La climatologie des champs stratosphériques a montré une augmentation du tourbillon potentiel à partir du mois d'août et s'intensifiant vers la fin de la période active AOH. Cette dynamique explique une relation directe avec le comportement du vortex polaire pendant cette période la plus active du vortex pendant l'hiver polaire, et avec le retour du rayonnement au printemps austral une diminution de ses activités.

Les moyennes mensuelles liées aux événements de diminution de l'AOH ont montré une augmentation progressive de l'APV d'août à novembre au cours des 42 années. L'anomalie mensuelle de ces événements a identifié cette progression progressive avec une augmentation du tourbillon potentiel, selon la survenance des événements, en septembre et octobre. L'anomalie incluant les 102 événements de diminution de l'AOH sur Santa Maria/RS a montré une influence considérable sur la région, avec des valeurs de PV élevées pendant la période d'août à novembre.

Le couplage des jets stratosphériques et troposphériques a montré une forte influence au cours de la période des données analysées. La section verticale de l'atmosphère de 1000 à 5 hPa présente dans la climatologie un schéma cohérent avec le comportement du vortex polaire, comme il a été dit précédemment, il est plus intense et stable jusqu'à la fin de la nuit polaire. Pendant toute la période, le jet troposphérique subtropical reste connecté au vortex polaire, expliquant ce mécanisme d'échanges de masse d'air entre stratosphère-troposphère pendant la période d'étude. La moyenne lors des événements d'influence AOH sur la région sud du Brésil caractérise cette forte connexion entre les jets stratosphériques et troposphériques au cours de la période analysée.

Les résultats de cette thèse mettent en évidence l'occurrence des événements d'influence de l'AOH sur la région de Santa Maria/RS avec des diminutions prédominantes entre 24 - 28,1 km d'altitude selon les profils verticaux, et une prédominance des événements dans les mois de septembre et octobre. Un autre point à souligner est l'importance du comportement synoptique des jets stratosphériques et troposphériques lors des événements de diminution d'O3 sur les régions des latitudes

moyennes. Le couplage entre elles, tel que le montre le modèle conceptuel présenté, met en évidence et explique le comportement des échanges entre les couches atmosphériques (stratosphère et troposphère). Ils présentent un effet d'entonnoir isentropique bien caractérisé sur la région de l'entrée équatoriale du jet subtropical, mettant en évidence cette influence entre les jets lors de l'apparition d'événements de diminution de la teneur en O3 aux latitudes moyennes.

5.1 FUTURE WORKS

Outre la publication de deux articles en lien avec le sujet de ce travail : Événement majeur d'influence du trou d'ozone antarctique dans le sud du Brésil en octobre 2016 : une analyse de la dynamique troposphérique et stratosphérique (2018) et Enquête sur le comportement de la dynamique atmosphérique au cours occurrences de l'effet secondaire du trou dans la couche d'ozone dans le sud du Brésil (2019), trois autres articles devraient être développés à partir des résultats présentés dans cette thèse de doctorat.

I. Analysis of vertical ozone profiles in South America: comparison of the last 17 years between subtropical and tropical latitudes
II. Climatologie de la colonne totale d'ozone et profil vertical pour 42 ans de données en Amérique du Sud: analyse de l'influence des événements du trou d'ozone antarctique
III. La dynamique stratosphérique et troposphérique des événements d'influence AOH aux latitudes moyennes.

Certains points méritent d'être analysés dans ces articles, comme l'utilisation du satellite AURA/MLS pour la comparaison avec les données du satellite TIMED/SABRE, en relation avec l'analyse du contenu vertical d'O3 sur Santa Maria/RS. L'analyse des tendances des données TCO dans la région d'étude pour la période de données devrait également être unpoint d'étude important, en particulier pour surveiller le comportement du TCO et quelle devrait être sa tendance dans les régions des latitudes moyennes d'Amérique du Sud.

BLIOGRAPHIC

ABALOS, M., POLVANI, L., CALVO, N., KINNISON, D., PLOEGER, F., RANDEL, W., & SOLOMON, S. **New Insights on The Impact of Ozone-Depleting Substances on The Brewer-Dobson Circulation**. Journal of Geophysical Research: Atmospheres,124, 2435–2451, 2019.

BATES, D. R.; NICOLET, M. **Atmospheric hydrogen.** Astron. Soc. Pac**.**, v. 62, p. 106-110, 1950.

BENCHERIF H., T. PORTAFAIX, J.L. BARAY, B. MOREL, S. BALDY, J. LEVEAU, A. HAUCHECORNE, P. KECKHUT, A. MOORGAWA, M.M. MICHAELIS, R. DIAB, **LIDAR observations of lower stratospheric aerosols over South Africa linked to large scale transport across the southern subtropical barrier**, Journal of Atmospheric and Solar-Terrestrial Physics 65, 2003.

BENCHERIF, H., EL AMRAOUI, L., KIRGIS, G., DE BELLEVUE, J. L., HAUCHECORNE, A., MZÉ, N., PORTAFAIX, T., PAZMINO, A., GOUTAIL, F. **Analysis of a rapid increase of stratospheric ozone during late austral summer 2008 over Kerguelen (49.4°S, 70.3°E)**. Atmos. Chem. Phys., v. 11, p. 363–373, 2011.

BENCHERIF, H., TOIHIR. A., MBATHA, N., SIVAKUMAR, V., DU PREEZ, D. **Ozone Variability and Trend Estimates from 20-Years of Ground-Based and Satellite Observations at Irene Station, South Africa**. Atmosphere, MDPI 2020, Tropospheric Ozone Observations, 2020.

BITTENCOURT, G. D., BRESCIANI, C., BAGESTON, J. V., PINHEIRO, D. K., SCHUCH, N. J., BENCHERIF, H., LEME, N. P., AND PEREZ, L. V.: **A Major Event of Antarctic Ozone Hole Influence in the Southern Brazil in October 2016: An Analysis of Tropospheric and Stratospheric Dynamics**, Annales Geophysicae, 2018.

____. **Investigation of the behavior of the atmospheric dynamics during occurrences of the ozone hole's secondary effect in southern Brazil**. Annales Geophysicae, v. 37, n. 6, p. 1049–1061, 2019.

BRESCIANI, C., BITTENCOURT, D. G., BAGESTON, V. J., PINHEIRO, K. D., BENCHERIF, H., SCHUCH, J. N., LEME, N. P., PERES, V. L., **Report of a Large Depletion in the Ozone Layer over the South Brazil and Uruguay by Using Multi – Instrumental Data**, Annales Geophysicae, 2018.

BREWER, A. W**. Evidence for a world circulation provided by the measurements of helium and water vapour distribution in the stratosphere**, Q. J. R. Meteorol. Soc., v.75, p. 351- 363, 1949. BIRNER, T., **Residual circulation, and the tropopause structure**. J. Atmos. Sc. 67, 2582-2600, 2011.

BONISCH, H., **Residual circulation trajectories and transit times into the extratropical lower most stratosphere**. Atmos. Chem. Phys.,**11,** 817-827, 2011.

BUKIN, O. A., SUAN An, N.; PAVLOV, A. N.; STOLYARCHUK, S. Y. and SHMIRKO, K.A.

Effect that Jet Streams Have on the Vertical Ozone Distribution and Characteristics of Tropopause Inversion Layer, Izvestiya Atmospheric and Oceanic Physics, v. 47, n. 5, p. 610–618, 2011.

BUTCHART, N. **The brewer-dobson circulation**. Reviews of Geophysics, v. 52, 06 2014.

CASICCIA, C.; ZAMORANO, F.; HERNANDEZ, A. **Erythemal irradiance at the Magellan's region and Antarctic ozone hole 1999-2005.**Atmosfera, v. 21 n.1, p. 1-12, 2008.

CRUTZEN, P. J. **The influence of nitrogen oxide on the atmospheric ozone content**. Q. J. R. Meteorol. Soc., v. 96, p. 320-327, 1970.

DESSLER, A. **The Chemistry and Physics of Stratospheric Ozone**. International geophysics series, v. 74, Academic Press, 2000.

DOBSON, G. M. B. **Observations of the amount of ozone in the earth's atmosphere and its relation to other geophysical conditions**. Proceedings of the Royal Society of London A, v. 129, n. 411, 1930.

DOBSON, G. M. B., **Forty years' research on atmospheric ozone at Oxford: A history.** Appl. Opt., v. 7, p. 387-405, 1968.

FARMAN, J. C.; GARDINER, B. G.; SHANKLIN, J. D. **Large losses of total ozone in Antarctica reveal seasonal ClOx/NOx interaction**. Nature. 315: 207-210, 1985.

FABRY, C.; BUISSON, M. L. **L'absorption de l'ultraviolet par l'ozone et la limite du spectre solaire**. Journal of Physics, v. 3, p. 196–206, 1913.

FISHMAN, J., WATSON, C. E., LARSEN, J. C., LOGAN, J. A. **Distribution of tropospheric ozone determined from satellite data**, J. Geophys. Res., 95, 3599–3617, doi:10.1029/JD095iD04p03599, 1990.

HADJINICOLAOU, P., PYLE, J. A., HARRIS, N. R. P., **The recent turnaround in stratospheric ozone over northern middle latitudes: A dynamical modeling perspective**, *Geophys. Res. Lett.*, 32, L12821, doi:10.1029/2005GL022476, 2005.

HOFMANN, D. J., OLTMANS, S. J., HARRIS, J. M., JOHNSON, B. J., LATHROP, J. A. **Ten years of ozone sonde measurements at the South Pole: Implications for recovery of springtime Antarctic ozone**. J. Geophys. Res-Atmos., v.102, p. 8931-8943, 1997.

HOLTON, J. R.; HAYNES, P. 'H.; MCINTYRE, M. E.; DOUGLASS, A. R.; ' ROOD, R. B.; PFISTER, L. **Stratosphere-troposphere Exchange,** Rev. Geophys.v.3, n.3, p.403-439, 1995.

HOSKINS, B. J.; McINTYRE, M. E.; ROBERTSON, A. W. **On the use and significance of isentropic potential vorticity maps**. Q. J. Roy. Metror. Soc., v. 111, p. 877-946, 1985.

KIRCHHOFF, V. W. J. H., SCHUCH, N. J., PINHEIRO, D. K., HARRIS, J. M. **Evidence for an ozone hole perturbation at 30º south.** Atmos. Environ., v. 33, n. 9, p. 1481-1488, 1996.

KUCHAR, A., SACHA, P., MIKSOVSKY, J. & PISOFT, P. **The 11-year solar cycle in current**

reanalyses: a (non)linear attribution study of the middle atmosphere. Atmos. Chem. Phys. 15, 6879–6895, 2015.

LARY, D., CHIPPERFILD, M., PYLE, J.; NORTON, W. RIISHOJGAARD. L. **Treedimensional tracer initialization and general diagnostics using equivalent PV latitude potential- temperature coordinates**, Q. J. Roy. Metror. Soc., v. 121, p. 187– 210, 1995.

LEE, H., AND A. K. SMITH, **Simulation of the combined effects of solar cycle, quasi-biennial oscillation, and volcanic forcingon stratospheric ozone changes in recent decades**, J. Geophys. Res.,108(D2), 4049, doi:10.1029/2001JD001503, 2003.

LONDON, J. **Observed distribution of atmospheric ozone and its variations**. In: WHITTEN, R. C.; PRASAD, S. S. (Ed.). Ozone in the free atmosphere. New York: Van Nostrand Reinhold Company, 1985.

MARCHAND, M.; BEKKI, S.; PAZMINO, A.; LEFÈVRE, F.; GODIN-BEEKMANN, S.; HAUCHECORNE, A. **Model simulations of the impact of the 2002 Antarctic ozone hole on midlatitudes**. Journal Atmos. Sci., v. 62, p. 871–884, 2005.

MLYNCZAK, Martin G. **Energetics of the mesosphere and lower thermosphere and the SABER experiment**, Advances in Space Research, Volume 20, Issue 6, 1997, Pages 1177-1183, ISSN 0273-1177, https://doi.org/10.1016/S0273-1177(97)00769-2, 1997.

MOLINA, M. J., ROWLAND, F. S. **Stratospheric sink for chlorofluoromethanes: Chlorine atom catalyzed destruction of ozone**. Nature, v. 249, p. 820-812, 1974.

NAIR, P. J., L. FROIDEVAUX, J. KUTTIPPURATH, J. M. ZAWODNY, J. M. RUSSELL III, W. STEINBRECHT, H. CLAUDE, T. LEBLANC, J.A.E. VAN GIJSEL, B. JOHNSON, D.P.J. SWART, A. THOMAS, R. QUEREL, R. WANG, and ANDERSON, J. **Subtropical and midlatitude ozone trends in the stratosphere: Implications for recovery.** J. Geophys. Res. Atmos., 120, 7247–7257, doi:10.1002/ 2014JD022371, 2015.

OMAN, L. D., A. R. DOUGLASS, J. R. ZIEMKE, J. M. RODRIGUEZ, D. W. WAUGH, AND J. E. NIELSEN, **The ozone response to ENSO in Aura satellite measurements and a chemistry-climate simulation**, J. Geophys. Res.,118, 965–976, 2013.

PINHEIRO, D. K. ; LEME, N. P. ; Peres, L. V. and Kall, E.. **Influence of the antarctic ozone hole over South of Brazil in 2008 and 2009**. **Nat. Inst. of Sce. and Tech. Ant. Env. Res.** v. 1, p. 33-37, 2011.

PERES, L. V.; REIS, N. C. S. dos.; SANTOS, L. O.; BITTENCOURT, G. D.; SCHUCH, A. P.; ANABOR, V ; PINHEIRO, D. K.; SCHUCH, N. J.; LEME, N. M. P. **Análise Atmosférica dos Eventos de Efeito Secundário do Buraco de Ozônio Antártico sobre o Sul do Brasil em 2012. Parte 2: Verificação Sinótica da Troposfera durante os eventos**. CeN. v. 36, p. 423-433, 2014.

PERES, V. L. **Monitoramento da coluna total de ozônio e a ocorrência de eventos de influência do Buraco de Ozônio Antártico sobre o Sul do Brasil**.Tese de Doutorado, 2016.

PERES, L. V., BENCHERIF, H., MBATHA, N., SCHUCH, A.P., TOIHIR, A. M., BÈGUE, N., PORTAFAIX, T., ANABOR, V., PINHEIRO, D. K, LEME, N. M.P., BAGESTON, J. V.,

SCHUCH, N. J. **Measurements of the total ozone column using a Brewer spectrophotometer and TOMS and OMI satellite instruments over the Southern Space Observatory in Brazil,** Ann. Geophysics., 35, 25-37, 2017.

SALBY, M. L. **Fund. Atmos. Phys**. International geophysics series, v. 61, Academic Press, 1996.

SALBY, M. L., TITOVA, E. A.; DESCHAMPS, L. **Changes of the Antarctic ozone hole: Controlling mechanisms, seasonal predictability, and evolution**. J. Geophys. Res-Atmos., v. 117, n. D10111, 2012.

SANTOS, L. O. **Troca Estratosfera - Troposfera e sua Influência no Conteúdo de Ozônio sobre a região Central do Rio Grande do Sul.** Dissertação de Mestrado, 2016.

SEINFELD, J. H.; PANDIS, S. N. **From Air Pollution to Climate Change**, 3rd edition, **Atmos. Chem. Phys.** John Wiley and Sons, Inc. 2016.

SEMANE, N.; BENCHERIF, H.; MOREL, B.; HAUCHECORNE, A.; DIAB, R. D. **An unusual stratospheric ozone decreases in Southern Hemisphere subtropics linked to isentropic air-mass transport as observed over Irene (25.5º S, 28.1º E) in mid-May 2002**. Atmos. Chem. Phys**.**, v. 6, p. 1927-1936, 2006.

SERVICE, C. C. C., **Copernicus Climate Change Service (2017): ERA5: Fifth generation of ECMWF atmospheric reanalyses of the global climate**. 2019.

SCHUCH, A. P., SANTOS, M. B., LIPINSKI, V. M., PERES, L. V, SANTOS C. P., CECHIN S. Z., SCHUCH, N. J., PINHEIRO, D. K., LORETO, E. L. S. **Identification of influential events concerning the Antarctic ozone hole over southern Brazil and the biological effects induced by UVB and UVA radiation in an endemic treefrog species.** Ecotoxicology & Environmental Safety, 2015.
SOLOMON, S., GARCIA, R. R., ROWLAND, F. S., WUEBBLES, D. J. **On the depletion of Antarctic ozone.** Nature, v. 321, p. 755-758, 1986.

SOLOMON, S. **Stratospheric ozone depletion: A review of concepts and history**. Reviews of Geophysics, v. 37, n. 3, p. 275–316, 1999.

STEFFENEL, L.A., ANABOR, V., KIRSCH P, D., GÚZMAN, L., BITTENCOURT, G. D., BENCHERIF, H. **Forecasting upper atmospheric scalars advection using deep learning: an O_3 experiment**. *Machine Learning*, https://doi.org/10.1007/s10994-020-05944-x, 2021.

STOLARSKI, R. S., CICERONE, R. J. **Stratospheric chlorine: A possible sink for ozone**, Can. J. Chem., v. 52, p. 1610-1615, 1974.

SOUKHAREV, B.E.; HOOD, L.L**. Solar cycle variation of stratospheric ozone: Multiple regression analysis of long –term satellite data sets and comparisons with models**. J. Geophys. Res., 111, D20314, 2006.

TOIHIR, A. M., PORTAFAIX T., SIVAKUMAR V., BENCHERIF, H., PAZMINO, A. **Variability and trend in ozone over the southern tropics and subtropics.** Annales Geophysicae, European Geosciences Union, 2018, 36 (2), pp.381-404. DOI: 10.5194/angeo-36-381-2018.

THOMPSON, A. M., WITTE, J. C., STERLING, C., JORDAN, A., JOHNSON, B. J., OLTMANS, S. J., …THIONGO, K. **First reprocessing of Southern Hemisphere Additional Ozonesondes (SHADOZ) ozone profiles (1998–2016): 2. Comparisons with satellites and ground-based instruments.** Journal of Geophysical Research: Atmospheres, 122, 13,000–13,025. https://doi.org/10.1002/ 2017JD027406, 2017.

WEI LIU, MICHAELA I. HEGGLIN, RAMIRO CHECA-GARCIA, SHOUWEI LI, NATHAN P. GILLETT, KEWEI LYU, XUEBIN ZHANG, NEIL C. SWART. **Stratospheric ozone depletion and tropospheric ozone increases drive Southern Ocean interior warming**. *Nature Climate Change*, https://www.nature.com/articles/s41558-022-01320-w, 2022.

WITTE, J. C., POSNY, F., THOMPSON, A. M., SMIT, H. J. G., FUJIWARA, M., COETZEE, G. J. R., NORTHAN, E. T., JOHNSON, B. J., STERLING, C. W., MOHAMAD, M., OGINO, S-Y., JORDAN, A., SILVA, F. R. First reprocessing of Southern Hemisphere Additional OZonesondes (SHADOZ) profile records (1998 - 2015): 1 Methodology and evaluation. Journal of Geophysical Research Atmospheres, 122, 12, 6611-6636, 10.1002/2016jd026403, 2017.

WOFSY, S.C., MCELROY, M. B., YUNG, Y. L. **The chemistry of atmospheric bromine,** Geophysics. Res. Lett., v. 2, p. 215-218, 1975.

WMO. World Meteorological Organization: **Scientific Assessment of Ozone Depletion**. Estados Unidos da América, 1996.

WMO. World Meteorological Organization: **Scientific Assessmentof Ozone Depletion**. Estados Unidos da América, 2006.

WMO. World Meteorological Organization: **Scientific Assessment of Ozone Depletion**. Estados Unidos da América, 2010.

WMO. World Meteorological Organization: **Scientific Assessmentof Ozone Depletion**. Estados Unidos da América, 2014.

Appendix

SECONDARY EFFECT EVENTS OF THE ANTARCTIC OZONE HOLE IDENTIFIED OVER THE SOUTHERN REGION OF BRAZIL BETWEEN 1979 TO 2020

09/29/1979

Figure A1: PVA fields for the 20 hPa in pressure levels, days 09/27/1979 to 09/30/1979.

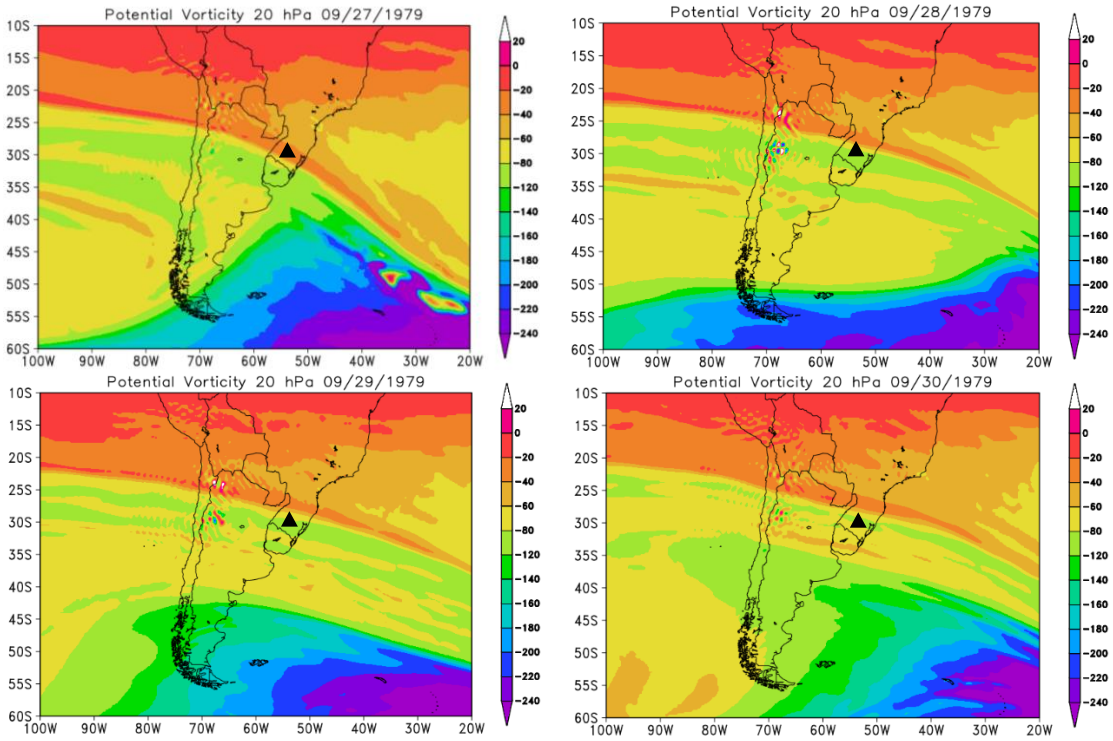

Source: The author.

Figure A2: a) Retroactive trajectory by the HYSPLIT/NOAA model, b) O3 content OMI satellite for South Pole view.

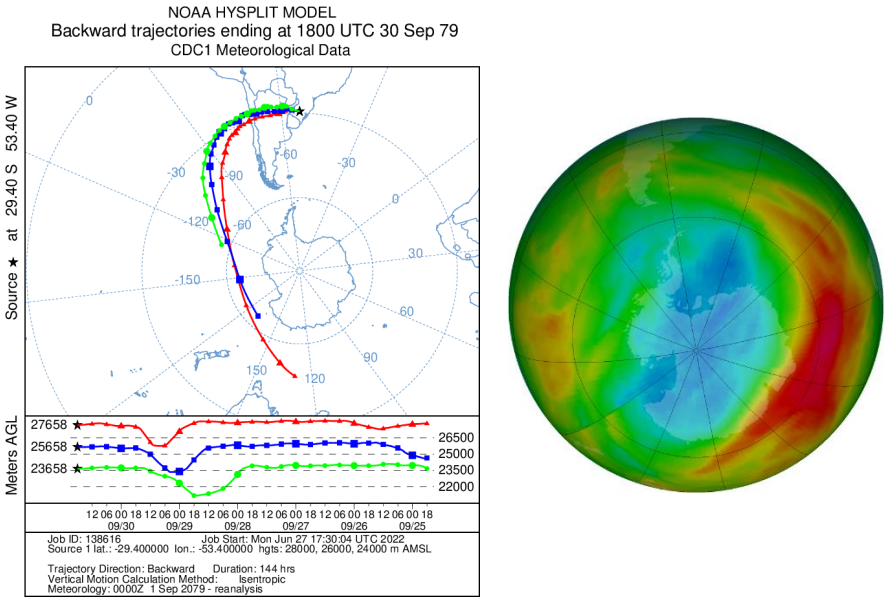

Source: HYPSPLIT/NOAA, NASA/OZONE WATCH

Figure A3: Vertical section of the atmosphere between 1000 and 5 hPa for the days of the event in September 1979.

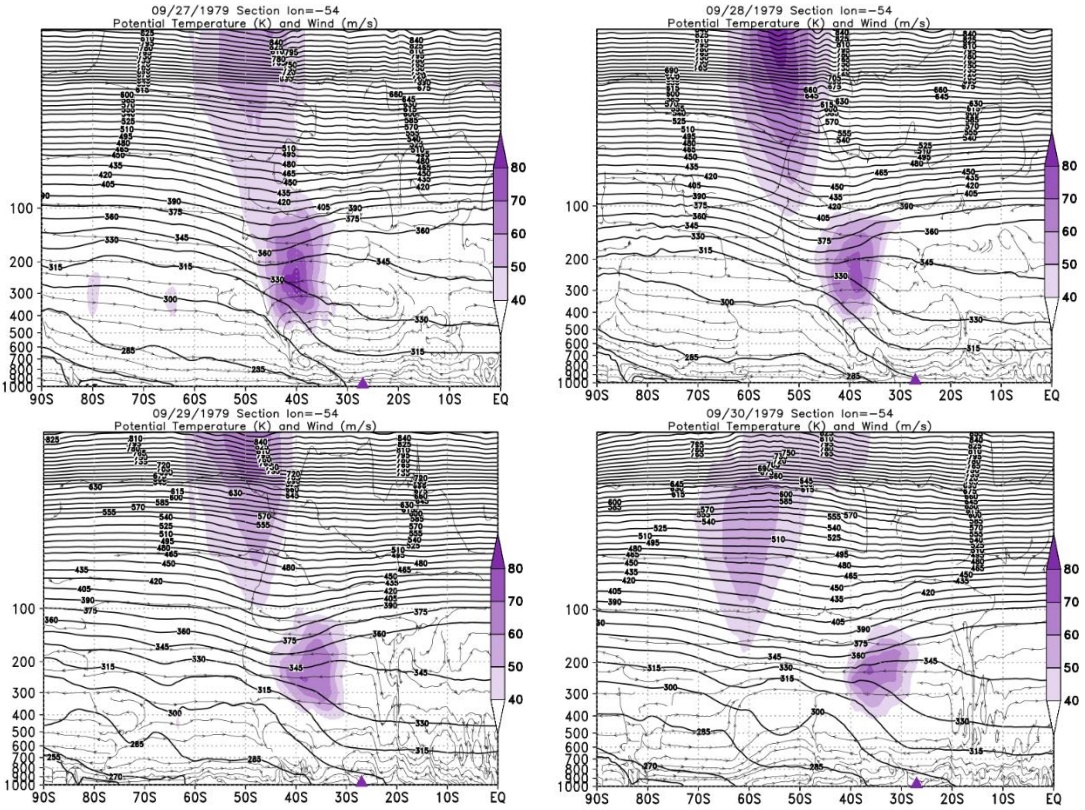

Source: The author.

08/05/1982

Figure A4: PVA fields for the 20 hPa in pressure levels, days 08/03/1982 to 08/06/1982.

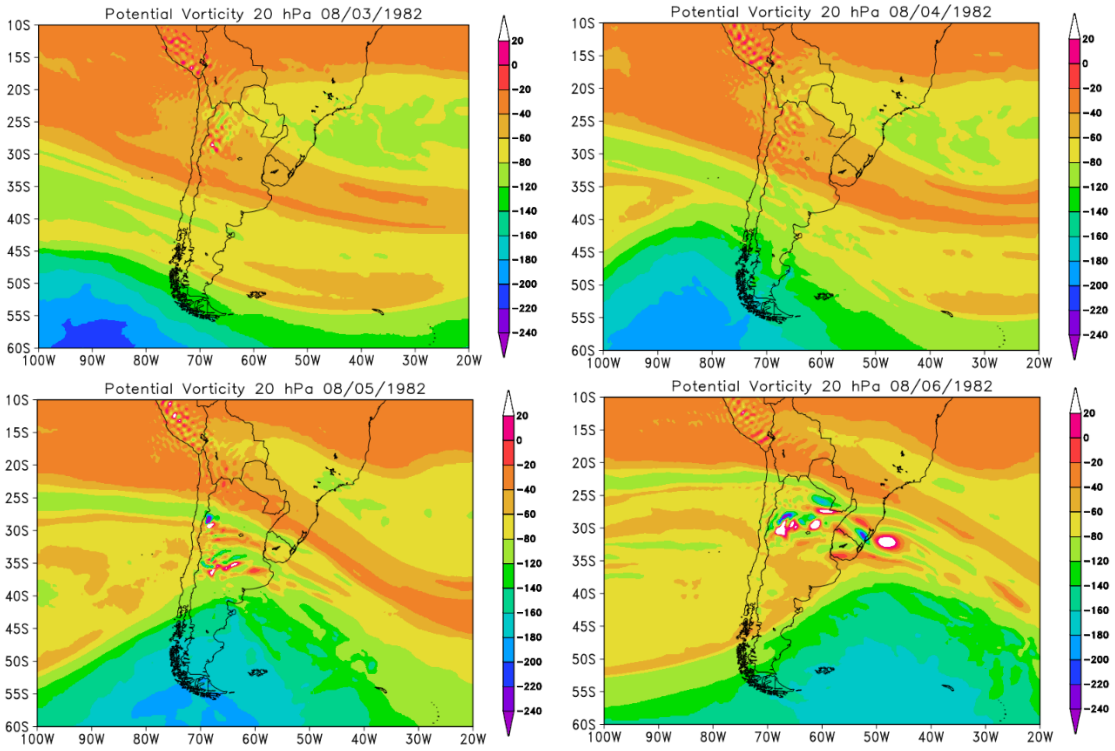

Source: The author.

Figure A5: a) Retroactive trajectory by the HYSPLIT/NOAA model, b) O3 content OMI satellite for South Pole view.

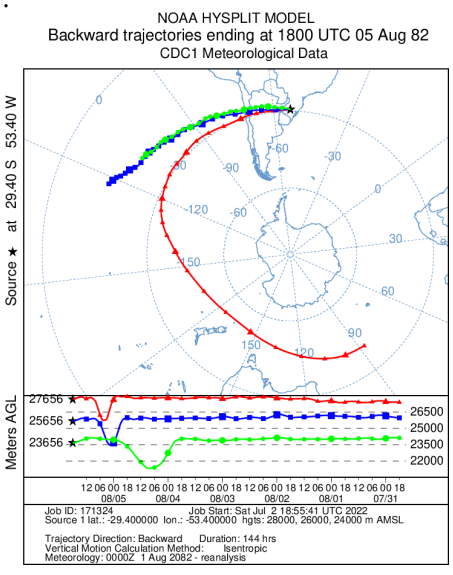

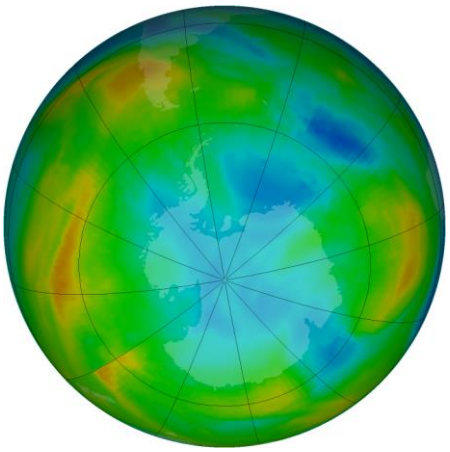

Source: HYPSPLIT/NOAA, NASA/OZONE WATCH

Figure A6: Vertical section of the atmosphere between 1000 and 5 hPa for the days of the event in August 1982.

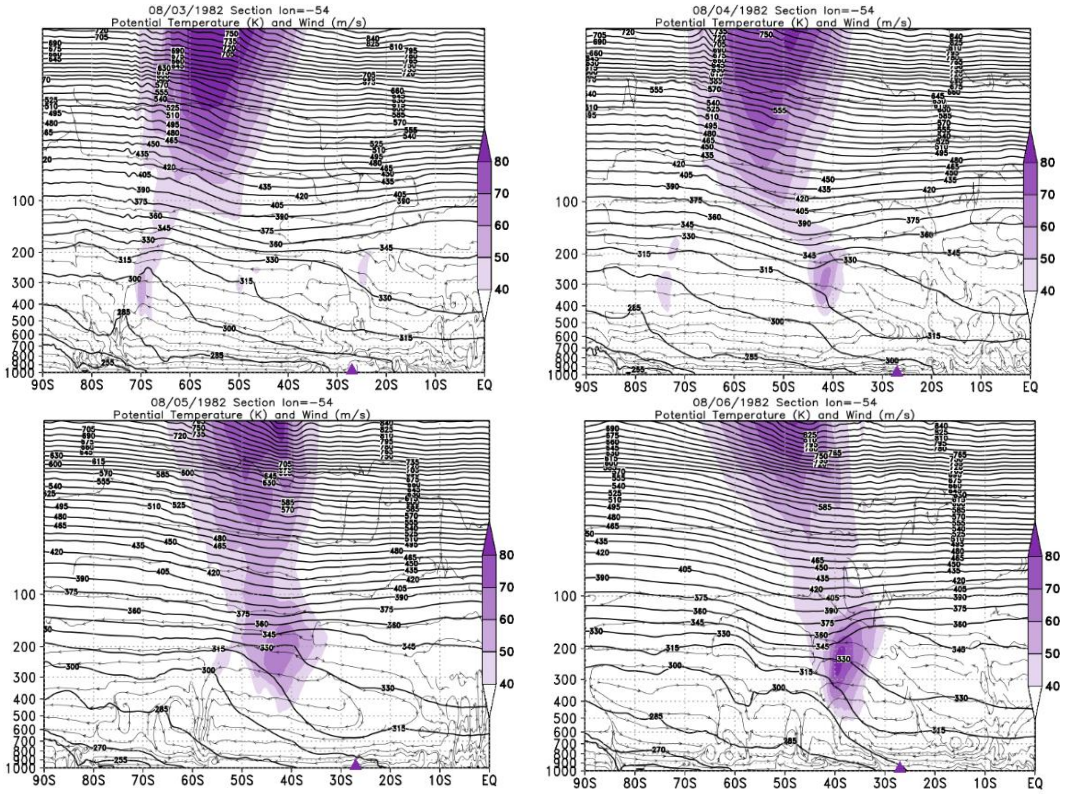

Source: The author.

09/09/1982

Figure A7: PVA fields for the 20 hPa in pressure levels, days 09/07/1982 to 09/10/1982.

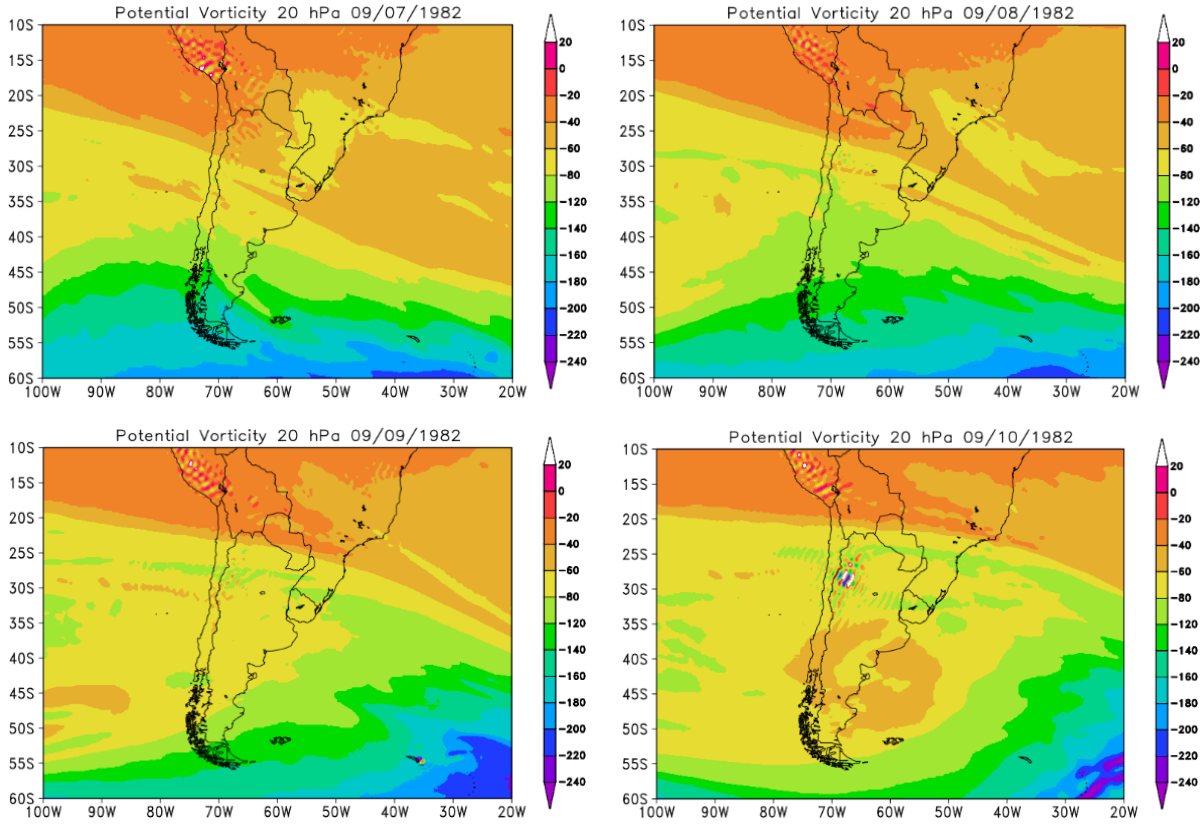

Source: The author.

Figure A8: a) Retroactive trajectory by the HYSPLIT/NOAA model, b) O3 content OMI satellite for South Pole view.

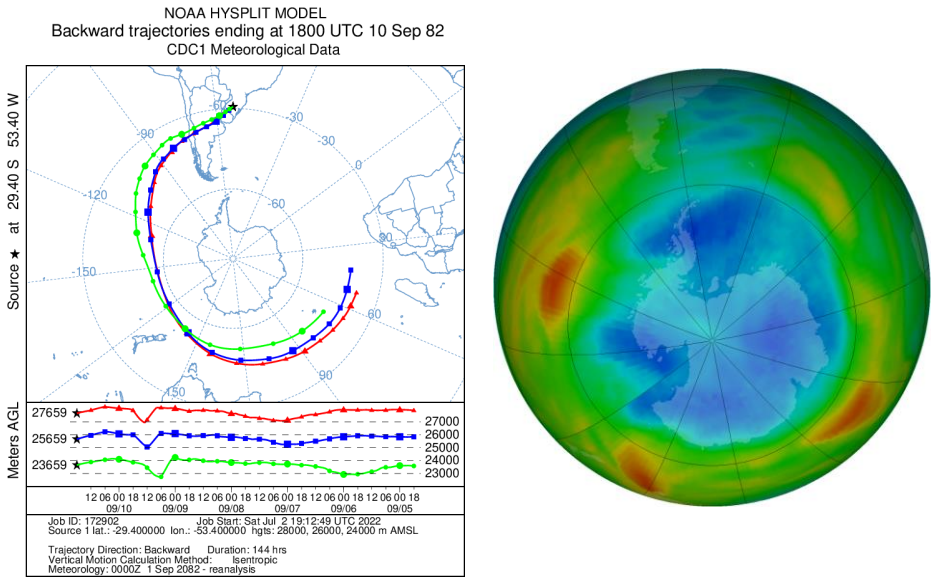

Source: HYSPLIT/NOAA, NASA/OZONE WATCH.

Figure A9: Vertical section of the atmosphere between 1000 and 5 hPa for the days of the event in September 1982.

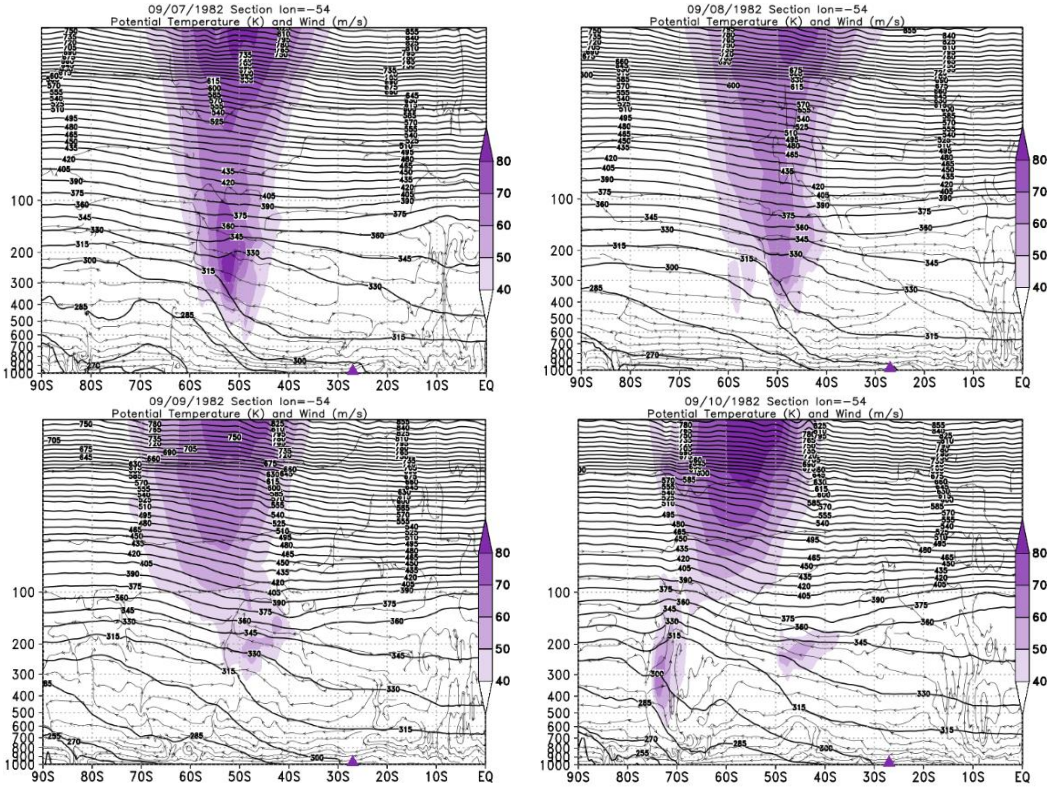

Source: The author.

09/24/1982

Figure A10: PVA fields for the 20 hPa in pressure levels, days 09/22/1982 to 09/24/1982.

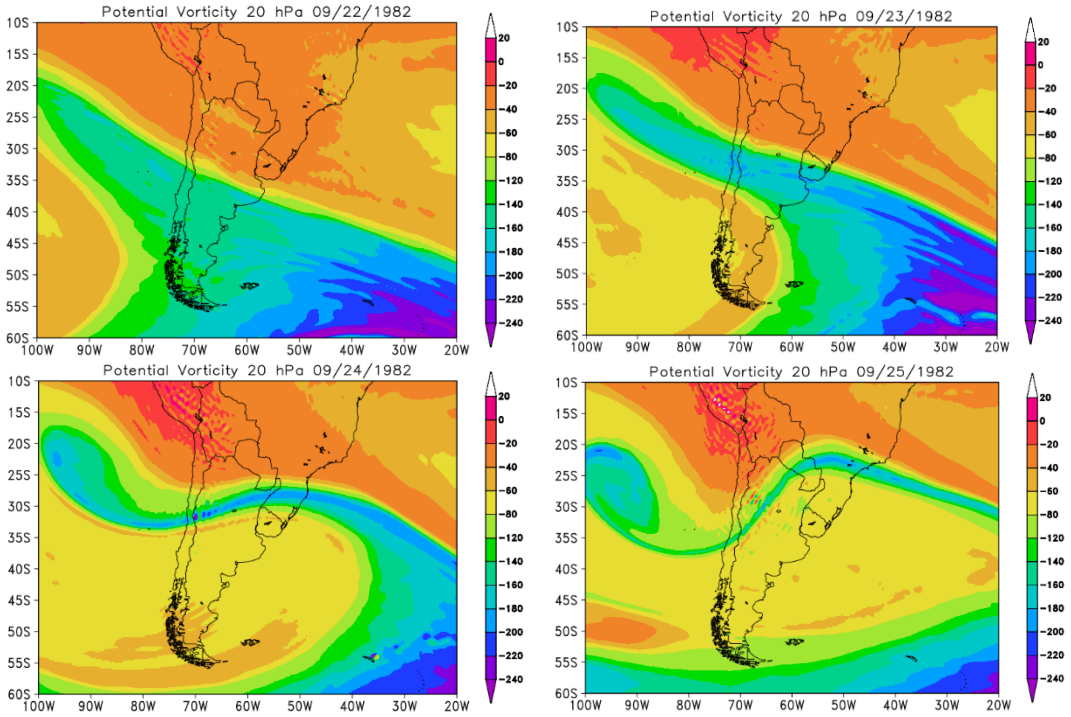

Source: The author.

Figure A11: a) Retroactive trajectory by the HYSPLIT/NOAA model, b) O3 content OMI satellite for South Pole view.

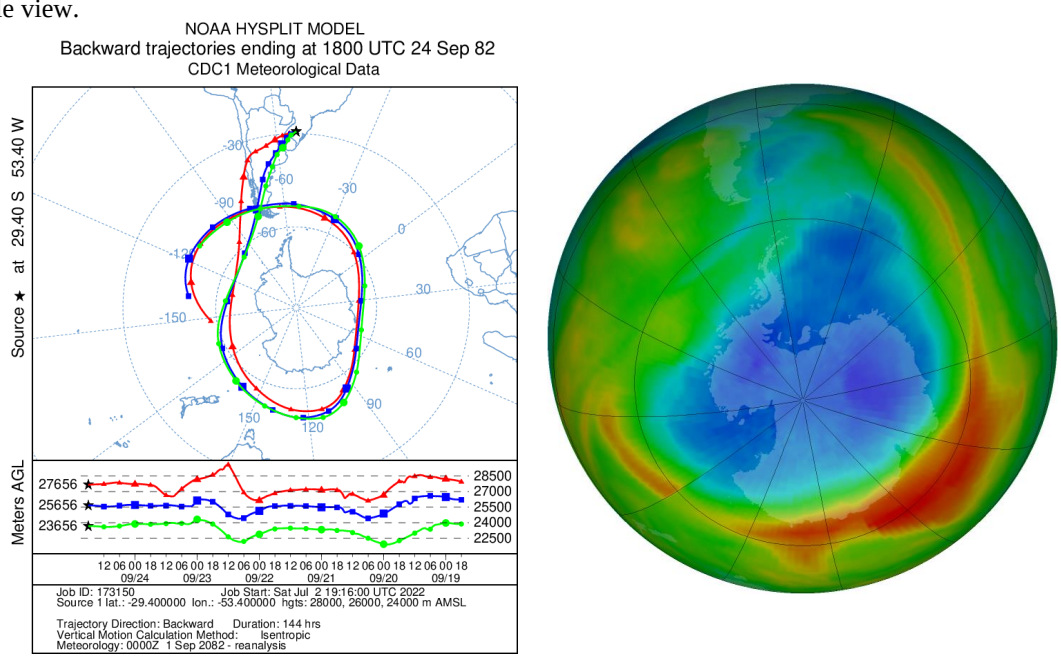

Source: HYSPLIT/NOAA, NASA/OZONE WATCH.

Figure A12: Vertical section of the atmosphere between 1000 and 5 hPa for the days of the event in September 1982.

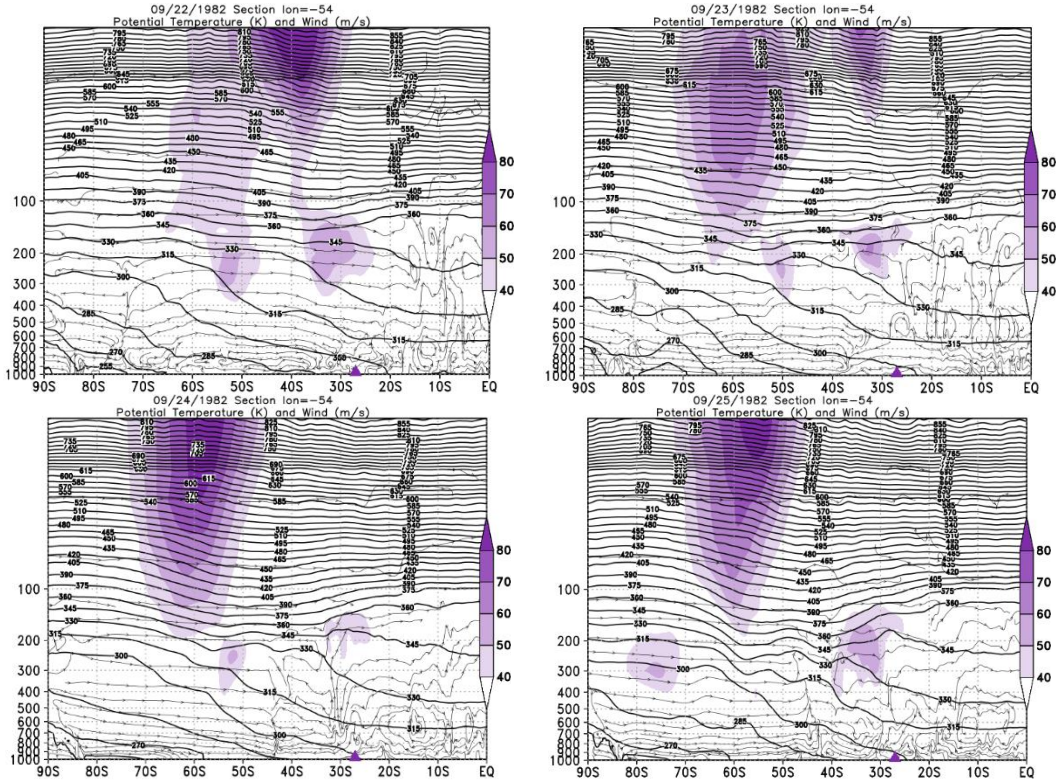

Source: The author.

10/08/1982

Figure A13: PVA fields for the 20 hPa in pressure levels, days 10/07/1982 to 10/09/1982.

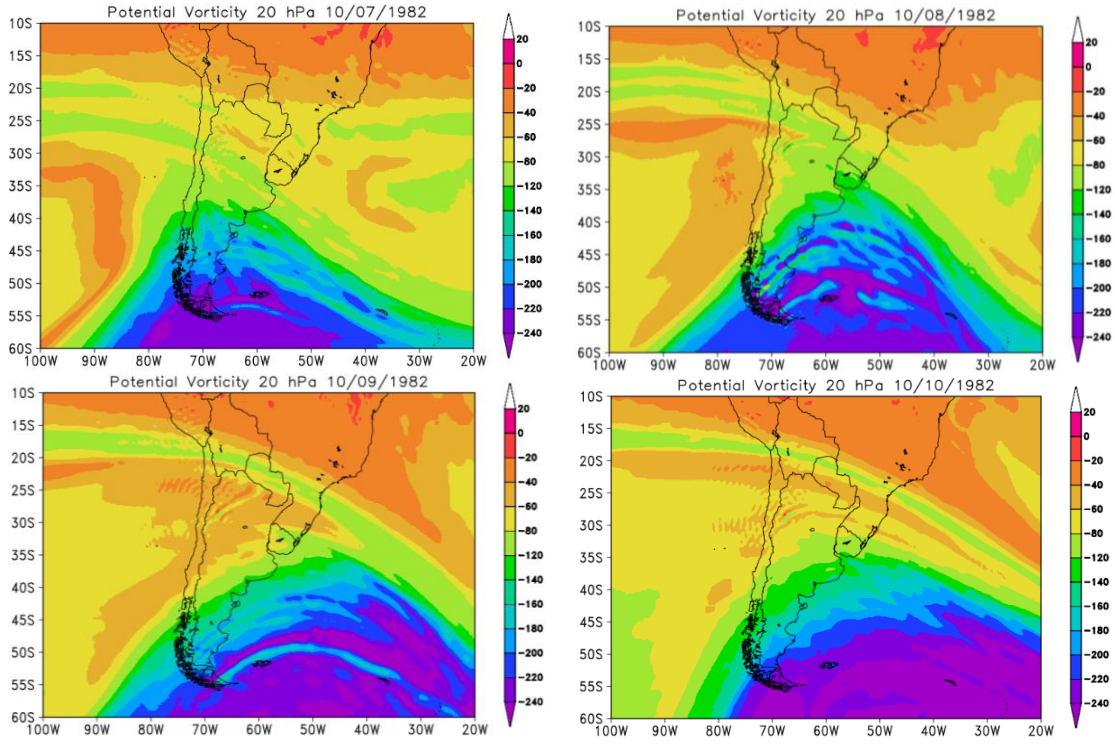

Source: The author.

Figure A14: a) Retroactive trajectory by the HYSPLIT/NOAA model, b) O3 content OMI satellite for South Pole view.

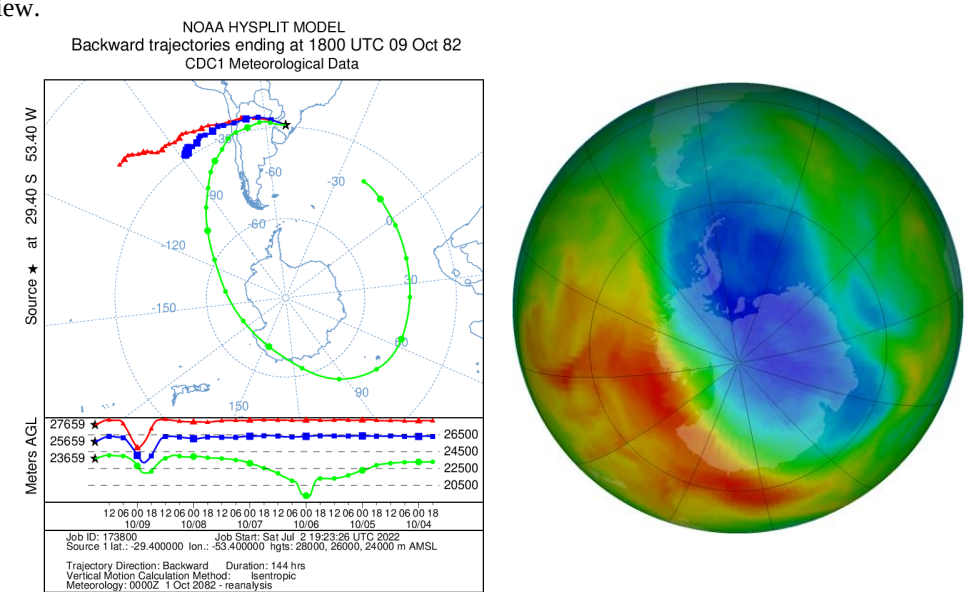

Source: HYSPLIT/NOAA, NASA/OZONE WATCH.

Figure A15: Vertical section of the atmosphere between 1000 and 5 hPa for the days of the event in October 1982.

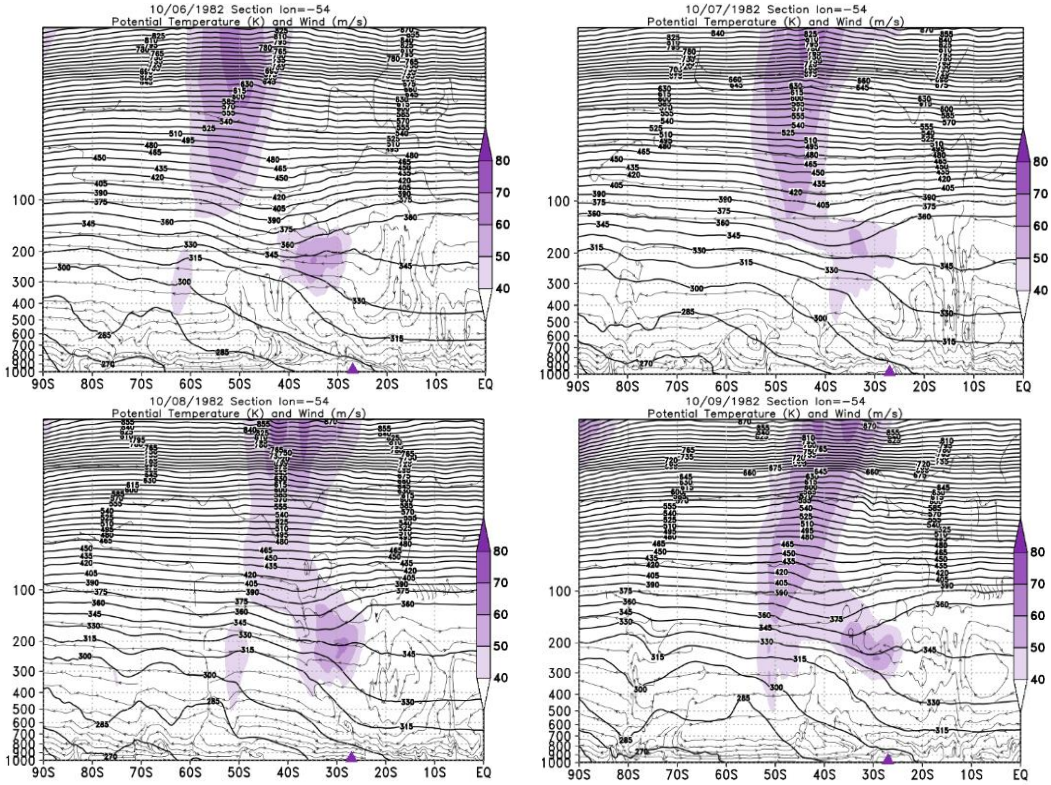

Source: The author.

10/15/1982

Figure A16: PVA fields for the 20 hPa in pressure levels, days 10/13/1982 to 10/15/1982.

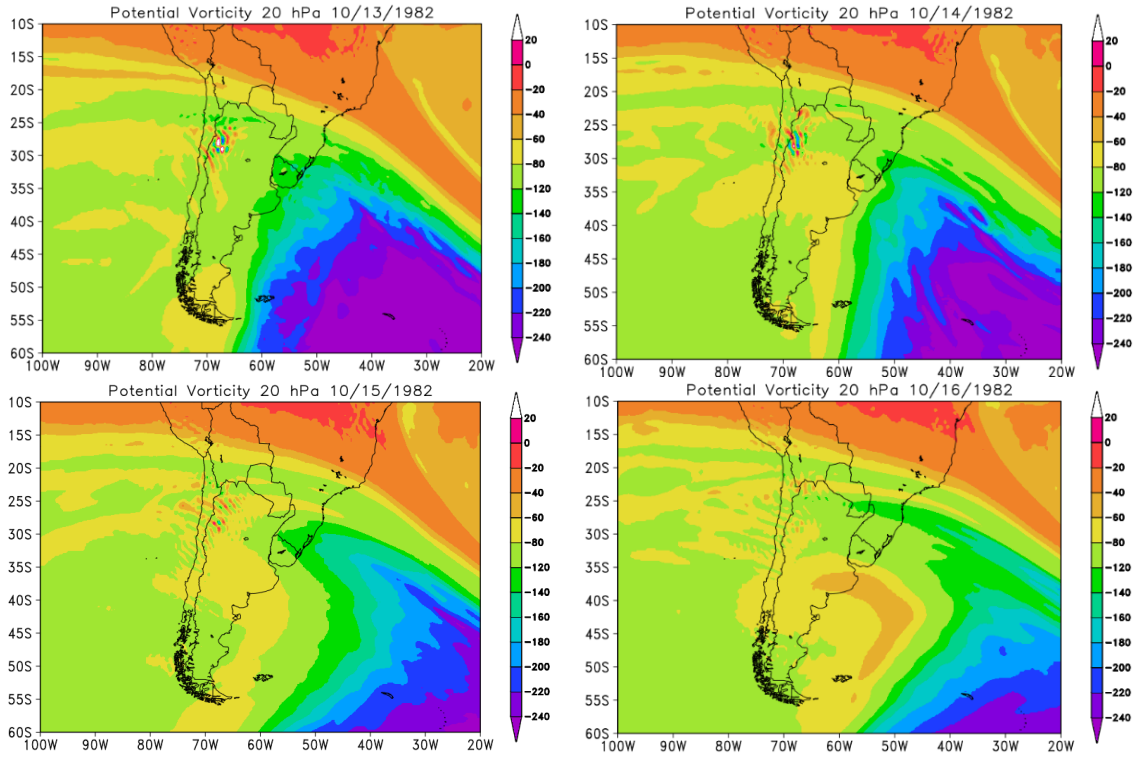

Source: The author.

Figure A17: a) Retroactive trajectory by the HYSPLIT/NOAA model, b) O3 content OMI satellite for South Pole view.

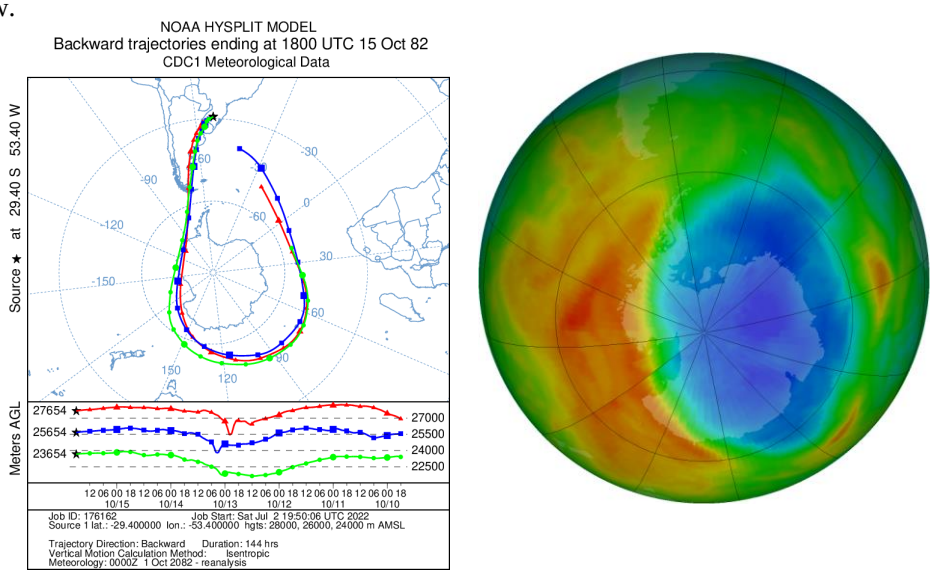

Source: HYSPLIT/NOAA, NASA/OZONE WATCH.

Figure A18: Vertical section of the atmosphere between 1000 and 5 hPa for the days of the event in October 1982.

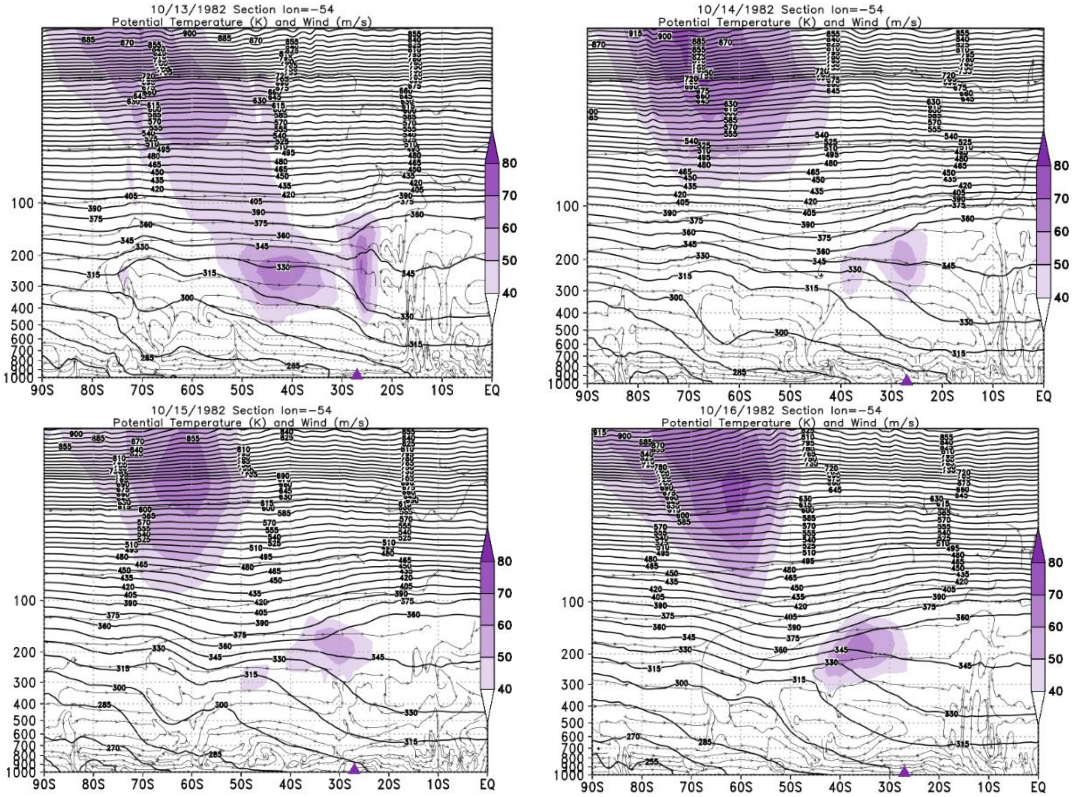

Source: The author.

09/30/1983

Figure A19: PVA fields for the 20 hPa in pressure levels, days 09/28/1983 to 10/01/1983.

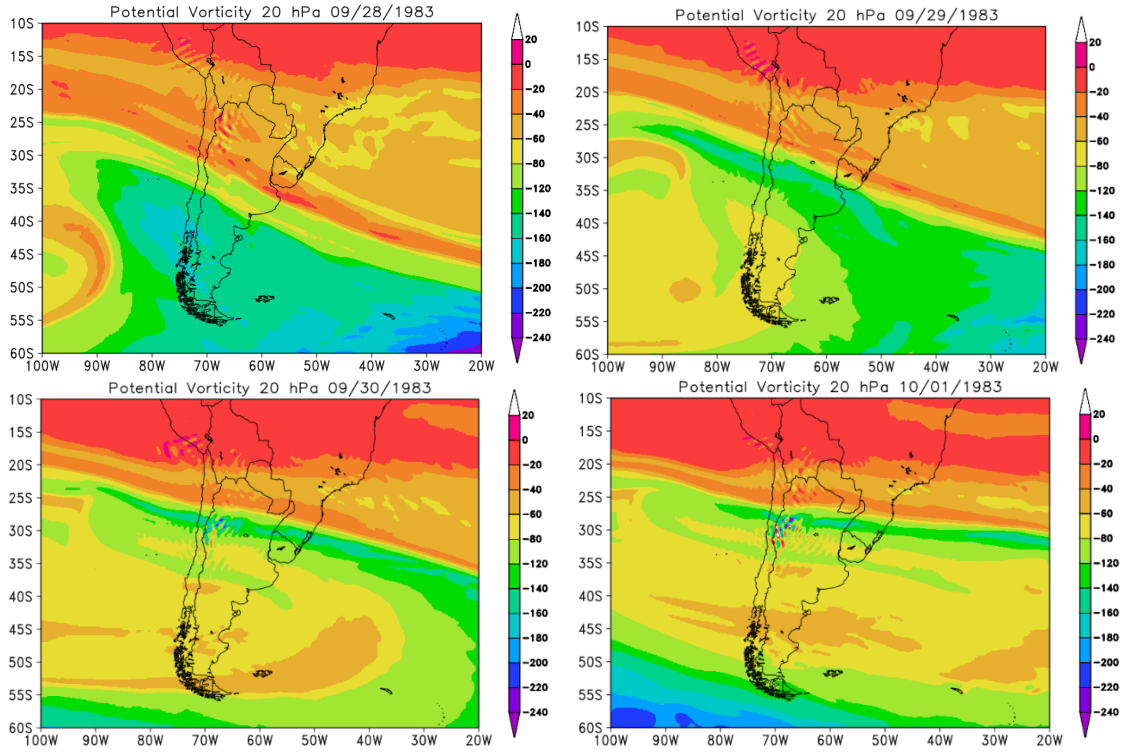

Source: The author.

Figure A20: a) Retroactive trajectory by the HYSPLIT/NOAA model, b) O3 content OMI satellite for South Pole view.

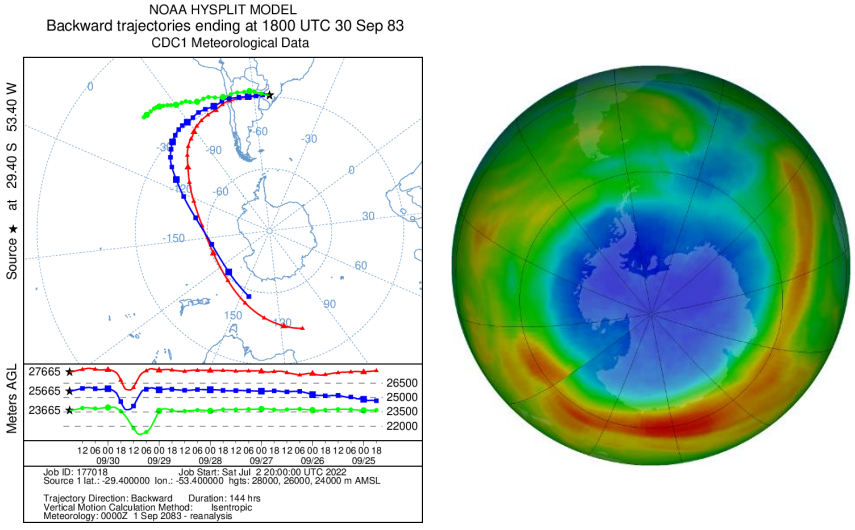

Source: HYSPLIT/NOAA, NASA/OZONE WATCH.

Figure A21: Vertical section of the atmosphere between 1000 and 5 hPa for the days of the event in September 1983.

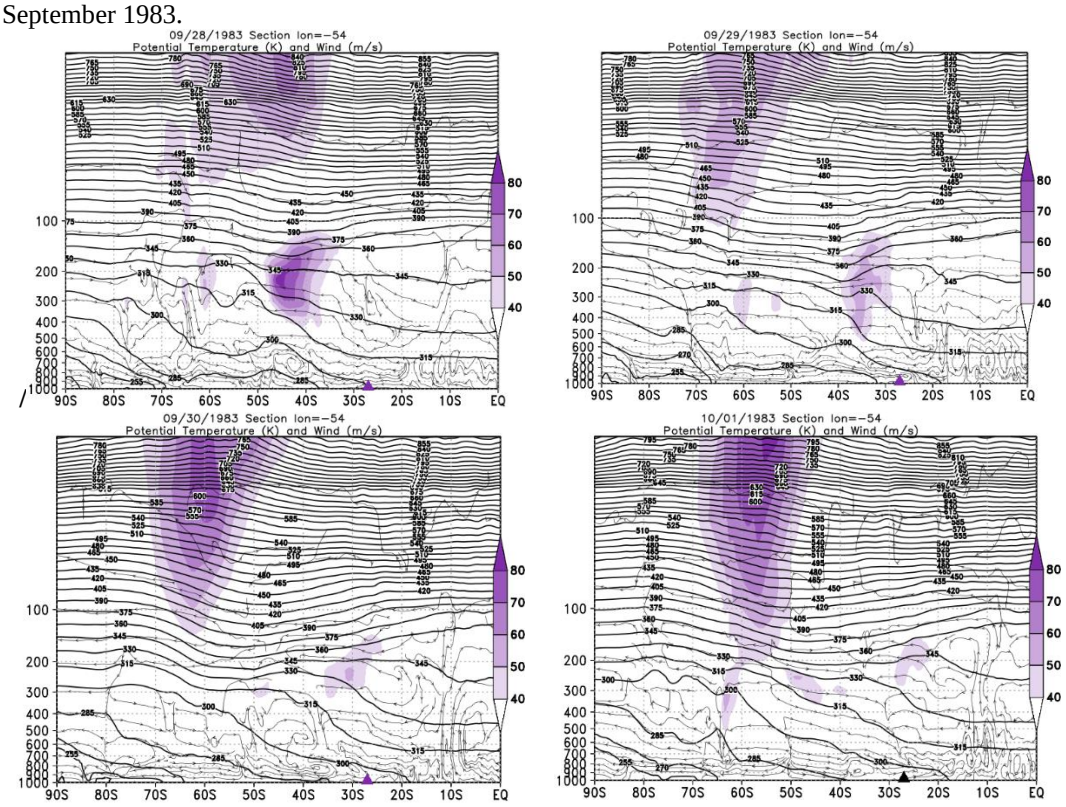

Source: The author.

10/14/1983

Figure A22: PVA fields for the 20 hPa in pressure levels, days 10/12/1983 to 10/15/1983.

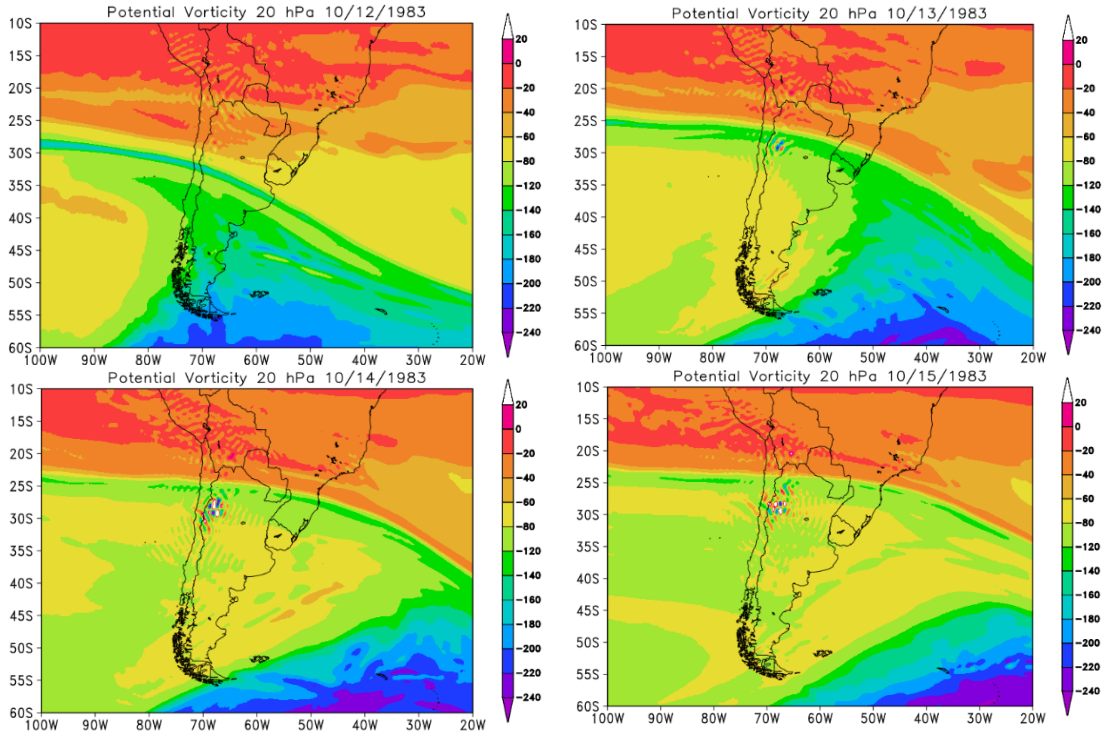

Source: The author.

Figure A23: a) Retroactive trajectory by the HYSPLIT/NOAA model, b) O3 content OMI satellite for South Pole view.

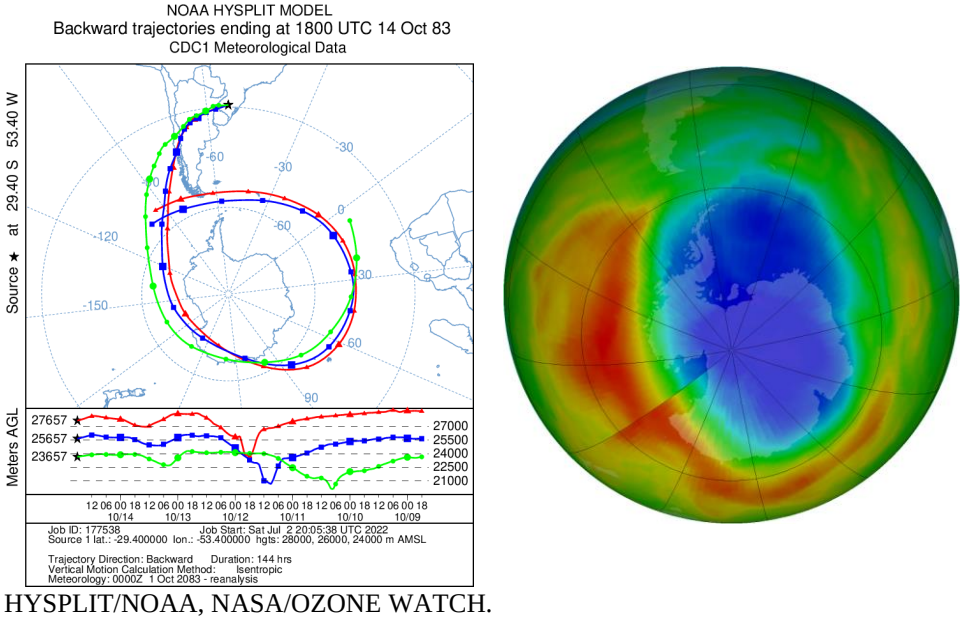

Source: HYSPLIT/NOAA, NASA/OZONE WATCH.

Figure A24: Vertical section of the atmosphere between 1000 and 5 hPa for the days of the event in October 2016.

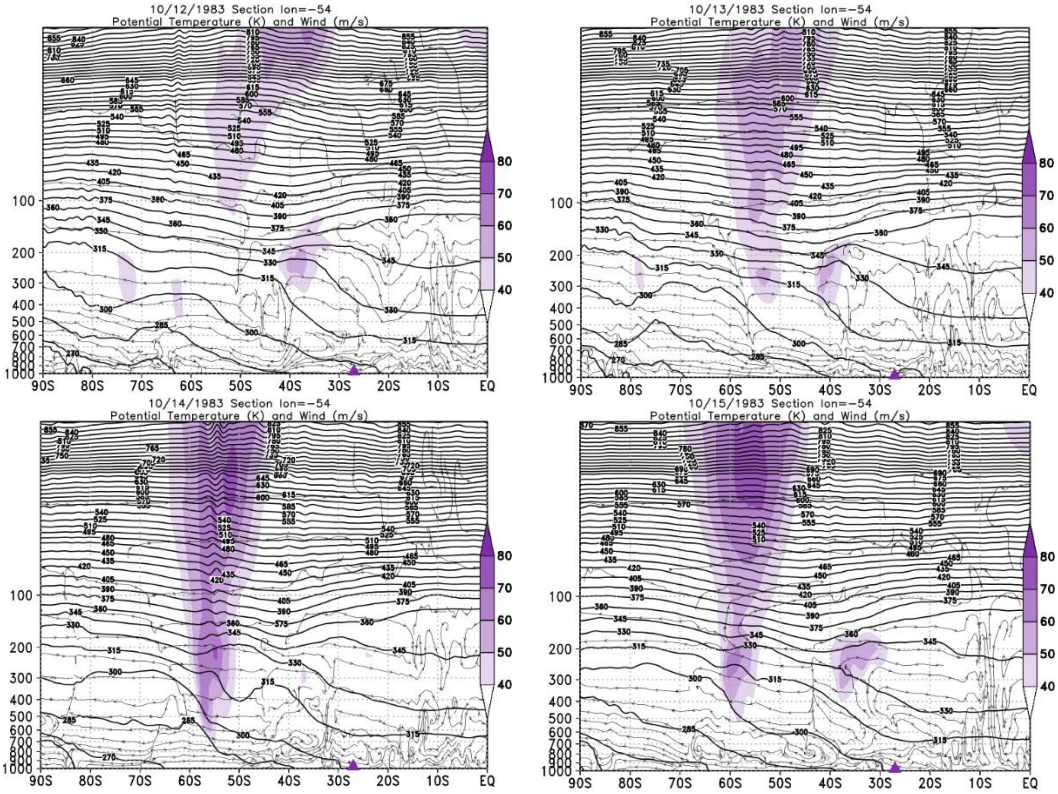

Source: The author.

10/16/1984

Figure A25: PVA fields for the 20 hPa in pressure levels, days 10/14/1984 to 10/17/1984.

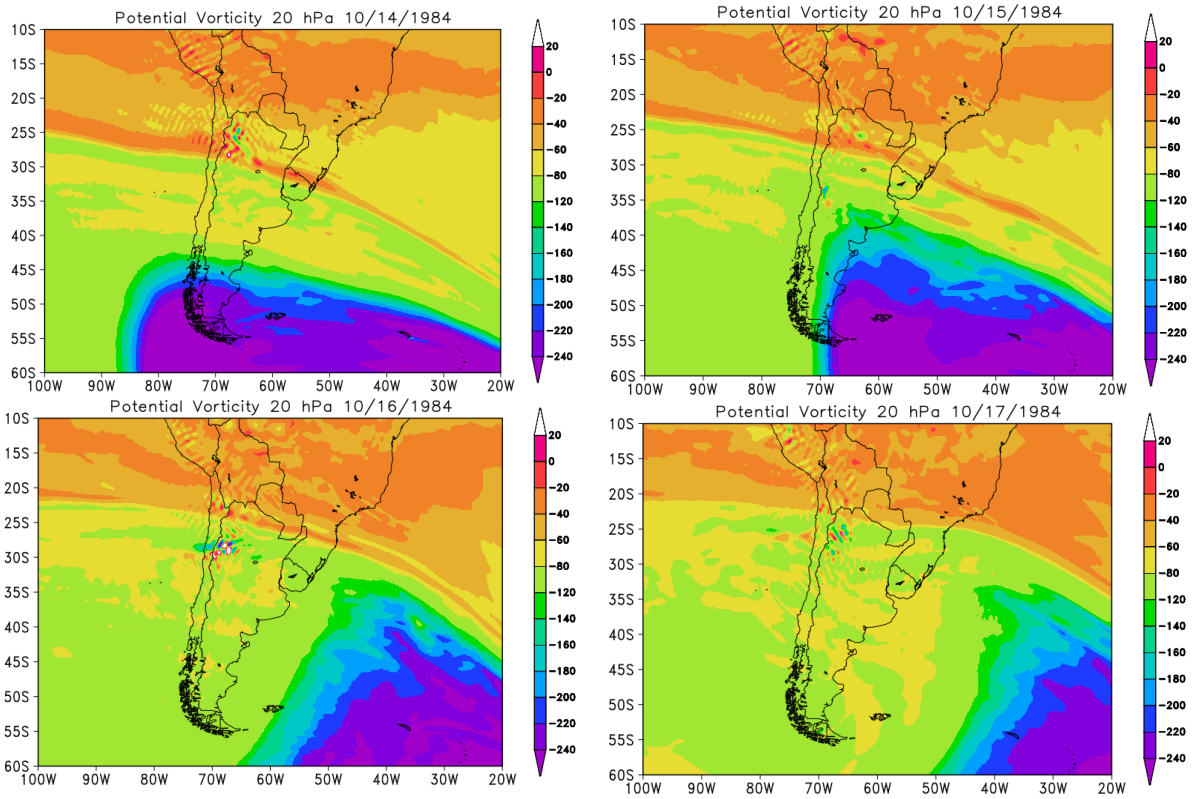

Source: The author.

Figure A26: a) Retroactive trajectory by the HYSPLIT/NOAA model, b) O3 content OMI satellite for South Pole view.

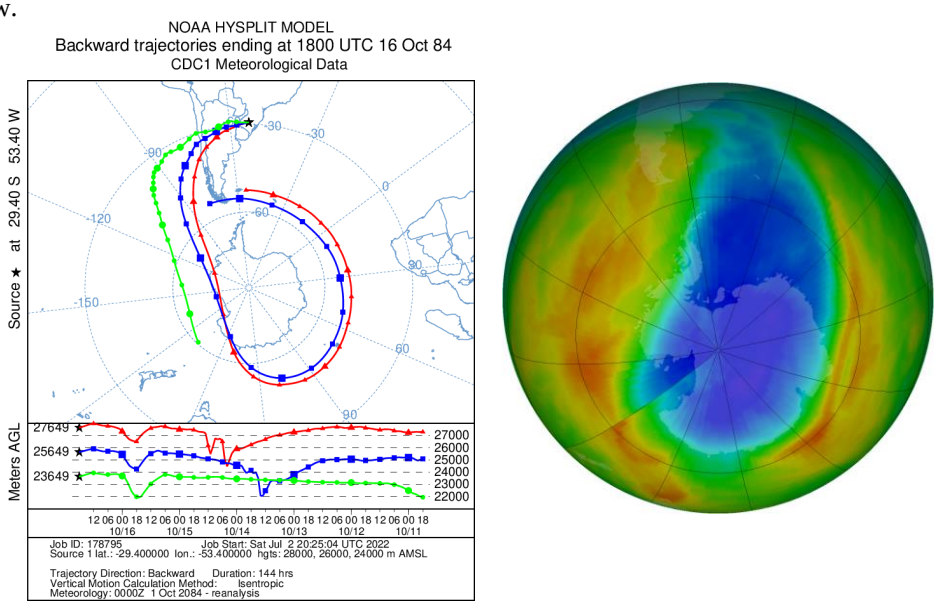

Source: HYSPLIT/NOAA, NASA/OZONE WATCH.

Figure A27: Vertical section of the atmosphere between 1000 and 5 hPa for the days of the event in October 1984.

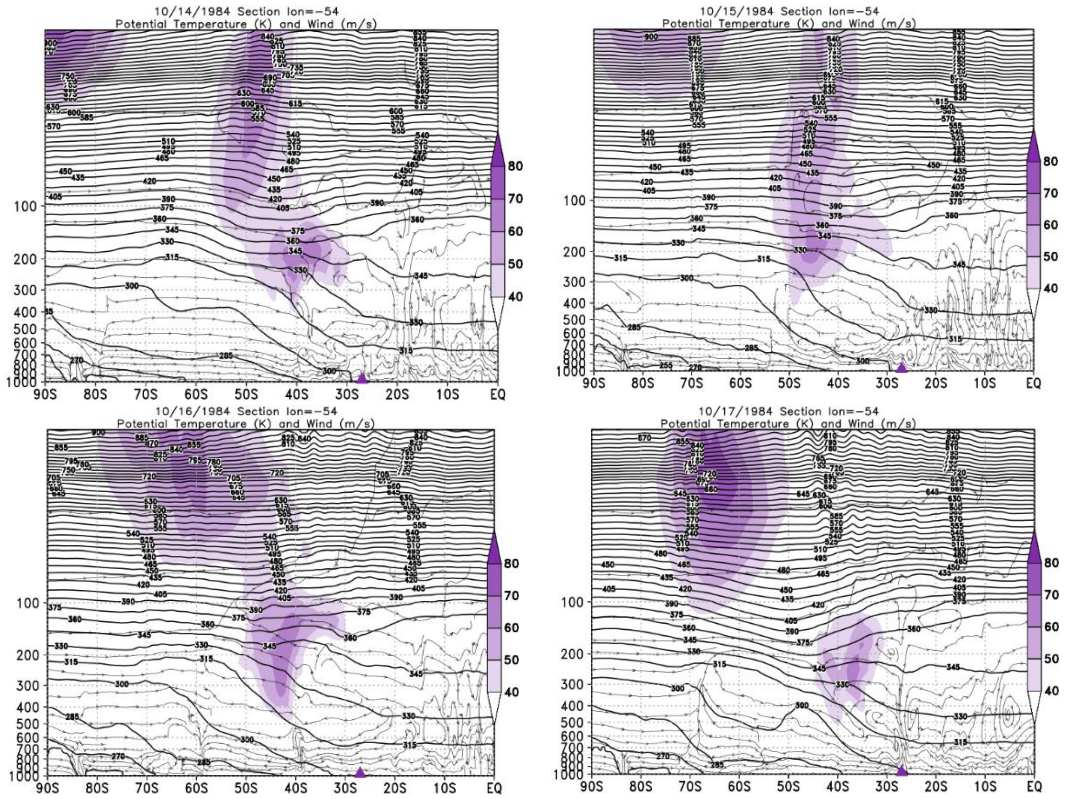

Source: The author.

11/05/1984

Figure A28: PVA fields for the 20 hPa in pressure levels, days 11/03/1984 to 11/06/1984.

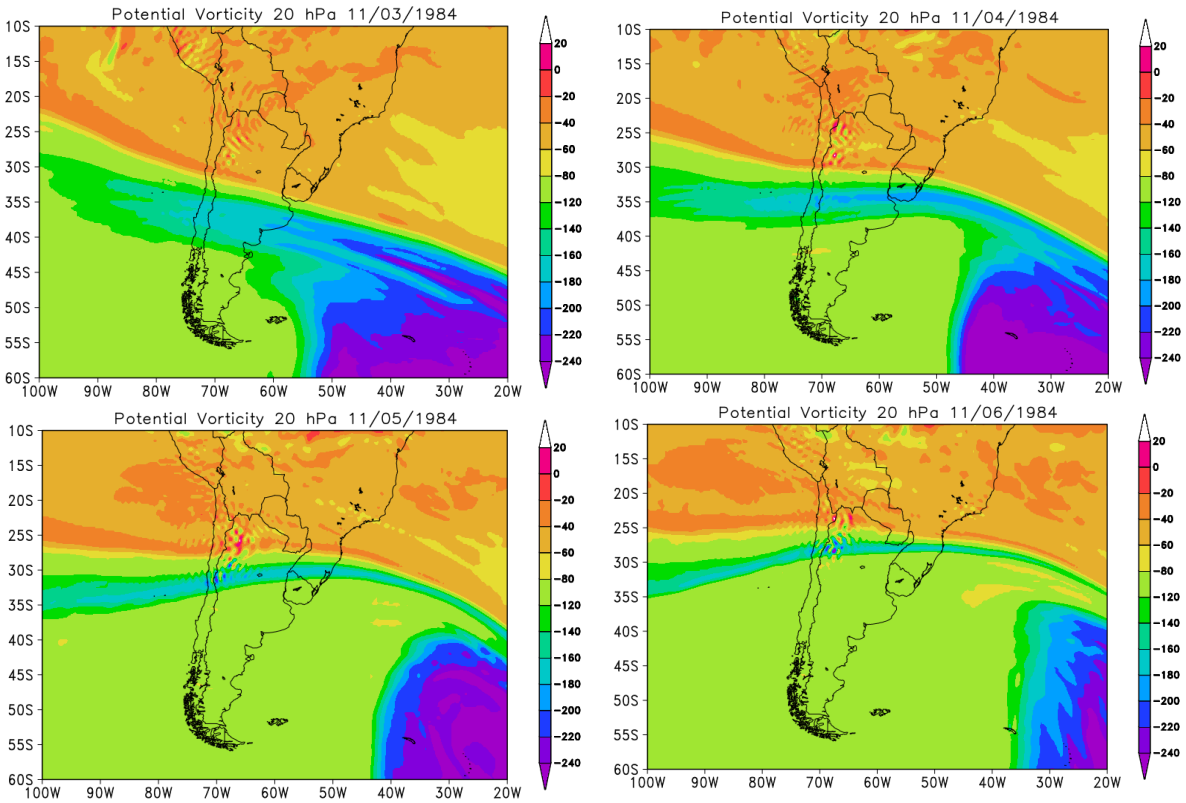

Source: The author.

Figure A29: O3 content NASA satellite for South Pole view in 11/05/1984.

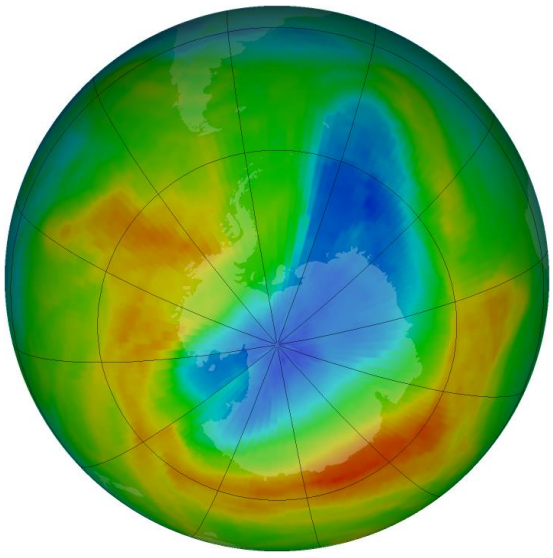

Source: NASA/OZONE WATCH.

Figure A30: Vertical section of the atmosphere between 1000 and 5 hPa for the days of the event in October 2016

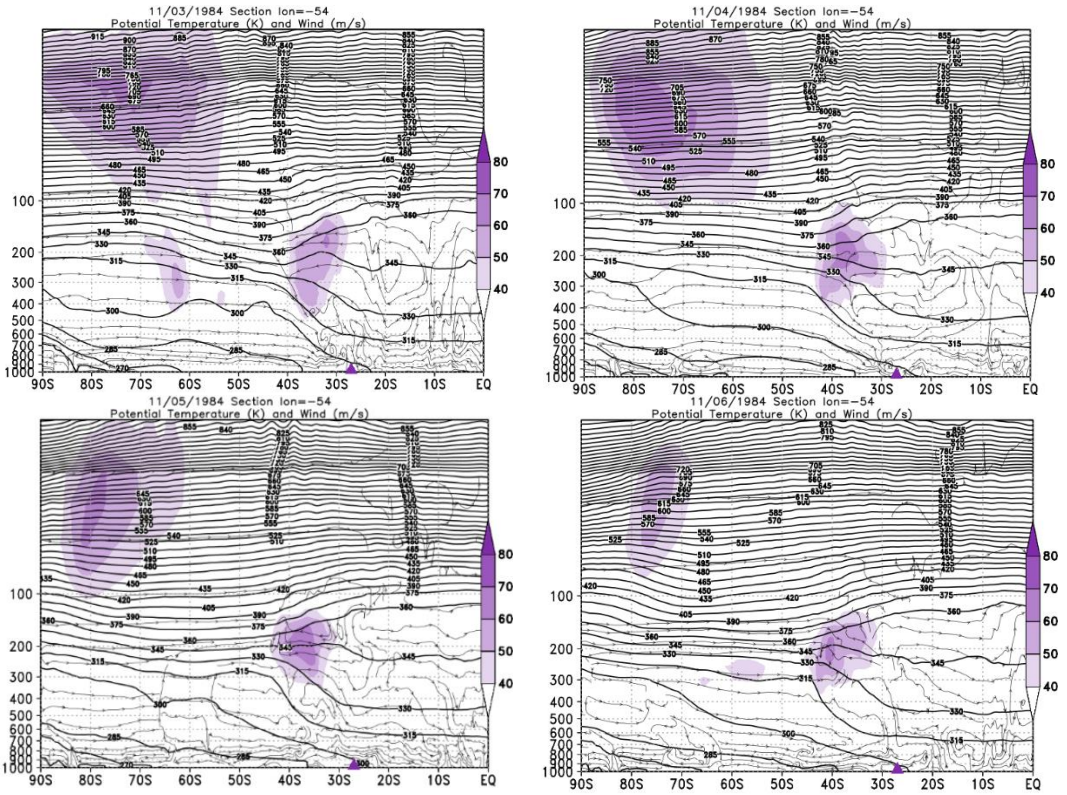

Source: The author.

08/09/1985

Figure A31: PVA fields for the 20 hPa in pressure levels, days 08/07/1985 to 08/10/1985.

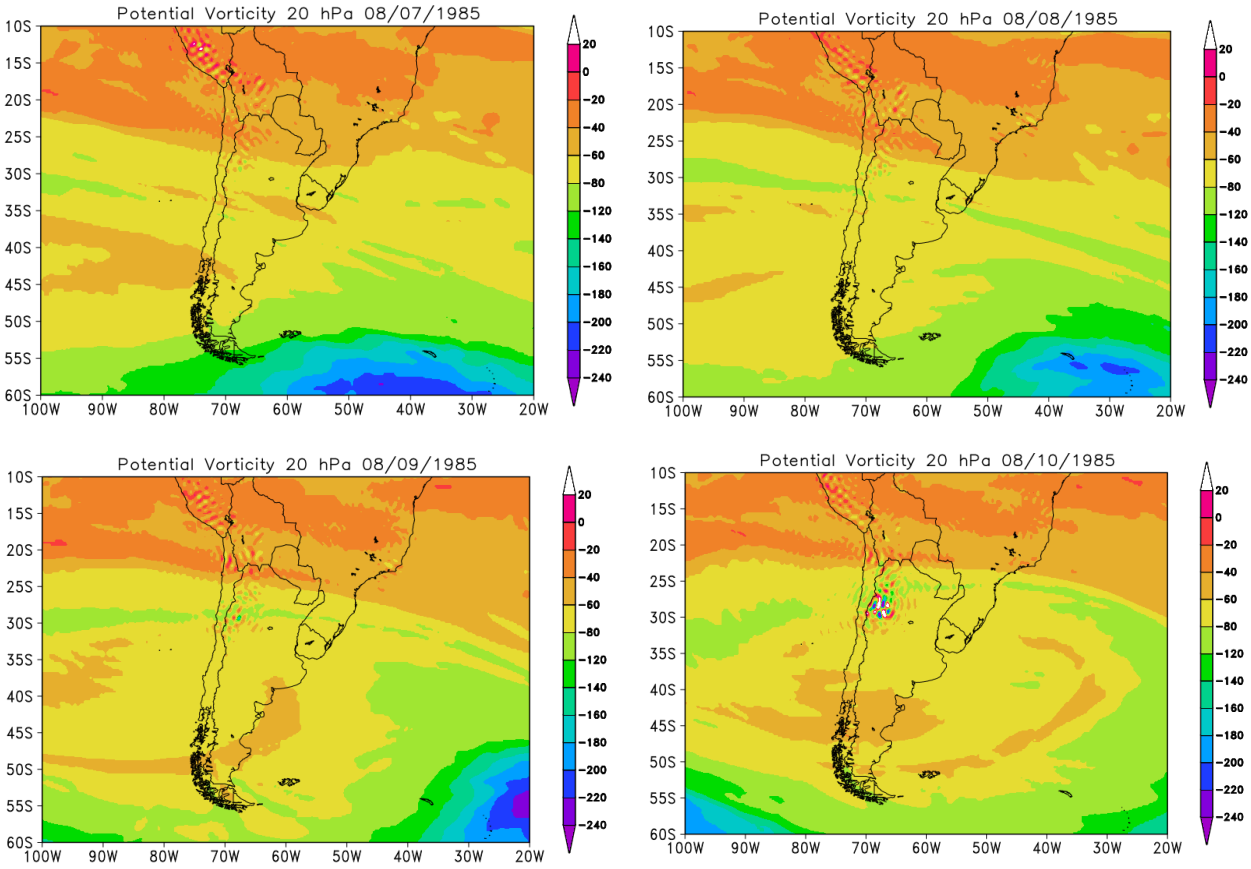

Source: The author.

Figure A32: a) Retroactive trajectory by the HYSPLIT/NOAA model, b) O3 content OMI satellite for South Pole, and global view.

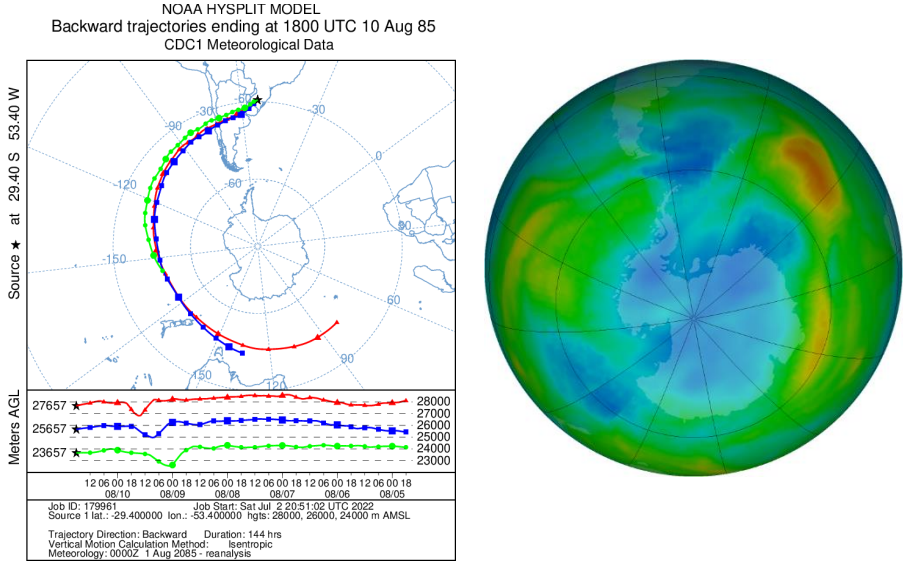

Source: HYSPLIT/NOAA, NASA/OZONE WATCH.

Figure A33: Vertical section of the atmosphere between 1000 and 5 hPa for the days of the event in August 1985.

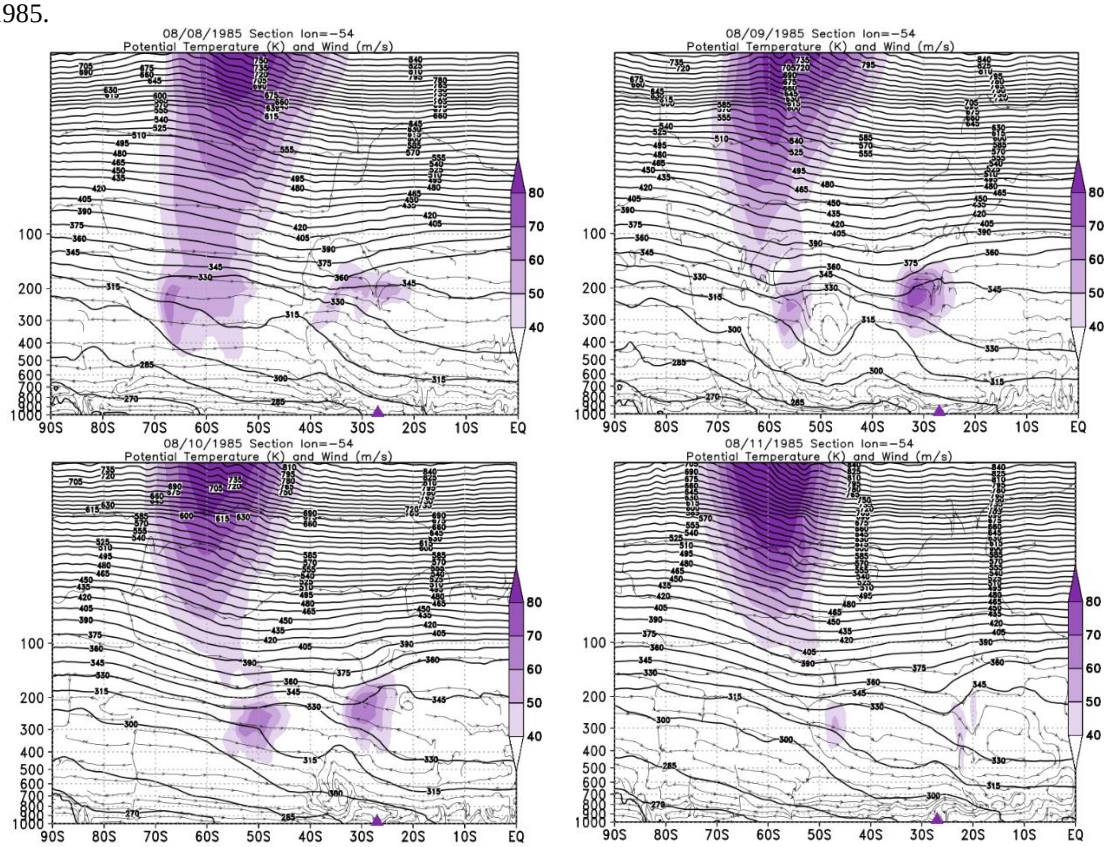

Source: The author.

08/23/1985

Figure A34: PVA fields for the 20 hPa in pressure levels, days 08/21/1985 to 08/24/1985.

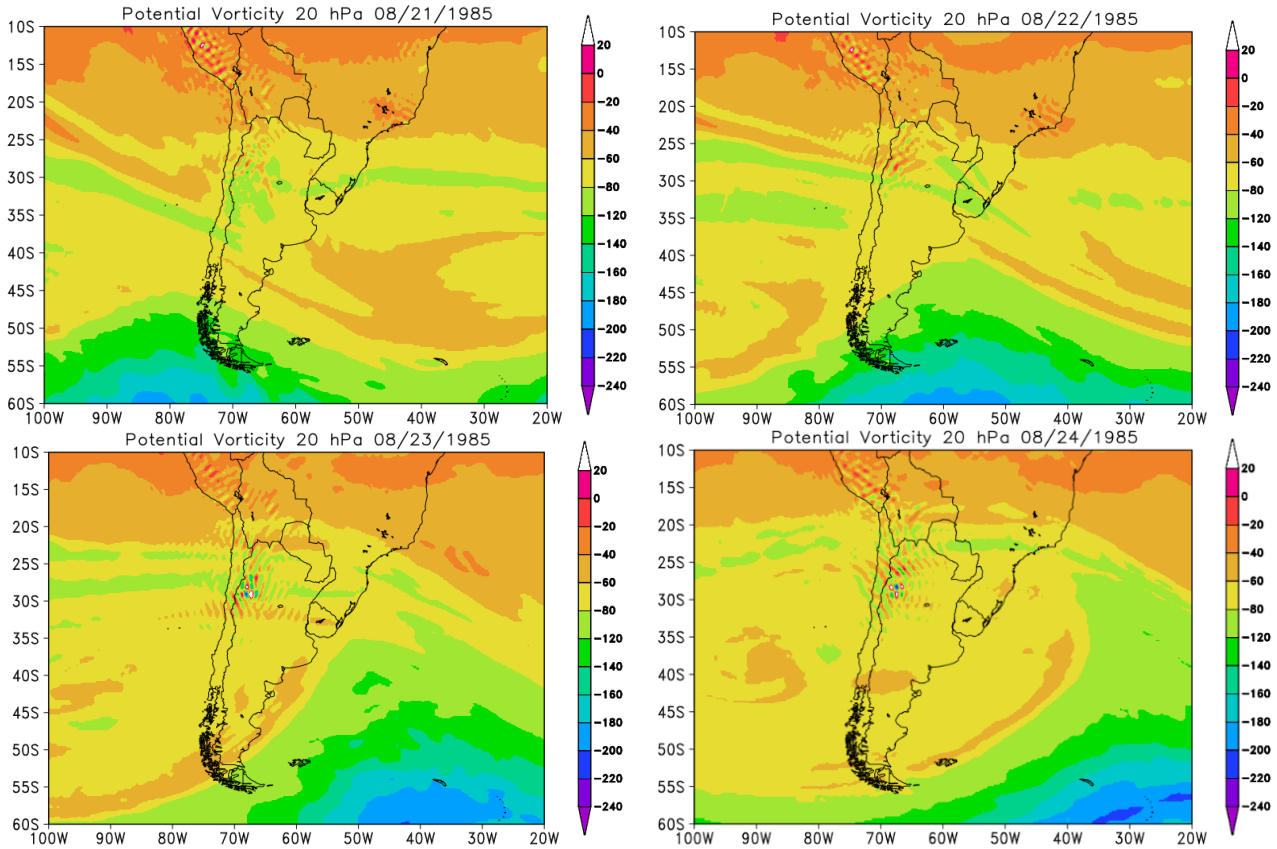

Source: The author.

Figure A35: a) Retroactive trajectory by the HYSPLIT/NOAA model, b) O3 content OMI satellite for South Pole view.

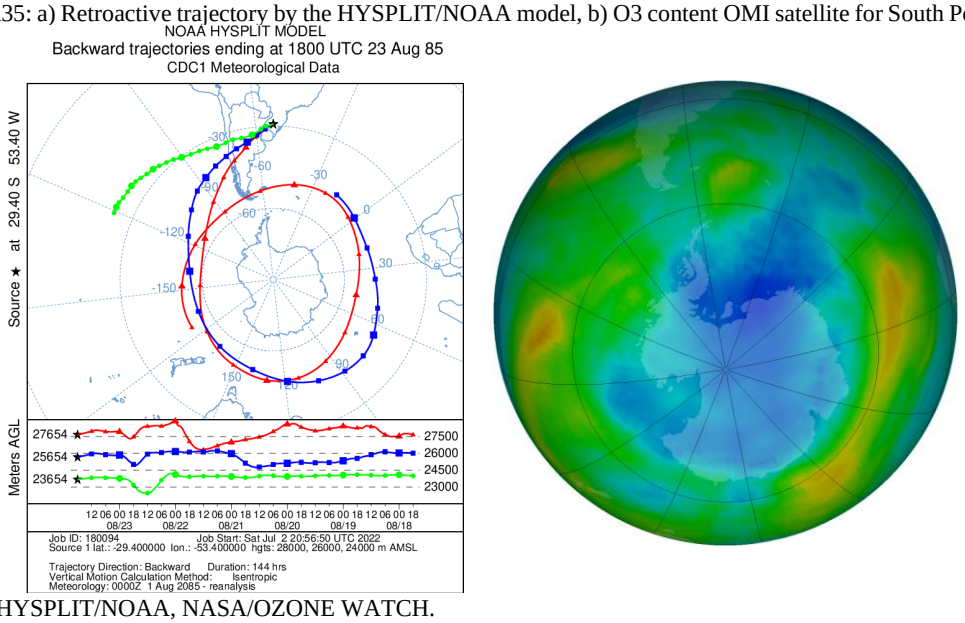

Source: HYSPLIT/NOAA, NASA/OZONE WATCH.

Figure A35: Vertical section of the atmosphere between 1000 and 5 hPa for the days of the event in August 1985.

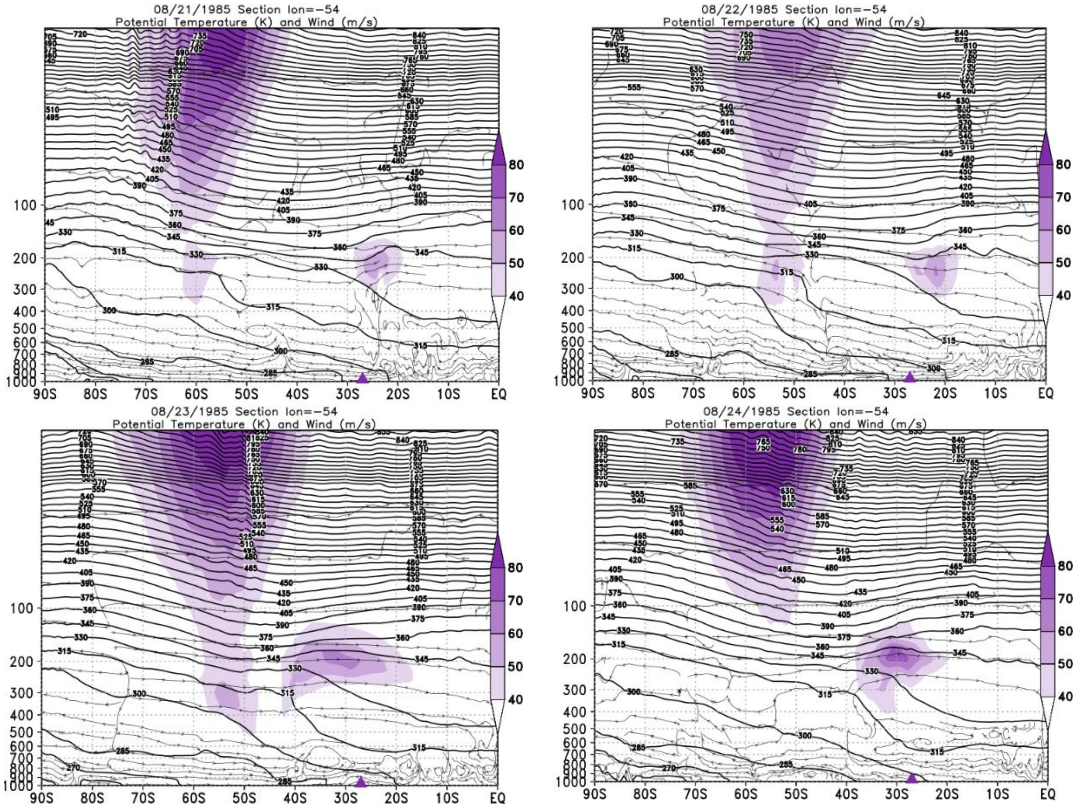

Source: The author.

09/03/1985

Figure A36: PVA fields for the 20 hPa in pressure levels, days 09/01/1985 to 09/04/1985

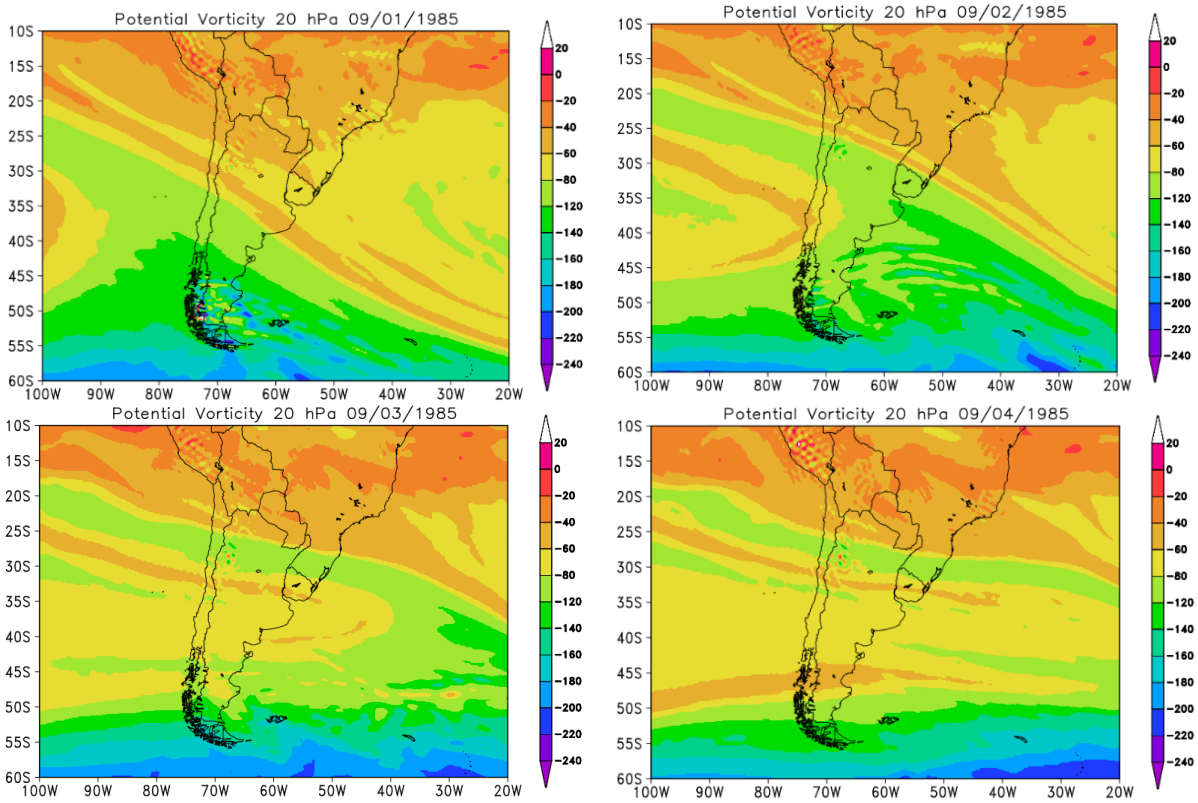

Source: The author.

Figure A37: a) Retroactive trajectory by the HYSPLIT/NOAA model, b) O3 content OMI satellite for South Pole view.

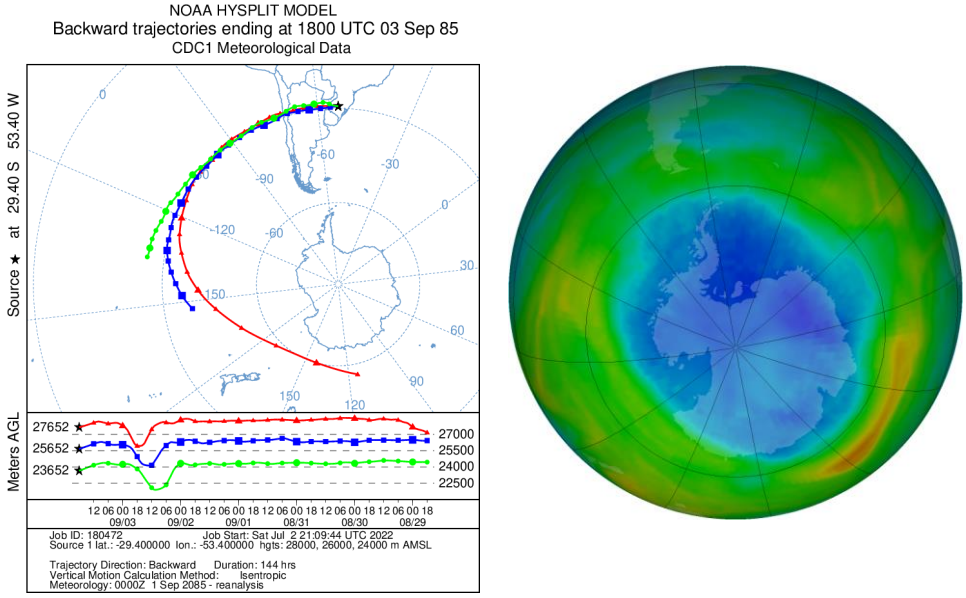

Source: HYSPLIT/NOAA, OZONE WATCH/NASA.

Figure A38: Vertical section of the atmosphere between 1000 and 5 hPa for the days of the event in September 1985.

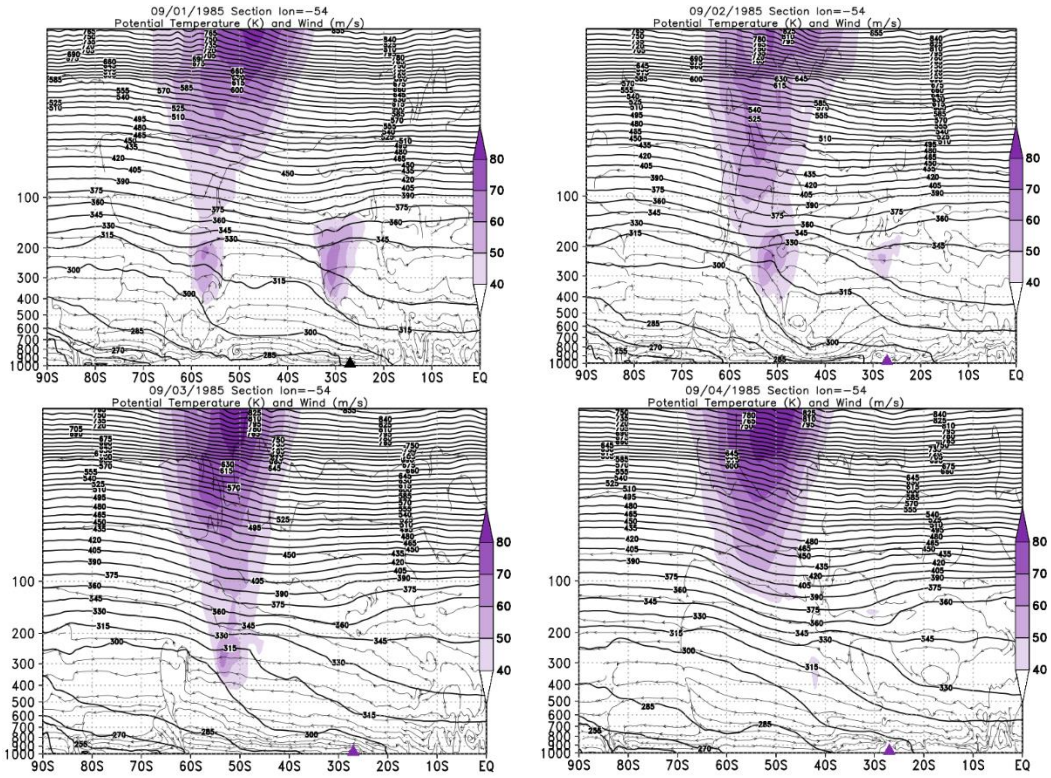

Source: The author.

10/15/1985

Figure A39: PVA fields for the 20 hPa in pressure levels, days 10/13/1985 to 10/16/1985.

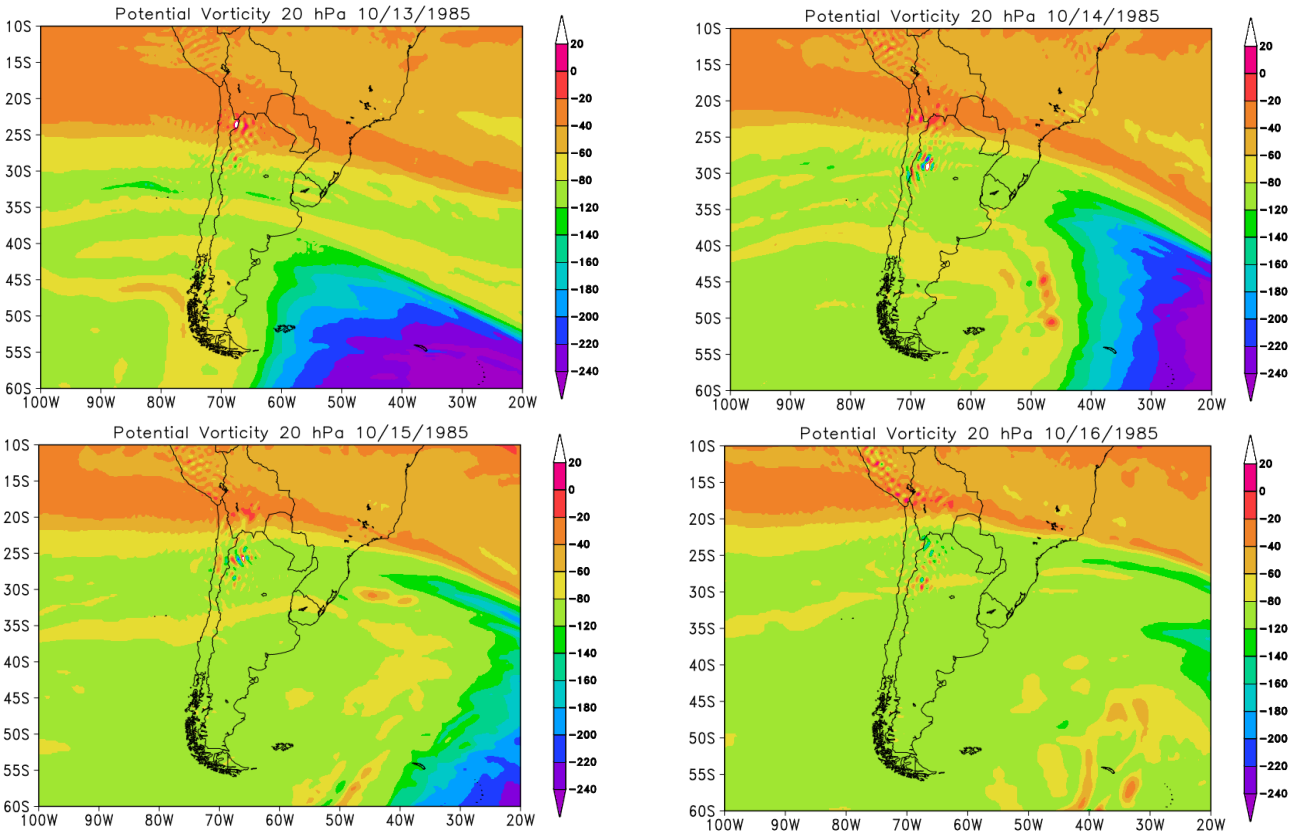

Source: The author.

Figure A40: a) Retroactive trajectory by the HYSPLIT/NOAA model, b) O3 content OMI satellite for South Pole view.

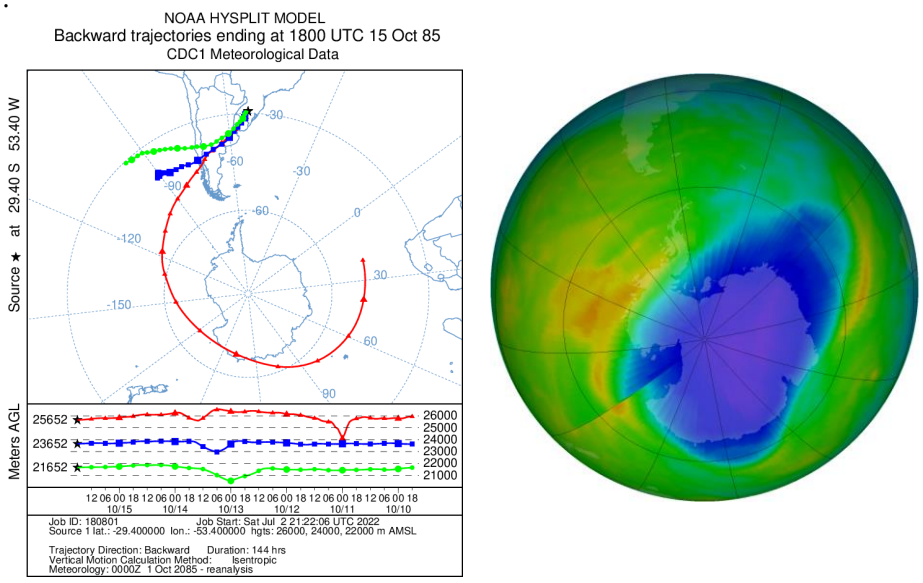

Source: HYSPLIT/NOAA, NASA/OZONE WATCH.
Figure A41: Vertical section of the atmosphere between 1000 and 5 hPa for the days of the event in October 1985.

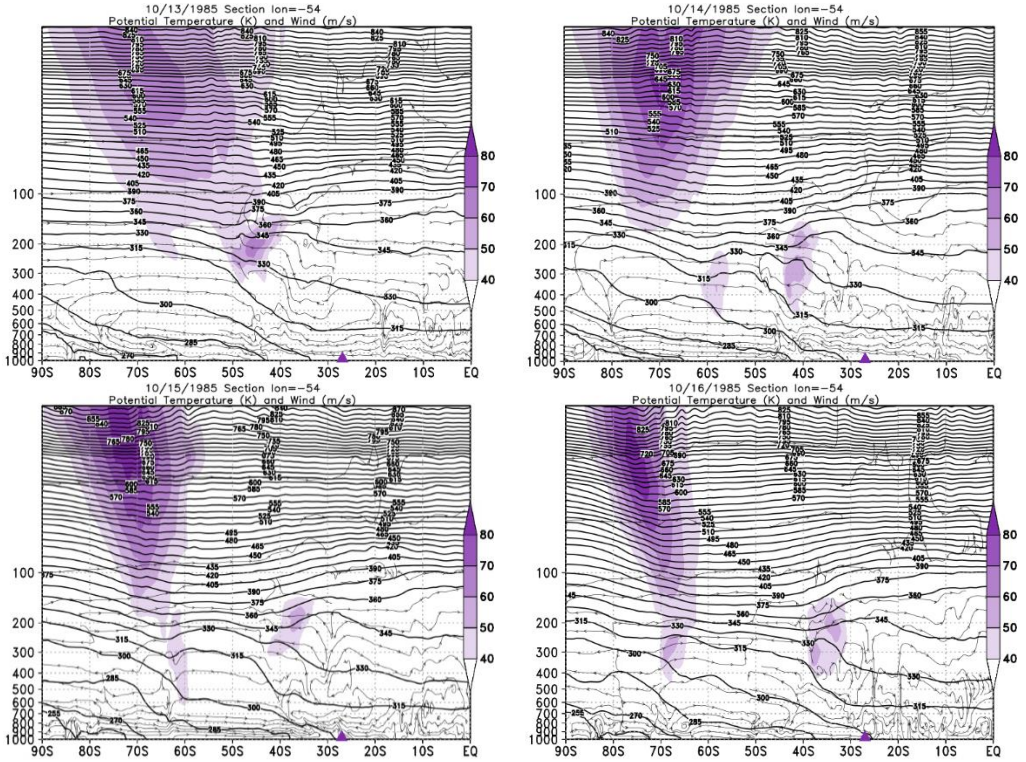

Source: The author.

11/07/1985

Figure A42: PVA fields for the 20 hPa in pressure levels, days 11/05/1985 to 11/08/1985.

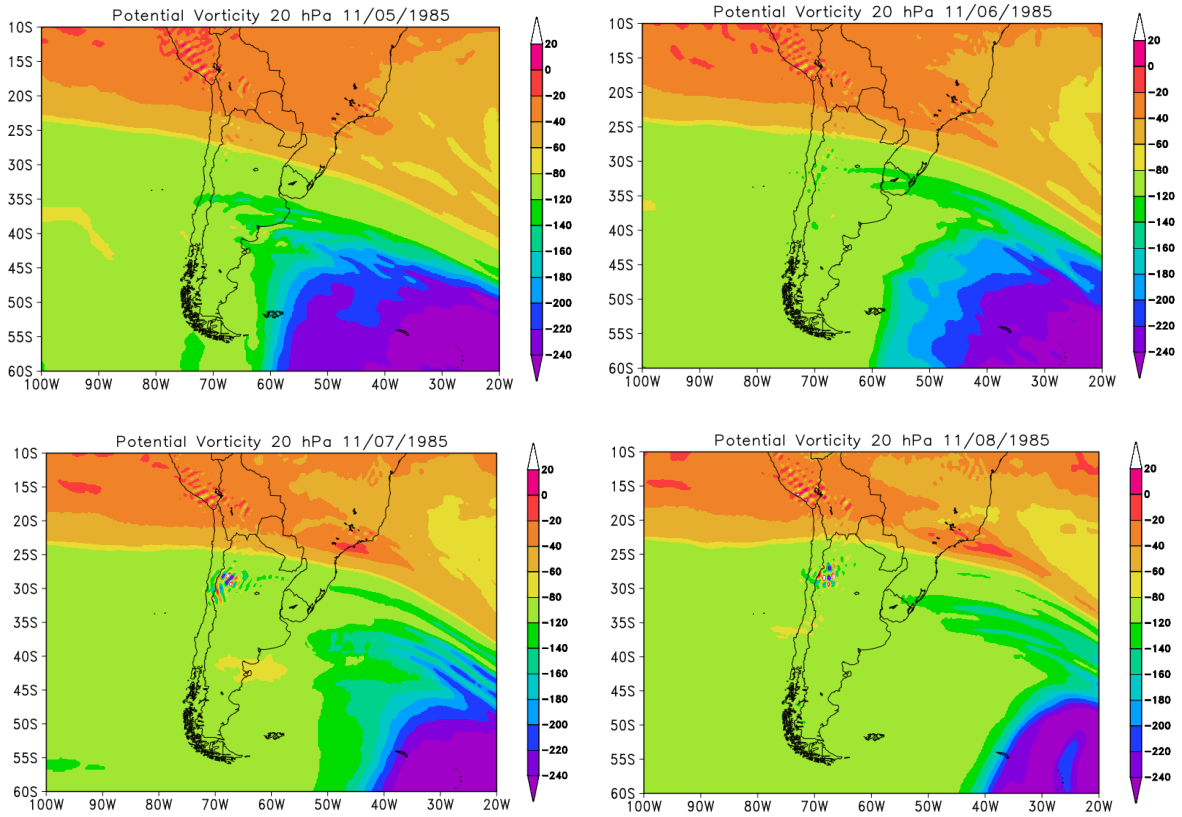

Source: The author.

Figure A43: a) Retroactive trajectory by the HYSPLIT/NOAA model, b) O3 content OMI satellite for South Pole view.

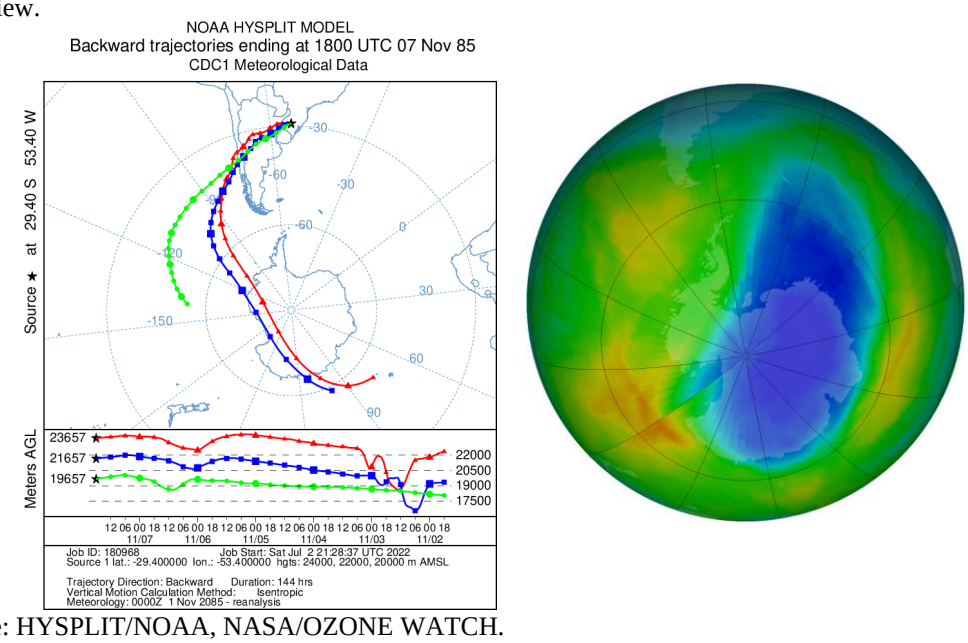

Source: HYSPLIT/NOAA, NASA/OZONE WATCH.

Figure A44: Vertical section of the atmosphere between 1000 and 5 hPa for the days of the event in November 1985.

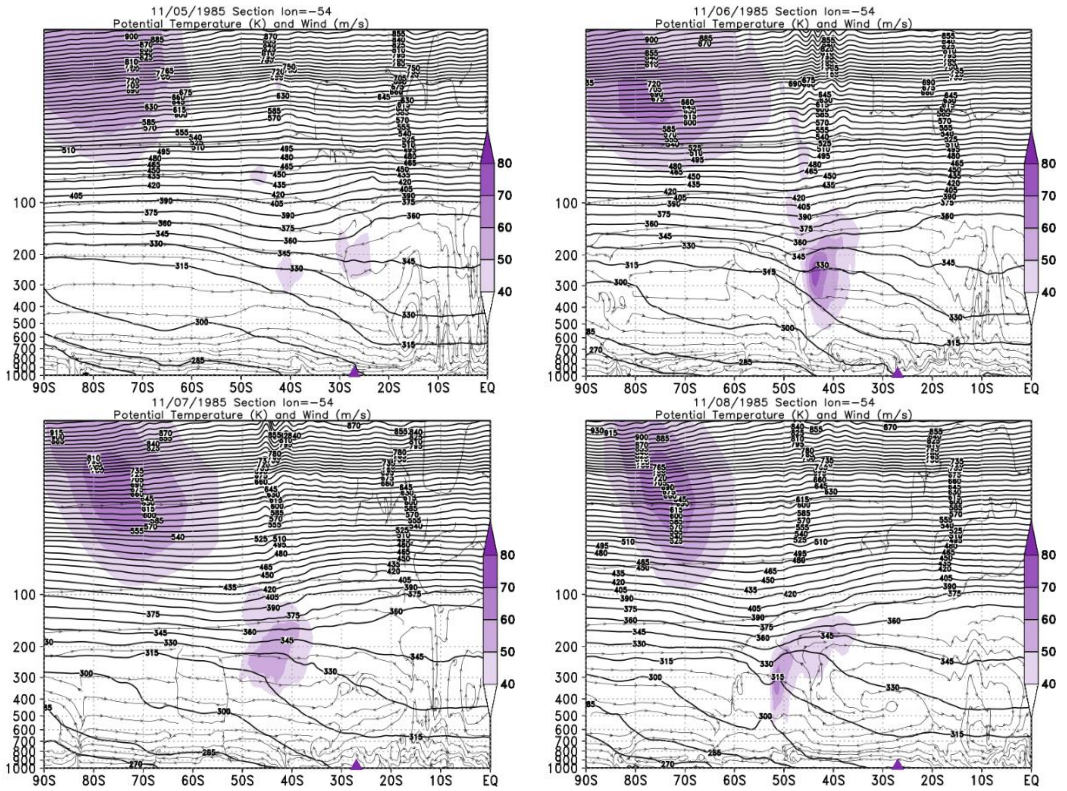

Source: The author.

08/09/1987

Figure A45: PVA fields for the 20 hPa in pressure levels, days 09/27/1979 to 09/30/1979.

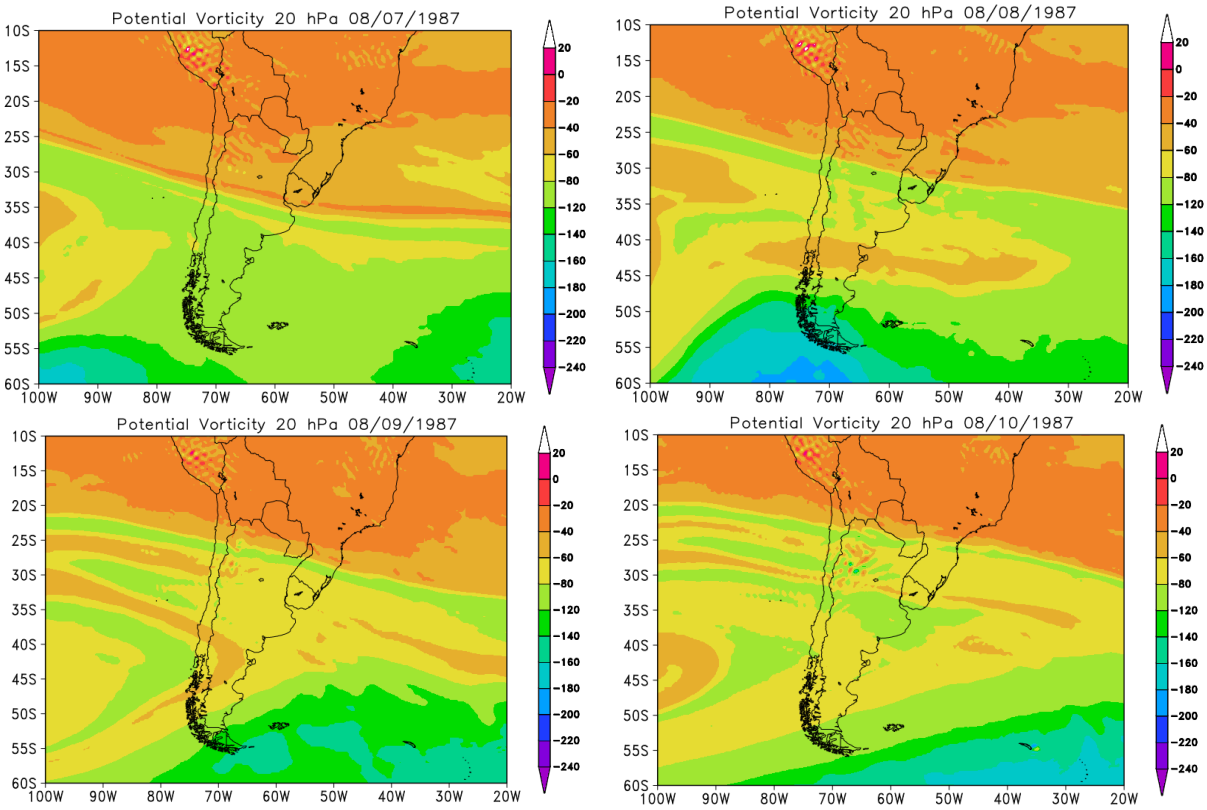

Source: The author.

Figure A46: a) Retroactive trajectory by the HYSPLIT/NOAA model, b) O3 content satellite for South Pole view.

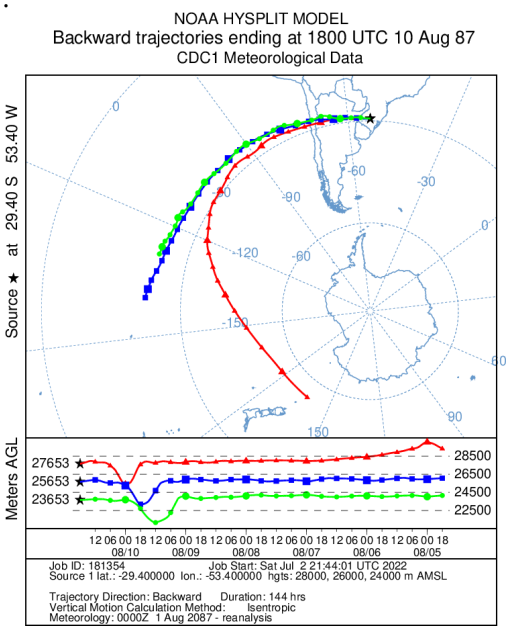

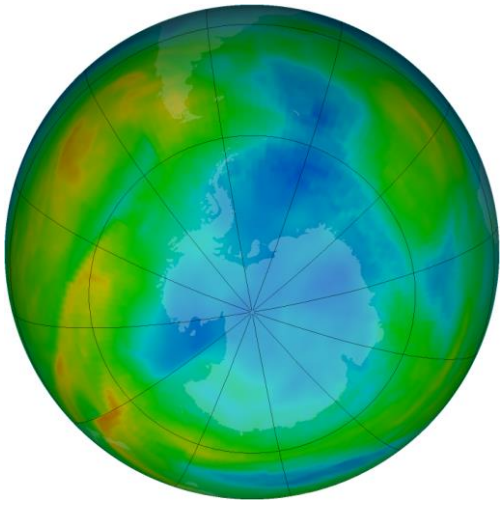

Source: HYSPLIT/NOAA, NASA/OZONE WATCH.

Figure A47: Vertical section of the atmosphere between 1000 and 5 hPa for the days of the event in August 1987.

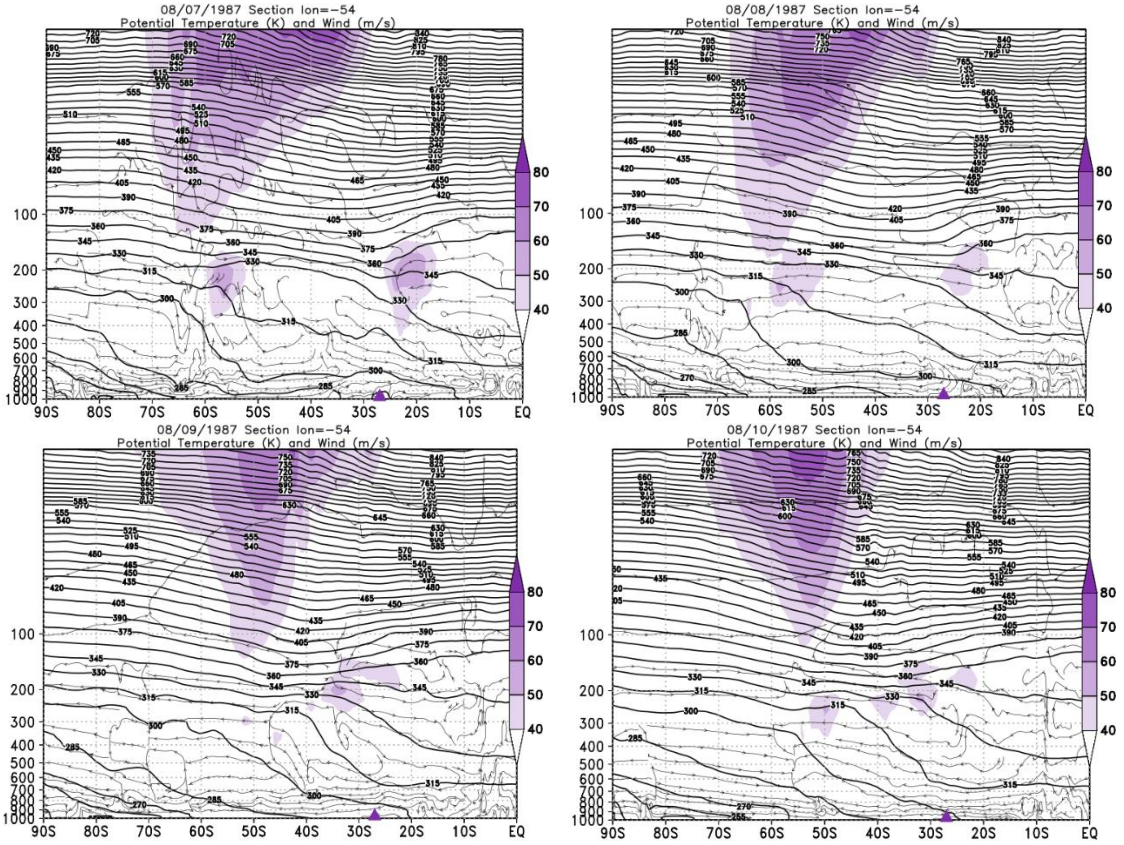

Source: The author.

10/07/1987

Figure A48: PVA fields for the 20 hPa in pressure levels, days 10/05/1987 to 10/08/1987.

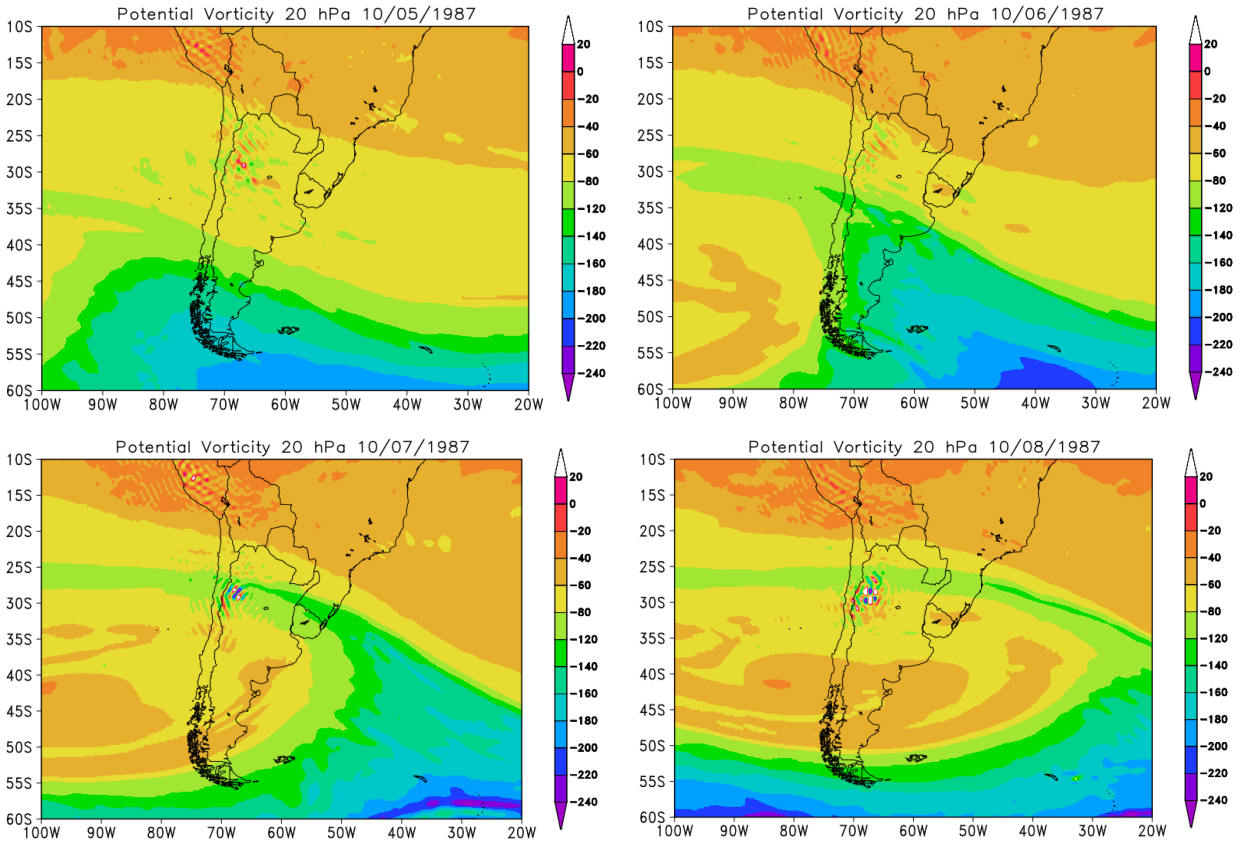

Source: The author.

Figure A49: Retroactive trajectory by the HYSPLIT/NOAA model, and O3 content satellite for South Pole view.

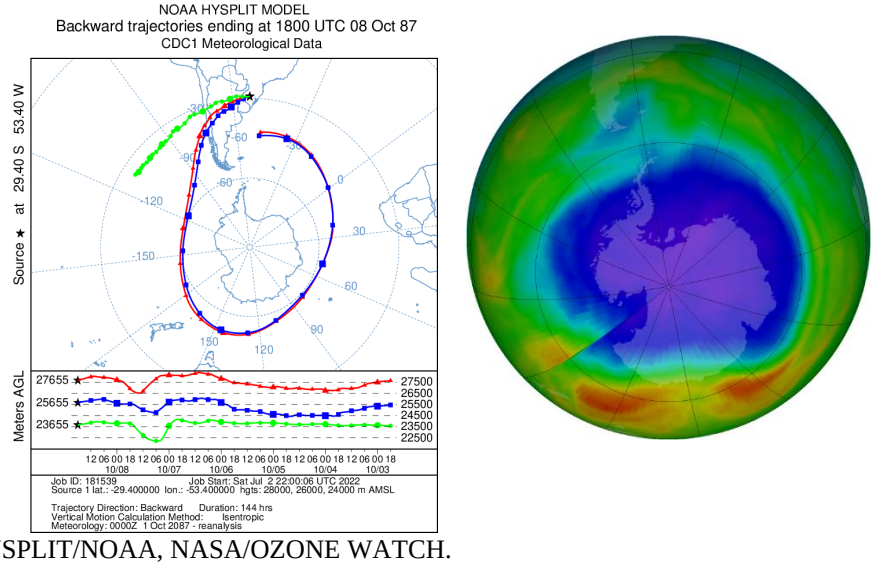

Source: HYSPLIT/NOAA, NASA/OZONE WATCH.

Figure A50: Vertical section of the atmosphere between 1000 and 5 hPa for the days of the event in October 1987.

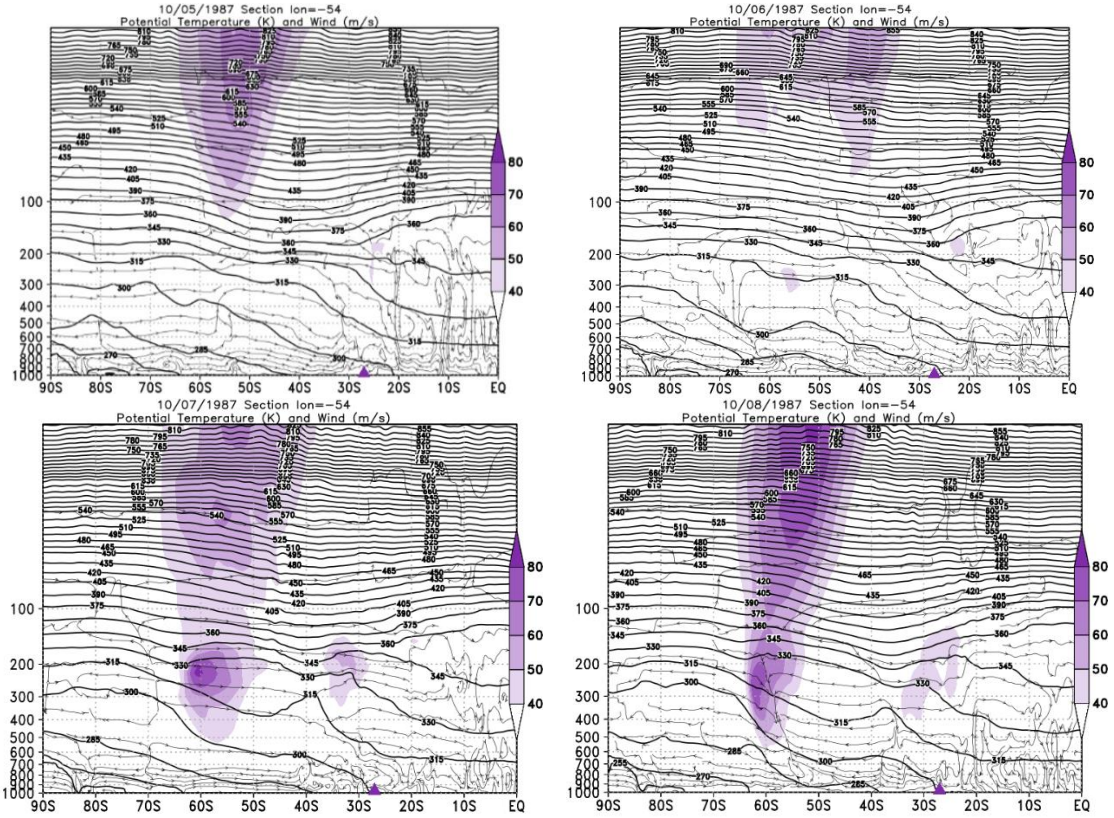

Source: The author.

10/16/1987

Figure A51: PVA fields for the 20 hPa in pressure levels, days 10/14/1987 to 10/17/1987.

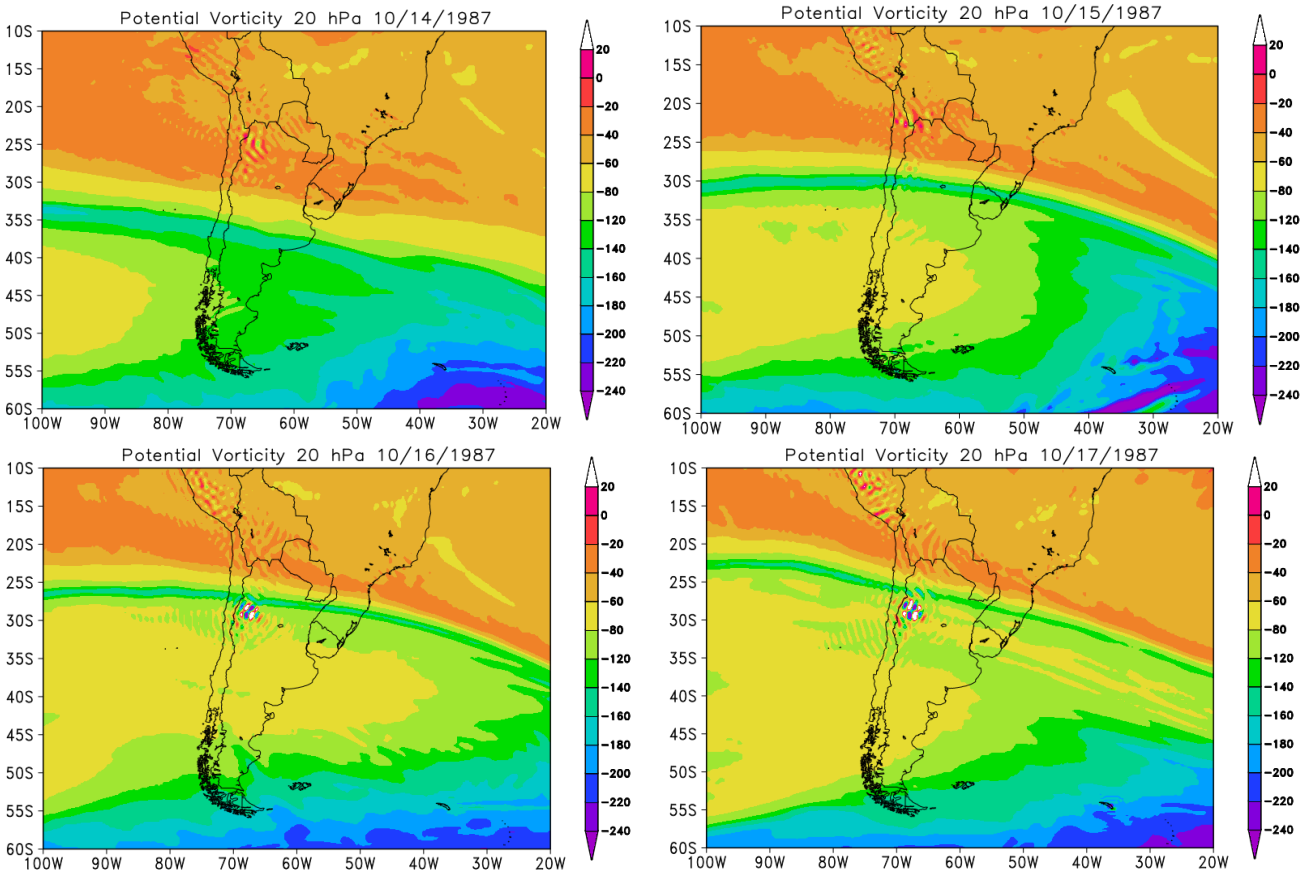

Source: The author.

Figure A52: Retroactive trajectory by the HYSPLIT/NOAA model, and O3 content satellite for South Pole view.

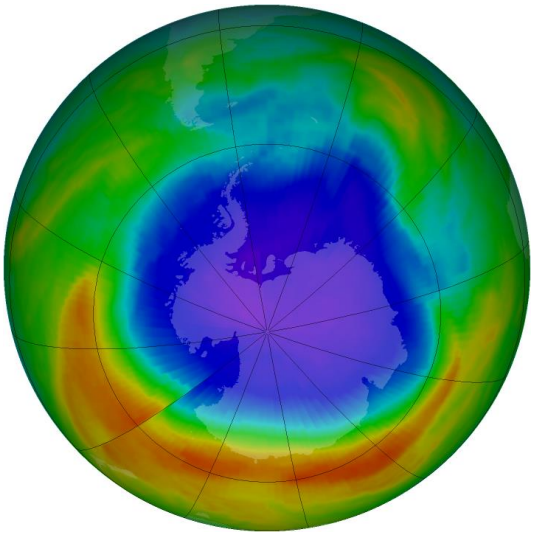

Source: NASA/OZONE WATCH.

Figure 53: Vertical section of the atmosphere between 1000 and 5 hPa for the days of the event in October 1987.

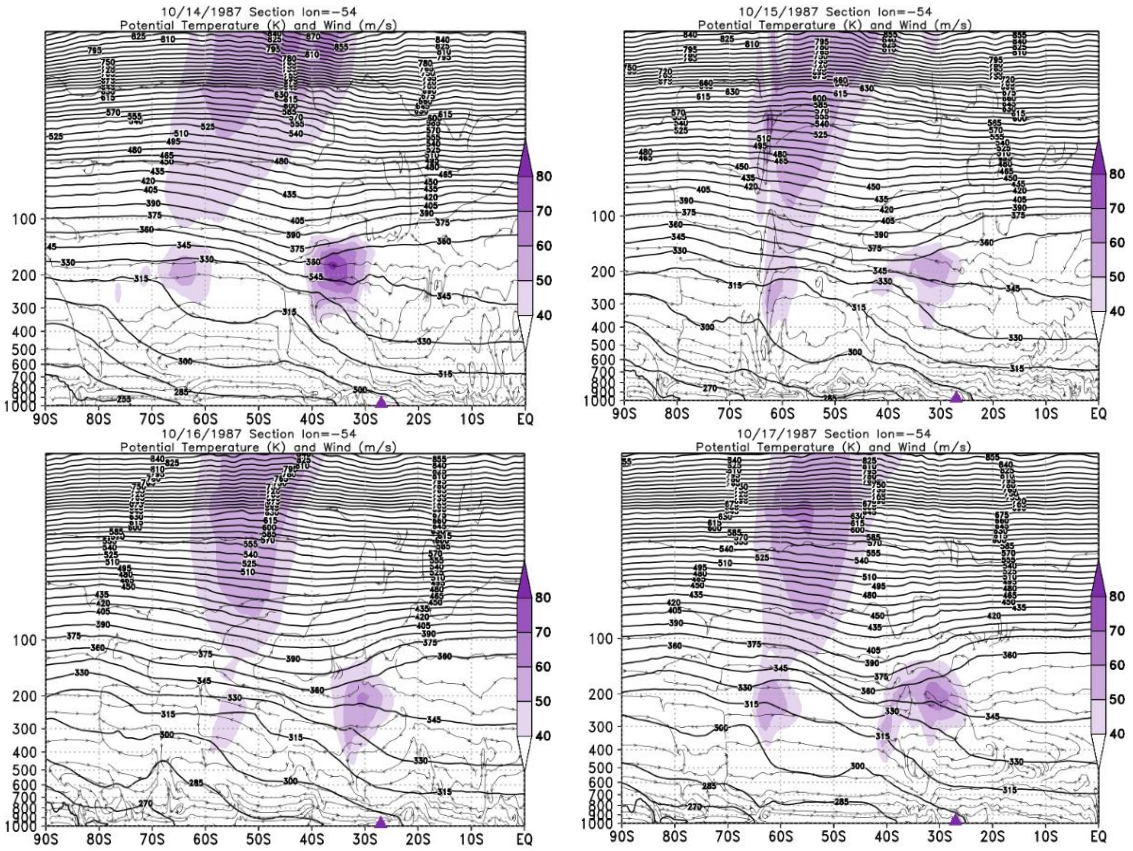

Source: The author.

09/02/1988

Figure A54: PVA fields for the 20 hPa in pressure levels, days 08/31/1988 to 09/03/1988.

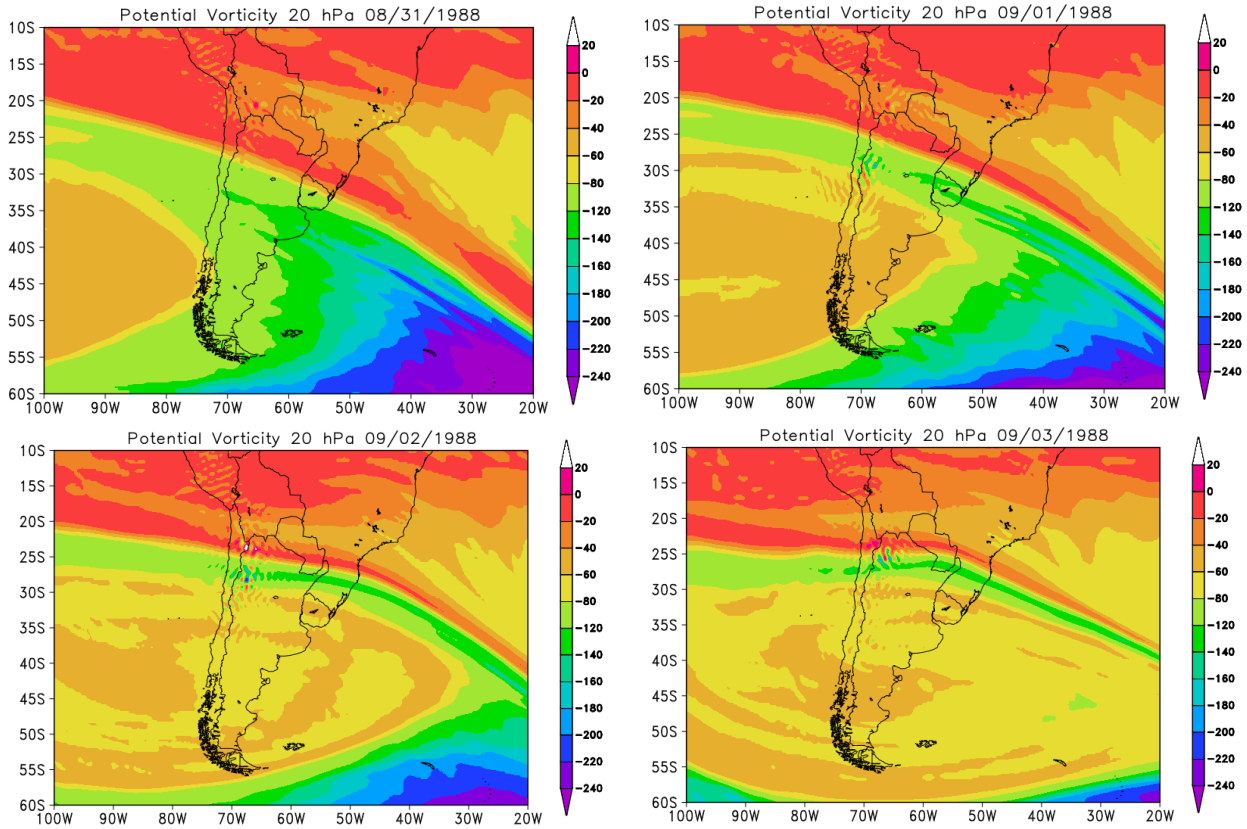

Source: The author.

Figure A55: Retroactive trajectory by the HYSPLIT/NOAA model, and O3 content satellite for South Pole view.

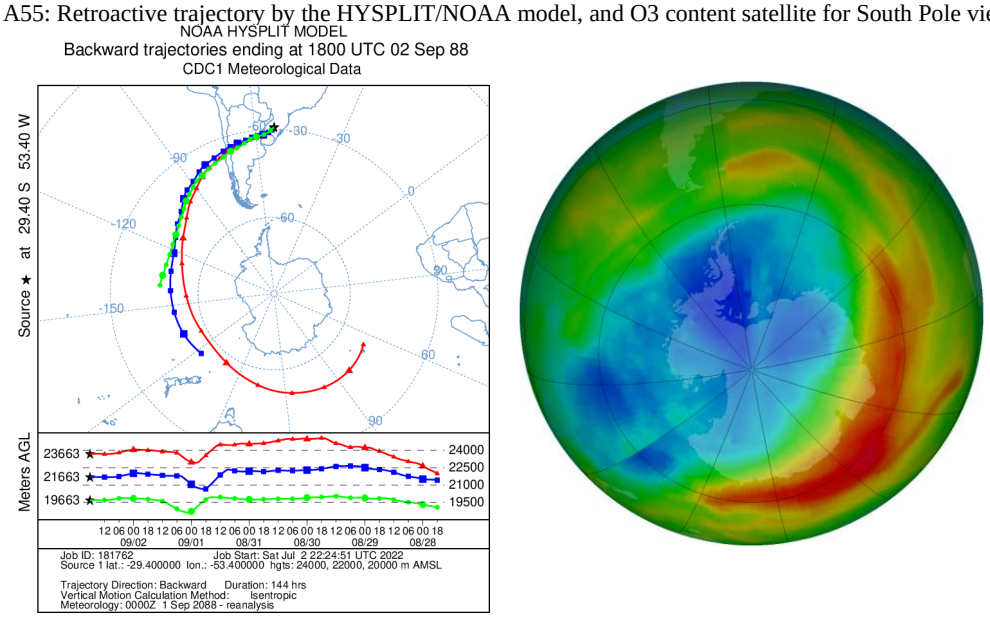

Source: HYSPLIT/NOAA, NASA/OZONE WATCH.

Figure A56: Vertical section of the atmosphere between 1000 and 5 hPa for the days of the event in September 1988

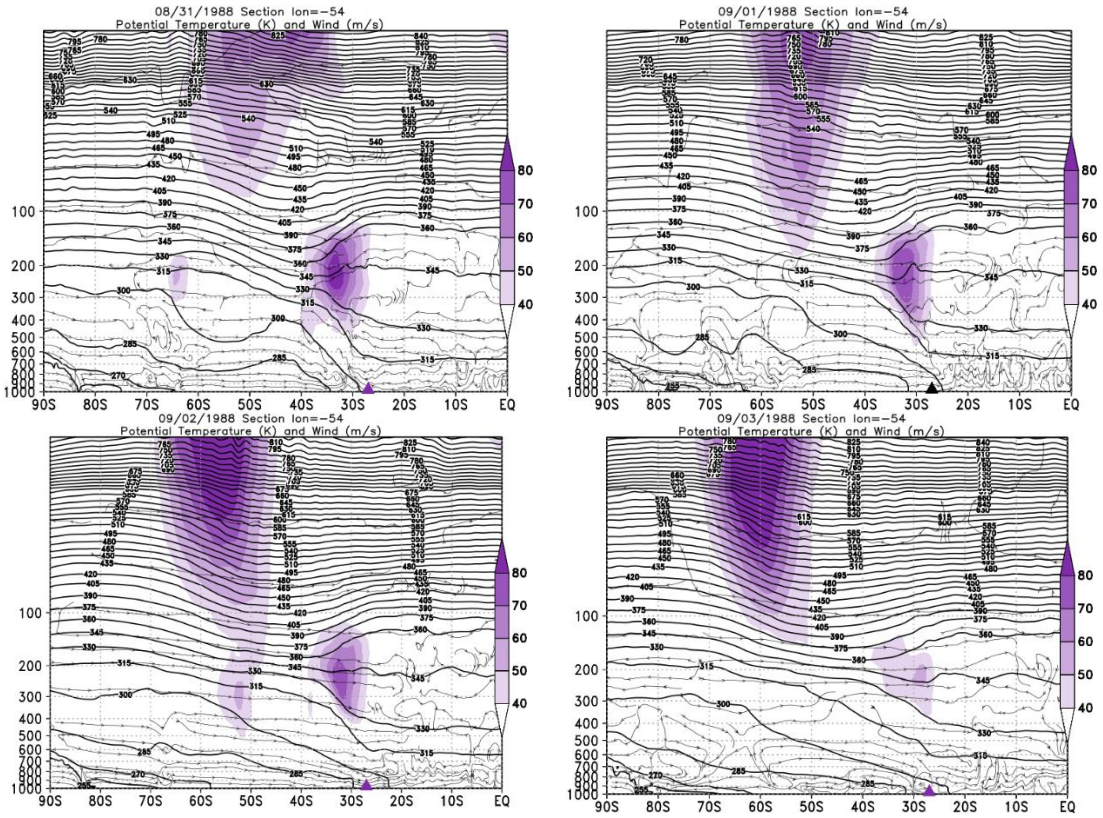

Source: The author.

08/24/1990

Figure A57: PVA fields for the 20 hPa in pressure levels, days 08/22/1990 to 08/25/1990.

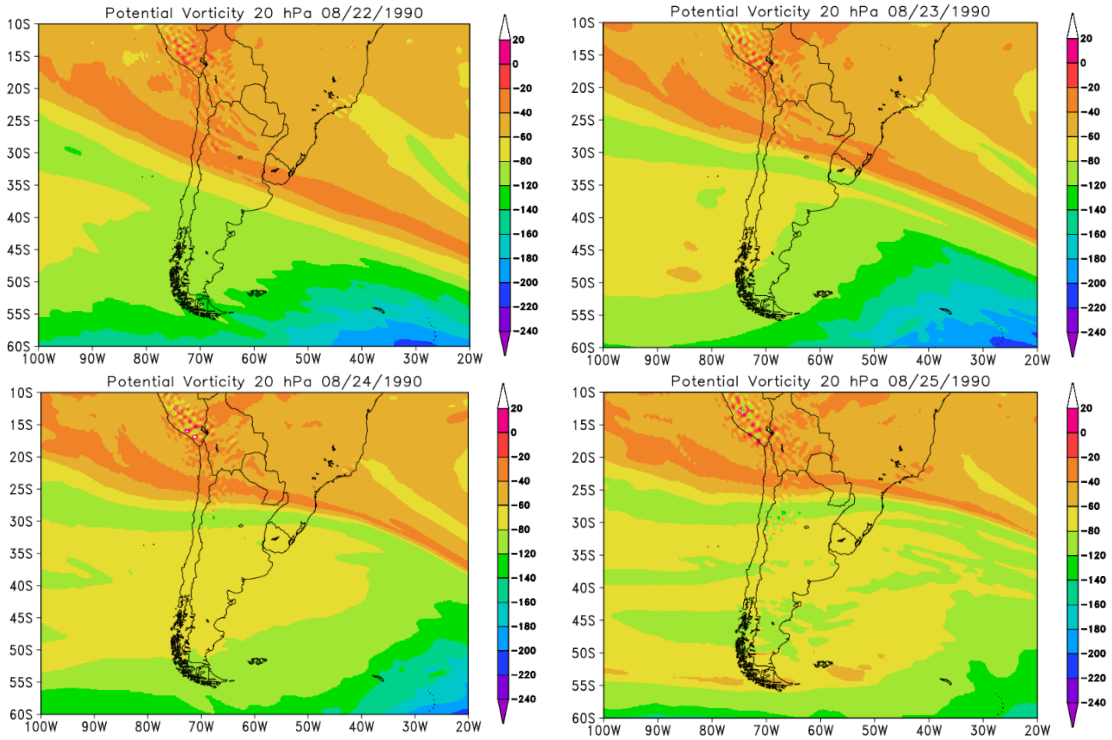

Source: The author.

Figure A58: Retroactive trajectory by the HYSPLIT/NOAA model, and O3 content satellite for South Pole view.

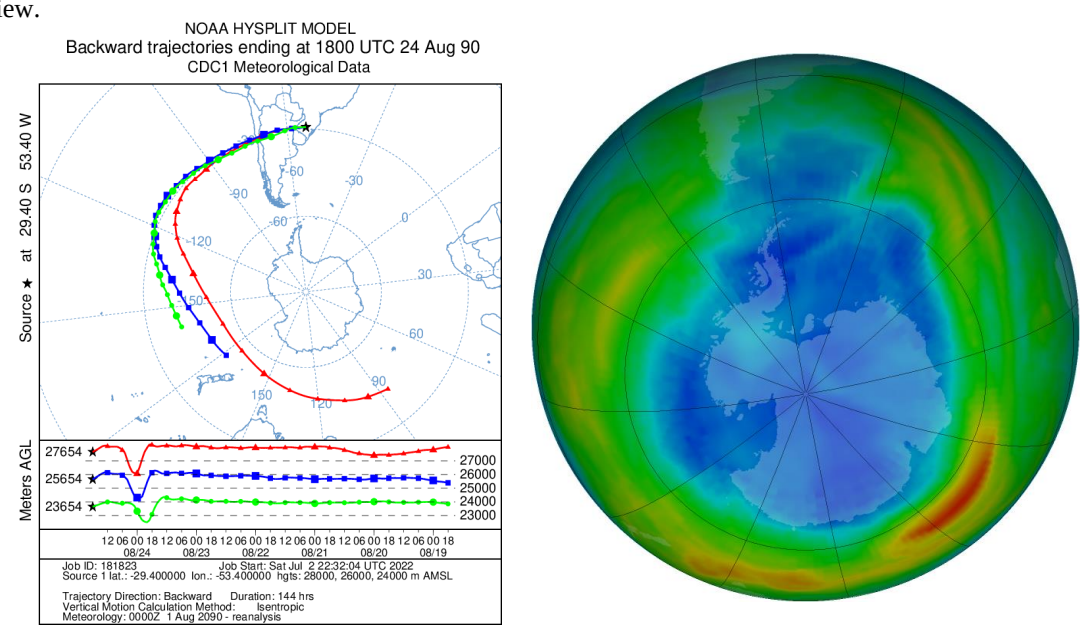

Source: HYSPLIT/NOAA, NASA/OZONE WATCH.

Figure 59: Vertical section of the atmosphere between 1000 and 5 hPa for the days of the event in August 1990.

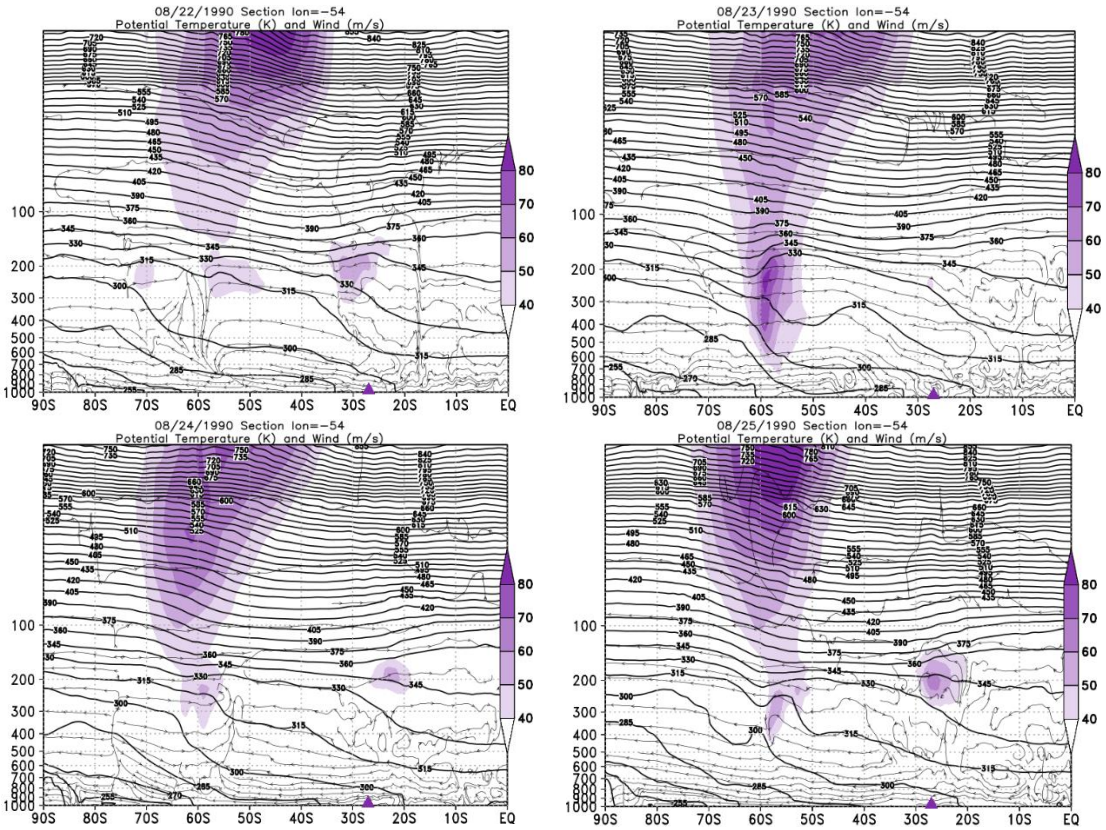

Source: The author.

09/06/1990

Figure 60: PVA fields for the 20 hPa in pressure levels, days 09/04/1990 to 09/07/1990.

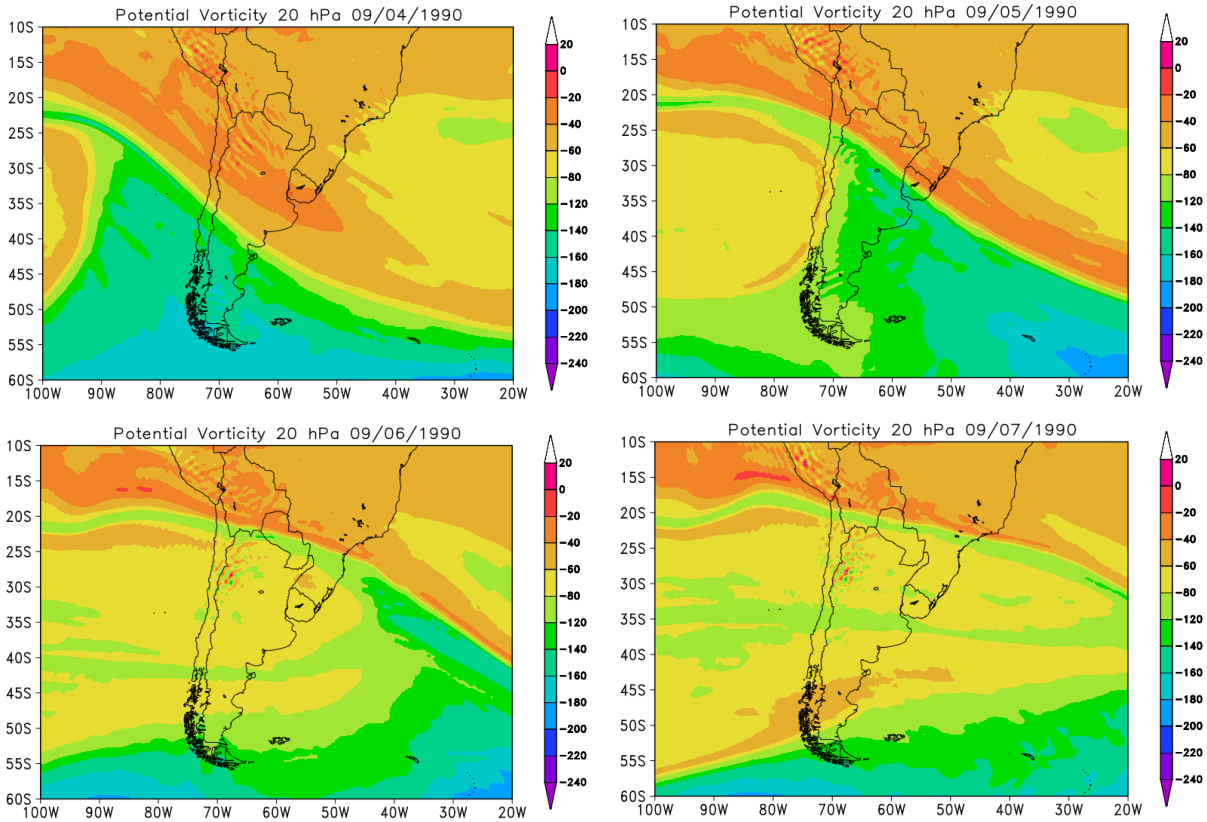

Source: The author.

Figure A61: Retroactive trajectory by the HYSPLIT/NOAA model, and O3 content satellite for South Pole view.

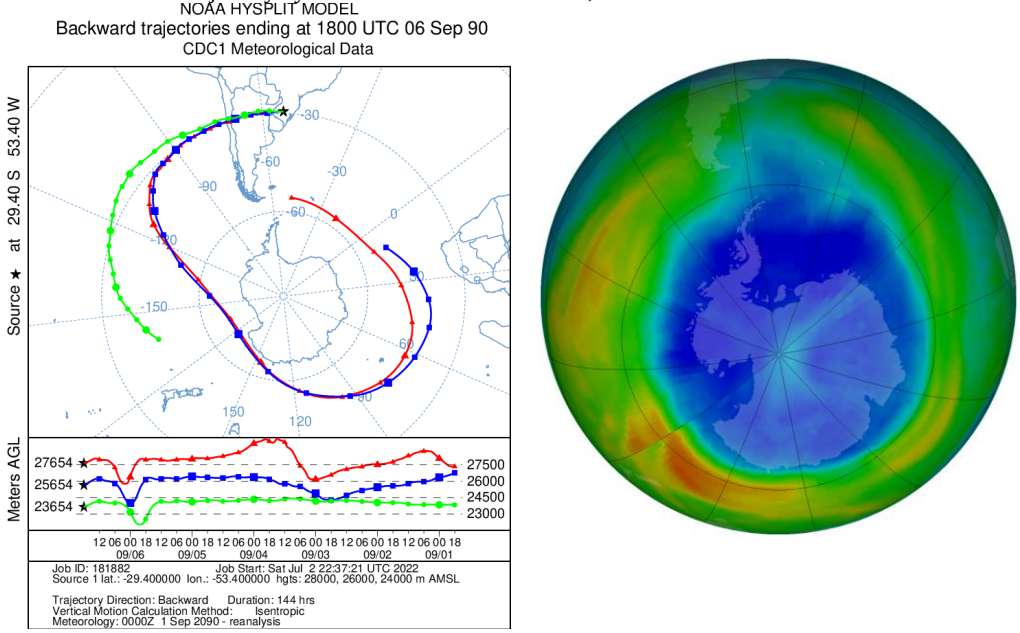

Source: HYSPLIT/NOAA, NASA/OZONE WATCH.

Figure A62: Vertical section of the atmosphere between 1000 and 5 hPa for the days of the event in September 1990.

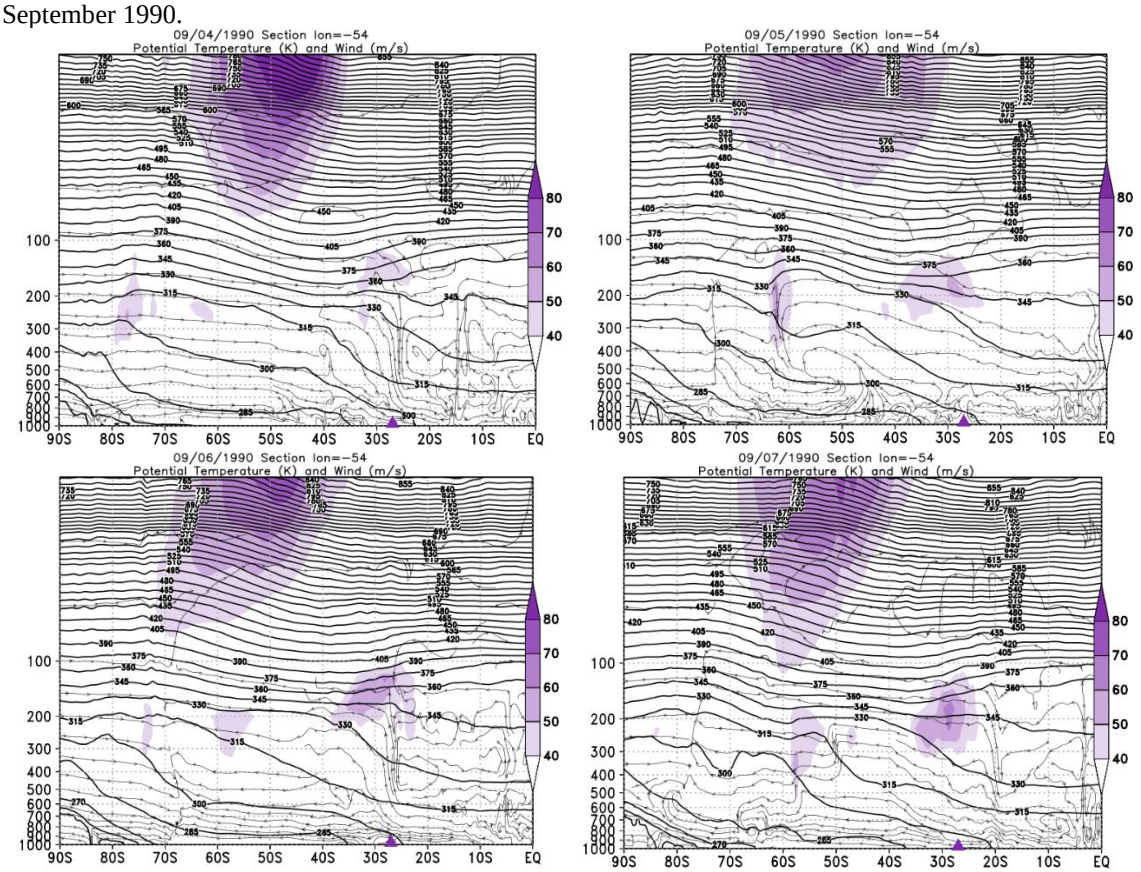

Source: The author.

09/16/1990

Figure A63: PVA fields for the 20 hPa in pressure levels, days 09/14/1990 to 09/17/1990.

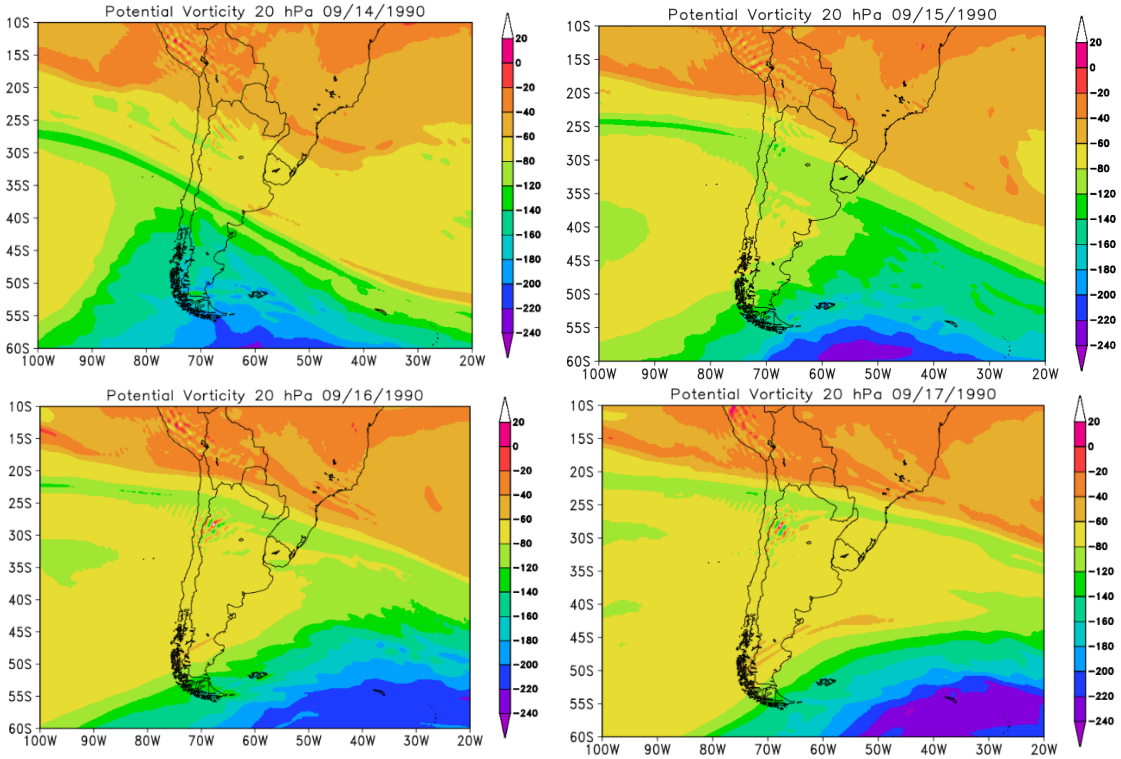

Source: The author.

Figure A64: Retroactive trajectory by the HYSPLIT/NOAA model, and O3 content satellite for South Pole view

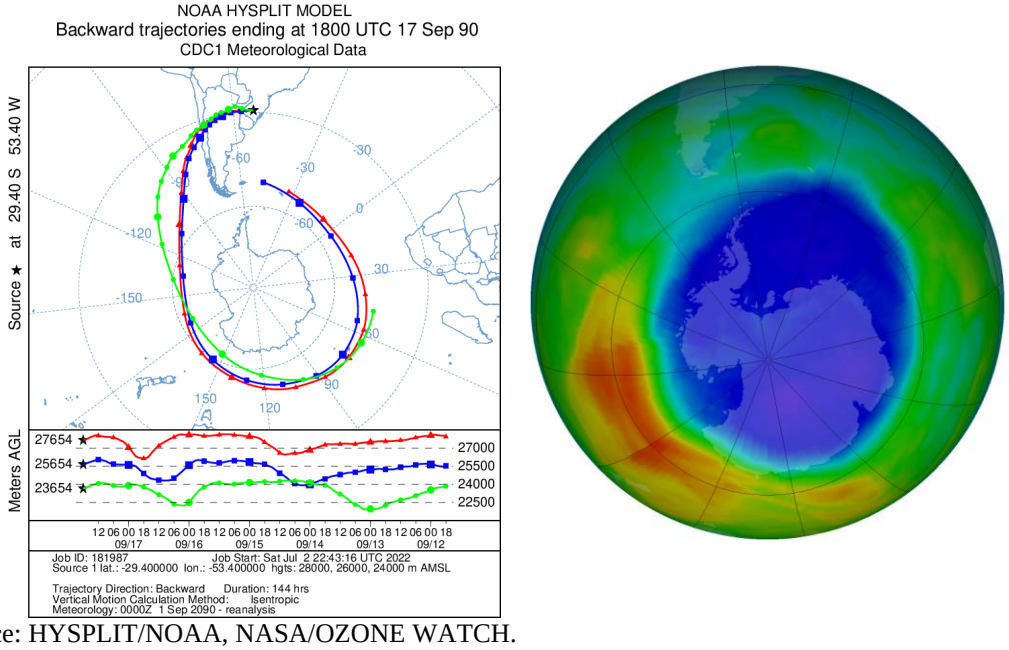

Source: HYSPLIT/NOAA, NASA/OZONE WATCH.

Figure 65: Vertical section of the atmosphere between 1000 and 5 hPa for the days of the event in September 1990.

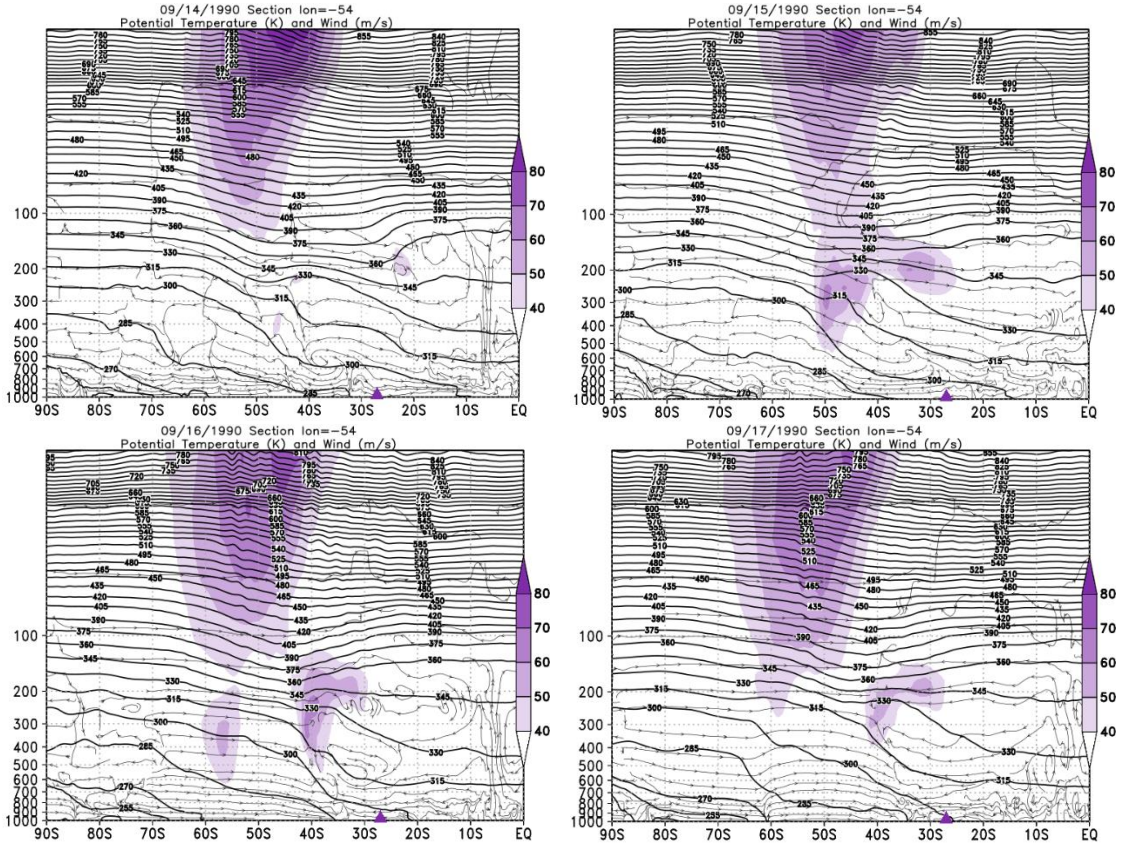

Source: The author.

10/01/1990

Figure A66: PVA fields for the 20 hPa in pressure levels, days 09/29/1990 to 10/02/1990.

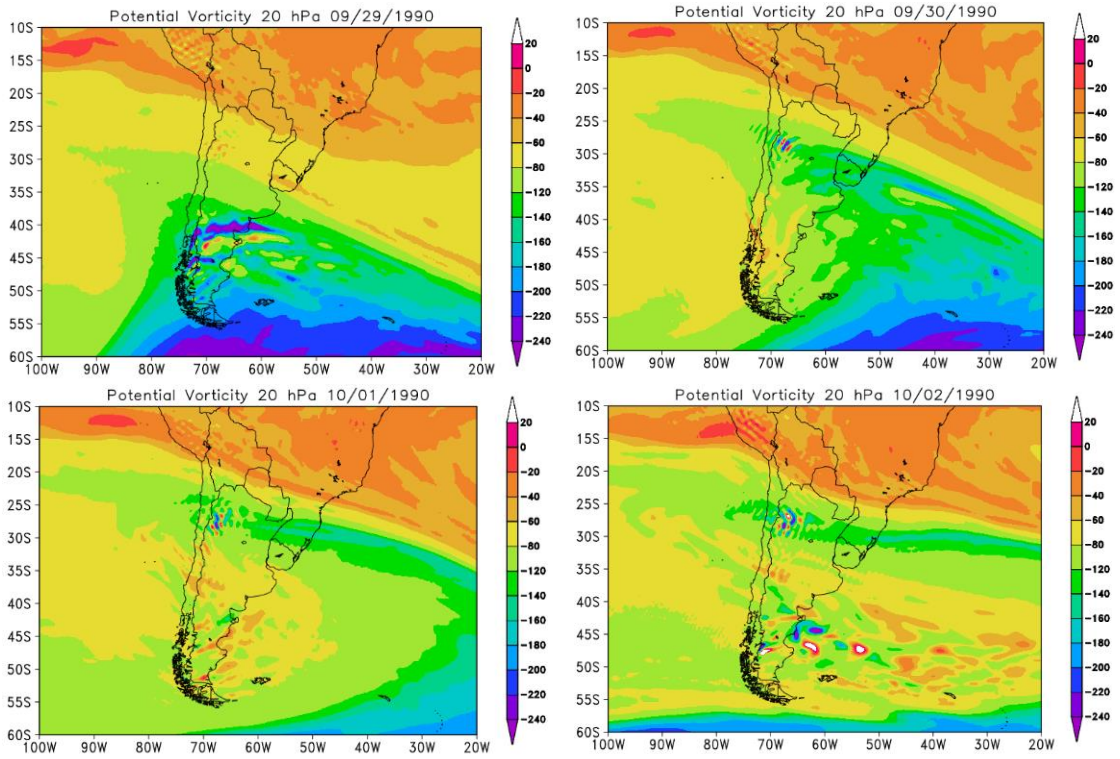

Source: The author.

Figure A67: Retroactive trajectory by the HYSPLIT/NOAA model, and O3 content satellite for South Pole view.

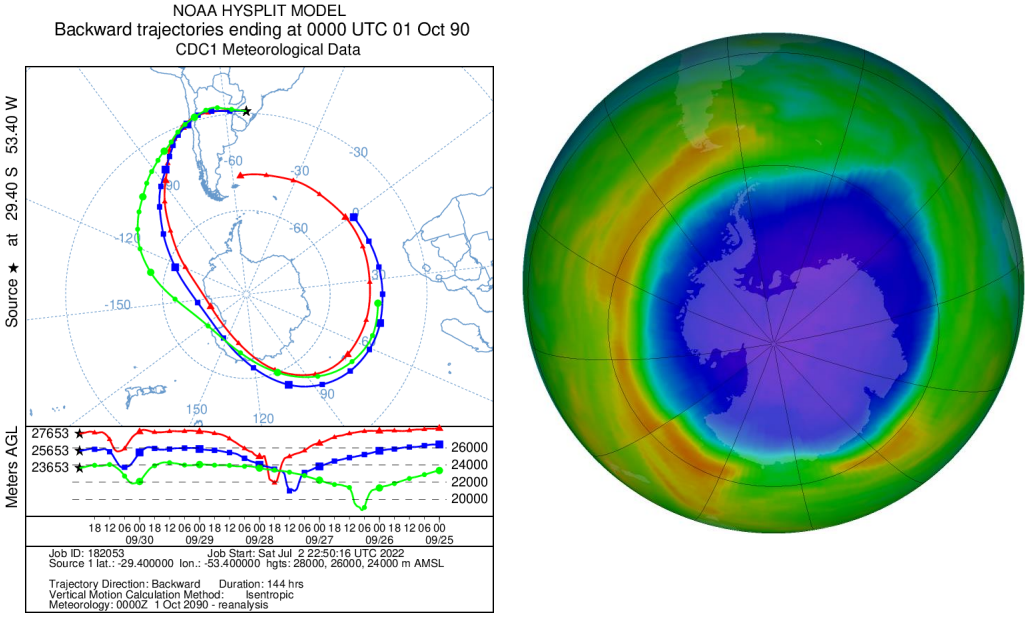

Source: HYSPLIT/NOAA, NASA/OZONE WATCH.

Figure A68: Vertical section of the atmosphere between 1000 and 5 hPa for the days of the event in October 1990.

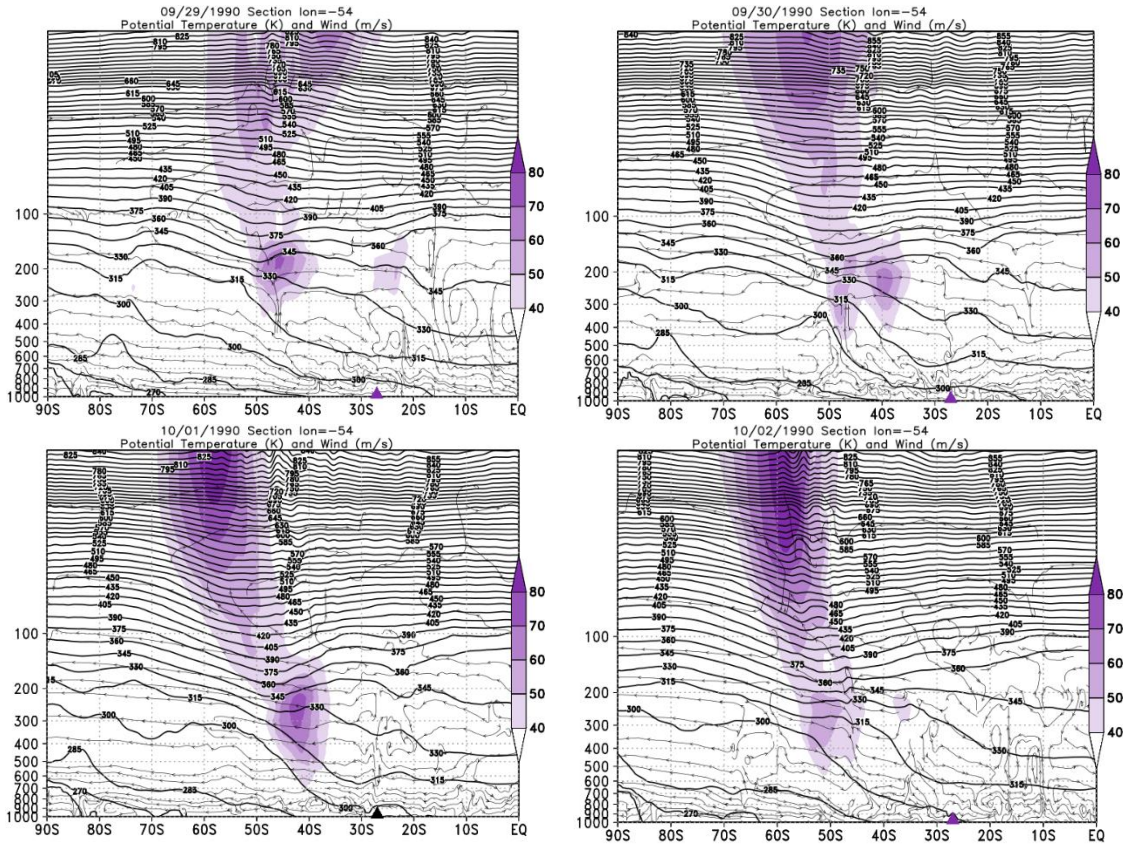

Source: The author.

10/16/1990

Figure A1: PVA fields for the 20 hPa in pressure levels, days 10/14/1990 to 10/17/1990.

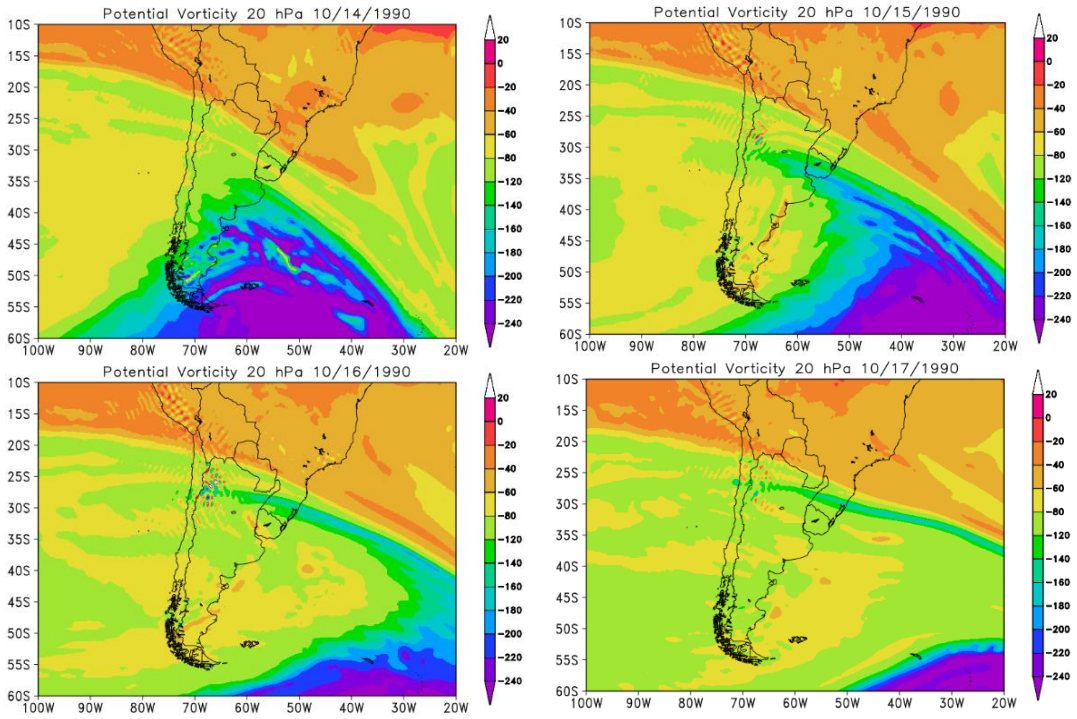

Source: The author.

Figure A70: Retroactive trajectory by the HYSPLIT/NOAA model, and O3 content satellite for South Pole view.

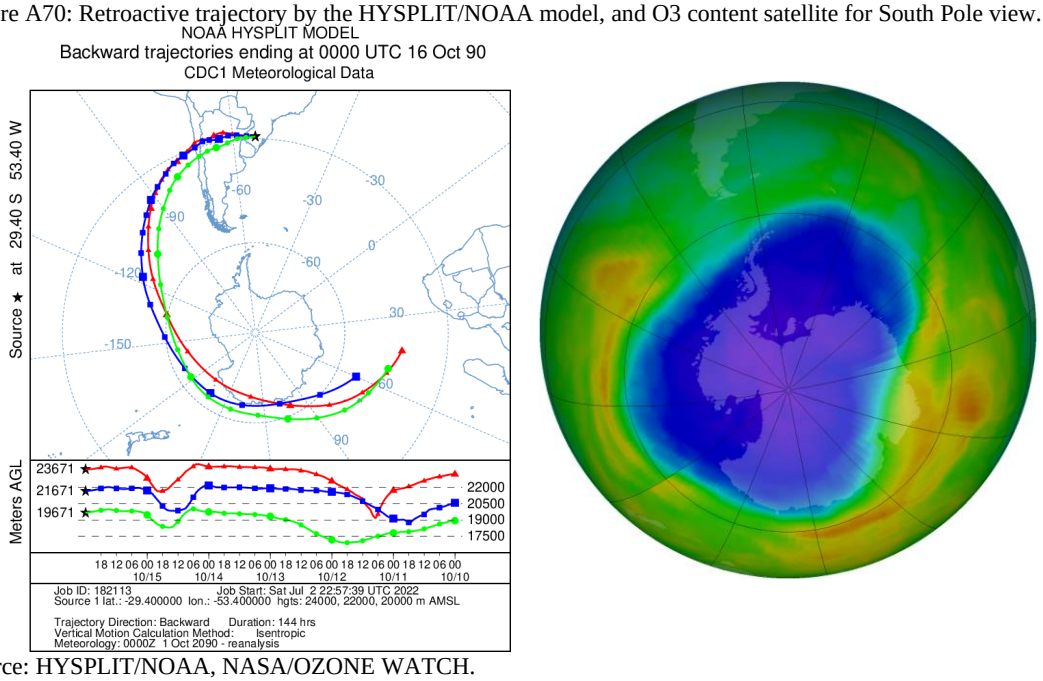

Source: HYSPLIT/NOAA, NASA/OZONE WATCH.

Figure A71: Vertical section of the atmosphere between 1000 and 5 hPa for the days of the event in October 2016

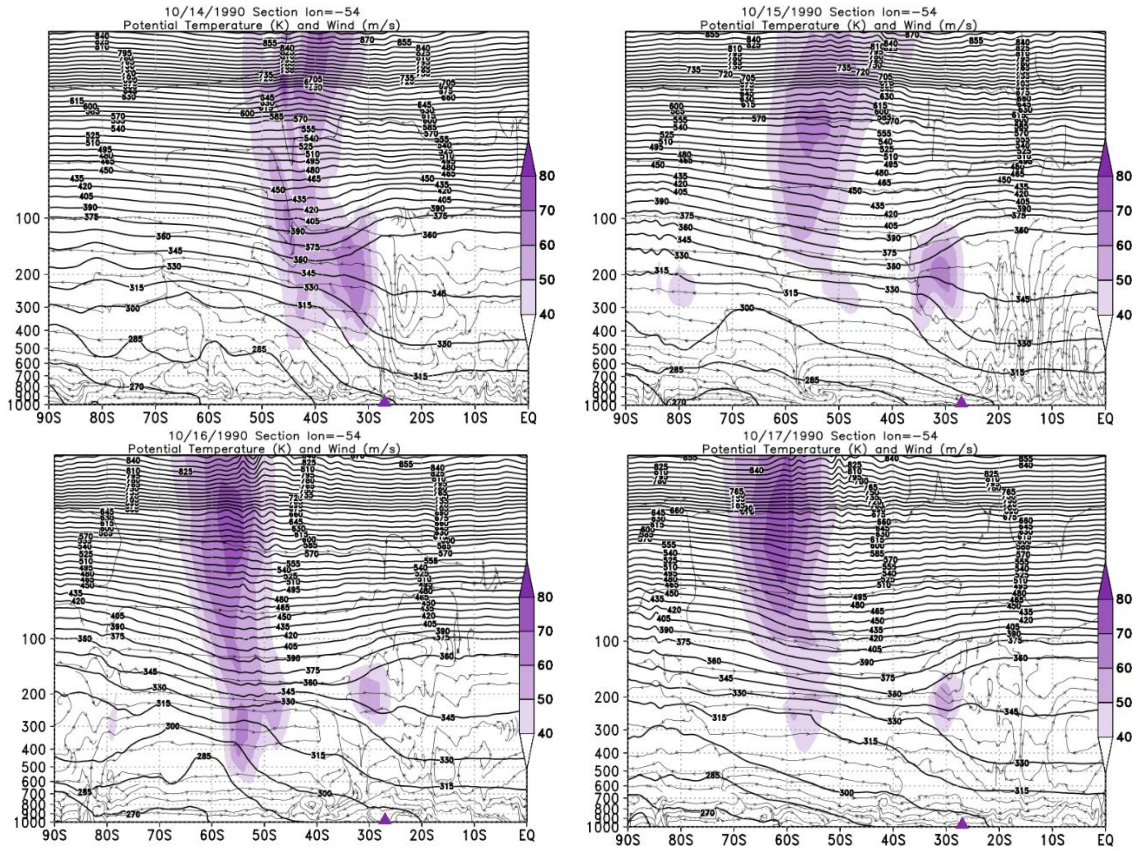

Source: The author.

09/03/1992

Figure A72: PVA fields for the 20 hPa in pressure levels, days 09/01/1992 to 09/04/1992.

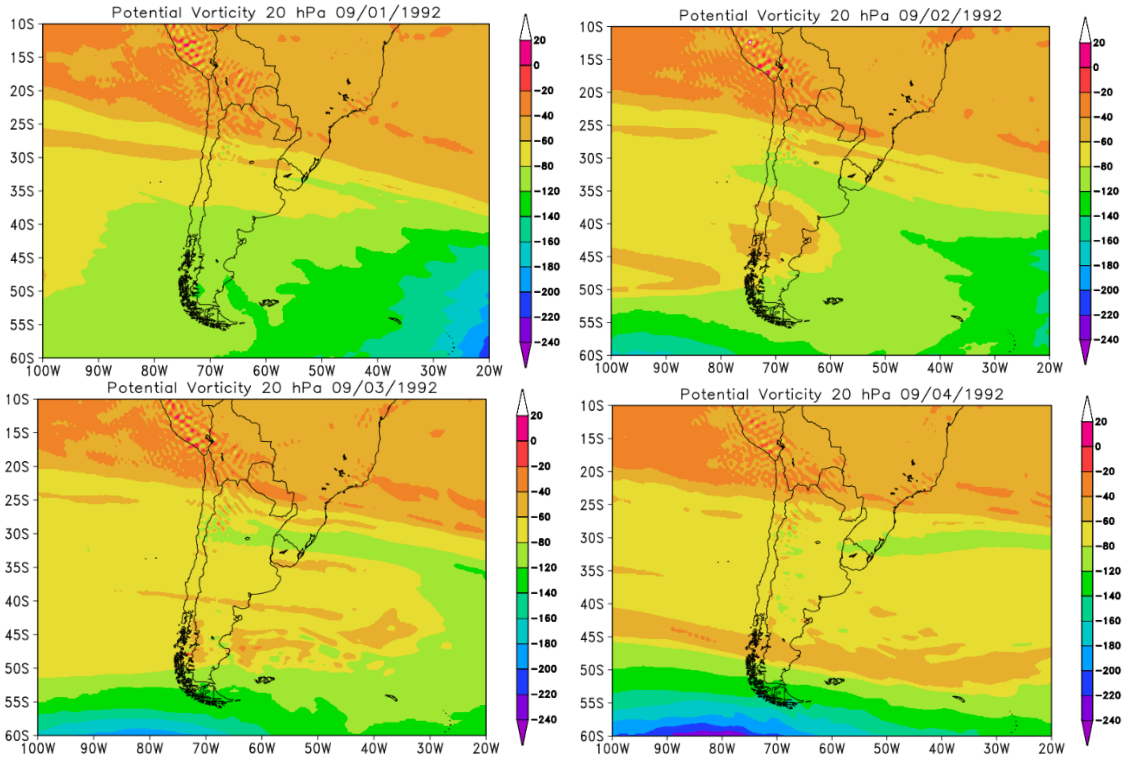

Source: The author.

Figure A73: Retroactive trajectory by the HYSPLIT/NOAA model, and O3 content satellite for South Pole view.

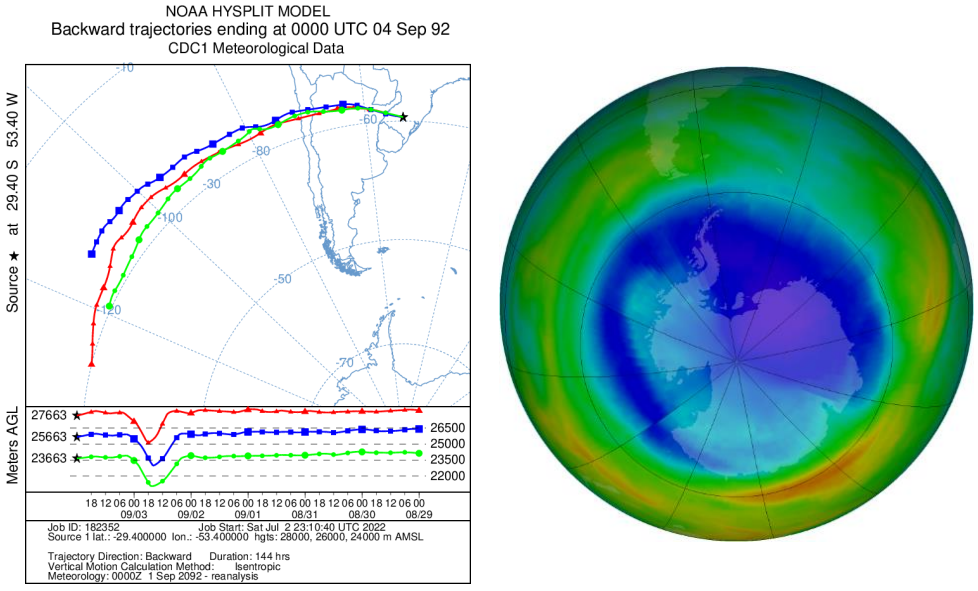

Source: HYSPLIT/NOAA, NASA/OZONE WATCH.

Figure A74: Vertical section of the atmosphere between 1000 and 5 hPa for the days of the event in September 1992.

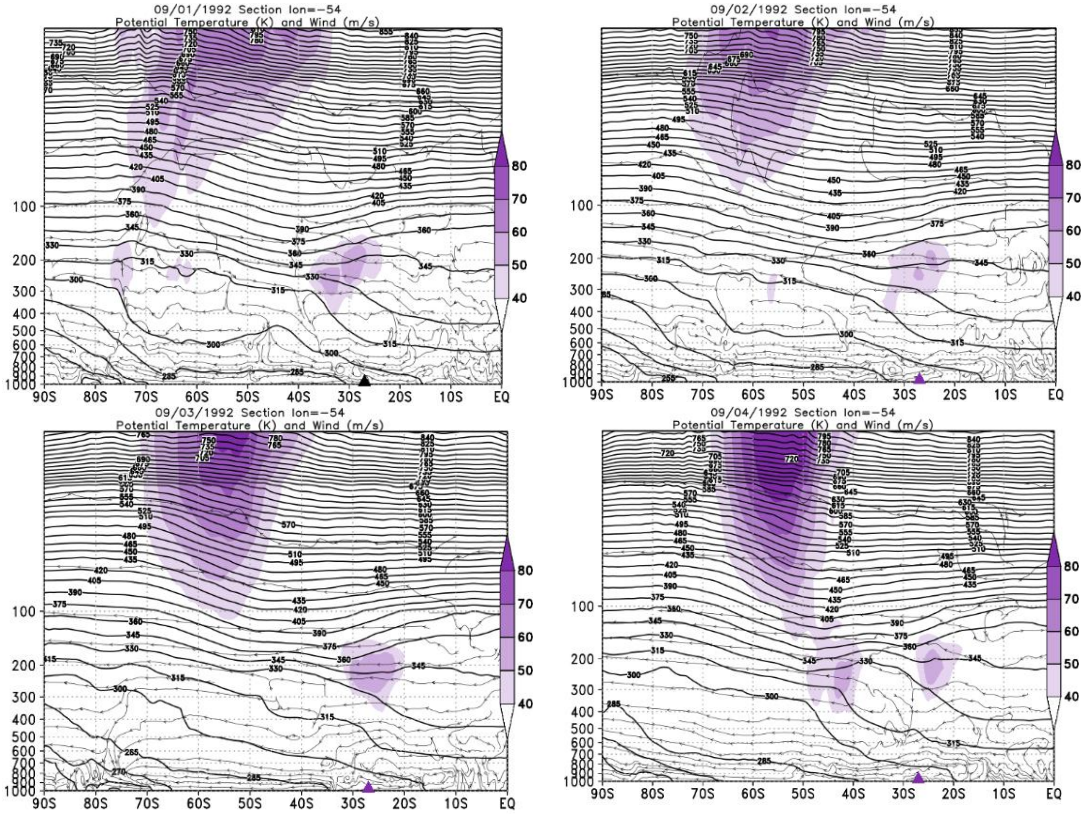

Source: The author.

10/10/1992

Figure A75: PVA fields for the 20 hPa in pressure levels, days 10/08/1992 to 10/11/1992.

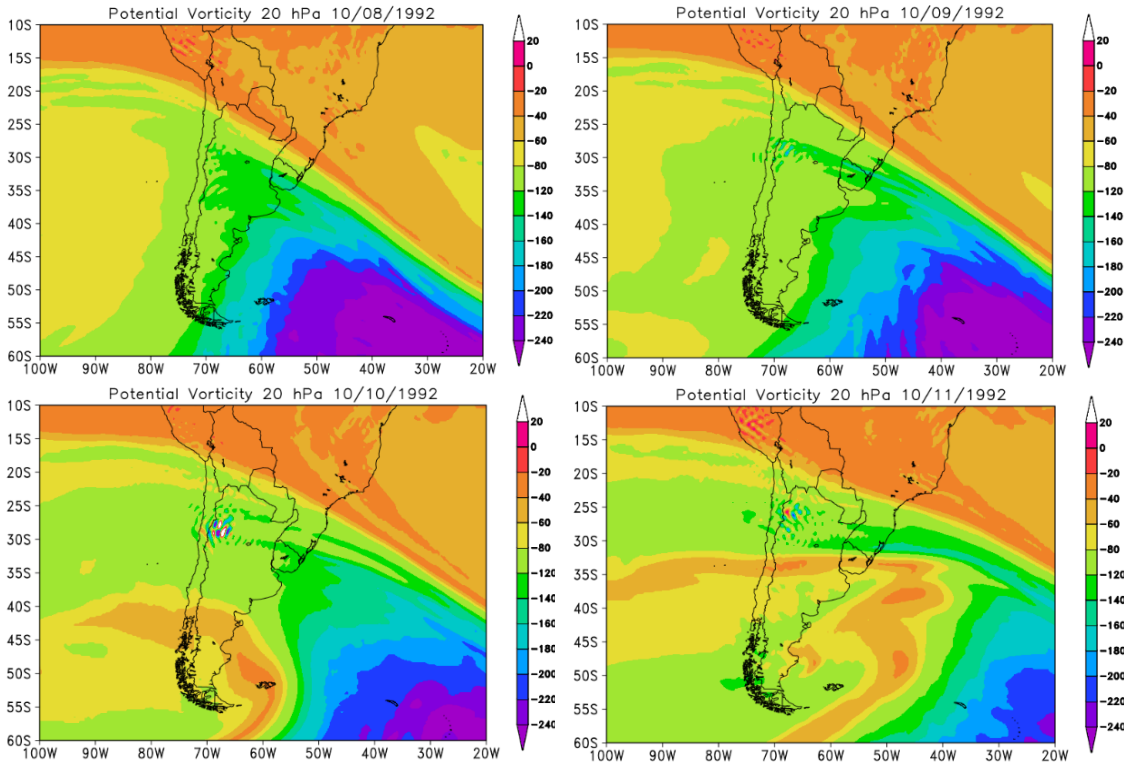

Source: The author.

Figure A76: Retroactive trajectory by the HYSPLIT/NOAA model, and O3 content satellite for South Pole view.

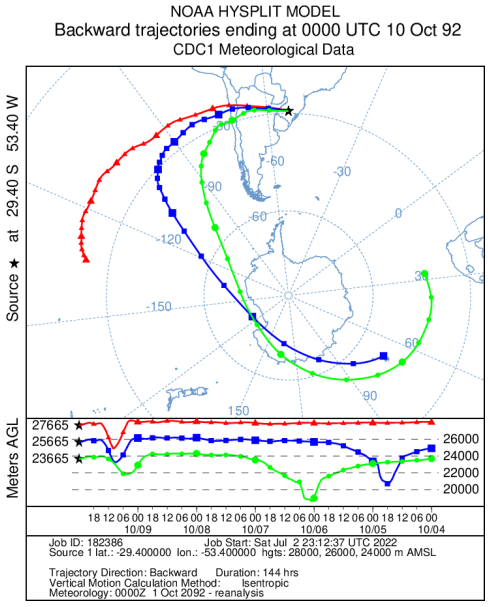

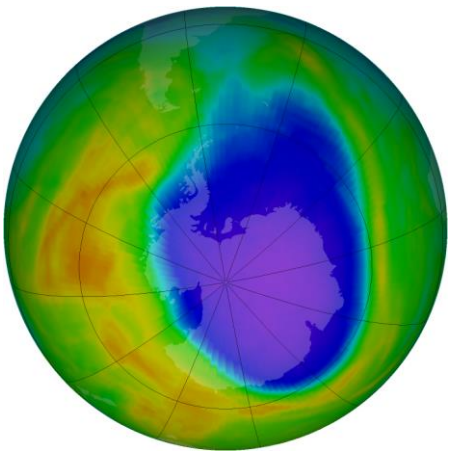

Source: HYSPLIT/NOAA, NASA/OZONE WATCH.

Figure A77: Vertical section of the atmosphere between 1000 and 5 hPa for the days of the event in October 1992.

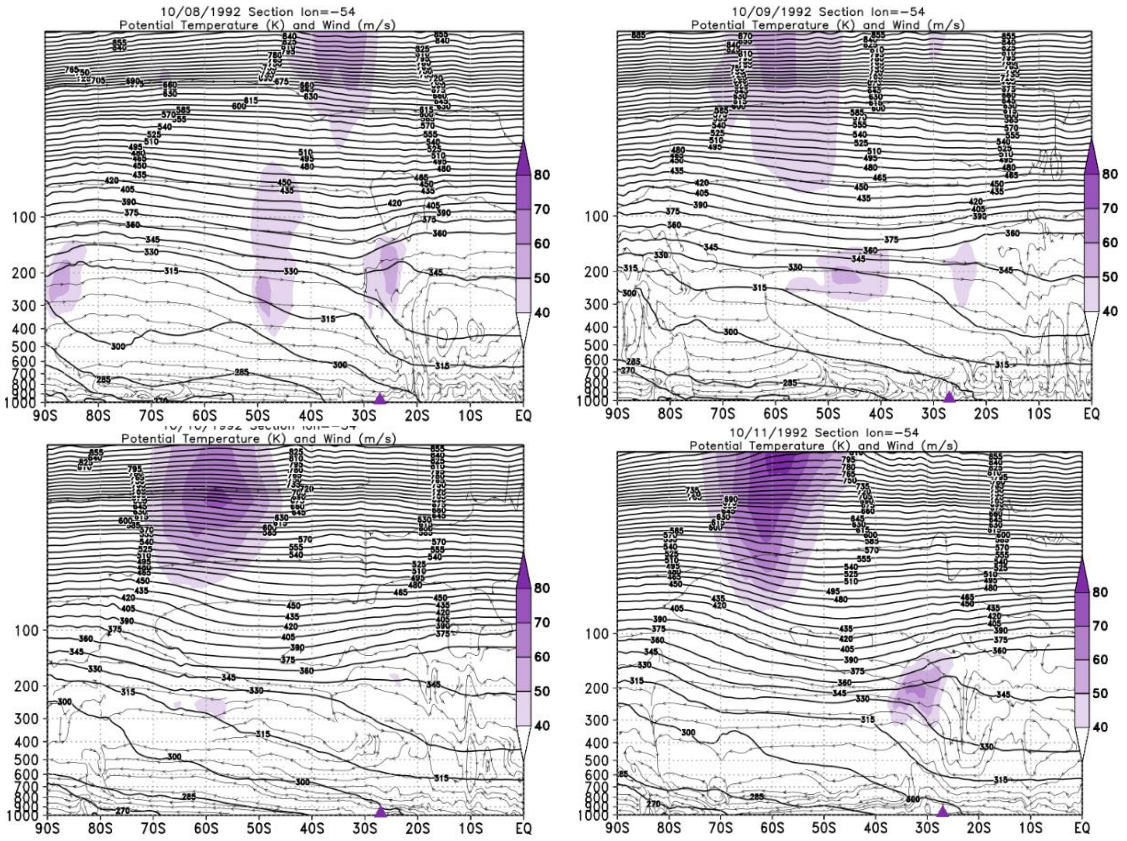

Source: The author.

08/15/1993

Figure A78: PVA fields for the 20 hPa in pressure levels, days 08/13/1993 to 08/16/1993.

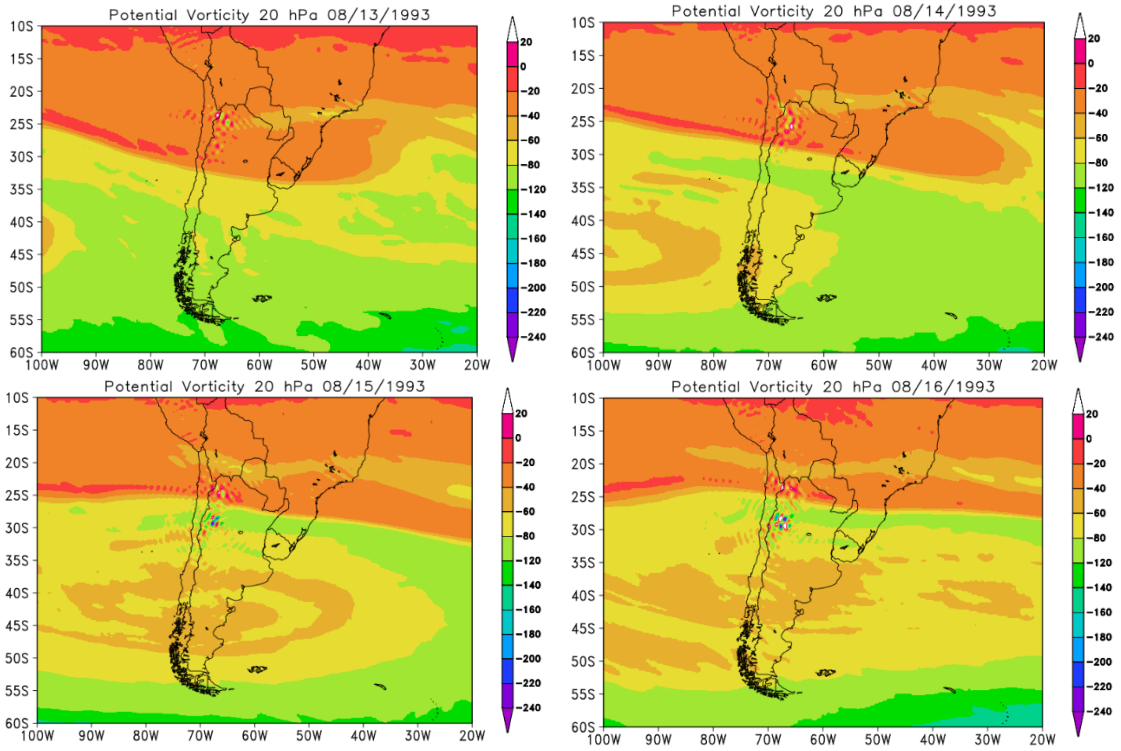

Source: The author.

Figure A79: Retroactive trajectory by the HYSPLIT/NOAA model, and O3 content satellite for South Pole view.

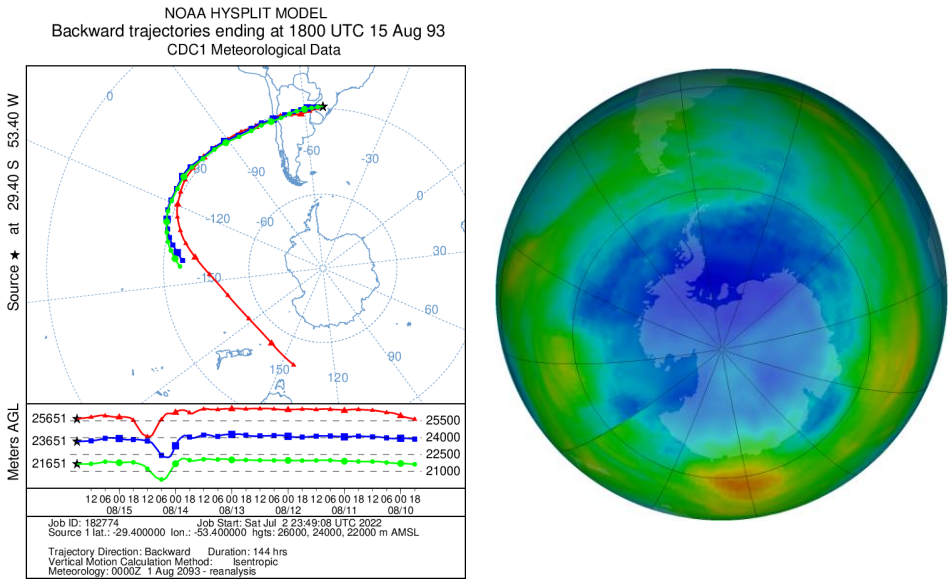

Source: HYSPLIT/NOAA, NASA/OZONE WATCH.

Figure 80: Vertical section of the atmosphere between 1000 and 5 hPa for the days of the event in August 1993.

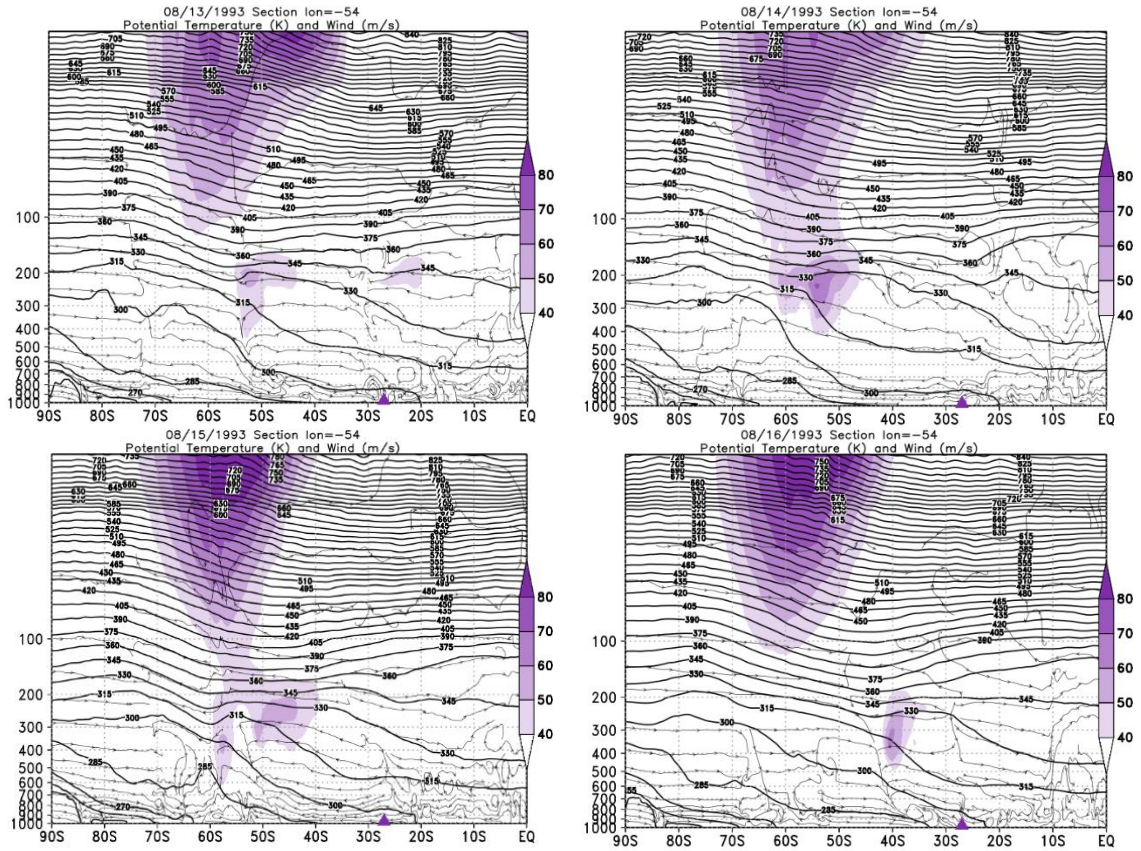

Source: The author.

08/25/1993

Figure 81: PVA fields for the 20 hPa in pressure levels, days 08/23//1993 to 08/26/1993.

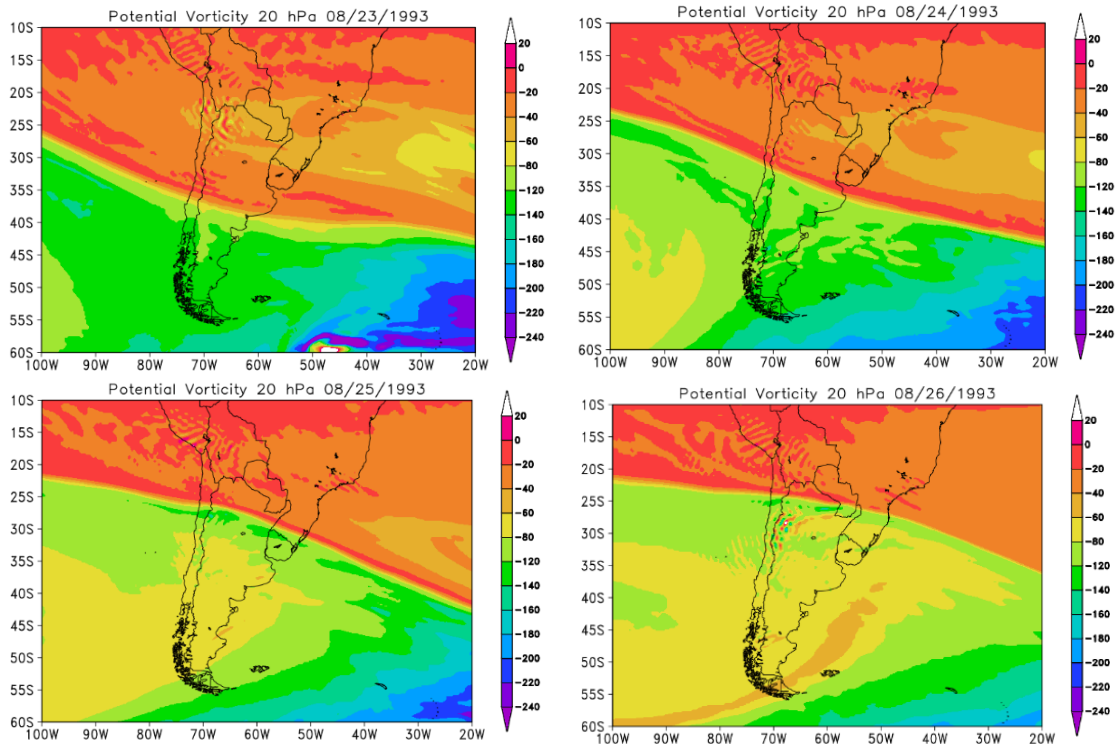

Source: The author.

Figure A82: Retroactive trajectory by the HYSPLIT/NOAA model, and O3 content satellite for South Pole view.

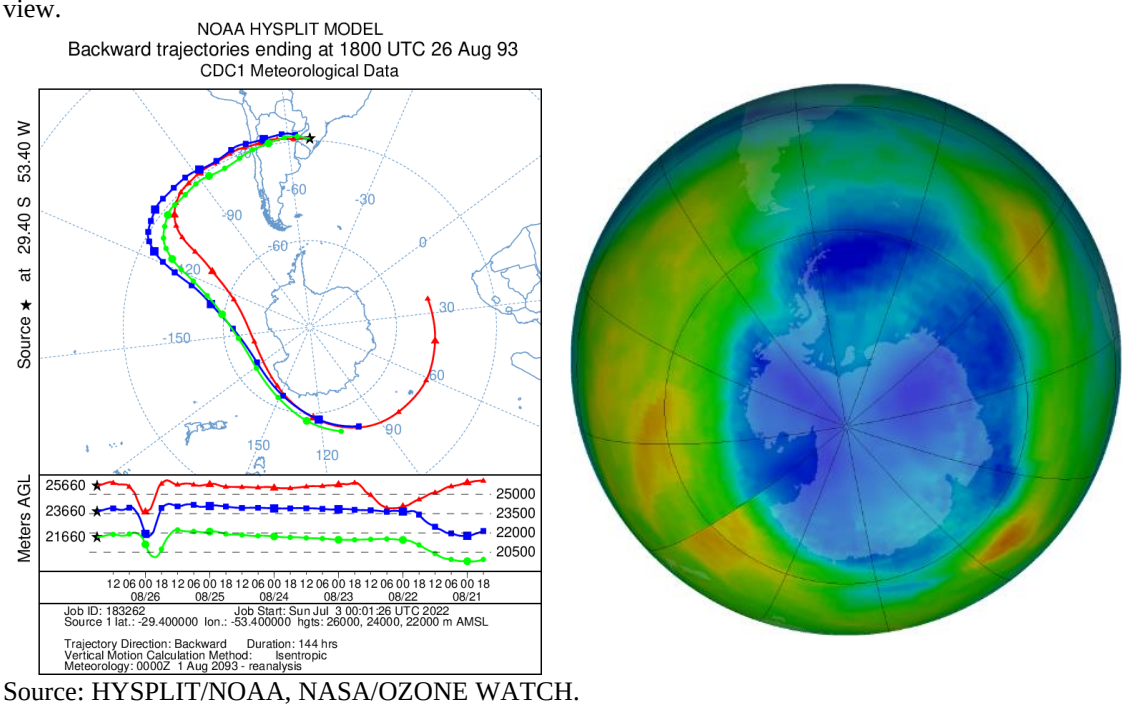

Source: HYSPLIT/NOAA, NASA/OZONE WATCH.

Figure A83: Vertical section of the atmosphere between 1000 and 5 hPa for the days of the event in August 1993.

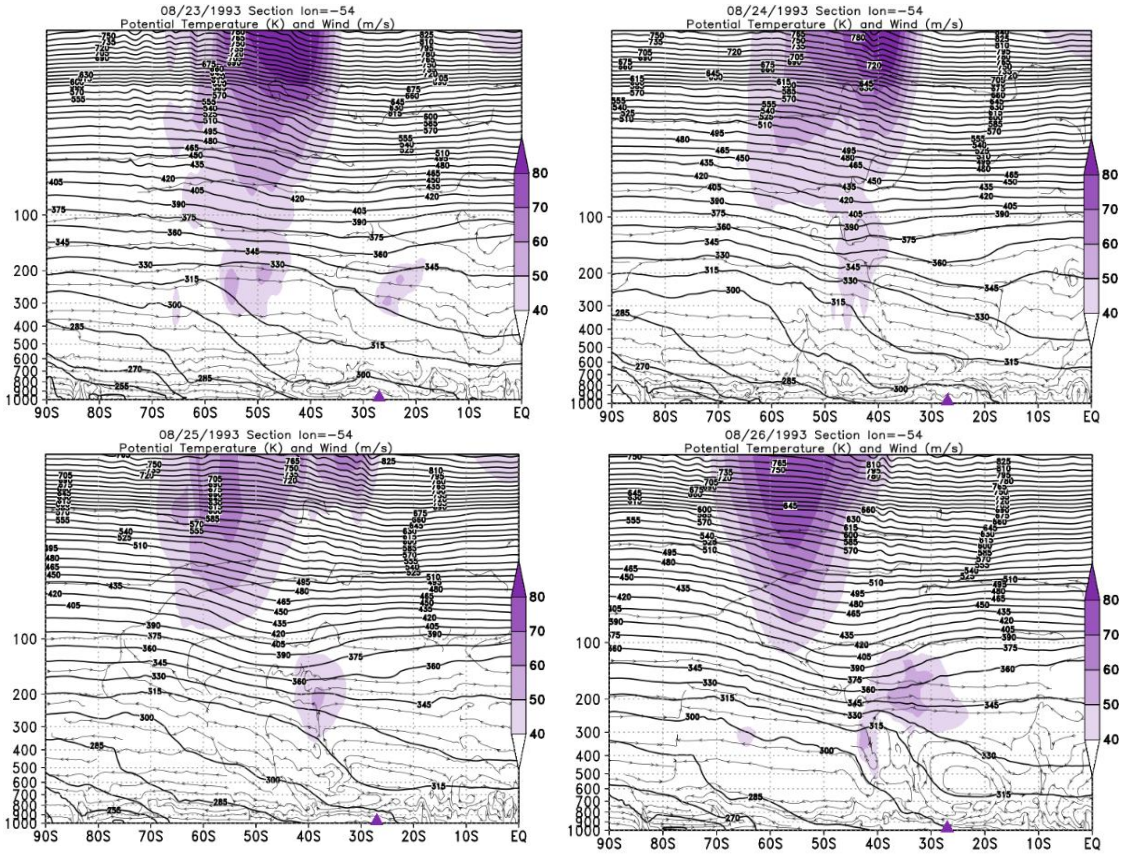

Source: The author.

10/19/1993

Figure A84: PVA fields for the 20 hPa in pressure levels, days 09/27/1979 to 09/30/1979.

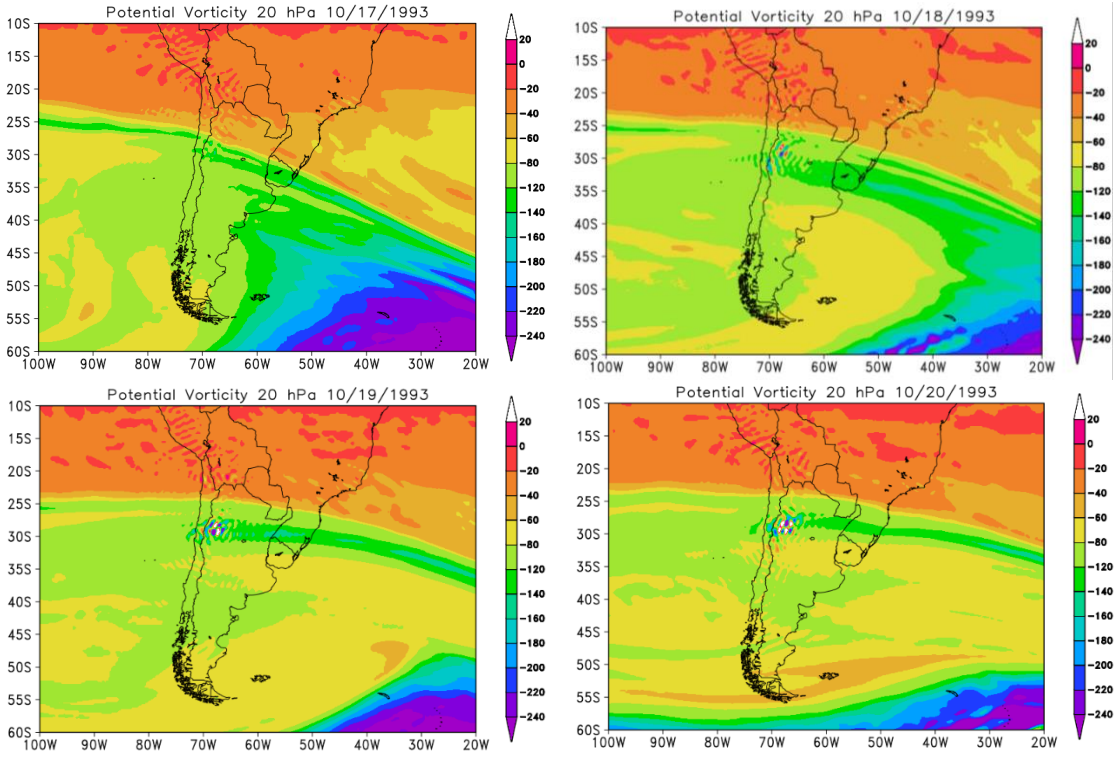

Source: The author.

Figure A85: Retroactive trajectory by the HYSPLIT/NOAA model.

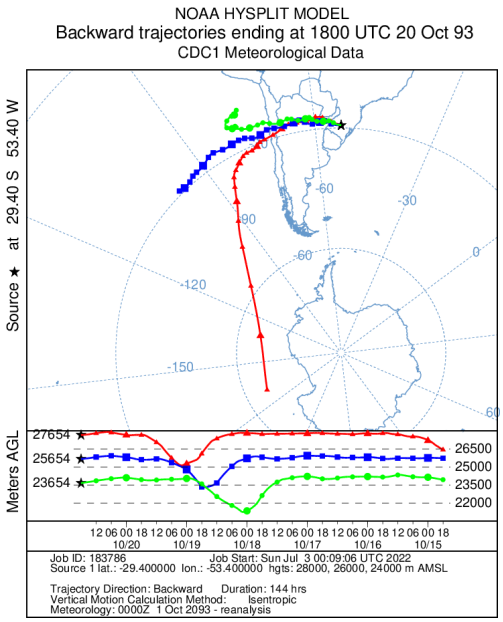

Source: HYSPLIT/NOAA.

Figure A86: Vertical section of the atmosphere between 1000 and 5 hPa for the days of the event in October 1993.

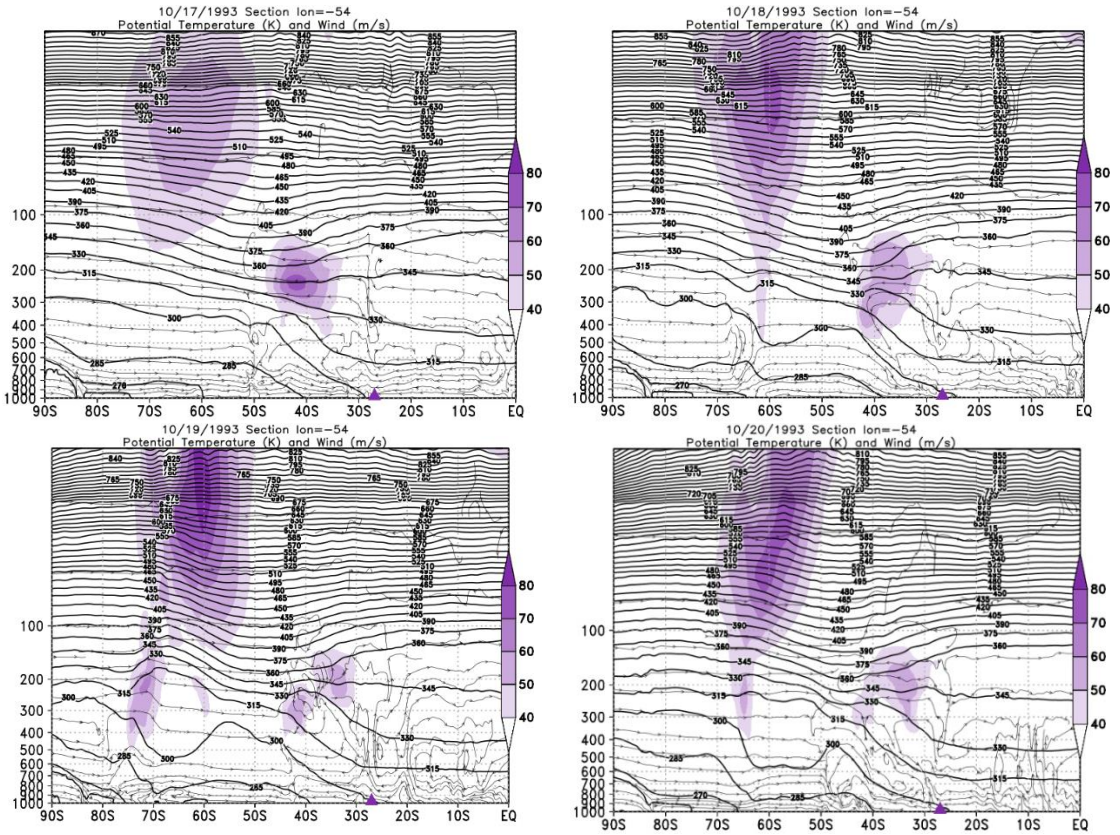

Source: The author.

10/31/1993

Figure A87: PVA fields for the 20 hPa in pressure levels, days 10/28/1993 to 10/31/1993.

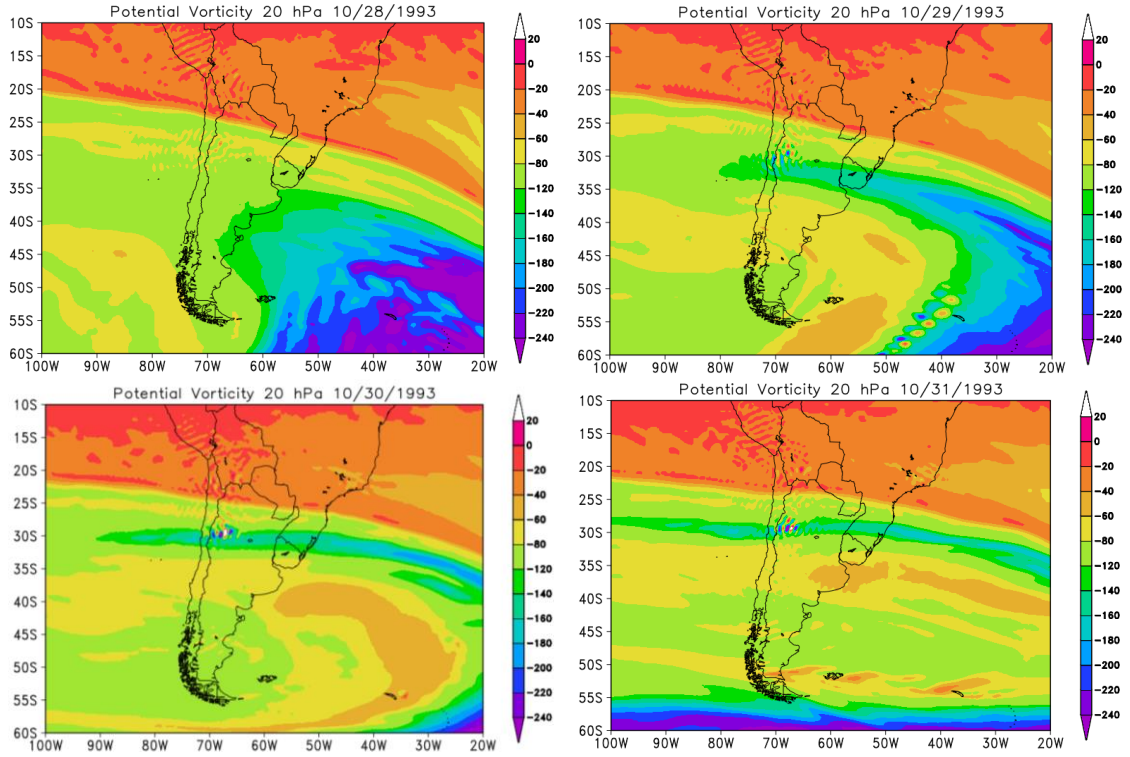

Source: The author.

Figure A88: Retroactive trajectory by the HYSPLIT/NOAA model, and O3 content satellite for South Pole view.

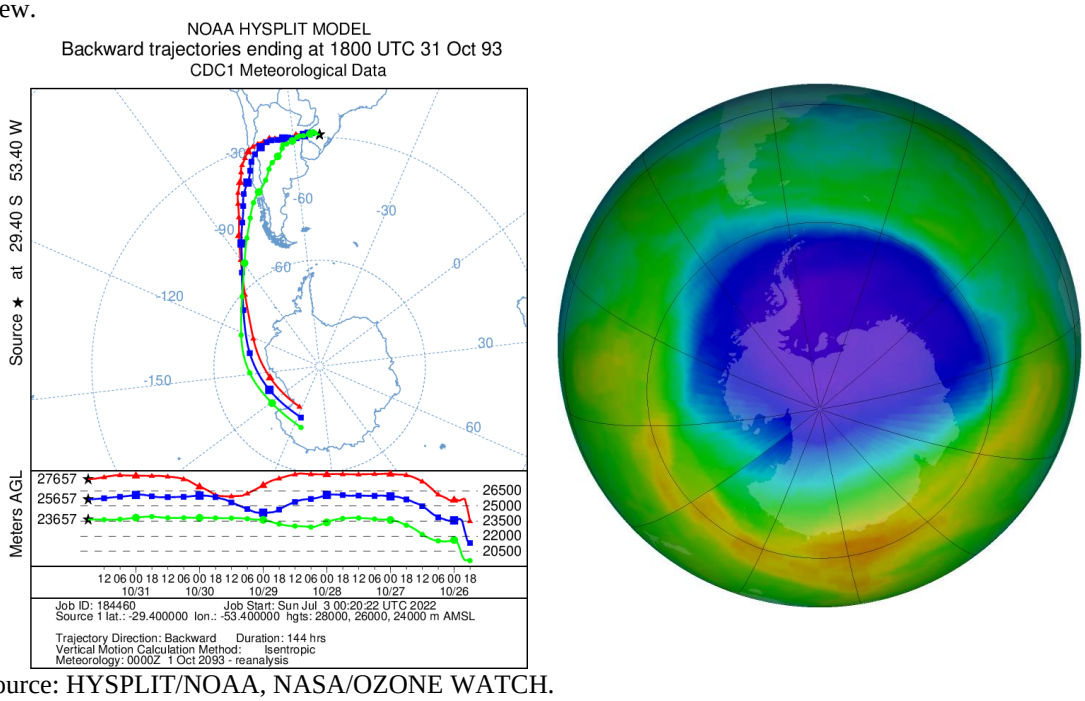

Source: HYSPLIT/NOAA, NASA/OZONE WATCH.

Figure A89: Vertical section of the atmosphere between 1000 and 5 hPa for the days of the event in October 1993.

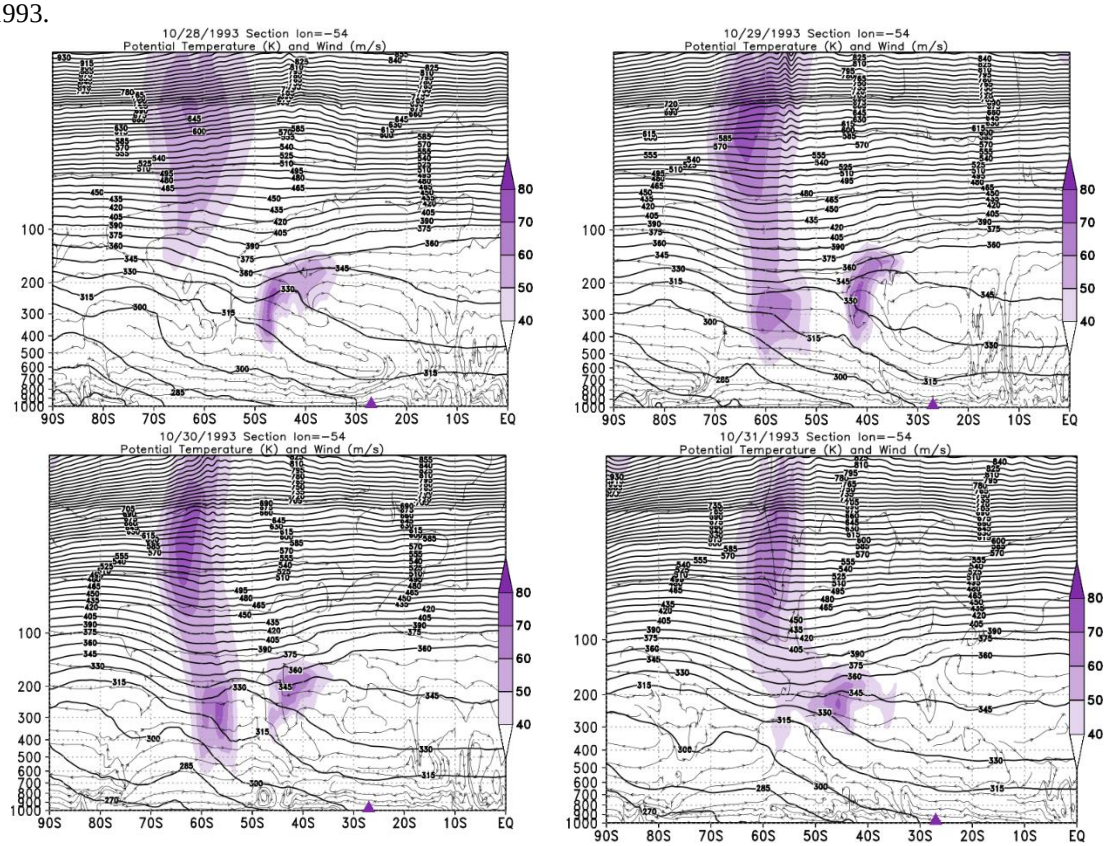

Source: The author.

08/16/1994

Figure A90: PVA fields for the 20 hPa in pressure levels, days 08/14/1994 to 08/17/1994.

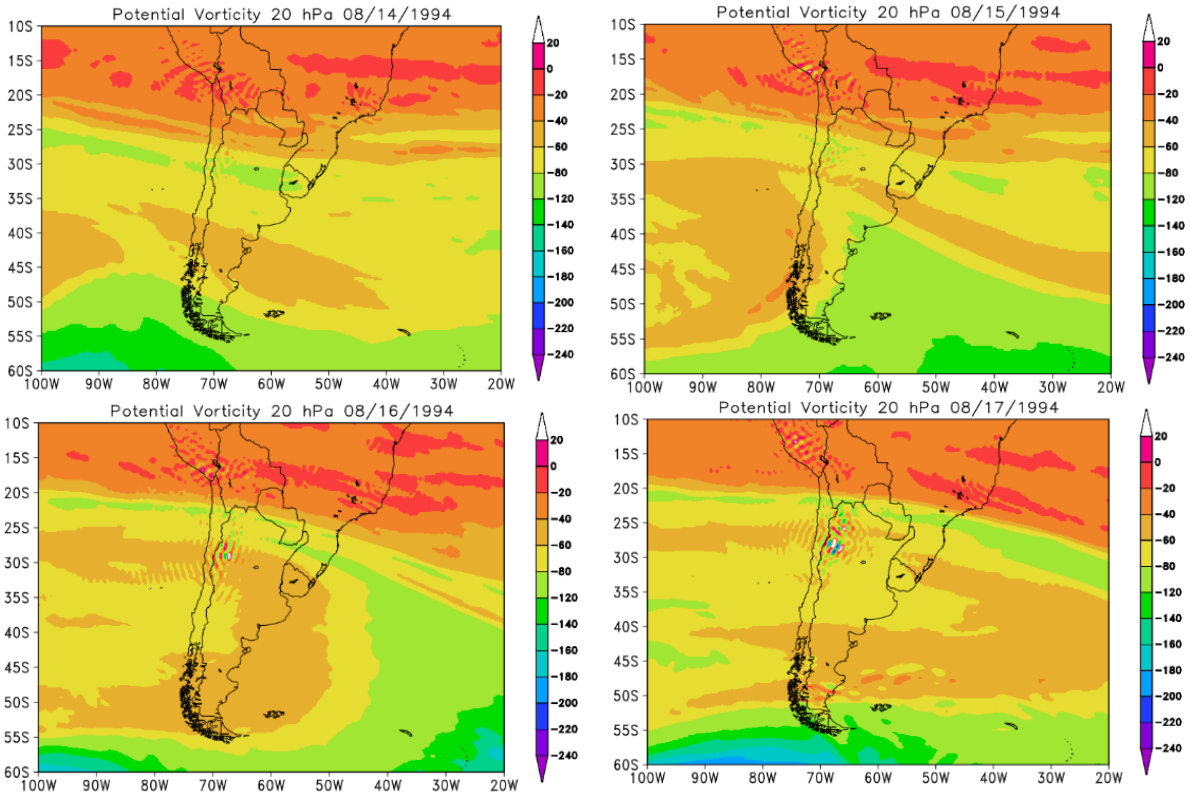

Source: The author.

Figure A91: Retroactive trajectory by the HYSPLIT/NOAA model.

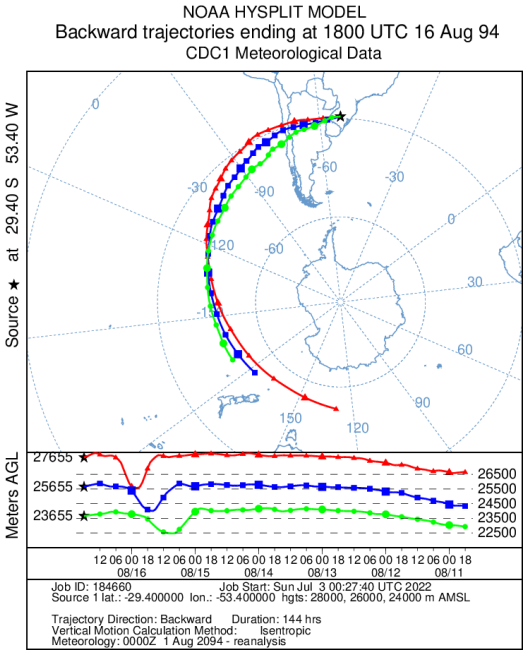

Source: HYSPLIT/NOAA.

Figure A92: Vertical section of the atmosphere between 1000 and 5 hPa for the days of the event in August 1994.

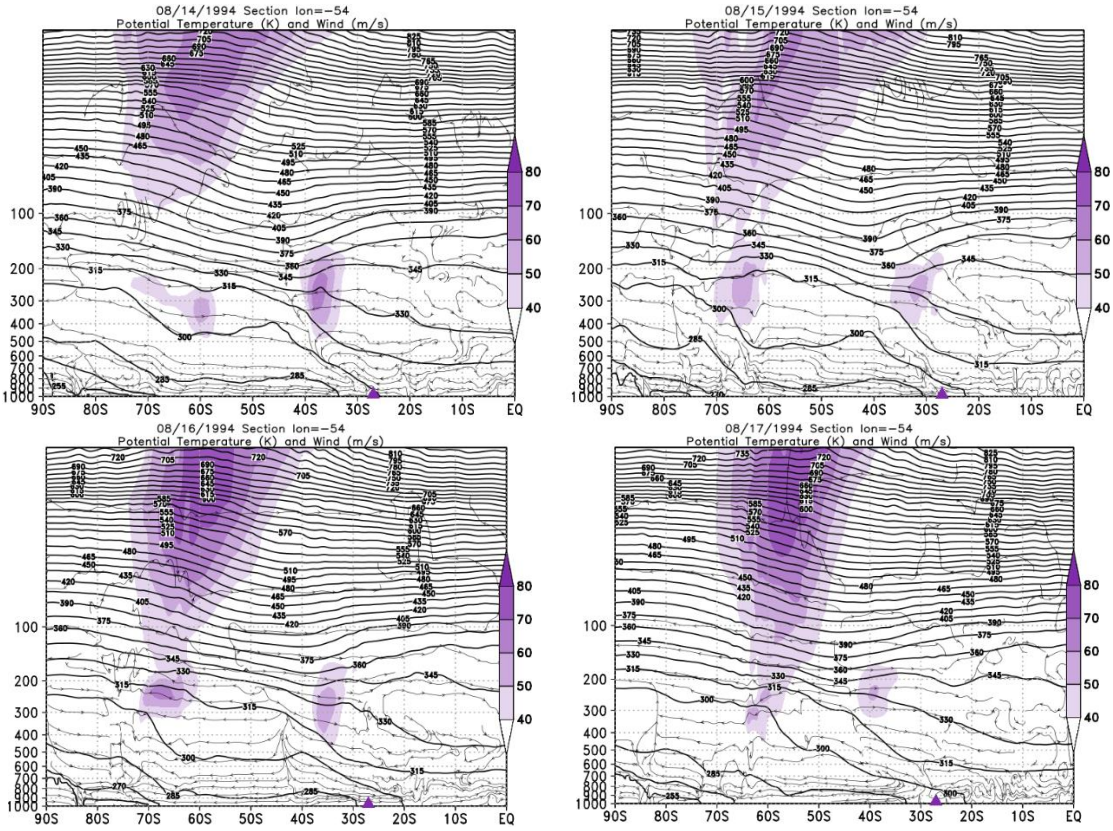

Source: The author.

09/17/1994

Figure A93: PVA fields for the 20 hPa in pressure levels, days 09/14/1994 to 09/18/1994.

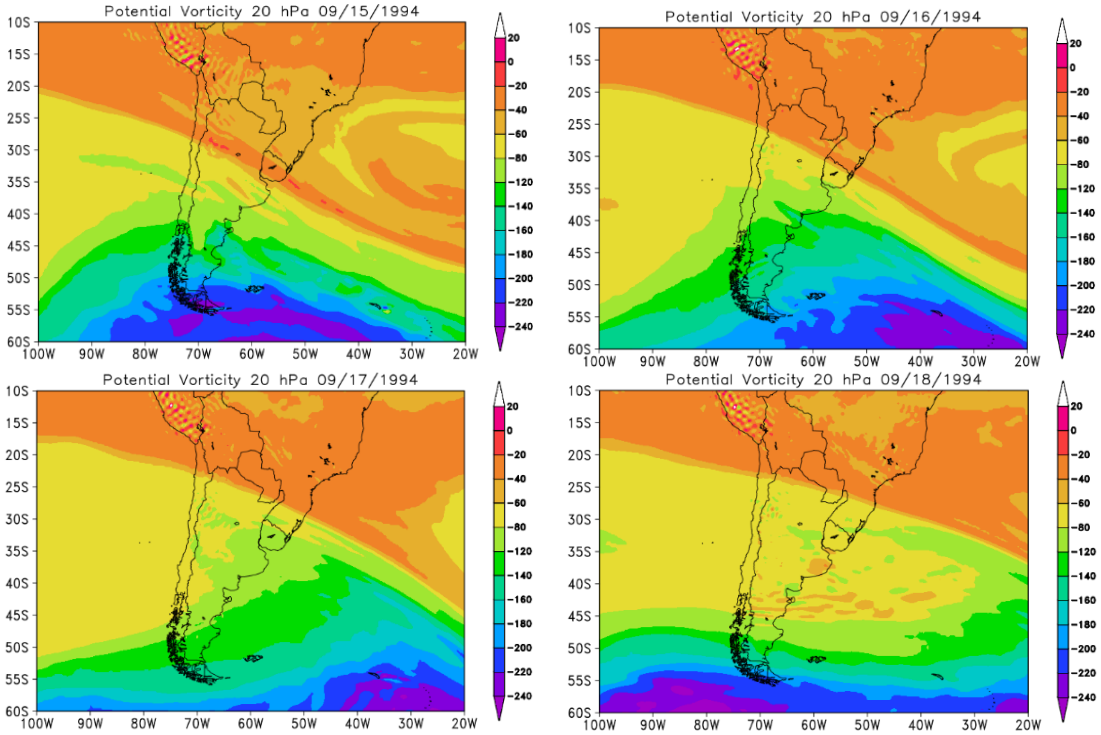

Source: The author.

Figure A94: Retroactive trajectory by the HYSPLIT/NOAA model, and O3 content satellite for South Pole view.

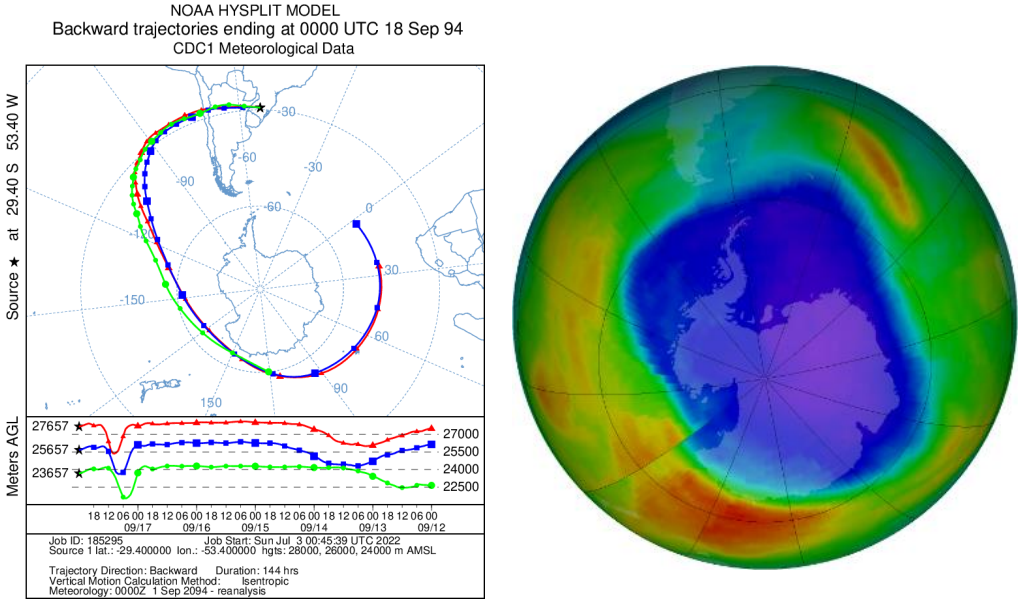

Source: HYSPLIT/NOAA, NASA/OZONE WATCH.

Figure A95: Vertical section of the atmosphere between 1000 and 5 hPa for the days of the event in September 1994.

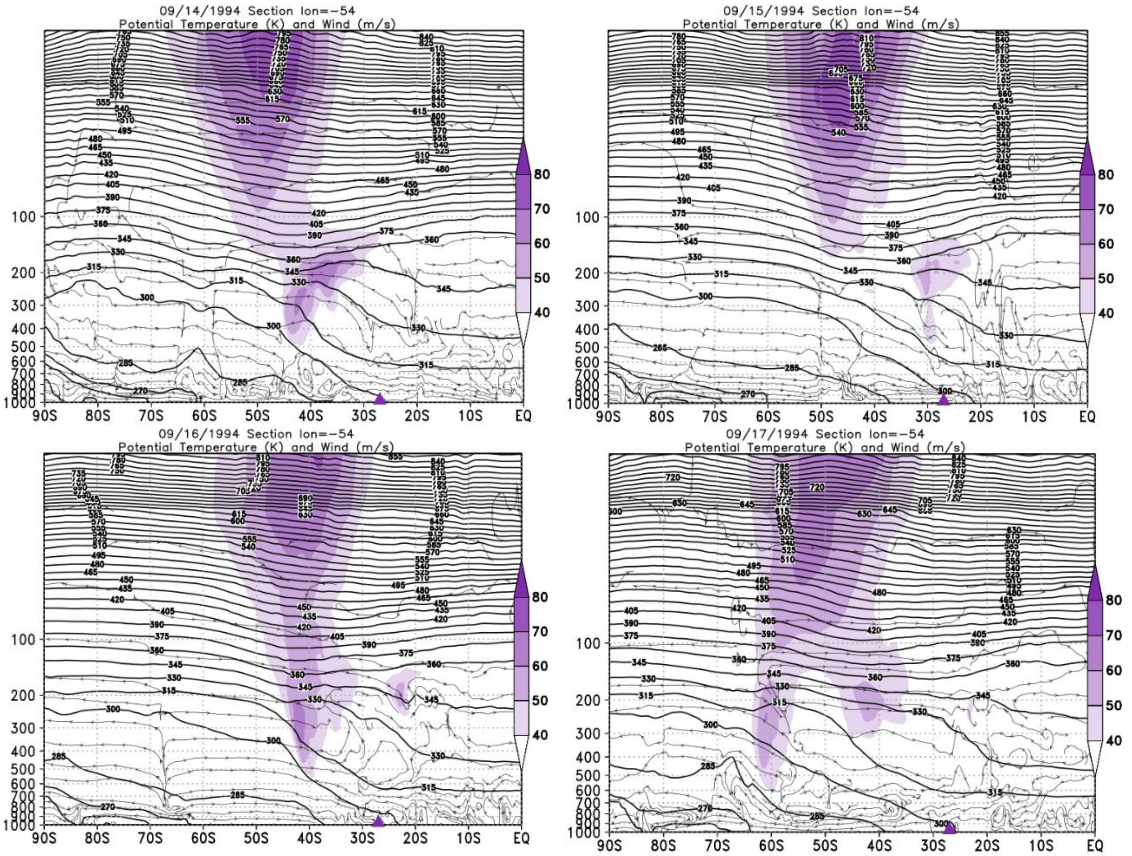

Source: The author.

10/01/1995

Figure A96: PVA fields for the 20 hPa in pressure levels, days 09/29/1995 10/02/1995.

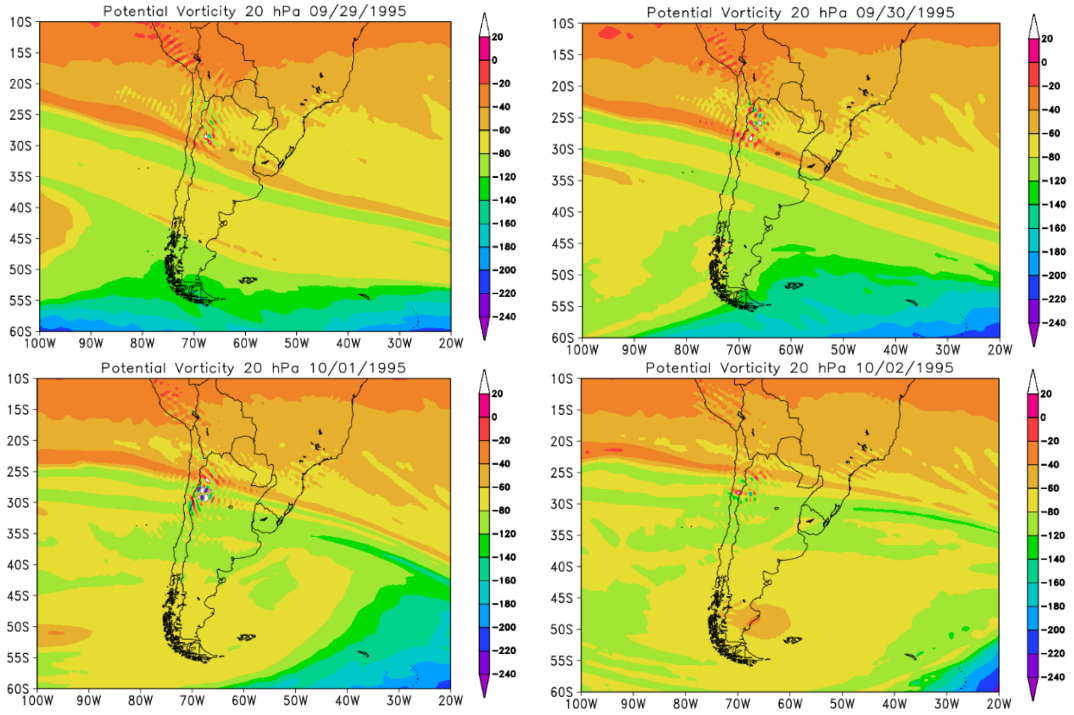

Source: The author.

Figure A97: Vertical section of the atmosphere between 1000 and 5 hPa for the days of the event in October 1996.

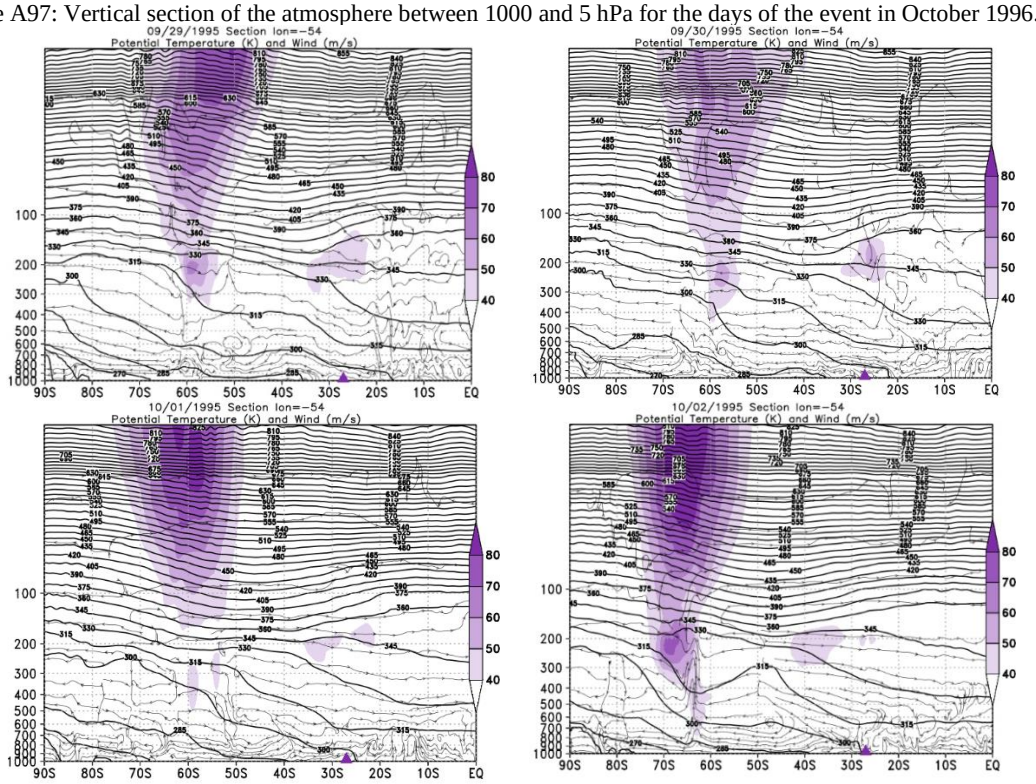

09/20/1996

Figure A98: PVA fields for the 20 hPa in pressure levels, days 09/18/1996 to 09/21/1996.

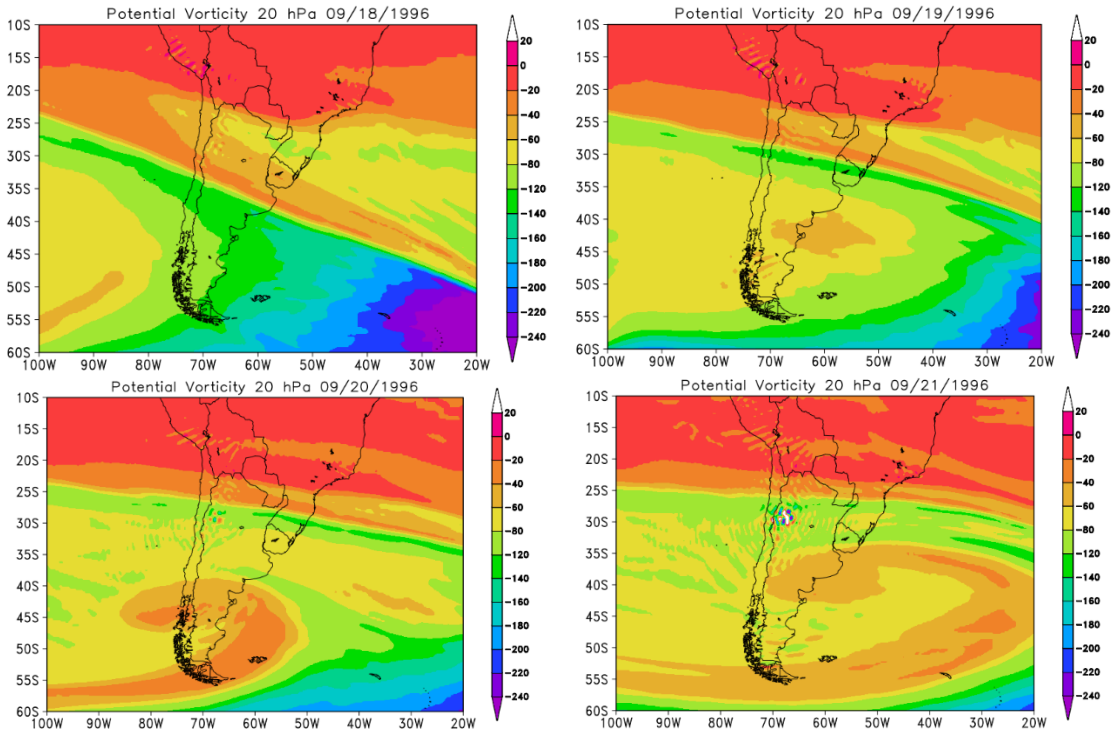

Source: The author.

Figure A99: Retroactive trajectory by the HYSPLIT/NOAA model, and O3 content satellite for South Pole view.

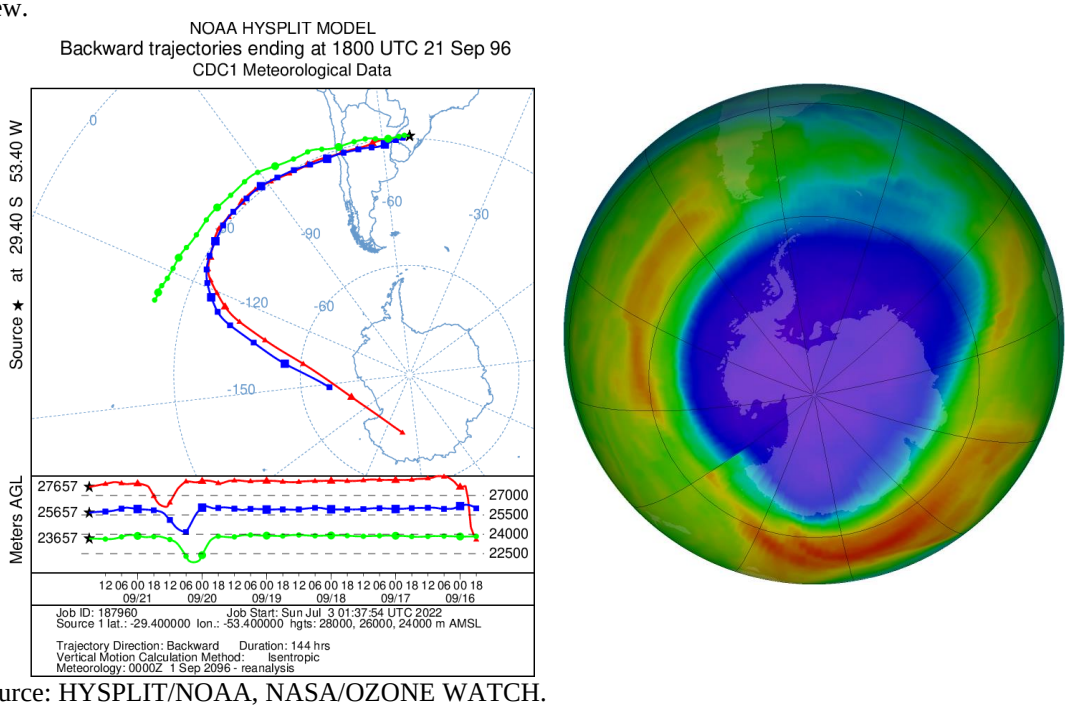

Source: HYSPLIT/NOAA, NASA/OZONE WATCH.

Figure A100: Vertical section of the atmosphere between 1000 and 5 hPa for the days of the event in October 1996.

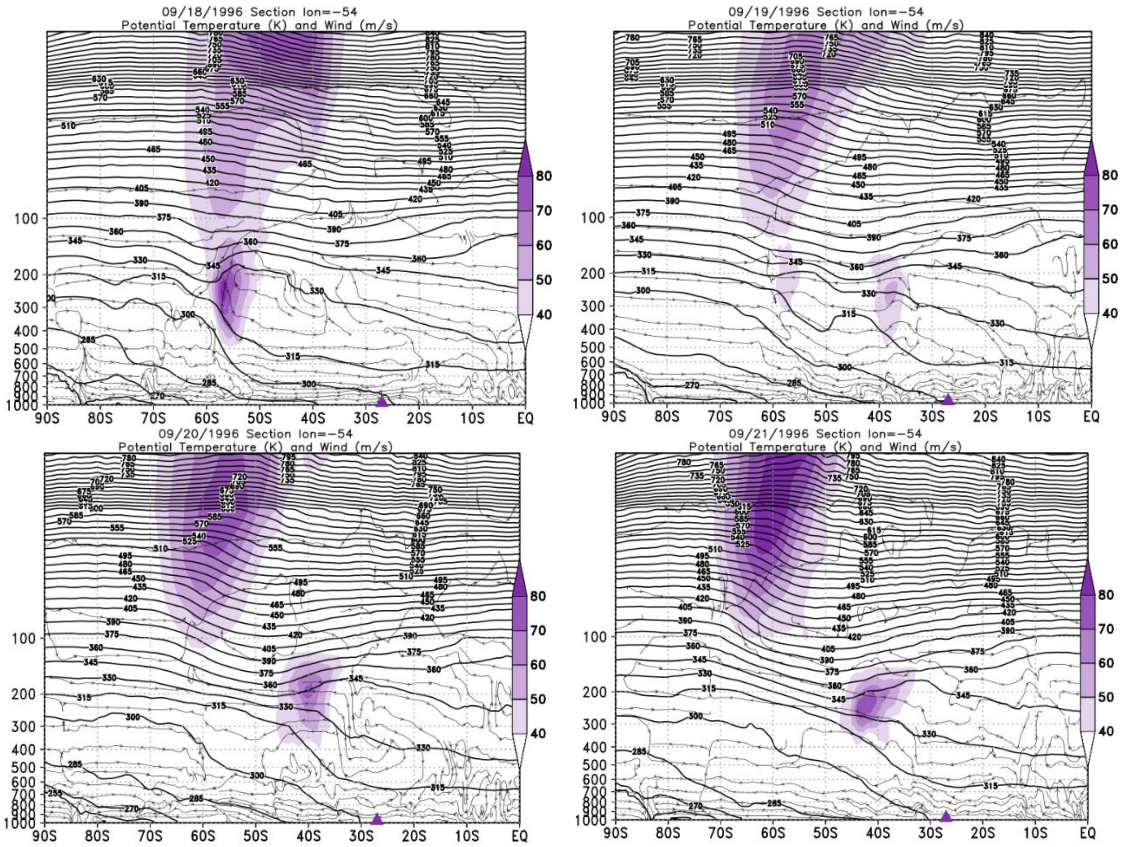

Source: The author.

08/18/1997

Figure A101: PVA fields for the 20 hPa in pressure levels, days 08/18/1997 to 08/21/1997.

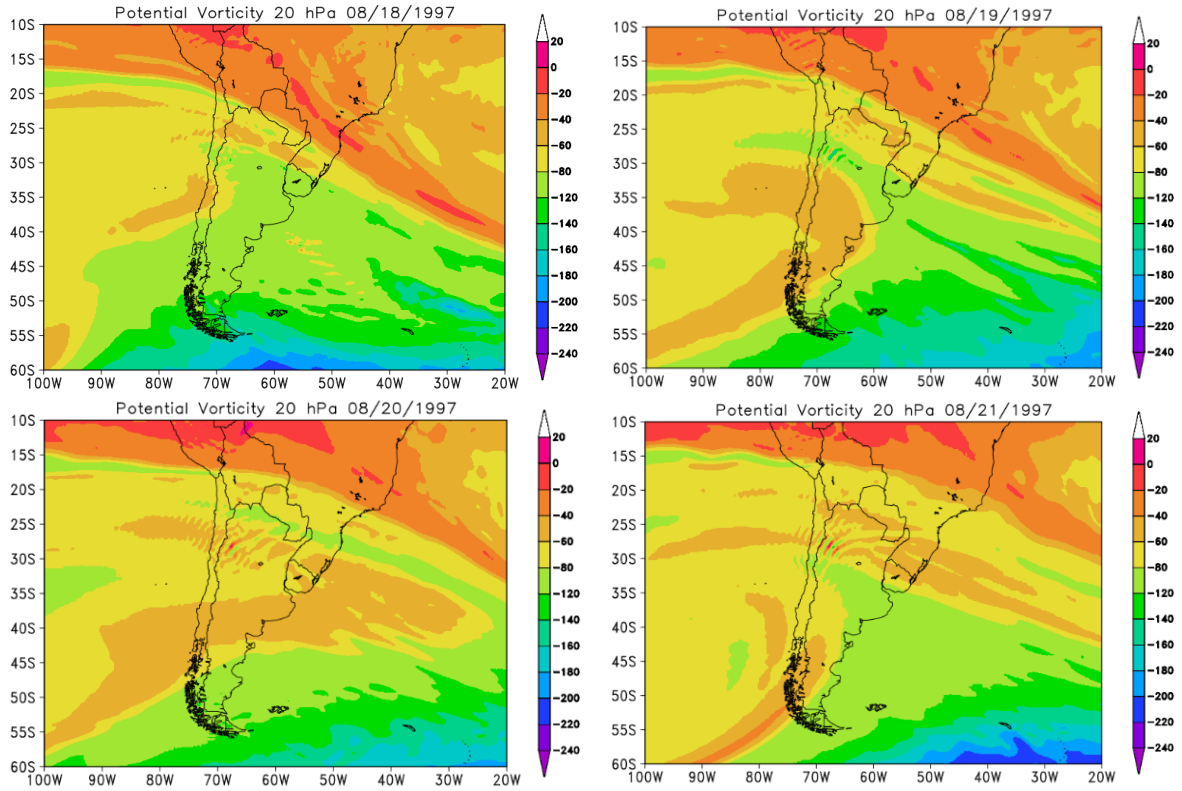

Figure A102: Retroactive trajectory by the HYSPLIT/NOAA model, and O3 content satellite for South Pole view.

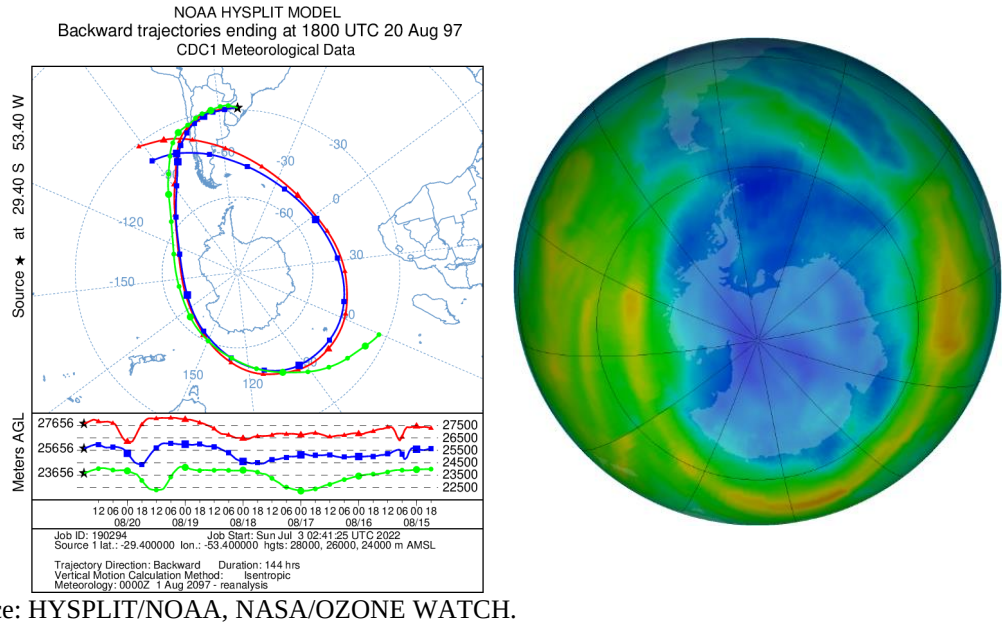

Source: HYSPLIT/NOAA, NASA/OZONE WATCH.

Figure A103: Vertical section of the atmosphere between 1000 and 5 hPa for the days of the event in October 2016

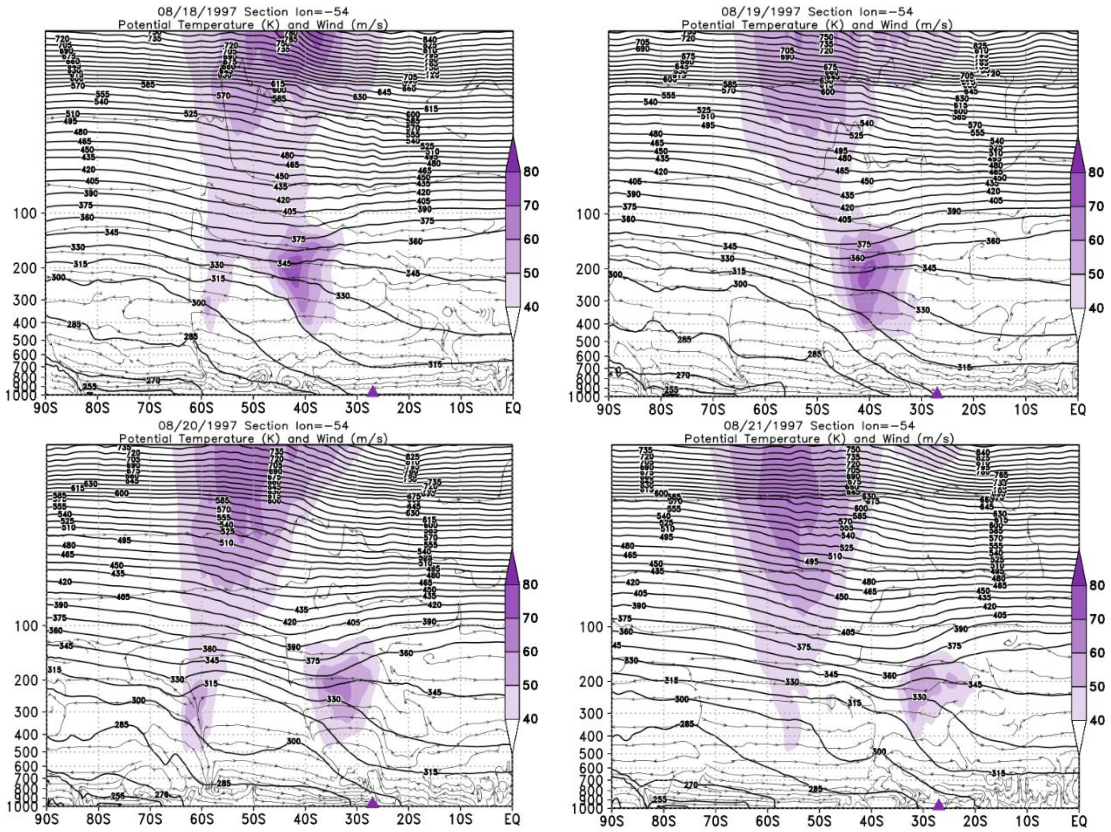

Source: The author.

09/14/1997

Figure A104: PVA fields for the 20 hPa in pressure levels, days 09/12/1997 to 09/15/1997.

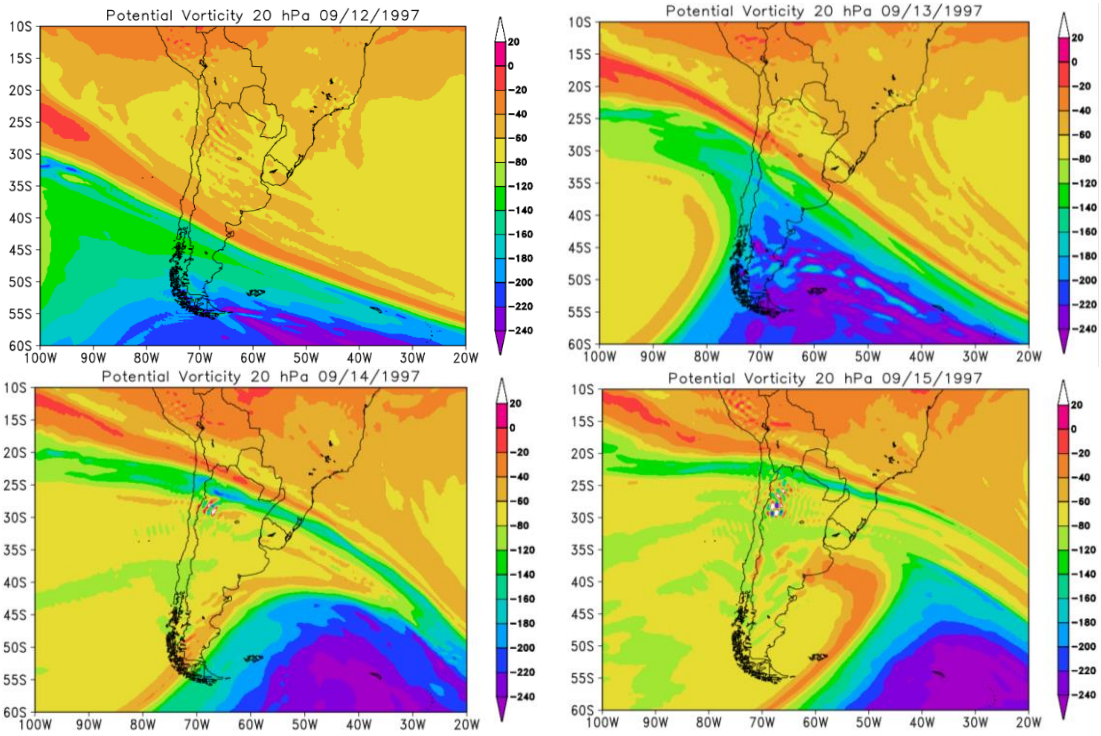

Figure A105: Retroactive trajectory by the HYSPLIT/NOAA model, and O3 content satellite for South Pole view.

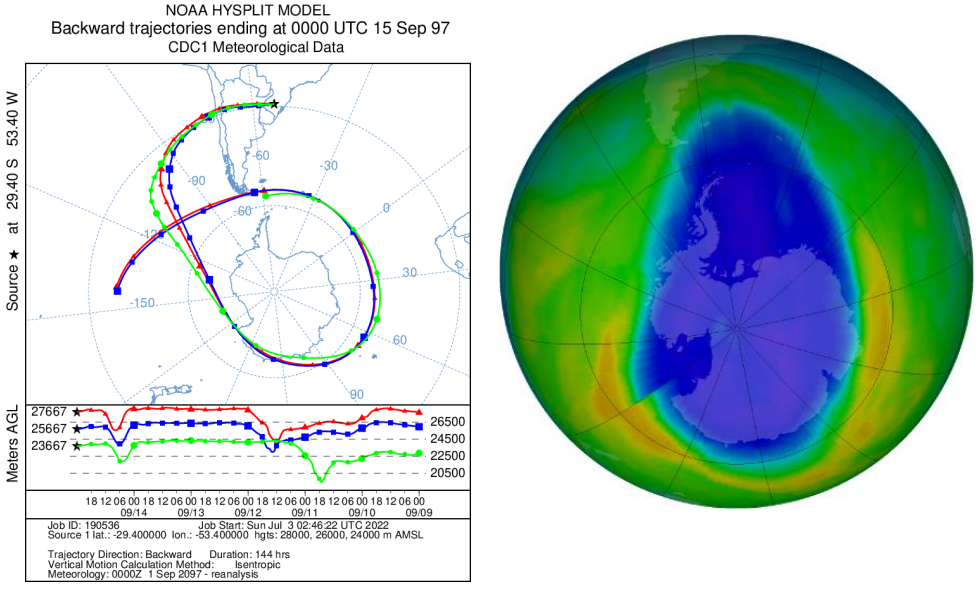

Source: HYSPLIT/NOAA, NASA/OZONE WATCH.

Figure A106: Vertical section of the atmosphere between 1000 and 5 hPa for the days of the event in September 1997.

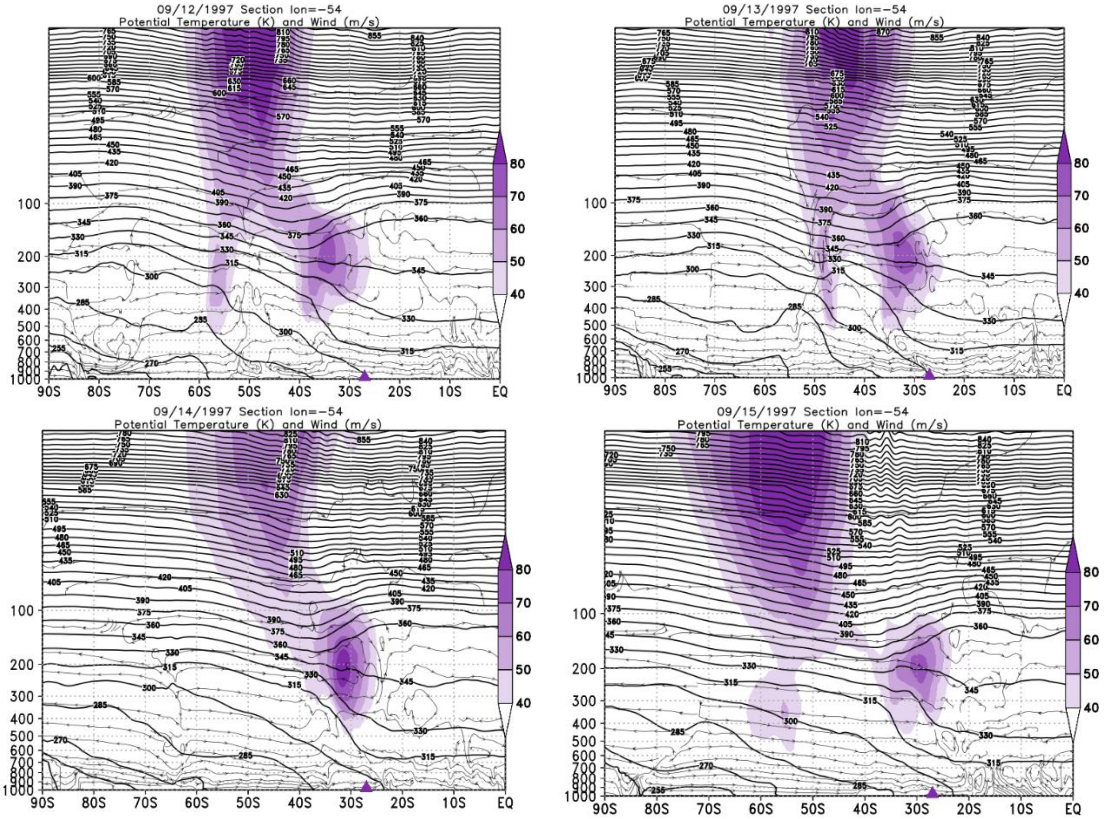

Source: The author.

10/16/1997

Figure A107: PVA fields for the 20 hPa in pressure levels, days 10/14/1997 to 10/17/1997.

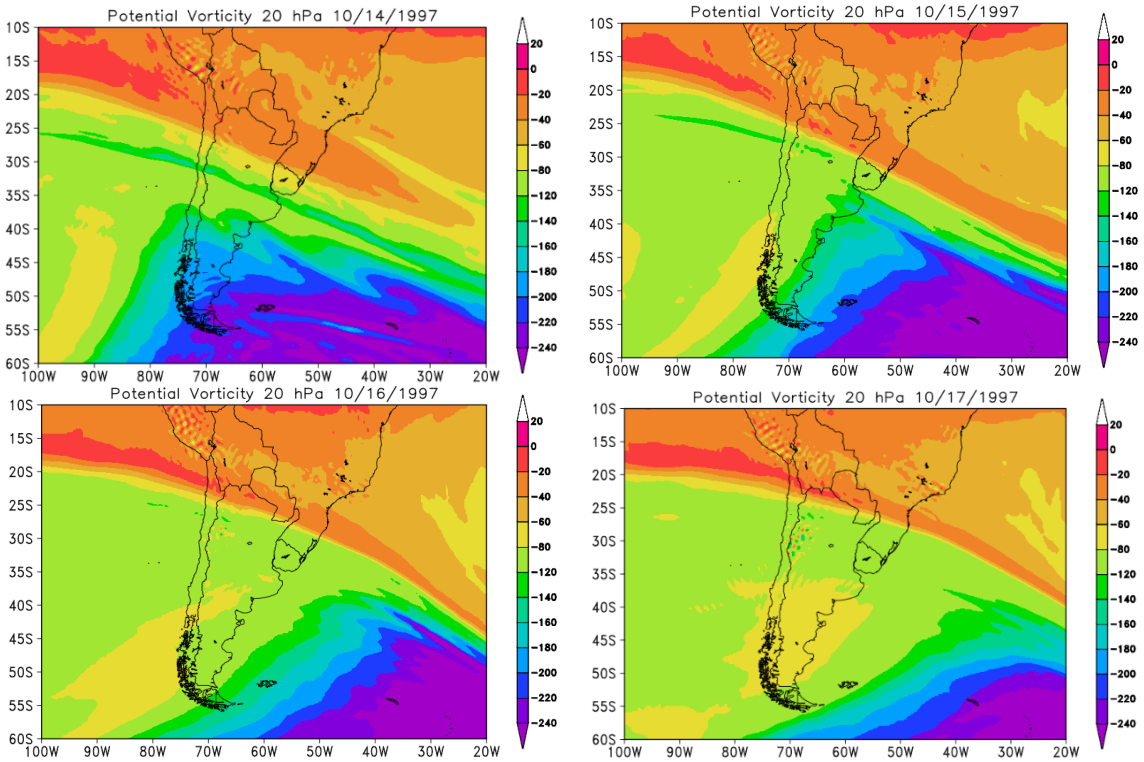

Figure A108: Retroactive trajectory by the HYSPLIT/NOAA model, and O3 content satellite for South Pole view.

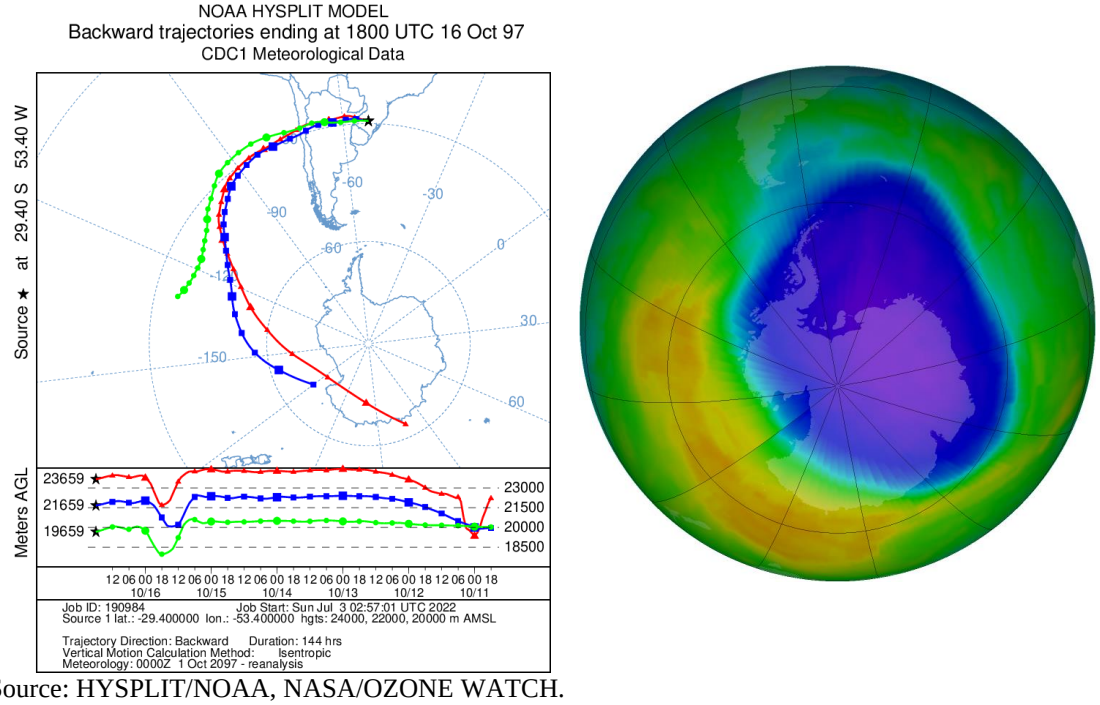

Source: HYSPLIT/NOAA, NASA/OZONE WATCH.

Figure A109: Vertical section of the atmosphere between 1000 and 5 hPa for the days of the event in October 1997.

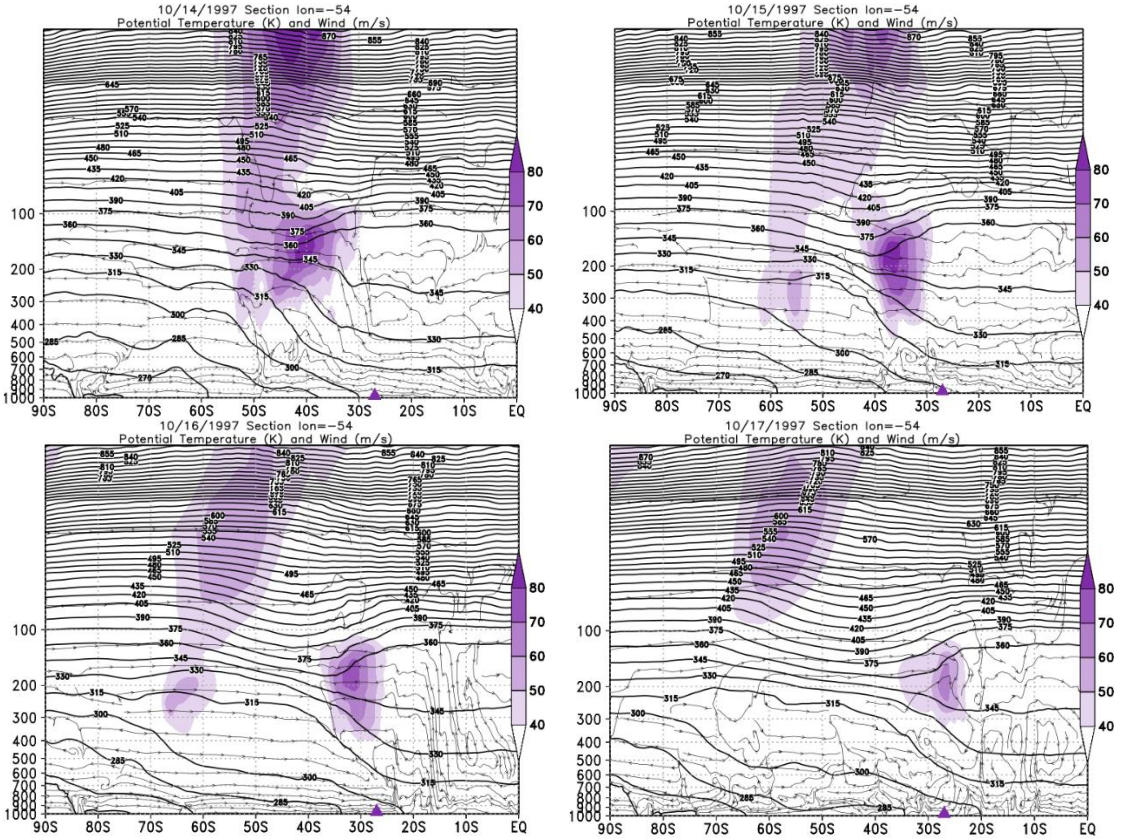

11/02/1997

Figure A110: PVA fields for the 20 hPa in pressure levels, days 10/31/1997 to 11/03/1997.

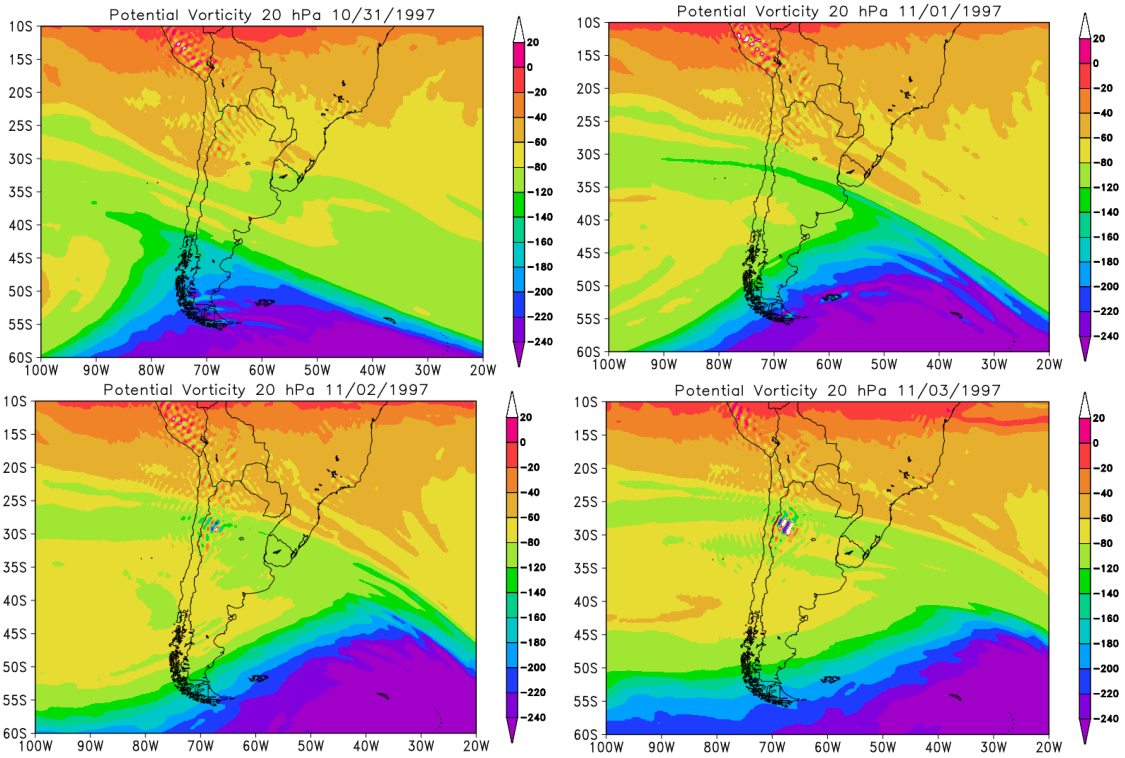

Figure A111: Retroactive trajectory by the HYSPLIT/NOAA model, and O3 content satellite for South Pole view.

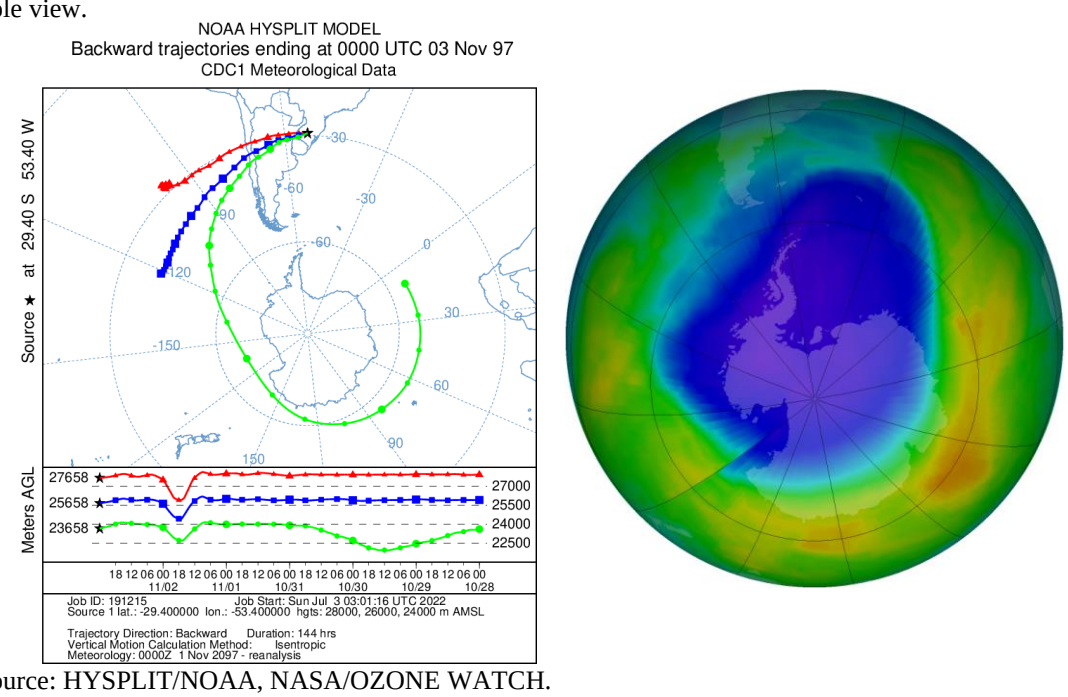

Source: HYSPLIT/NOAA, NASA/OZONE WATCH.

Figure A107: Vertical section of the atmosphere between 1000 and 5 hPa for the days of the event in November 1997.

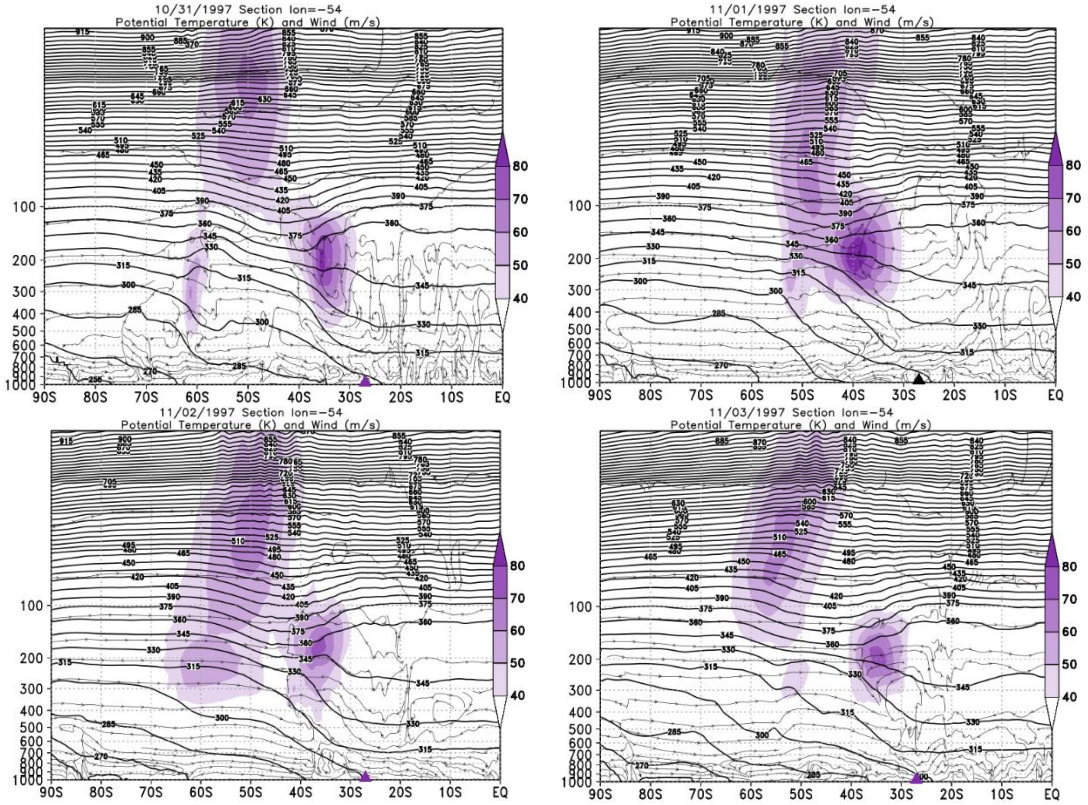

11/19/1997

Figure A108: PVA fields for the 20 hPa in pressure levels, days 11/17/1997 to 11/20/1997.

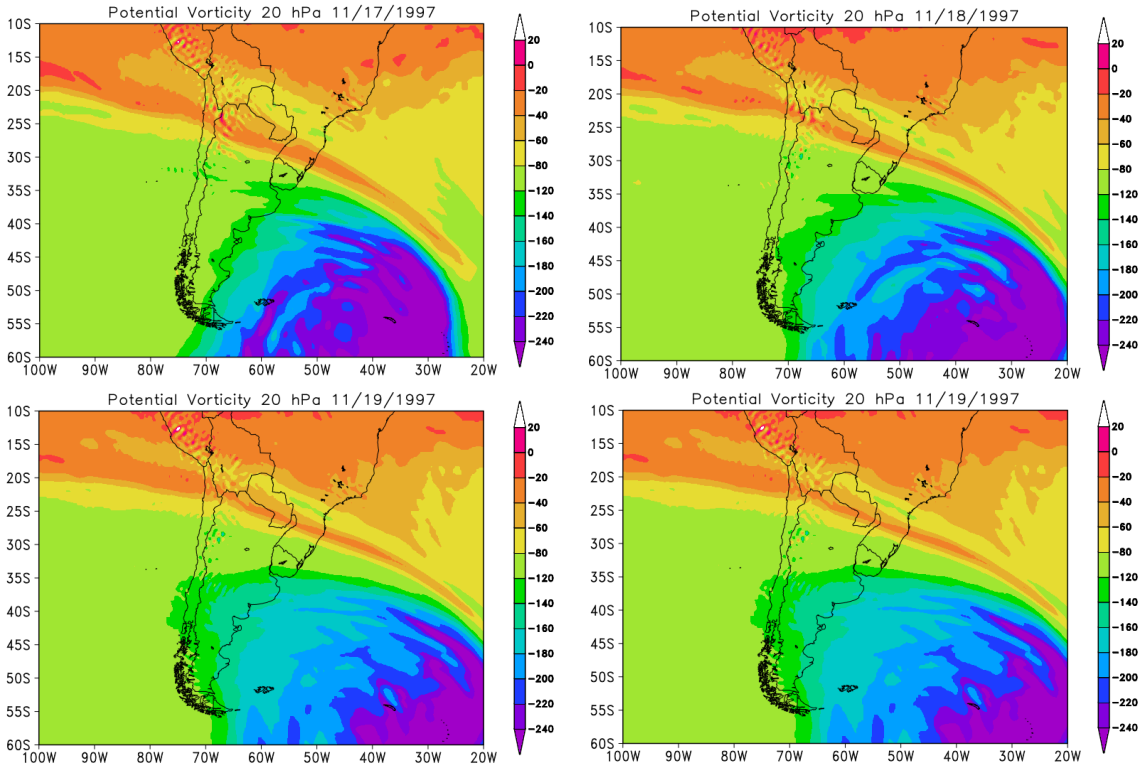

Figure A109: Retroactive trajectory by the HYSPLIT/NOAA model, and O3 content satellite for South Pole view.

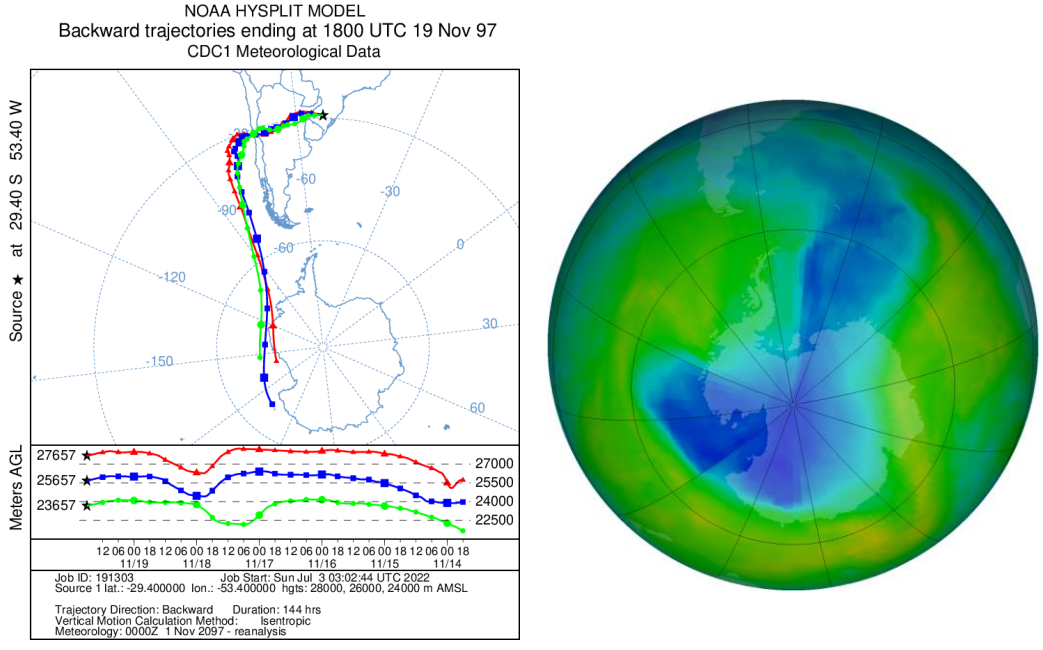

Source: HYSPLIT/NOAA, NASA/OZONE WATCH.

Figure 110: Vertical section of the atmosphere between 1000 and 5 hPa for the days of the event in October 2016.

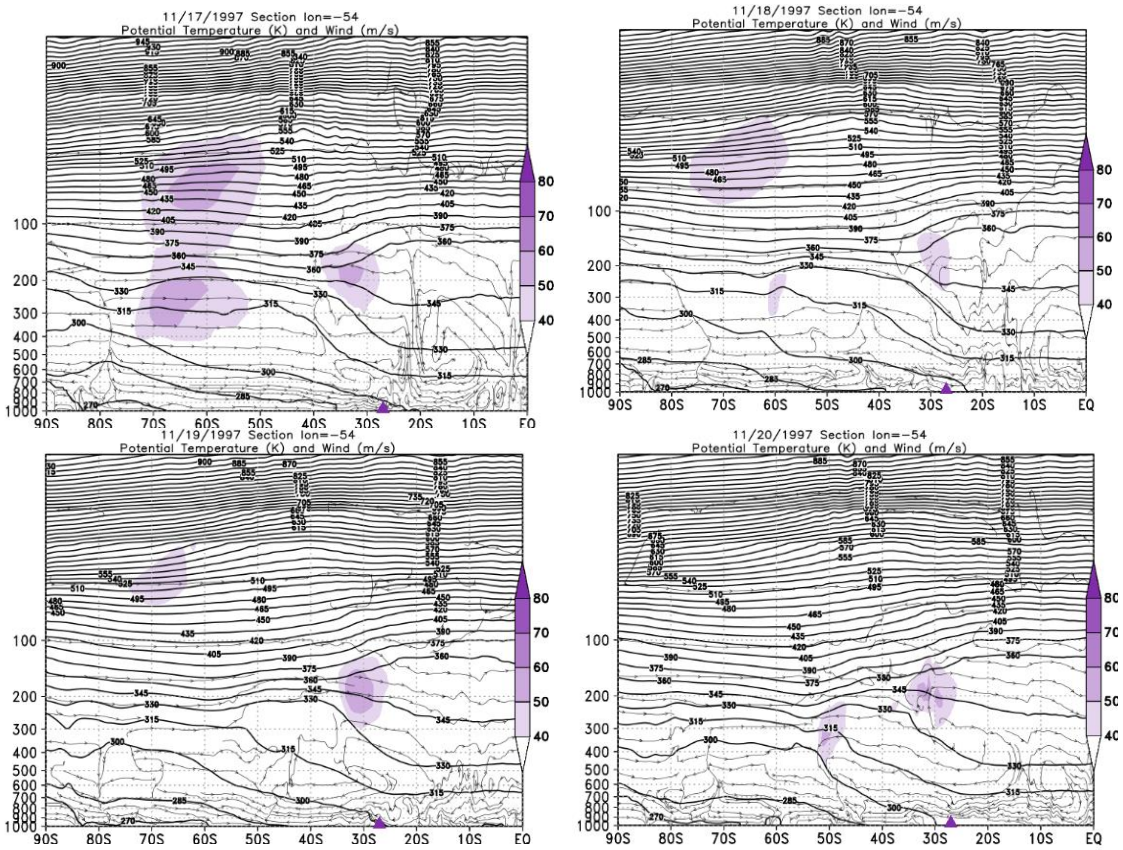

Source: The author.

10/24/1998

Figure A111: PVA fields for the 20 hPa in pressure levels, days 10/22/1998 to 10/25/1998.

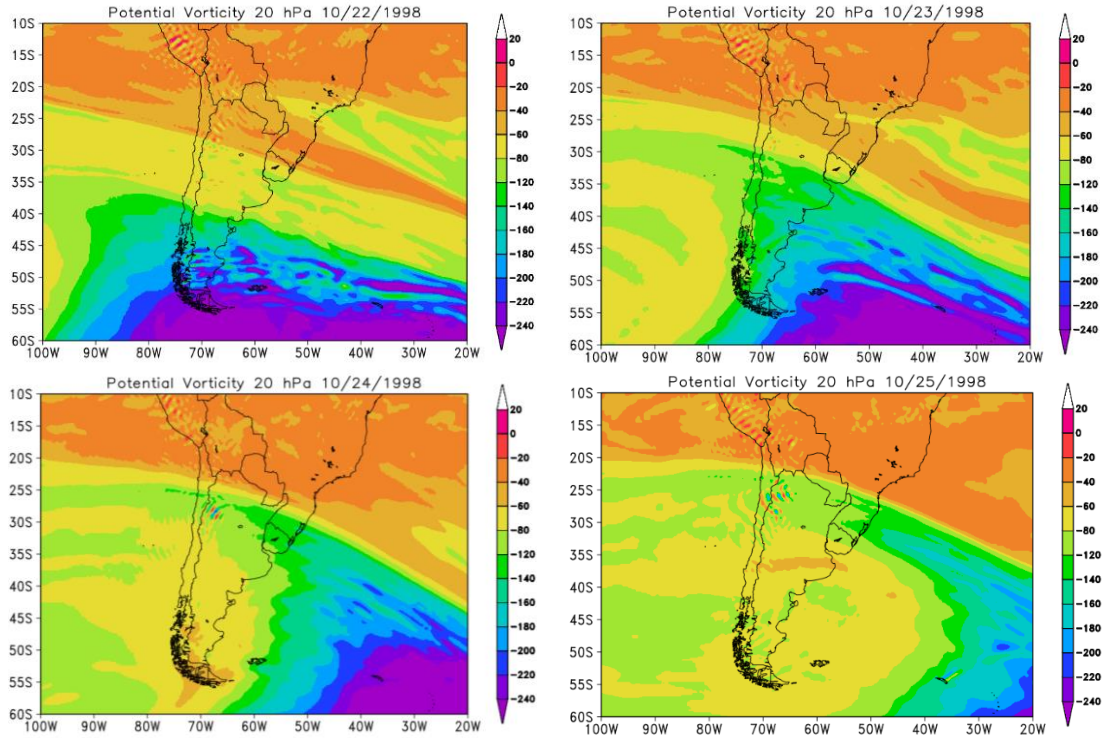

Figure A112: Retroactive trajectory by the HYSPLIT/NOAA model, and O3 content satellite for South Pole view.

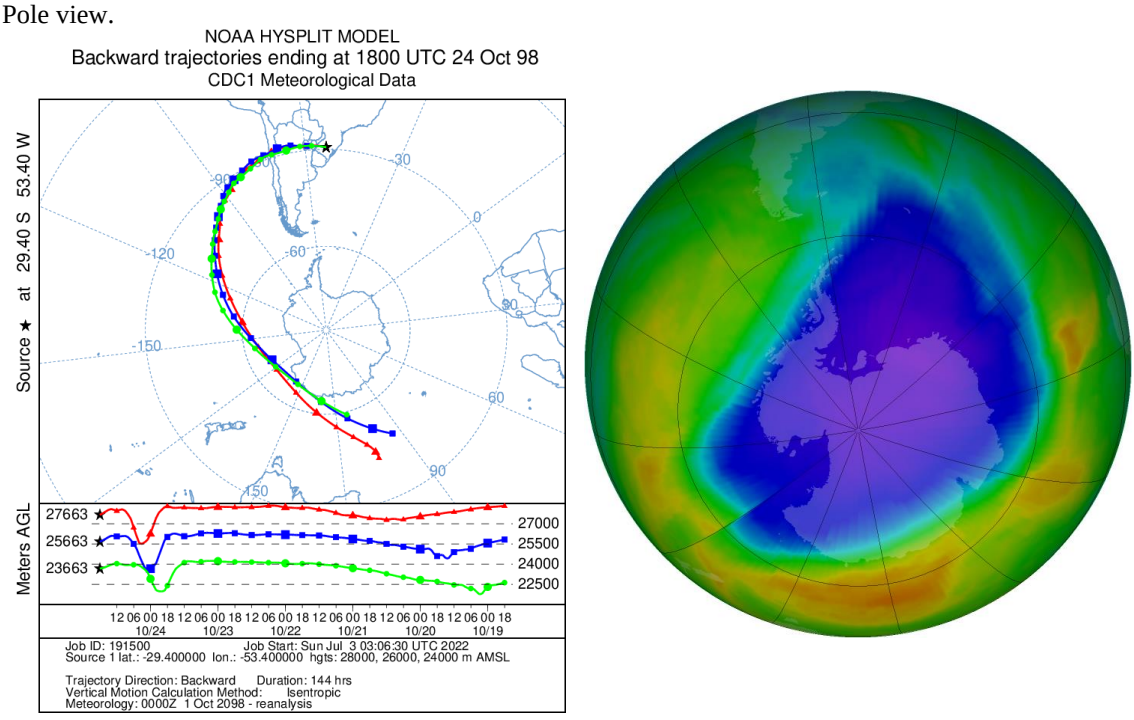

Source: HYSPLIT/NOAA, NASA/OZONE WATCH.

Figure A113: Vertical section of the atmosphere between 1000 and 5 hPa for the days of the event in October 21998.

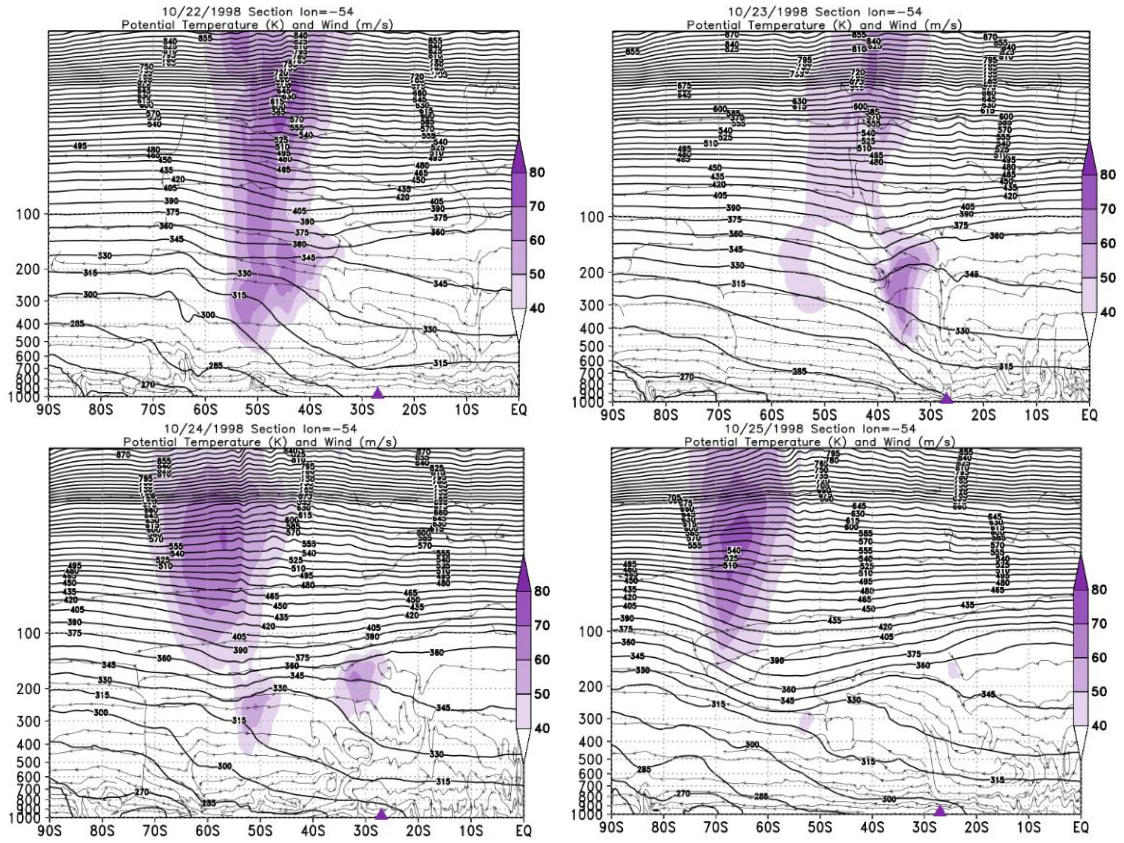

Source: The author.

08/21/1999

Figure A114: PVA fields for the 20 hPa in pressure levels, days 08/19/1999 to 08/22/1999.

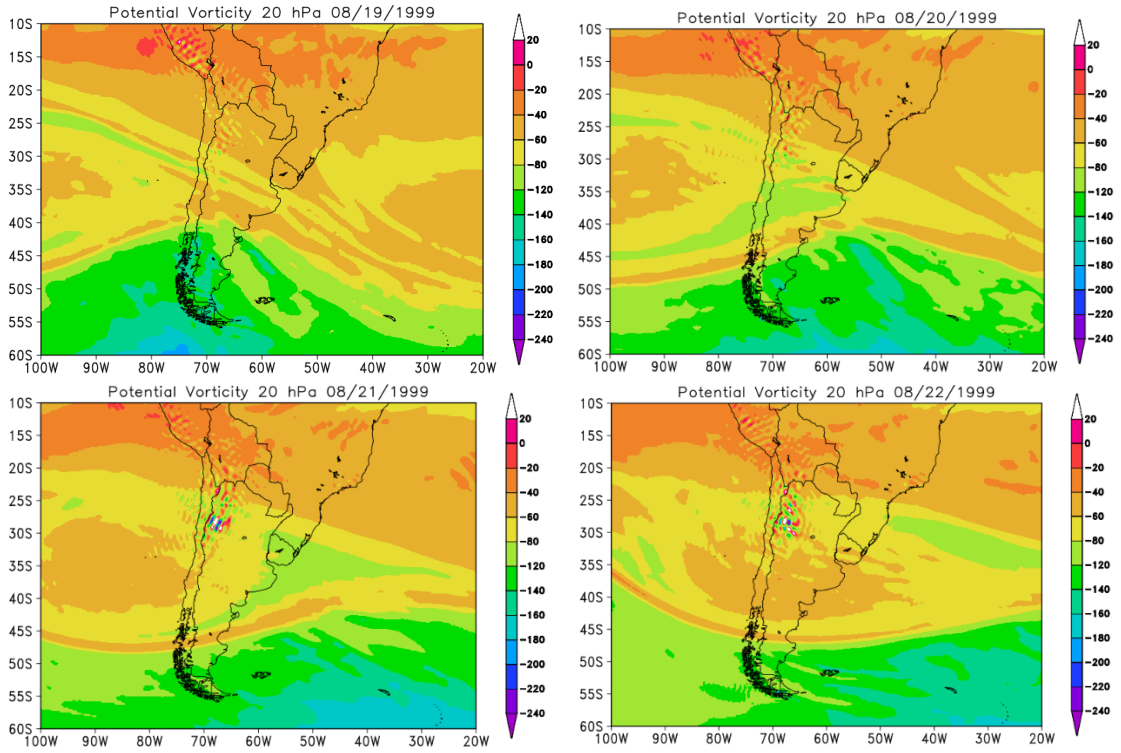

Figure A115: Retroactive trajectory by the HYSPLIT/NOAA model, and O3 content satellite for South Pole view.

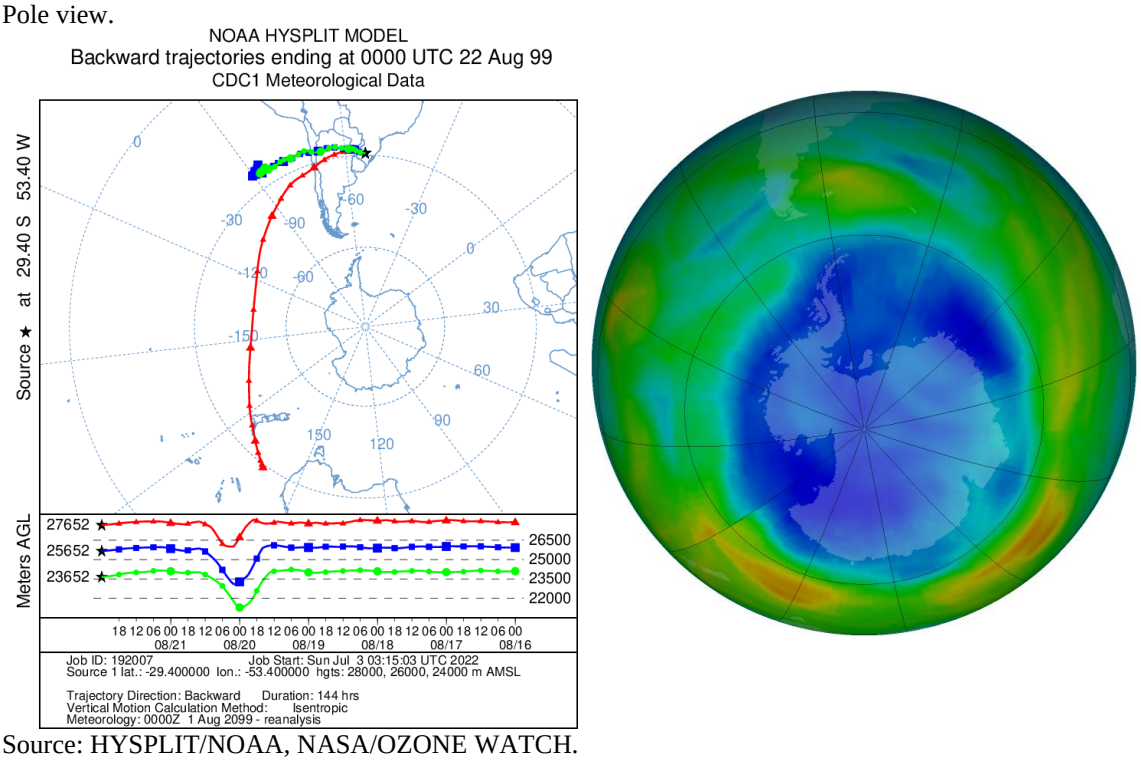

Source: HYSPLIT/NOAA, NASA/OZONE WATCH.

Figure A116: Vertical section of the atmosphere between 1000 and 5 hPa for the days of the event in August 1999.

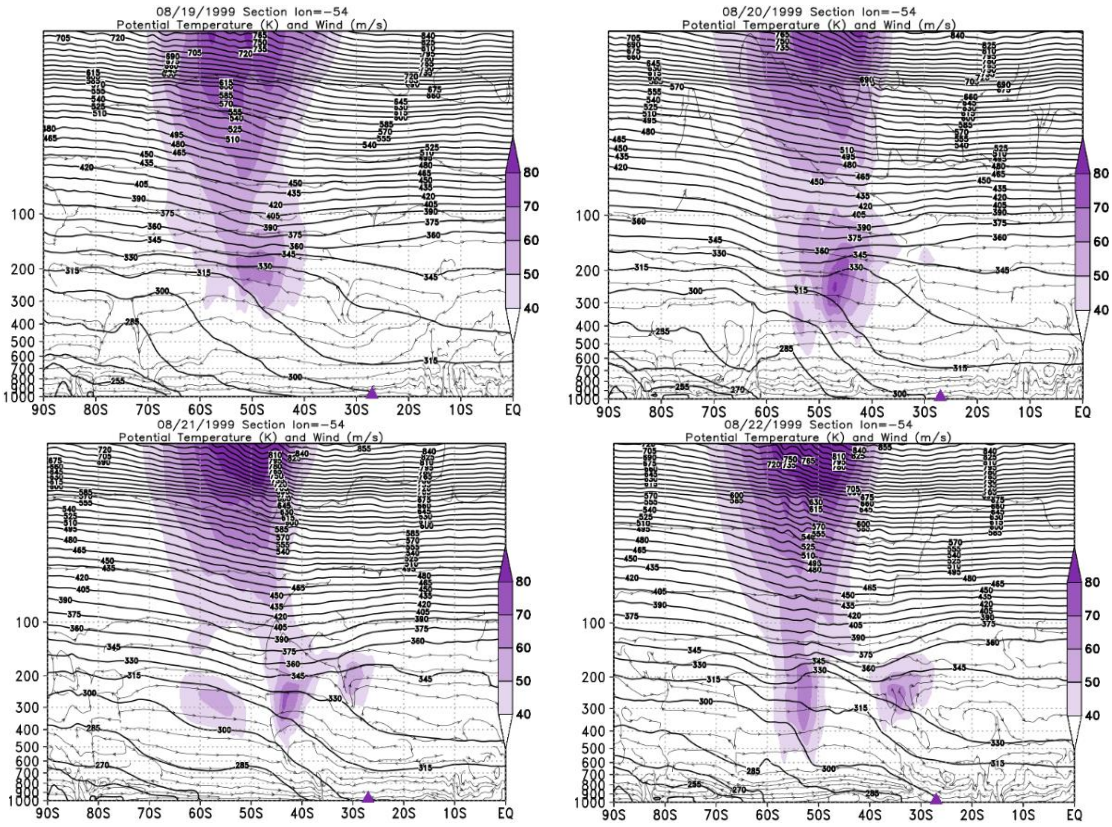

10/07/1999

Figure A117: PVA fields for the 20 hPa in pressure levels, days 10/05/1999 to 10/08/1999.

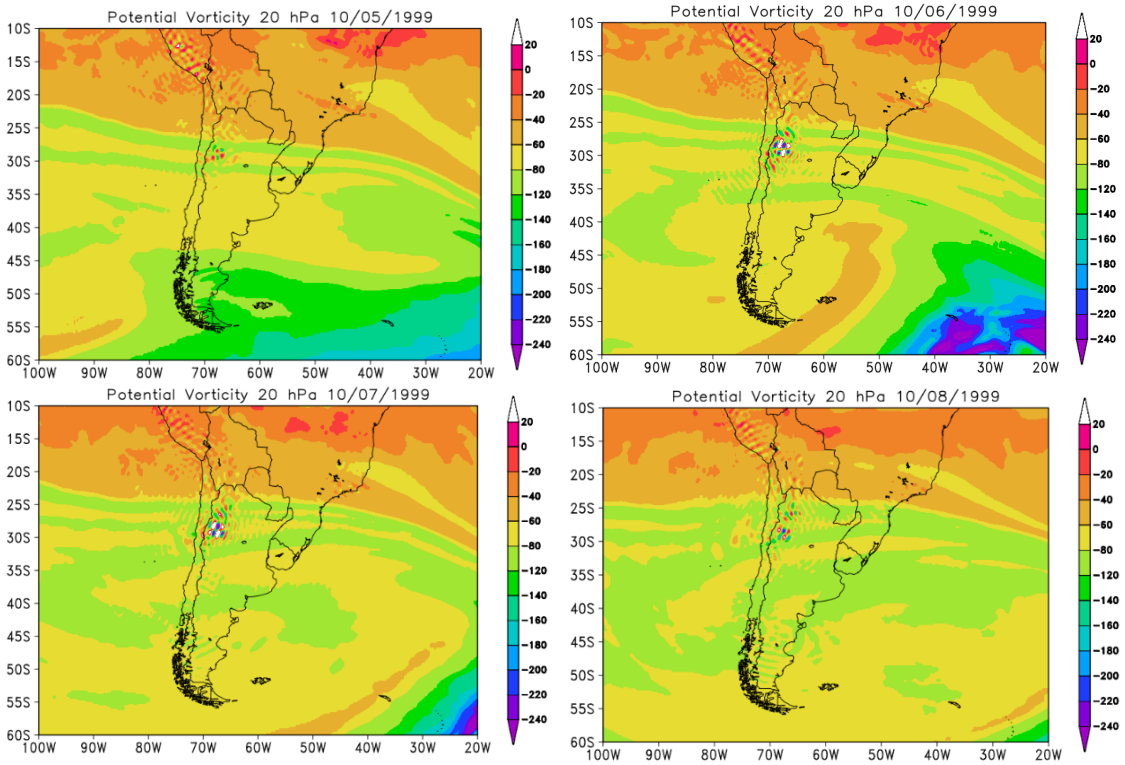

Figure A118: Retroactive trajectory by the HYSPLIT/NOAA model, and O3 content satellite for South Pole view.

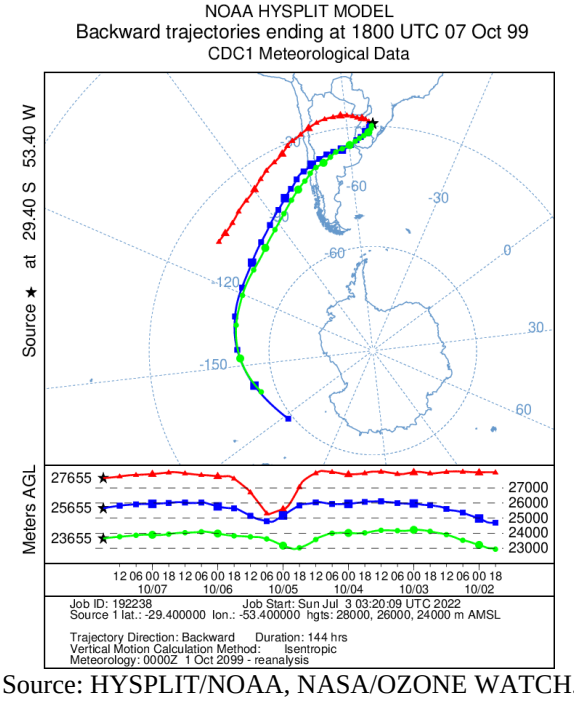

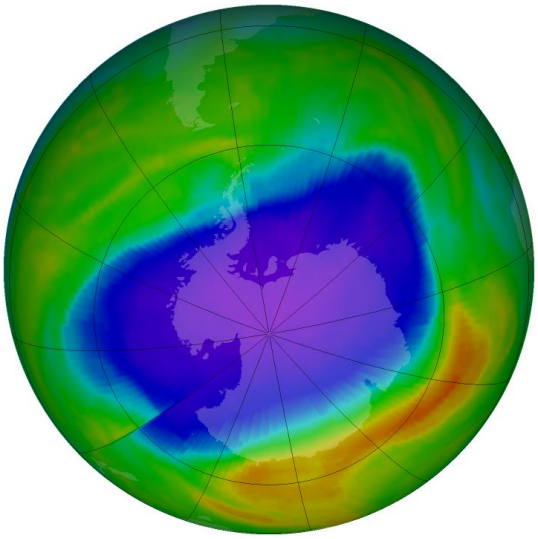

Source: HYSPLIT/NOAA, NASA/OZONE WATCH.

Figure A119: Vertical section of the atmosphere between 1000 and 5 hPa for the days of the event in October 1999.

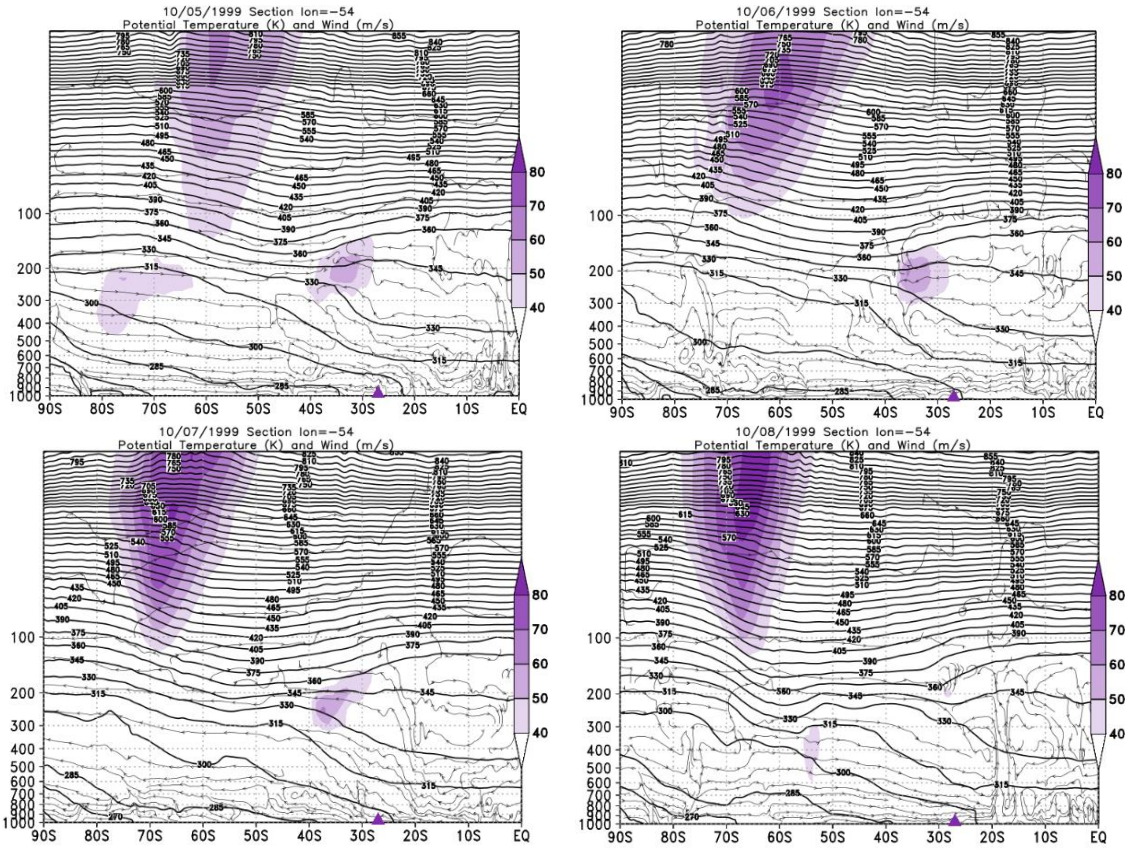

Source: The author.

09/23/2000

Figure A120: PVA fields for the 20 hPa in pressure levels, days 09/23/2000 to 09/24/2000.

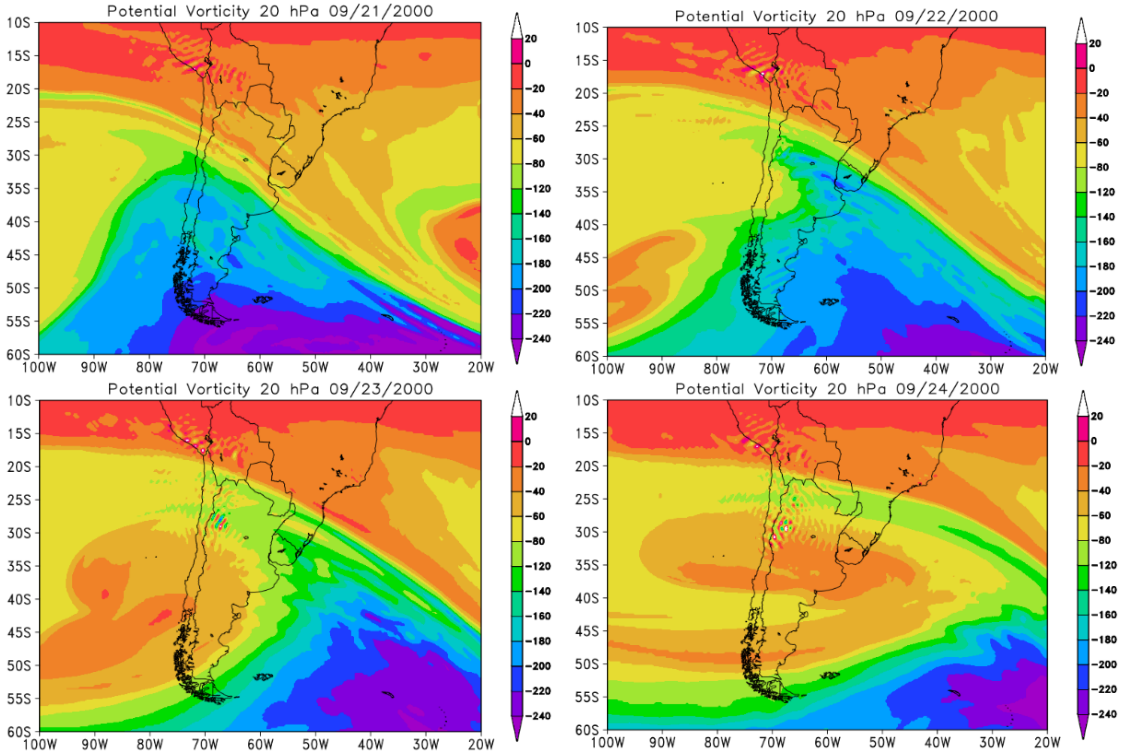

Figure A121: Retroactive trajectory by the HYSPLIT/NOAA model, and O3 content satellite for South Pole view.

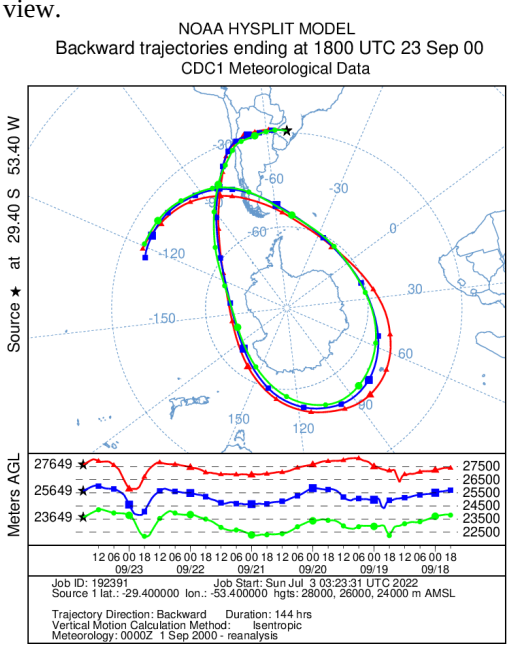

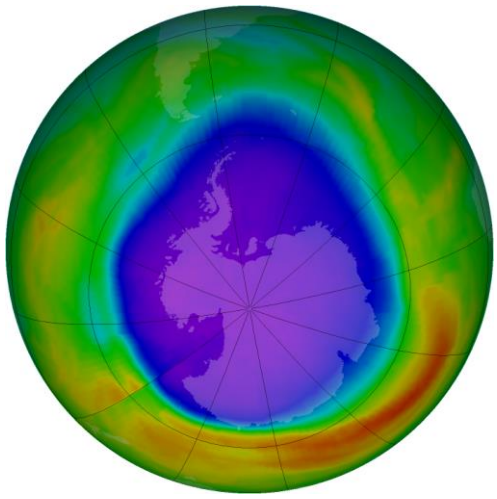

Source: HYSPLIT/NOAA, NASA/OZONE WATCH.

Figure A122: Vertical section of the atmosphere between 1000 and 5 hPa for the days of the event in October 2000.

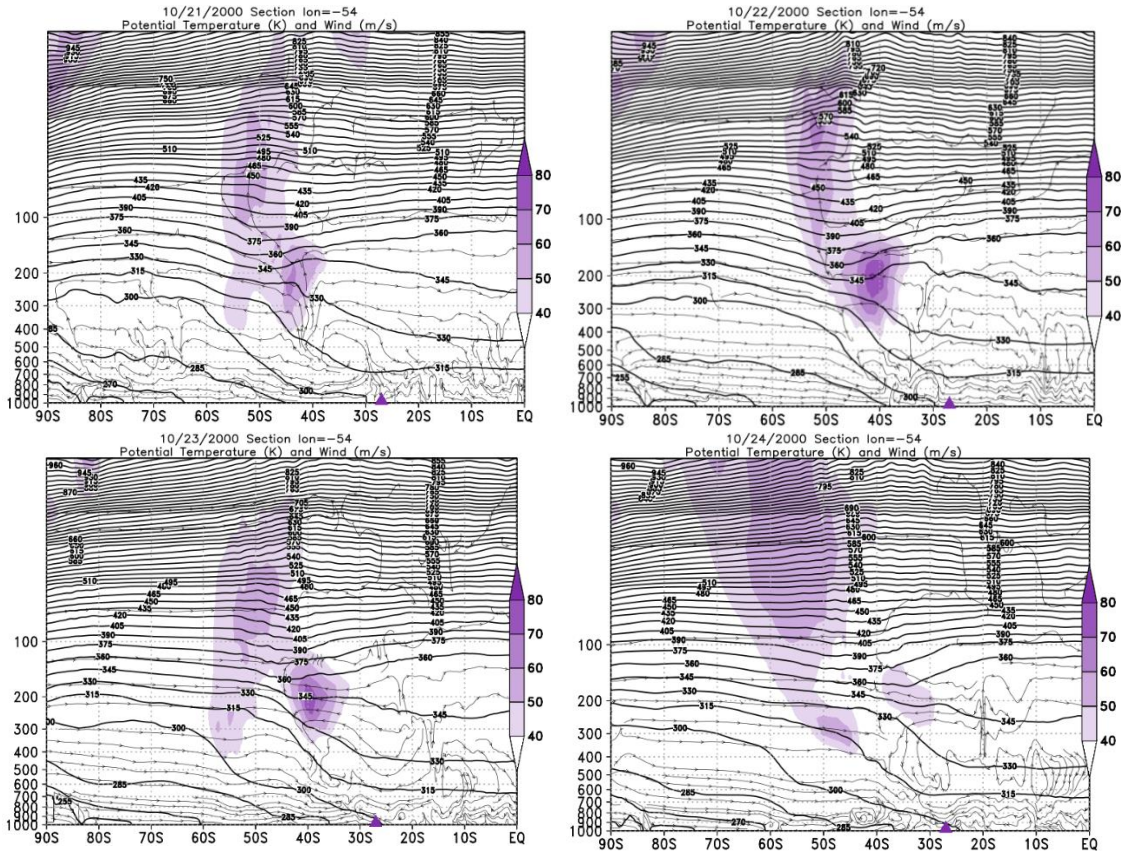

Source: The author.

10/12/2000

Figure A123: PVA fields for the 20 hPa in pressure levels, days 10/08/2000 to 10/12/2000, and HYSPLIT model.

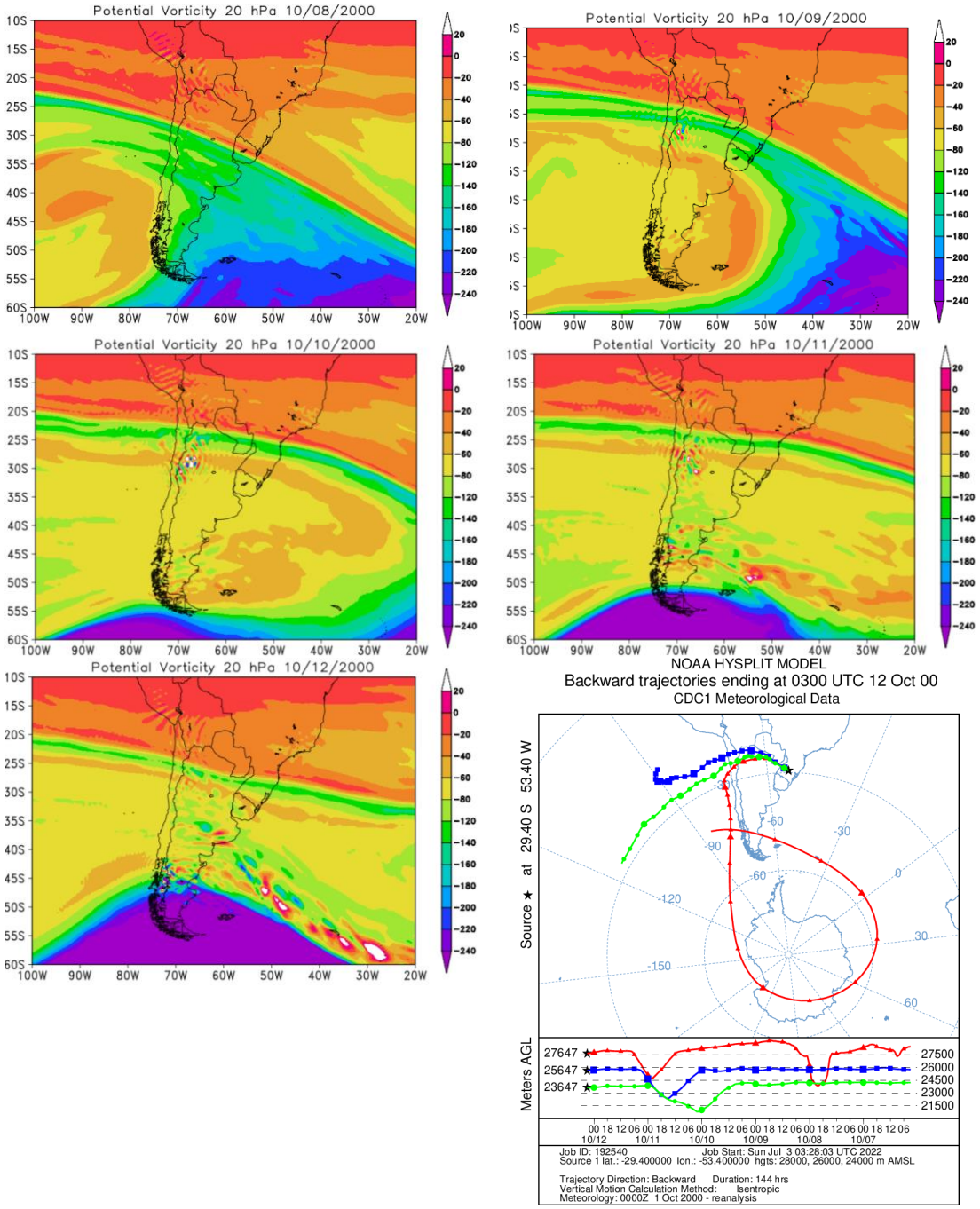

Source: The author, HYSPLIT/NOAA.

Figure A124: Vertical section of the atmosphere between 1000 and 5 hPa for the days of the event in October 2000.

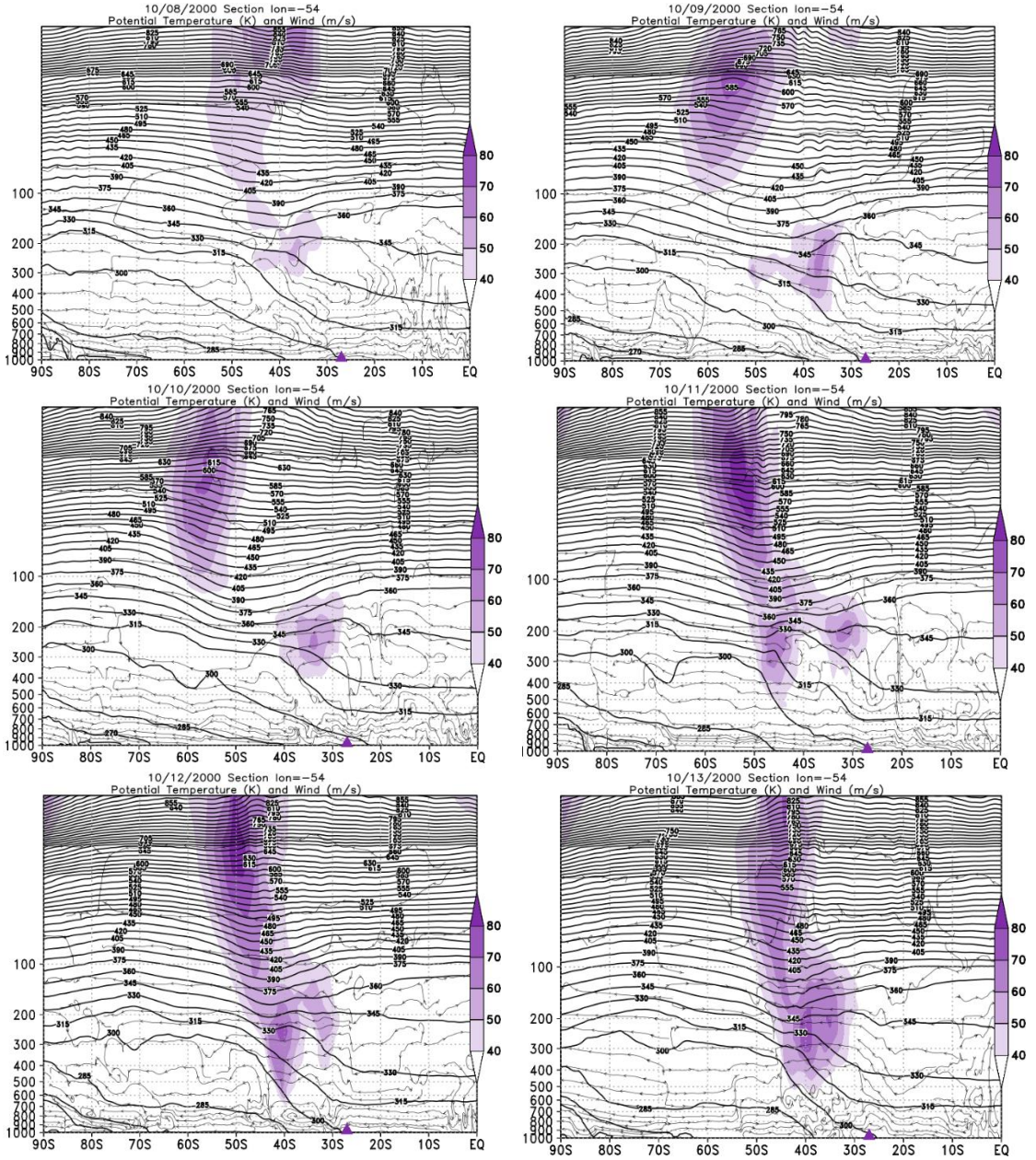

Source: The author.

10/26/2000

Figure A125: PVA fields for the 20 hPa in pressure levels, days 10/24/2000 to 10/27/2000.

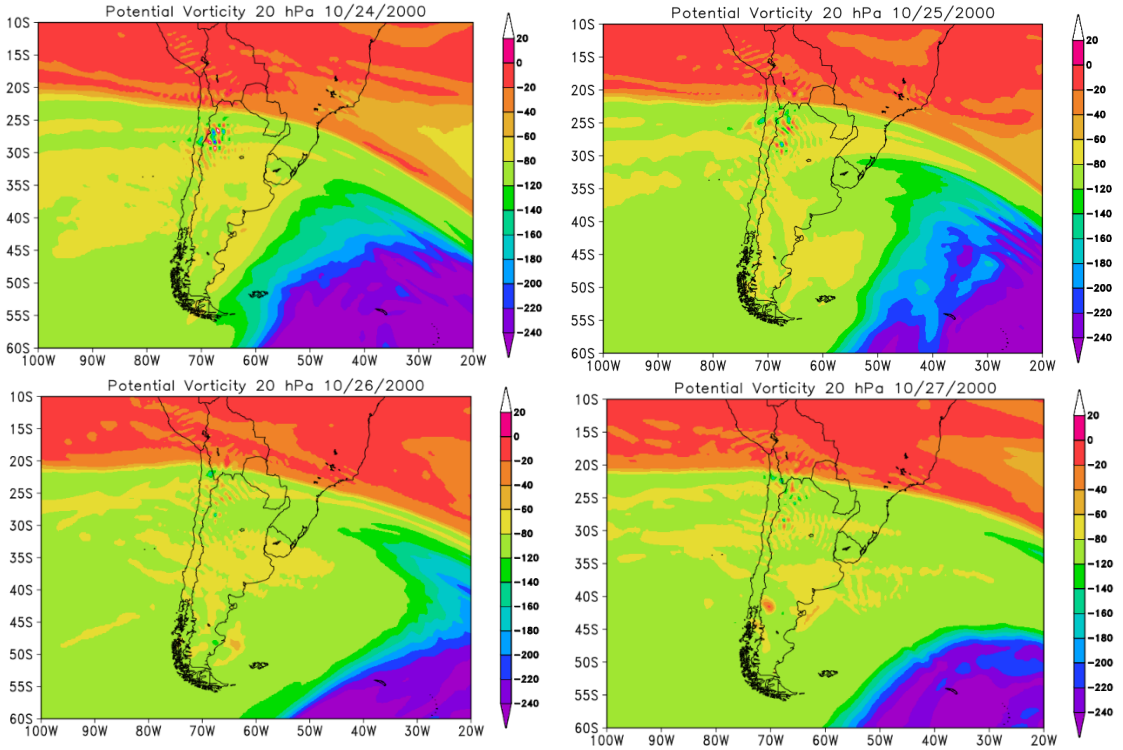

Figure A126: Retroactive trajectory by the HYSPLIT/NOAA model, and O3 content satellite for South Pole view.

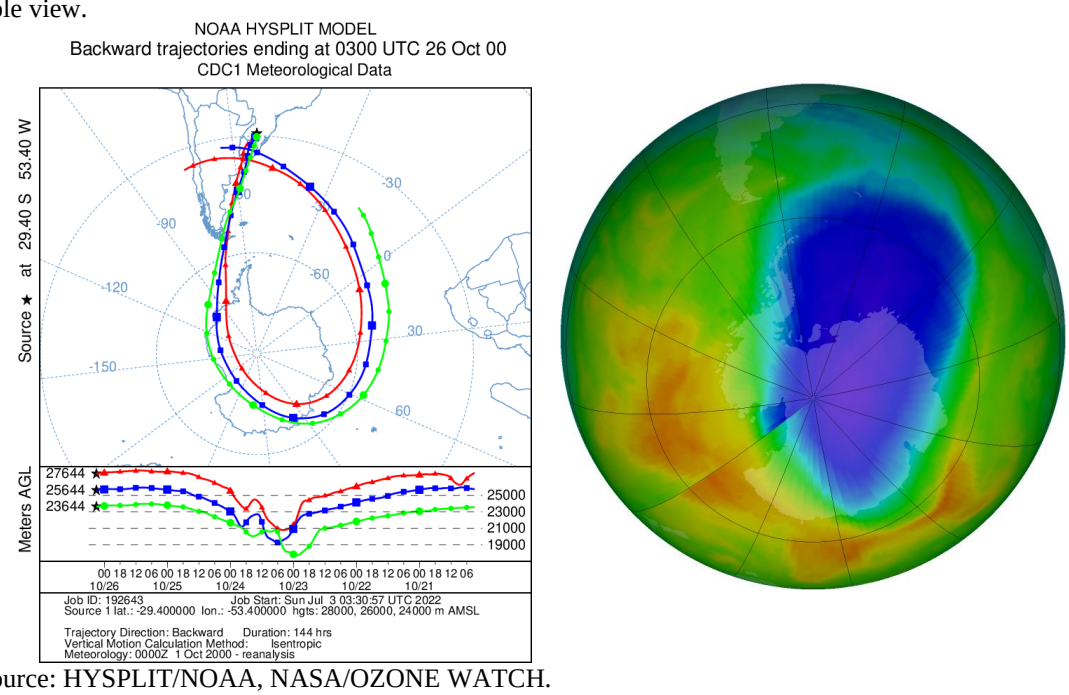

Source: HYSPLIT/NOAA, NASA/OZONE WATCH.

Figure A127: Vertical section of the atmosphere between 1000 and 5 hPa for the days of the event in October 2000.

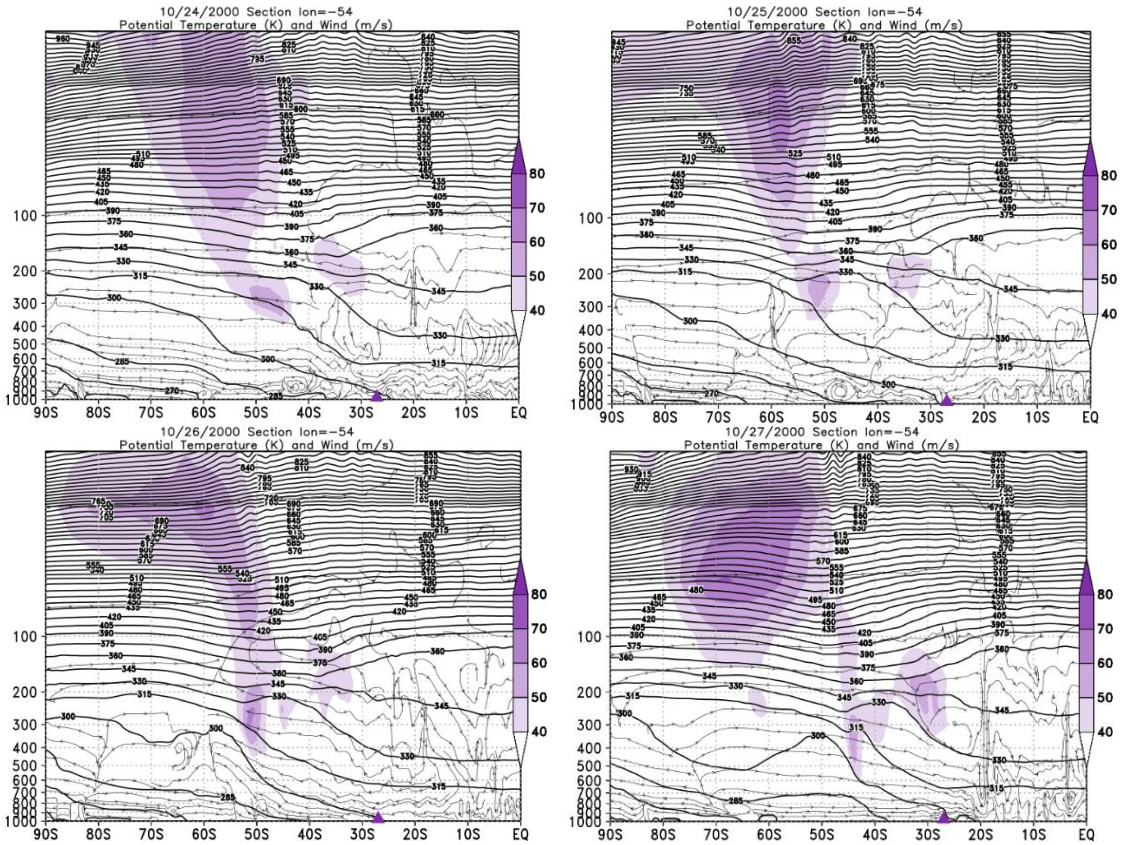

Source: The author.

08/15/2001

Figure A1: PVA fields for the 20 hPa in pressure levels, days 08/13/2001 to 08/16/2001.

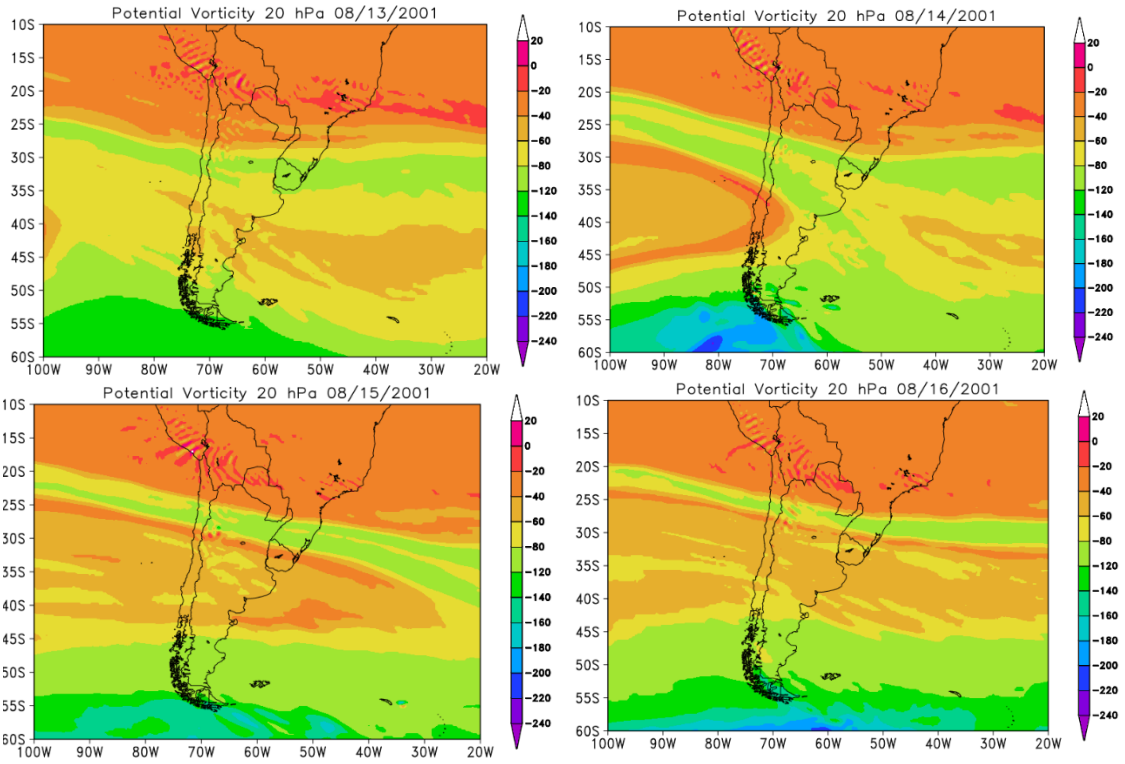

Source: The author.

Figure A129: Retroactive trajectory by the HYSPLIT/NOAA model, and O3 content satellite for South Pole view.

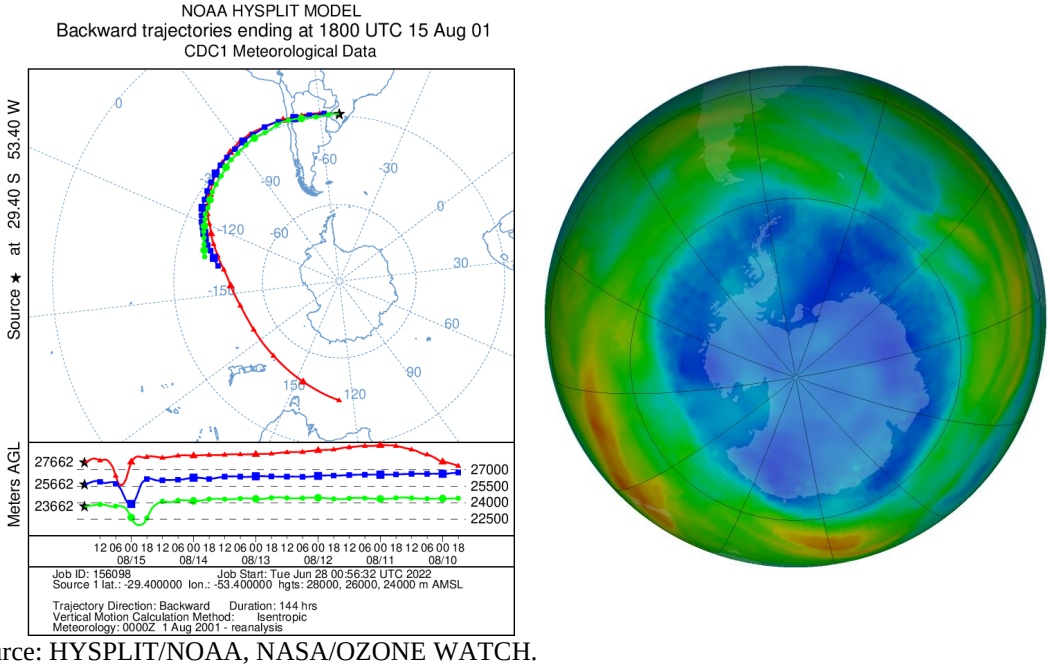

Source: HYSPLIT/NOAA, NASA/OZONE WATCH.

Figure A130: Vertical section of the atmosphere between 1000 and 5 hPa for the days of the event in August 2001.

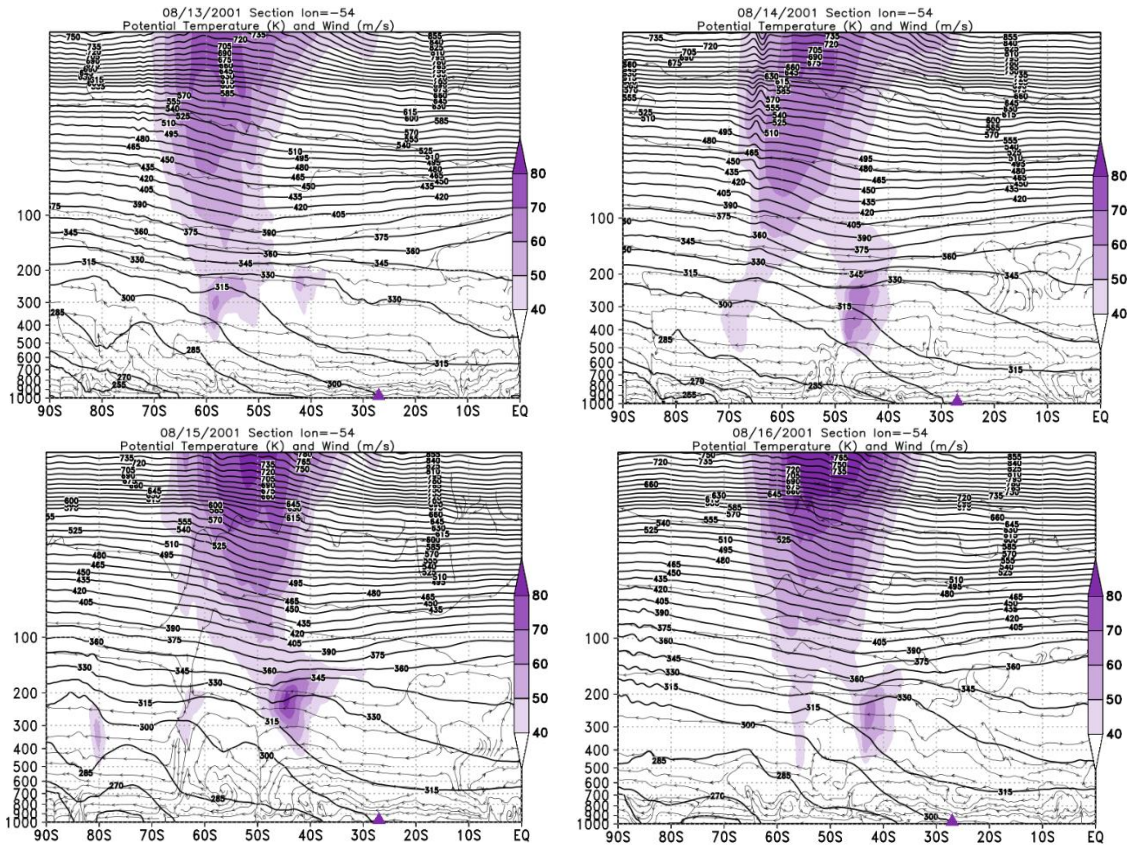

Source: The author.

09/23/2001

Figure A131: PVA fields for the 20 hPa in pressure levels, days 09/21/2001 to 09/24/2001.

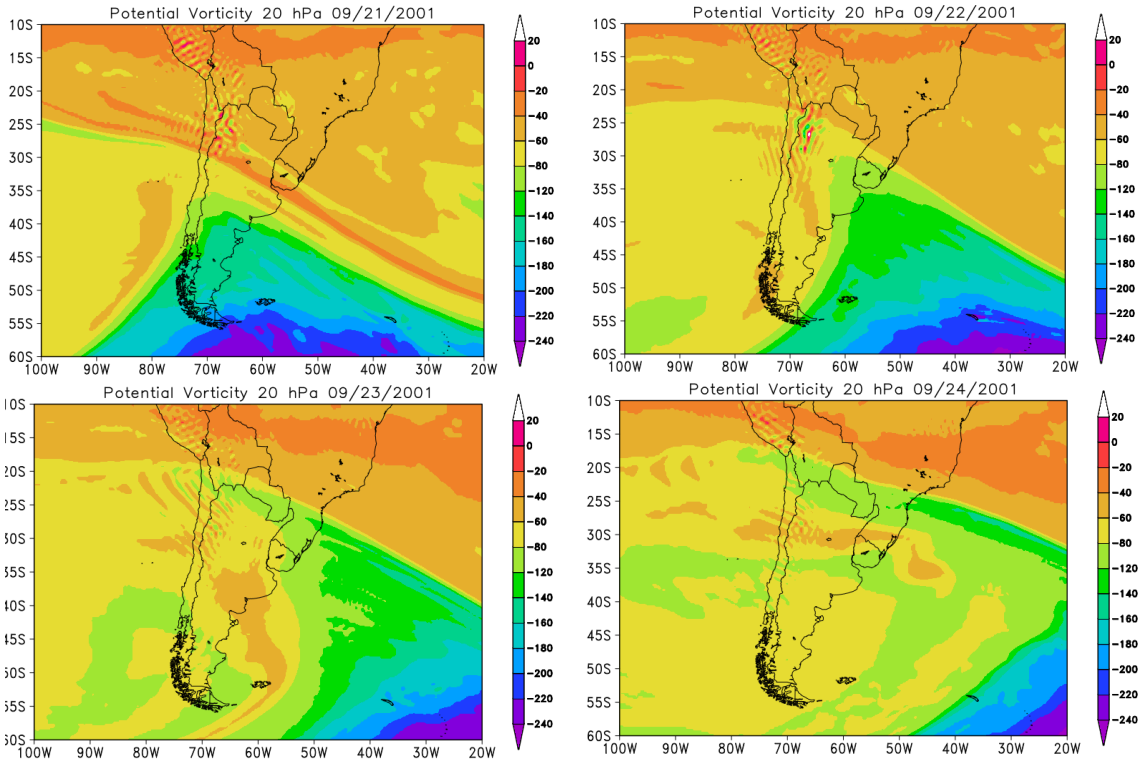

Figure A132: Retroactive trajectory by the HYSPLIT/NOAA model, and O3 content satellite for South Pole view.

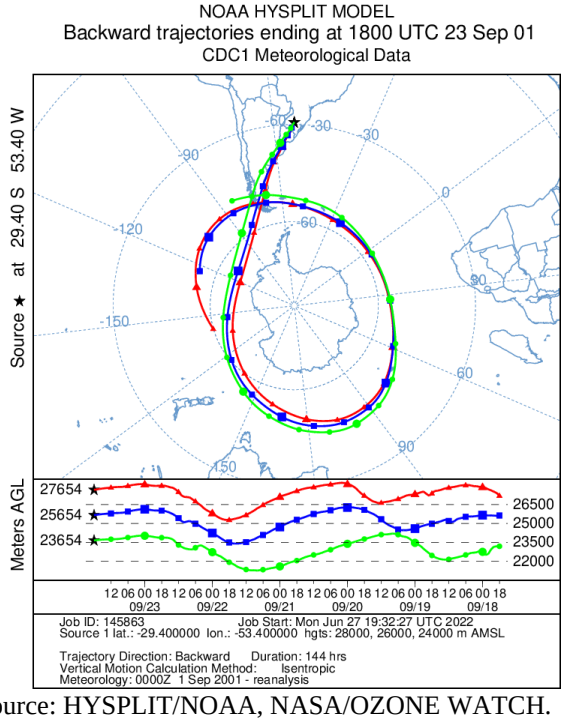

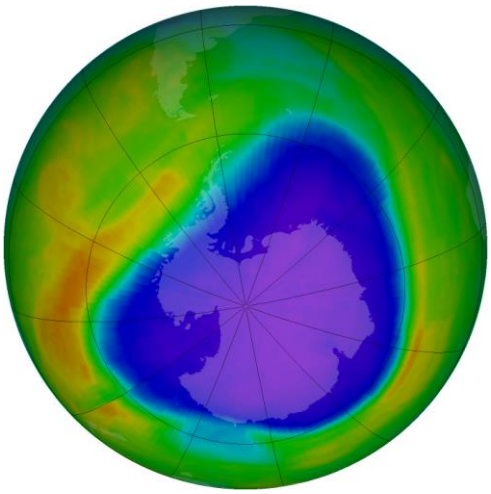

Source: HYSPLIT/NOAA, NASA/OZONE WATCH.

Figure A133: Vertical section of the atmosphere between 1000 and 5 hPa for the days of the event in September 2001

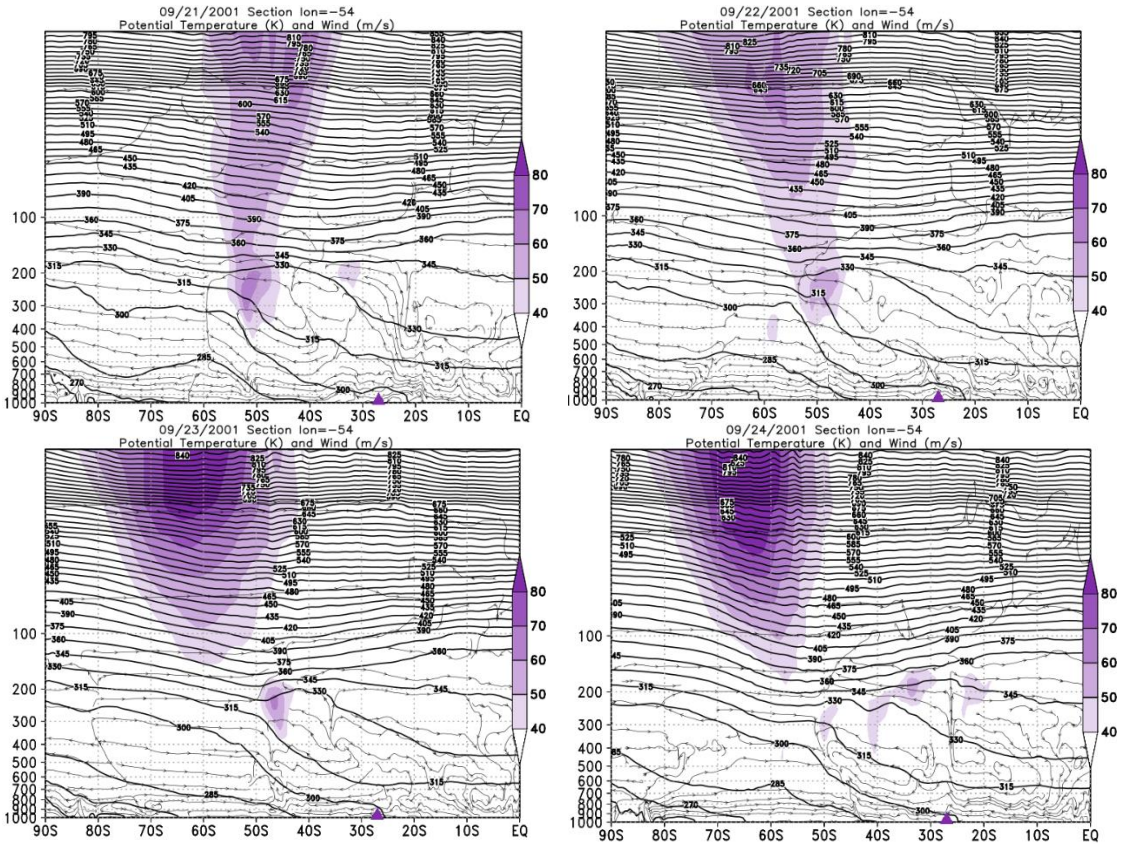

Source: The author.

08/18/2002

Figure A134: PVA fields for the 20 hPa in pressure levels, days 08/16/2002 to 08/19/2002.

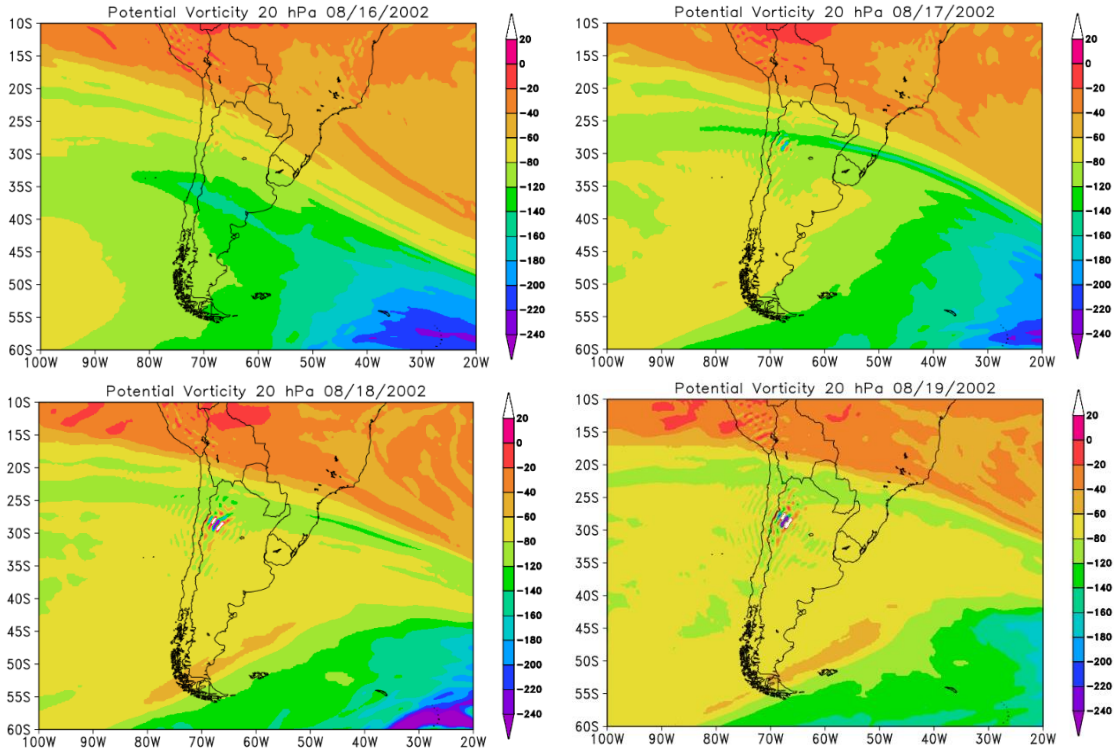

Source: The author.

Figure A135: Retroactive trajectory by the HYSPLIT/NOAA model, and O3 content satellite for South Pole view.

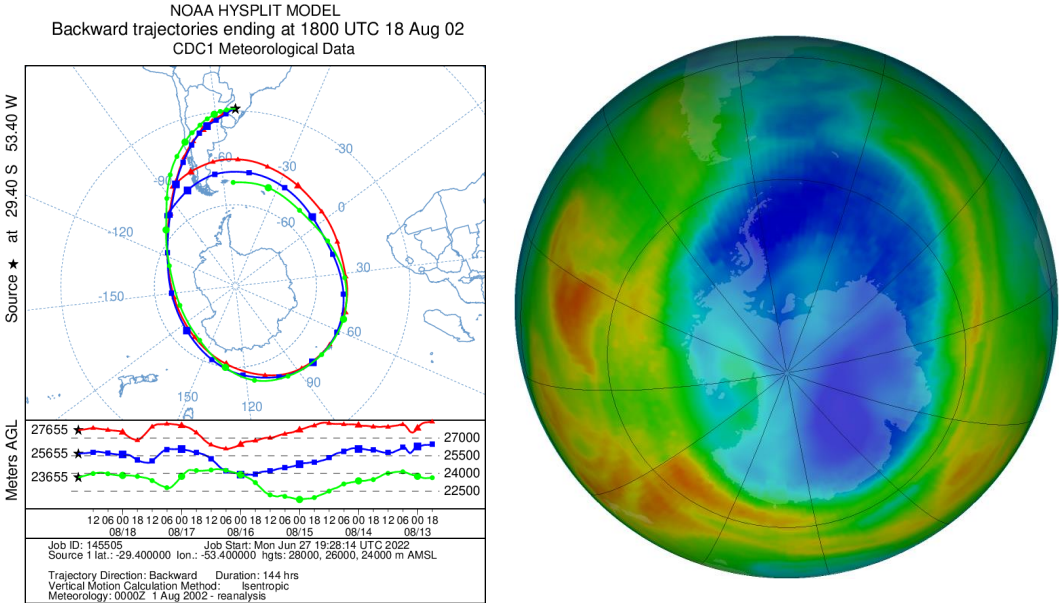

Source: HYSPLIT/NOAA, NASA/OZONE WATCH.

Figure A136: Vertical section of the atmosphere between 1000 and 5 hPa for the days of the event in October 2016.

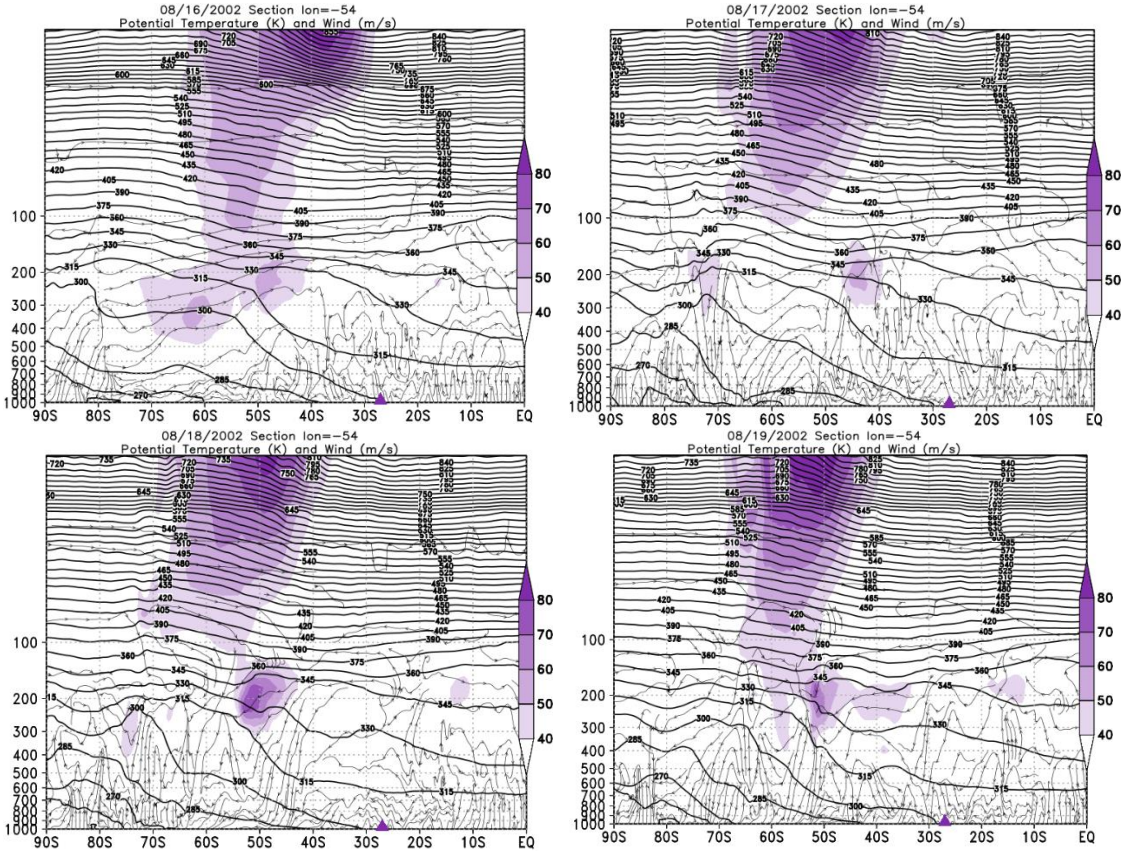

Source: The author.

10/15/2003

Figure A137: PVA fields for the 20 hPa in pressure levels, days 10/13/2003 to 10/16/2003.

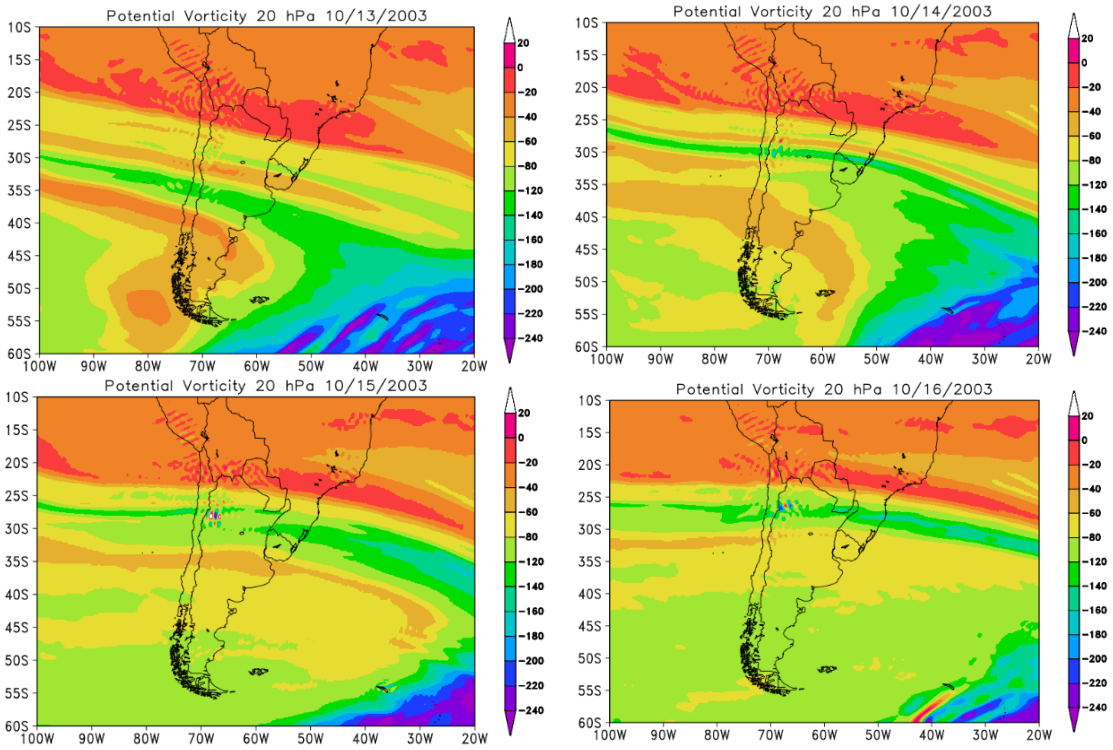

Figure A138: Retroactive trajectory by the HYSPLIT/NOAA model, and O3 content satellite for South Pole view.

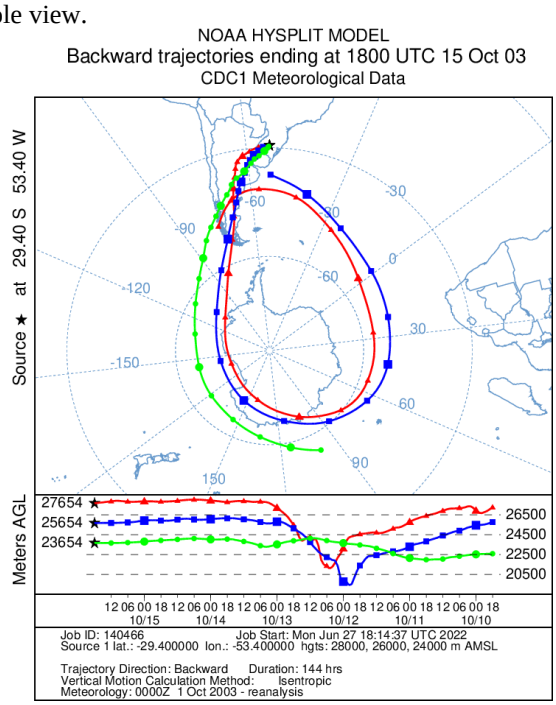

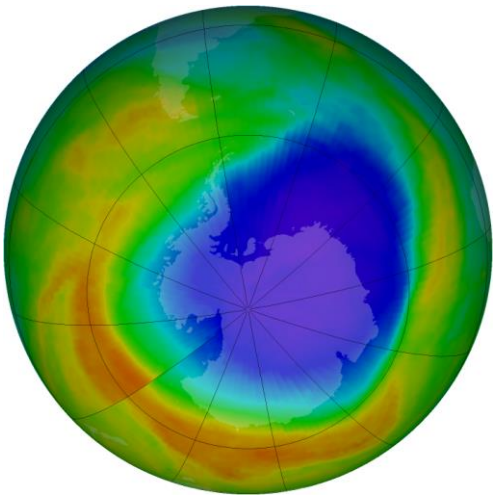

Source: HYSPLIT/NOAA, NASA/OZONE WATCH.

Figure A139: Vertical profile of O_3 by the SABER satellite for the October 15, 2003 (in red) and climatology for the month of October (in black).

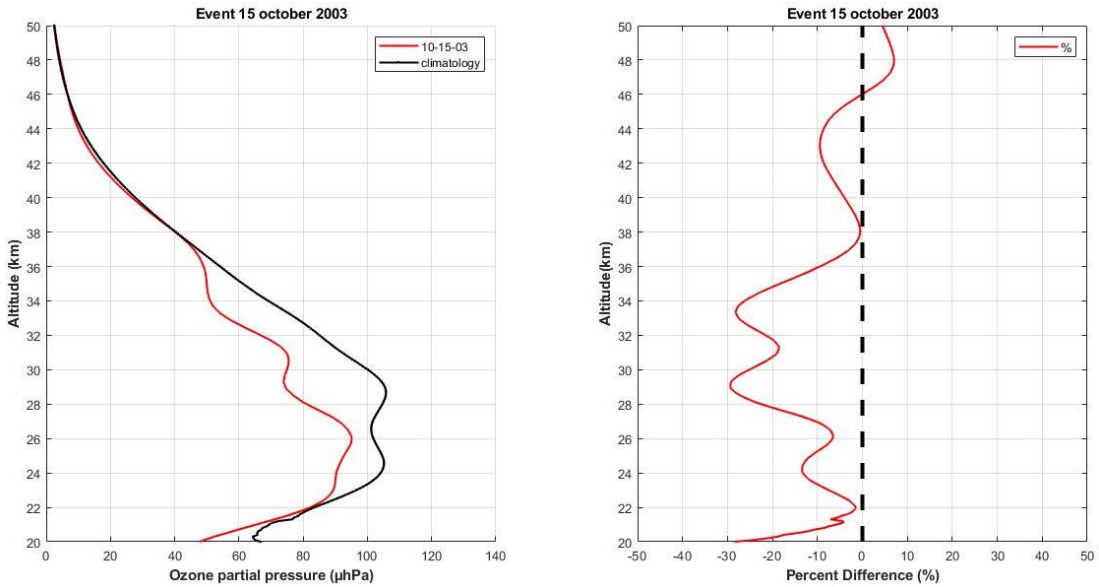

Figure A140: Vertical section of the atmosphere between 1000 and 5 hPa for the days of the event in October 2003.

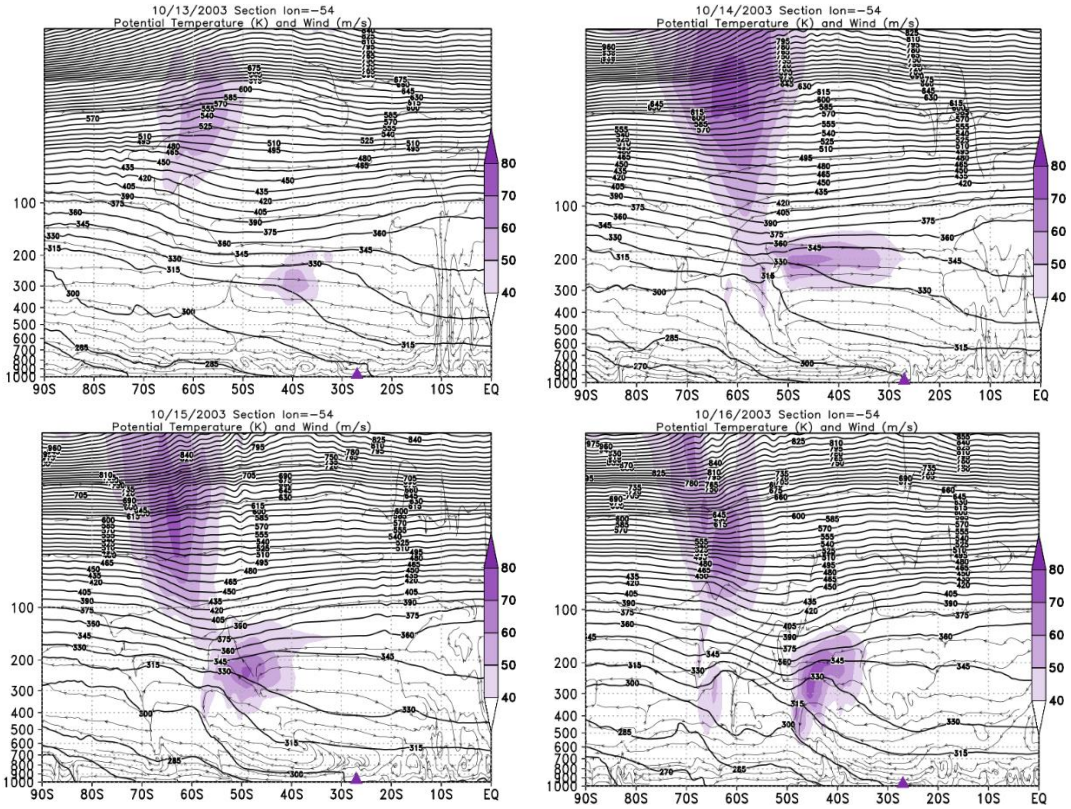

Source: The author.

08/22/2004

Figure A141: PVA fields for the 20 hPa in pressure levels, days 08/19/2004 to 08/22/2004.

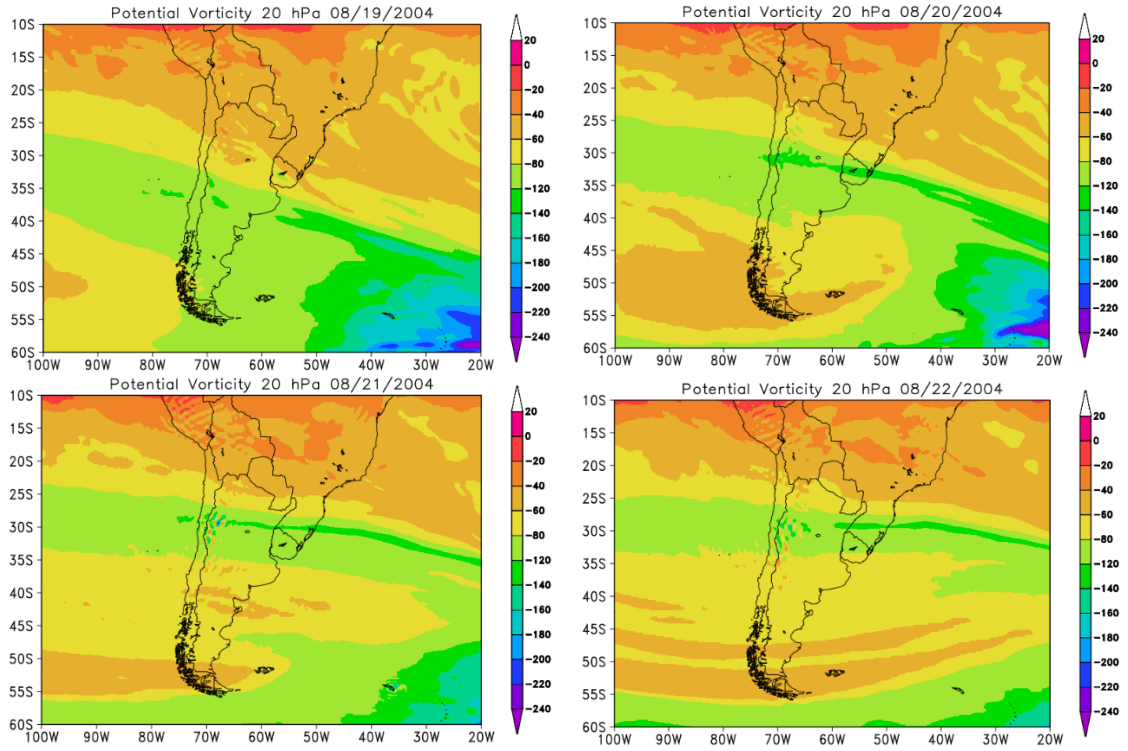

Source: The author.

Figure A142: Retroactive trajectory by the HYSPLIT/NOAA model, and O3 content satellite for South Pole view.

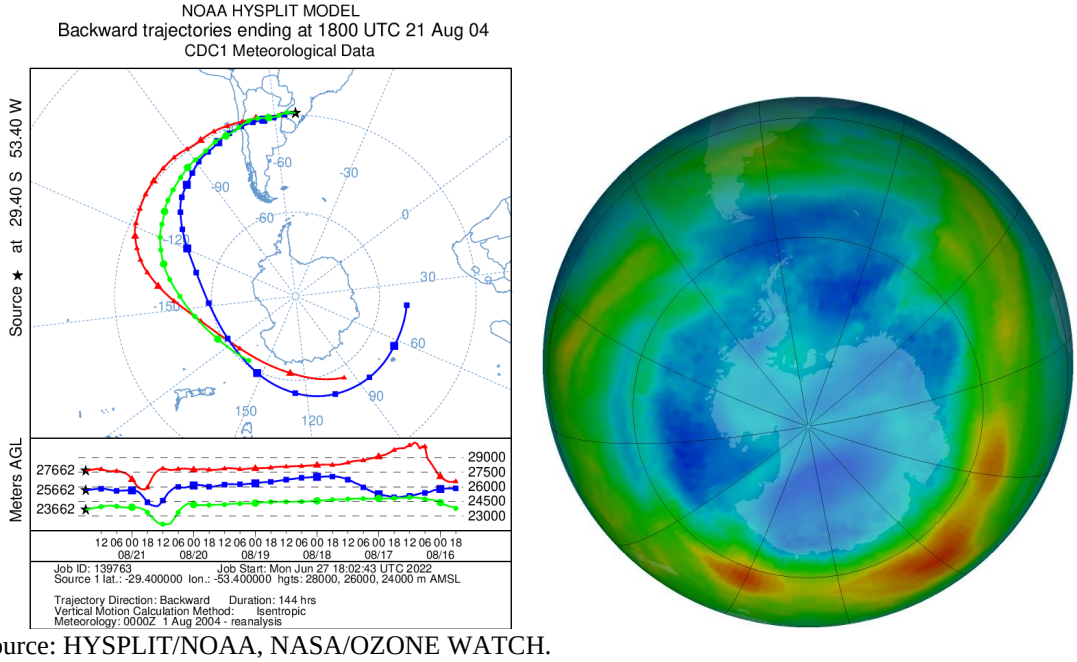

Source: HYSPLIT/NOAA, NASA/OZONE WATCH.

Figure A143: Vertical profile of O_3 by the SABER satellite for the August 23, 2004 (in red) and climatology for the month of October (in black).

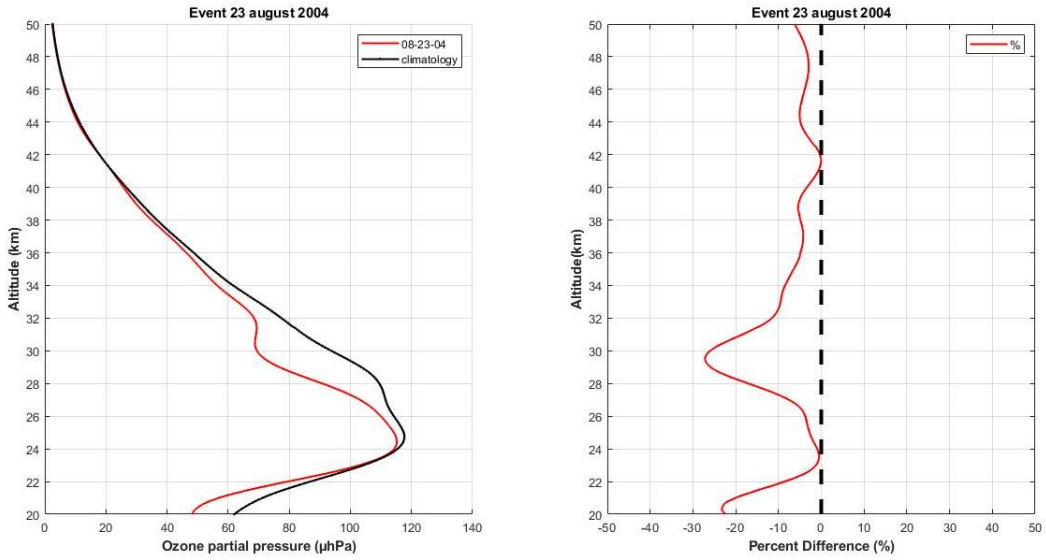

Figure A144: Vertical section of the atmosphere between 1000 and 5 hPa for the days of the event in August 2004.

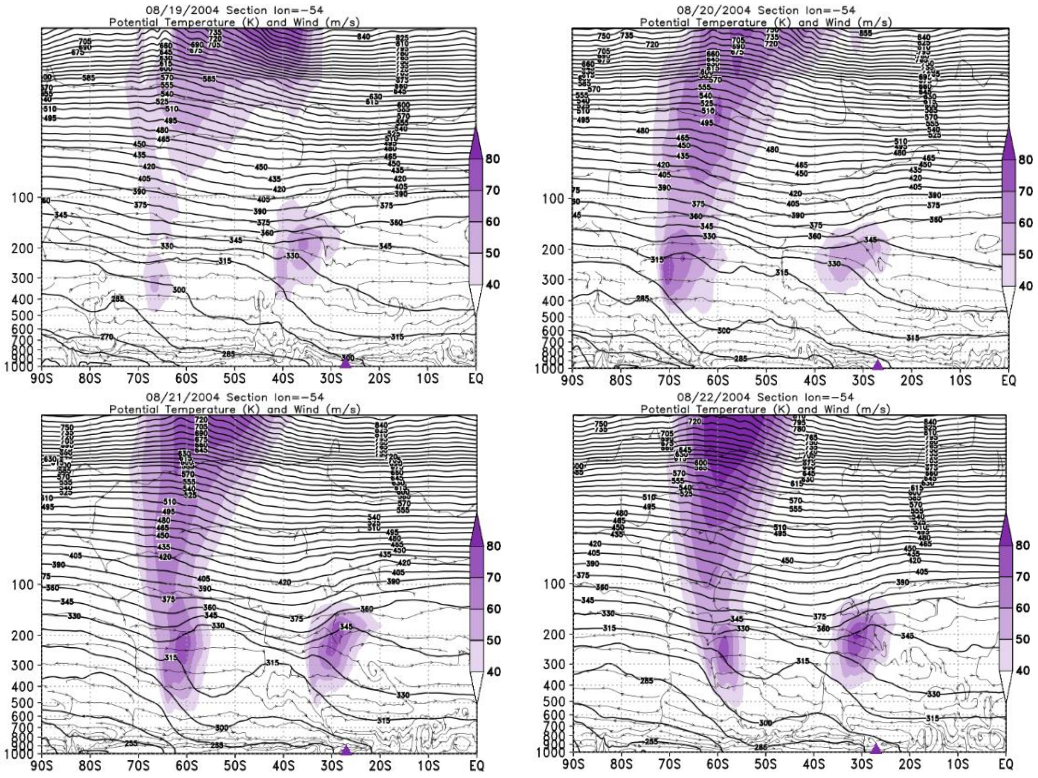

Source: The author.

09/12/2004

Figure A145: PVA fields for the 20 hPa in pressure levels, days 09/10/2004 to 09/13/2004.

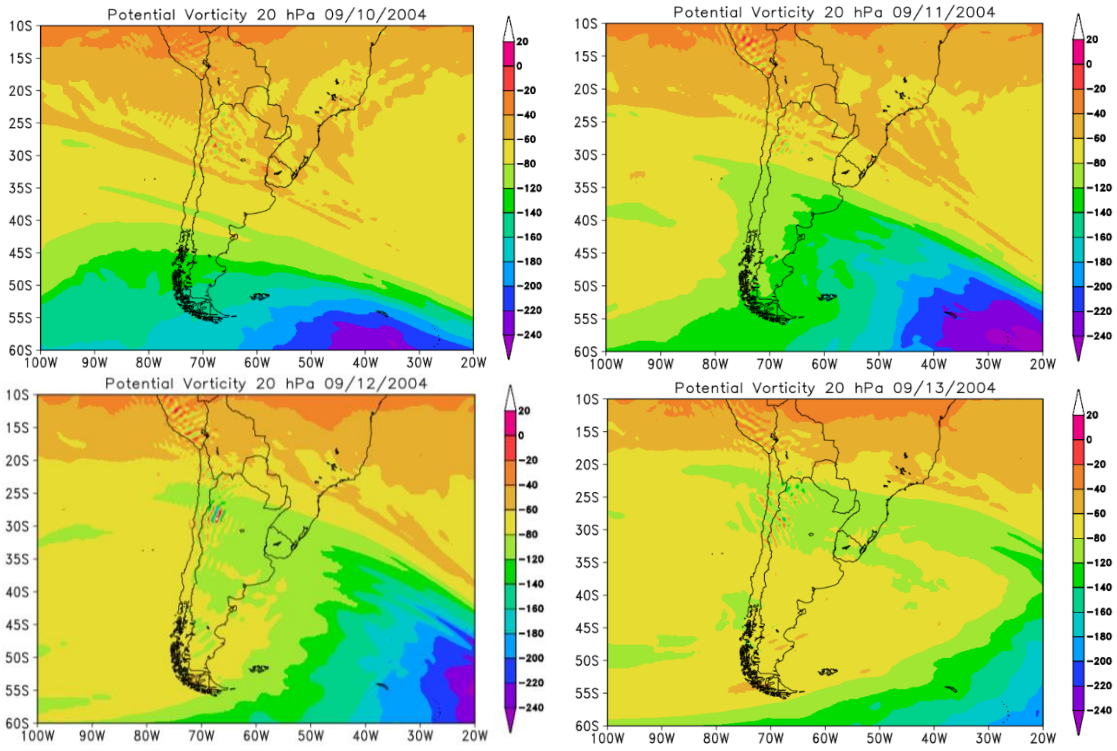

Figure A146: Retroactive trajectory by the HYSPLIT/NOAA model, and O3 content satellite for South Pole view.

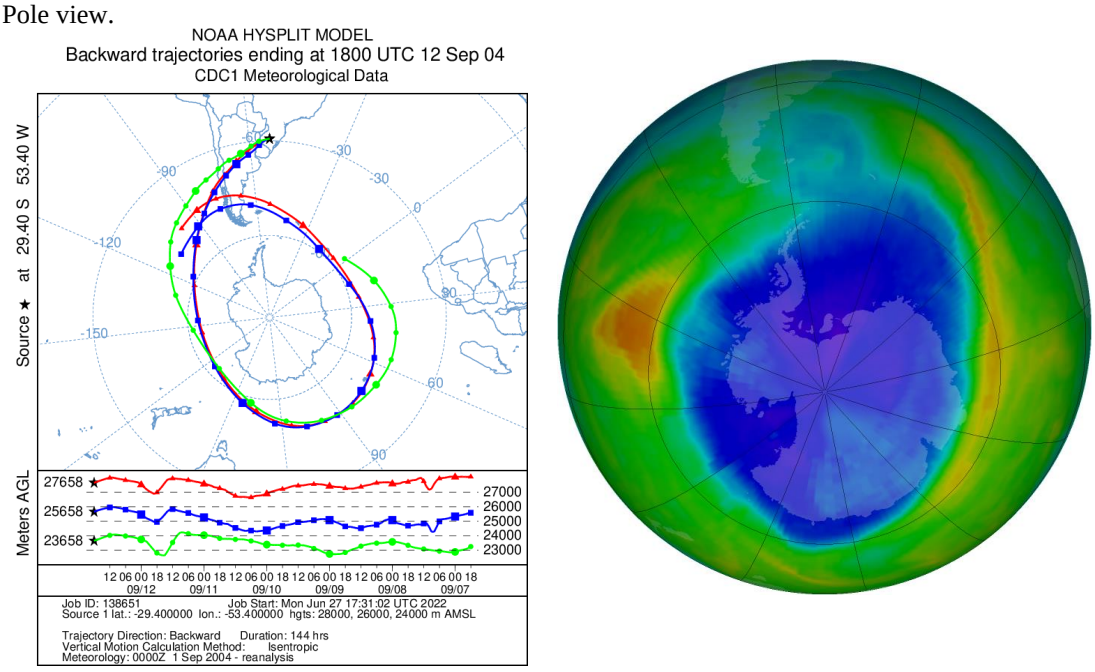

Source: HYSPLIT/NOAA, NASA/OZONE WATCH.

Figure A147: Vertical profile of O_3 by the SABER satellite for the September 13, 2004 (in red) and climatology for the month of October (in black).

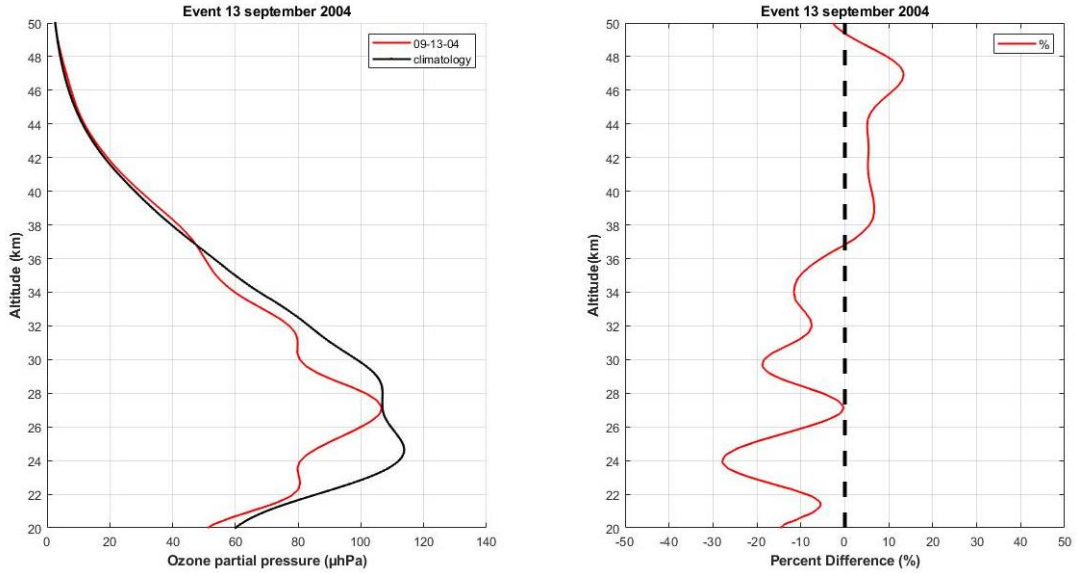

Figure A148: Vertical section of the atmosphere between 1000 and 5 hPa for the days of the event in September 2004.

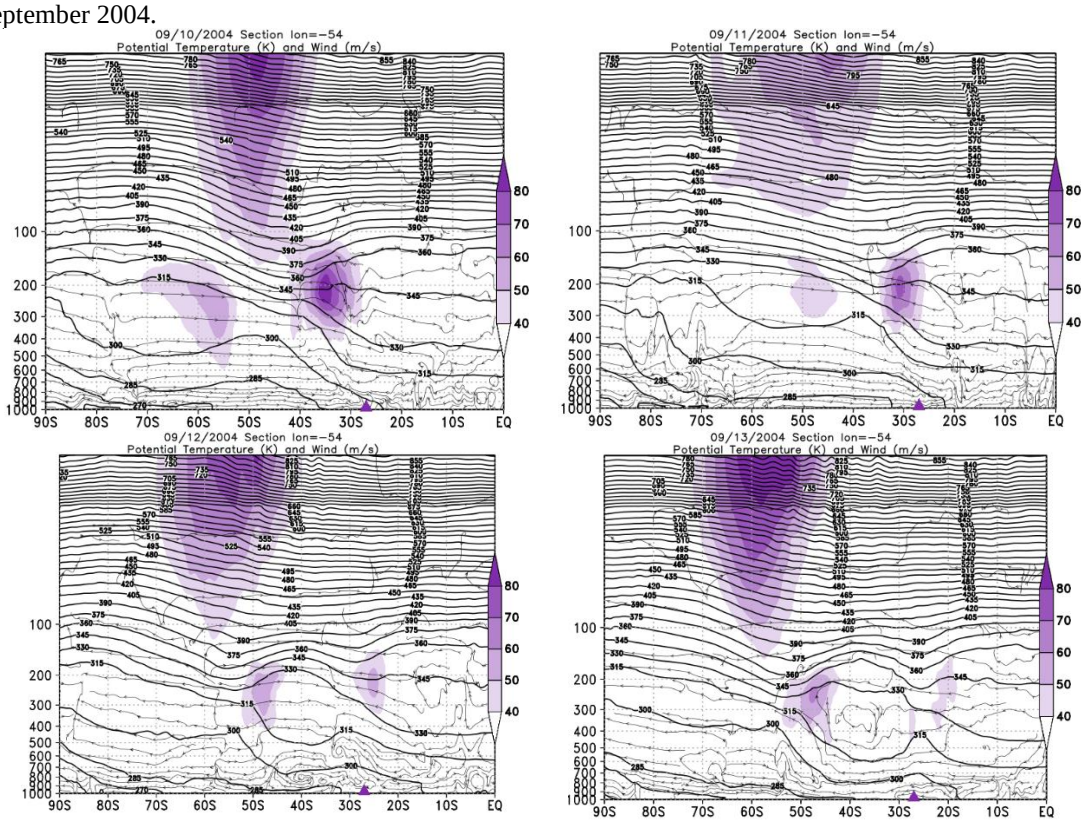

Source: The author.

10/03/2004

Figure A149: PVA fields for the 20 hPa in pressure levels, days 10/01/2004 to 10/04/2004.

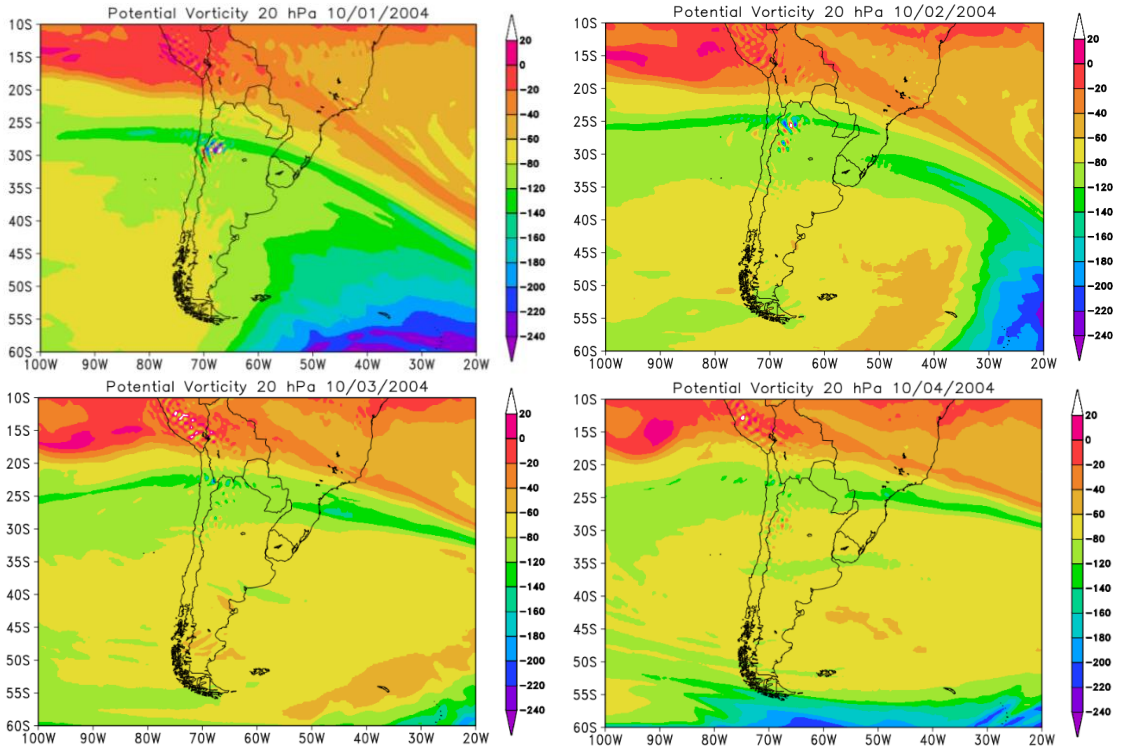

Figure A150: Retroactive trajectory by the HYSPLIT/NOAA model, and O3 content OMI satellite for South Pole, and global view.

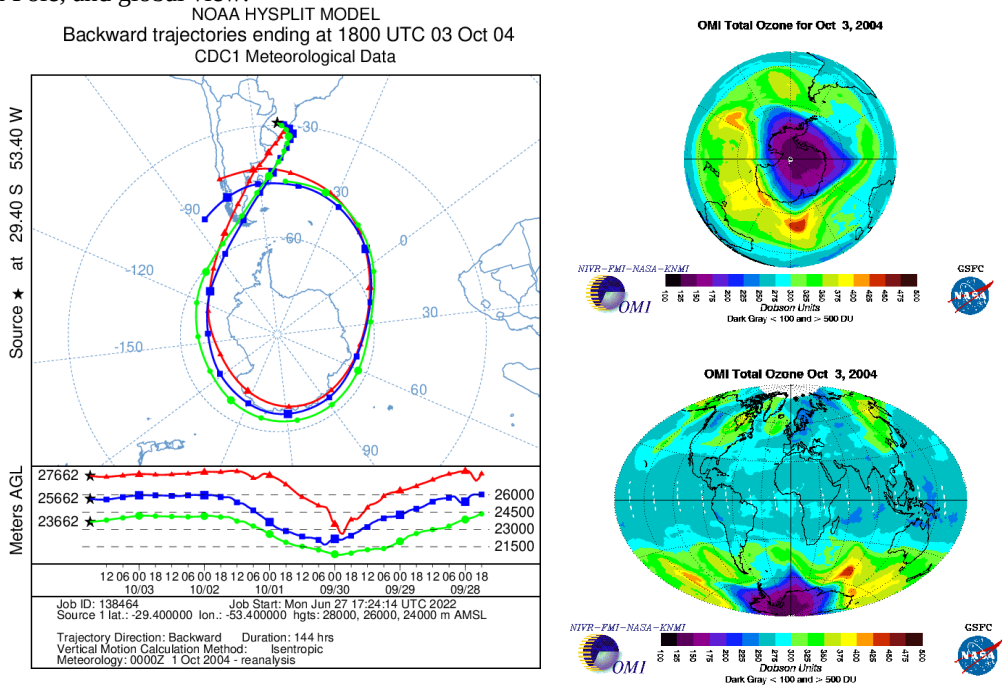

Source: HYSPLIT/NOAA, OMI/NASA.

Figure A151: Vertical profile of O_3 by the SABER satellite for the October 03, 2004 (in red) and climatology for the month of October (in black).

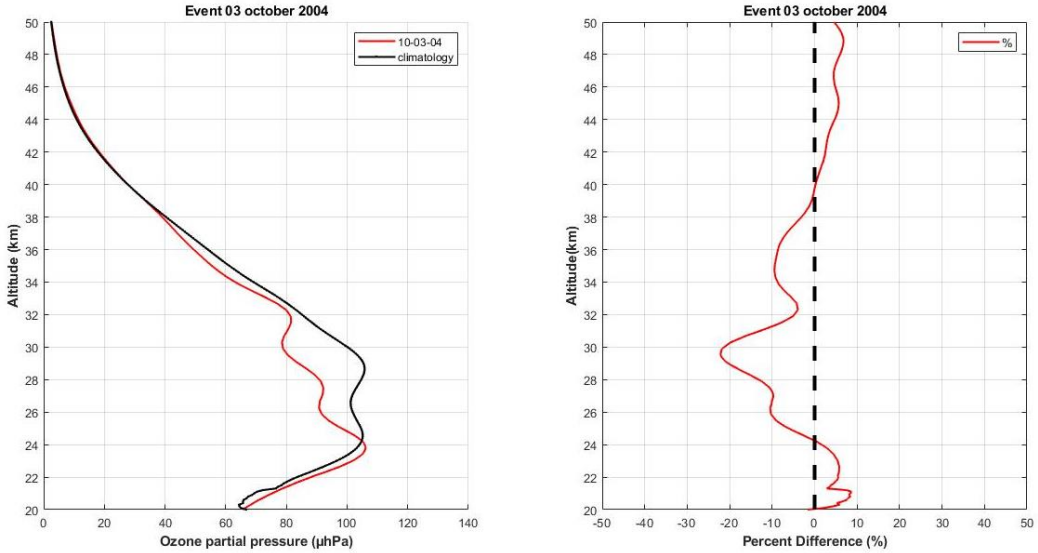

Figure A152: Vertical section of the atmosphere between 1000 and 5 hPa for the days of the event in October 2004.

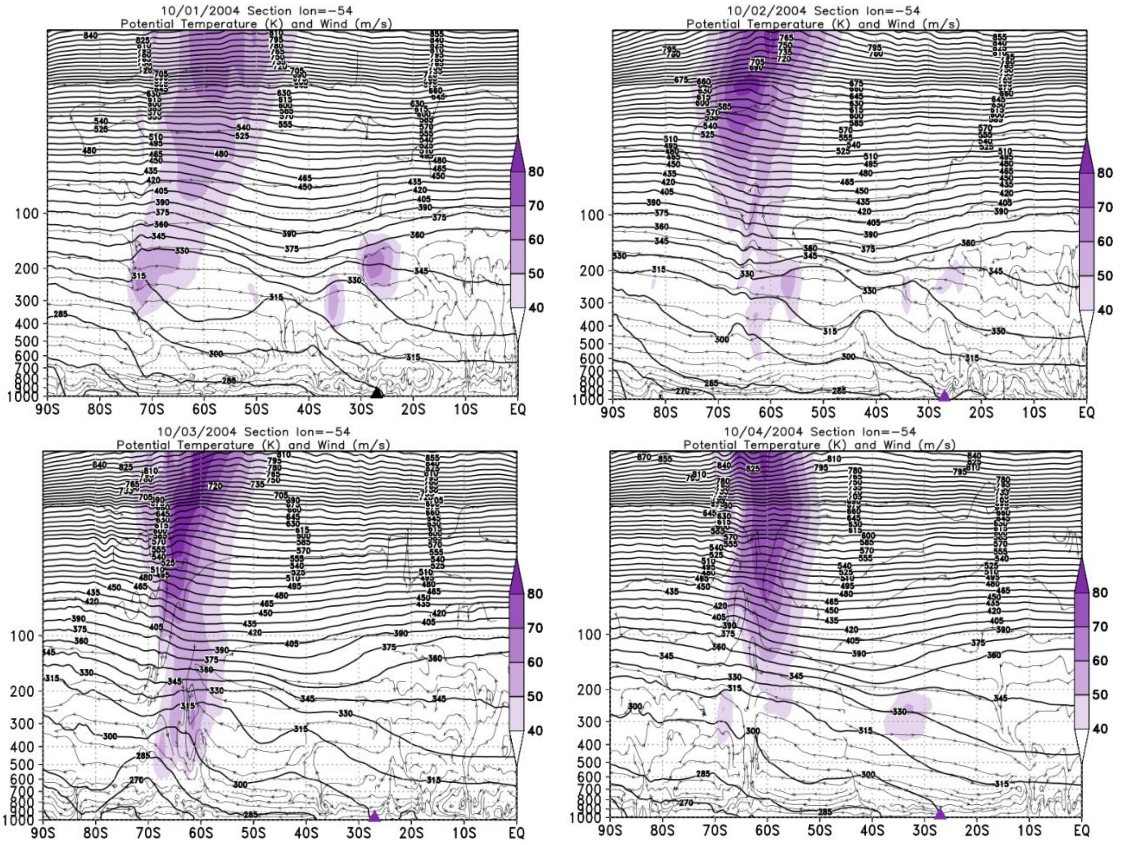

10/16/2004

Figure A153: PVA fields for the 20 hPa in pressure levels, days 10/14/2004 to 10/17/2004.

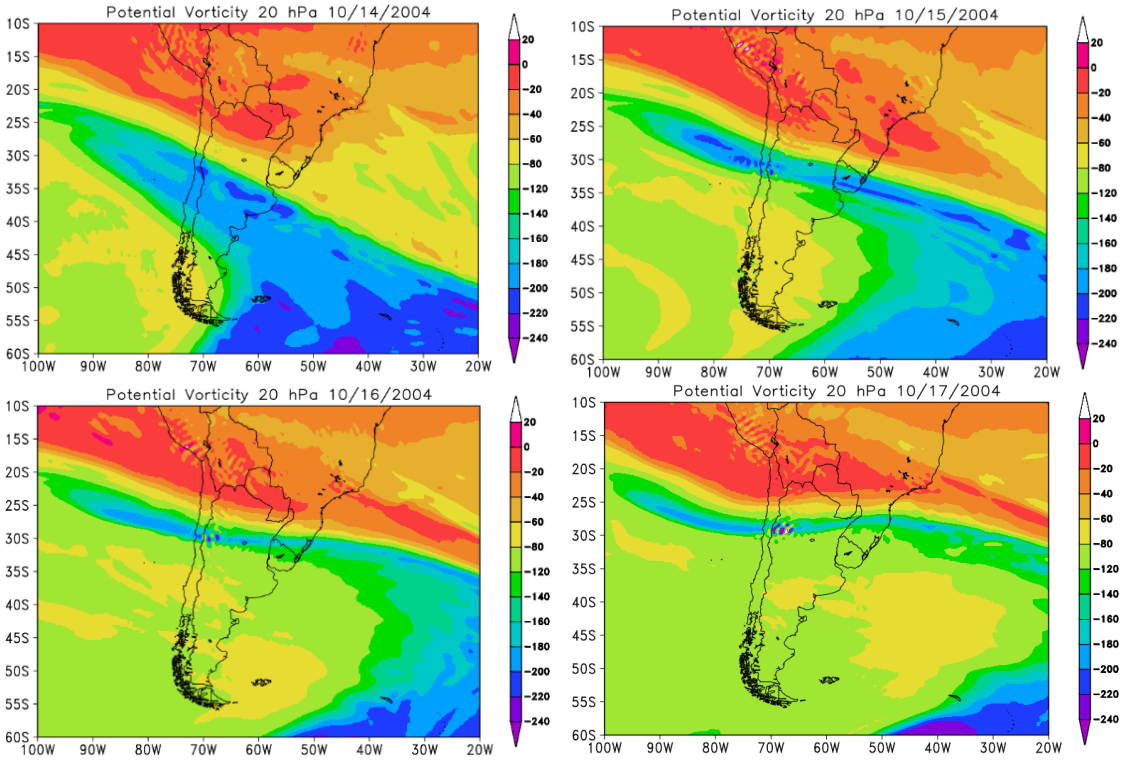

Figure A154: Retroactive trajectory by the HYSPLIT/NOAA model, and O3 content OMI satellite for South Pole, and global view.

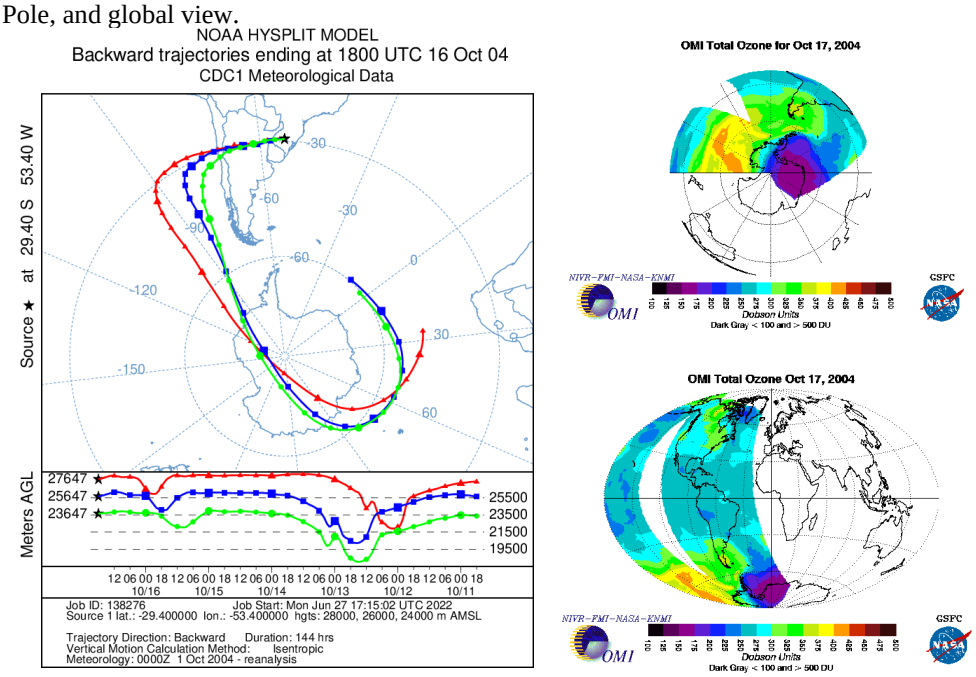

Source: HYSPLIT/NOAA, OMI/NASA.

Figure A155: Vertical profile of O_3 by the SABER satellite for the October 17, 2004 (in red) and climatology for the month of October (in black).

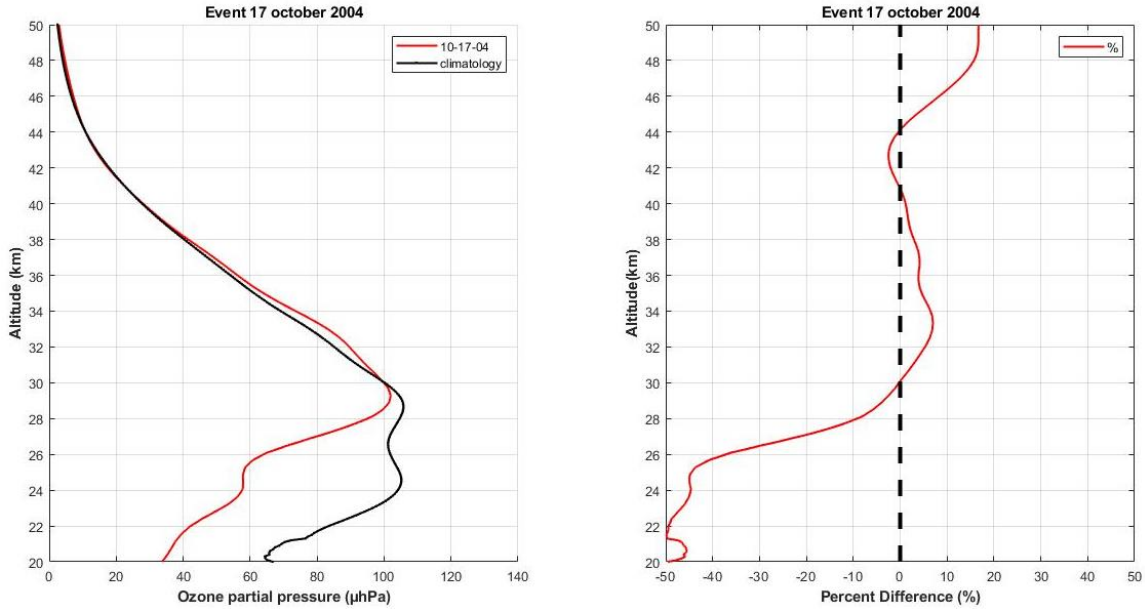

Figure A156: Vertical section of the atmosphere between 1000 and 5 hPa for the days of the event in October 2004.

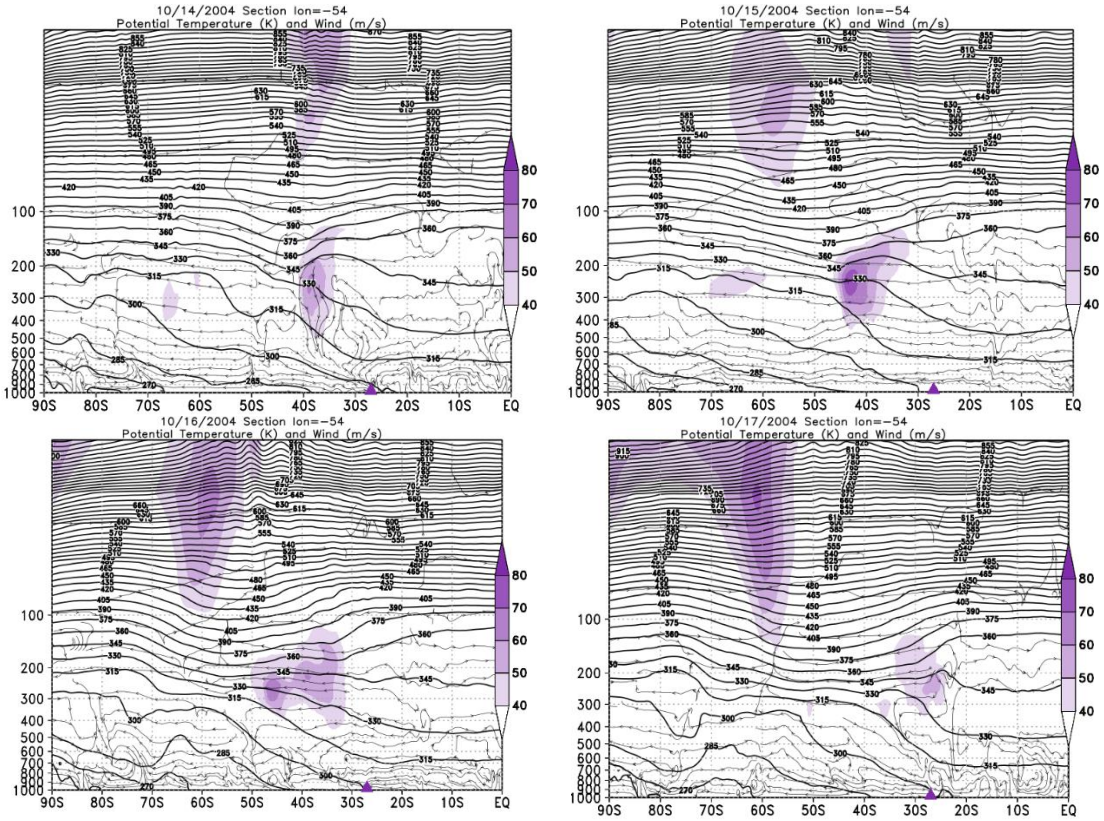

Source: The author.

09/29/2005

Figure A157: PVA fields for the 20 hPa in pressure levels, days 09/27/2005 to 09/30/2005.

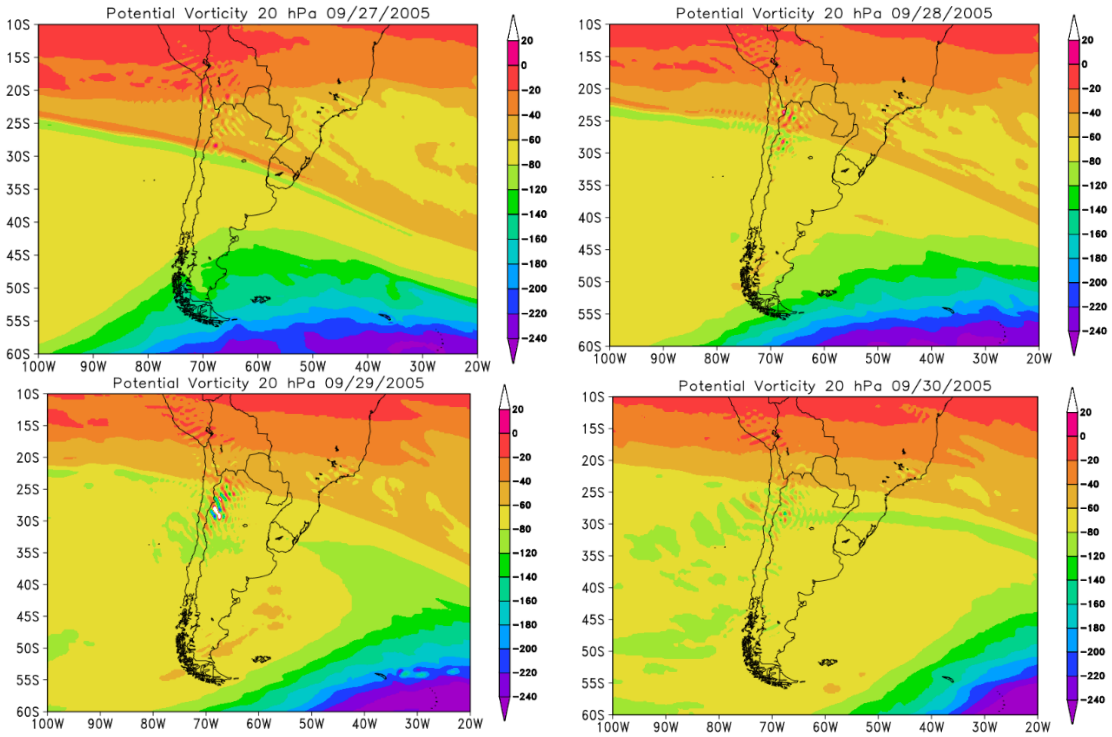

Figure A158: Retroactive trajectory by the HYSPLIT/NOAA model, and O3 content OMI satellite for South Pole, and global view

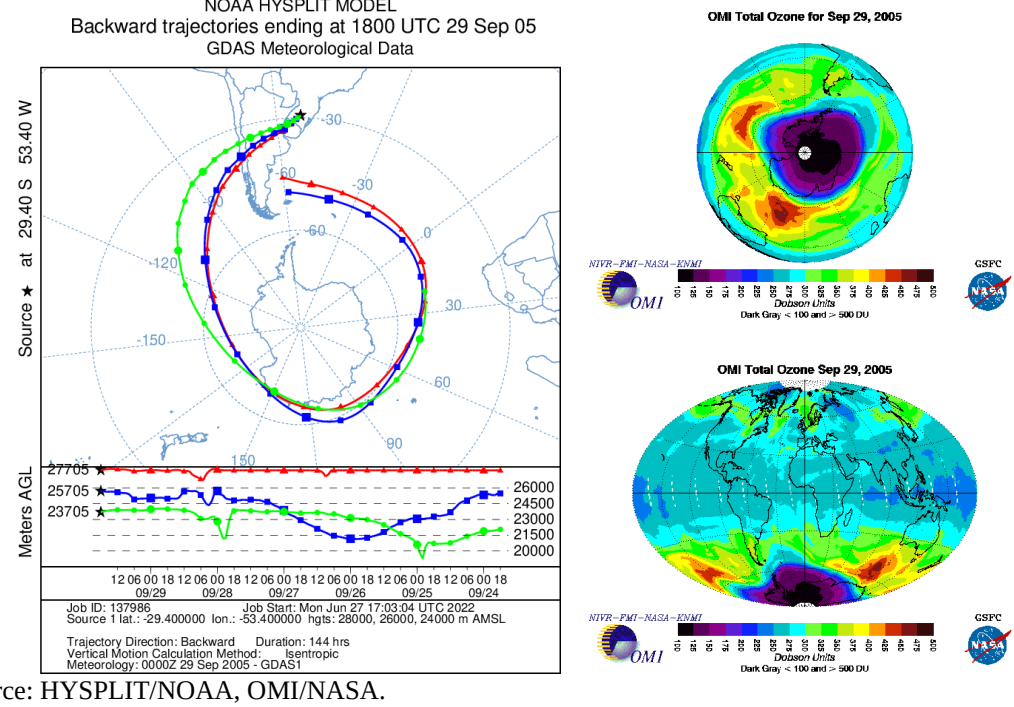

Source: HYSPLIT/NOAA, OMI/NASA.

Figure A159: Vertical section of the atmosphere between 1000 and 5 hPa for the days of the event in September 2005.

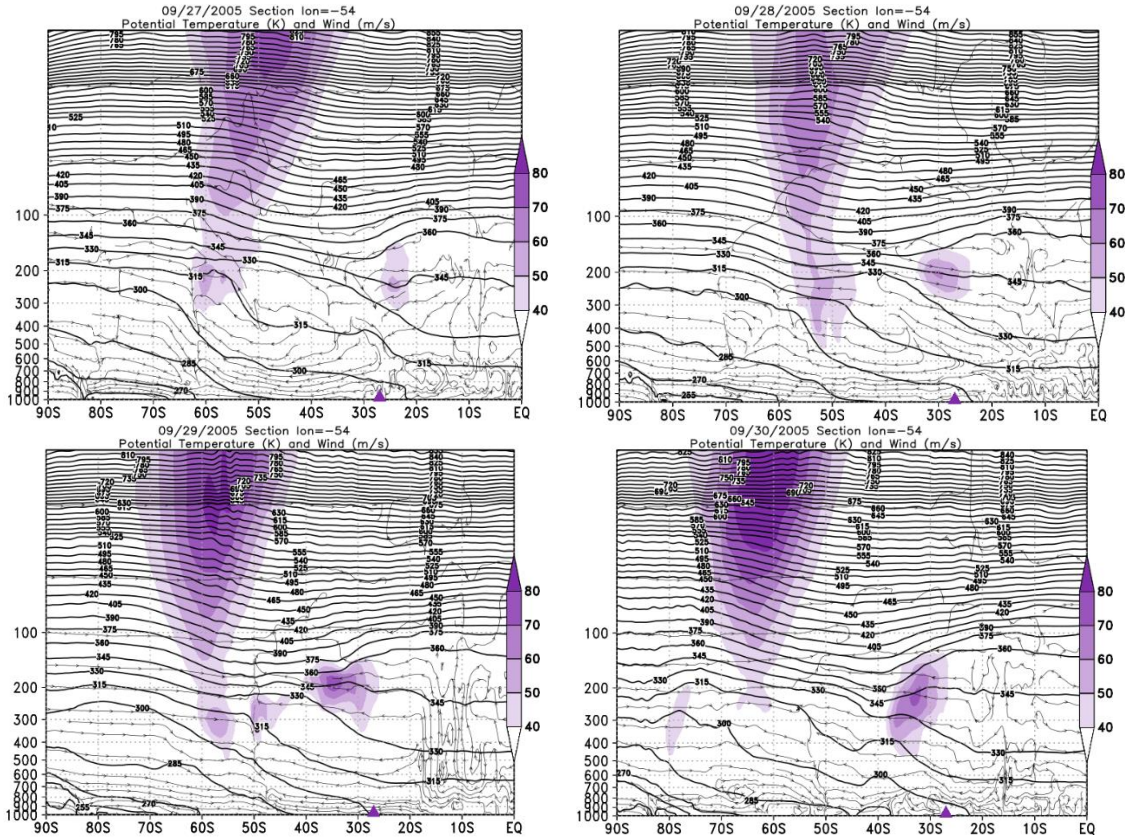

Source: The author.

10/11/2005

Figure A160: PVA fields for the 20 hPa in pressure levels, days 10/09/2005 to 10/12/2005.

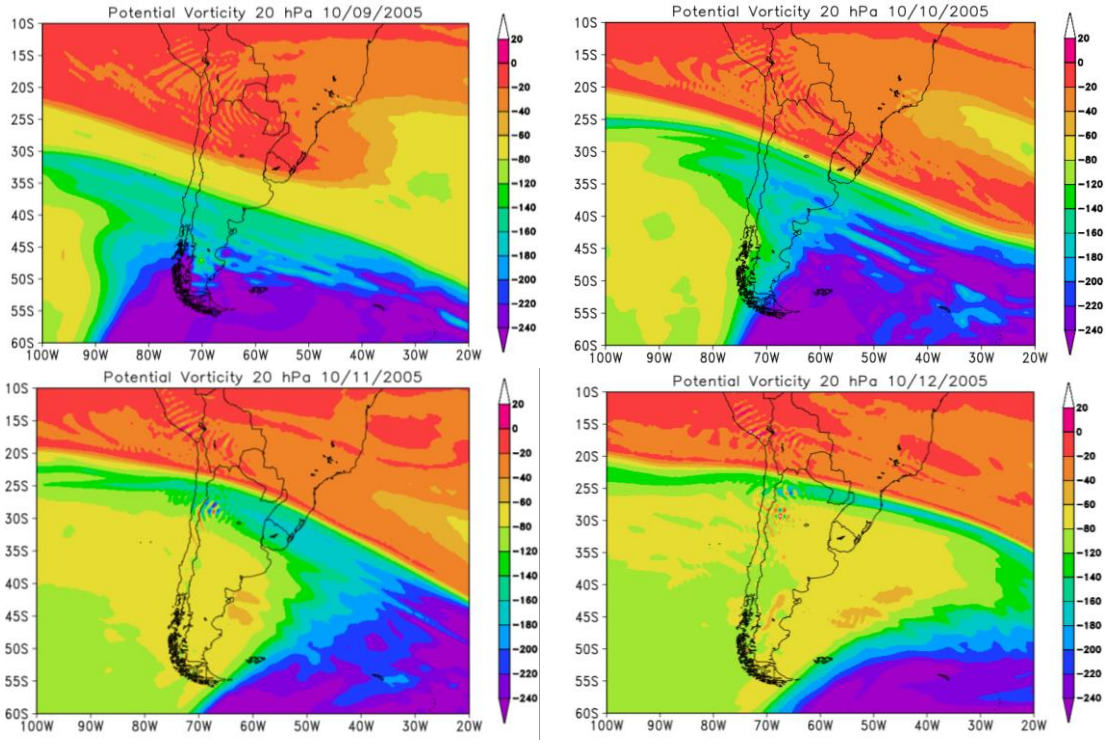

Figure A161: Retroactive trajectory by the HYSPLIT/NOAA model, and O3 content OMI satellite for South Pole, and global view.

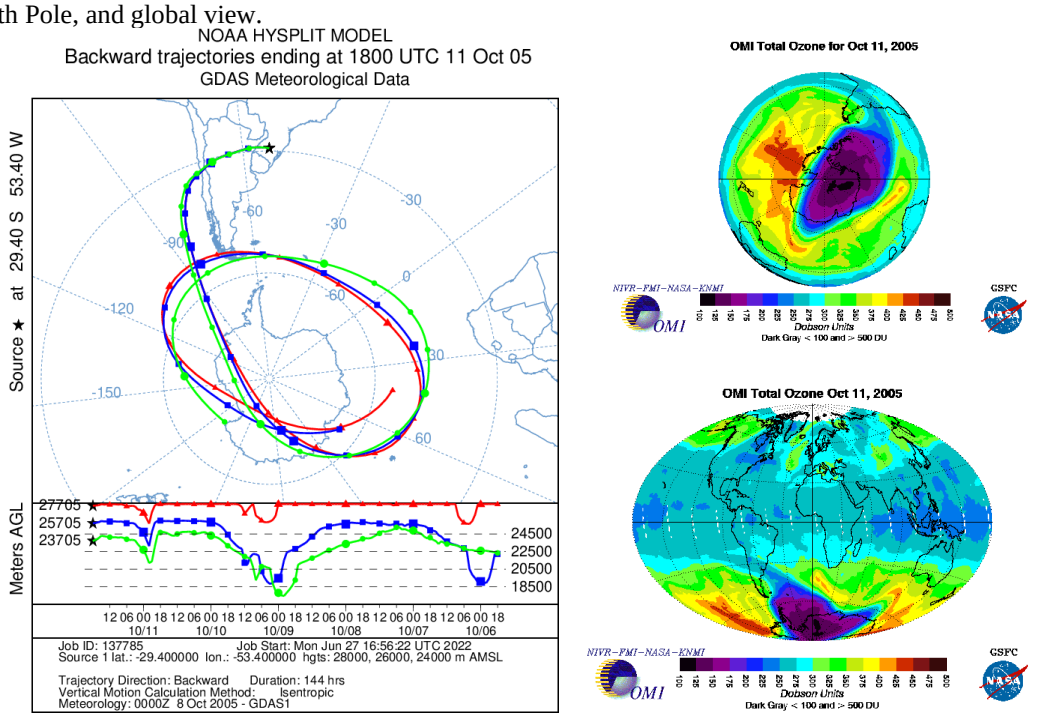

Source: HYSPLIT/NOAA, OMI/NASA.

Figure A162: Vertical profile of O_3 by the SABER satellite for the October 11, 2005 (in red) and climatology for the month of October (in black).

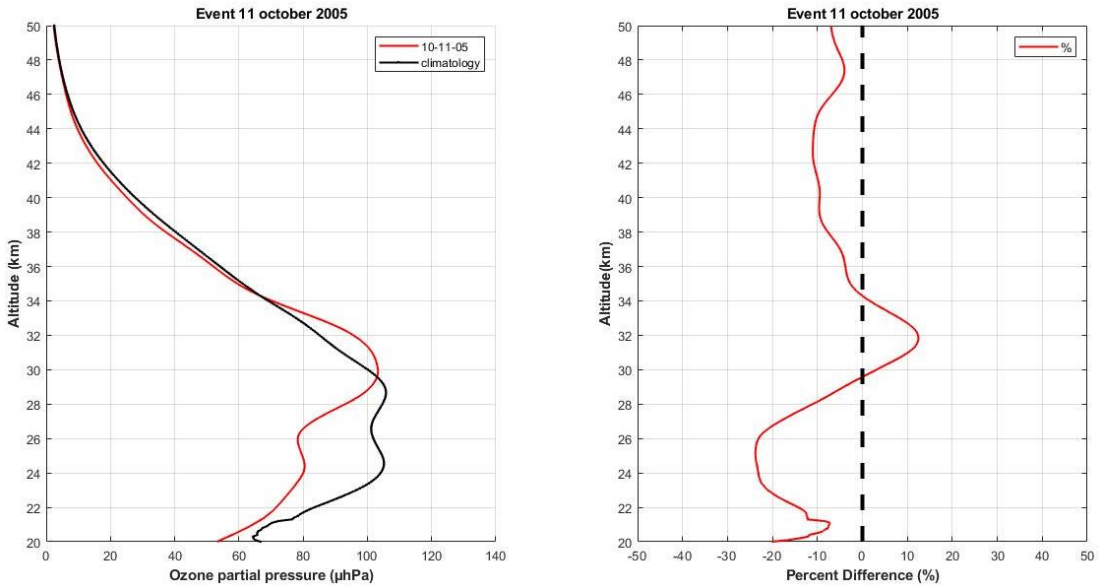

Source: The author.

Figure A163: Vertical section of the atmosphere between 1000 and 5 hPa for the days of the event in October 2016

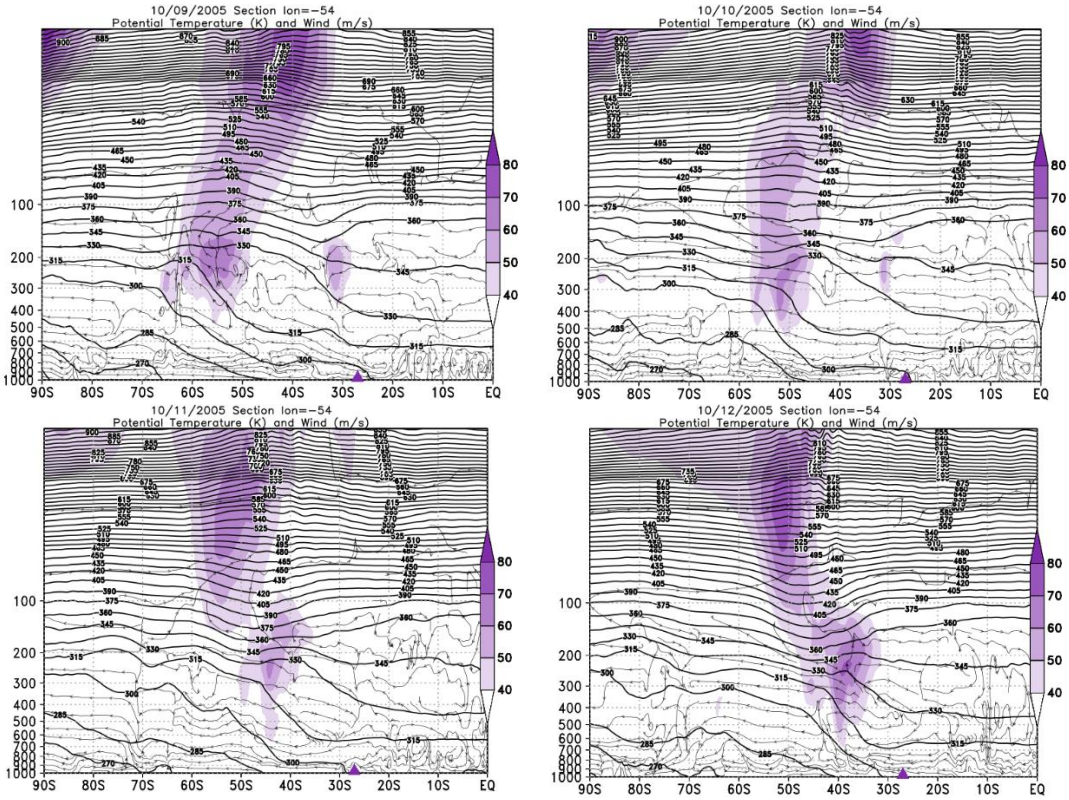

Source: The author.

11/16/2005

Figure A164: PVA fields for the 20 hPa in pressure levels, days 11/14/2005 to 11/17/2005.

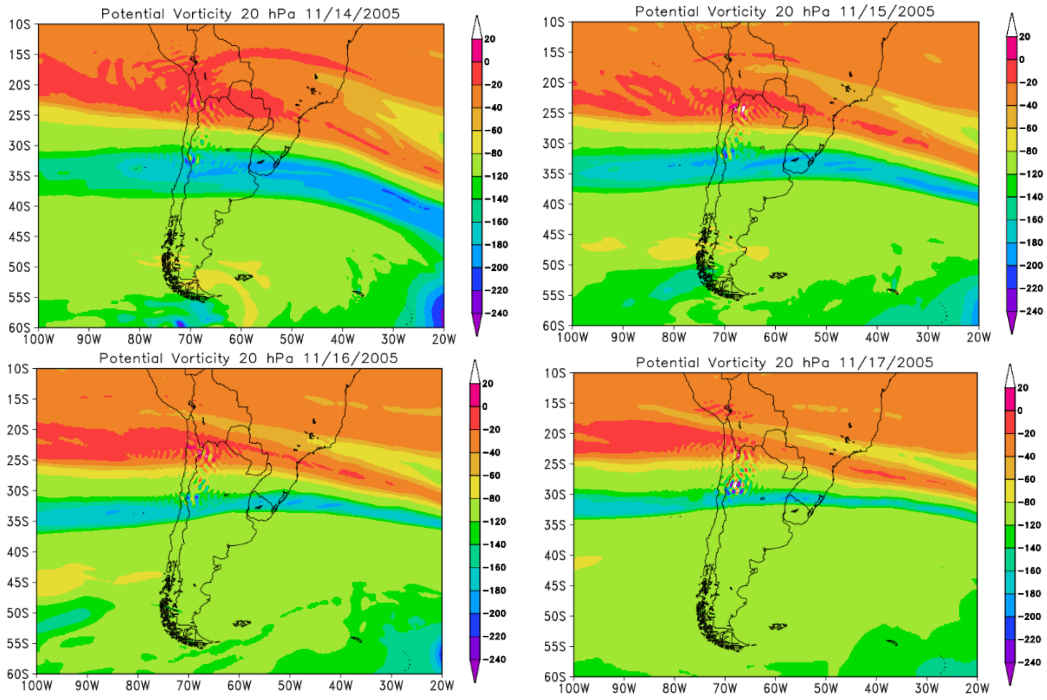

Figure A165: Retroactive trajectory by the HYSPLIT/NOAA model, and O3 content OMI satellite for South Pole, and global view.

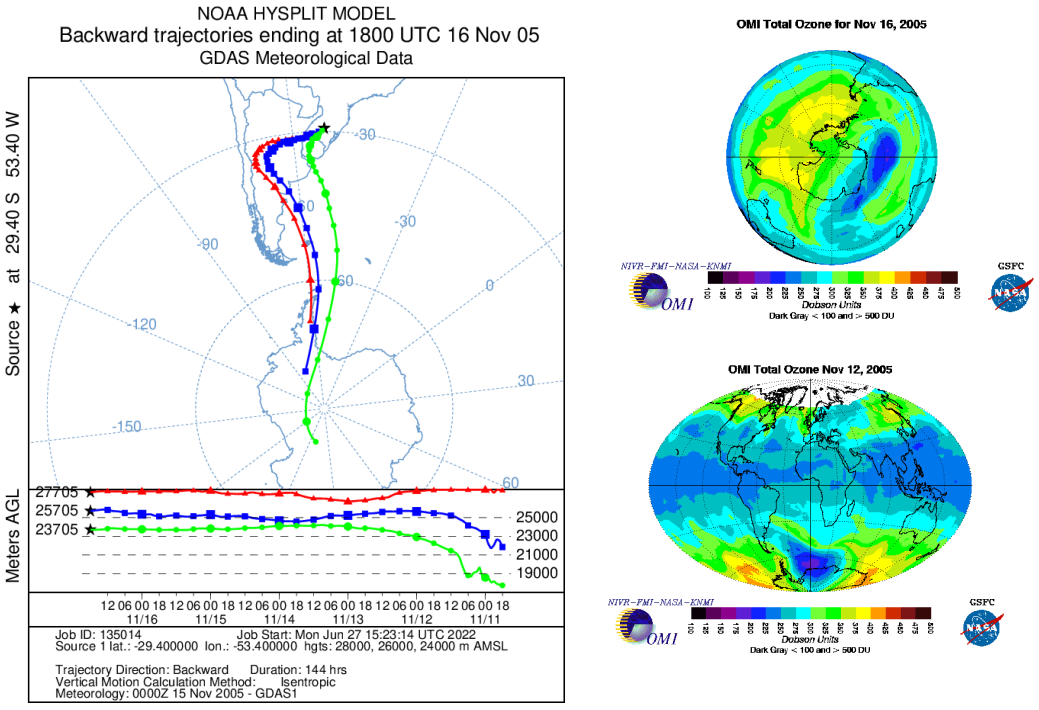

Source: HYSPLIT/NOAA, OMI/NASA.

Figure A166: Vertical profile of O_3 by the SABER satellite for the November 17, 2005 (in red) and climatology for the month of October (in black).

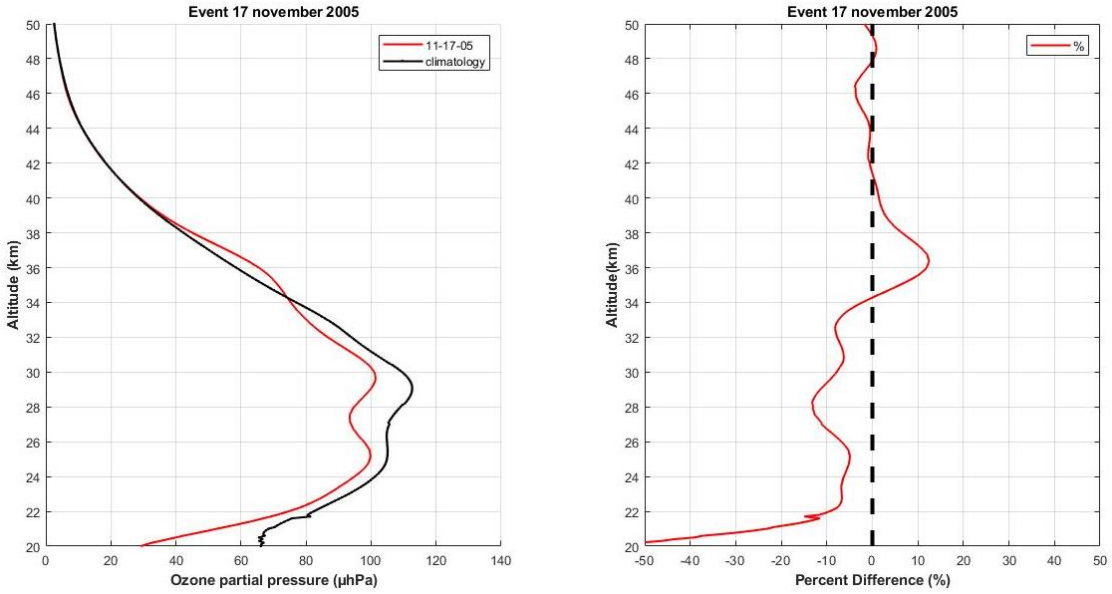

Figure A167: Vertical section of the atmosphere between 1000 and 5 hPa for the days of the event in November 2005.

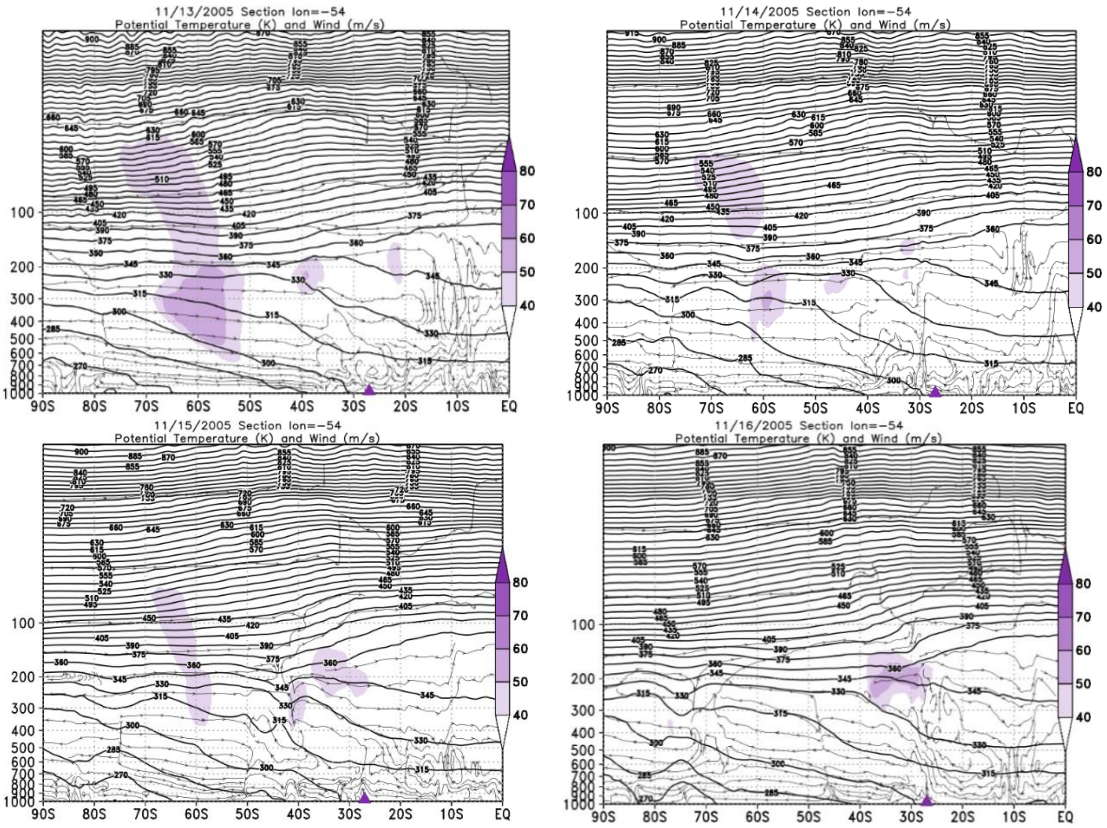

Source: The author.

08/07/2006

Figure A168: PVA fields for the 20 hPa in pressure levels, days 08/05/2006 to 08/08/2006.

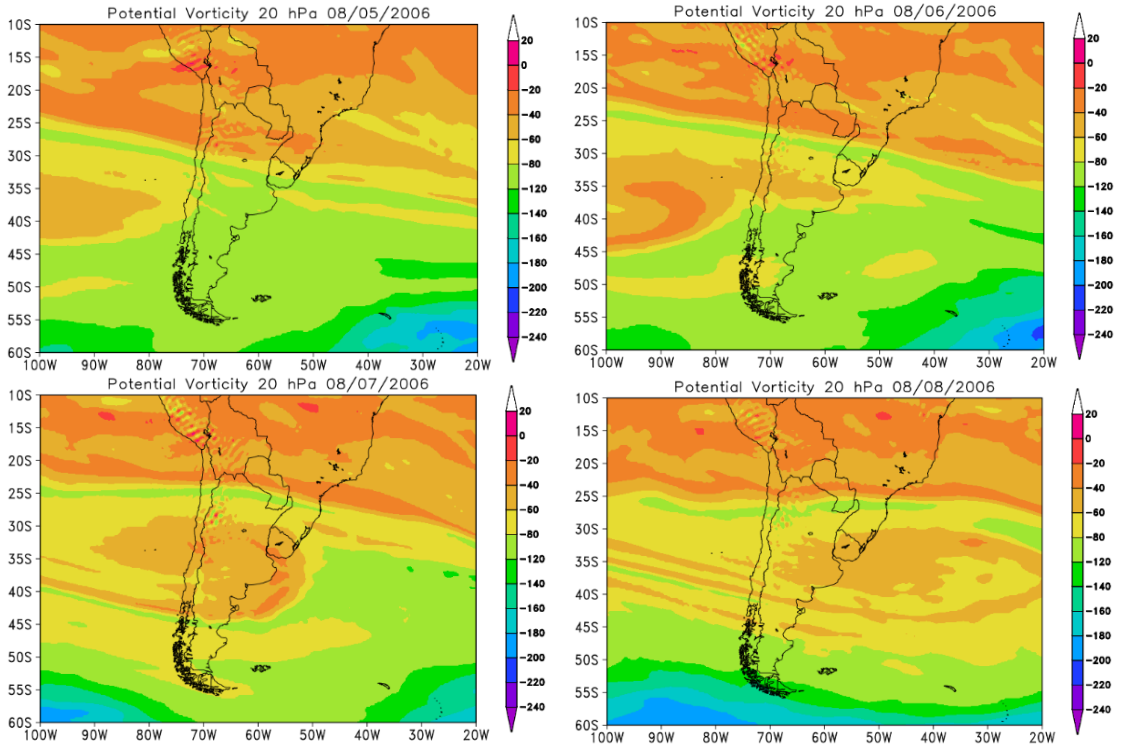

Figure A169: Retroactive trajectory by the HYSPLIT/NOAA model, and O3 content OMI satellite for South Pole, and global view.

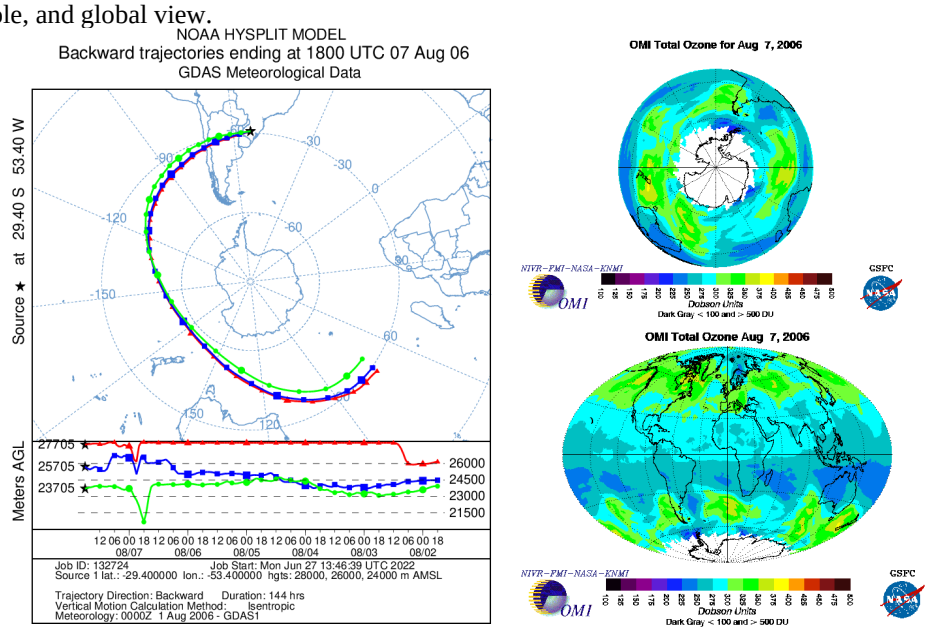

Figure A170: Vertical profile of O_3 by the SABER satellite for the August 06, 2006 (in red) and climatology for the month of October (in black).

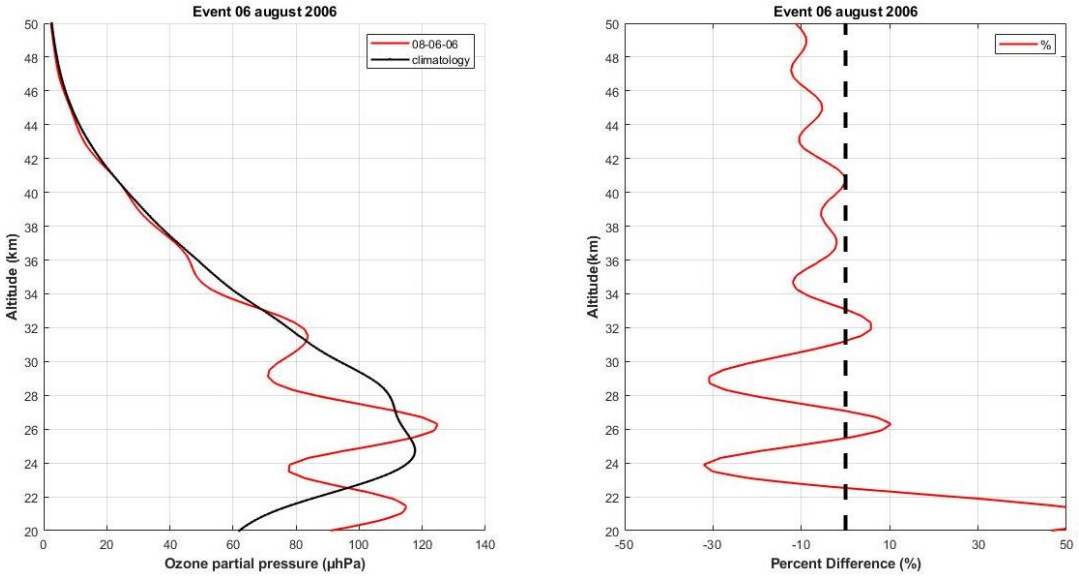

Figure A170: Vertical section of the atmosphere between 1000 and 5 hPa for the days of the event in August 2006.

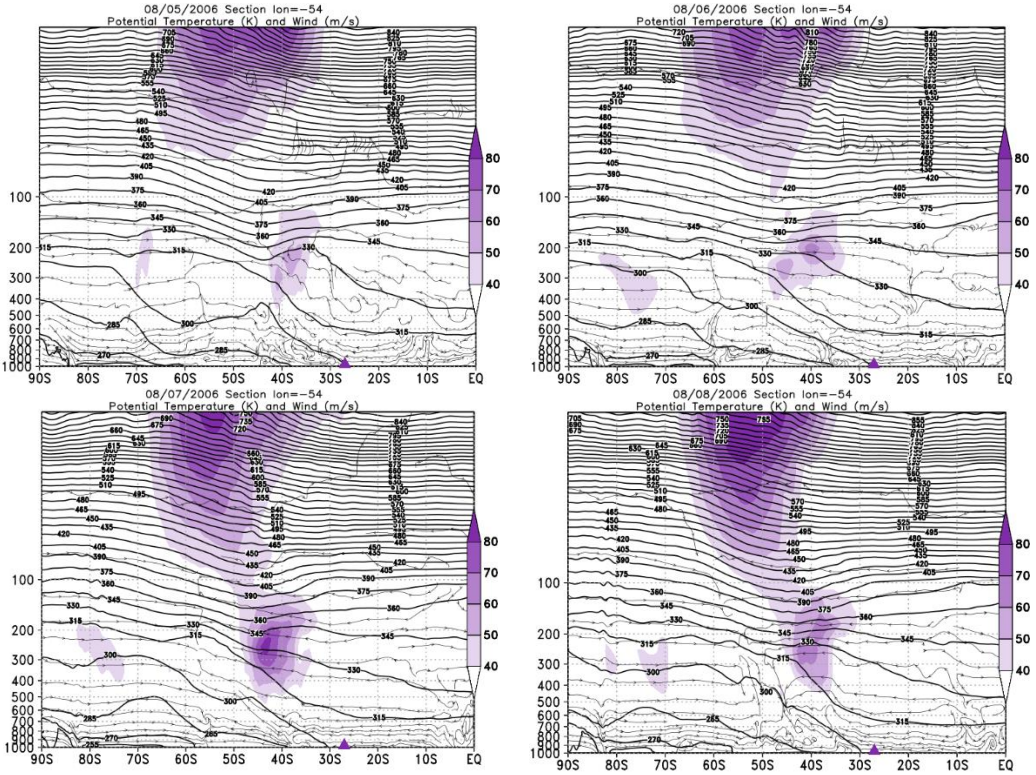

Source: The author.

08/23/2006

Figure A171: PVA fields for the 20 hPa in pressure levels, days 08/21/2006 to 08/24/2006.

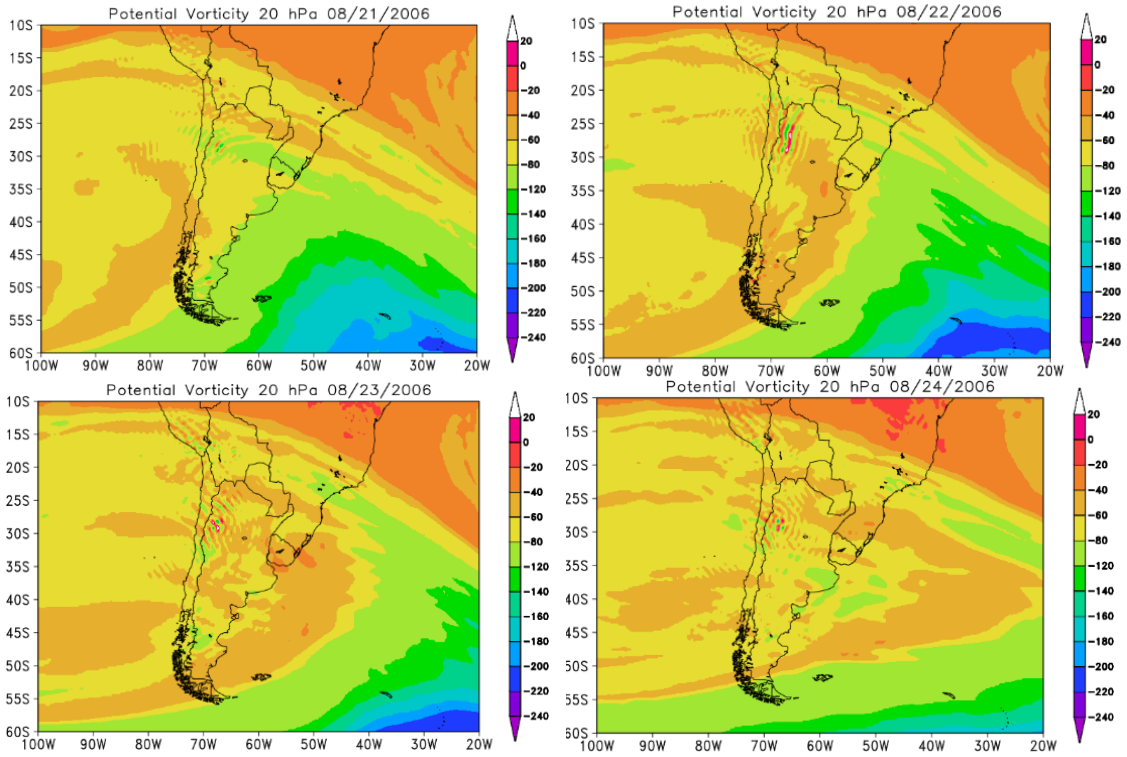

Figure A172: Retroactive trajectory by the HYSPLIT/NOAA model, and O3 content OMI satellite for South Pole, and global view.

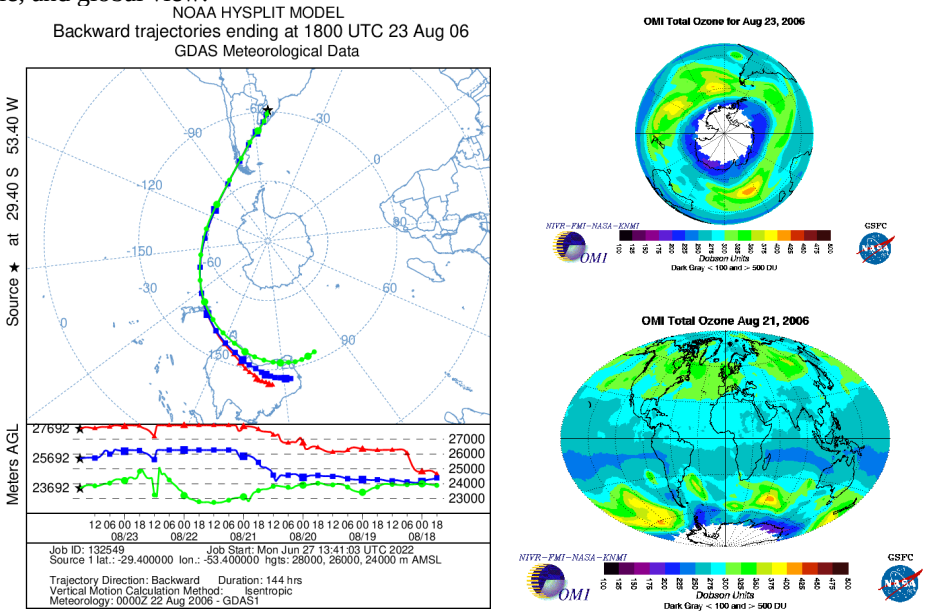

Figure A173: Vertical profile of O_3 by the SABER satellite for the August 22, 2006 (in red) and climatology

for the month of October (in black).

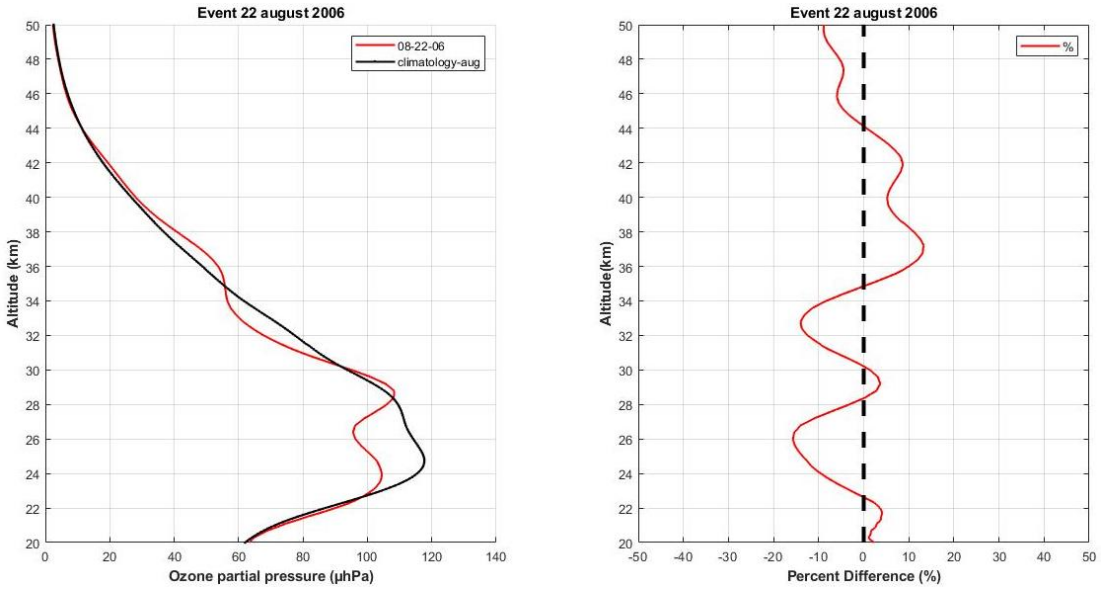

Source: The author.

Figure A174: Vertical section of the atmosphere between 1000 and 5 hPa for the days of the event in August 2006.

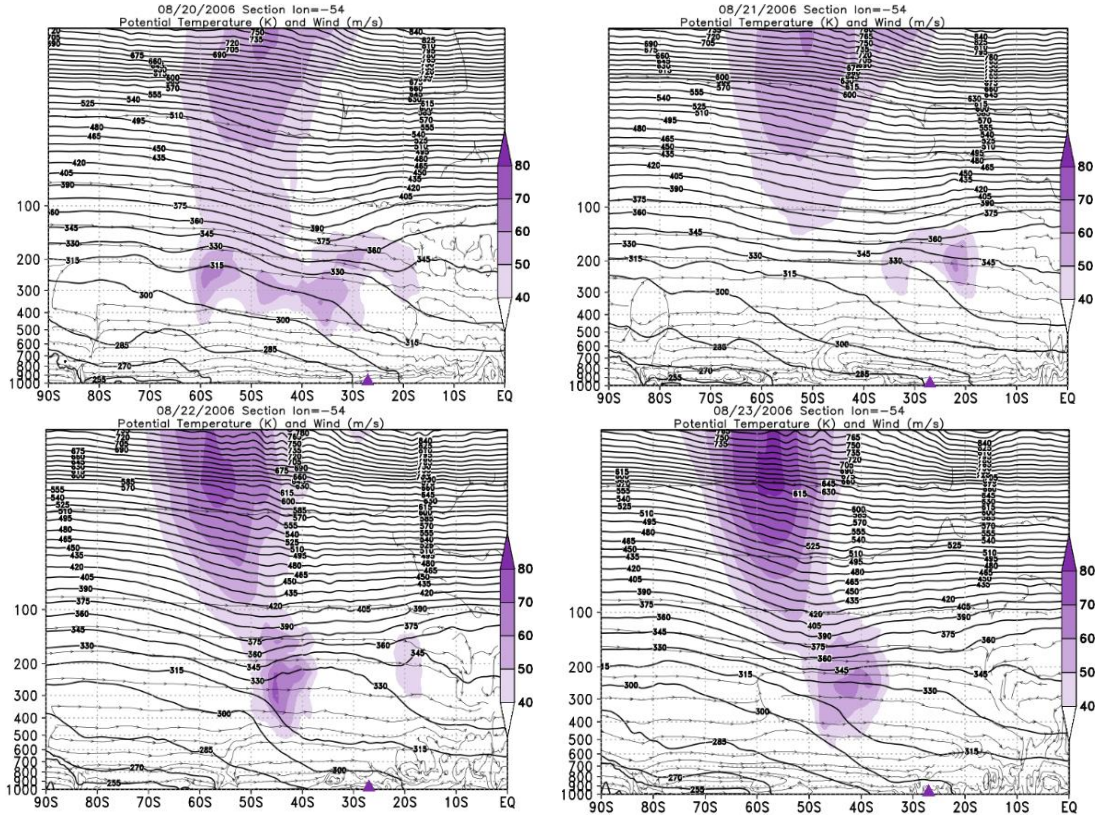

Source: The author.

09/19/2006

Figure A175: PVA fields for the 20 hPa in pressure levels, days 09/18/2006 to 09/21/2006.

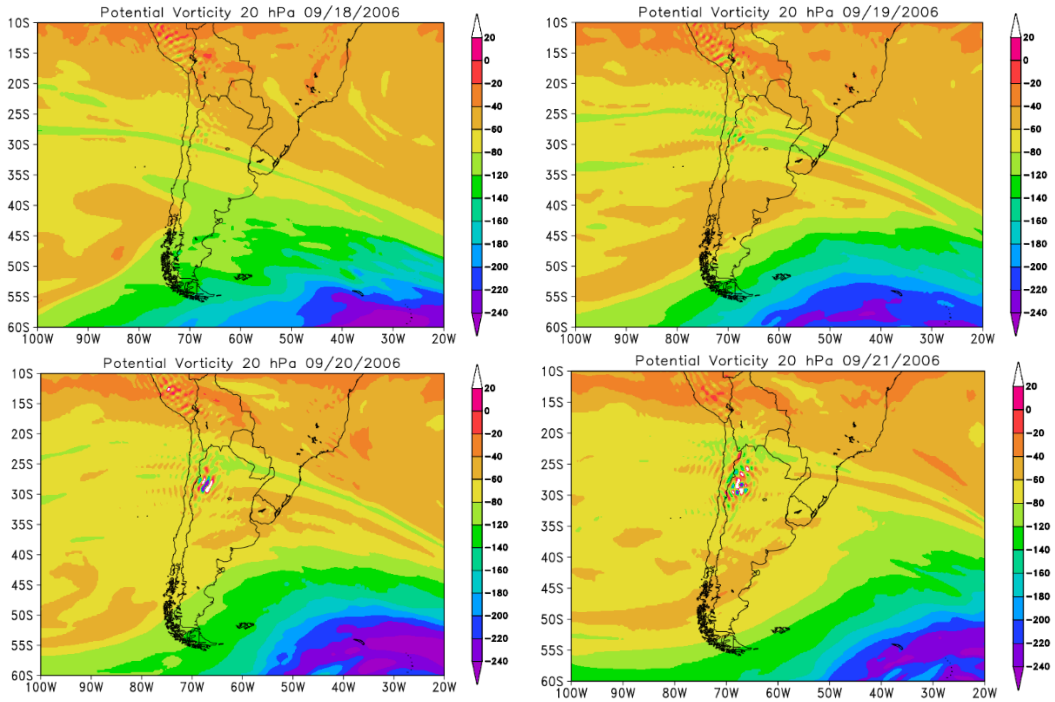

Source: The author.

Figure A176: Retroactive trajectory by the HYSPLIT/NOAA model, and O3 content OMI satellite for South Pole, and global view.

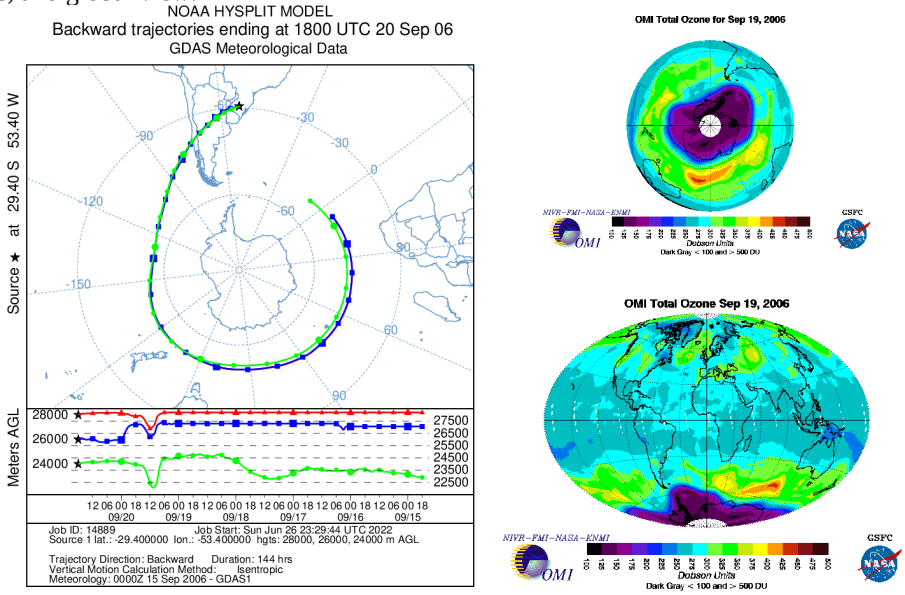

Figure A177: Vertical profile of O_3 by the SABER satellite for the September 21, 2006 (in red) and climatology for the month of October (in black).

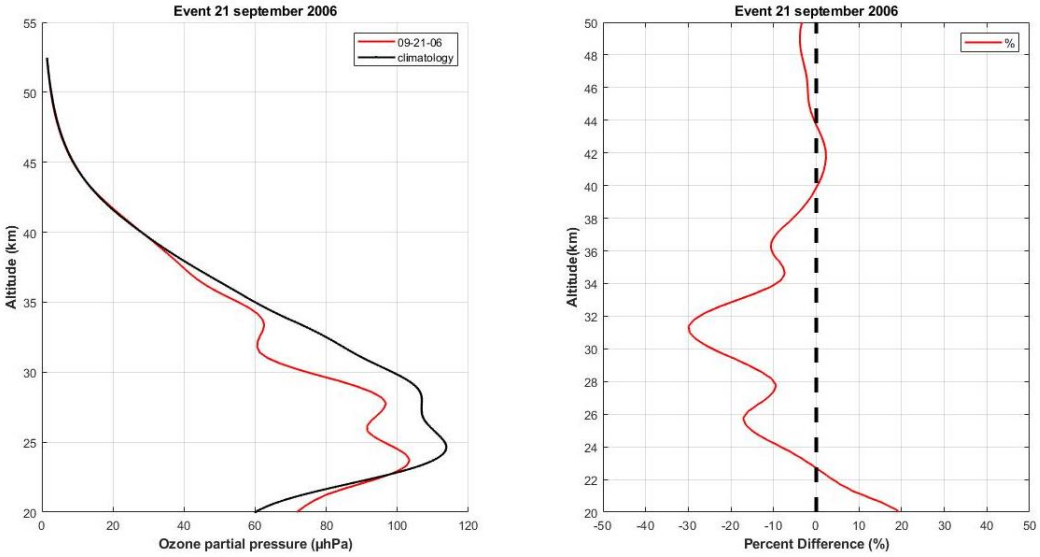

Source: The author.

Figure A178: Vertical section of the atmosphere between 1000 and 5 hPa for the days of the event in September 2006.

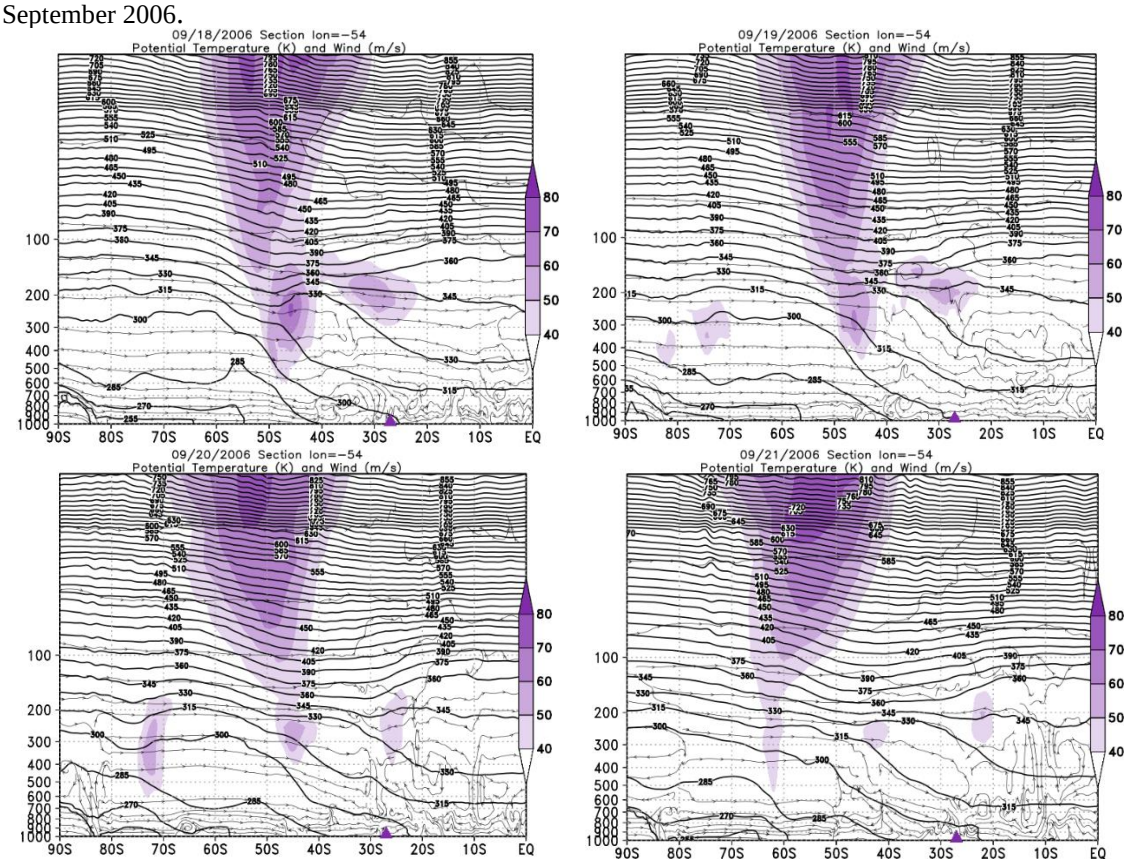

Source: The author.

10/07/2006

Figure A179: PVA fields for the 20 hPa in pressure levels, days 10/05/2006 to 10/08/2006.

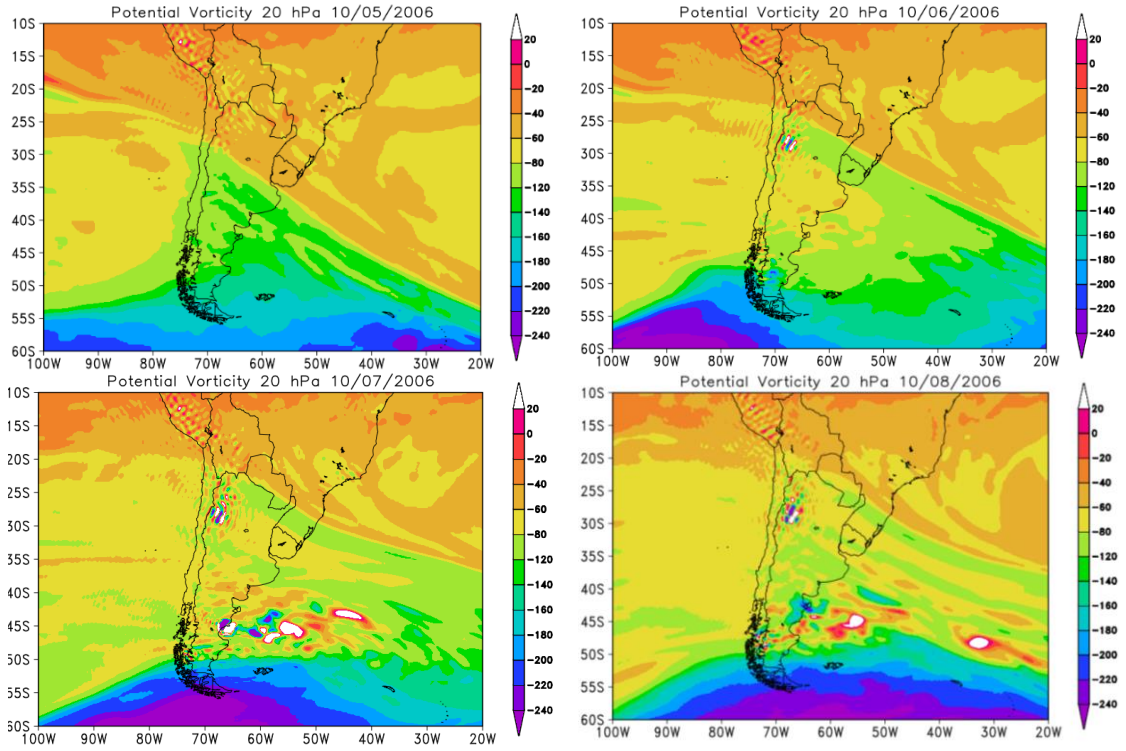

Source: The author.

Figure A180: Retroactive trajectory by the HYSPLIT/NOAA model, and O3 content OMI satellite for South Pole, and global view.

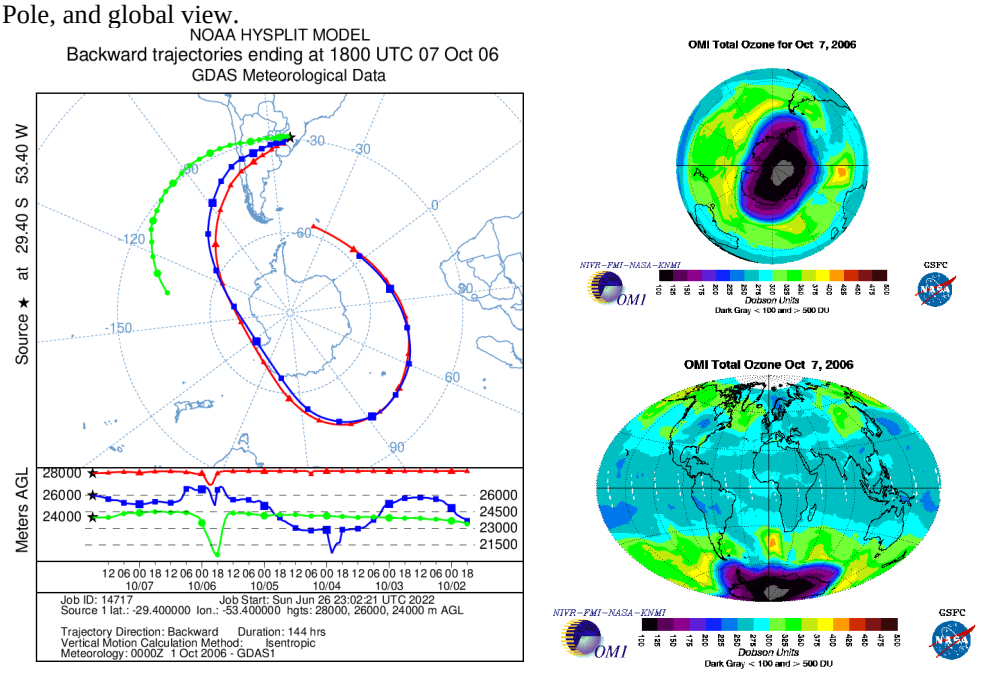

Figure A181: Vertical profile of O_3 by the SABER satellite for the October 06, 2006 (in red) and climatology for the month of October (in black).

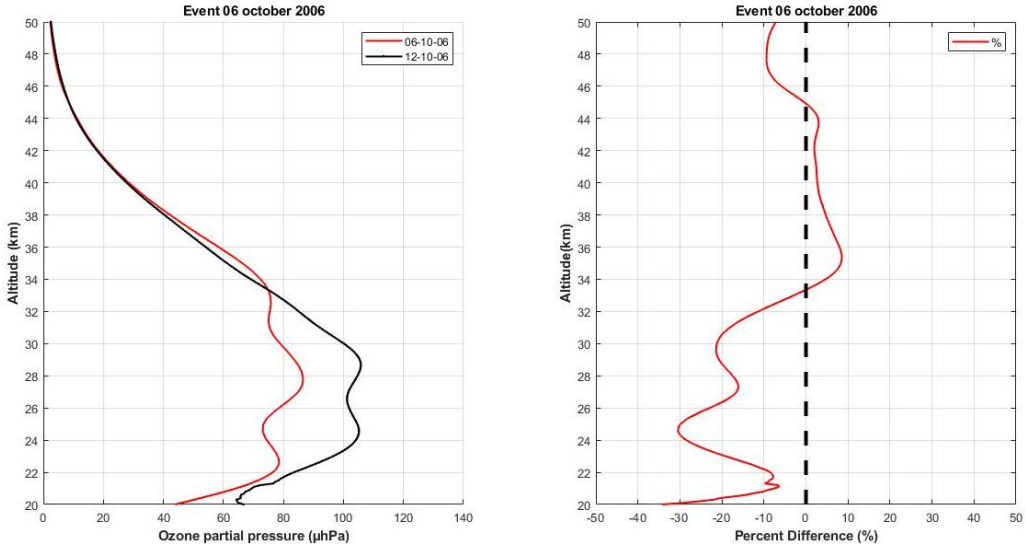

Source: The author.

Figure A182: Vertical section of the atmosphere between 1000 and 5 hPa for the days of the event in October 2016.

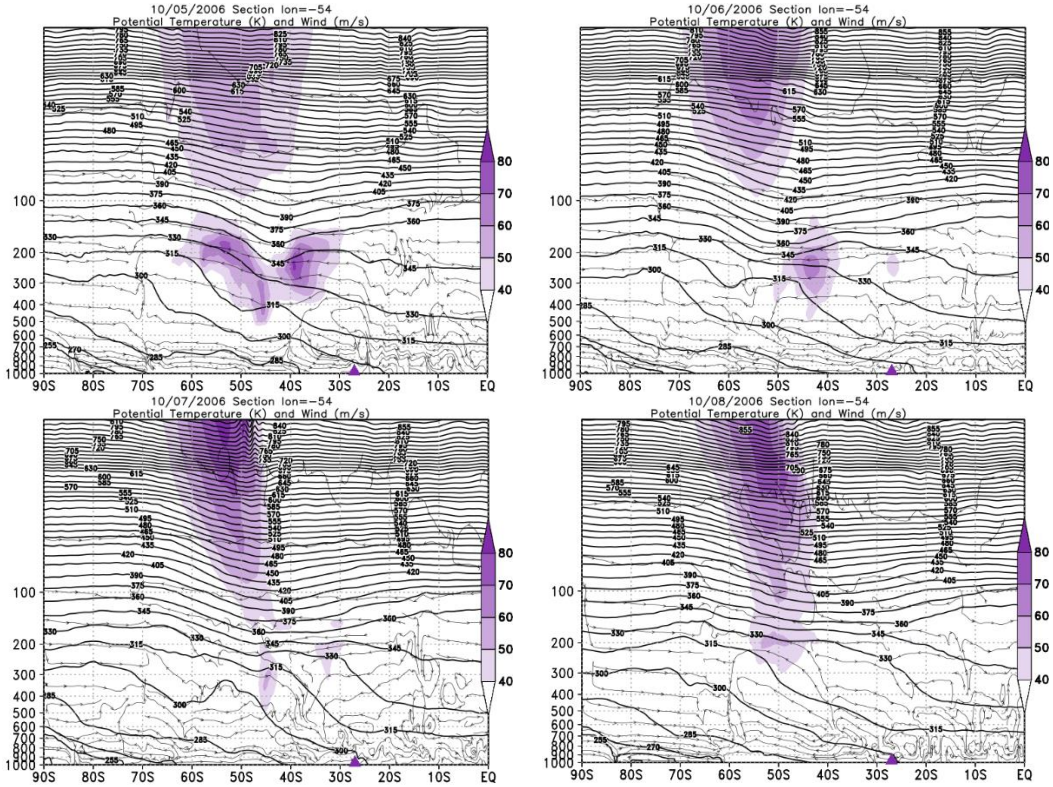

Source: The author.

10/12/2006

Figure A183: PVA fields for the 20 hPa in pressure levels, days 10/10/2006 to 10/13/2006.

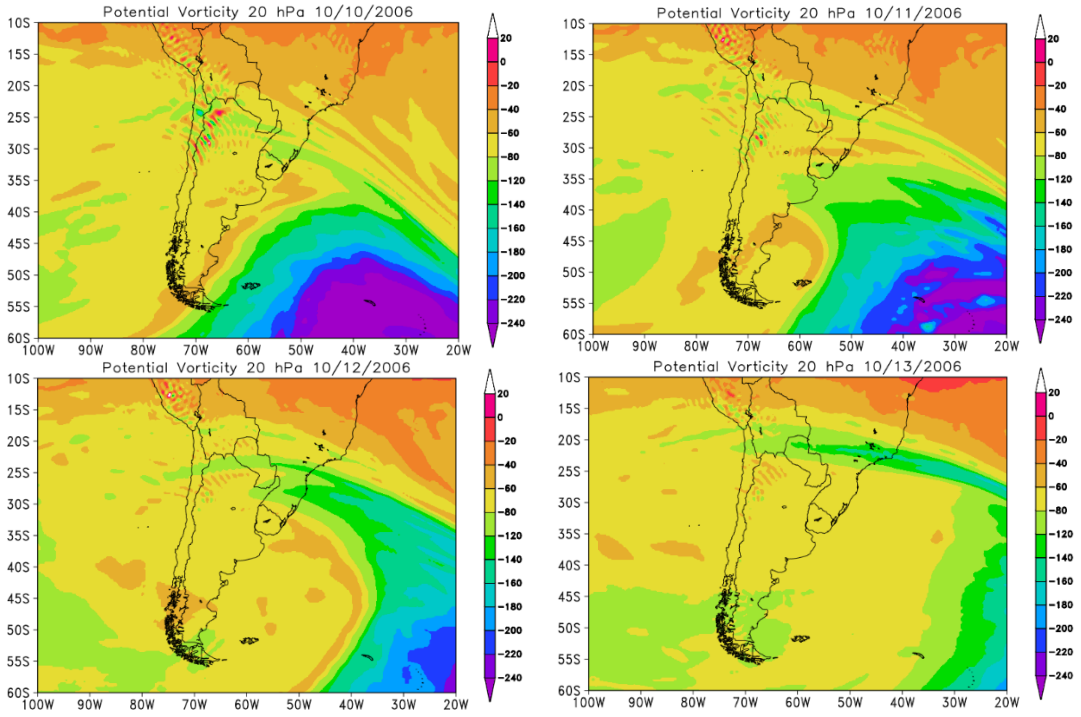

Figure A184: Retroactive trajectory by the HYSPLIT/NOAA model, and O3 content OMI satellite for South Pole, and global view.

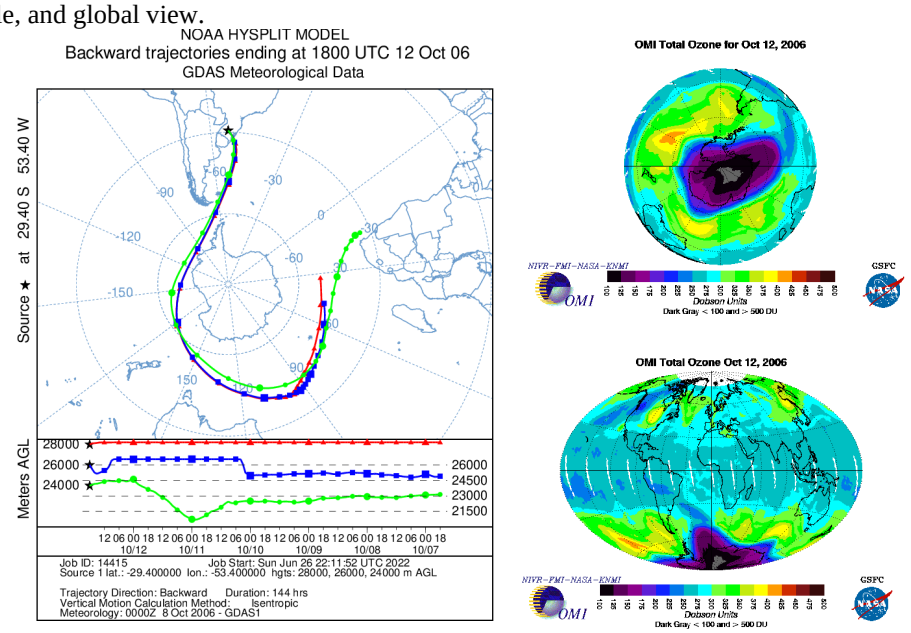

Figure A185: Vertical profile of O_3 by the SABER satellite for the October 20, 2016 (in red) and climatology for the month of October (in black).

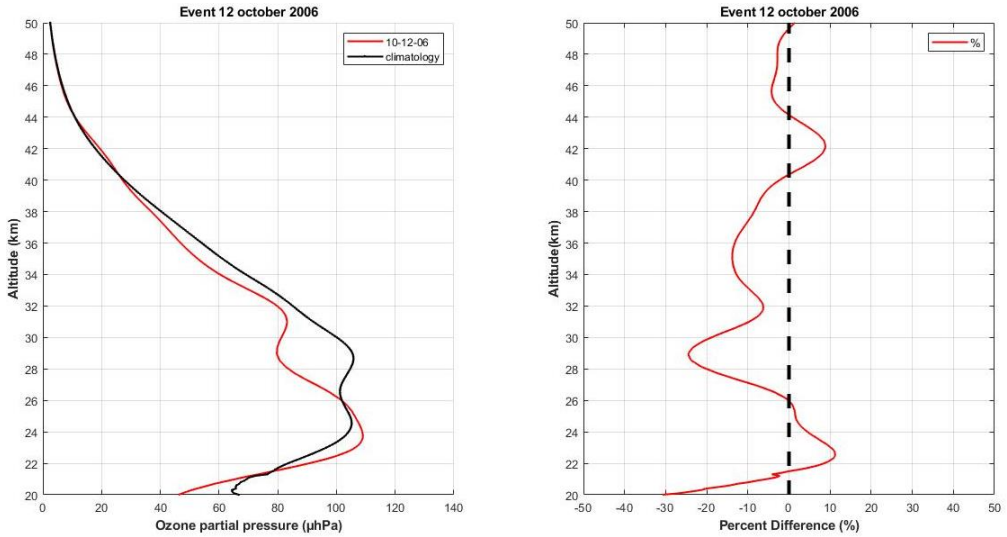

Source: The author.

Figure A186: Vertical section of the atmosphere between 1000 and 5 hPa for the days of the event in October 2006.

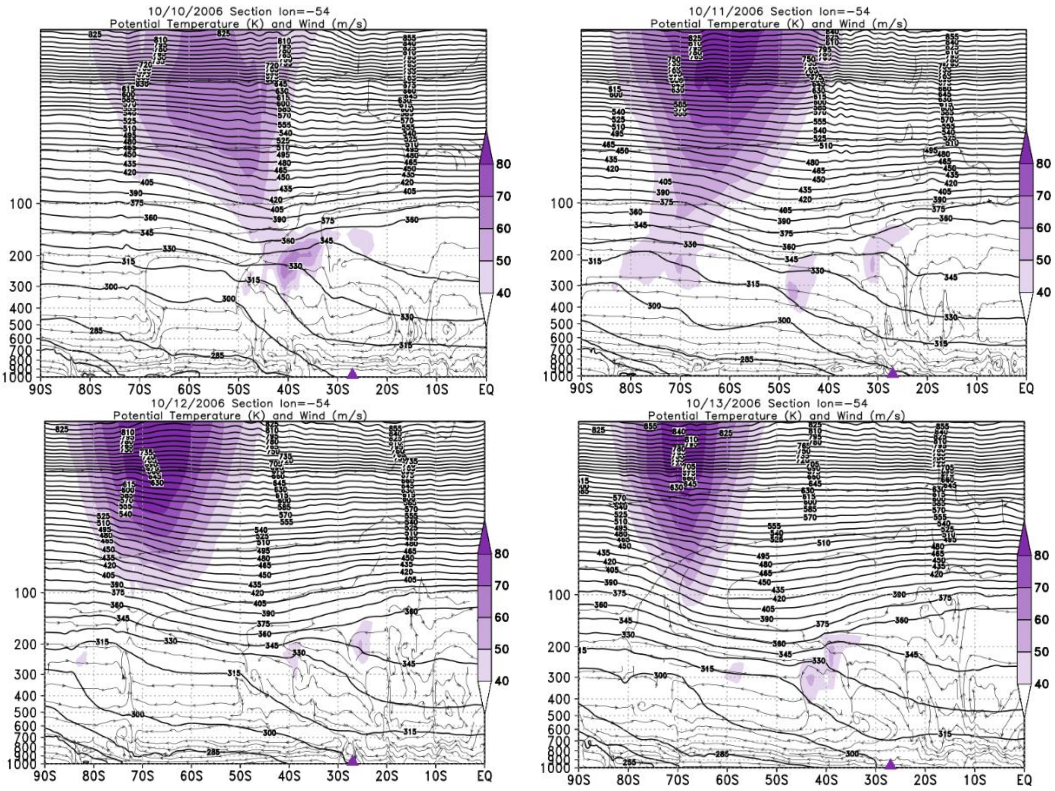

Source: The author.

08/16/2007

Figure A187: PVA fields for the 20 hPa in pressure levels, days 08/14/2007 to 08/17/2007.

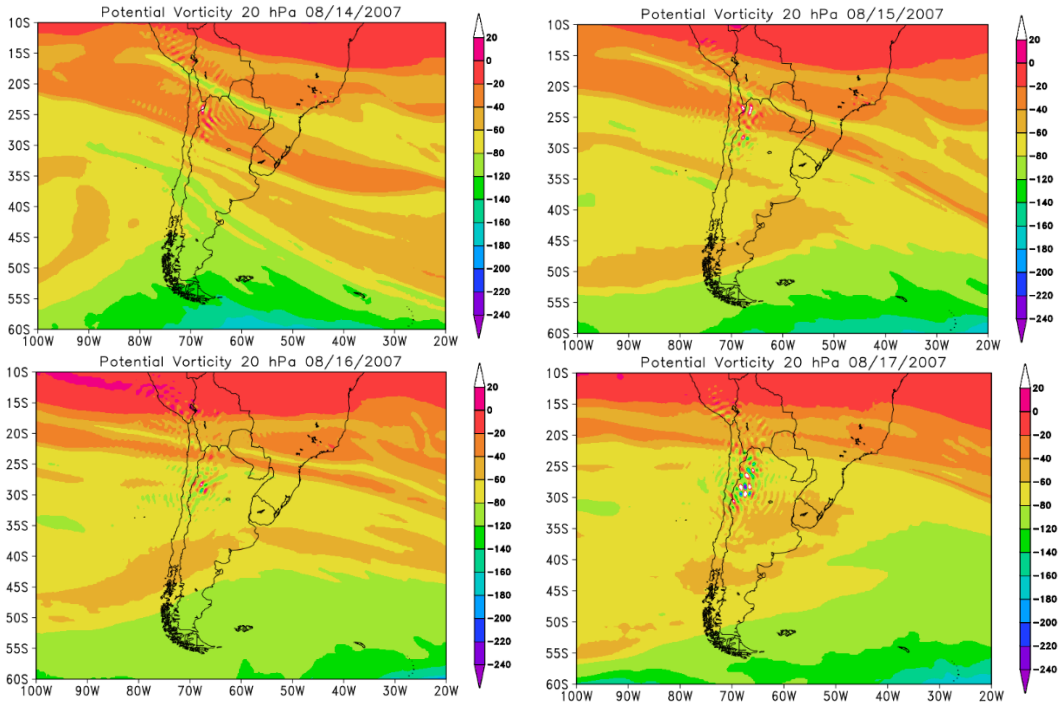

Source: The author.

Figure A188: Retroactive trajectory by the HYSPLIT/NOAA model, and O3 content OMI satellite for South Pole, and global view.

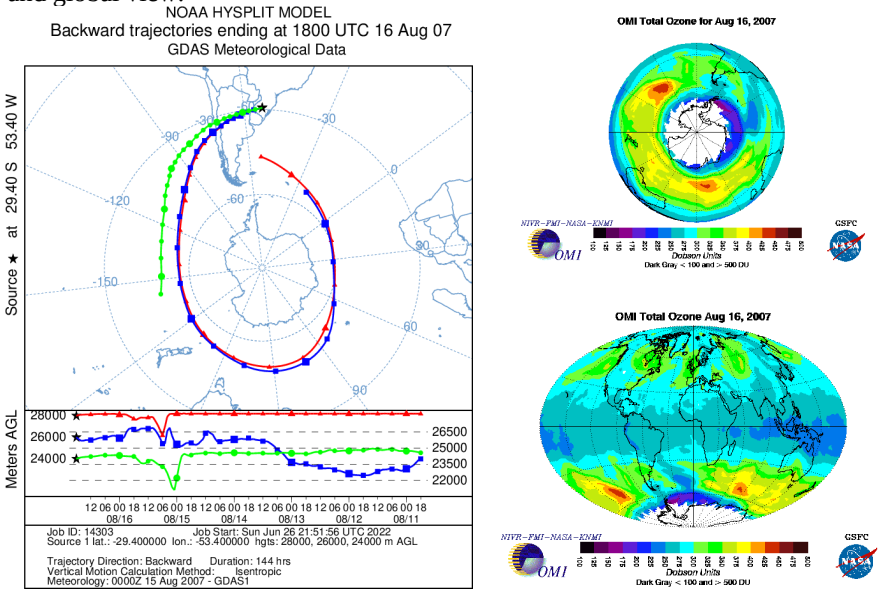

Figure A189: Vertical profile of O_3 by the SABER satellite for the August 15, 2007 (in red) and climatology

for the month of October (in black).

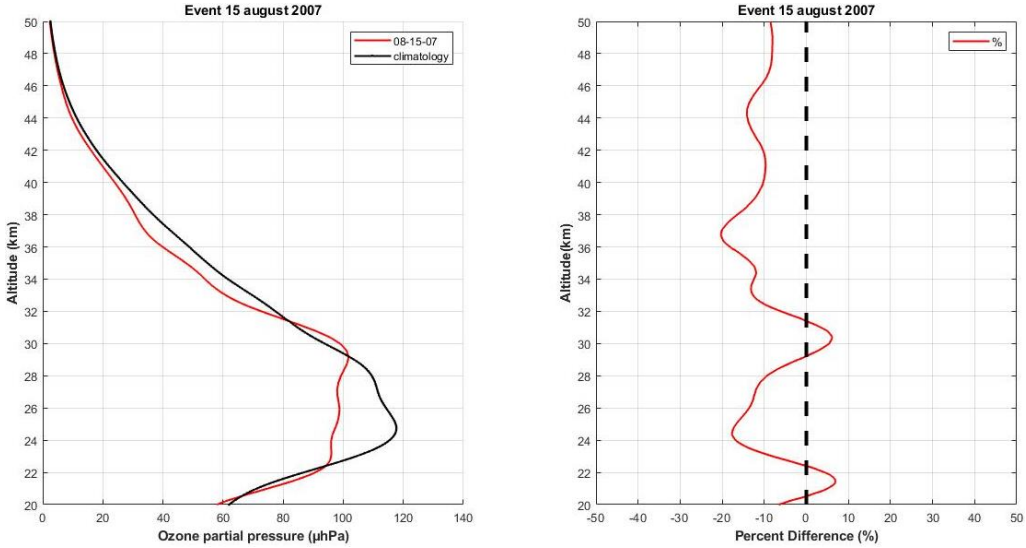

Source: The author.

Figure A190: Vertical section of the atmosphere between 1000 and 5 hPa for the days of the event in October 2016.

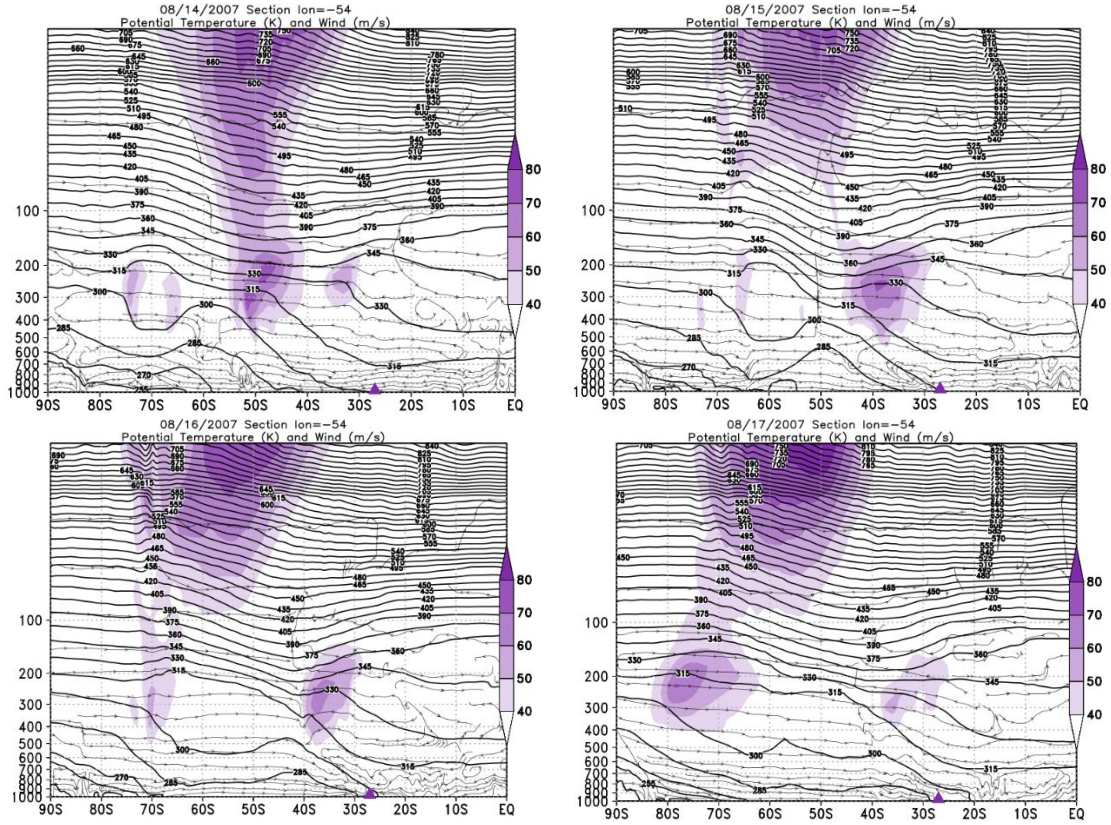

Source: The author.

09/13/2007

Figure A191: PVA fields for the 20 hPa in pressure levels, days 09/11/2007 to 09/14/2007.

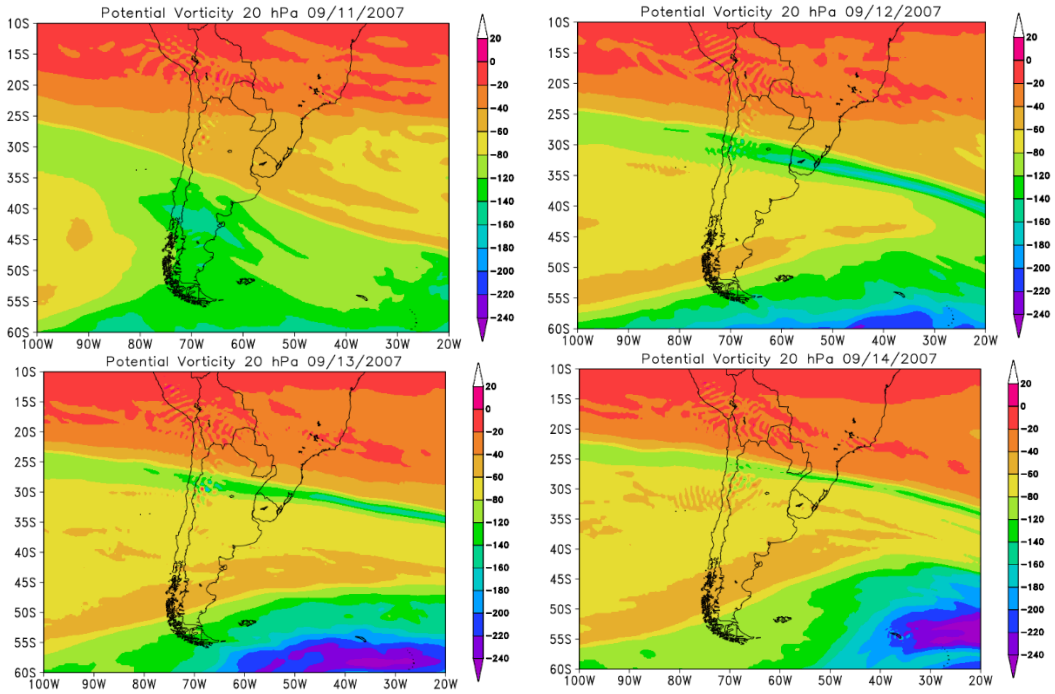

Figure A192: Retroactive trajectory by the HYSPLIT/NOAA model, and O3 content OMI satellite for South Pole, and global view.

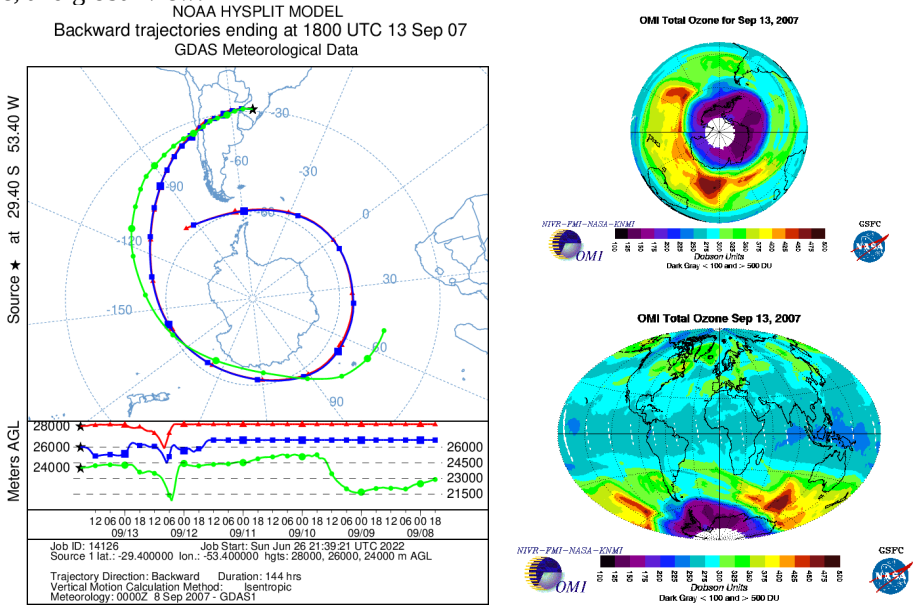

Figure A193: Vertical profile of O_3 by the SABER satellite for the September 13, 2007 (in red) and climatology for the month of October (in black).

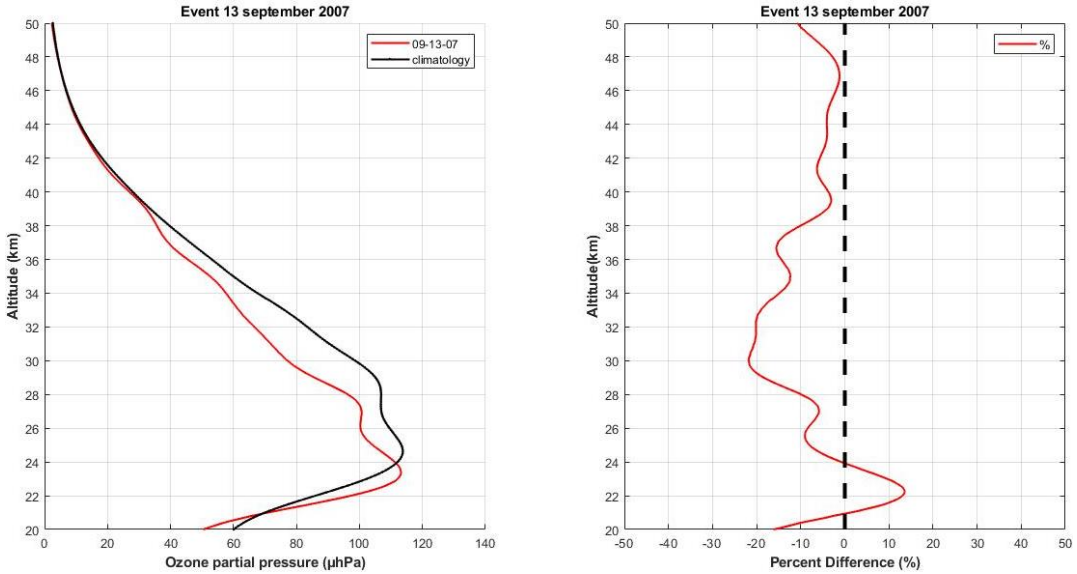

Source: The author.

Figure A194: Vertical section of the atmosphere between 1000 and 5 hPa for the days of the event in September 2007.

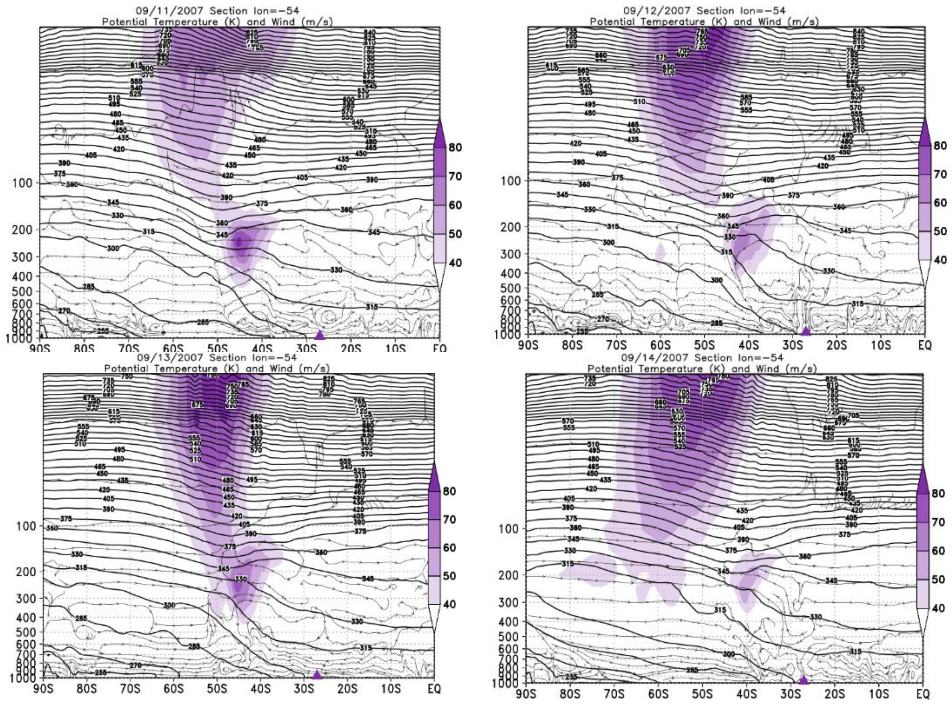

Source: The author.

10/07/2007

Figure A195: PVA fields for the 20 hPa in pressure levels, days 10/06/2007 to 10/09/1997.

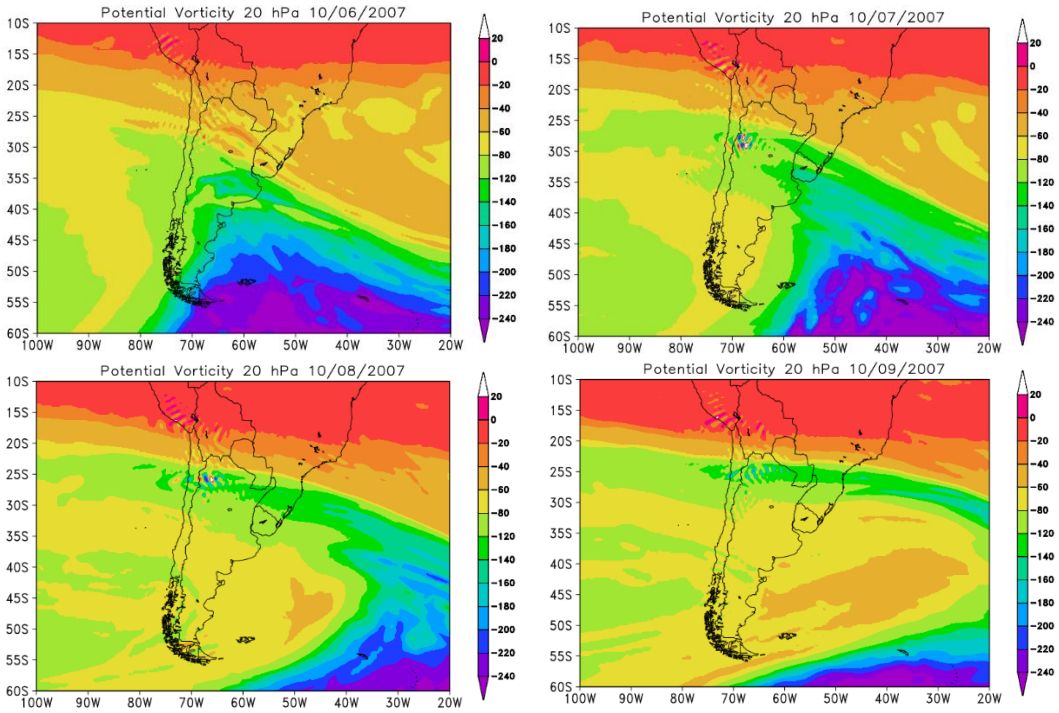

Figure A196: Retroactive trajectory by the HYSPLIT/NOAA model, and O3 content OMI satellite for South Pole, and global view.

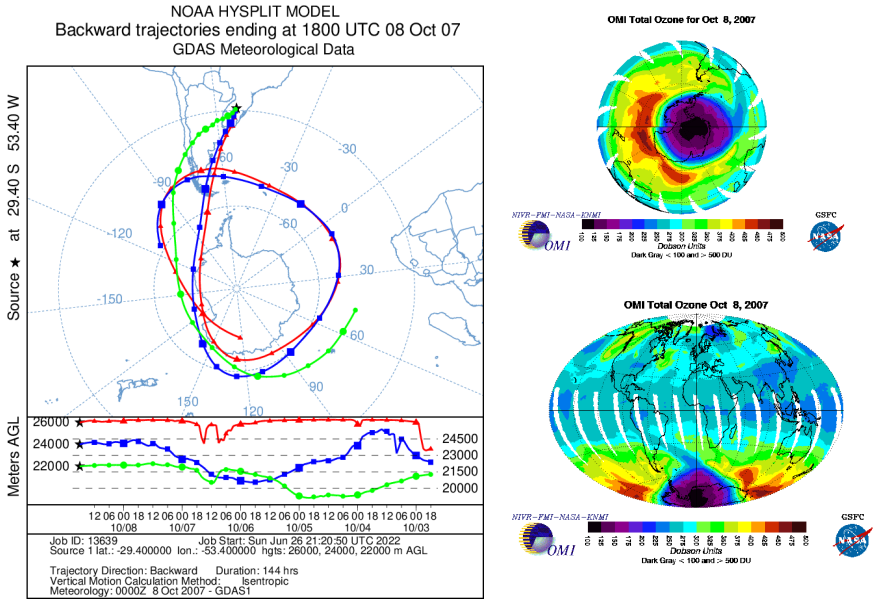

Figure A197: Vertical profile of O_3 by the SABER satellite for the October 08, 2007 (in red) and climatology for the month of October (in black).

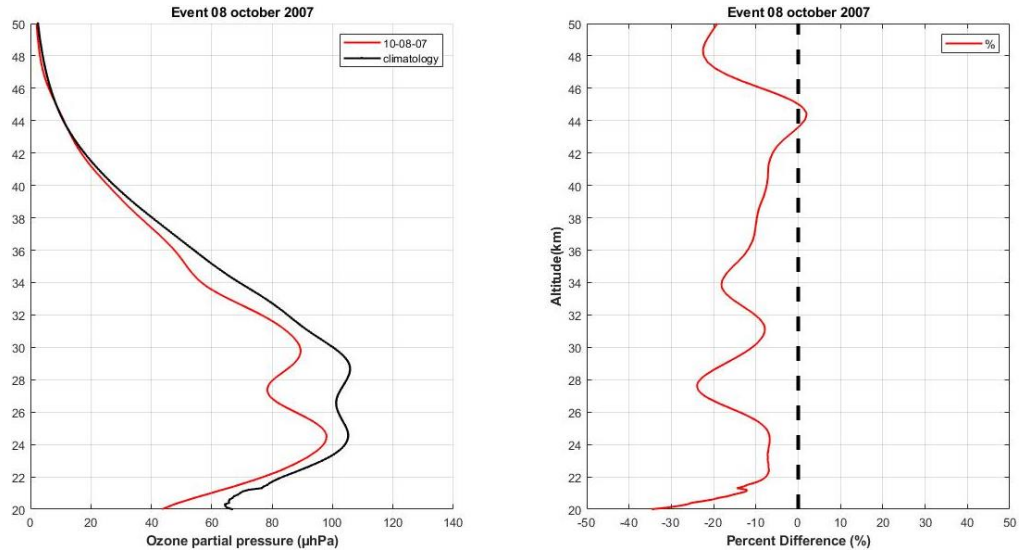

Source: The author.

Figure A198: Vertical section of the atmosphere between 1000 and 5 hPa for the days of the event in October 2007.

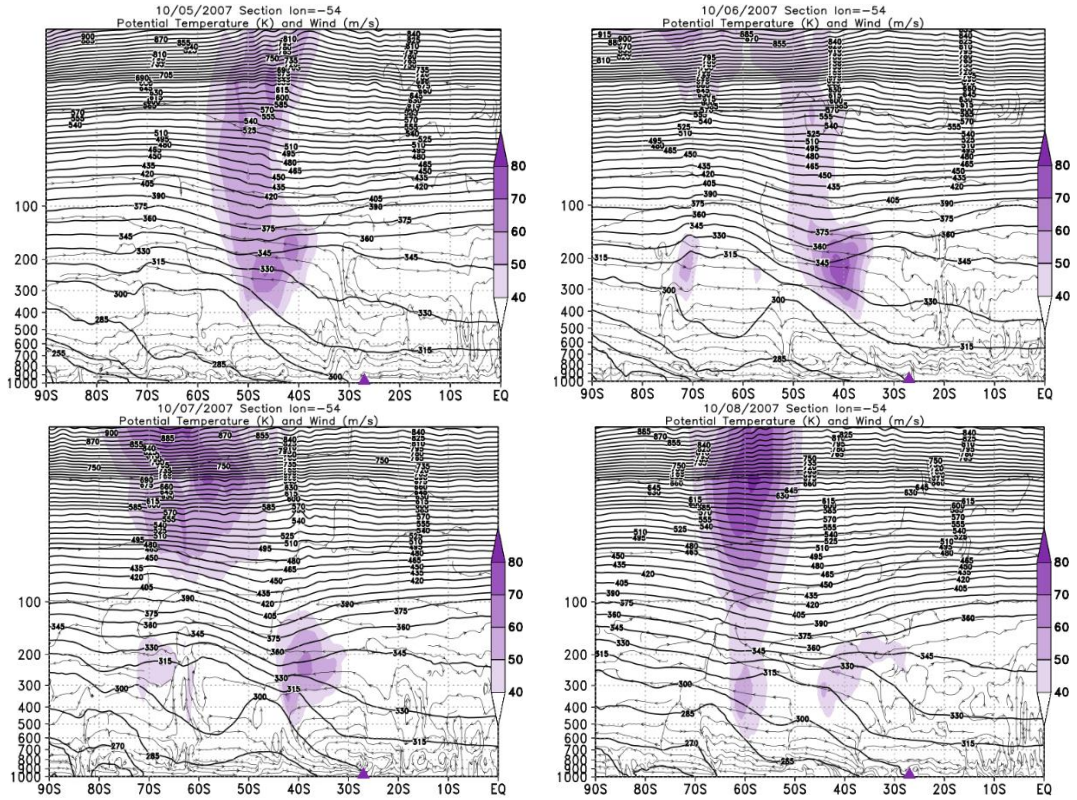

Source: The author.

10/12/2008

Figure A199: PVA fields for the 20 hPa in pressure levels, days 10/10/2008 to 10/13/2008.

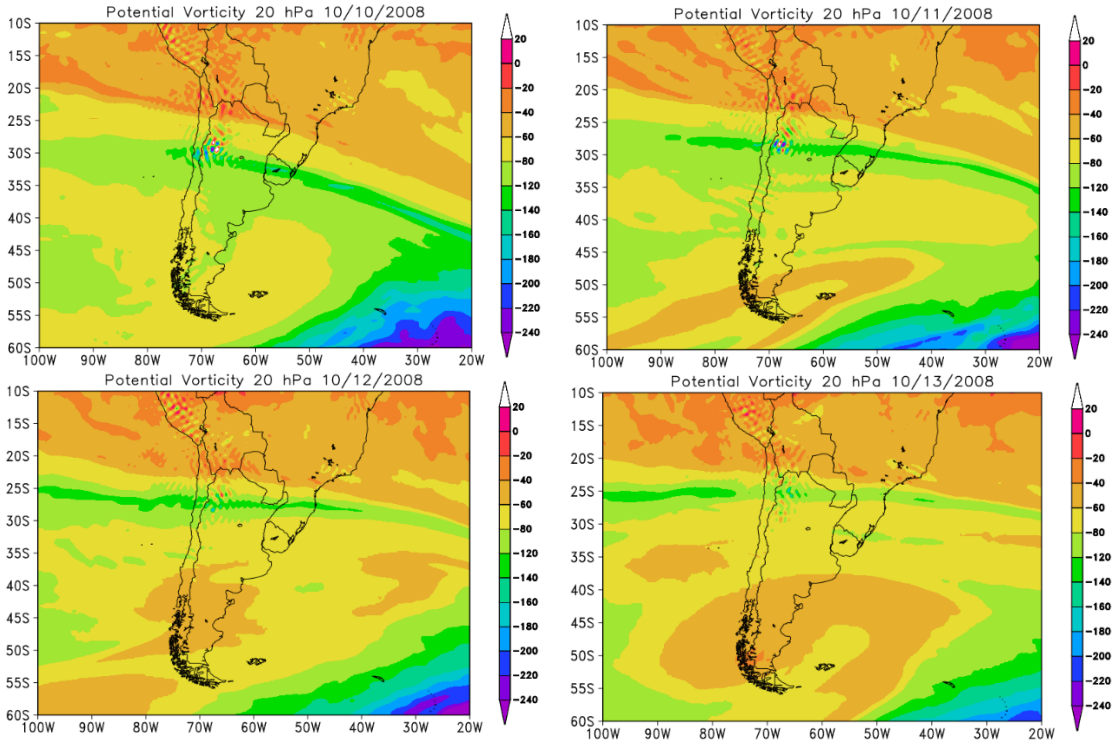

Figure A200: Retroactive trajectory by the HYSPLIT/NOAA model, and O3 content OMI satellite for South Pole, and global view.

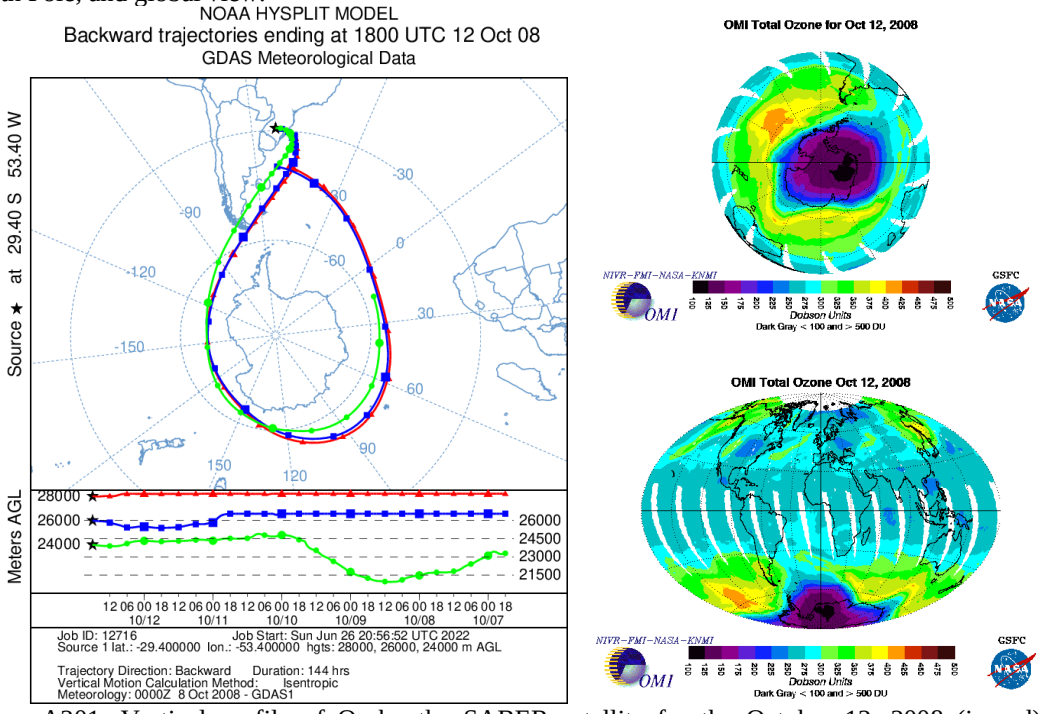

Figure A201: Vertical profile of O_3 by the SABER satellite for the October 12, 2008 (in red) and

climatology for the month of October (in black).

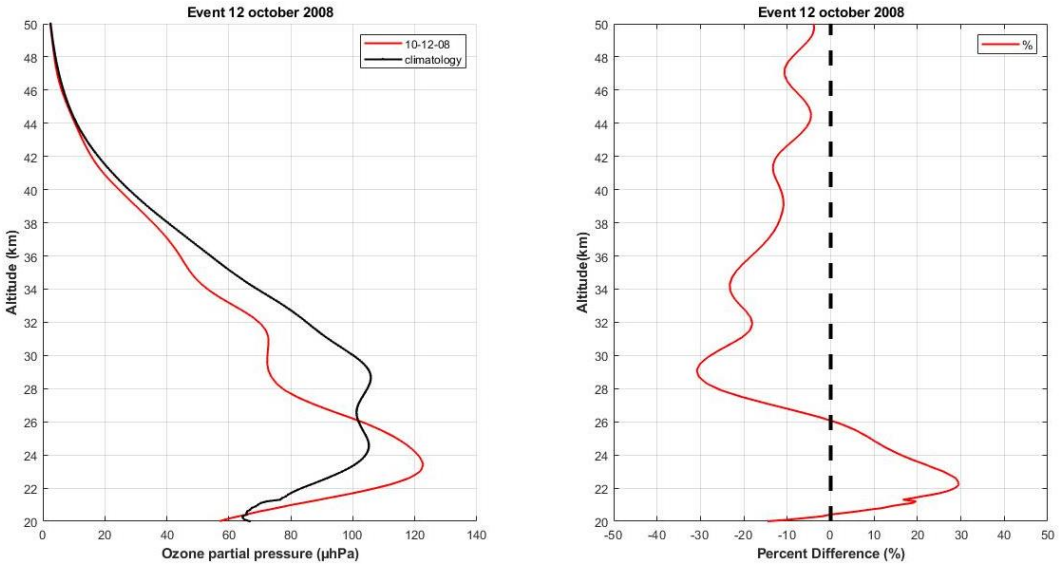

Source: The author.

Figure A202: Vertical section of the atmosphere between 1000 and 5 hPa for the days of the event in October 2008.

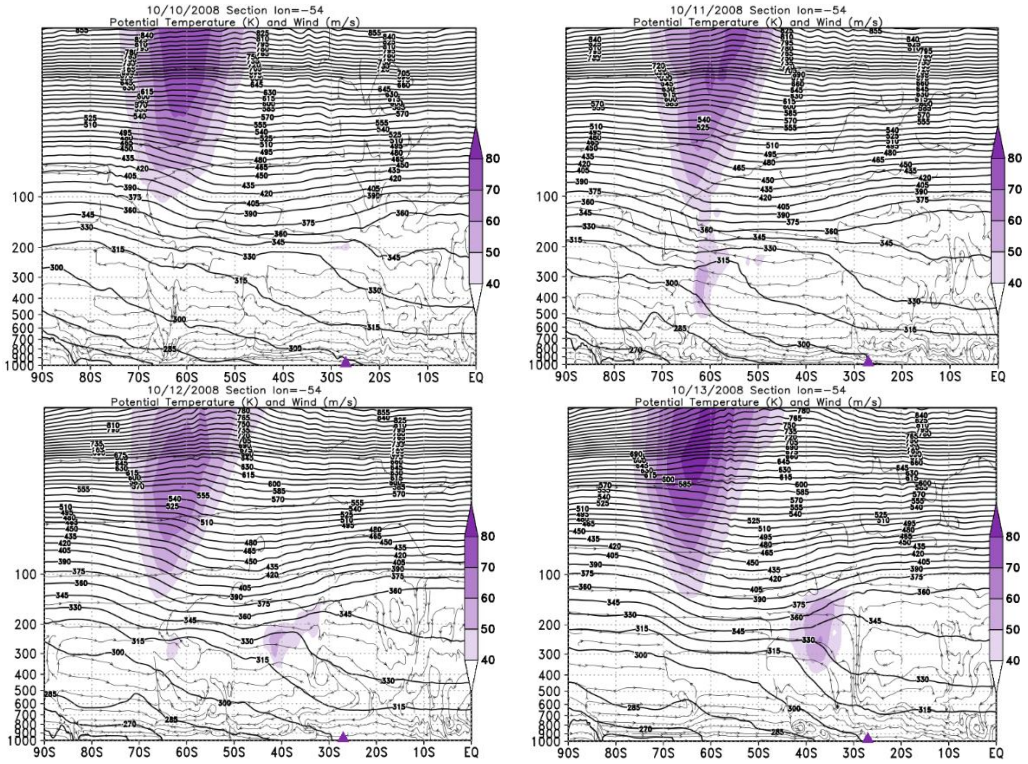

Source: The author.

10/26/2008

Figure A203: PVA fields for the 20 hPa in pressure levels, days 10/24/2008 to 10/27/2008.

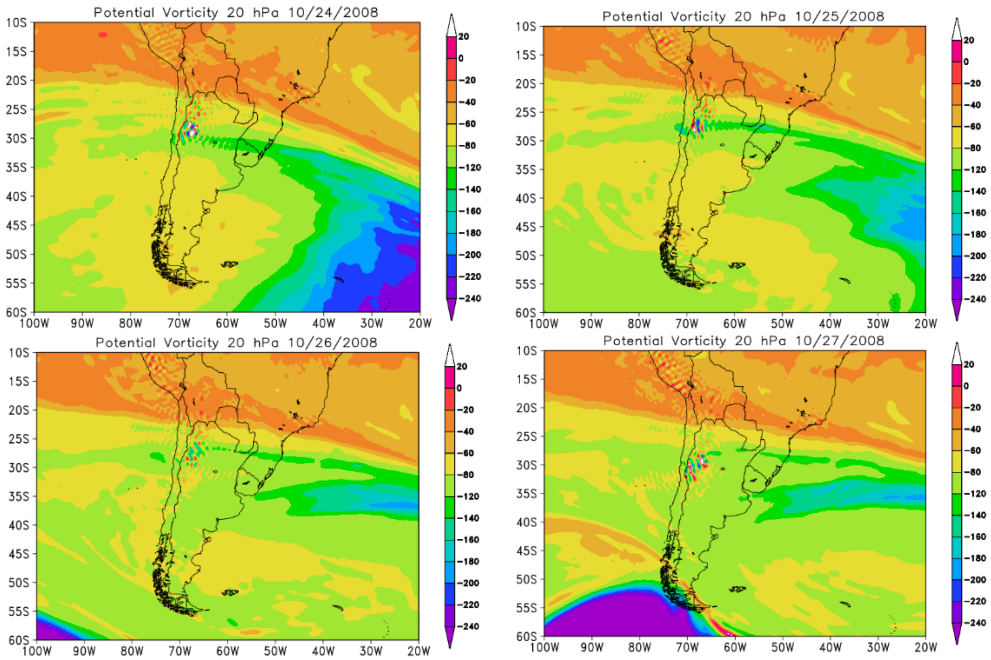

Figure A204: Retroactive trajectory by the HYSPLIT/NOAA model, and O3 content OMI satellite for South Pole, and global view.

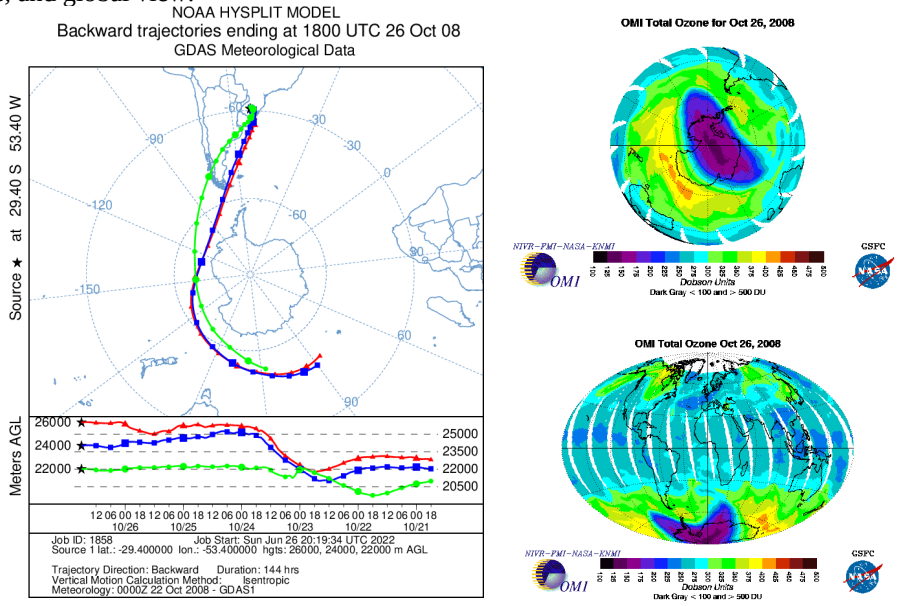

Figure A205: Vertical profile of O_3 by the SABER satellite for the October 26, 2008 (in red) and climatology for the month of October (in black).

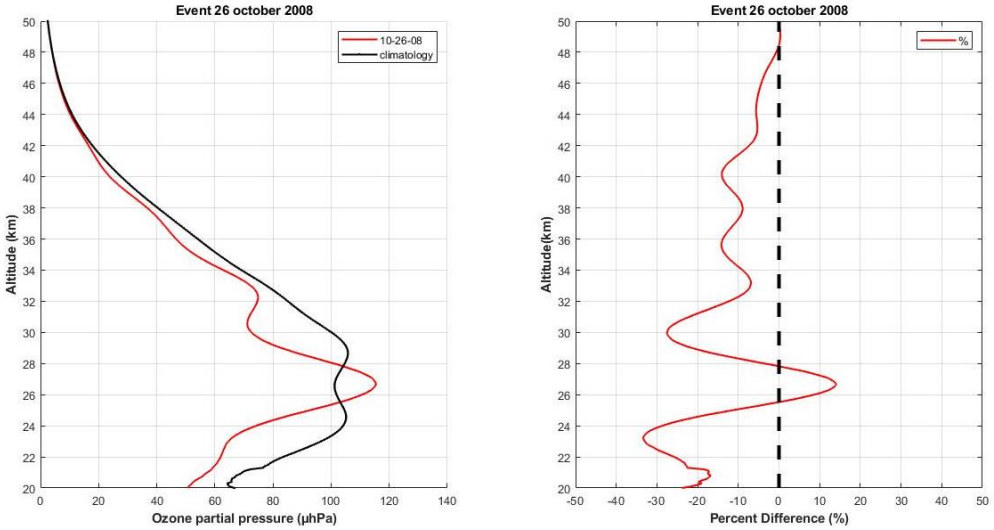

Source: The author.

Figure A206: Vertical section of the atmosphere between 1000 and 5 hPa for the days of the event in October 2008.

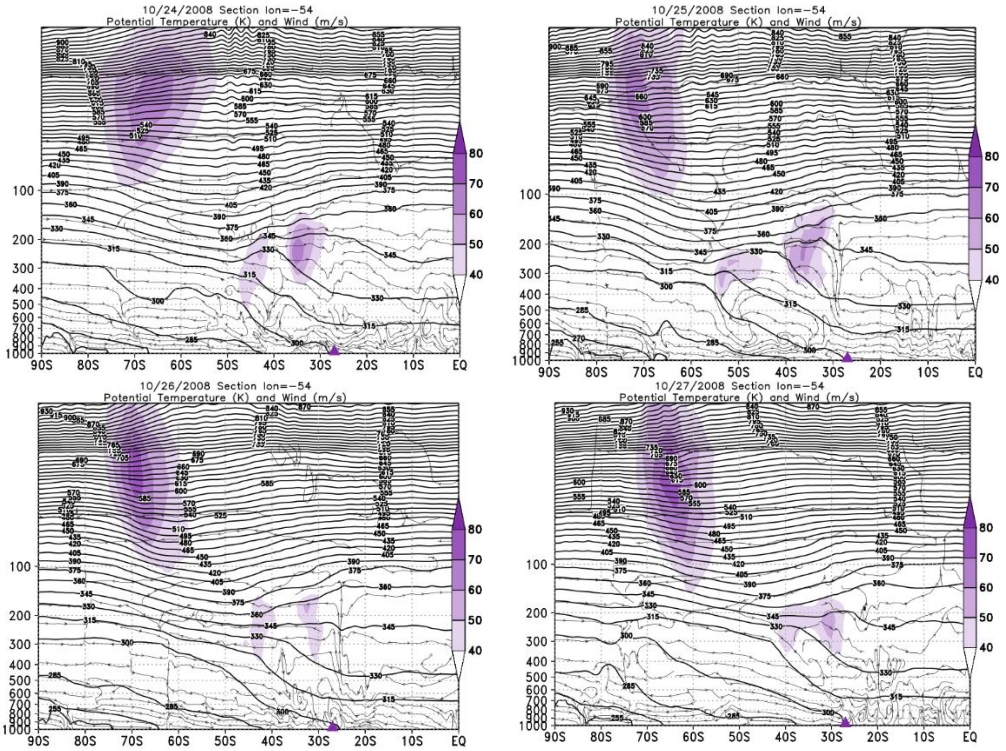

Source: The author.

11/01/2008

Figure A207: PVA fields for the 20 hPa in pressure levels, days 10/30/2008 to 11/02/2008.

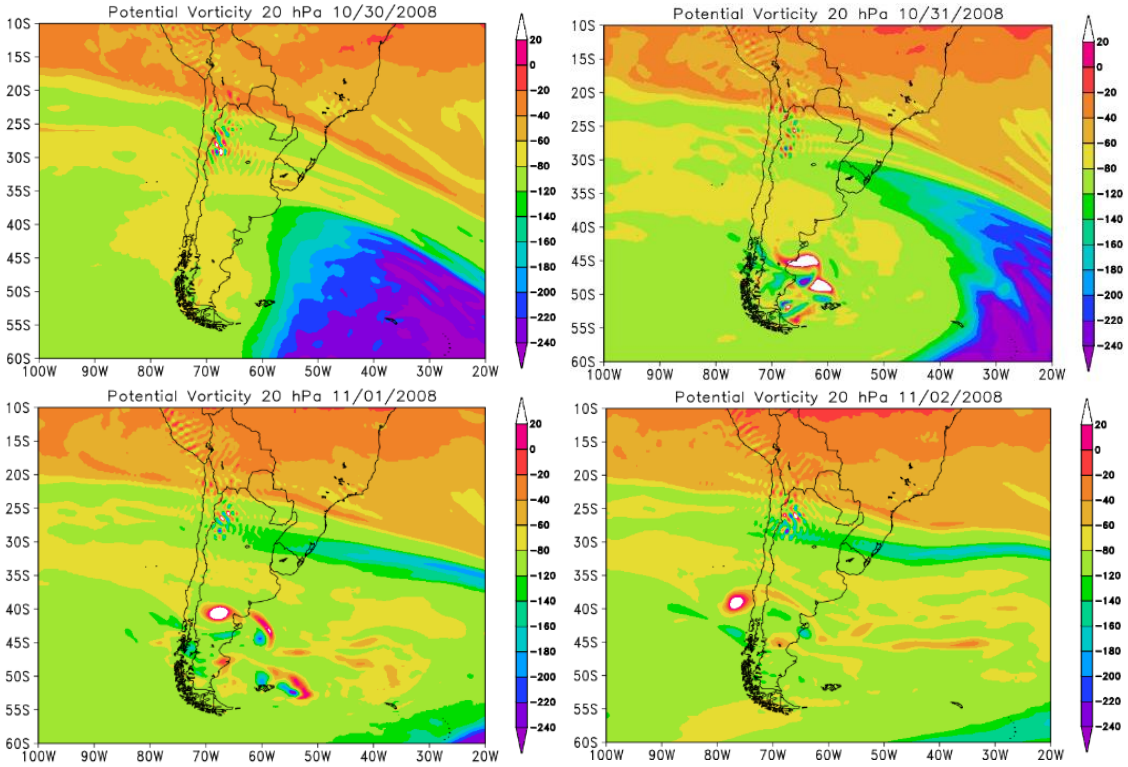

Source: The author.

Figure A208: Retroactive trajectory by the HYSPLIT/NOAA model, and O3 content OMI satellite for South Pole, and global view.

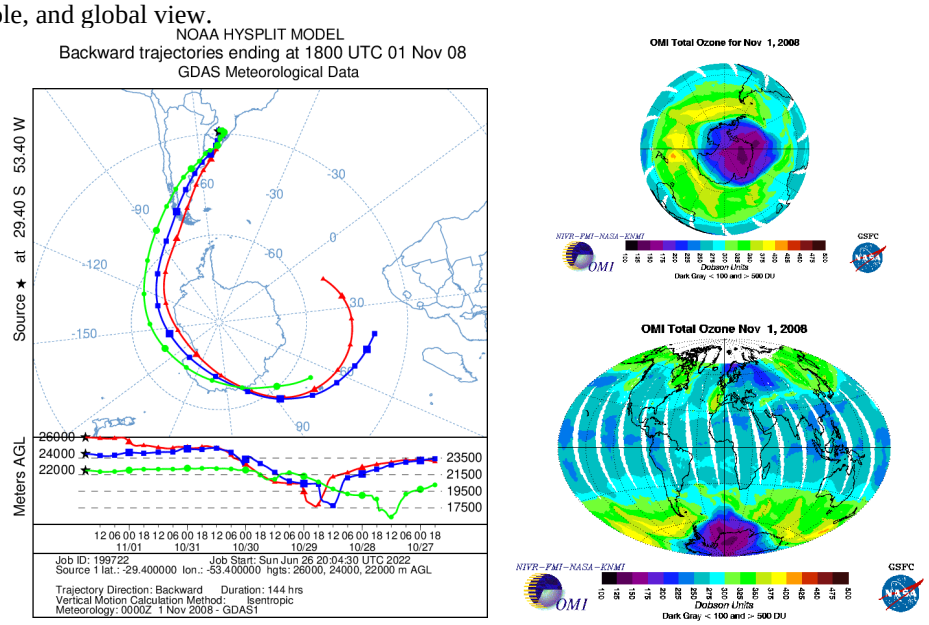

Figure A209: Vertical profile of O_3 by the SABER satellite for the November 02, 2008 (in red) and climatology for the month of October (in black).

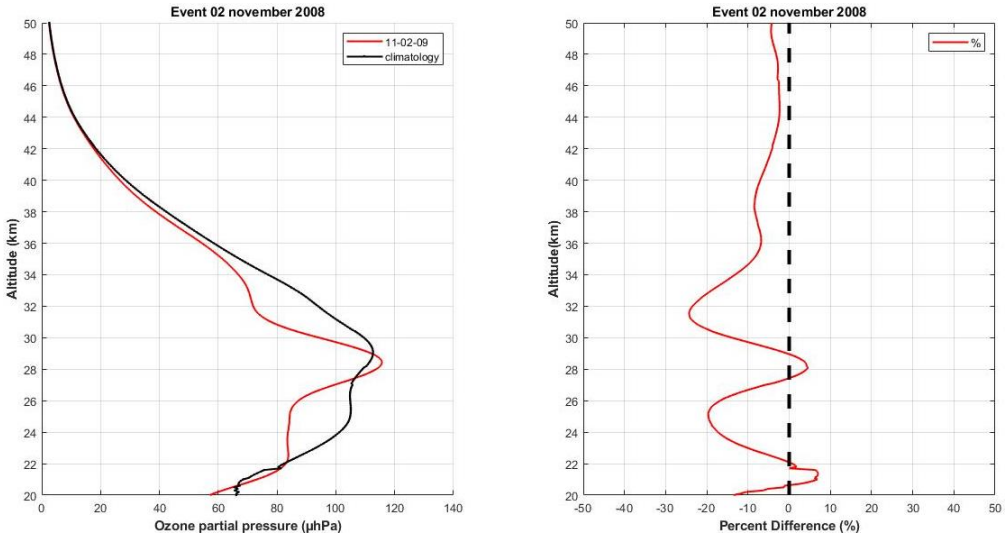

Source: The author.

Figure A210: Vertical section of the atmosphere between 1000 and 5 hPa for the days of the event in October 2016.

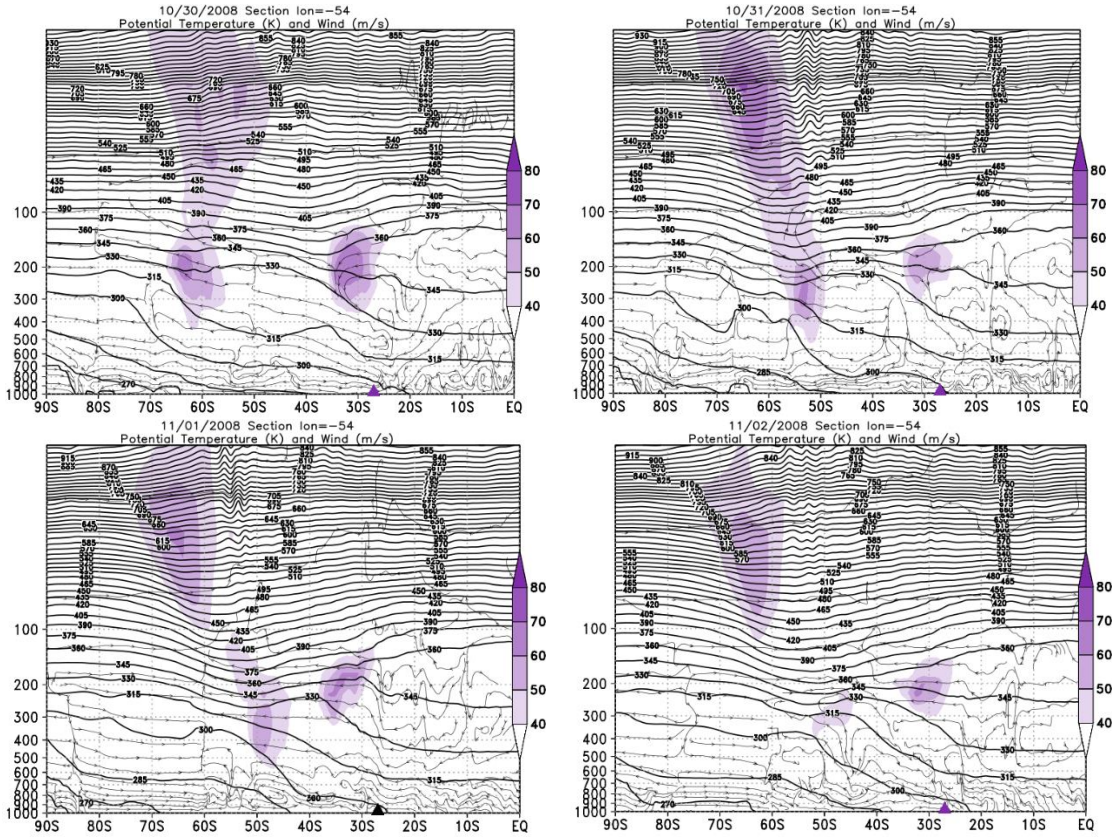

Source: The author.

09/04/2009

Figure A211: PVA fields for the 20 hPa in pressure levels, days 09/02/2009 to 09/05/2009.

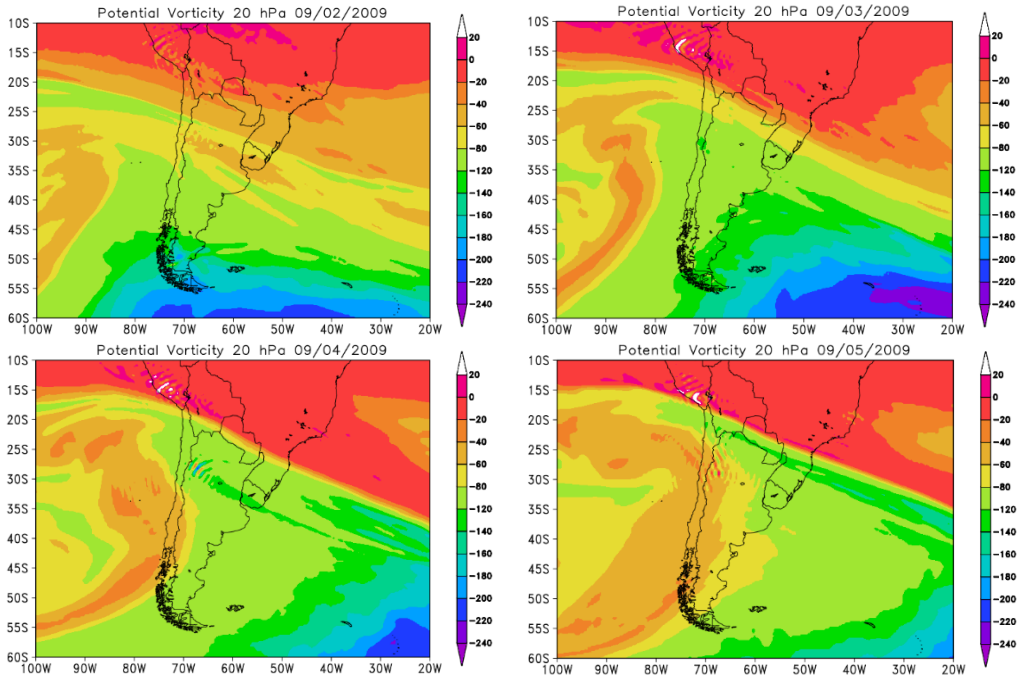

Source: The author.

Figure A212: Retroactive trajectory by the HYSPLIT/NOAA model, and O3 content OMI satellite for South Pole, and global view.

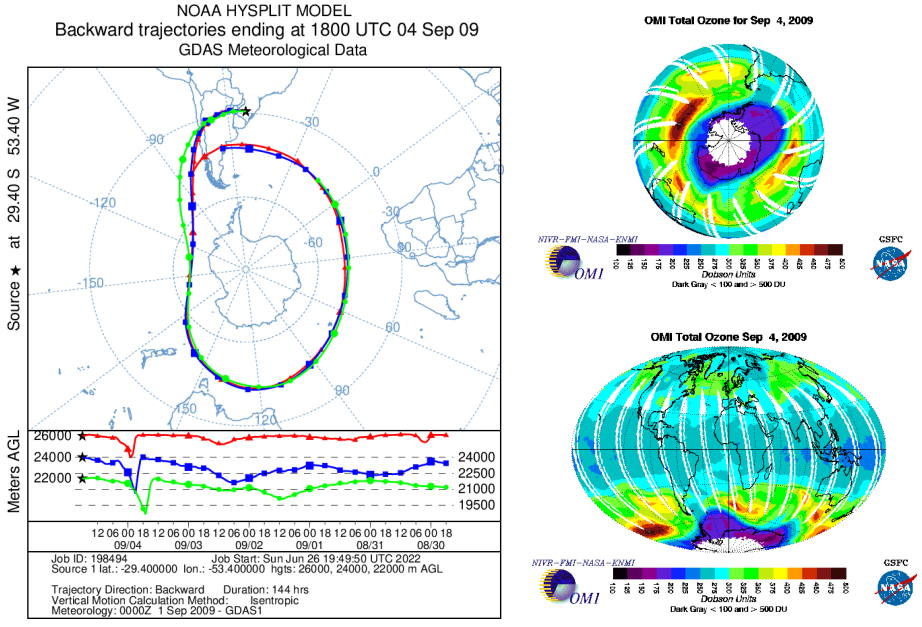

Figure A213: Vertical profile of O_3 by the SABER satellite for the September 02, 2009 (in red) and

climatology for the month of October (in black).

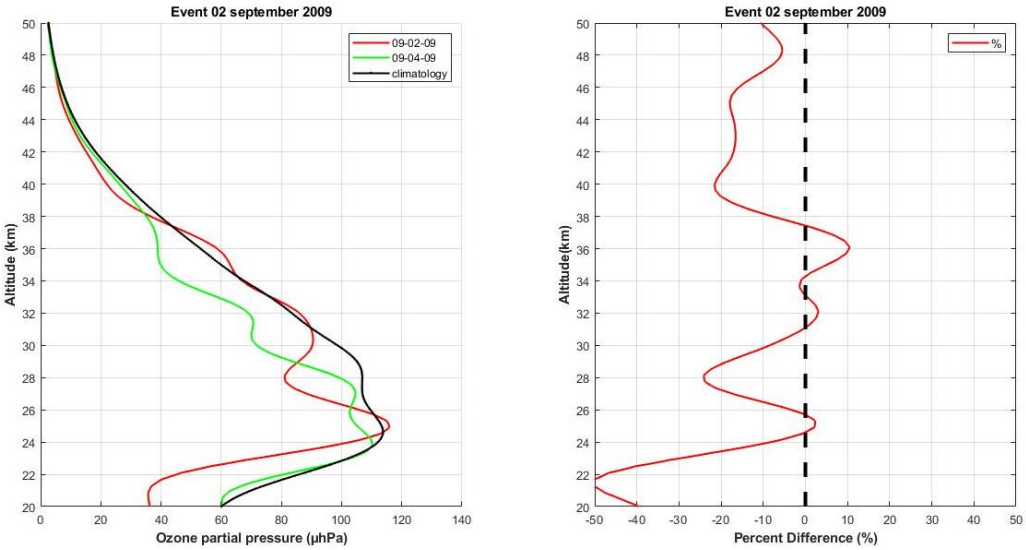

Source: The author.

Figure A214: Vertical section of the atmosphere between 1000 and 5 hPa for the days of the event in September 2009.

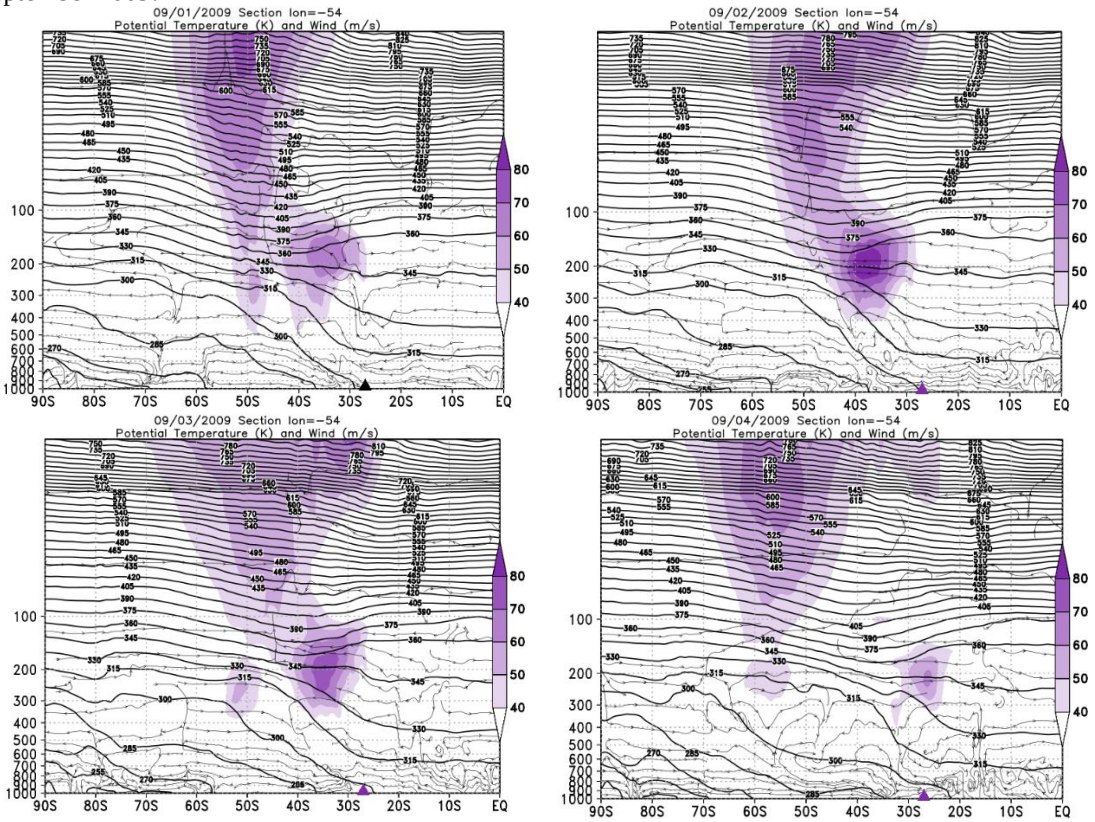

Source: The author.

09/29/2009

Figure A215: PVA fields for the 20 hPa in pressure levels, days 09/27/2009 to 09/30/2009.

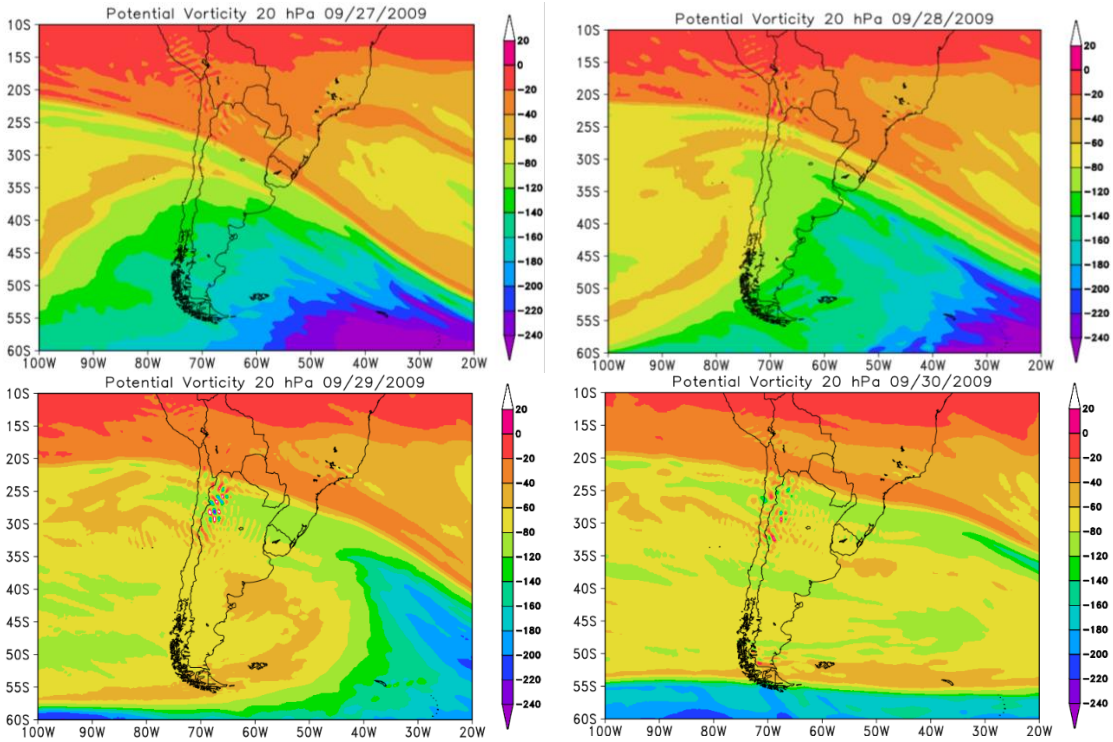

Source: The author.

Figure A216: Retroactive trajectory by the HYSPLIT/NOAA model, and O3 content OMI satellite for South Pole, and global view.

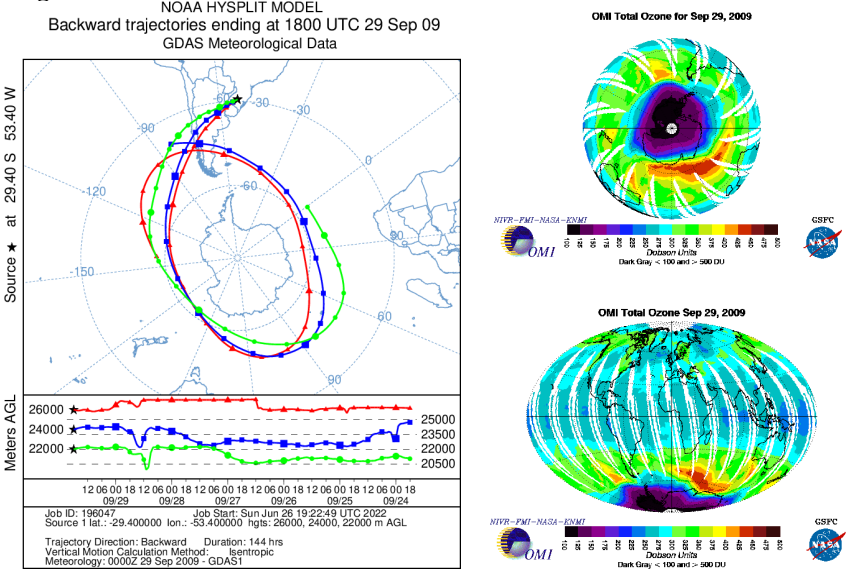

Figure A217: Vertical profile of O_3 by the SABER satellite for the September 29, 2009 (in red) and climatology for the month of October (in black).

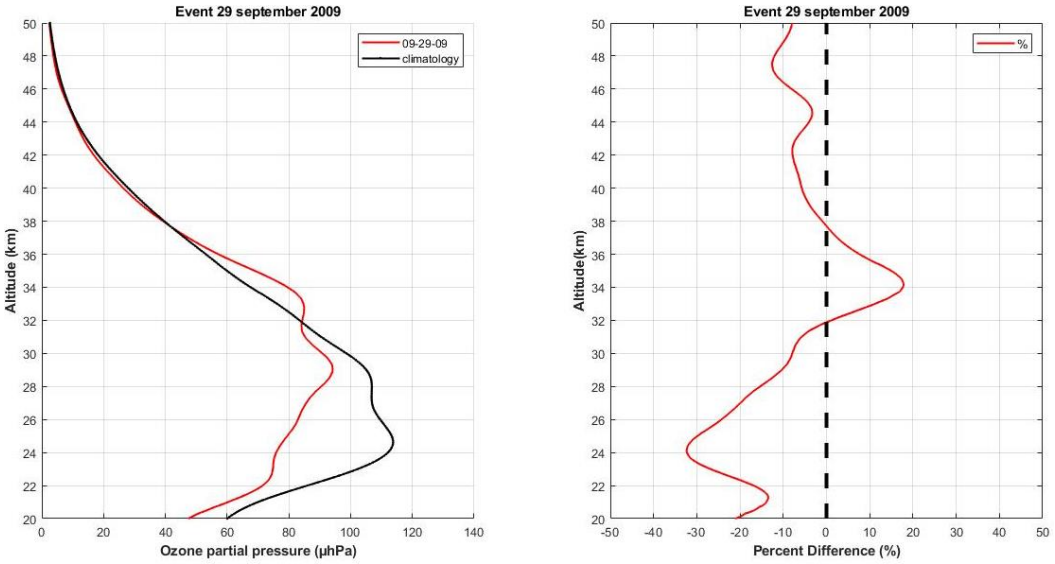

Source: The author.

Figure A218: Vertical section of the atmosphere between 1000 and 5 hPa for the days of the event in September 2009.

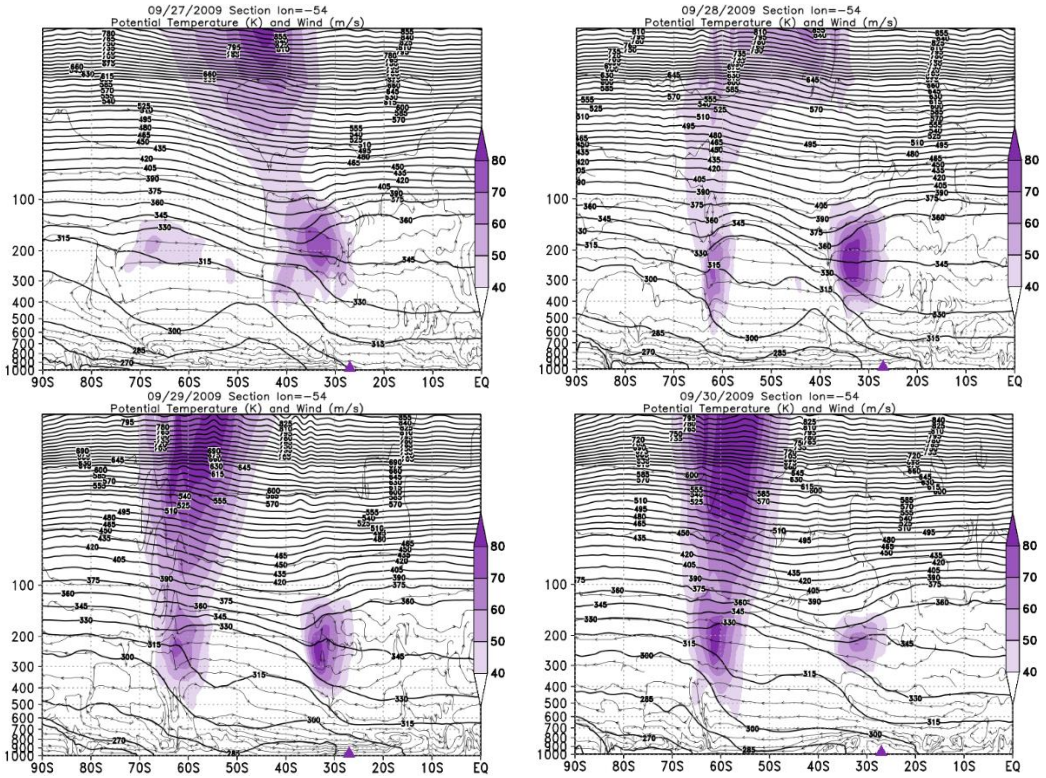

Source: The author.

09/09/2010

Figure A219: PVA fields for the 20 hPa in pressure levels, days 09/07/2010 to 09/10/2010.

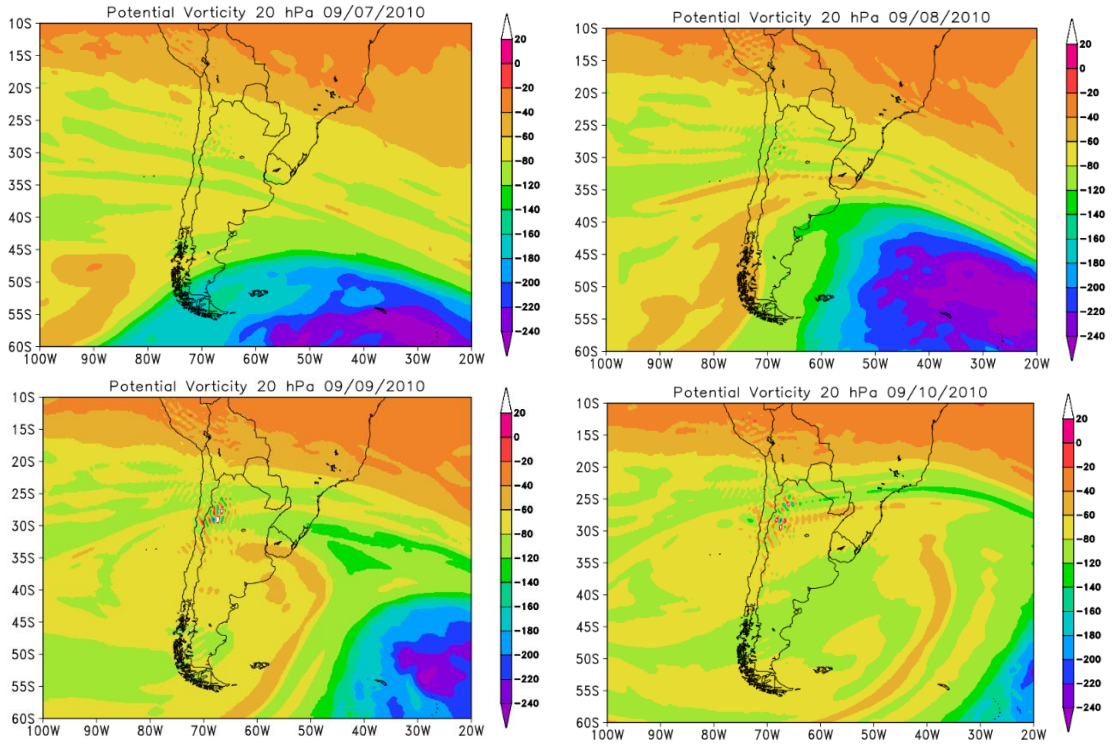

Figure A220: Retroactive trajectory by the HYSPLIT/NOAA model, and O3 content OMI satellite for South Pole, and global view.

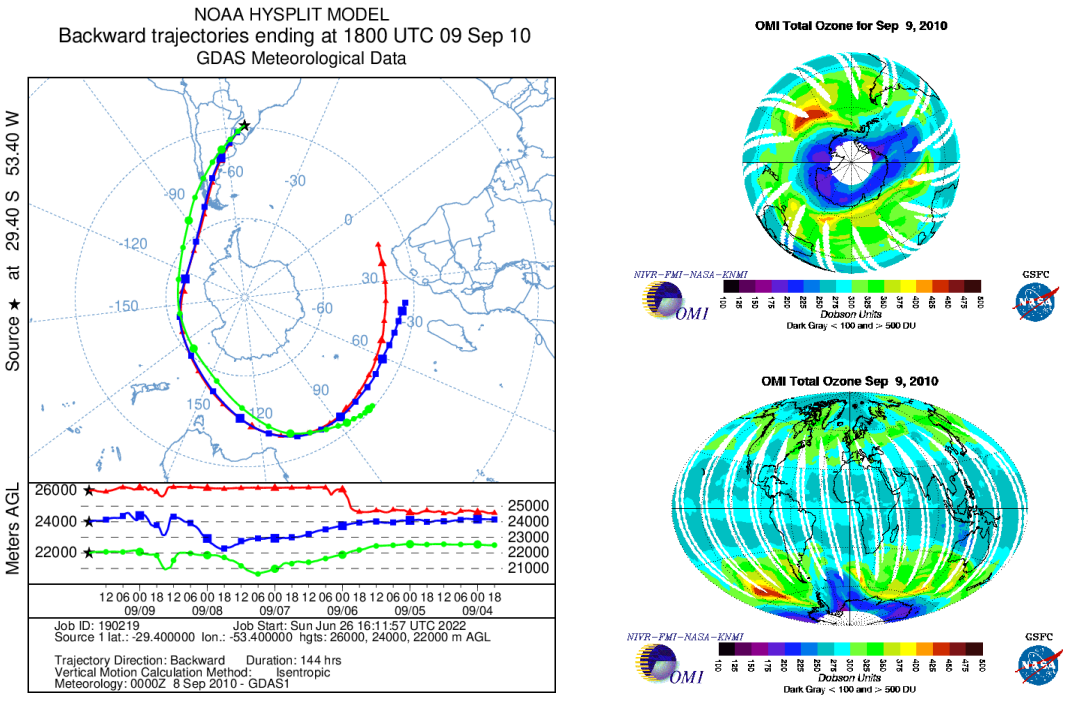

Figure A221: Vertical profile of O_3 by the SABER satellite for the September 08, 2010 (in red) and climatology for the month of October (in black).

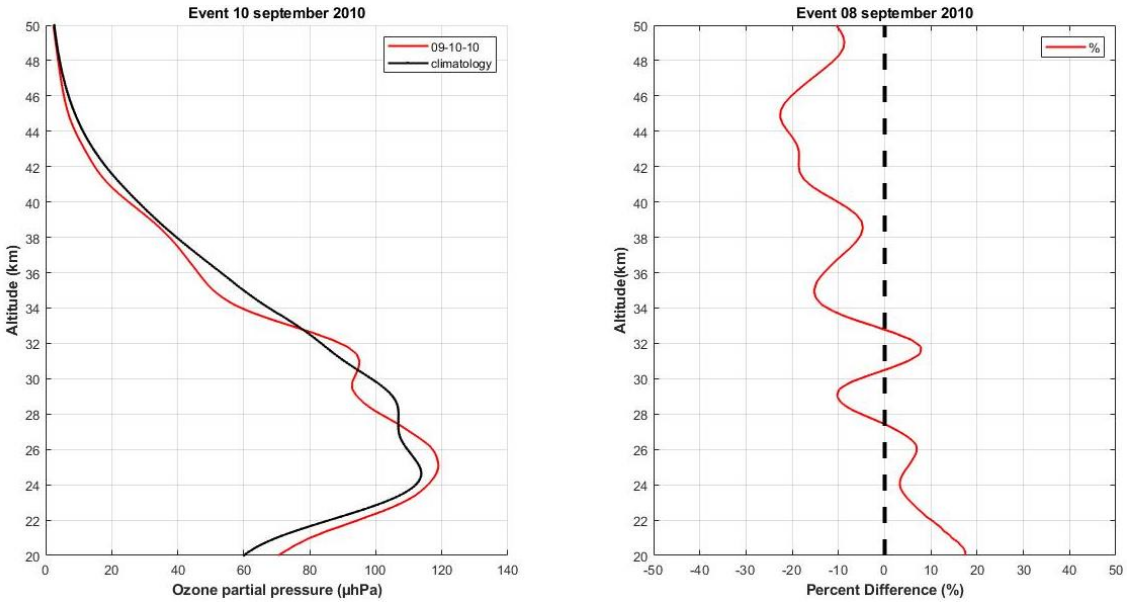

Source: The author.

Figure A222: Vertical section of the atmosphere between 1000 and 5 hPa for the days of the event in September 2010.

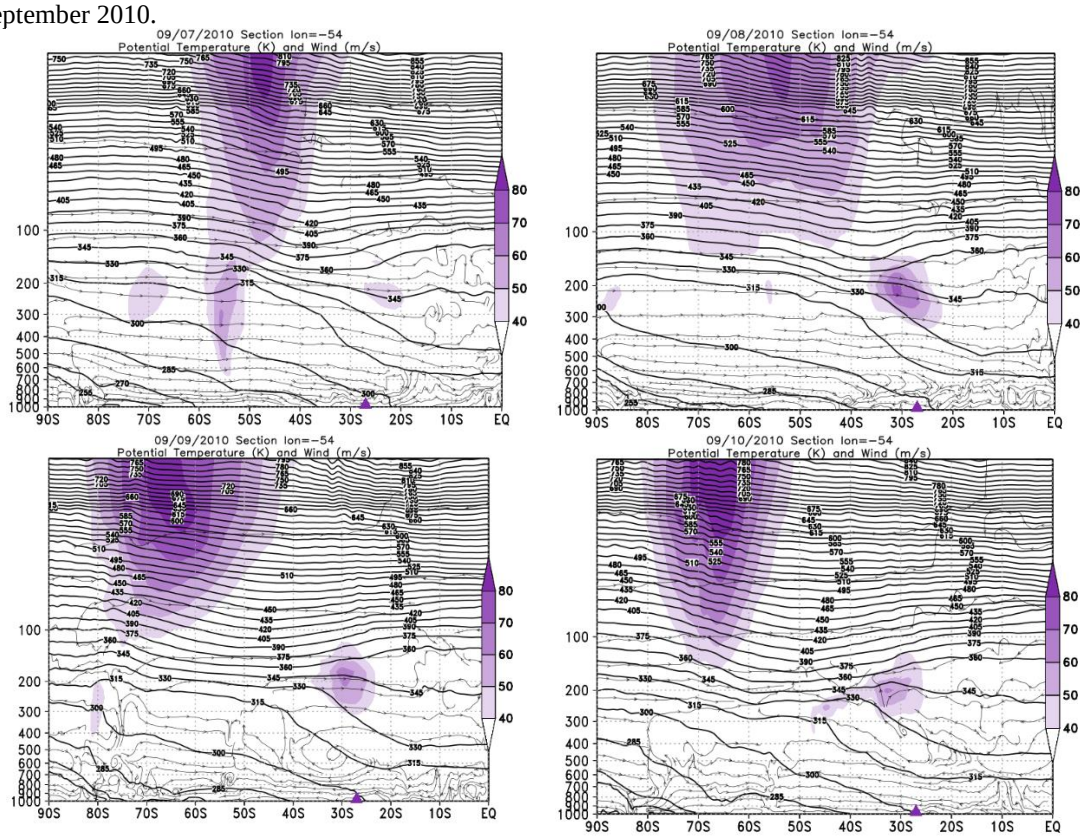

Source: The author.

10/13/2010

Figure A224: PVA fields for the 20 hPa in pressure levels, days 10/11/2010 to 10/14/2010.

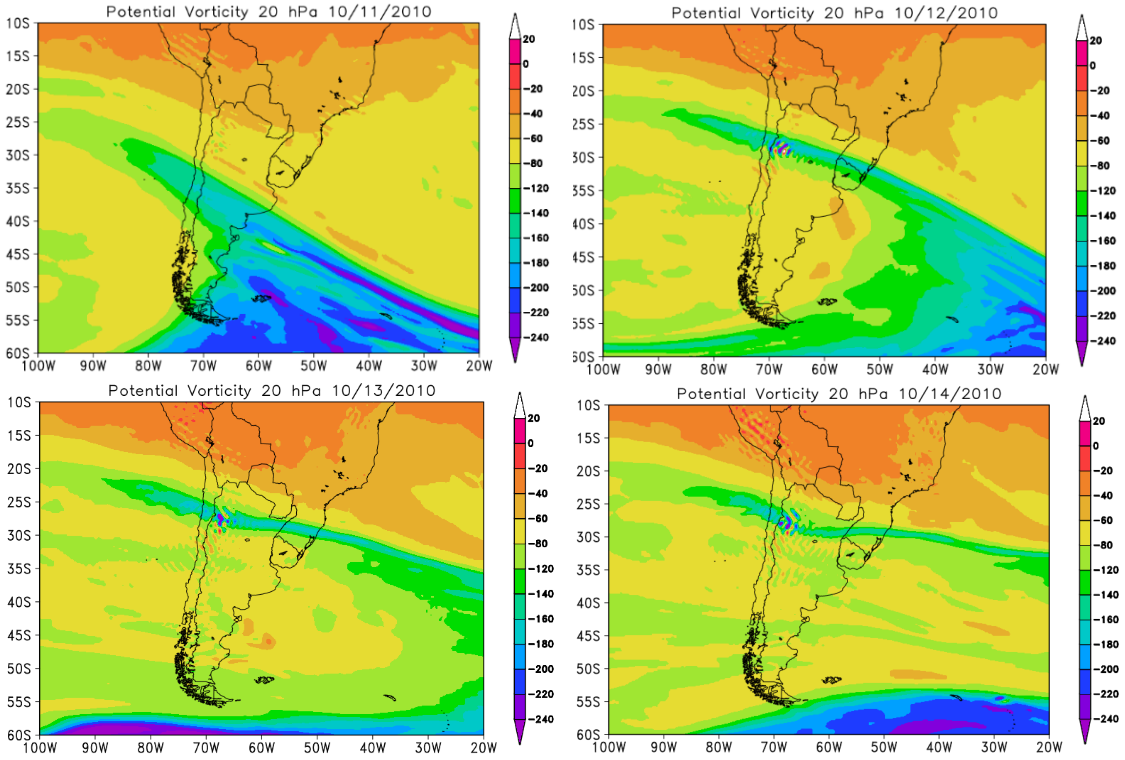

Figure A225: Retroactive trajectory by the HYSPLIT/NOAA model, and O3 content OMI satellite for South Pole, and global view.

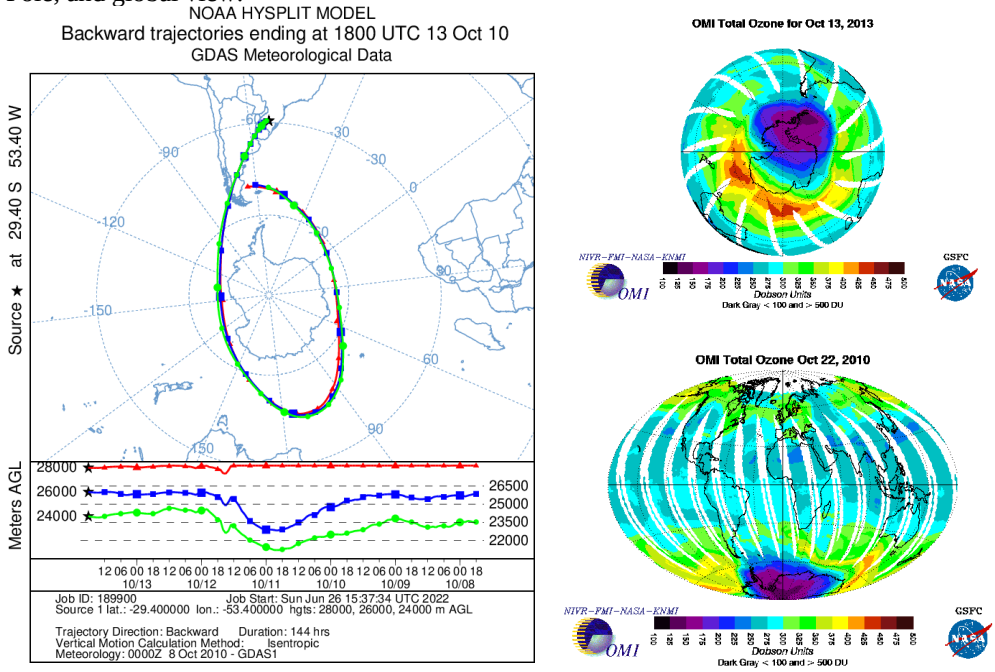

Figure A226: Vertical profile of O_3 by the SABER satellite for the October 13, 2010 (in red) and climatology for the month of October (in black).

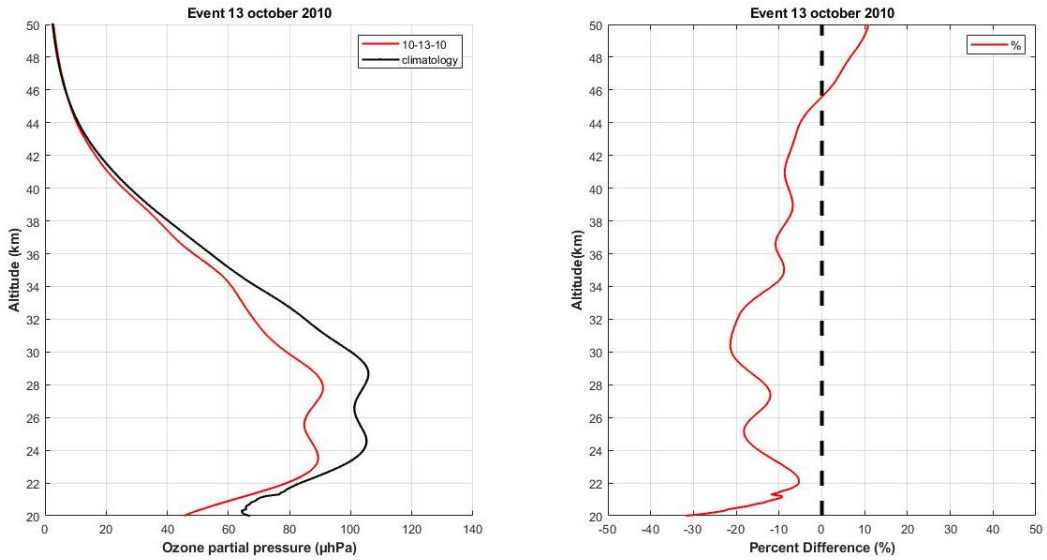

Source: The author.

Figure A227: Vertical section of the atmosphere between 1000 and 5 hPa for the days of the event in October 2010.

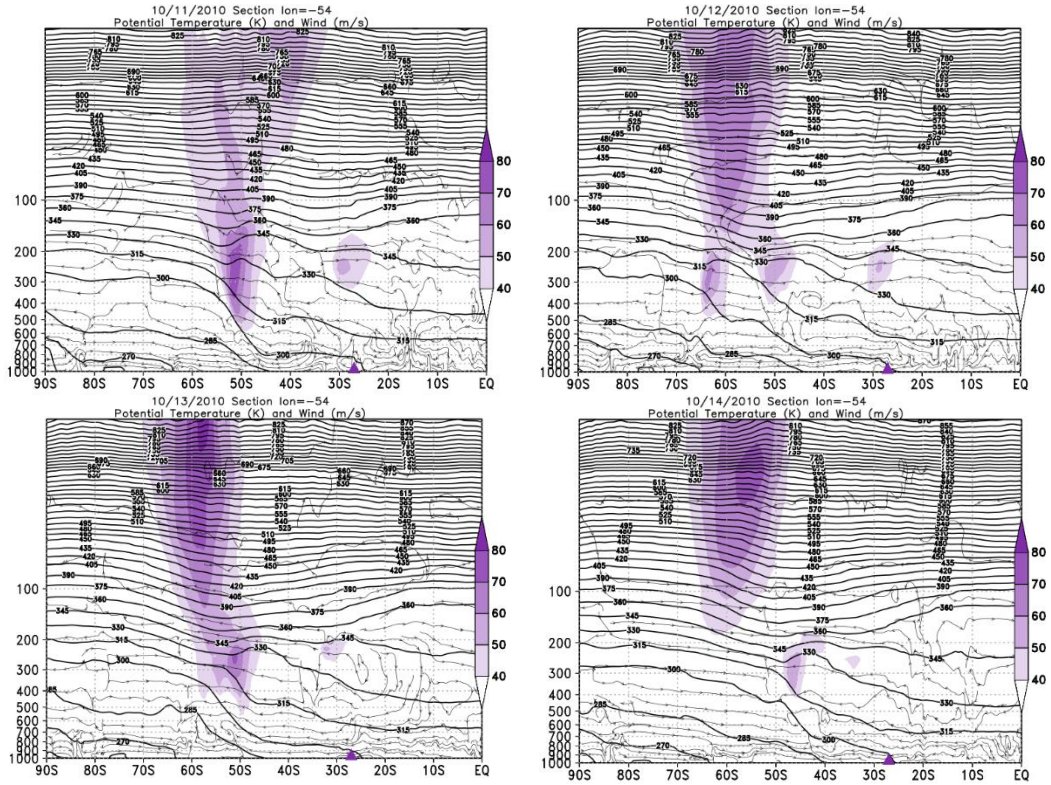

Source: The author.

10/22/2010

Figure A228: PVA fields for the 20 hPa in pressure levels, days 10/20/2010 to 10/23/2010.

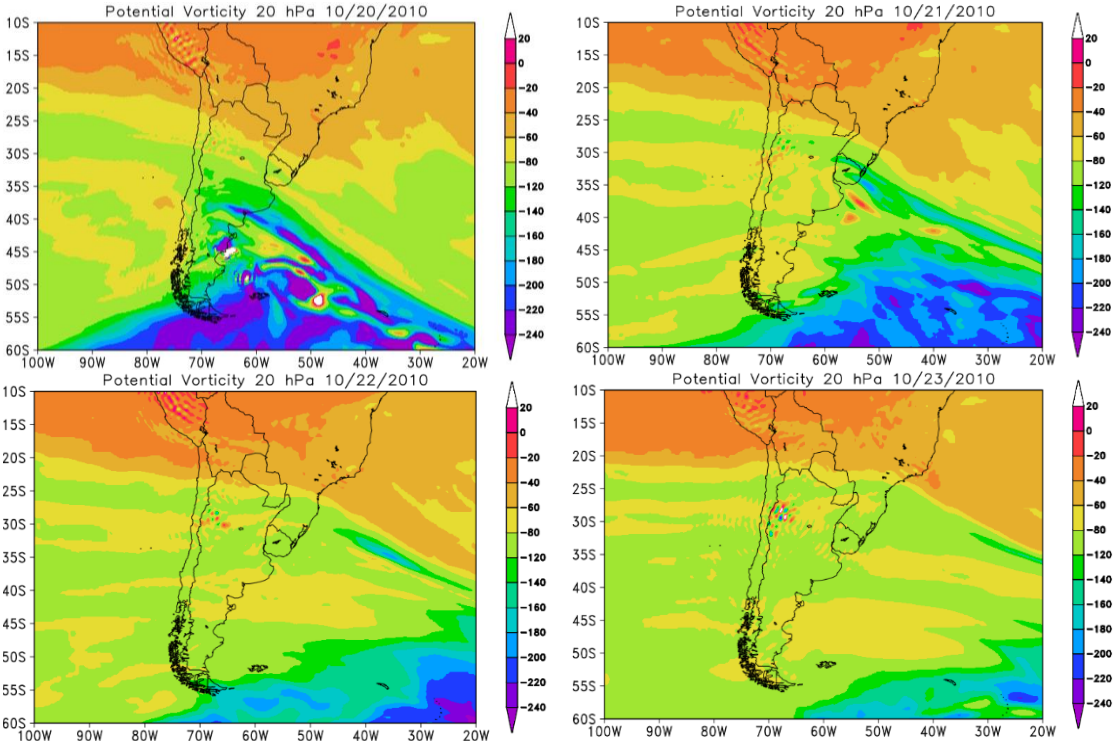

Source: The author.

Figure A229: Retroactive trajectory by the HYSPLIT/NOAA model, and O3 content OMI satellite for South Pole, and global view.

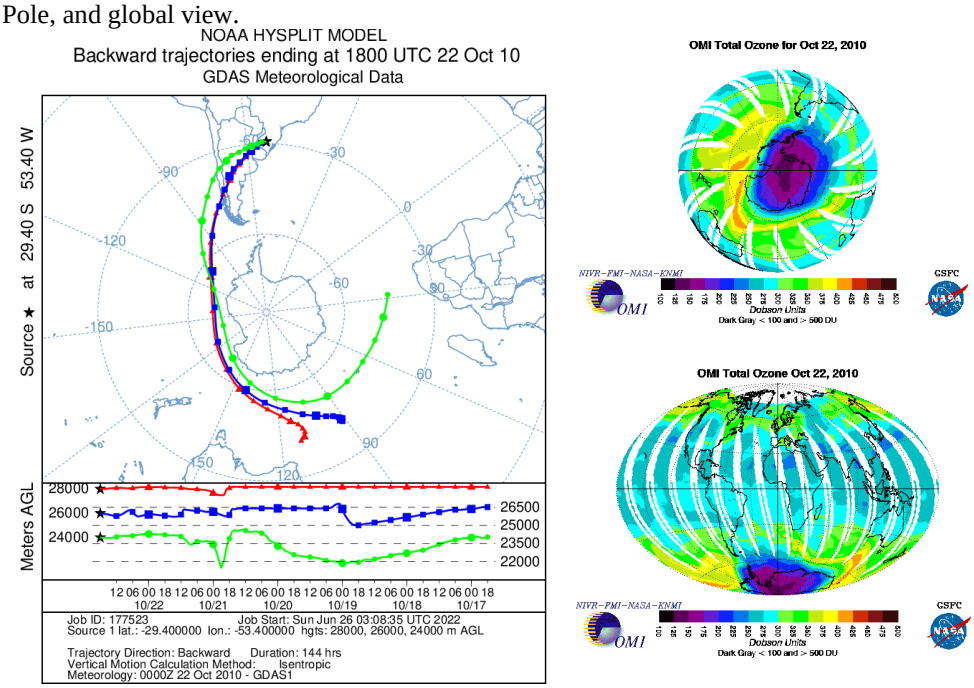

Figure A230: Vertical profile of O_3 by the SABER satellite for the October 22, 2010 (in red) and climatology for the month of October (in black).

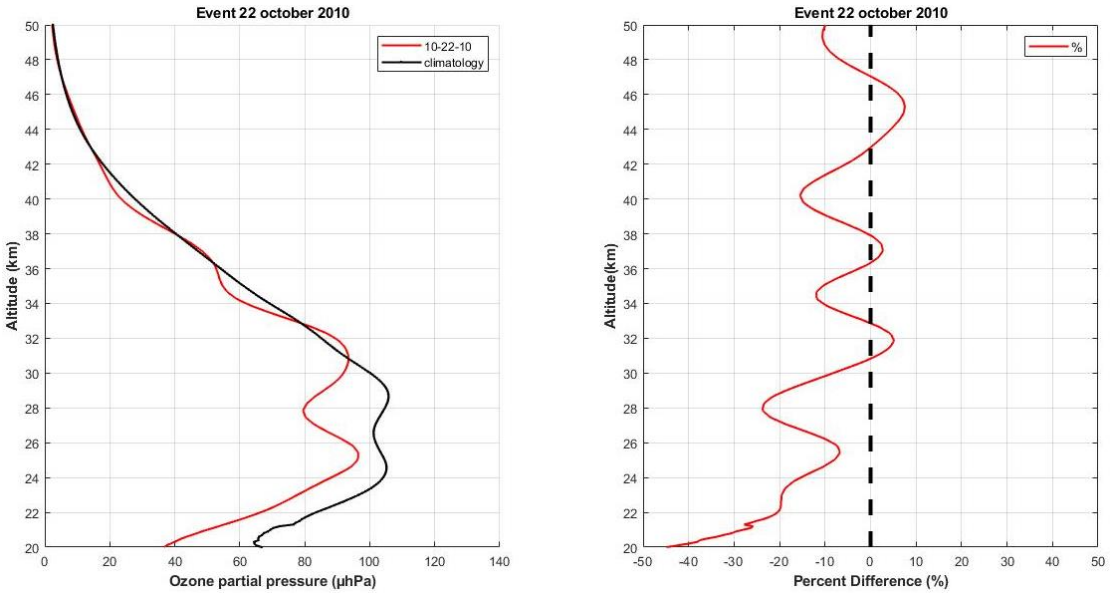

Source: The author.

Figure A231: Vertical section of the atmosphere between 1000 and 5 hPa for the days of the event in October 2010.

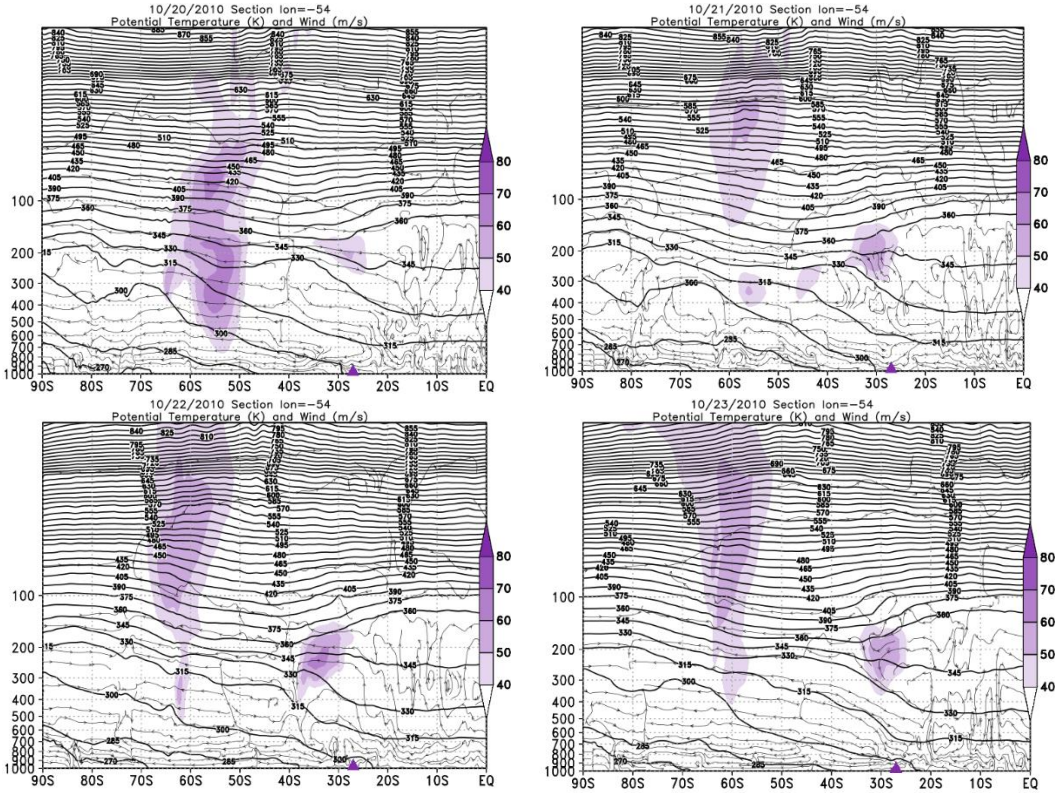

Source: The author.

09/05/2011

Figure A232: PVA fields for the 20 hPa in pressure levels, days 09/03/2011 to 09/06/2011.

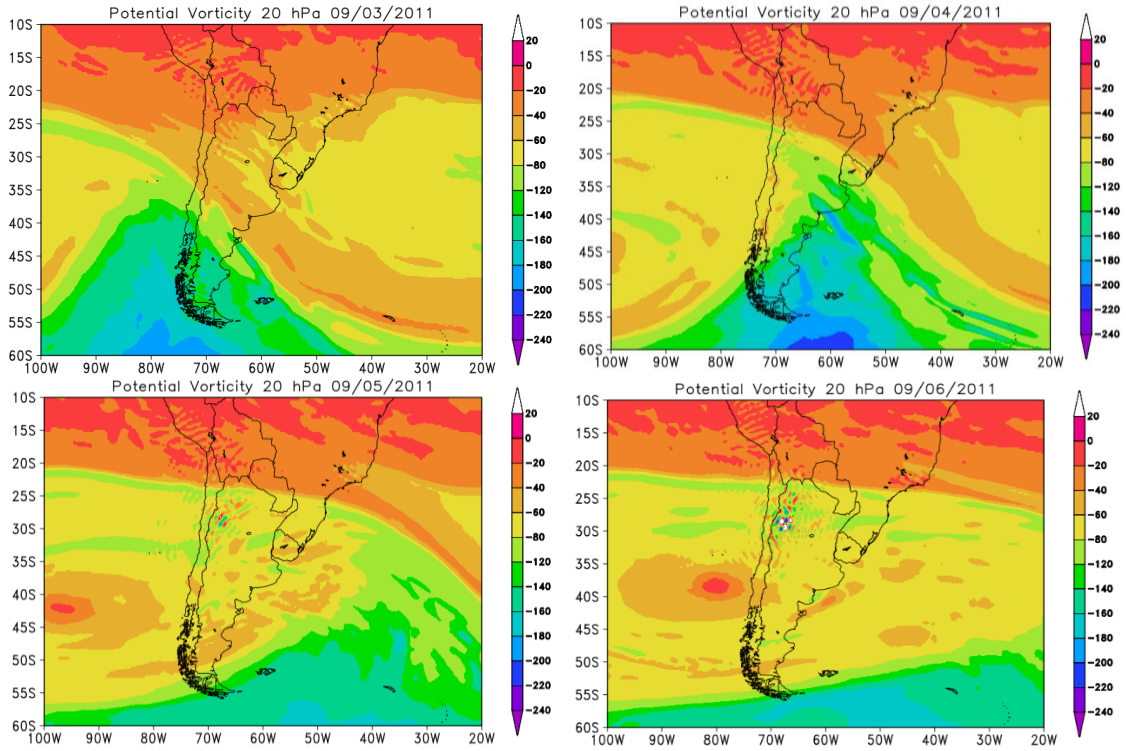

Source: The author.

Figure A233: Retroactive trajectory by the HYSPLIT/NOAA model, and O3 content OMI satellite for South Pole, and global view.

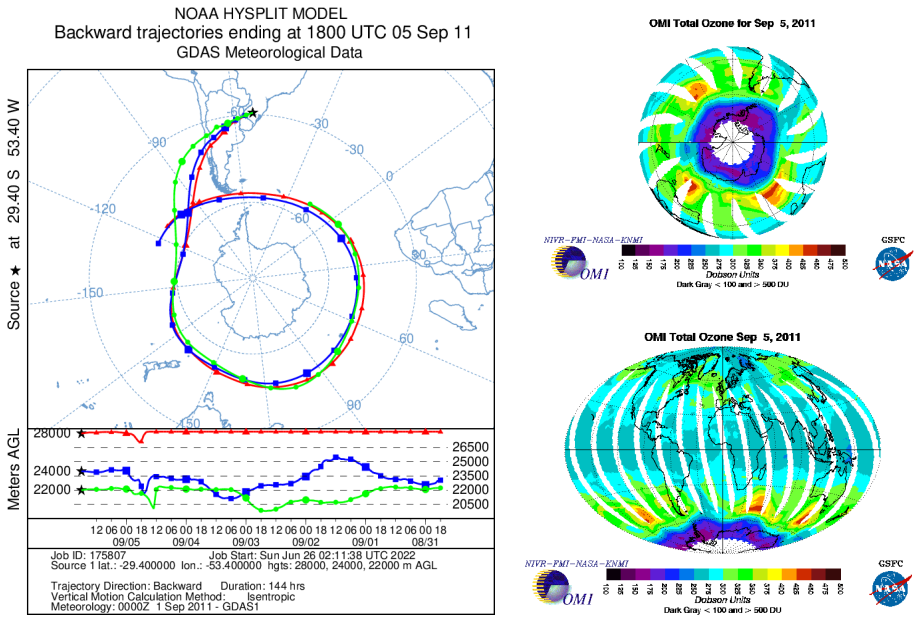

Figure A234: Vertical profile of O_3 by the SABER satellite for the September 05, 2011 (in red) and climatology for the month of October (in black).

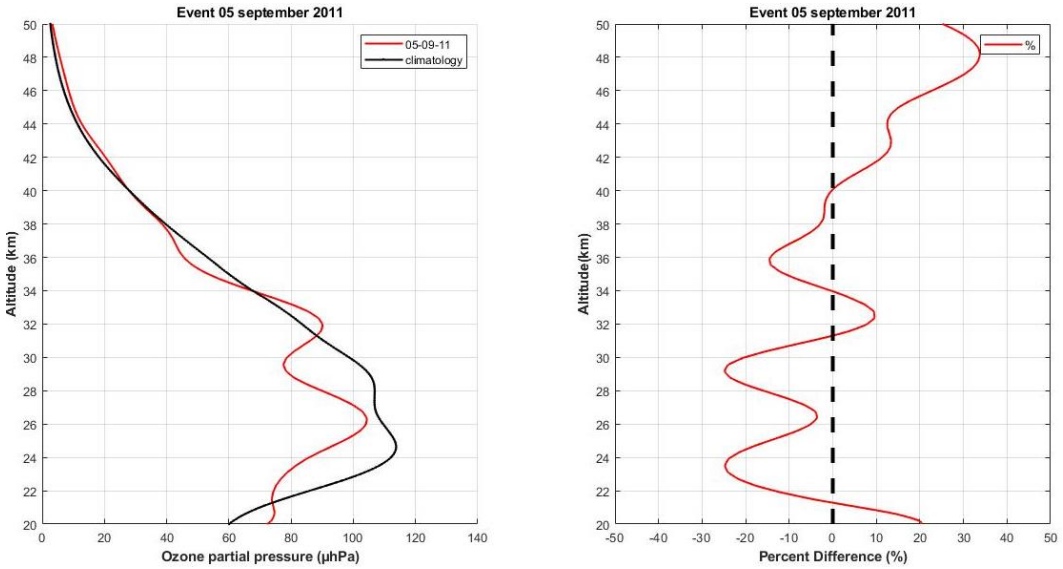

Source: The author.

Figure A235: Vertical section of the atmosphere between 1000 and 5 hPa for the days of the event in September 2011.

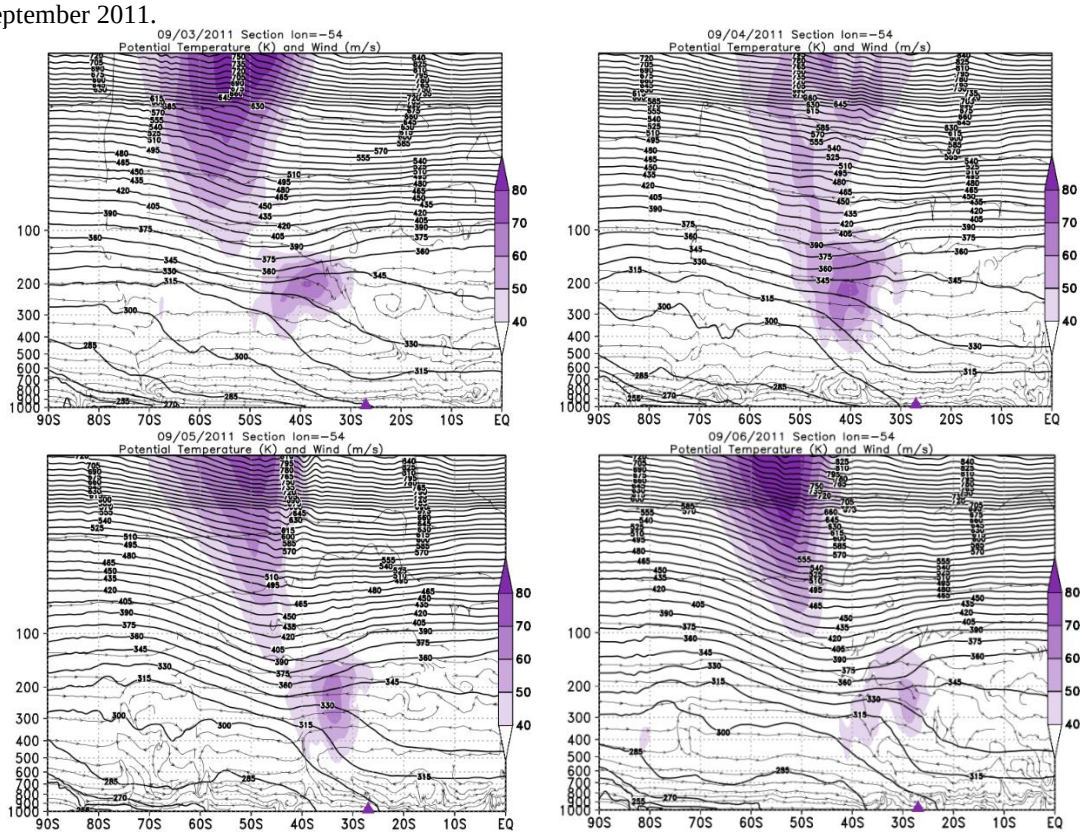

Source: The author.

09/14/2012

Figure A236: PVA fields for the 20 hPa in pressure levels, days 09/12/2012 to 09/15/2012.

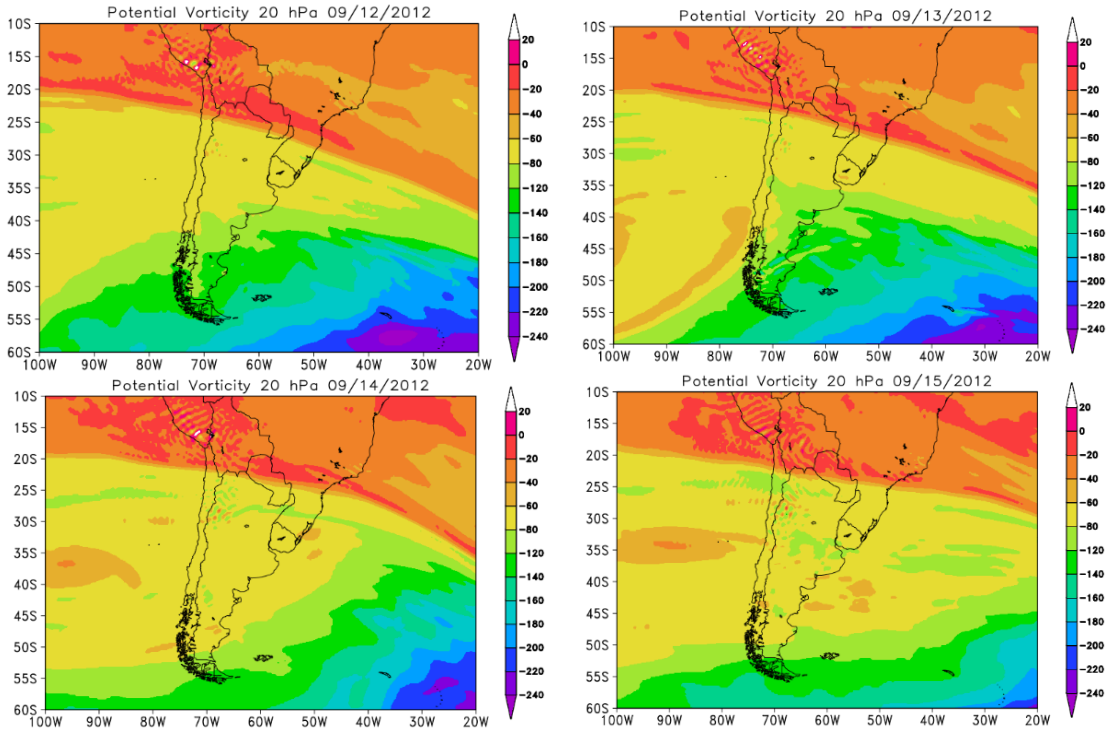

Figure A237: Retroactive trajectory by the HYSPLIT/NOAA model, and O3 content OMI satellite for South Pole, and global view.

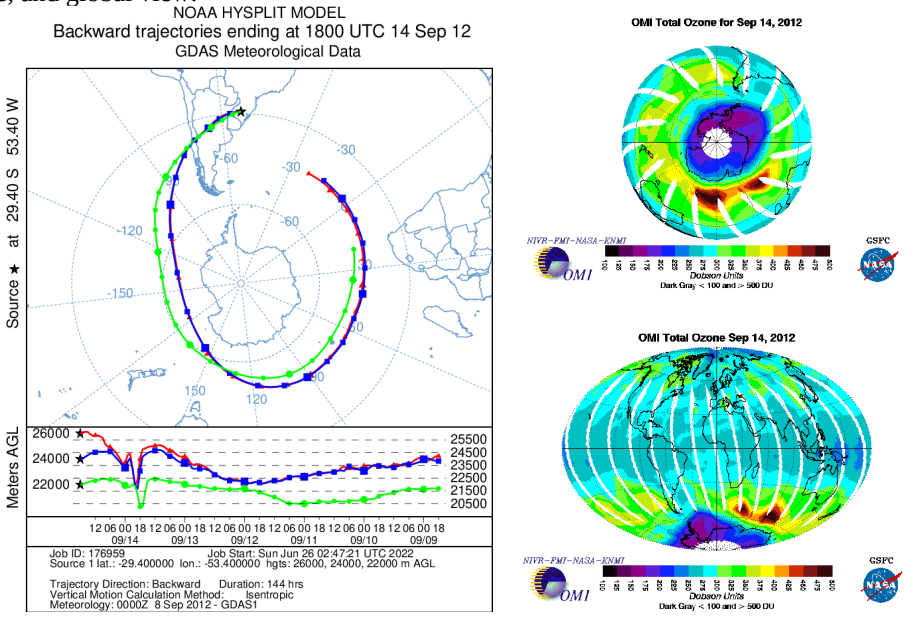

Figure A238: Vertical profile of O_3 by the SABER satellite for the September 14, 2012 (in red) and climatology for the month of October (in black).

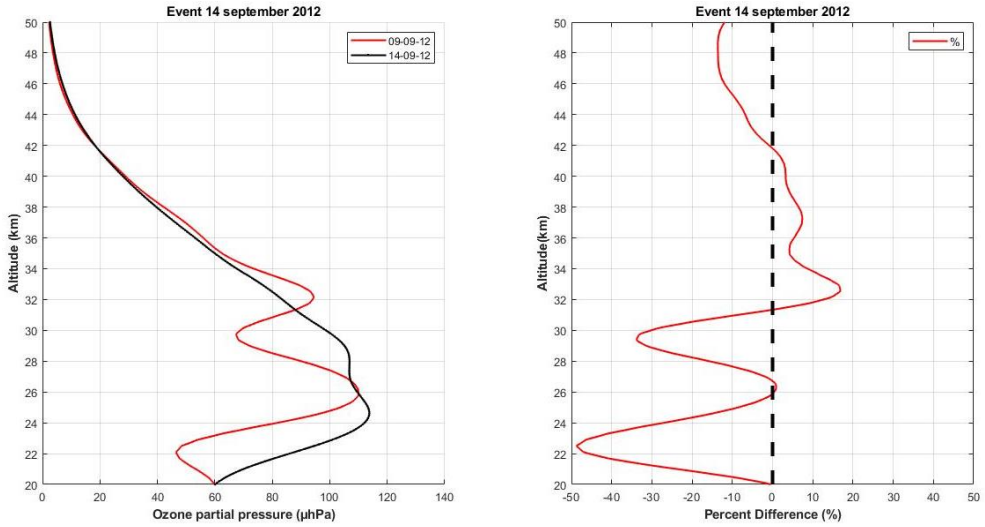

Source: The author.

Figure A239: Vertical section of the atmosphere between 1000 and 5 hPa for the days of the event in September 2012.

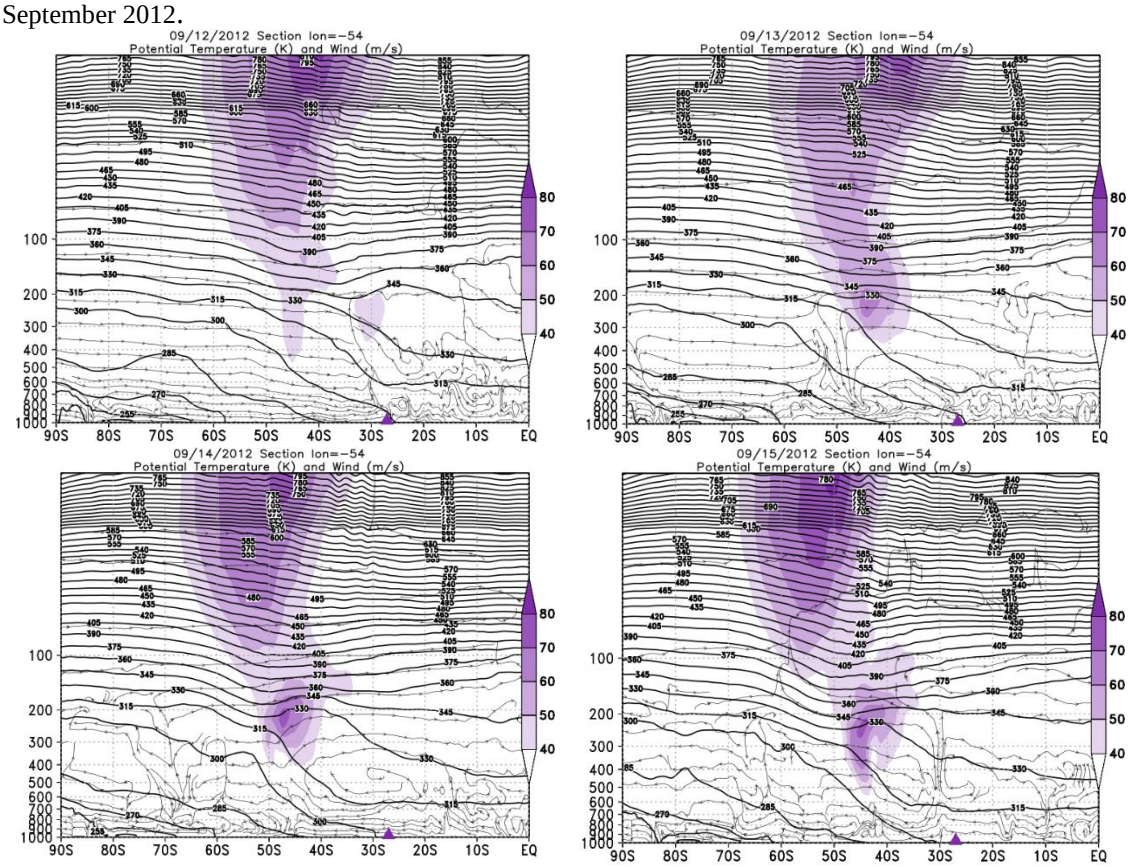

Source: The author.

10/14/2012

Figure A240: PVA fields for the 20 hPa in pressure levels, days 10/12/2012 to 10/15/2012.

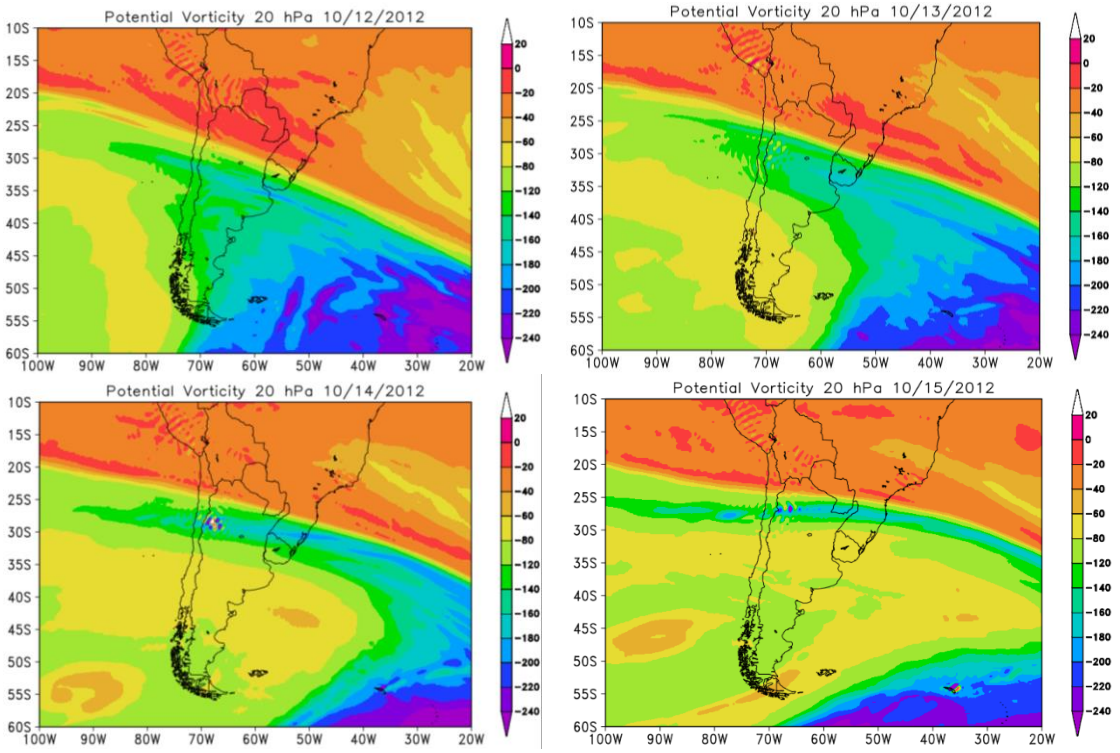

Figure A241: Retroactive trajectory by the HYSPLIT/NOAA model, and O3 content OMI satellite for South Pole, and global view.

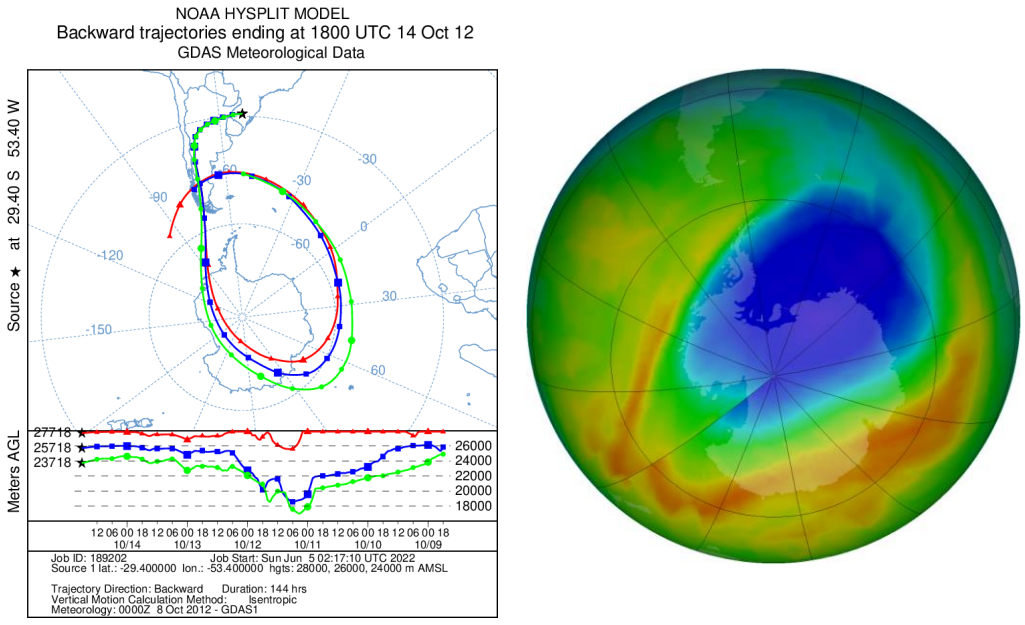

Figure A242: Vertical profile of O_3 by the SABER satellite for the October 15, 2012 (in red) and climatology for the month of October (in black).

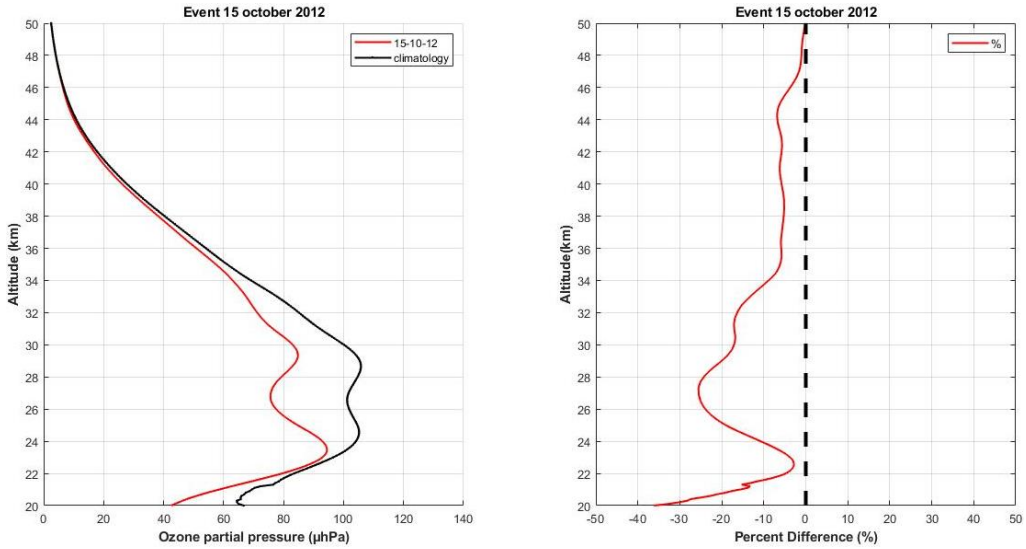

Source: The author.

Figure A243: Vertical section of the atmosphere between 1000 and 5 hPa for the days of the event in October 2012

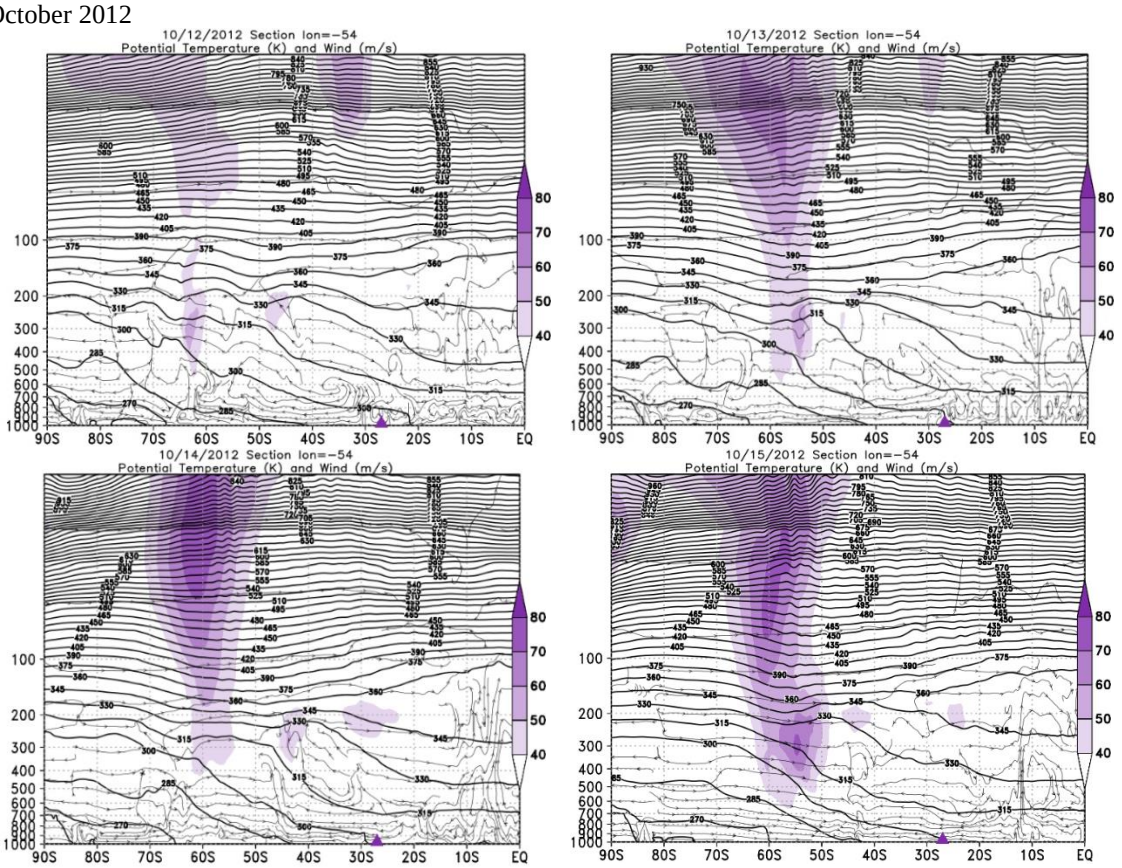

Source: The author.

10/23/2013

Figure A244: PVA fields for the 20 hPa in pressure levels, days 10/21/2013 to 10/24/2013.

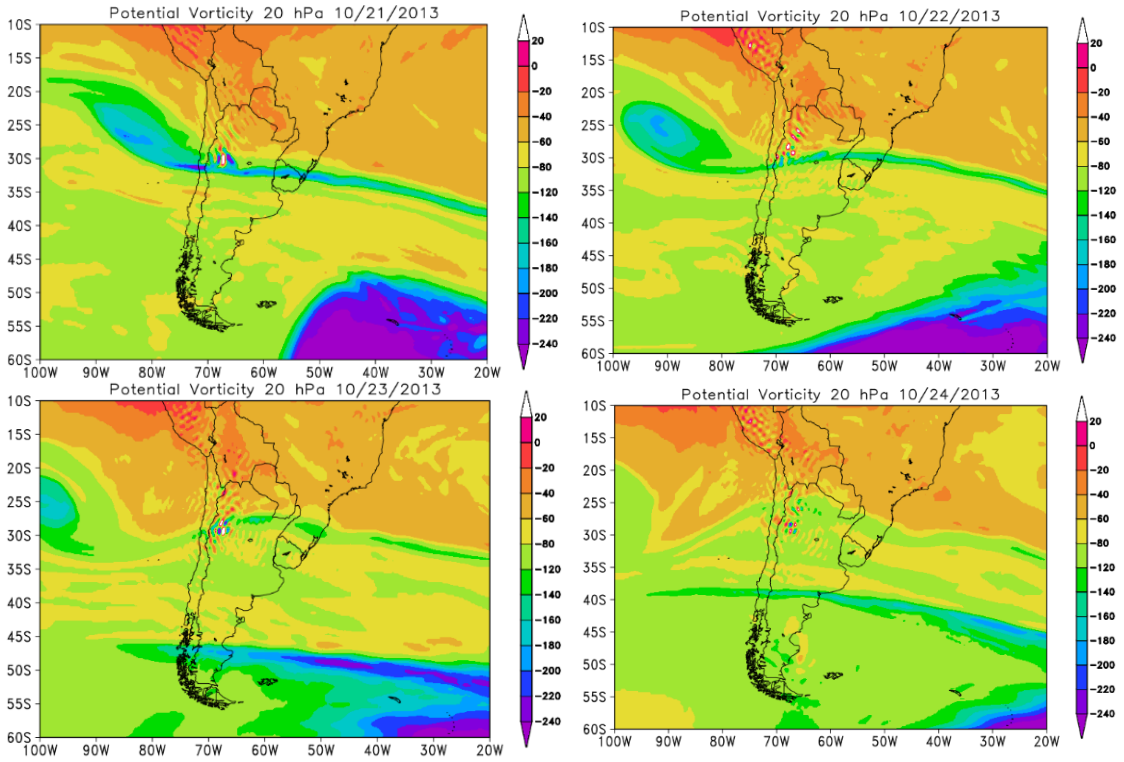

Figure A245: Retroactive trajectory by the HYSPLIT/NOAA model, and O3 content OMI satellite for South Pole, and global view.

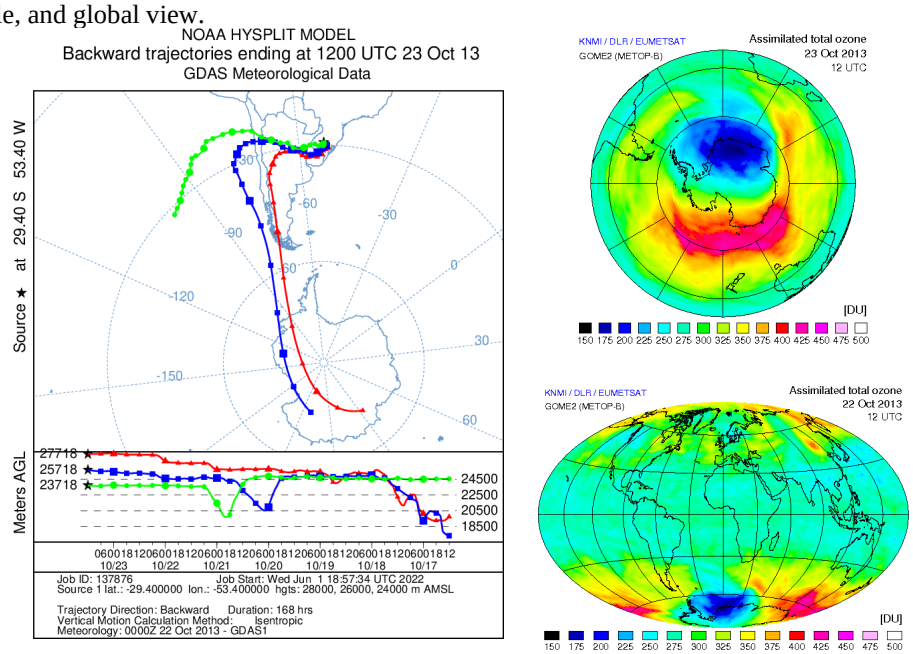

Figure A246: Vertical profile of O_3 by the SABER satellite for the October 23, 2013 (in red) and

climatology for the month of October (in black).

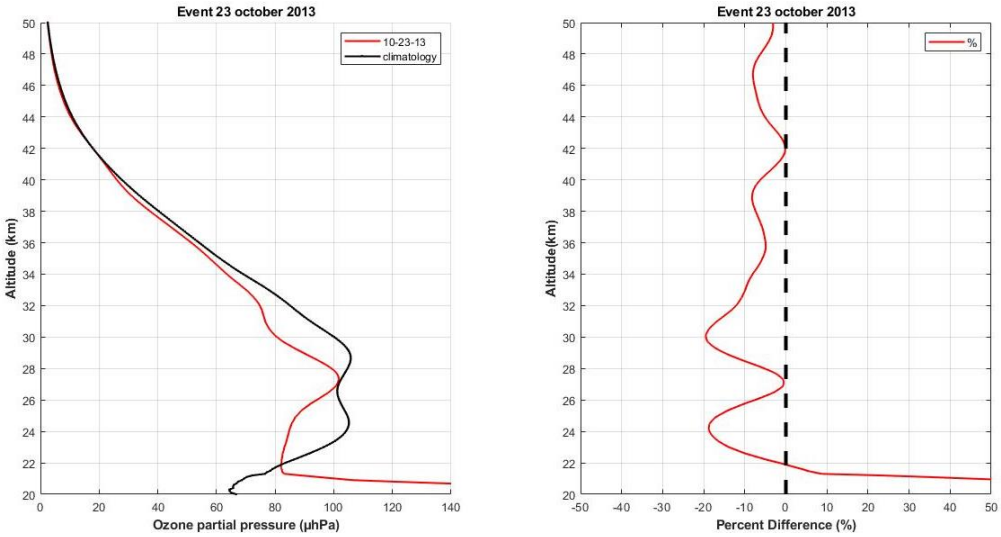

Source: The author.

Figure A247: Vertical section of the atmosphere between 1000 and 5 hPa for the days of the event in October 2013.

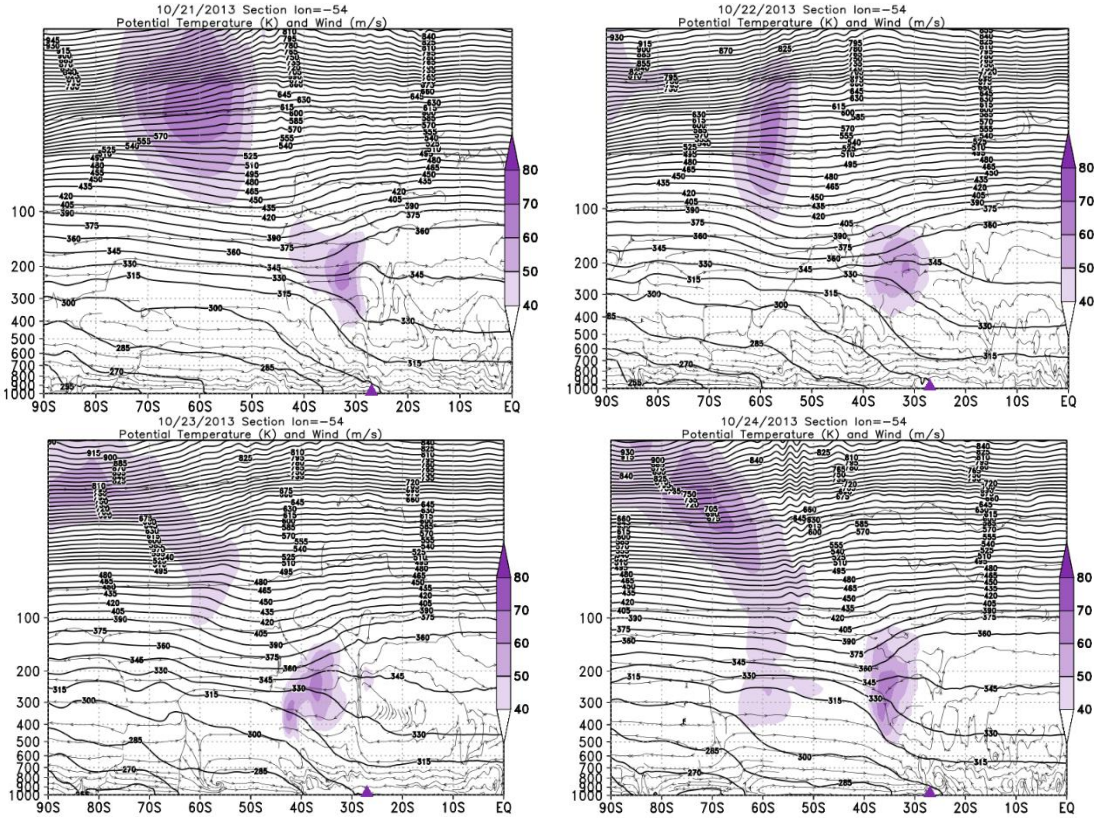

Source: The author.

08/10/2014

Figure A248: PVA fields for the 20 hPa in pressure levels, days 08/08/2014 to 08/11/2014.

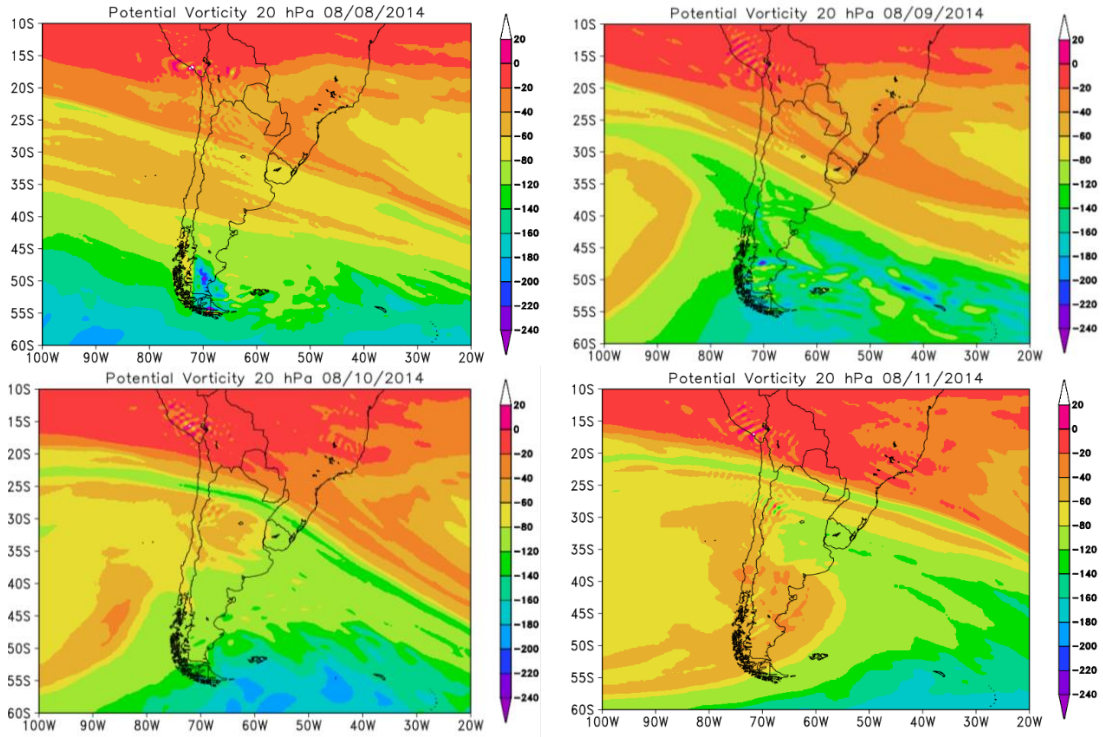

Source: The author.

Figure A249: Retroactive trajectory by the HYSPLIT/NOAA model, and O3 content OMI satellite for South Pole, and global view.

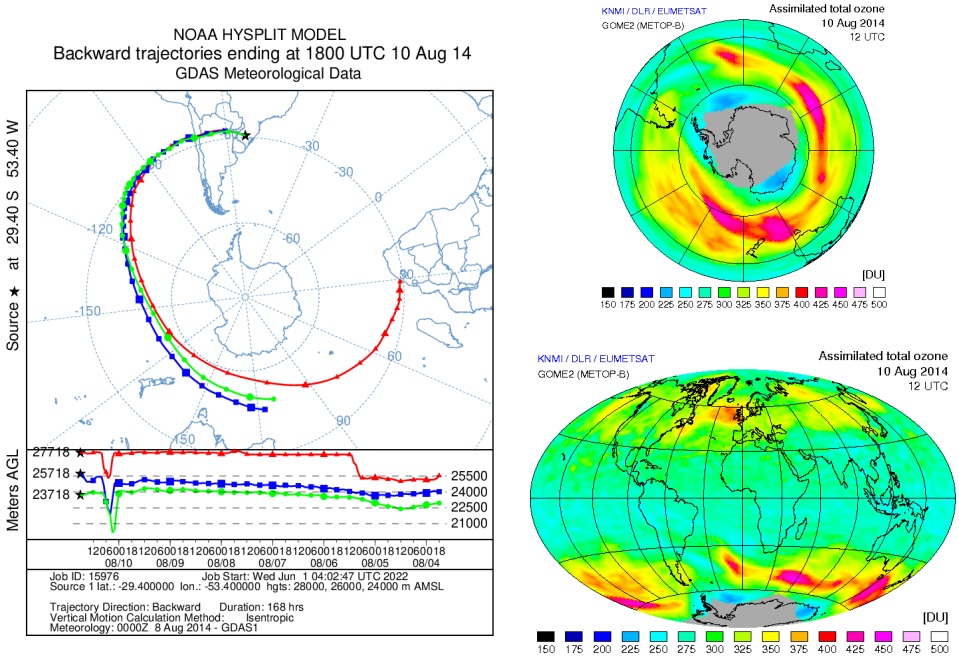

Figure A250: Vertical section of the atmosphere between 1000 and 5 hPa for the days of the event in August 2014.

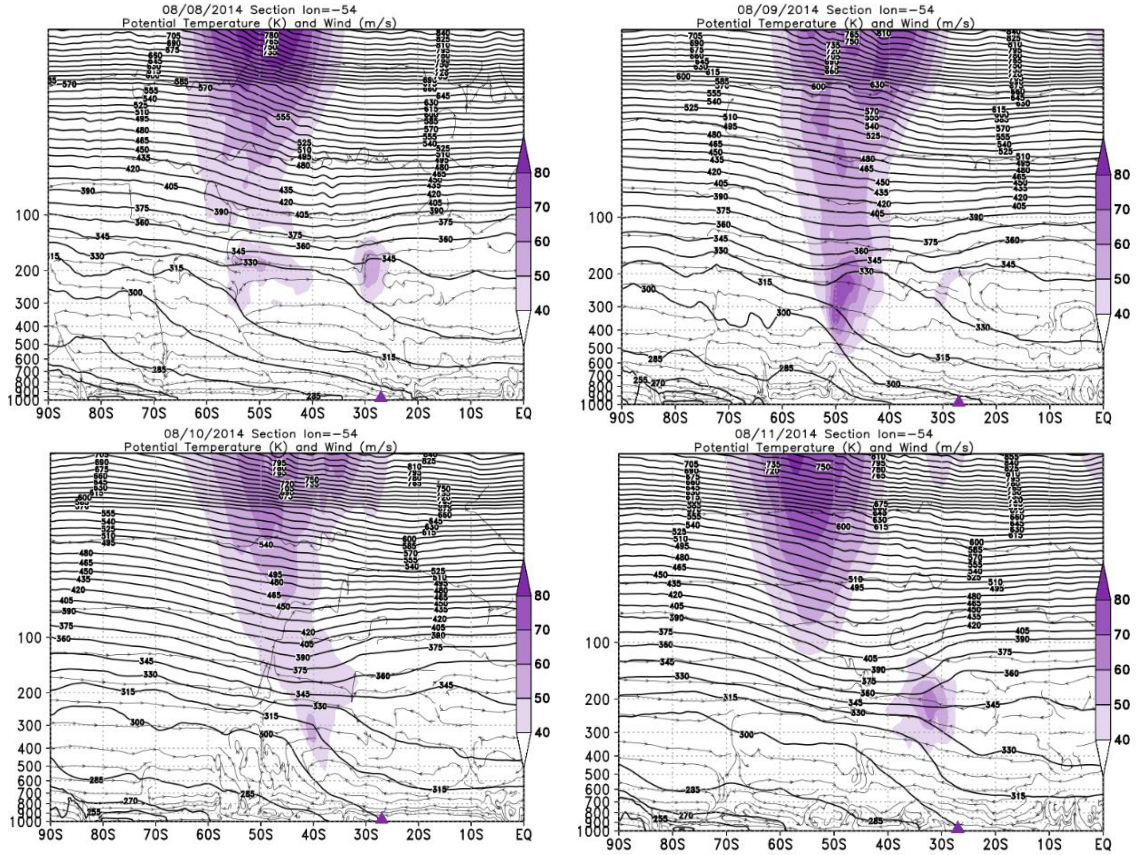

Source: The author.

10/16/2014

Figure A251: PVA fields for the 20 hPa in pressure levels, days 10/14/2014 to 10/17/2014.

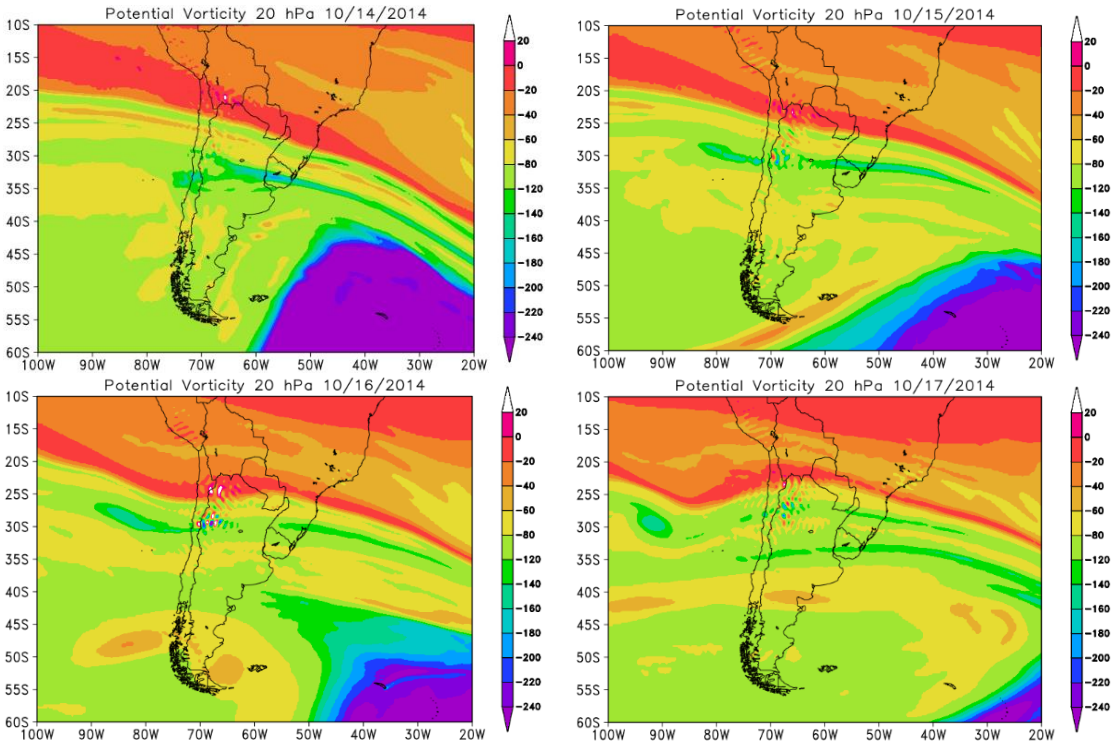

Source: The author.

Figure A252: Retroactive trajectory by the HYSPLIT/NOAA model, and O3 content OMI satellite for South Pole, and global view.

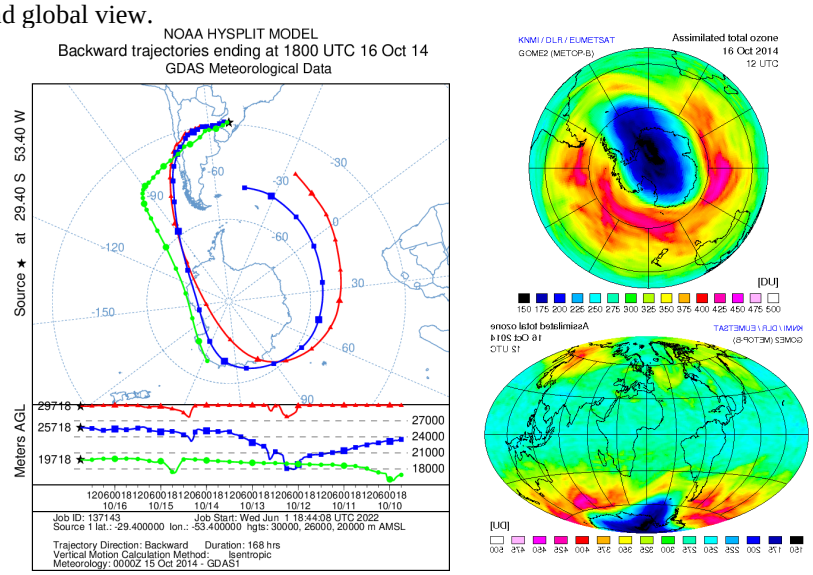

Figure A253: Vertical profile of O_3 by the SABER satellite for the October 16, 2014 (in red) and climatology for the month of October (in black).

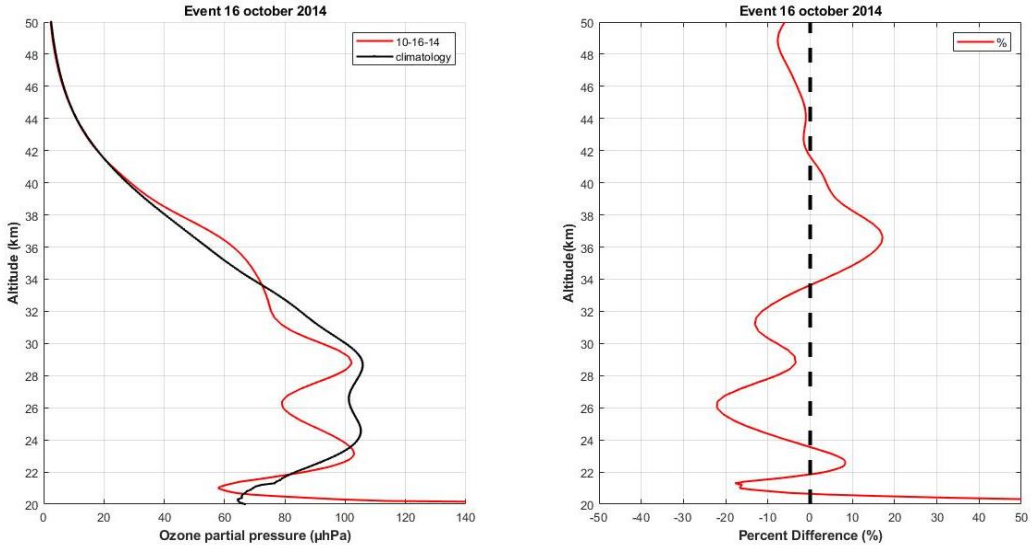

Source: The author.

Figure A254: Vertical section of the atmosphere between 1000 and 5 hPa for the days of the event in October 2014

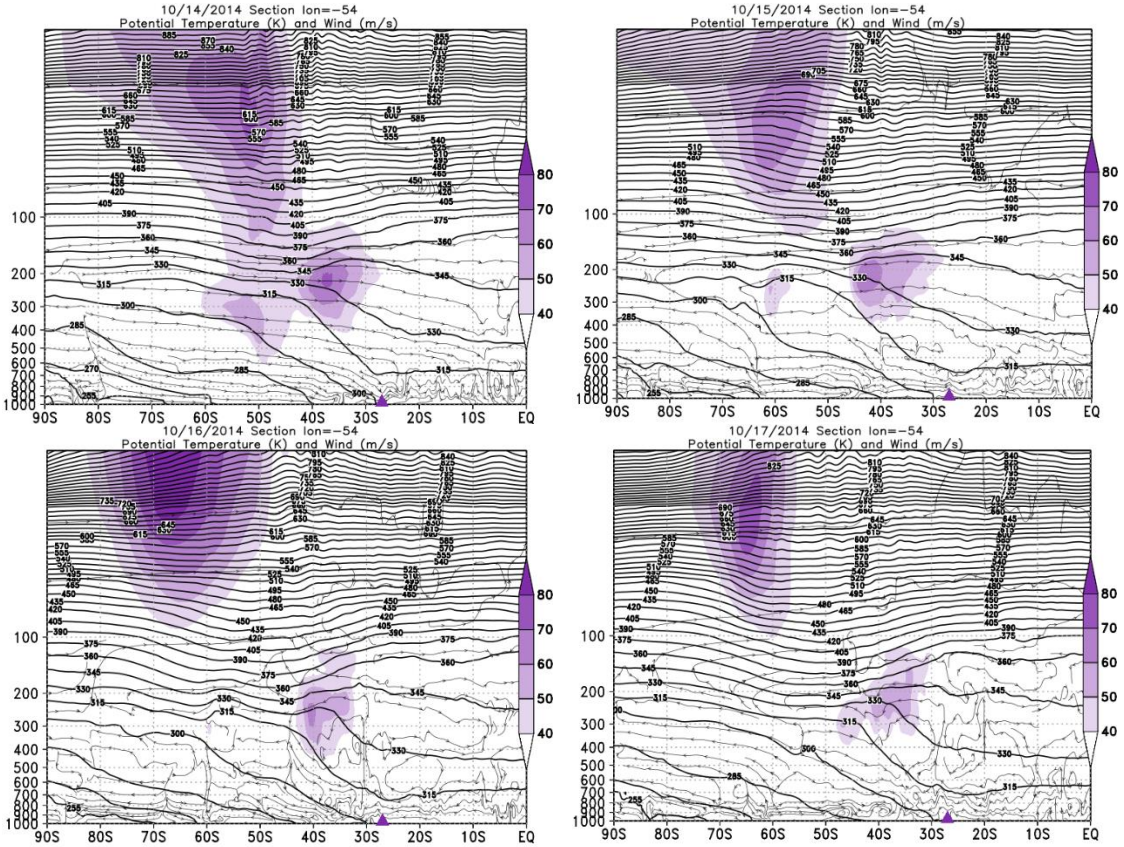

Source: The author.

11/03/2014

Figure A255: PVA fields for the 20 hPa in pressure levels, days 11/01/2014 to 11/04/2014.

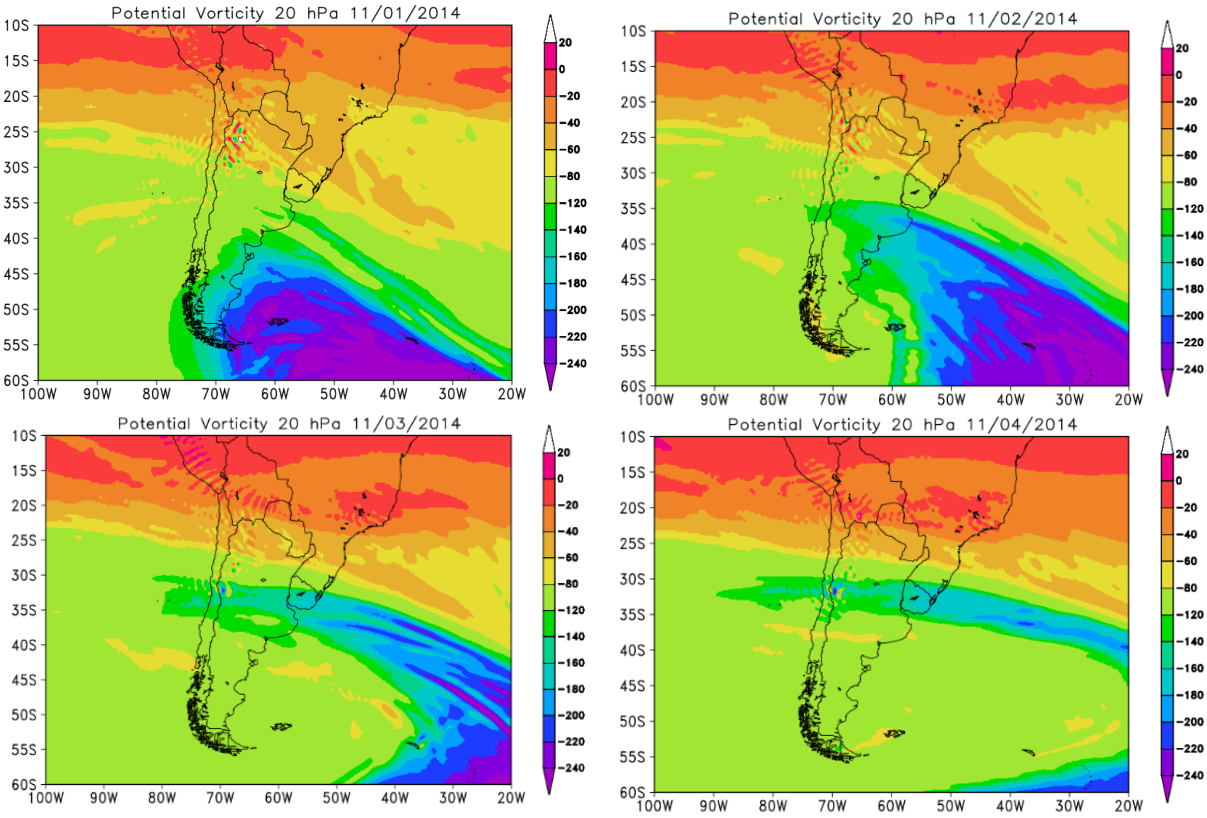

Figure A256: Retroactive trajectory by the HYSPLIT/NOAA model, O3 content OMI satellite for South Pole, and global view.

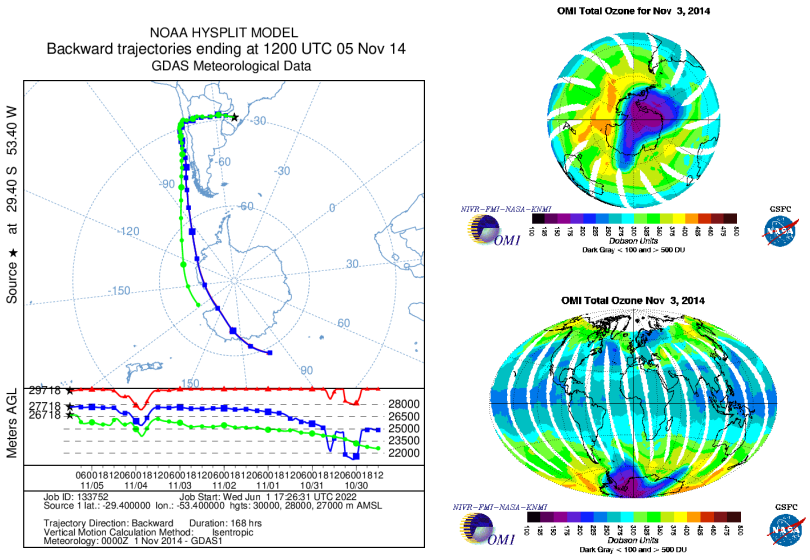

Source: HYSPLIT/NOAA, OMI/NASA.

Figure A257: Vertical profile of O_3 by the SABER satellite for the November 05, 2014 (in red) and climatology for the month of October (in black).

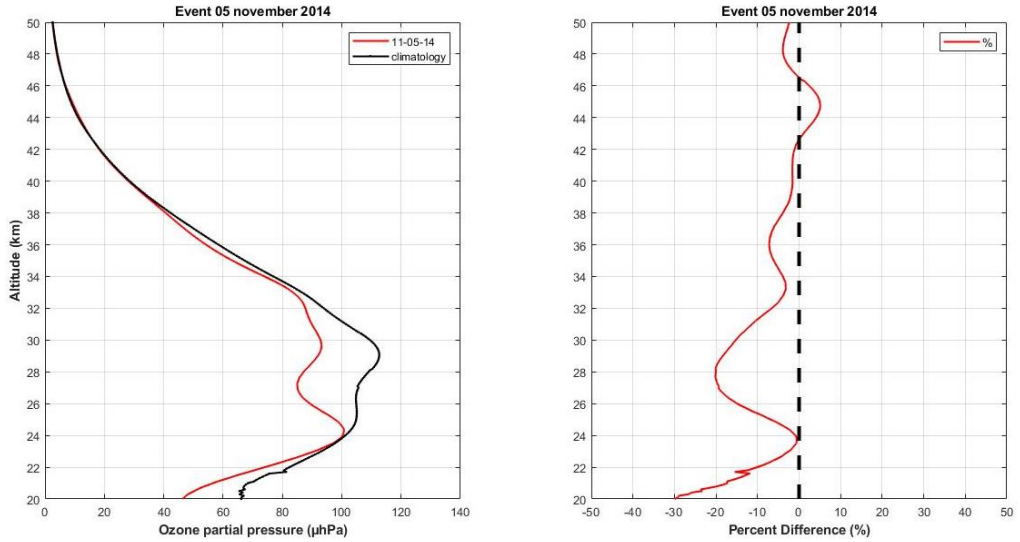

Source: The author.

Figure A258: Vertical section of the atmosphere between 1000 and 5 hPa for the days of the event in October 2016

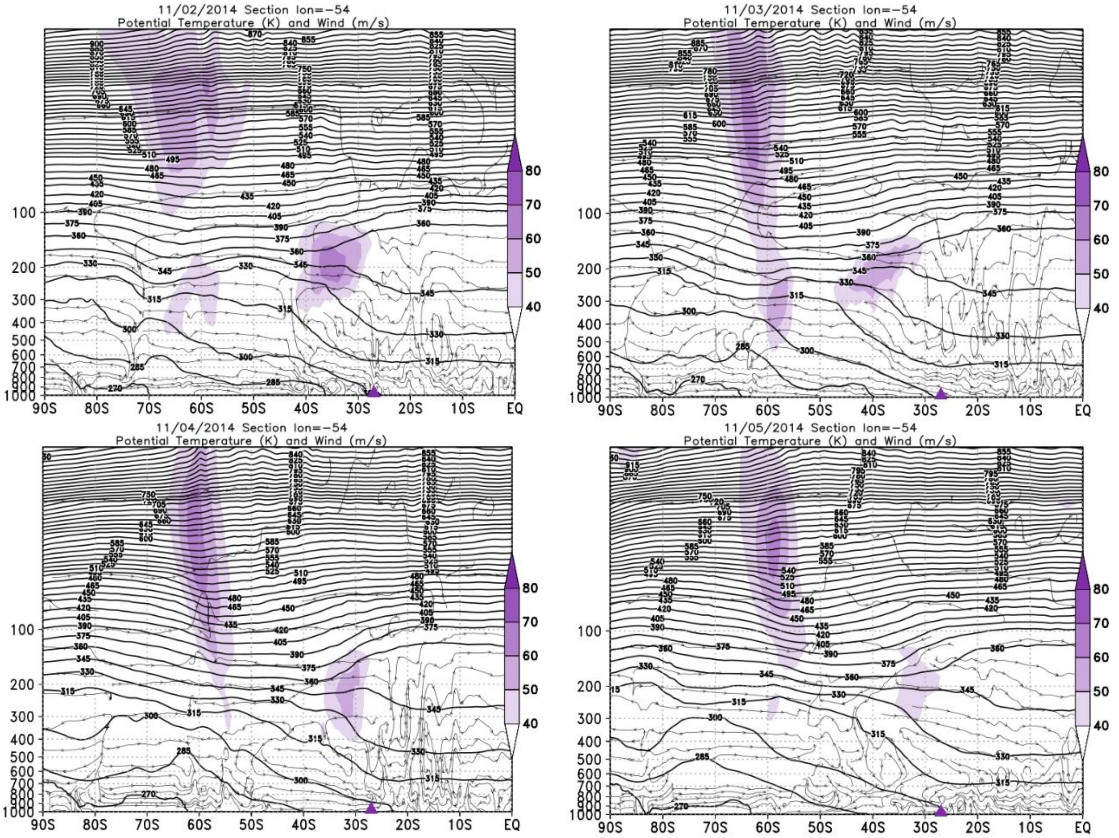

Source: The author

09/22/2015

Figure A259: PVA fields for the 20 hPa in pressure levels, days 09/20/2015 to 09/23/2015.

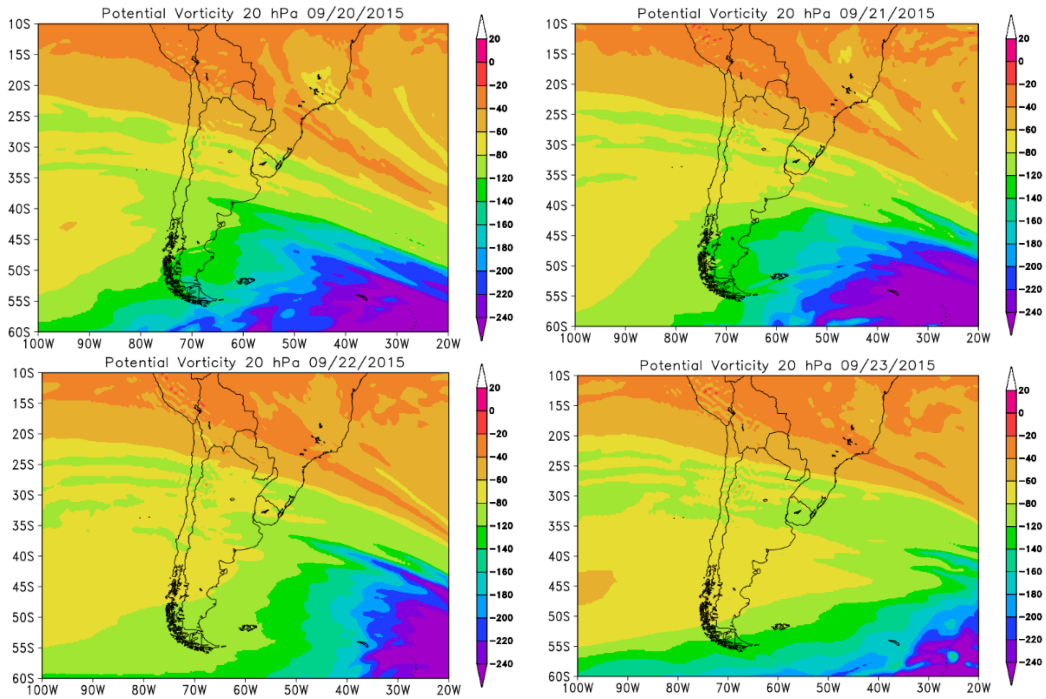

Source: The author.

Figure A260: Retroactive trajectory by the HYSPLIT/NOAA model, and O3 content OMI satellite for South Pole, and global view.

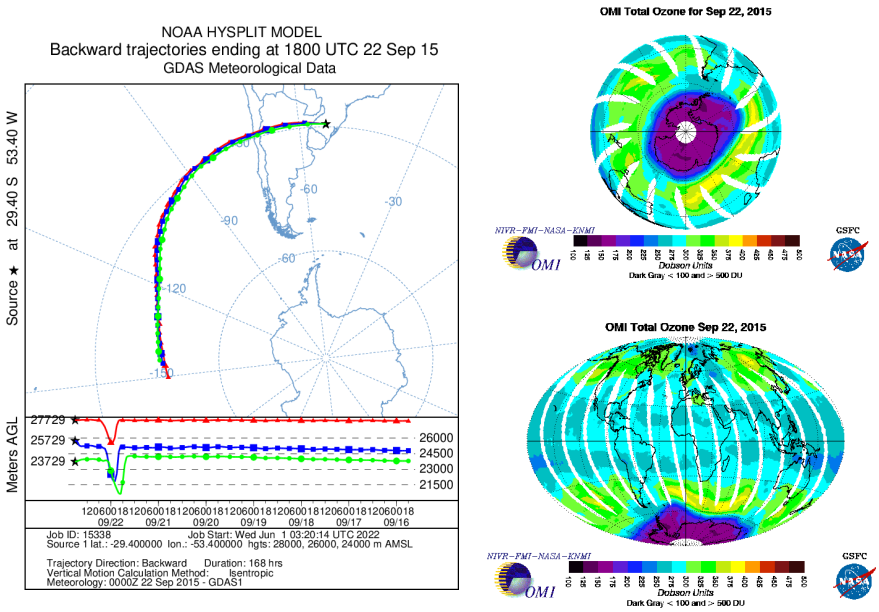

Source: HYSPLIT/NOAA, OMI/NASA.

Figure A261: Vertical profile of O_3 by the SABER satellite for the September 22, 2015 (in red) and climatology for the month of October (in black).

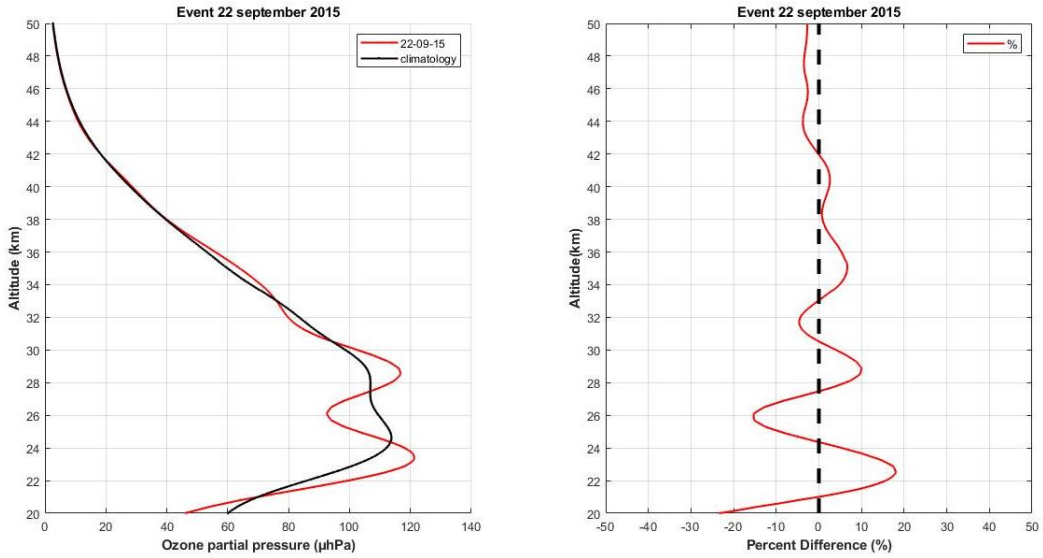

Source: The author.

Figure A262: Vertical section of the atmosphere between 1000 and 5 hPa for the days of the event in September 2015.

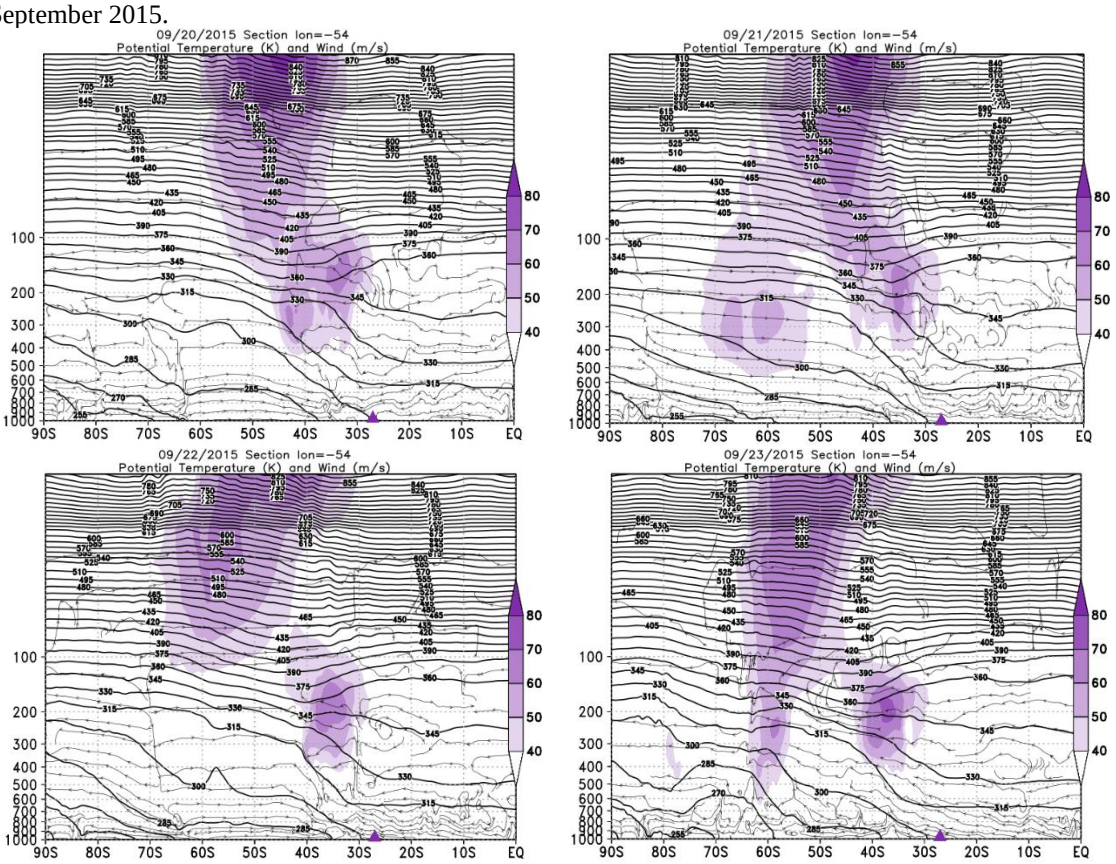

Source: The author.

11/03/2015

Figure A263: PVA fields for the 20 hPa in pressure levels, days 11/02/2015 to 11/04/2015.

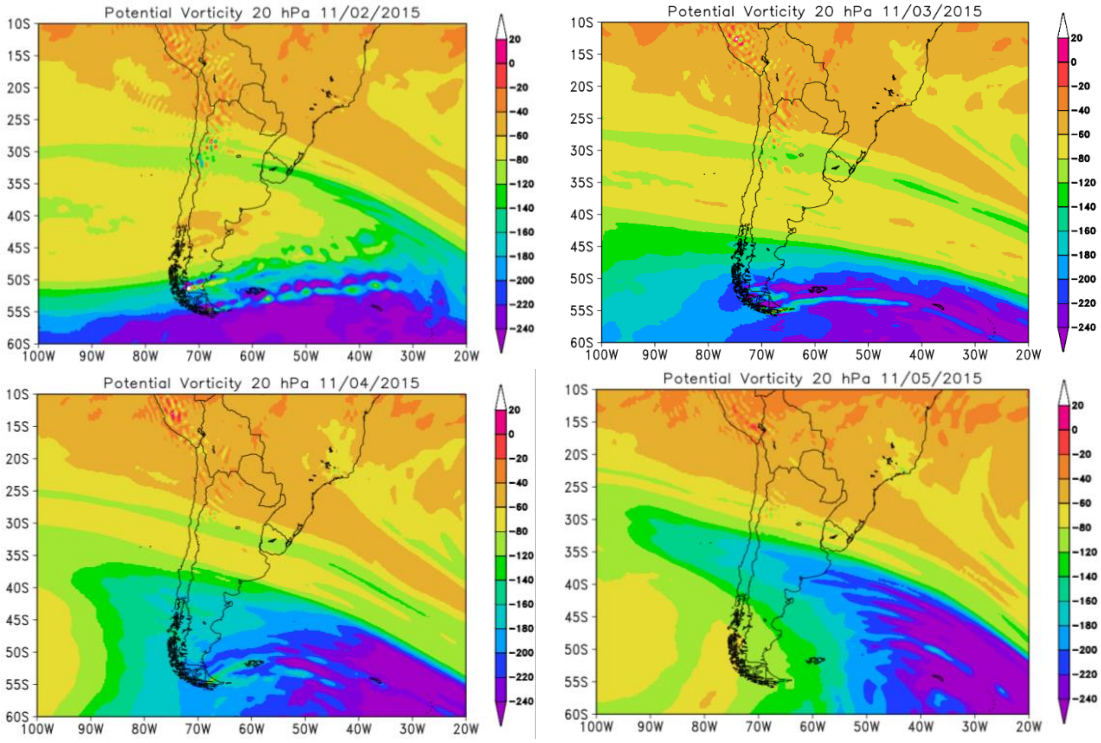

Source: The author.

Figure A264: O3 content OMI satellite for South Pole, and global view.

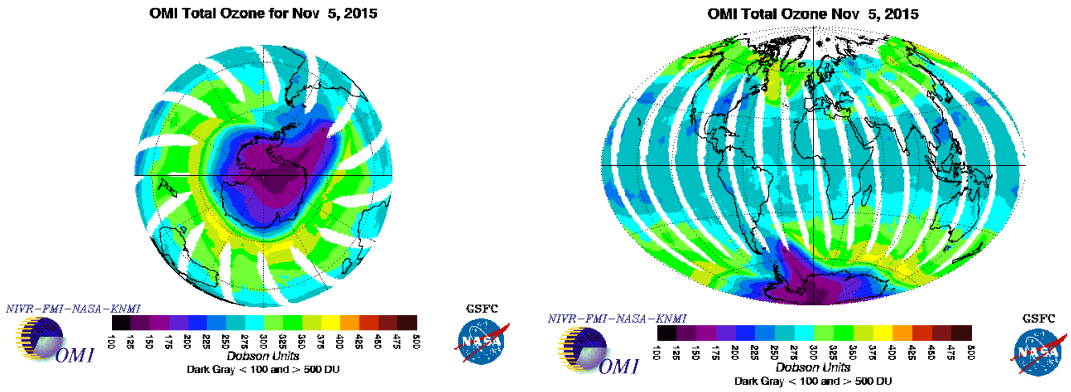

Source: OMI/NASA.

Figure A265: Vertical profile of O_3 by the SABER satellite for the November 04, 2015 (in red) and climatology for the month of October (in black).

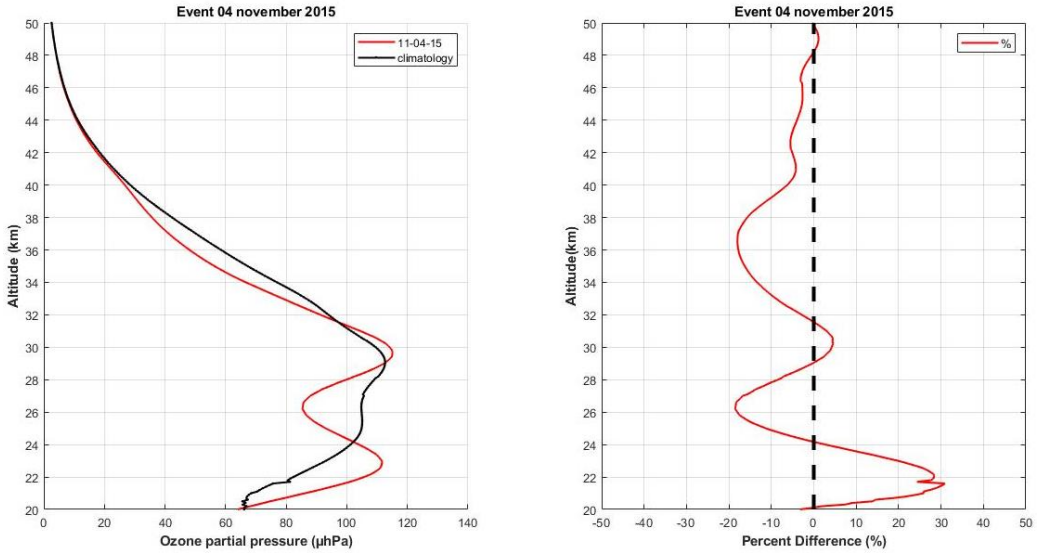

Source: The author.

Figure A266: Vertical section of the atmosphere between 1000 and 5 hPa for the days of the event in November 2015.

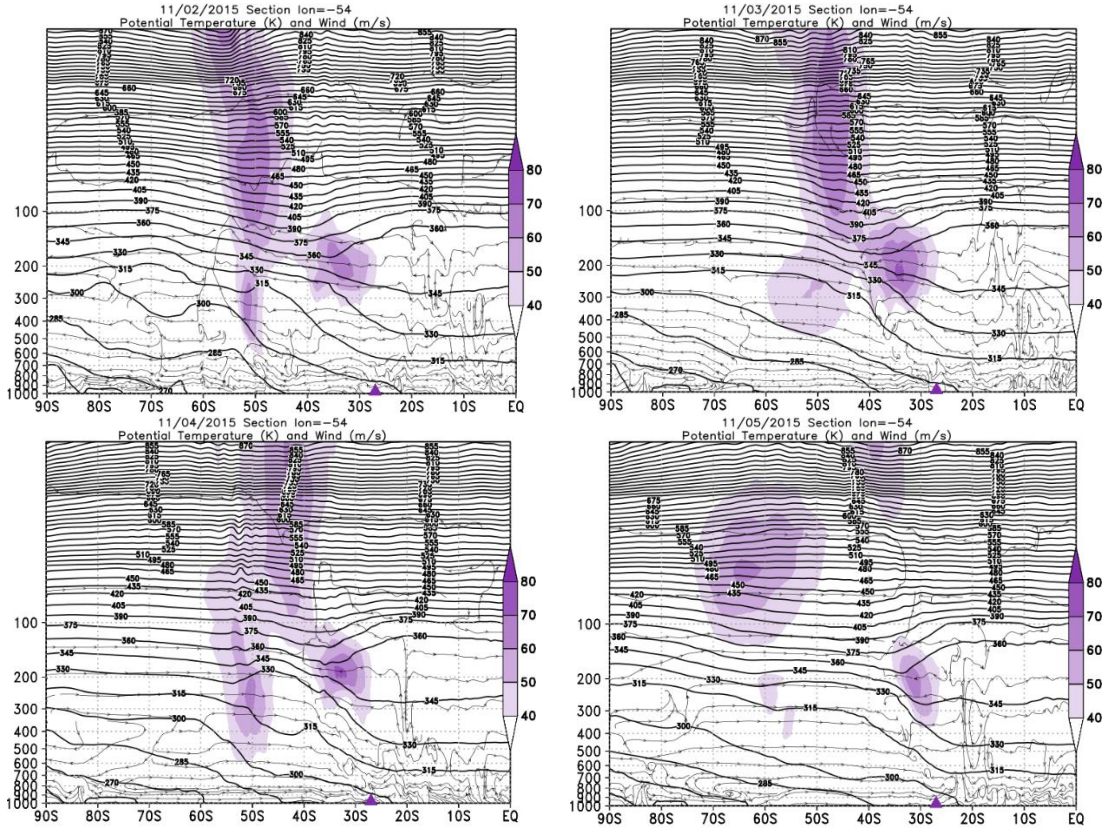

Source: The author.

09/05/2016

Figure A267: PVA fields for the 20 hPa in pressure levels, days 09/02/2016 to 09/05/2016.

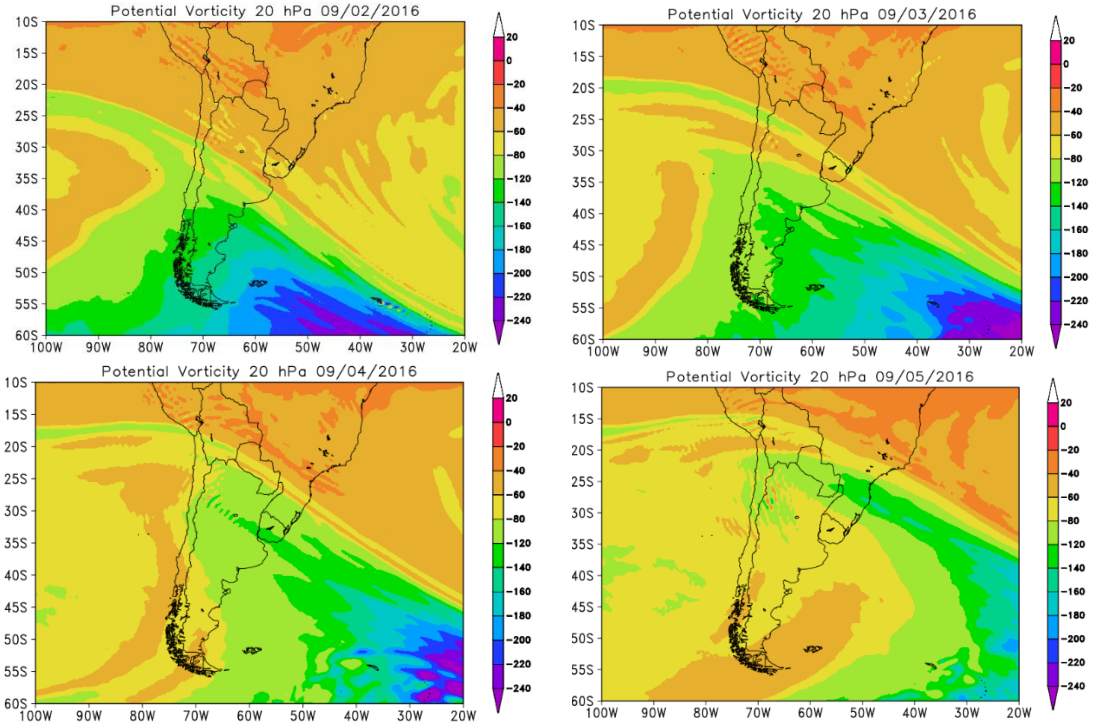

Source: The author.

Figure A268: Retroactive trajectory by the HYSPLIT/NOAA model, O3 content OMI satellite for South Pole, and global view.

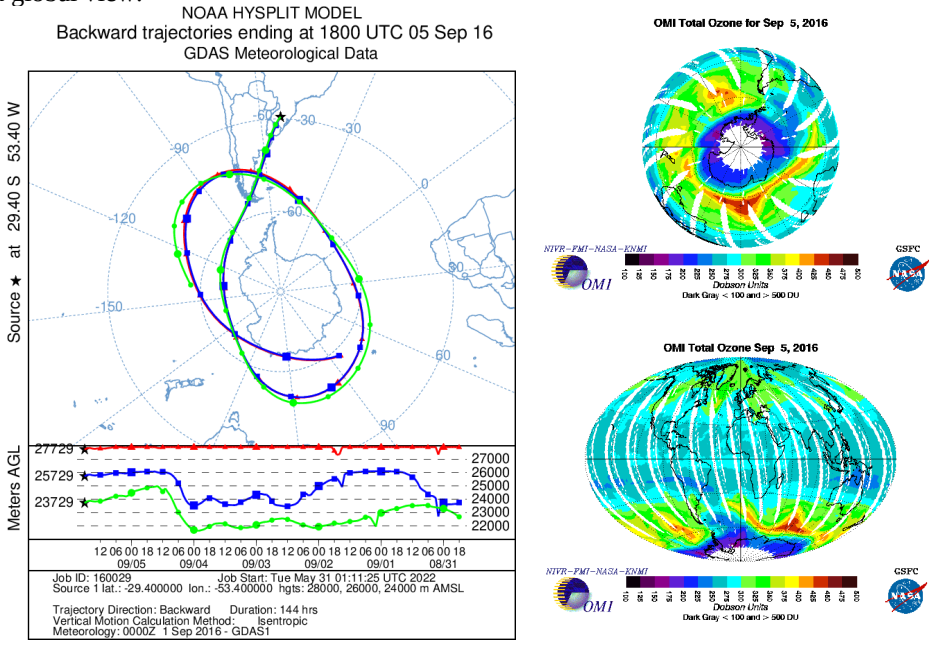

Source: HYSPLIT/NOAA, OMI/NASA.

Figure A269: Vertical profile of O_3 by the SABER satellite for the September 04, 2016 (in red) and

climatology for the month of October (in black).

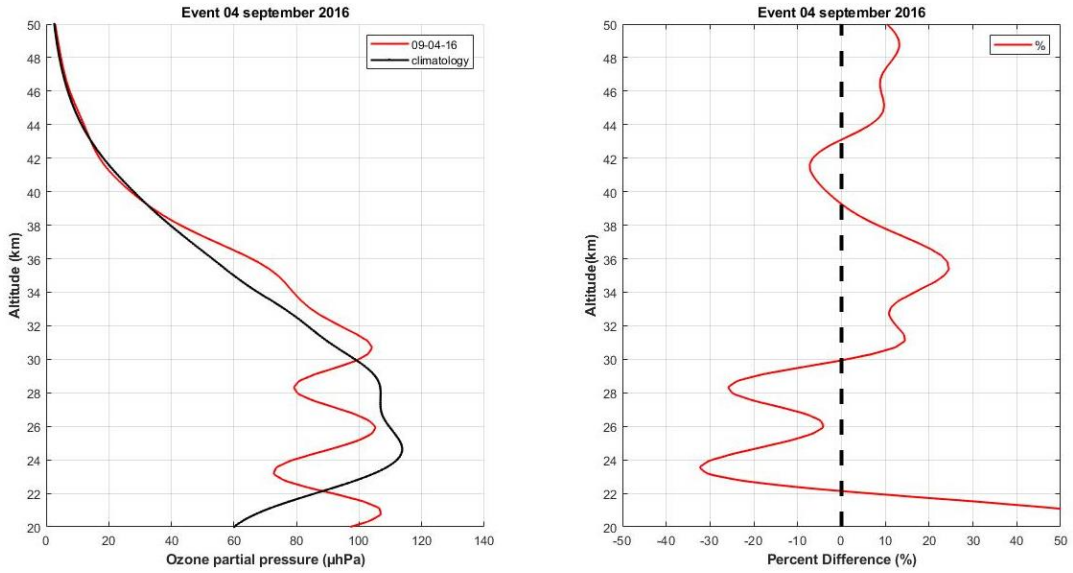

Source: The author.

Figure A270: Vertical section of the atmosphere between 1000 and 5 hPa for the days of the event in October 2016

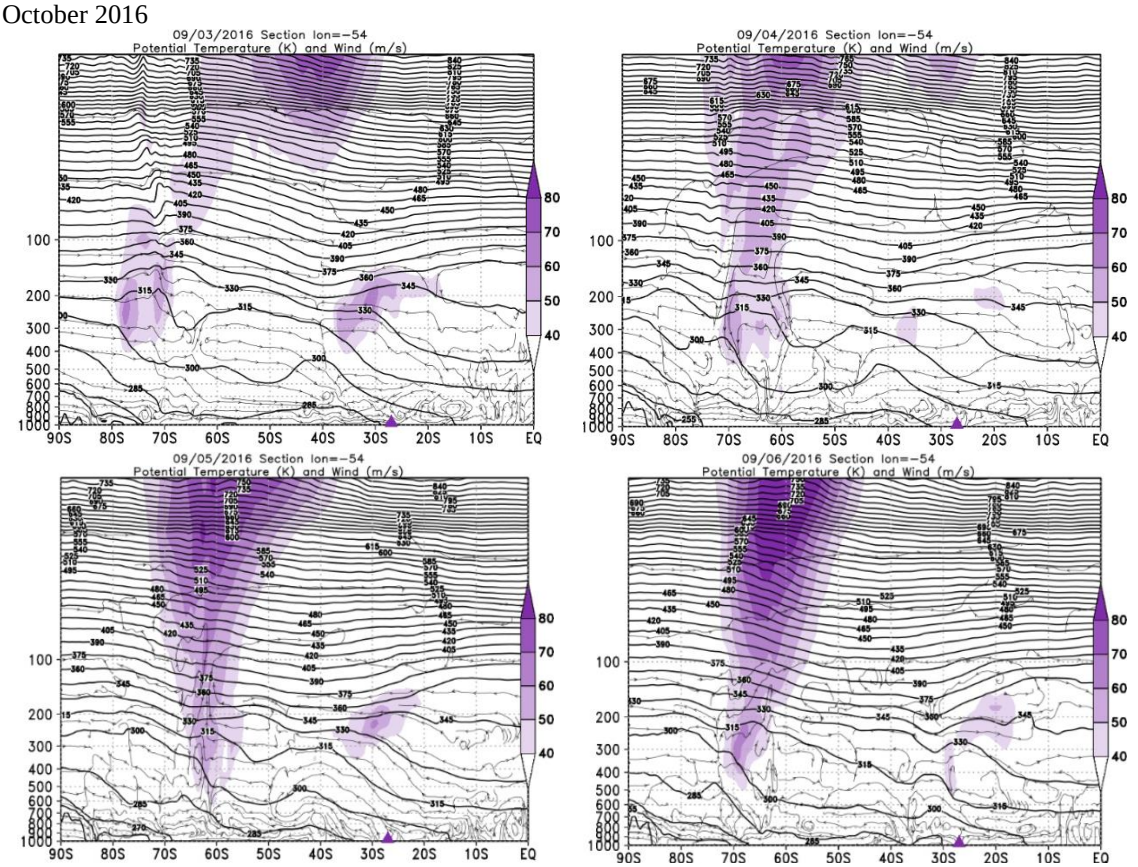

Source: The author.

08/26/2017

Figure A271: PVA fields for the 20 hPa in pressure levels, days 08/24/2017 to 08/27/2017.

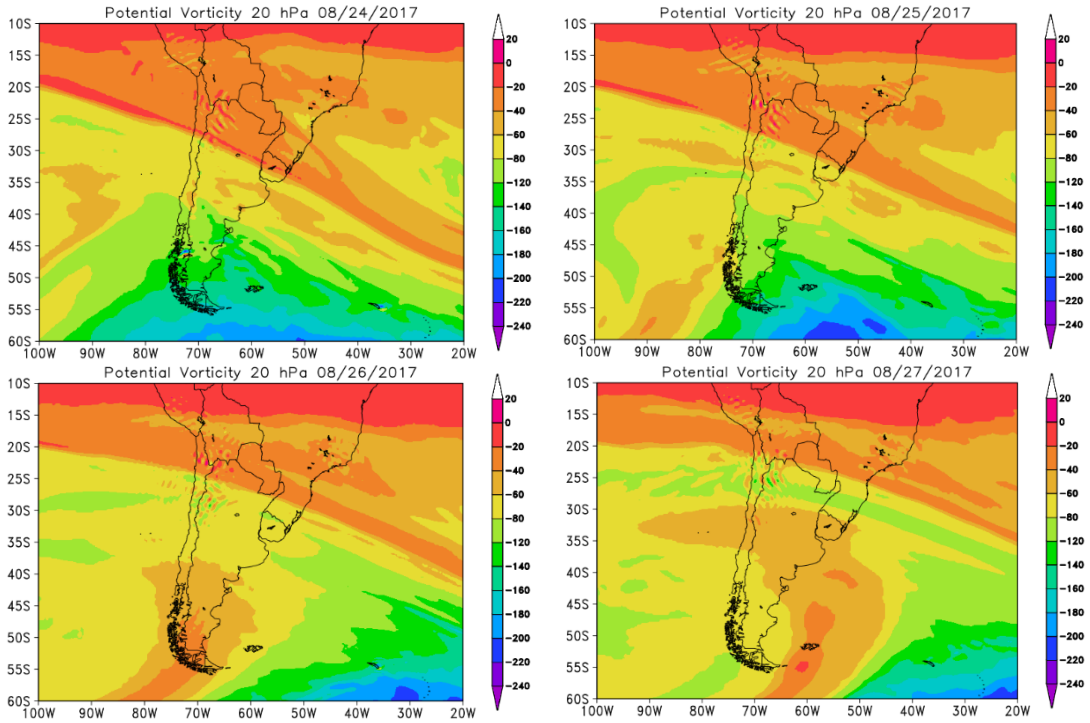

Source: The author.

Figure A272: Retroactive trajectory by the HYSPLIT/NOAA model, O3 content OMI satellite for South Pole, and global view.

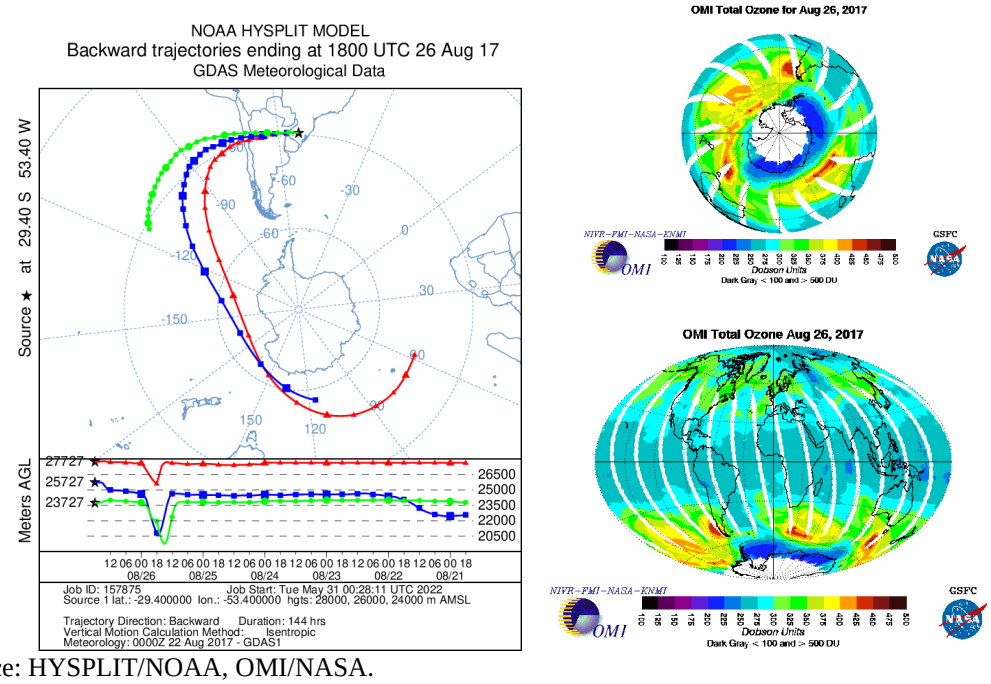

Source: HYSPLIT/NOAA, OMI/NASA.

Figure A273: Vertical profile of O_3 by the SABER satellite for the August 25, 2017 (in red) and climatology for the month of October (in black).

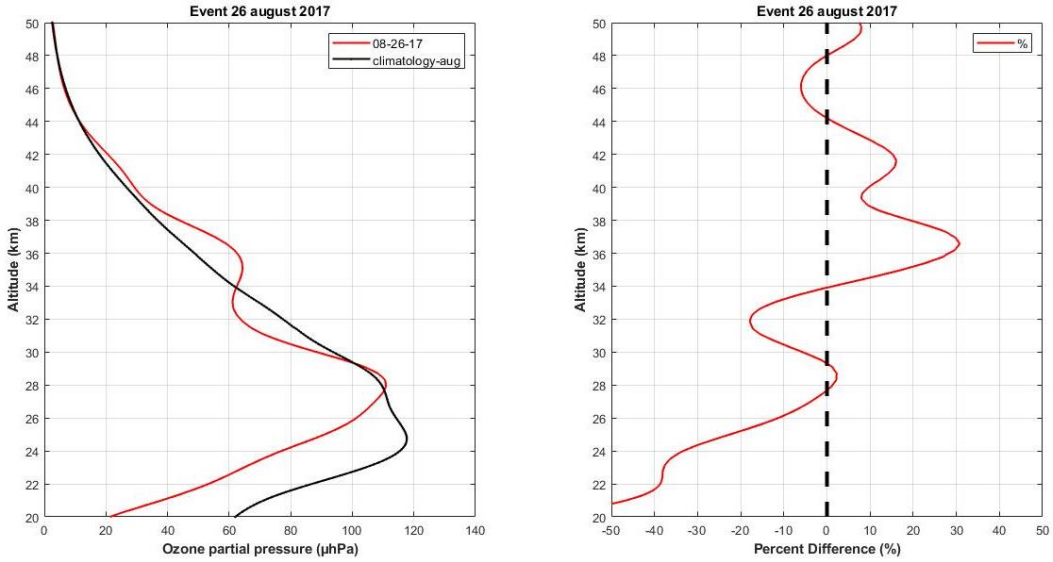

Source: The author.

Figure A274: Vertical section of the atmosphere between 1000 and 5 hPa for the days of the event in August 2017.

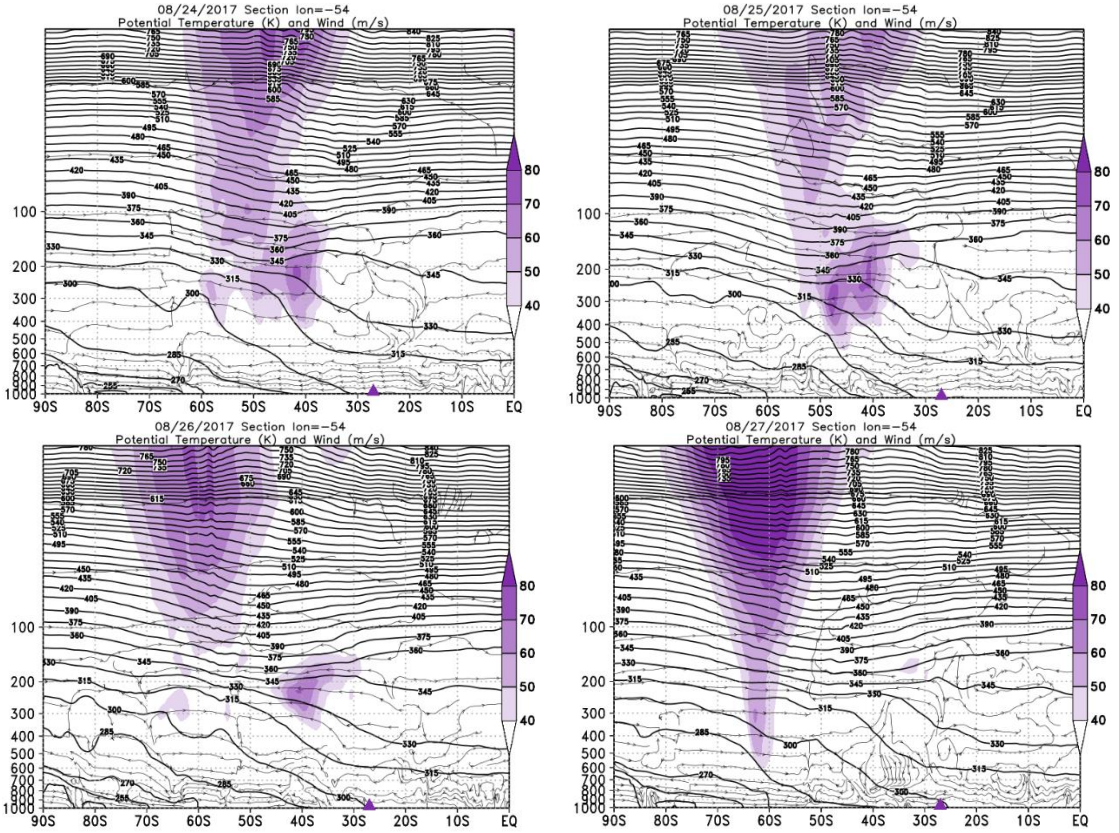

Source: The author.

09/18/2017

Figure A275: PVA fields for the 20 hPa in pressure levels, days 09/16/2017 to 09/19/2017.

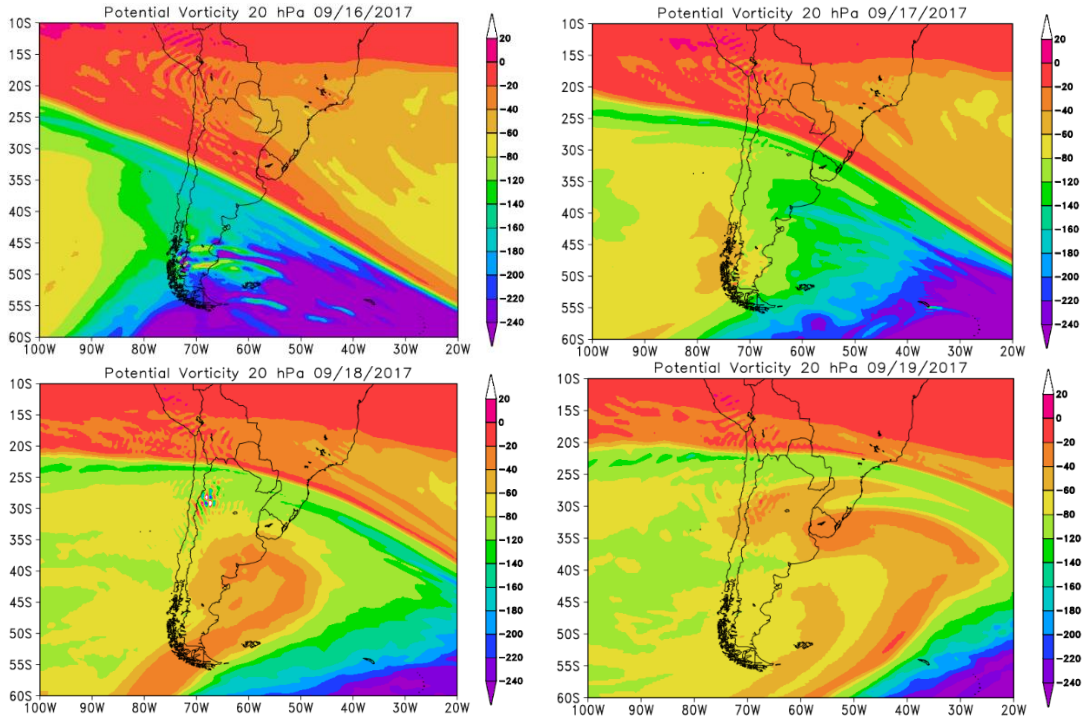

Source: The author.

Figure A276: Retroactive trajectory by the HYSPLIT/NOAA model, O3 content OMI satellite for South Pole, and global view.

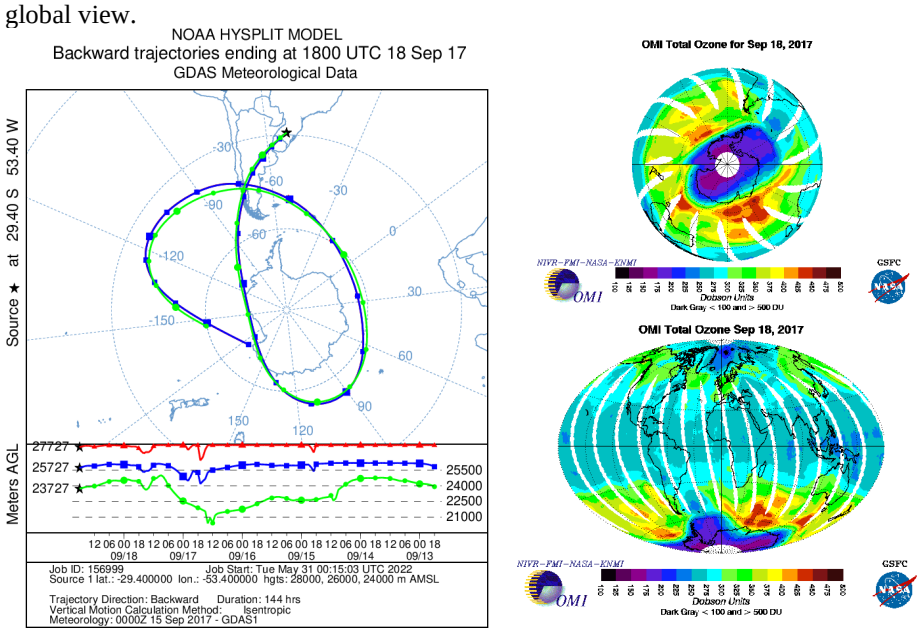

Source: HYSPLIT/NOAA, OMI/NASA.

Figure A277: Vertical profile of O_3 by the SABER satellite for the September 18, 2017 (in red) and climatology for the month of October (in black).

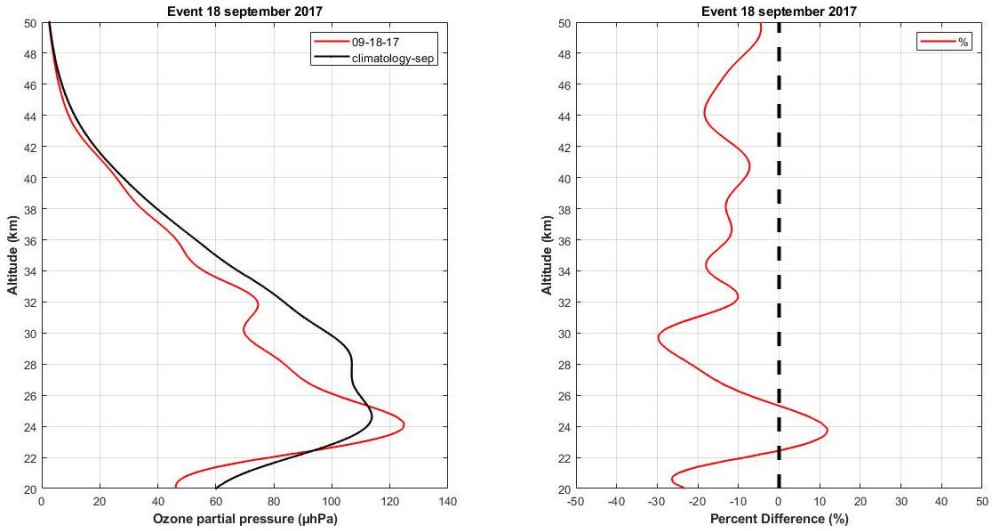

Source: The author.

Figure A278: Vertical section of the atmosphere between 1000 and 5 hPa for the days of the event in September 2017.

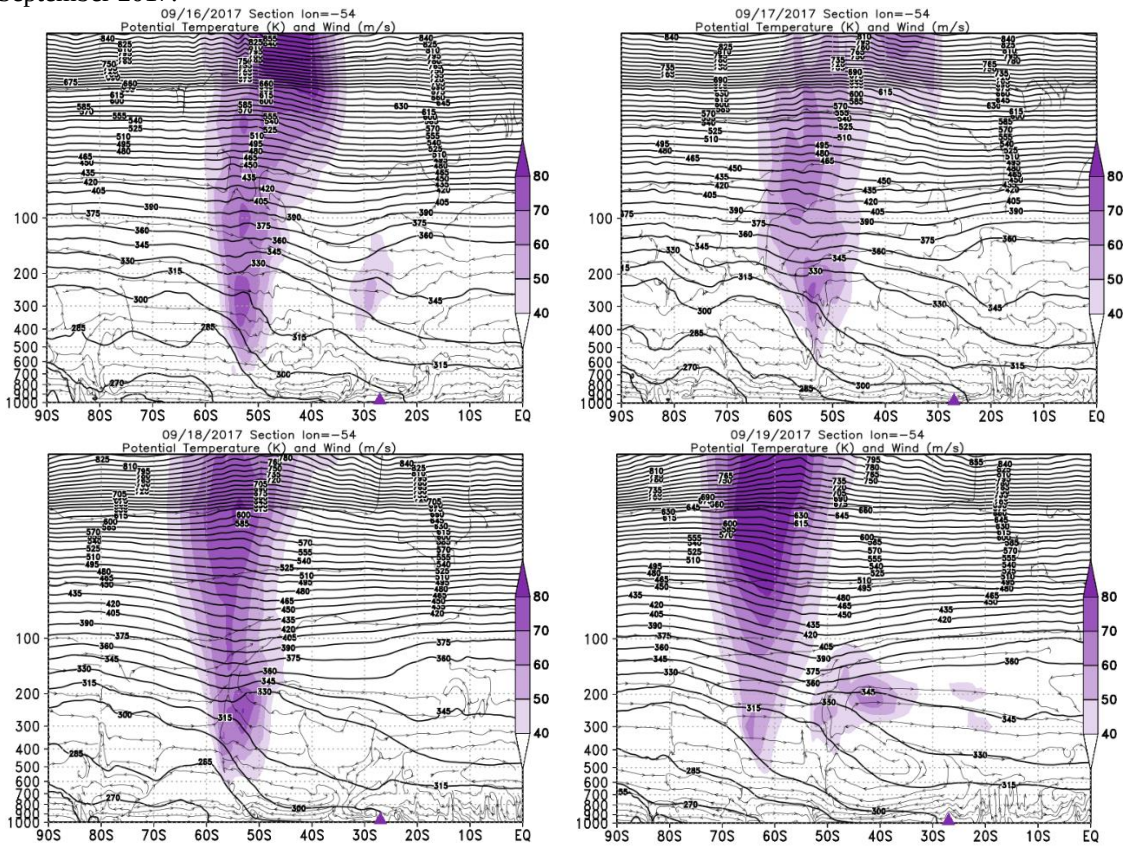

Source: The author.

11/11/2018

Figure A279: PVA fields for the 20 hPa in pressure levels, days 11/09/2018 to 11/12/2018.

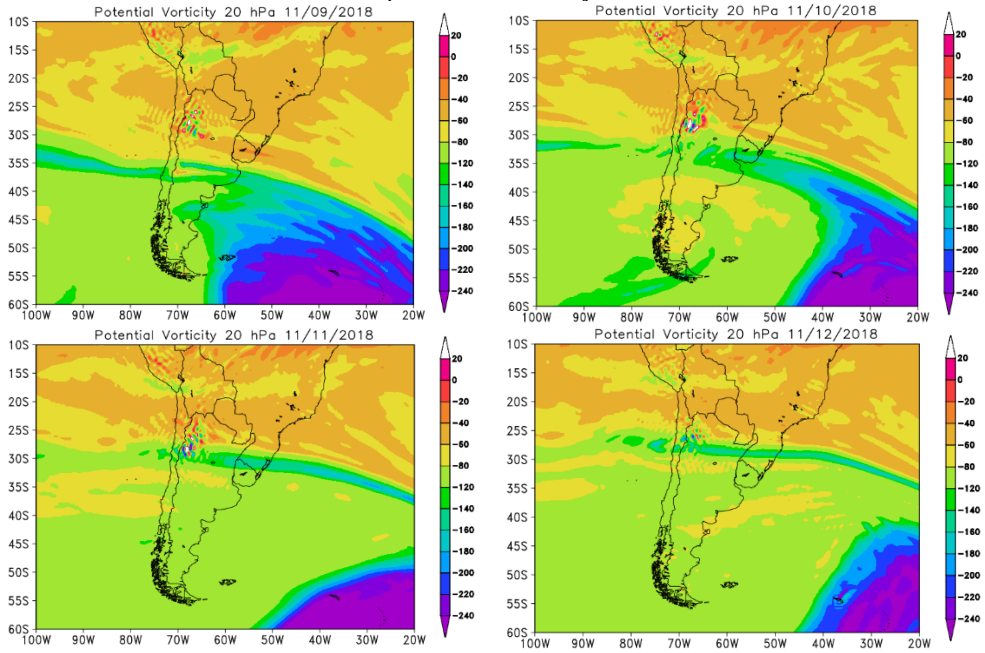

Source: The author.

Figure A280: Retroactive trajectory by the HYSPLIT/NOAA model, O3 content OMI satellite for South Pole, and global view.

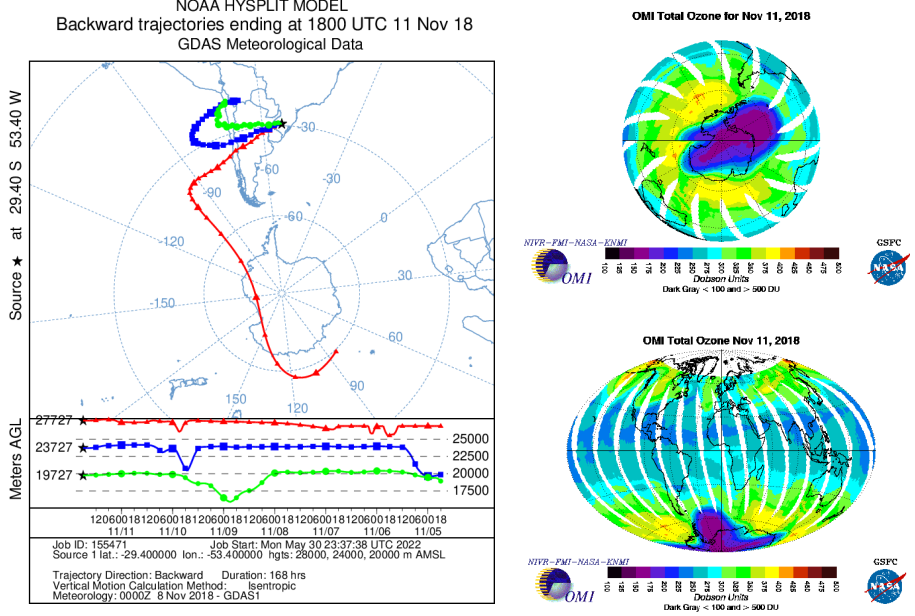

Source: HYSPLIT/NOAA, OMI/NASA.

Figure A281: Vertical profile of O_3 by the SABER satellite for the November 11, 2019 (in red) and climatology for the month of October (in black).

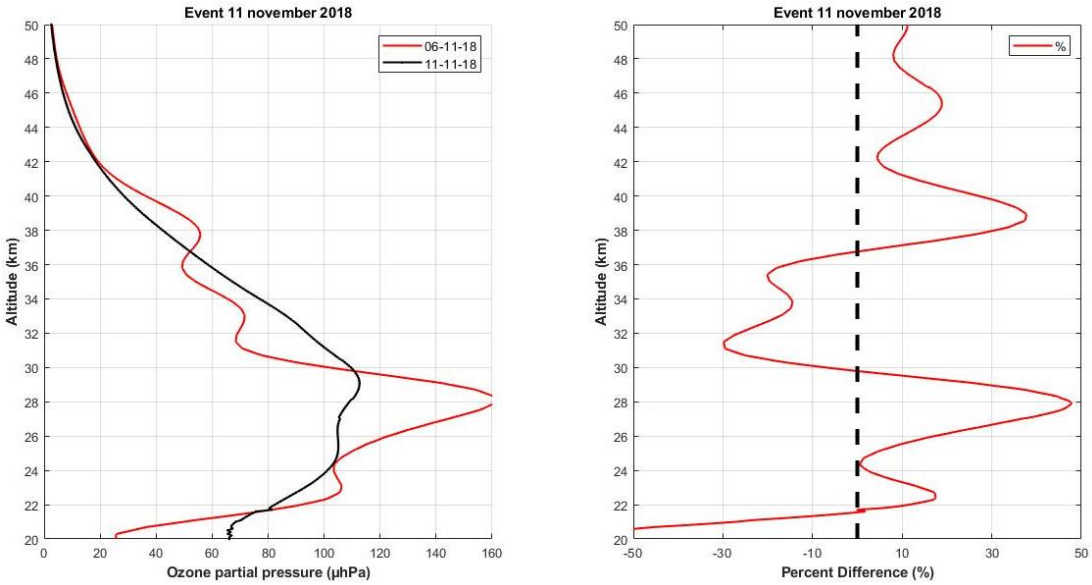

Source: The author.

Figure A282: Vertical section of the atmosphere between 1000 and 5 hPa for the days of the event in November 2018.

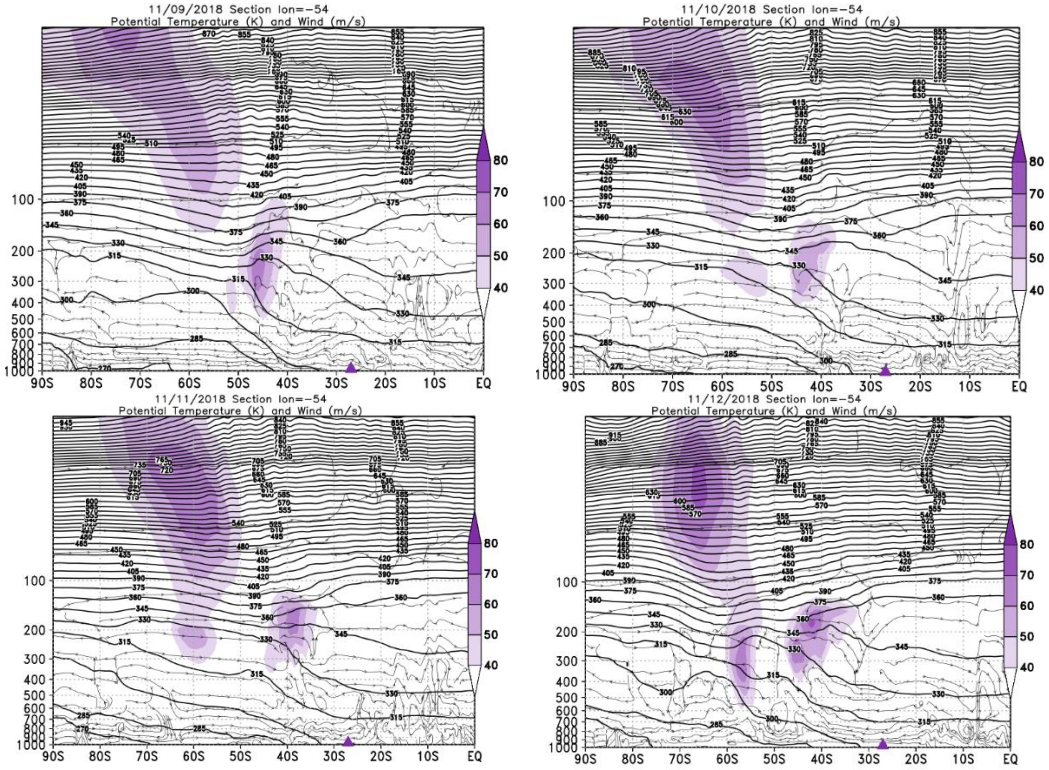

Source: The author.

09/16/2019

Figure A283: PVA fields for the 20 hPa in pressure levels, days 09/16/2019 to 09/19/2019.

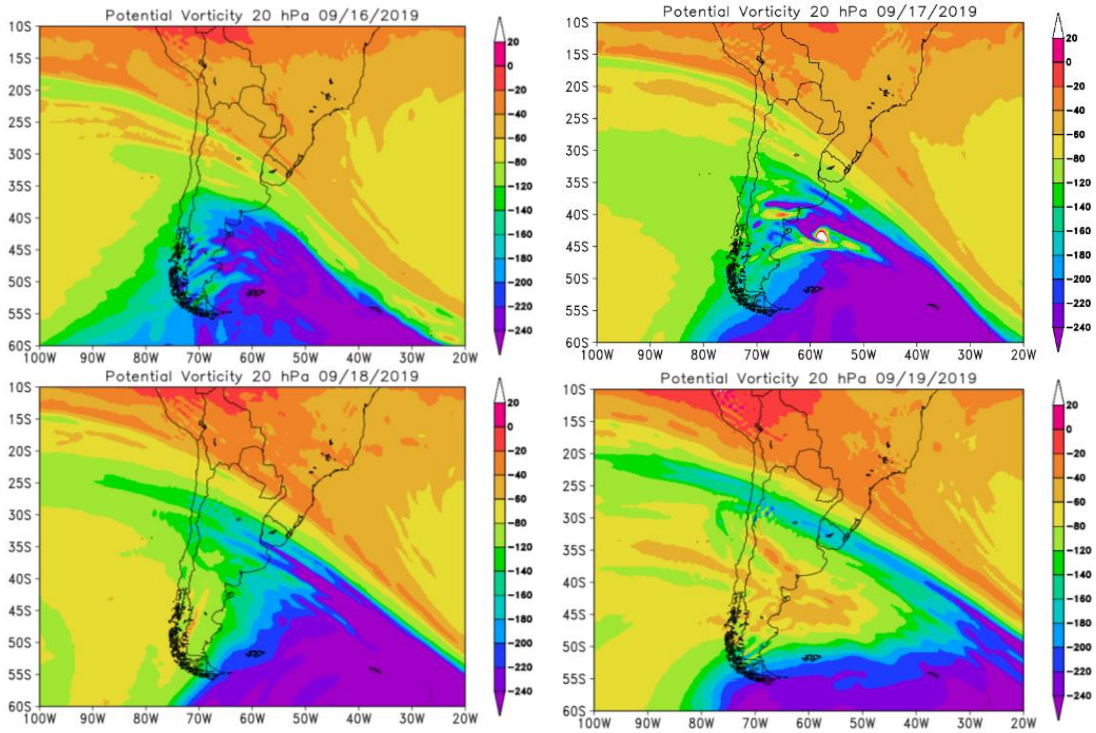

Source: The author.

Figure A284: a) Retroactive trajectory by the HYSPLIT/NOAA model, b) O3 content OMI satellite for South Pole, and global view.

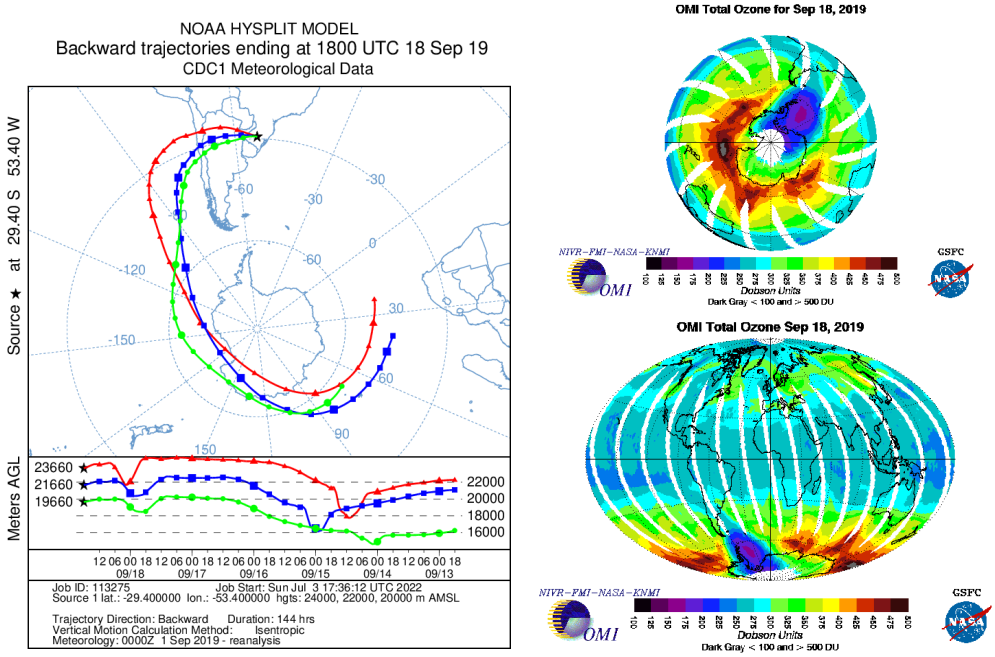

Source: HYSPLIT/NOAA, OMI/NASA.

Figure A285: Vertical section of the atmosphere between 1000 and 5 hPa for the days of the event in September 2019.

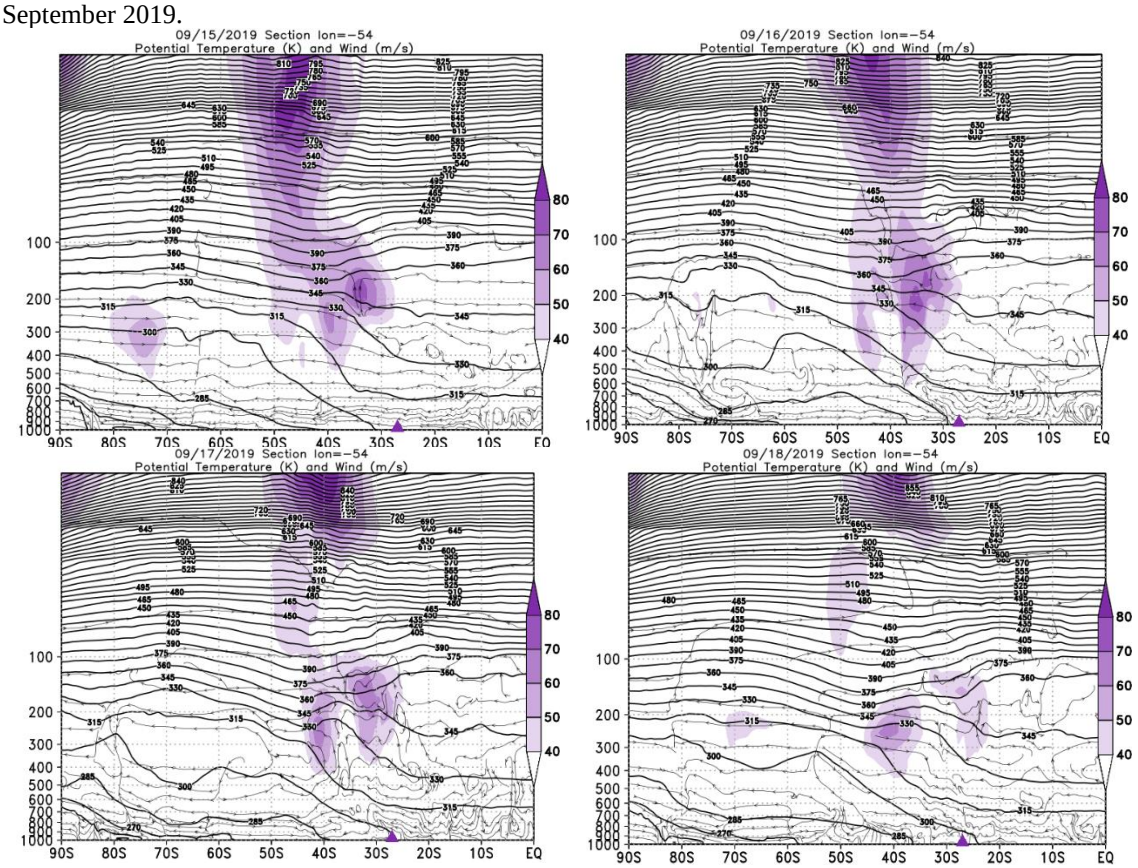

Source: The author.

08/28/2020

Figure A286: PVA fields for the 20 hPa in pressure levels, days 08/26/2020 to 08/29/2020.

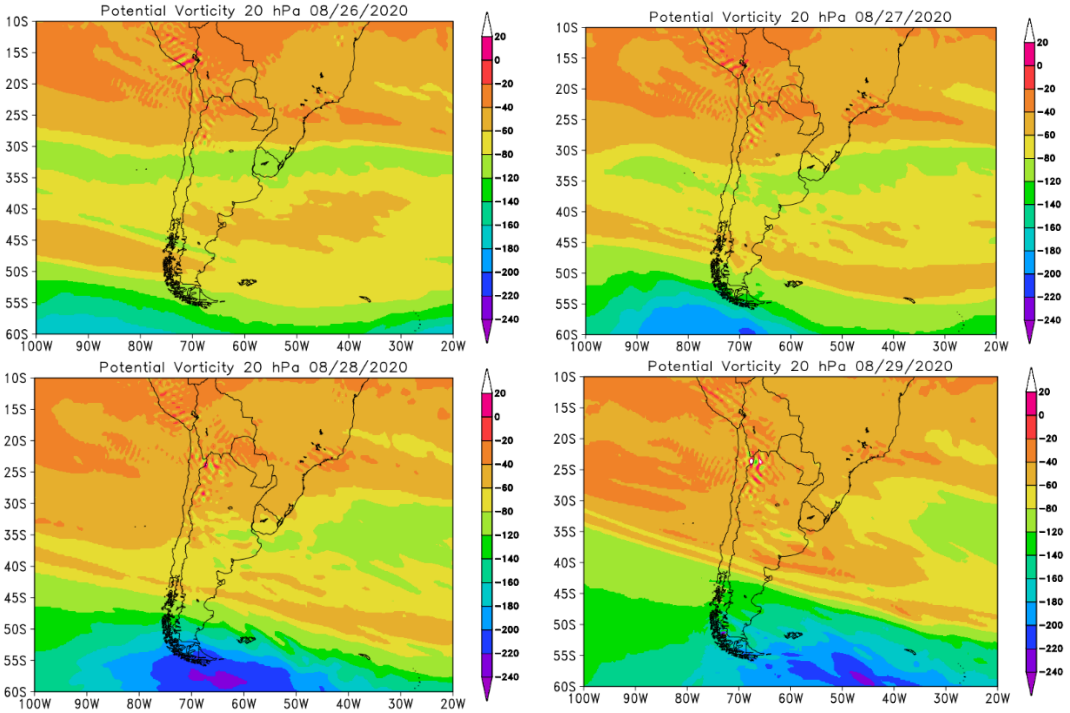

Source: The author.

Figure A287: Retroactive trajectory by the HYSPLIT/NOAA model, O3 content OMI satellite for South Pole, and global view.

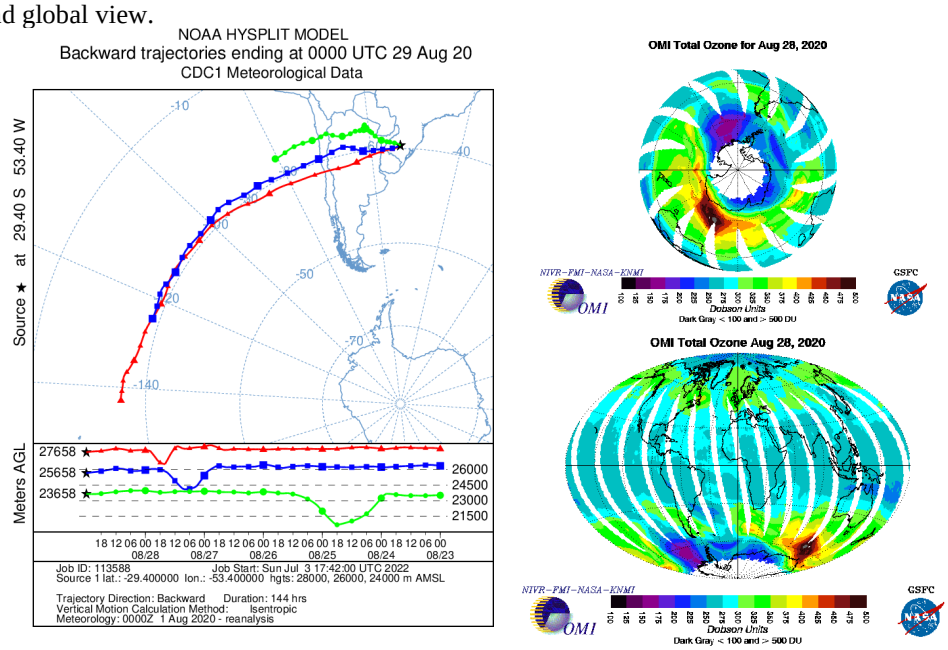

Source: HYSPLIT/NOAA, OMI/NASA.

Figure A288: Vertical section of the atmosphere between 1000 and 5 hPa for the days of the event in August 2020.

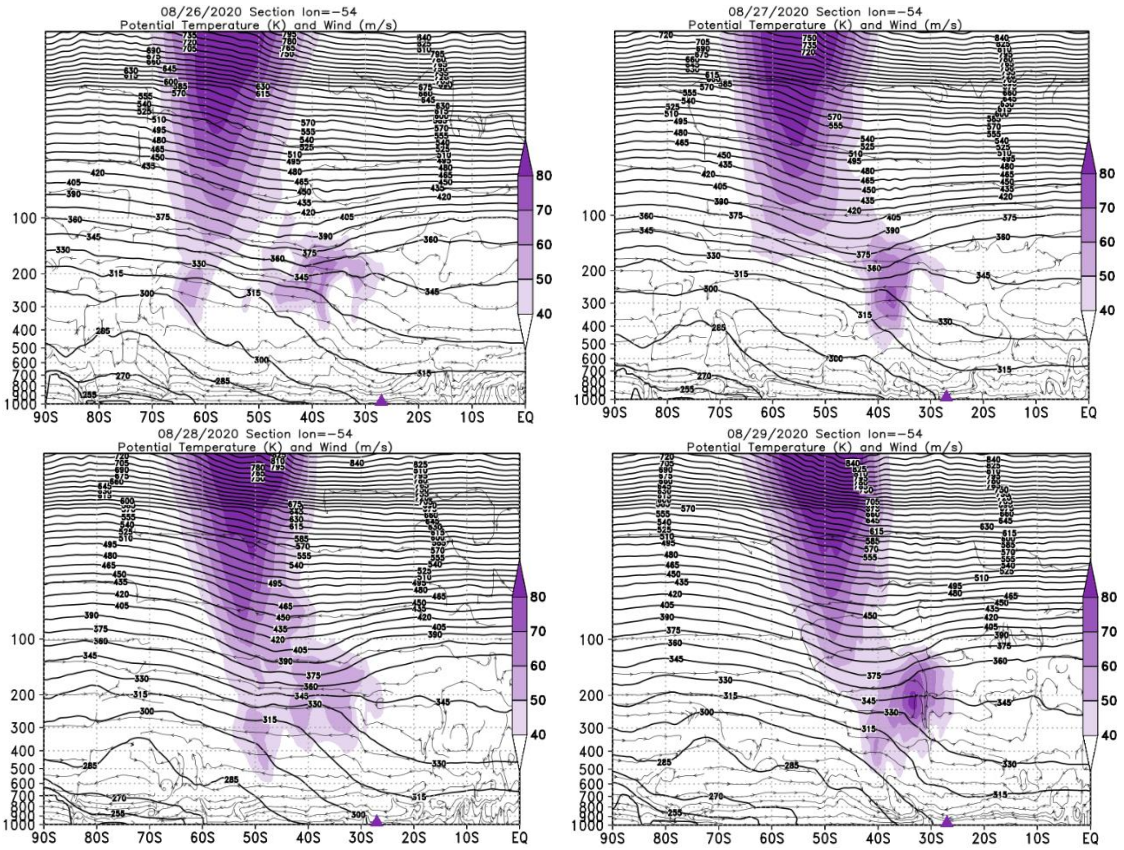

Source: The author.

09/03/2020

Figure A289: PVA fields for the 20 hPa in pressure levels, days 09/01/2020 to 09/04/2020.

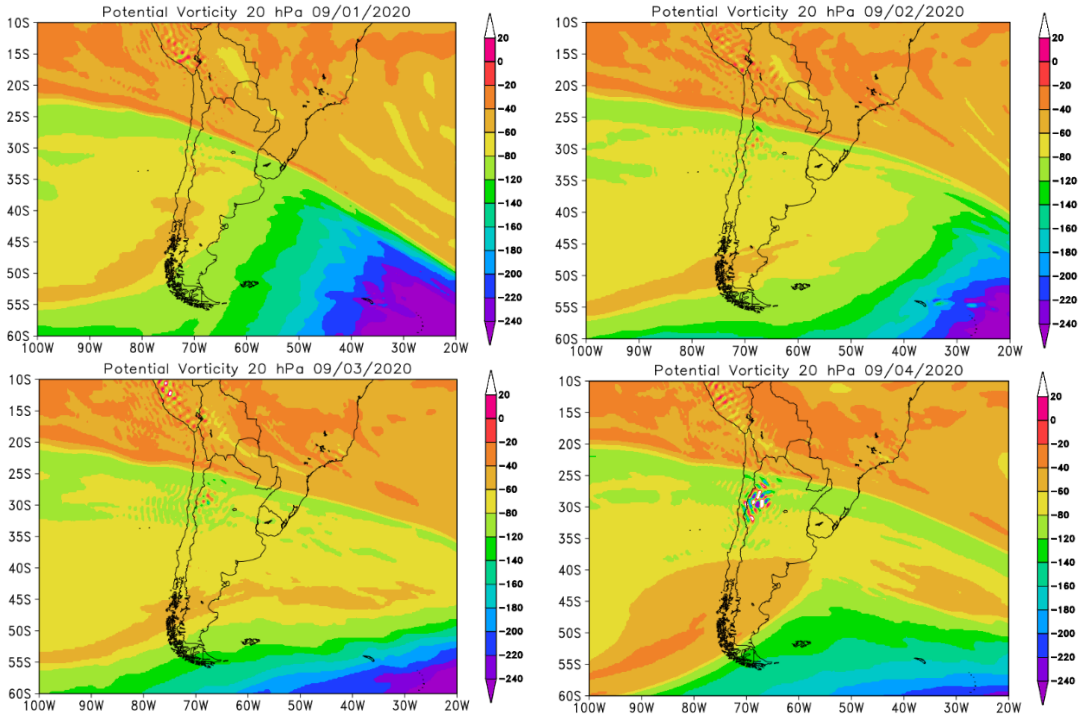

Source: The author.

Figure A290: Retroactive trajectory by the HYSPLIT/NOAA model, O3 content OMI satellite for South Pole, and global view.

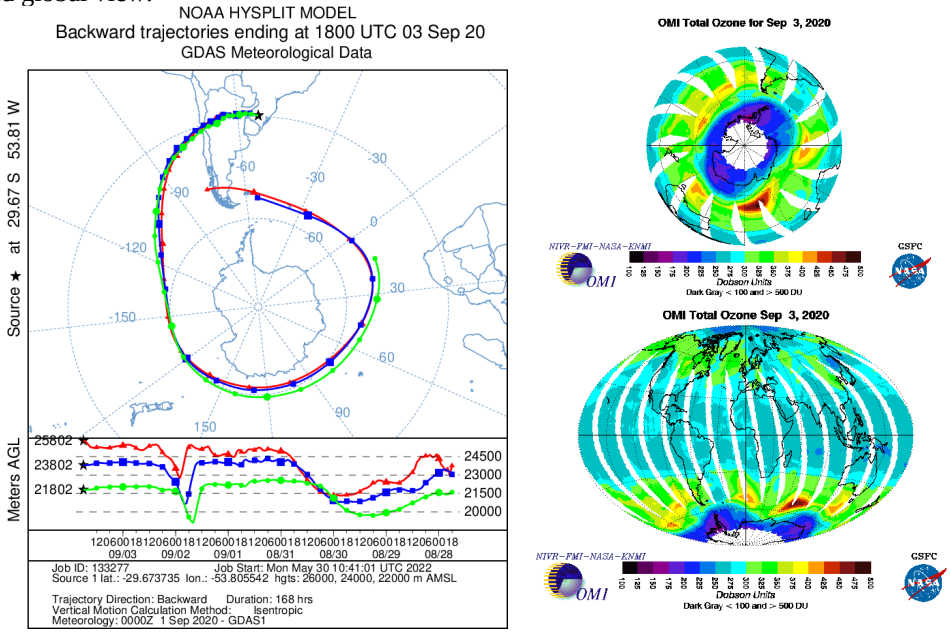

Source: HYSPLIT/NOAA, OMI/NASA.

Figure A291: Vertical section of the atmosphere between 1000 and 5 hPa for the days of the event in September 2020.

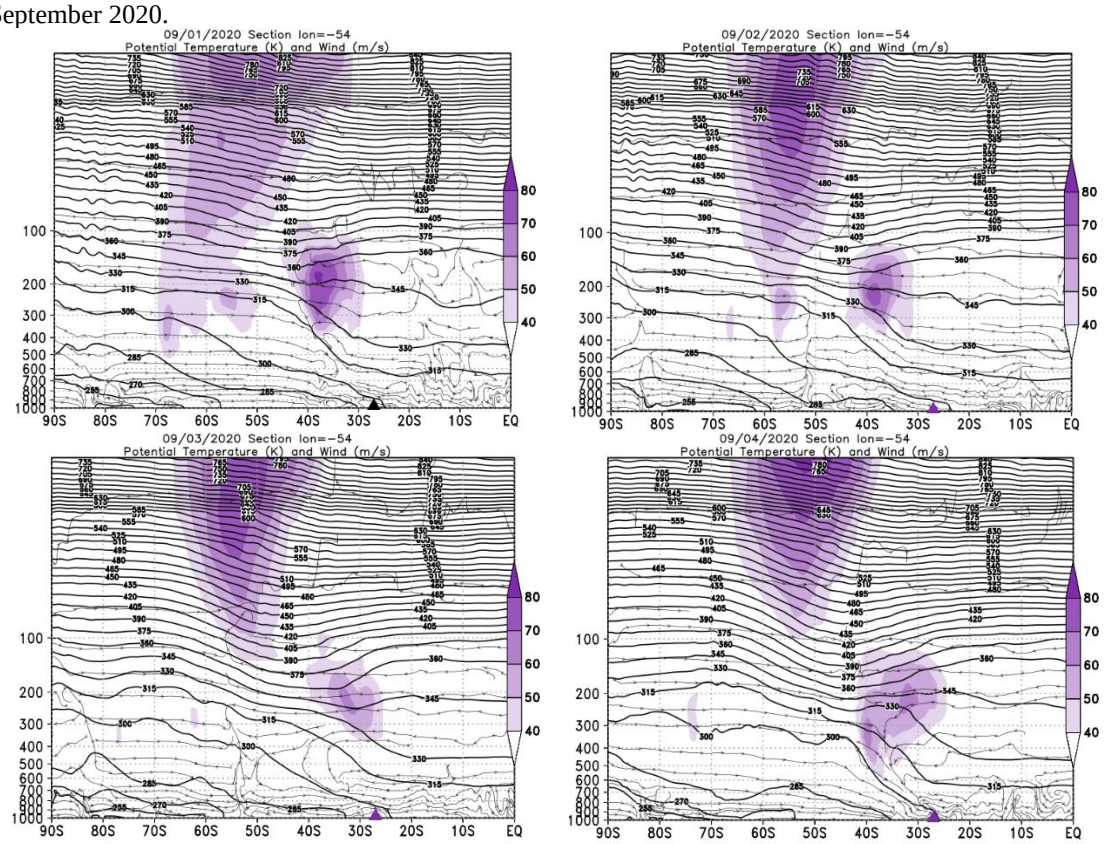

Source: The author.

10/21/2020

Figure A292: PVA fields for the 20 hPa in pressure levels, days 10/19/2020 to 10/22/2020.

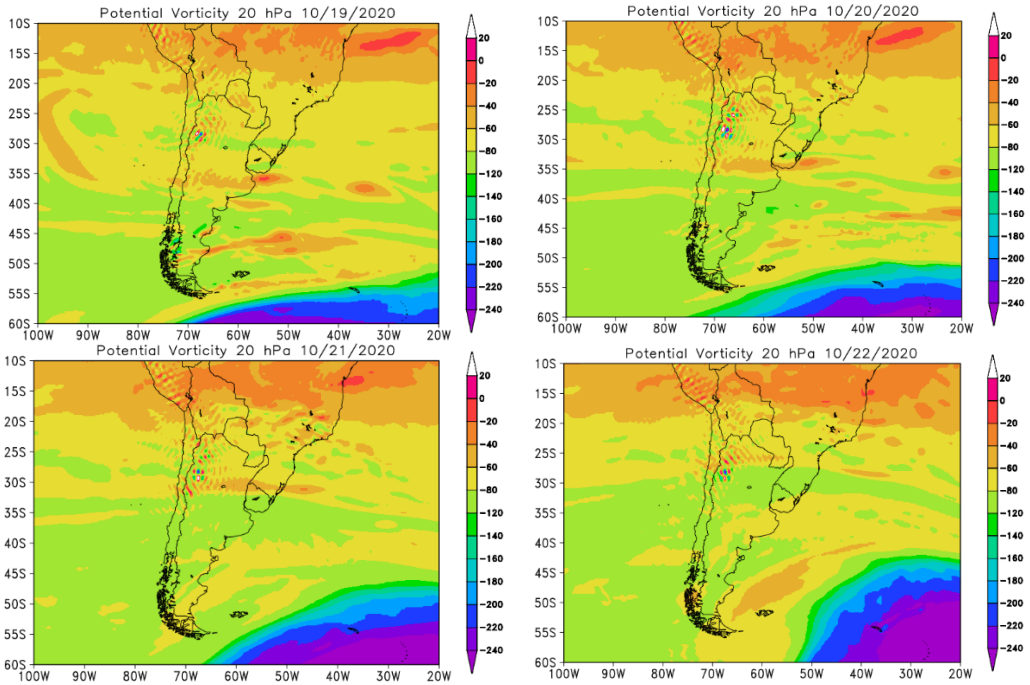

Source: The author.

Figure A293: Retroactive trajectory by the HYSPLIT/NOAA model, O3 content OMI satellite for South Pole, and global view.

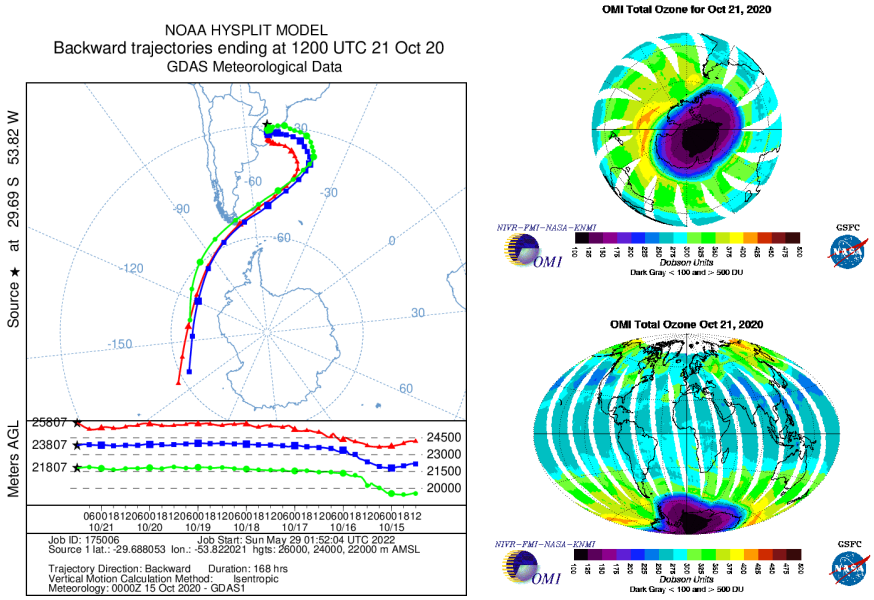

Source: HYSPLIT/NOAA, OMI/NASA.

Figure A294: Vertical section of the atmosphere between 1000 and 5 hPa for the days of the event in October 2020.

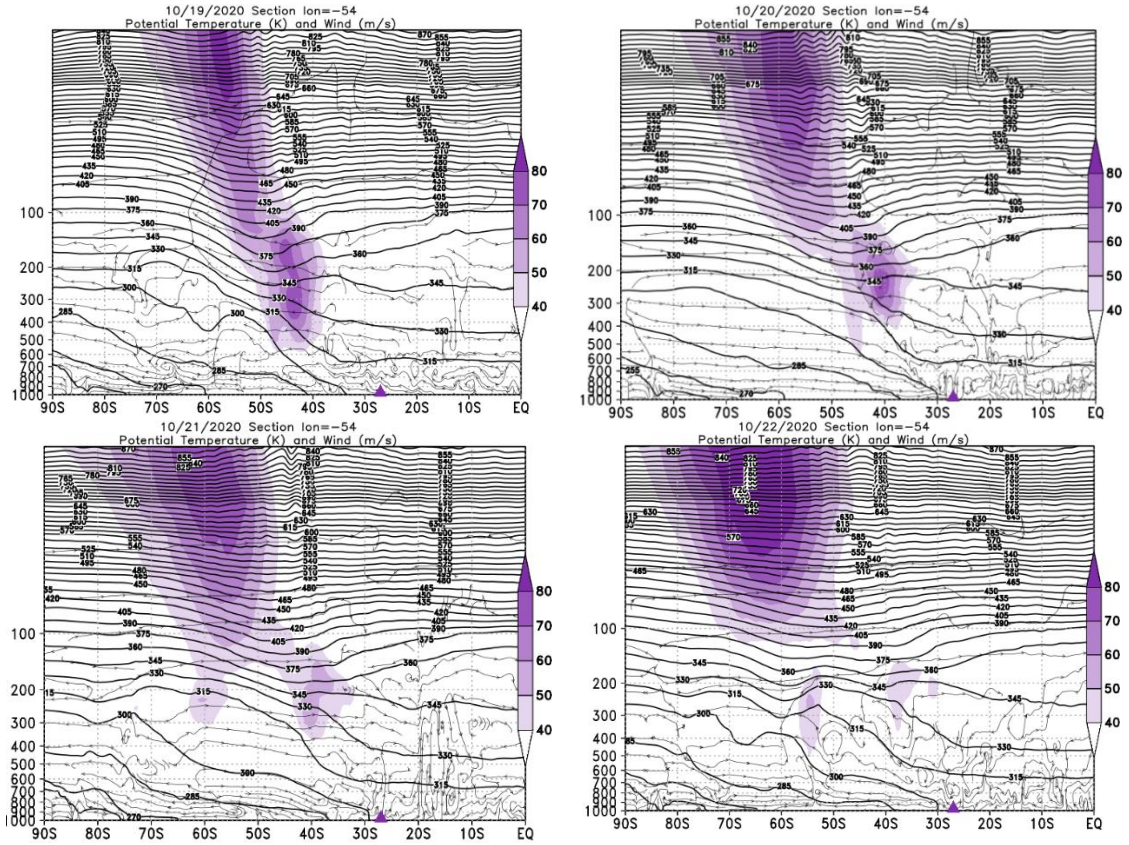

Source: The author.

11/22/2020

Figure A295: PVA fields for the 20 hPa in pressure levels, days 11/20/2020 to 11/23/2020.

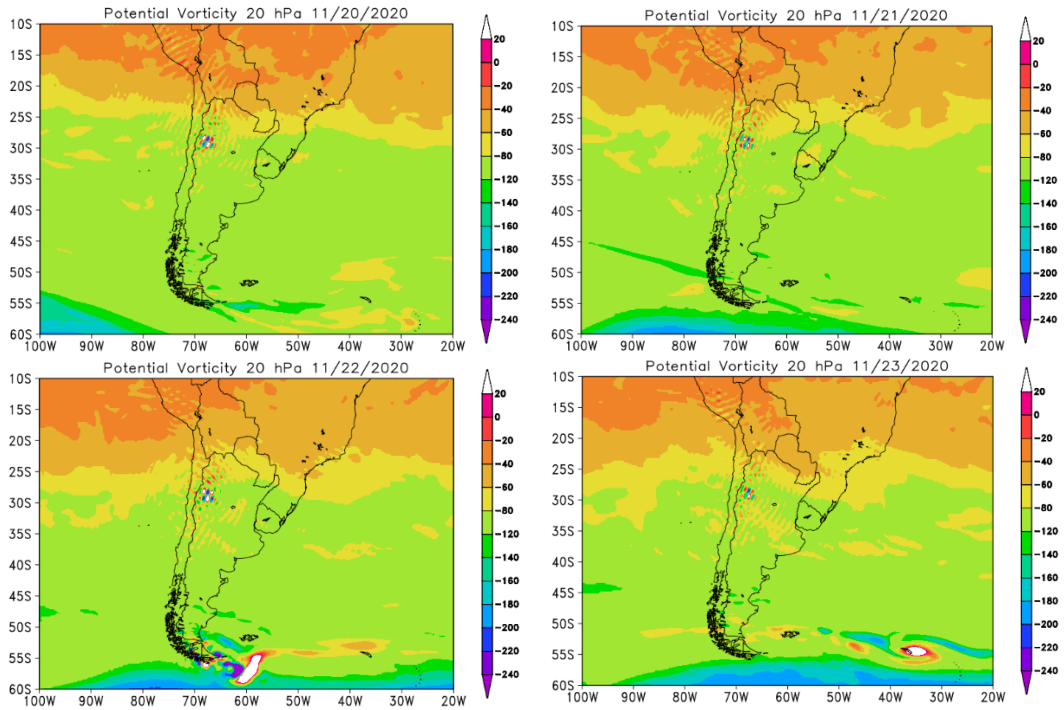

Source: The author.

Figure A296: O3 content OMI satellite for South Pole, and global view.

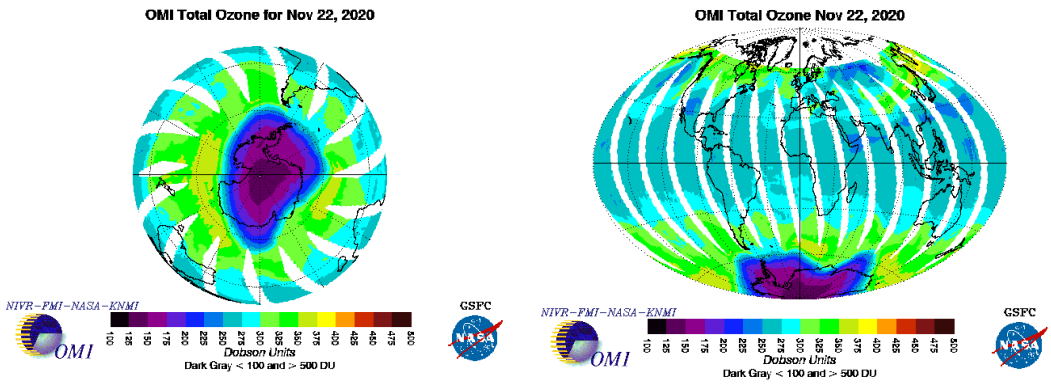

Source: OMI/NASA.

Figure A297: Vertical section of the atmosphere between 1000 and 5 hPa for the days of the event in November 2020.

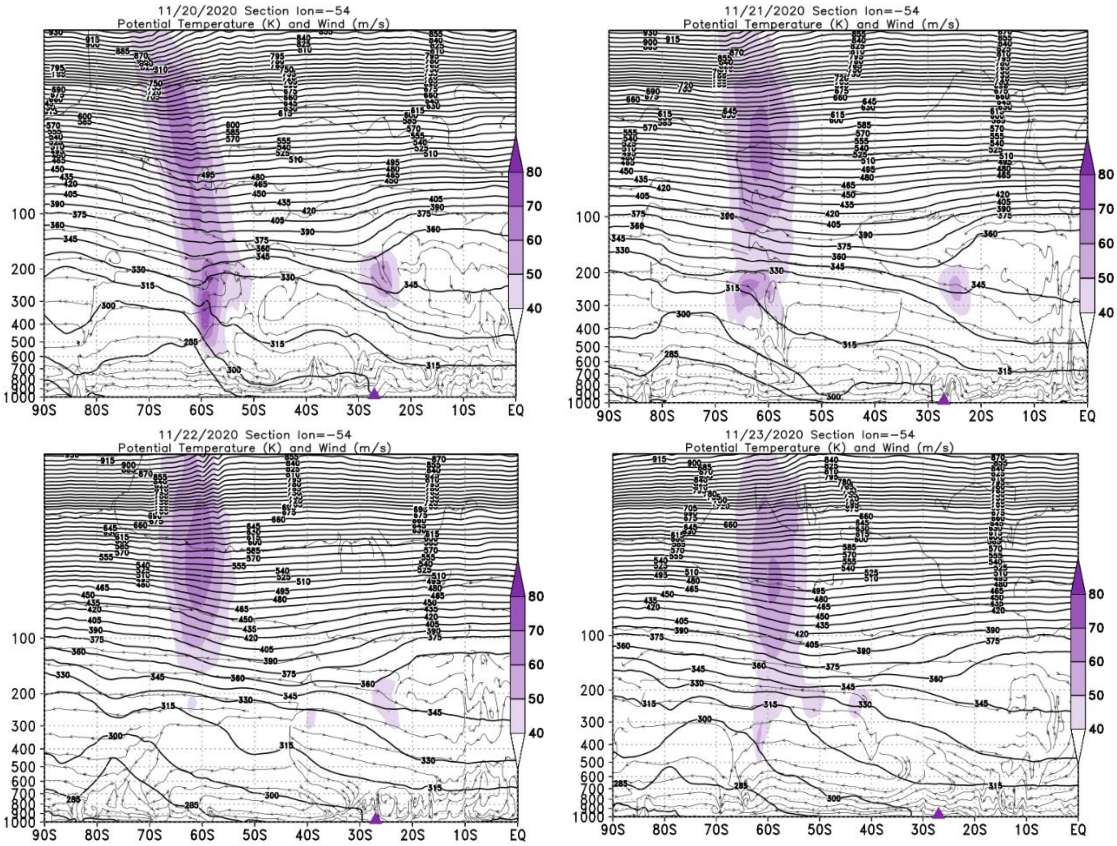

Source: The author.